CHEMICAL ENGINEERING SCIENCE
GENIE CHIMIQUE

VOL. 16 1961 Nos. 3 and 4

Determination of the Conditions at Minimum Reflux when the keys are the most and least volatile components

J. A. McDonough and C. D. Holland

Department of Chemical Engineering, A. and M. College of Texas, College Station, Texas, U.S.A.

and

H. L. Bauni

Humble Oil and Refining Company, Baytown, Texas, U.S.A.

(*Received* 18 *July* 1960; *in revised form* 24 *January* 1961)

Abstract—Proofs of the relationships between the temperature and composition of the feed and those of the pinches are given for feeds having any one of five general thermal conditions. In the application of these relationships a procedure for the calculation of the product distributions at specified distillate and reflux rates is presented.

Résumé—L'auteur donne des preuves des relations existant entre la température et la composition de l'alimentation et celles des " pinches " pour des alimentations ayant l'une ou l'autre des 5 conditions thermiques générales.

Dans le cadre de l'application de ces relations, l'auteur présente un procédé pour le calcul des distributions de produit et des taux de reflux pour un distillat déterminé.

Zusammenfassung—Für die Beziehungen zwischen der Temperatur und der Zusammensetzung des Zulaufs und den Werten der Zwickelbereiche werden Bestätigungen für Zuläufe für irgendeine der fünf allgemeinen thermischen Bedingungen angegeben. Bei der Anwendung dieser Beziehungen wird eine Methode für die Berechnung der Produktverteilung bei speziellen Destillier- und Rücklaufgeschwindigkeiten mitgeteilt.

The relationships which are proved herein apply at minimum reflux to distillation columns when the keys are the most and least volatile components of the mixture. These components are also for convenience referred to as the lightest and heaviest, respectively. The columns considered contain a single feed plate and two withdrawals, the distillate and bottoms.

The term " pinch " is used to denote the existence of a limit for the vapour and for the liquid mole fractions as the number of plates is increased without bound. Following the proofs a few applications are given. These applications represent a different approach than that taken by Shiras *et al.* [1] and Bachelor [2]. These authors solved the problem in which the separations of two components are specified and the minimum reflux ratio (L_0/D) required to effect the separation is determined. In the applications presented the distillate rate, D, and the overhead vapour rate, V_1, (or L_0) are specified and the corresponding product distribution is determined, provided the keys are the most and least volatile components of the mixture.

As discussed by Gilliland [3], when two components other than the lightest and heaviest are designated as the key components, the rectifying pinch occurs infinite plates above the feed plate after all components less volatile than the heavy key have been separated. The pinch

in the stripping section occurs infinite plates below the feed plate. It occurs in the limit as all components lighter than the light key have been separated.

When the keys are specified as the most and least volatile components of the mixture, the rectifying pinch occurs adjacent to the feed plate and the stripping pinch occurs at and generally includes the feed plate, as shown in Figs. 1–5. This has been discussed by Jenny [4] and Underwood [5].

Feeds having any one of five general thermal conditions are considered herein. The action assumed to occur at the feed plate for each type of feed is given by the following definitions. A boiling-point liquid feed is defined as one that enters the column as a liquid at its boiling point at the column pressure. A subcooled feed is defined as one which enters the column as a liquid at a temperature below its bubble point at the column pressure. For boiling-point and subcooled feeds it is assumed that the liquid upon entering the column mixes perfectly with the liquid on the feed plate and comes to equilibrium with the vapour immediately above it. A dew point vapour feed is one which enters the column as a vapour at its dew point at the column pressure. A superheated feed is defined as one which enters the column as a vapour at a temperature above its dew point at the column pressure.

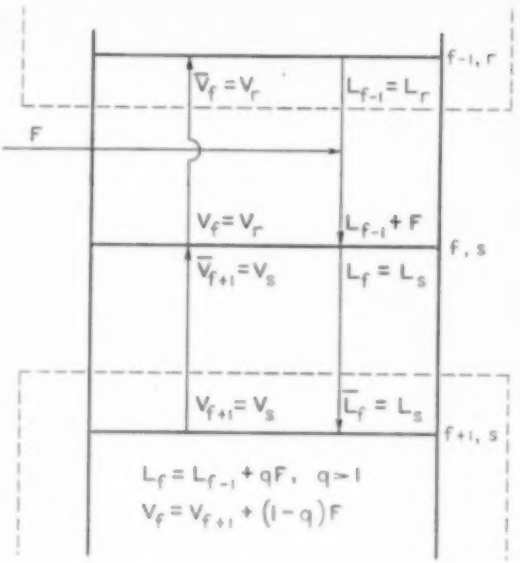

Fig. 2. Conditions on the feed plate for subcooled feeds.

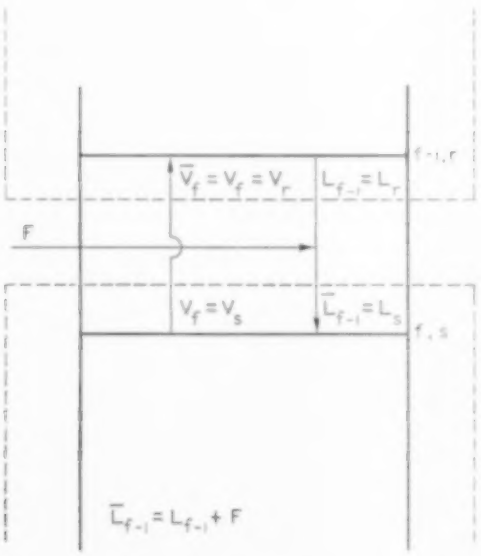

Fig. 1. Conditions on the feed plate for bubble-point liquid feeds.

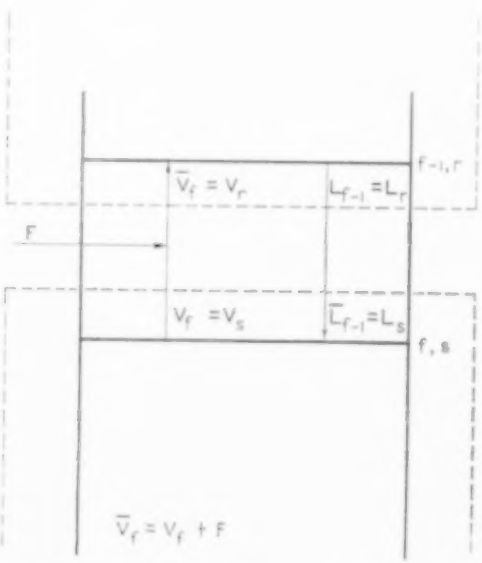

Fig. 3. Conditions on the feed plate for a dew-point vapour feed.

VOL. 16 1962

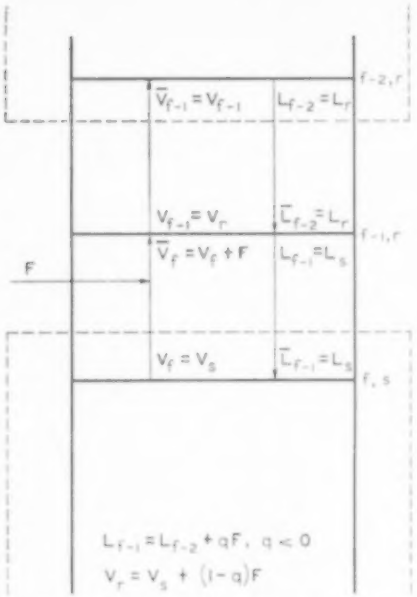

FIG. 4. Conditions on the feed plate for a superheated feed.

For dew point and superheated feeds it is assumed that the vapour upon entering the column mixes perfectly with the vapour rising from the feed plate and enters the plate above. (Equilibrium between the mixed vapour and the liquid on the feed plate is not assumed). A partially vapourized feed is defined as one which consists of an equilibrium mixture of liquid and vapour at the temperature T_F and at the column pressure. As illustrated in Fig. 5 the liquid part of the feed flows onto the feed plate, mixes perfectly with the liquid on the tray and comes to equilibrium with the vapour immediately above it. The vapour part of the feed is considered to mix perfectly with the vapour rising from the feed plate and then to enter the plate above the feed plate.

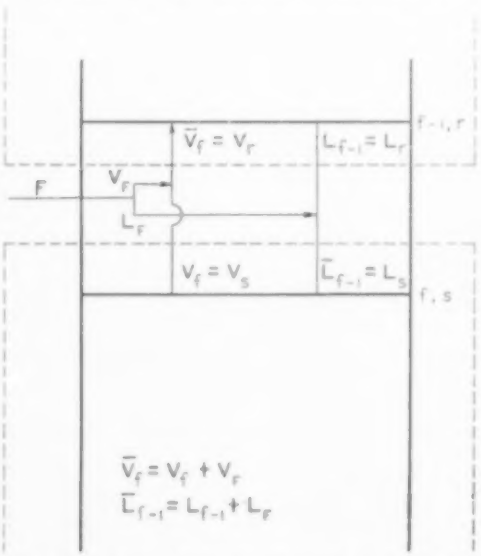

FIG. 5. Conditions on the feed plate for a partially-vapourized feed.

In the proofs which follow the equilibrium constants in Henry's law are taken to be positive functions of temperature and pressure. Throughout the pinches, the compositions are constant for each component i. For the rectifying pinch this is expressed as follows:

$$\lim_{j\to\infty} y_{ji} = y_{ri} \quad \text{and} \quad \lim_{j\to\infty} x_{ji} = x_{ri}$$

Thus the temperatures are constant throughout each pinch. Since the enthalpies are functions of the compositions and temperatures of the respective pinches it follows that the enthalpies as well as the flow rates remain constant throughout each pinch.

The relationships of the pinch compositions and temperatures with each other and with those of the feed are given in Table 1 for feeds having any one of the five thermal conditions. Except for a partially-vapourized feed, which is treated in a subsequent section, the relationships shown in Table 1 are obtained in a similar manner to that shown for a boiling-point liquid feed. For such a feed, $v_{fi} = v_{ri}$ and $v_{ri} = v_{si}$. Thus, $y_{ri} = y_{si}$ and since equilibrium exists at each pinch, $x_{ri} = x_{si}$ and $T_r = T_s$. For subcooled and superheated feeds the equality of the pinch compositions follows from the equilibrium relationships given in Table 2. The composition of the feed is related to those of the pinches by equation (3), which is based on the following material balance:

$$FX_{Fi} + L_r x_{ri} + V_s y_{si} = V_r y_{ri} + L_s x_{si} \qquad (1)$$

Let the thermal condition of the feed be defined in terms of q as follows:

$$L_s = L_r + qF, \quad \text{or} \quad V_r - V_s = (1-q)F \qquad (2)$$

Table 1. Relationships necessary for the keys to be the most and least volatile components of the feed

Thermal condition of the feed	*Relationships*	*Inequality*
Boiling-point liquid	$y_{ri} = y_{si}$, $x_{ri} = x_{si}$, $X_{Fi} = x_{ri}$ and $T_F = T_r = T_s$	$K_1^* - K_c^* < \dfrac{F}{V_r}$
Subcooled liquid	$y_{ri} = y_{si}$, $x_{ri} = x_{si}$, $T_r = T_s$ and T_r is given by Eq. [5]	$K_1 - K_c < \dfrac{(1-q)\,FK_1}{V_r} + \dfrac{qF}{V_r}$
Partially vapourized	$y_{ri} = y_{si} = y_{Fi}$, $x_{ri} = x_{si} = x_{Fi}$ and $T_r = T_s = T_F$	$K_1 - K_c < \dfrac{(1-q)\,FK_1}{V_r} + \dfrac{qF}{V_r}$
Dew-point vapour	$x_{ri} = x_{si}$, $y_{ri} = y_{si}$, $T_r = T_s$, $X_{Fi} = y_{ri}$ and $T_F = T_r = T_s$	$K_1 - K_c < \dfrac{K_1 F}{V_r}$
Superheated vapour	$x_{ri} = x_{si}$, $y_{ri} = y_{si}$, $T_r = T_s$ and T_r is given by equation (3)	$K_1 - K_c < \dfrac{(1-q)\,FK_1}{V_r} + \dfrac{qF}{V_r}$

*Where the components of the feed are numbered in the order of decreasing volatility; the most volatile component is denoted by "1" and the least volatile by "c."

Table 2. Formulae needed for the calculation of b_i/d_i

Thermal condition of the feed	*Calculation of b_i/d_i*
Boiling-point liquid	$\dfrac{b_i}{d_i} = \dfrac{(v_{fi}/d_i)}{(v_{fi}/b_i)}$, $\dfrac{v_{fi}}{d_i} = \dfrac{v_{fi}}{d_i}$, $\dfrac{v_{fi}}{b_i} = \dfrac{v_{si}}{b_i}$
Subcooled liquid	$\dfrac{b_i}{d_i} = \dfrac{(v_{fi}/d_i)}{(v_{fi}/b_i)}$, $\dfrac{v_{fi}}{d_i} = \dfrac{v_{ri}}{d_i}$, $\dfrac{v_{fi}}{b_i} = \left(\dfrac{V_r}{V_s}\right)(S_{si})\left(\dfrac{l_{si}}{b_i}\right)$
Partially vapourized	$\dfrac{b_i}{d_i} = \dfrac{(l_{f-1,i}/d_i) + (l_{Fi}/FX_{Fi})}{(v_{fi}/b_i) + (v_{Fi}/FX_{Fi})}$, $\dfrac{l_{f-1,i}}{d_i} = \dfrac{l_{ri}}{d_i}$, $\dfrac{v_{fi}}{b_i} = \dfrac{v_{si}}{b_i}$
Dew-point vapour	$\dfrac{b_i}{d_i} = \dfrac{(l_{f-1,i}/d_i)}{(l_{f-1,i}/b_i)}$, $\dfrac{l_{j-1,i}}{d_i} = \dfrac{l_{ri}}{d_i}$, $\dfrac{l_{f-1,i}}{b_i} = \dfrac{l_{si}}{b_i}$
Superheated vapour	$\dfrac{b_i}{d_i} = \dfrac{(l_{f-1,i}/d_i)}{(l_{f-1,i}/b_i)}$, $\dfrac{l_{f-1,i}}{d_i} = \left(\dfrac{L_s}{L_r}\right)(A_{ri})\left(\dfrac{v_{ri}}{d_i}\right)$, $\dfrac{l_{f-1,i}}{b_i} = \dfrac{l_{si}}{b_i}$

General pinch equations for a feed of any thermal condition

Rectifying section	*Stripping section*
$\dfrac{v_{ri}}{d_i} = \dfrac{1}{1 - A_{ri}}$, $\dfrac{l_{ri}}{d_i} = A_{ri}\left(\dfrac{v_{ri}}{d_i}\right)$	$\dfrac{l_{si}}{b_i} = \dfrac{1}{1 - S_{si}}$, $\dfrac{v_{si}}{b_i} = S_{si}\left(\dfrac{l_{si}}{b_i}\right)$

Once it has been shown that $y_{ri} = y_{si}$ and $x_{ri} = x_{si}$ equations (1) and (2) may be combined to give the expression for the familiar q-line.

$$X_{Fi} = (1 - q)\, y_{ri} + q x_{ri} \tag{3}$$

Since $q = 1$ for a boiling-point liquid feed it follows from equation (3) that $X_{Fi} = x_{ri}$ and thus $T_F = T_r$. For subcooled and superheated feeds T_r is determined by use of equation (5), which is developed in the following manner. Equation (3) may be solved for x_{ri} to give

$$x_{ri} = \frac{X_{Fi}}{(1 - q)\, K_{ri} + q} \tag{4}$$

VOL. 16 1962

Summation of both sides of this expression over all components leads to the function $p(T)$, where

$$p(T) = \sum_{i=1}^{c} \frac{X_{Fi}}{(1 - q)\, K_{ri} + q} - 1 \tag{5}$$

The temperature which gives $p(T) = 0$ is $T = T_r = T_s$.

Partially-vapourized Feeds

For systems with a feed of this type in which the keys are the lightest and heaviest components it is to be shown that at minimum reflux

(1) $T_F = T_r = T_s$

(2) $y_{Fi} = y_{ri} = y_{si}$ and $x_{Fi} = x_{ri} = x_{si}$

The equality of the temperatures is established by means of an indirect proof. In the first part of the proof it will be shown that $T_F = T_r$. In order to prove this it is supposed that $T_F < T_r$ and then a contradiction is obtained. Next it is supposed that $T_F > T_r$ and again a contradiction is obtained. This leads to the conclusion that $T_F = T_r$. In the second part of the proof it is shown in a similar manner that $T_F = T_s$. In the final part of the proof the equality of the compositions is shown. The development of certain relationships needed in the proofs follows. The conditions at the feed plate are described by the following equations:

$$\bar{y}_{fi} = y_{ri},\ x_{f-1,i} = x_{ri},\ \bar{x}_{f-1,i} = x_{si},\ y_{fi} = y_{si} \tag{6}$$

$$y_{Fi} = K_{Fi} x_{Fi},\quad y_{fi} = K_{fi} x_{fi} \tag{7}$$

$$V_r\, \bar{y}_{fi} = V_s\, y_{fi} + V_F\, y_{Fi} \tag{8}$$

$$L_s\, \bar{x}_{f-1,i} = L_r\, x_{f-1,i} + L_F\, x_{Fi} \tag{9}$$

$$V_r = V_s + V_F,\quad L_s = L_r + L_F \tag{10}$$

Also since the feed plate is in the stripping section $T_f = T_s$, but it remains to be shown that $T_r = T_s$. Equations (6) and (8) may be combined to give

$$V_r\, y_{ri} = V_s\, y_{si} + V_F\, y_{Fi} \tag{11}$$

Division of each member of this equation by K_{ri}, followed by the summation over all components gives

$$V_r = V_s \sum_{i=1}^{c} \frac{y_{si}}{K_{ri}} + V_F \sum_{i=1}^{c} \frac{y_{Fi}}{K_{ri}},\ \text{since} \sum_{i=1}^{c} \frac{y_{ri}}{K_{ri}} = 1.$$

This expression for V_r may be combined with equation (10) to give

$$\frac{V_s}{V_F} = \frac{\left[\sum_{i=1}^{c} (y_{Fi}/K_{ri})\right] - 1}{1 - \left[\sum_{i=1}^{c} (y_{si}/K_{ri})\right]} \tag{12}$$

Commencing with equations (6), (9) and (10), the expression for L_r/L_F is developed in an analogous manner to that shown for V_s/V_F.

$$\frac{L_r}{L_F} = \frac{\sum_{i=1}^{c} K_{ri} x_F - \sum_{i=1}^{c} K_{ri} x_{si}}{\sum_{i=1}^{c} K_{ri} x_{si} - 1} \tag{13}$$

Equations (12) and (13) are used in the proofs which follow.

Part I – To prove: $T_F = T_r$

Proof. Suppose $T_F < T_r$. Consideration of equation (12) on the basis of this supposition shows that

$$\sum_{i=1}^{c} \frac{y_{Fi}}{K_{ri}} < 1$$

Since all flow rates are positive $V_s/V_F > 0$. These two results require that

$$\sum_{i=1}^{c} \frac{y_{si}}{K_{ri}} > 1,$$

which is satisfied provided

$$T_r < T_s \tag{14}$$

Consideration of equation (13) under the same supposition, $T_F < T_r$, gives

$$\sum_{i=1}^{c} K_{ri} x_{Fi} > 1$$

and since $L_r/L_F > 0$, it is necessary that

$$1 < \sum_{i=1}^{c} K_{ri} x_{si} < \sum_{i=1}^{c} K_{ri} x_{Fi}$$

in order for equation (13) to be satisfied. Since by this inequality

$$\sum_{i=1}^{c} K_{ri} x_{si} > 1$$

it follows that

$$T_r > T_s \tag{15}$$

This result constitutes a contradiction to the previous one (equation (14)). Therefore, the supposition $T_F < T_r$ is false. Thus, T_F must be either equal to or greater than T_r. That T_F can not be greater than T_r is proved next.

Suppose $T_F > T_r$. By a method analogous to that used to obtain equation (14) it is readily shown that equation (12) leads to the following conclusion

$$T_s < T_r \tag{16}$$

Similarly, consideration of equation (13) on the basis of the supposition that $T_F > T_r$ leads to the relationship.

$$T_s > T_r \tag{17}$$

This result contradicts the previous one (equation (16)). Therefore the supposition $T_F > T_r$ is false. Hence, T_F must be either less than or equal to T_r. When this conclusion is compared with the previous one which follows equation (15) the desired conclusion

$$T_F = T_r \tag{18}$$

is obtained.

Part II – To prove: $T_F = T_s$

In an analogous manner to that shown for the development of equations (12) and (13) the following relationships are readily obtained:

$$\frac{V_s}{V_F} = \frac{\sum_{i=1}^{c} (y_{Fi}/K_{si}) - \sum_{i=1}^{c} (y_{ri}/K_{si})}{\sum_{i=1}^{c} (y_{ri}/K_{si}) - 1} \tag{19}$$

$$\frac{L_r}{L_F} = \frac{\sum_{i=1}^{c} K_{si} x_{Fi} - 1}{1 - \sum_{i=1}^{c} K_{ri} x_{ri}} \tag{20}$$

Proof. Because of the repetition involved only an outline of the proof is given. Suppose $T_F < T_s$. In an analogous manner to that shown for the supposition that $T_F < T_r$ of Part I, it is readily deduced that T_F is either equal to or greater than T_s. Similarly, when it is supposed that $T_F > T_s$, it is found that T_F is either less than or equal to T_s. Therefore

$$T_F = T_s \tag{21}$$

In view of equations (18), (21) and the fact that $T_f = T_s$ the desired result

$$T_F = T_f = T_r = T_s$$

is obtained.

Part III – To prove: $y_{Fi} = y_{ri} = y_{si}$ and $x_{Fi} = x_{ri} = x_{si}$

Proof. By use of the previous result, $T_F = T_r = T_s$, it will be shown that $y_{si} = y_{Fi}$. Beginning with $v_{ri}/d_i = l_{ri}/d_i + l$ and $v_{ri} = v_{si} + v_{Fi}$, it is readily shown that

$$\frac{b_i}{d_i} = \frac{(l_{ri}/d_i) + (l_{Fi}/FX_{Fi})}{(v_{si}/b_i) + (v_{Fi}/FX_{Fi})} \tag{22}$$

Also, at the stripping pinch v_{si} is given by

$$v_{si} = \left(\frac{S_{si}}{1 - S_{si}}\right) b_i \tag{23}$$

An over-all material balance for component i may be rearranged to the following form:

$$b_i = \frac{FX_{Fi}}{1 + (d_i/b_i)} \tag{24}$$

Furthermore, since

$$\frac{l_{ri}}{d_i} = \frac{A_{ri}}{1 - A_{ri}} \tag{25}$$

and $K_{ri} = K_{si}$, $V_r = V_s + V_F$ and $L_s = L_r + L_F$, equations (22)–(25) may be solved to give

$$v_{si} = v_{Fi} \frac{\left[1 + (V_r L_F / V_F L_r)\right]}{\left[(V_r L_s / V_s L_r) - 1\right]} = \frac{V_s}{V_F} v_{Fi} \tag{26}$$

Therefore, $y_{si} = y_{Fi}$. By use of this result and equations (10) and (11) it follows that $y_{ri} = y_{si}$. Hence,

$$y_{ri} = y_{si} = y_{Fi} \tag{27}$$

Since $T_F = T_r = T_s$ division of each member of equation (27) by K_{Fi} yields

$$x_{ri} = x_{si} = x_{Fi} \tag{28}$$

Applications

In the following treatment of a system at minimum reflux it is supposed that D, V_1, the thermal condition of the feed and the column pressure are specified and that the keys are designated as the most and least volatile components of the mixture. For this set of specifications it is desired to find the product distribution at infinite plates in both sections. Systems in which L/V remains constant throughout each section of the column and those where L/V may vary in each section of the column are considered.

Constant molal overflows in each section

When the specifications are as stated previously the product distribution is readily obtained, provided it exists; that is a set of values for D and V_1 may be specified such that it is impossible for the keys to be the lightest and heaviest components of the mixture. In which case one or both of the pinches occur away from the feed plate. A system may be examined to determine whether or not it is possible at the specified values of D and V_1 for the keys to be the lightest and heaviest components. Since the flow rates of all components in the pinches are greater than zero it is necessary that A_{ri} and S_{si} be less than unity. The quantity A_{ri} is largest when $i = c$, the heaviest component, and S_{si} is largest for $i = 1$, the lightest component. These conditions and similar ones for feeds of other thermal conditions lead to the inequalities stated in Table 1. If the inequality corresponding to a given feed condition is satisfied for a given set of specifications a solution is said to exist. It is to be observed that either the heaviest (or lightest) component ceases to be a key as it becomes completely separated in the limit as A_{rc} (or S_{s1}) approaches unity.

When the thermal condition of the feed is either boiling-point liquid, dew-point vapour or partially vapourized the product distribution is calculated by use of the formulae given in Table 2, as illustrated by Example 1 of Table 3. For systems with feeds having one of these thermal conditions a direct solution exists because the temperature of the feed is equal to that of the pinches.

For the case of either a superheated or a

Table 3. Statement and solution of example 1

Statement

Comp. no.	K_{Fi}	FX_{Fi}	*Specifications*
1	1·5	33·3333	Thermal condition of feed = boiling-point liquid
2	1·0	33·3333	
3	0·5	33·3333	$D = 50$, $V_1 = V_r = 90$, (Thus, $L_r = 40$, $L_s = 140$, $V_s = 90$) The keys are components "1" and "3"

Solution

Comp. no.	$A_{ri} = \frac{L_r}{K_{Fi}V_r}$	$S_{si} = \frac{K_{Fi}V_s}{L_s}$	$\frac{b_i}{d_i}$	$d_i = \frac{FX_{Fi}}{1 + b_i/d_i}$
1	0·296296	0·964286	0·052632	31·666666
2	0·444444	0·642857	1·000000	16·666666
3	0·888889	0·321429	19·000000	1·666666

subcooled feed, the formulae given in Tables 1 and 2 are applicable, but some trial is involved since neither T_r nor T_s is known, only that $T_r = T_s$. The value of T to be employed is the one for which $p(T) = 0$, equation (5). It is to be observed that this T is a function of the thermal condition of the feed alone and independent of V_r, D and L_r. However, in order for a solution to exist at the specific values of D and V_1 it is necessary for the appropriate inequality given in Table 1 to be satisfied at the T which gives $p(T) = 0$. If the inequality is not satisfied it is impossible for the keys to be the lightest and heaviest components of the mixture.

In the solution of Example 2, Table 4, equation (5) was used to determine the temperature of the pinches. The results obtained for Examples 1 and 2 were checked by use of the formulae stated by Murdoch and Holland [6]. In the application of their formulae the values of b_i/d_i for components 1 and 3 obtained for Examples 1 and 2 were taken as the specifications. The corresponding values of D and L_0/D were then computed and found to be in agreement with those specified for Examples 1 and 2.

Variable overflows

For the case of variable overflows the calculational procedure for the determination of the product distribution at specified values of D and V_1 follows closely that described for systems in which the molal overflows remained constant within each section of the column, except that the flow rates at the pinches are determined by use of enthalpy and material balances.

When the thermal condition of the feed is either boiling-point liquid, dew-point vapour or partially vapourized the following general procedure is recommended. On the basis of an assumed value for V_r which satisfies the appropriate inequality of Table 1 b_i, d_i for each component is computed by use of the appropriate formula given in Table 2. Then by use of an over-all material balance, equation (24), the product rates for each component are calculated. After these have been computed the compositions needed in the enthalpy balances are calculated. After the temperature (or temperatures) of the distillate and the top plate have been determined by means of the appropriate equilibrium (bubble point or dew point) and material balance calculations the condenser duty is found by making an enthalpy balance around the condenser. The vapour and liquid rates at the rectifying pinch are calculated by means of enthalpy and material balances around the condenser and the rectifying

Table 4. Statement and solution of example 2

Comp. no.	α_i	FX_{Fi}	*Specifications*
1	3·0	33·3333	Superheated feed : $q = -0{\cdot}05$. $D = 50$, $V_1 = V_r = 120$
2	2·0	33·3333	(Thus, $L_0 = L_r = 70$, $L_s = 65$). The keys are components 1 and 3. (Note, for constant $-\alpha$ problems it is convenient to replace K_i of equation (5) by $\alpha_i K_b$ and find the value of K_b which gives $p(T) = 0$)
3	1·0	33·3333	

Solution

Comp. no.	K_i (by equation (5) $K_b = 0{\cdot}61768375$)	b_i	d_i
1	1·85305125	6·54185	26·791482
2	1·2353675	12·420323	20·913010
3	0·61768375	31·037828	2·295505

pinch. After these rates have been determined the flow rates at the stripping pinch are readily determined by use of the appropriate material balances.

Instead of using the particular value of V_r (computed by means of enthalpy balances) for the next trial a better value to be employed is the one given by interpolation (*regula falsi*), as described by SOKOLNIKOFF [7]. Before this value of V_r may be used it is necessary to determine whether or not it satisfies the appropriate inequality of Table 1. If it does not the value of V_r to be assumed for the next trail is obtained by adjusting the computed value as required to satisfy the inequality. The correct product distribution has been obtained when the assumed and calculated values of V_r are in agreement. If it is impossible to obtain agreement between these values and to satisfy the given inequality simultaneously a solution does not exist as discussed in the preceding section.

In order to illustrate the use of the equations for variable L/V problems Example 3 shown in Table 5 was solved by two different methods, direct interation and interpolation. In the method of direct interation the assumed value of

VOL. 16 1962

Table 5. Statement and solution of example 3

Component	FX_{Fi}	*Specifications*
C_3H_1	20·0	Boiling-point liquid feed (267·34°F at 400 p.s.i.a.).
$i\,C_4H_{10}$	20·0	$D = 40$, $V_1 = 55$, $L_0 = 15$. The keys are C_3H_8 and
$n\,C_4H_{10}$	20·0	$n\,C_5H_{12}$. (Curve-fits for the equilibrium data are given
$i\,C_5H_{12}$	20·0	in Table 6 and those for the enthalpies are given in
$n\,C_5H_{12}$	20·0	Ref. [8].)

Solution

Trial no.	$(V_r)_{assumed}$	$(V_r)_{calculated}$	*Component*	d_i
1	55	54·499	C_3H_8	17·168039
2	54·499	54·852	$i\,C_4H_{10}$	9·501945
3	54·7058*	54·7060	$n\,C_4H_{10}$	7·361634
4	54·7058	54·7059**	$i\,C_5H_{12}$	3·440505
			$n\,C_5H_{12}$	2·527875

*For all trials after the second the assumed value was determined by interpolation.
†In order to obtain this same accuracy by direct intertion thirteen additional trials were required.

*Table 6. Equilibrium data**

Comp.	$a_1 \times 10^2$	$a_2 \times 10^5$	$a_3 \times 10^7$	$a_4 = 10^{10}$
C_3H_8	− 27·980091	118·11943	− 10·935041	3·5180421
$i\,C_4$	− 23·209137	87·122379	− 6·6100972	1·6677740
$n\,C_4$	− 23·203344	83·753226	− 6·177436	1·5243376
$i\,C_5$	− 6·981454	8·8862037	3·9689556	− 2·9075073
$n\,C_5$	3·7103008	− 36·257004	9·9113800	− 5·444111

$(K_i/T)^{1/3} = a_{1i} + a_{2i}\,T + a_{3i}\,T^2 + a_{4i}\,T^3$, ($T$ in °R)
*See Ref. [9].

V_r for the next trial was taken equal to the one calculated by the previous trial. As shown in Table 5 more rapid convergence is obtained by use of interpolation.

Acknowledgments—The assistance given by Mr. W. M. Harp and Dr. K. K. McMillin of the Humble Oil and Refining Company is appreciated. The authors at the college wish to acknowledge the additional support given to them either individually or collectively by the E. I. du Pont de Nemours and Company, the National Science Foundation and the Texas Engineering Experiment Station, and for the encouragement given by Dr. E. C. Klipple of the college.

Notations

A_{ji} = absorption factor for plate j and component i. $A_{r,i}$ = absorption factor for component i in the rectification pinch

b_i = molal withdrawal rate of component i in the bottom product

B = molal withdrawal rate of bottoms

c = total number of components : the least volatile component

d_i = molal withdrawal rate of component i in the distillate

D = molal withdrawal rate of distillate

f = feed plate

F = molal rate of flow of the entering feed

K_{ji} = the Henry-law constant ($y = Kx$) for component i at the temperature of plate j. For the rectifying pinch $j = r$ and for the stripping pinch $j = s$

l_{ji} = molal rate at which component i in the liquid state leaves plate j. $l_{f-1,i}$ = molal rate of flow of component i in the liquid state onto plate f.

l_{Fi} = molal rate of flow of component i in the liquid part of a partially-vapourized feed

L_j = total molal rate of flow of liquid from plate j. L_{f-1} = total molal rate of flow of liquid onto the feed plate

L_F = molal rate of flow of the liquid part of the feed. For boiling-point liquid and subcooled feeds $L_F = F$, and for dew-point vapour and superheated feeds $L_F = 0$

$p(T)$ = function of temperature : defined by equation (5)

q = a measure of the thermal condition of the feed : defined by equation (2)

S_{ji} = stripping factor for component i and for plate j

T = temperature in °R

v_{ji} = molal rate at which component i in the vapour state leaves plate j. v_{fi} = molal rate at which component i in the vapour state enters plate $f - 1$

v_{Fi} = molal rate of flow of component i in the vapour part of a partially vapourized feed

V_j = total molal rate of flow of vapour from plate j. V_f = total molal rate at which vapour enters plate $f - 1$.

V_F = molal rate of flow of the vapour part of the feed. For boiling-point liquid and subcooled feeds $V_F = 0$, and for dew-point vapour and superheated feeds $V_F = F$.

x_{Fi} = mole fraction of component i in the liquid part of a partially vapourized feed.

x_{ji}, $\bar{x}_{ji}$ = mole fraction of component i in the liquid leaving plate j and mole fraction of component i in the liquid flowing onto plate $j + 1$, respectively

X_{Di} = mole fraction of component i in the distillate regardless of state in which it is withdrawn

X_{Fi} = total mole fraction of component i in the total feed F, regardless of state

y_{Fi} = mole fraction of component i in the vapour part of a partially vapourized feed

y_{ji}, $\bar{y}_{ji}$ = mole fraction of component i in the vapour leaving plate j and mole fraction of component i in the vapour entering plate $j - 1$, respectively

α = relative volatility ; $\alpha_i = K_i/K_b$,

where $K_b = \dfrac{1}{\sum_{i=1}^{c} \alpha_i x_i} = \sum_{i=1}^{c} y_i/\alpha_i$ = value of K for the base component

References

[1] Shiras R. N., Hanson D. N. and Gibson G. H. *Industr. Engng. Chem.* 1950 **42** 871.
[2] Bachelor J. B. *Petrol. Refin.* 1957 **36** 161.
[3] Gilliland E. R. *Industr. Engng. Chem.* 1940 **32** 1019.
[4] Jenny F. J. *Trans. Amer. Inst. Chem. Engrs.* 1939 **35** 641.
[5] Underwood A. J. V. *Trans. Inst. Chem. Engrs.* 1932 **10** 112.
[6] Murdoch P. G. and Holland C. D. *Chem. Engr. Progr.* 1952 **48** 287.
[7] Sokolnikoff I. S. and Sokolnikoff E. S. *Higher Mathematics for Engineers and Physicists* p. 101 McGraw Hill, New York 1941.
[8] Lyster W. N., Sullivan S. L. Jr., Billingsley D. S. and Holland C. D. *Petrol. Refin.* 1959 **36** 221.
[9] *Equilibrium Ratio Data Book*. Natural Gasoline Association of America, Tulsa, Oklahoma 1957.

Chemical Engineering Science, 1961, Vol. 16, pp. 153 to 180. Pergamon Press Ltd., London. Printed in Great Britain.

The fluidization of light solids by gases under pressure and heavy solids by water

A study of the transition between aggregative and particulate fluidization

H. C. Simpson and B. W. Rodger

Imperial Chemical Industiers Ltd., Nobel Division,
Research and Development Department, Stevenston.

(*Received* 9 *September* 1960 ; *in revised form* 9 *February* 1961)

Abstract—As the result of an experimental study of the fluidization of light solids by gases under various pressures and the fluidization of heavy solids by water, a general family of curves has been produced relating a generalized fluid velocity to a bed porosity function for a series of values of a parameter P involving the fluid and solid properties only. This correlation satisfies both liquid- and gas-fluidised beds and indicates that there is no fundamental difference in mechanism between a liquid-fluidized bed and a gas-fluidized bed. It also enables direct comparison to be made between flow through a fluidized bed and flow through a fixed bed of similar porosity.

By treating an aggregatively-fluidized bed as a two-phase system and making reasonable assumptions about the rise of bubbles the general bed expansion correlation is used to produce general correlations of mean bubble velocities, frequencies, concentrations and volumes in terms of the mean bed porosity and the parameter P. These correlations predict that a gas system normally has a comparatively small number of large bubbles and appears to fluidize aggregatively. A liquid system may have a large number of small bubbles and appear to fluidize particulately although certain liquid–solid systems will fluidize aggregatively. The values of the bubble characteristics for both liquid and gas systems are in approximate agreement with those observed. These correlations can also be used to predict the fraction of fluid passing through the bed in bubble form and hence gives assistance to the estimation of the efficiency of the fluidized bed as a chemical reactor. The effect of gas pressure on this efficiency is also discussed.

Résumé—L'étude expérimentale de la fluidisation de solides lègers par des gaz sous différentes pressions, et de la fluidisation de solides lourds par l'eau a permis d'obtenir un ensemble de courbes reliant la vitesse généralisée du fluide à la porosité du lit pour une série de valeurs du paramètre P faisant seulement intervenir les propriétés du solide et du fluide. Cette correlation concerne à la fois les lits fluidisés liquides et gazeux et montre qu'il n'y a pas de différence fondamentale entre les mécanismes des deux systèmes. Elle permet aussi une comparaison directe entre un écoulement dans un lit fluidisé et un écoulement dans un lit fixe de porosité identique.

En considérant un lit fluidisé aggloméré comme un système à deux phases et en faisant des hypothèses raisonnables sur la formation des bulles la relation générale d'expansion du lit donne les relations générales des vitesses moyennes des bulles, fréquences, concentrations et volumes en fonction de la porosité moyenne du lit et du parametrè P. Ces relations prévoient qu'un système gazeux a normalement et comparativement un petit nombre de grosses bulles et fluidise par agglomération. Un système liquide peut avoir un grand nombre de petites bulles et se fluidise par particules bien que certains systèmes liquides fluidisent par agglomérats. Les caractéristiques des bulles pour les systèmes gazeux et pour les systèmes liquides sont en assez bon accord avec l'observation. Les relations peuvent servir à prévoir la fraction de fluide qui traverse le lit sous forme de bulles et par là à estimer l'efficacité d'un lit fluidisé pour un réacteur chimique. Les auteurs discutent également l'effet de la pression du gaz sur l'efficacité.

Zusammenfassung—Als Ergebnis experimenteller Untersuchungen von Wirbelschichten aus leichten Feststoffen und Gasen bei verschiedenen Drucken und aus schweren Feststoffen und Wasser wurde eine generelle Schar von Kurven erhalten, in welchen eine verallgemeinerte Strömungs-

geschwindigkeit mit der Bettporositätsfunktion für eine Reihe von Werten des Parameters P in Beziehung steht, wobei P nur Eigenschaften des strömenden Mediums und des Feststoffes enthält. Diese Korrelation genügt sowohl den Flüssigkeits- als auch den Gaswirbelschichten und zeigt damit, dass kein grundsätzlicher Unterschied im Mechanismus zwischen beiden besteht. Ausserdem gestattet die Beziehung einen direkten Vergleich zwischen der Strömung durch eine Wirbelschicht und der durch ein Festbett ähnlicher Porosität.

Durch die Behandlung eines inhomogenen Wirbelbettes als zweiphasiges System und durch das Treffen plausibler Annahmen über den Aufstieg von Blasen, konnte die allgemeine Beziehung über die Bettausdehnung benutzt werden, um allgemeine Korrelationen für die Blasengeschwindigkeiten, Frequenzen, Konzentrationen und Volumen in Ausdrücken für die mittlere Bettporosität und den Parameter P aufzustellen. Diese Korrelationen sagen voraus, dass ein Gassystem normalerweise eine vergleichsweise kleine Zahl von grossen Blasen enthält, und dass es inhomogen zu wirbeln scheint. Ein Flüssigkeitssystem kann eine grosse Zahl kleiner Blasen haben und scheint homogen zu wirbeln, obwohl bestimmte Flüssigkeits-Feststoff-Systeme inhomogen wirbeln. Die Werte für die Blasencharackteristika für Flüssigkeits- und Gassysteme sind in angenäherter Übereinstimmung mit den beobachteten Werten. Diese Beziehungen können auch dazu benutzy werden, den Anteil des strömenden Mediums zu berechnen, der in Form von Blasen aufsteigt. Damit ist ein Hilfsmittel für die Bestimmung des Wirkungsgrades Wirbelschicht als chemischer Reaktor gegeben. Der Einfluss des Gasdruckes auf diesen Wirkungsgrad wird ebenfalls diskutiert.

VOL
16
196

Introduction

Originally introduced for the catalytic cracking of petroleum fluidized beds have found extensive use in other heterogeneous reactions, in the distillation of materials producing tarry residues, in the drying of solids and as crystallizers, blenders and conveyors. The literature on the characteristics and applications of fluidization is vast but some of it has been summarized by Othmer [1], Reboux [2] and Leva [3]. Despite the wide range of application of the technique the mechanics of the process are not understood. The only reliable calculation that can be made is the estimation of the fluid velocity required for incipient fluidization in terms of the fluid and solid properties and the bed porosity.

In general, if a liquid is used to fluidize a solid, the concentration of solid particles throughout the expanded bed appears to be roughly uniform. The fluidization is particulate. If a gas is used to fluidize a solid pockets or bubbles of the gas rise rapidly through the otherwise uniformly fluidized bed. This is aggregative fluidization. Yasui and Johanson [4] observed the passage of bubbles between two light probes immersed in a gas-fluidized bed and concluded that bubbles increase in size by coalescence as they rise, the large ones overtaking the slow ones. However, the origin of the bubbles cannot be regarded as established since Yasui and Johanson were not able to detect bubbles less than $\frac{1}{2}$ in. in diameter. It is thus not known whether the bubbles are formed immediately above the distributor or throughout the bed depth although Rice and Wilhelm [5] have shown theoretically that the lower surface of a fluidized bed is unstable when lifted above the distributor and have calculated the wavelength of a disturbance of maximum rate of growth in terms of the effective bed viscosity.

Davidson *et al.* [6] have shown that the bubbles rise at the same rate as in an inviscid liquid of low surface tension. This suggests that the bubbles are true voids and contain few particles but throws no light on the forces stabilizing these bubbles.

It appears then that before a reliable theory of bubble formation, growth and history can be developed more must be known about the differences between aggregative and particulate fluidization.

Preliminary experiments in which sand was fluidized by air at atmospheric pressure in beds 6·5 cm in diameter and 15 cm tall, with sintered glass plates of several porosities used as gas distributors, showed no noticeable difference in the character of the fluidization when the ratio of the pressure drop in the distributor to that in the bed ranged between 0·35 and 15·5. It thus seemed likely that the transition from particulate

to aggregative fluidization was a problem of the hydrodynamic stability of the particulate fluidization and was not strongly affected by the distributor. It was the purpose of this work to define and find experimentally parameters separating one type of fluidization from another.

It is clear that since most gas–solid systems fluidize aggregatively and most liquid–solid systems particulately, and since the most outstanding difference between the two systems is the ratio ρ_s/ρ_f where ρ_s is the solids density and ρ_f the fluid density a promising approach would be to attempt to fluidize gas–solid systems particulately by working with systems of low ρ_s/ρ_f, and to fluidize liquid–solid systems aggregatively by using systems with high ρ_s/ρ_f. This was the approach adopted here.

Flow through a fixed bed

The results of the studies on fluidization were interpreted on the basis of flow through a fixed bed. Useful surveys on packed-bed flow have been provided by Carmen [7] and Scheidegger [8] but the clearest theory is that which treats the bed as a random bundle of capillary tubes, as follows.

The pressure gradient (dp/dL) for flow of an incompressible fluid down a channel of circular cross-section and diameter d_e is given by

$$-\frac{dp}{dL} = \frac{2 f_e \bar{v}^2 \rho_f}{g_c d_e}$$

where $\bar{v}$ is the linear velocity of the fluid, g_c is the units conversion factor, and f_e the friction factor is a function of the Reynolds number $d_e \bar{v} \rho_f/\mu_f$, ρ_f the fluid density and μ_f the fluid viscosity. If there are n channels/unit cross-section of bed the linear velocity $\bar{v}$ can be evaluated in terms of the fluid superficial velocity

$$V = \frac{\pi d_e^2}{4} \bar{v} n.$$

Furthermore, for a given geometry of packing the channel diameter d_e can be evaluated in terms of the bed porosity ϵ and the surface area of the particles per unit volume of the particles S_0 according to the porportionalities $\epsilon \propto n d_e^2$ and $(1-\epsilon) S_0 \propto n d_e$. Finally if a shape factor ϕ is defined so that S_0 is related to the particle diameter d by the equation $S_0 = 6 d \phi$, it is possible to eliminate n, d_e, $\bar{v}$ and S_0 to yield the basic equation for flow through a fixed bed. Written in dimensionless form with all the terms involving velocity on one side this equation is of the form

$$\left(\frac{f \mathrm{Re}}{90}\right)\left(\frac{\mathrm{Re}}{\mathrm{Gr}}\right) = \frac{1}{180}\left(\frac{\Delta P}{L}\right)_R \frac{\epsilon^3}{(1-\epsilon)^2} \qquad (1)$$

where the friction factor f includes the constants of proportionality and is a function of the Reynolds number Re defined as

$$\mathrm{Re} = \frac{(d/\phi)\, V \rho_f}{(1-\epsilon)\mu_f} \qquad (2)$$

where Gr is a number similar to the Grashof number used in natural convection and is defined as

$$\mathrm{Gr} = \frac{(d/\phi)^3 \rho_f^2 g}{\mu_f^2} \frac{\rho_s - \rho_f}{\rho_f} \qquad (3)$$

and $(\Delta P/L)_R$ is the reduced pressure gradient defined as

$$\left(\frac{\Delta P}{L}\right)_R = -\frac{dp/dL}{(\rho_s - \rho_f)(1-\epsilon)} \frac{g_c}{g} \qquad (4)$$

Empirical curves have been obtained for f in terms of Re (equation 2). In general, for streamline flow (i.e. $\mathrm{Re} < 10$) $f = 90/\mathrm{Re}$. Equation (1) then reduces to the Carman–Kozeny equation for flow through a packed bed modified by the shape factor ϕ as recommended by Leva *et al.* [9]. For turbulent flow (i.e. $\mathrm{Re} > 100$) $f \sim 0{\cdot}5$ and equation (1) again reduces to the form used by Leva *et al.* [9]. For regions of transitional flow Leva *et al.* used a different friction factor and Reynolds number, but the Reynolds number defined by equation (2) with the porosity has a clear physical meaning based on the channel theory of flow through a packed bed.

Equation (1) forms the basis for the analysis of the data presented below. Other porosity functions have been proposed [10] but none appears better than the Carman–Kozeny function $\epsilon^3/(1-\epsilon)^2$ which also has the advantage of having a definite physical meaning as described above. At high porosities the channel theory

breaks down and a different porosity function must be used, e.g. that proposed by Brinkman [11]. However, Carman [7] claims that the function $\epsilon^3/(1-\epsilon)^2$ is valid up to a porosity of 0·7, well beyond the porosities of most fluidized beds.

Flow through a fluidised bed

Consider a bed fluidized aggregatively or particulately. In general the mean porosity ϵ of the bed as measured by the bed height will depend on the fluid velocity V, viscosity μ_f and density ρ_f; the particle diameter d, density ρ_s, shape factor ϕ and some dimensionless measure x of the surface roughness; the gravitational constant g, the bed diameter D and the initial bed height L_0. By dimensional analysis these ten independent variables can be collected into seven independent groups to give

$$\frac{\epsilon^3}{(1-\epsilon)^2}\left(\frac{\Delta P}{L}\right)_R = \phi_1\left(\frac{f\,\mathrm{Re}^2}{90\,\mathrm{Gr}}, G, \frac{\rho_s-\rho_f}{\rho_f}, \frac{d/\phi}{D}, \frac{L_0}{D}, \phi, x\right) \qquad (5)$$

where the porosity and velocity groups are chosen to agree with equation (1), $(\rho_s-\rho_f)/\rho_f$ is a group strongly dependent on pressure when a given solid is fluidized by gas and G, defined by the equation

$$G = \frac{(d/\phi)^3\, g\,(\rho_s-\rho_f)^2}{{\mu_f}^2} = \mathrm{Gr}\Big/\frac{\rho_f}{\rho_s-\rho_f}, \qquad (6)$$

is a group largely independent of gas pressure.

Experimental method

Two apparatus were constructed, one for fluidizing solids with various gases under pressure and the other for fluidizing solids with liquids.

The gas fluidization apparatus is shown in Fig. 1. The bed was made from a length of mild steel rod 11in. long and 3½ in. square with a 2½ in. diameter hole bored down the centre to form the bed space. Steel flanges 2½ in. in diameter and $\frac{3}{16}$ in. thick were bolted on to similar flanges welded on to a piece converging to the outlet pipe at the top and on to the distributor column at the bottom. Slots 1 in. wide and 9½ in. long were cut in two opposite sides of the bed and the open space filled with Perspex to give transparent windows roughly 1½ in. thick which were clamped on to the bed by means of ½ in. mild steel plate with similar slots cut in them. The distributor column was filled with ⅛ in. lead shot to a height of 6 in. and the bed was supported on a layer of porous nickel sheet (permeability $92{\cdot}5 \times 10^{-10}$ cm²; pore diameter 4–8 μ; thickness 0·022 in.) sealed on to a layer of 16 mesh, 26 w.g. brass gauze. The pressure drop through the column and sintered nickel reached a maximum of 120 g/cm², roughly 8 to 16 times the pressure drop through the bed depending on the weight of the bed.

The pump was placed inside a cylindrical steel shell so that the outside and inside of the pump could be raised to 100 p.s.i.g. and was driven externally by a 1 h.p. motor via a belt drive. The flow rate through the bed was controlled by passing some of the gas through a by-pass line shown in Fig. 1 and the speed of the pump was changed by changing the pulley ratio on the drive.

The basic measurements were gas pressure, pressure drop across the bed, gas flow rate and bed height. The pressure drop across the distributor and the pressure rise across the pump were also noted during some runs. The gas pressure was measured by a 0–100 p.s.i.g. Bourdon gauge and the pressure drop across the bed was measured in an inclined manometer filled with either a bromoform–alcohol mixture or water, depending on the density of the solid being studied. The pressure drop across the distributor and the pump were both measured by a Foxboro recording manometer (range 0–320 in. H_2O) with a system of valves shown in Fig. 1 for changing the manometer from the distributor to the pump. The gas flow rate was measured in two rotameters in parallel for which general calibration curves were drawn. The bed height was measured visually by means of a scale attached to one of the Perspex windows. When the upper surface of the bed bumped up and down at high gas velocities a mean value of the bed height was recorded.

The liquid fluidization apparatus, similar in principle to the gas apparatus, is shown in Fig. 2. The bed itself was glass, i.d. 3 in., o.d. 3½ in. and length 60 in., with Q.V.F. glass flanges 5 in. in diameter at the ends. The distributor column, made from mild steel piping (i.d. 3 in., height 12 in.), was filled with ⅛ in. lead shot contained between 30 mesh 26 w.g. brass gauze. The pressure drop through the distributor reached a maximum of 30 cm Hg, ranging between 4 and 70 times the bed weight depending on the bed height and the material being fluidized. Pressure drops, bed heights and volumetric flow rates were measured as above.

The solids fluidized in the high pressure gas bed were sieved between three consecutive B.S.S. meshes and the material in the middle sieve used for fluidization. The particle diameter was estimated by taking a mean of about 200 different particles measured in two directions at right angles on photomicrographs. The percentage deviation of particle diameter about the mean value was less than ± 10 per cent. The particle diameter of the larger solids fluidized in the liquid bed was measured directly on a micrometer. These particles were uniform in size and spherical in shape.

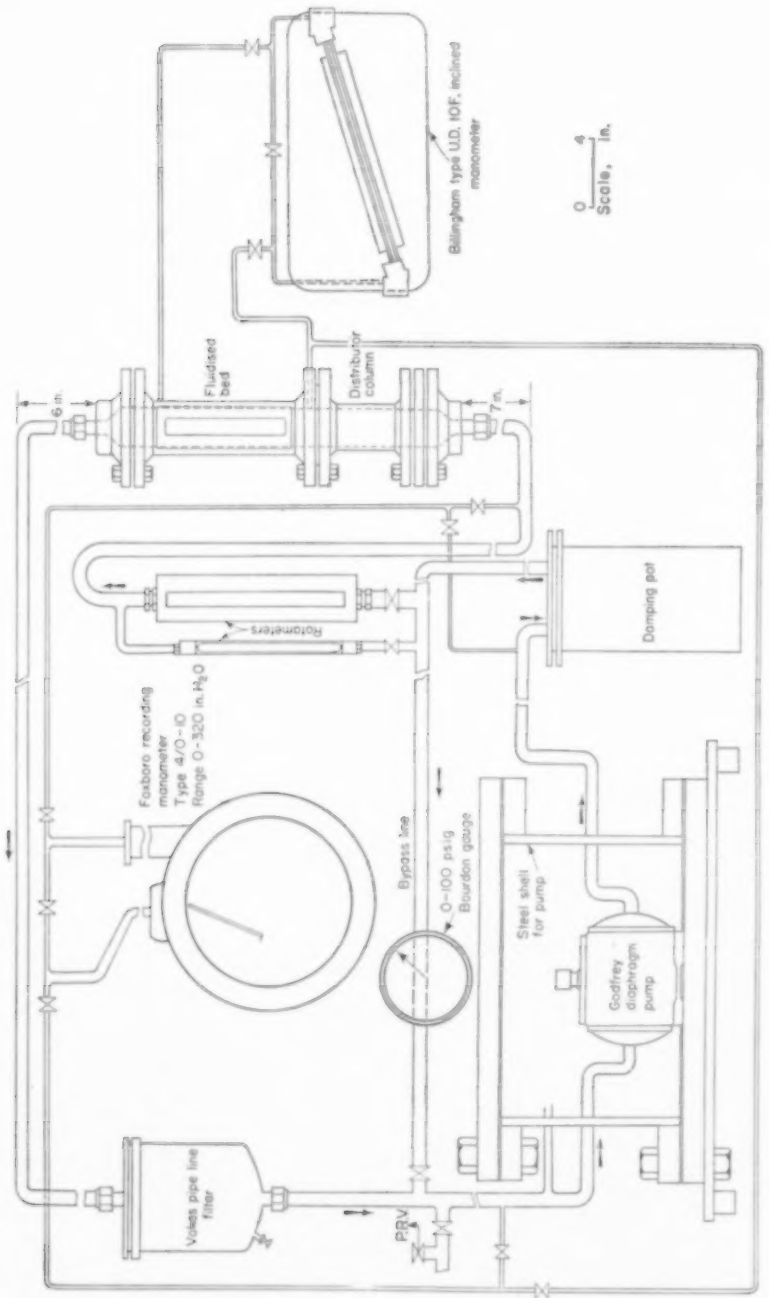

FIG. 1. Diagram of high pressure gas fluidization apparatus.

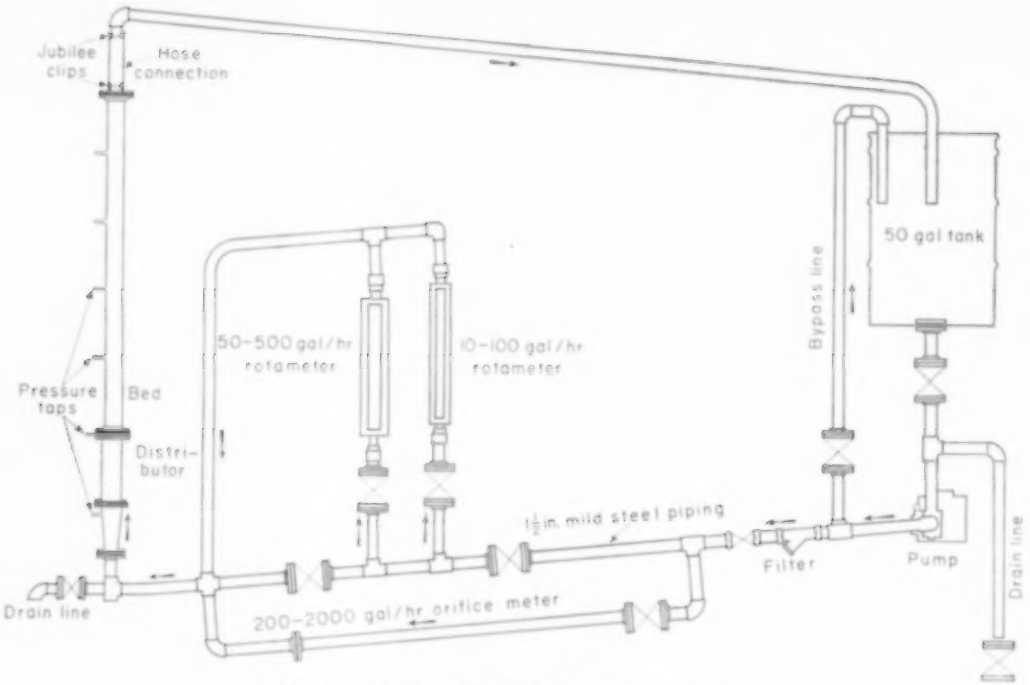

Fig. 2. Diagram of liquid fluidization apparatus.

Experimental Results

In the high pressure bed seven different solids were fluidized by air, argon, Arcton 6 (CCl_2F_2) and sometimes Arcton 33 ($C_2Cl_2F_4$) over a range of pressures. The properties of the fluidized beds studied in the various experiments are listed in Table 1. In the liquid bed, glass beads, steel spheres and lead shot were fluidized by water. The properties of the three systems are listed in Table 2.

All the gas–solid data were plotted in the form of

$$\frac{f\,\mathrm{Re}^2}{90\,\mathrm{Gr}} \text{ vs. } \left(\frac{\Delta P}{L}\right)_R \frac{\epsilon^3}{(1-\epsilon)^2}.$$

The results obtained for the sand and polyvinyl chloride (PVC) are typical and are shown in Figs. 3 and 4.* The ordinate, a generalized velocity term, can be written as $(f\,\mathrm{Re}/90)(\mathrm{Re}/\mathrm{Gr})$ where the correction factor $(f\,\mathrm{Re}/90)$ is 1·0 for streamline flow (i.e. $\mathrm{Re} < 10$) and greater than 1·0 for higher Reynolds number. This factor is plotted in Fig. 5 from the Carman friction factor curve presented by Reboux [2]. The abscissa

$$\left(\frac{\Delta P}{L}\right)_R \frac{\epsilon^3}{(1-\epsilon)^2}$$

represents the increase in pressure gradient across the bed in the static bed region (ϵ constant) and the growth of the voidage factor $\epsilon^3/(1-\epsilon)^2$ in the fluidized bed region ($[\Delta P/L]_R = 1$) as the fluid velocity increases. In the intermediate region of transition from static bed flow to fully developed fluidization both groups in the abscissa change. The limits of this transition region are also shown in Figs. 3 and 4.

Each family of curves represents a given solid fluidized by a given gas at a series of pressures. Since the fluid viscosity μ_f and the density difference $(\rho_s - \rho_f)$ are virtually independent of pressure for each gas the group G is constant for

*Because of the large number of systems studied and the limitations of space it is impossible to publish all the original bed height/fluid velocity/pressure drop data. However, since some of the systems are unusual, and may be of interest to other workers, these data are available on application to the Physical Chemistry Section, Research and Development Department, Nobel Division, I.C.I. Ltd.

Table 1. *Properties of gas fluidized beds*

(Data of SIMPSON and RODGER)

Solid	*Gas*	μ_f (*P*)	*G*	*Pressure* (p.s.i.g.)	ρ_f (g/cm³)	ρ_s/ρ_f	Gr	ϵ_0	*Run No.*
		$\times 10^{-4}$	$\times 10^5$		$\times 10^{-3}$	$\times 10^2$	$\times 10^2$		
				0	1·67	15·76	2·94	0·438	31
				20	3·95	6·68	6·94	0·412	32
	Argon	2·20	4·64	40	6·21	4·24	10·91	0·404	33
				60	8·49	3·10	14·91	0·398	34
				80	10·75	2·45	18·88	0·392	35
				96	12·37	2·09	22·05	0·392	36
		$\times 10^{-4}$	$\times 10^5$		$\times 10^{-3}$	$\times 10^2$	$\times 10^2$		
				0	1·205	21·83	3·03	0·434	18
				20	2·842	9·25	7·39	0·404	19
	Air	1·81	6·84	40	4·49	5·87	11·64	0·398	20
				60	6·12	4·30	15·89	0·393	21
				80	7·76	3·39	20·18	0·406	27
Sand				96	9·06	2·90	23·58	0·394	28
		$\times 10^{-4}$	$\times 10^5$		$\times 10^{-3}$	$\times 10^2$	$\times 10^2$		
									24
	Air +	1·373	11·92	0	3·76	7·00	17·02	0·423	25
	Arcton 6	1·373	11·92	20	9·06	2·90	41·1	0·409	23
		1·373	11·92	38	14·21	1·850	64·1	0·394	22
		1·302	13·45	50	20·02	1·315	101·6	0·398	26
		$\times 10^{-4}$	$\times 10^5$		$\times 10^{-3}$	$\times 10^2$	$\times 10^2$		
	Air +		16·29	0	6·936	3·86	42·1	0·412	30
	Arcton 33	1·160		10	11·66	2·26	71·6	0·398	29
		$\times 10^{-4}$	$\times 10^4$		$\times 10^{-3}$	$\times 10^2$	$\times 10$		
				0	1·676	7·17	5·96	0·414	61
				20	3·96	3·04	14·02	0·393	62
P.V.A.	Argon	2·19	4·29	30	5·11	2·35	18·14	0·393	63
				60	8·55	1·405	30·3	0·393	65
				80	10·84	1·109	38·3	0·411	66
		$\times 10^{-4}$	$\times 10^4$		$\times 10^{-3}$	$\times 10^2$	$\times 10$		
	Air	1·81	6·29	0	1·205	9·98	6·29	0·410	41
				20	2·842	4·23	14·81	0·397	42
				40	4·49	2·68	23·3	0·391	44

Table 1—*contd.*

Solid	*Gas*	μ_f (P)	G	*Pressure* (p.s.i.g.)	ρ_f (g/cm^3)	ρ_a/ρ_f	Gr	ϵ_0	*Run No.*
		$\times 10^{-4}$	$\times 10^5$		$\times 10^{-3}$	$\times 10^2$	$\times 10^2$		
				0	1·676	17·02	4·99	0·425	99
				20	3·960	7·21	11·81	0·390	98
	Argon	2·19	8·54	40	6·220	4·59	18·59	0·398	97
				60	8·550	3·34	25·45	0·387	100
				80	10·84	2·63	32·35	0·387	101
		$\times 10^{-4}$	$\times 10^6$		$\times 10^{-3}$	$\times 10^2$	$\times 10^2$		
				0	1·209	23·60	5·36	0·415	86
				20	2·865	9·96	12·61	0·398	87
Glass (A) (197·9)	Air	1·80	1·261	40	4·500	6·34	19·91	0·385	88
				60	6·125	4·66	27·0	0·396	89
				80	7·764	3·675	34·4	0·396	102
		$\times 10^{-4}$	$\times 10^6$		$\times 10^{-3}$	$\times 10^2$	$\times 10^2$		
				0	4·45	6·29	41·9	0·428	94
				10	7·85	3·635	72·4	0·425	90
	Arcton 6	1·24	2·632	20	11·25	2·538	103·7	0·425	93
				30	14·79	1·931	135·8	0·430	92
				40	18·47	1·546	169·1	0·409	91
				49	21·45	1·329	196·8	0·396	95
		$\times 10^{-4}$	$\times 10^5$		$\times 10^{-3}$	$\times 10^2$			
				0	1·209	23·60	61·6	0·462	103
Glass (B) (83·8)	Air	1·80	1·452	20	2·865	9·96	145·8	0·442	104
				40	4·500	6·34	229·0	0·448	105
				60	6·125	4·66	321·0	0·436	106
				80	7·764	3·675	395·0	0·436	107
		$\times 10^{-4}$	$\times 10^6$		$\times 10^{-3}$	$\times 10^2$	$\times 10^3$		
				0	1·209	23·60	2·60	0·390	108
	Air	1·80	6·14	40	4·500	6·34	9·66	0·376	109
Glass (C) (313·3)				80	7·764	3·675	16·69	0·376	110
		$\times 10^{-4}$	$\times 10^6$		$\times 10^{-3}$	$\times 10^2$	$\times 10^4$		
				20	11·25	2·538	5·08	0·380	111
	Arcton 6	1·24	12·89	30	14·79	1·931	6·64	0·376	112
				40	18·47	1·548	8·27	0·380	113

Table 1—contd.

Solid	*Gas*	μ_f (P)	G	*Pressure* (p.s.i.g.)	ρ_f (g/cm³)	ρ_s/ρ_f	Gr	ϵ_0	*Run No.*
		$\times 10^{-4}$	$\times 10^4$		$\times 10^{-3}$	$\times 10^2$	$\times 10$		
				0	1·676	7·08	3·52	0·639	80
				20	3·960	2·995	8·31	0·623	81
	Argon	2·19	2·49	40	6·220	1·909	13·02	0·617	82
				60	8·55	1·389	17·61	0·614	83
				80	10·84	1·092	22·58	0·617	84
		$\times 10^{-4}$	$\times 10^4$		$\times 10^{-3}$	$\times 10^2$	$\times 10$		
				0	1·205	9·81	3·75	0·652	67, 75
				20	2·842	4·16	8·84	0·624	68, 76
P.V.C.	Air	1·80	3·68	40	4·49	2·64	13·91	0·628	69, 78
				60	6·12	1·931	18·99	0·634	79
				80	7·76	1·522	24·05	0·610	85
		$\times 10^{-4}$	$\times 10^4$		$\times 10^{-3}$	$\times 10^2$	$\times 10$		
				0	4·54	2·62	29·4	0·643	70
				10	7·85	1·512	50·7	0·641	71
	Arcton 6	1·24	7·72	20	11·25	1·054	72·6	0·649	72
				30	14·79	0·804	95·1	0·641	73
				40	18·47	0·644	118·2	0·647	74
		$\times 10^{-4}$	$\times 10^3$		$\times 10^{-3}$	$\times 10^2$	$\times 10$		
Bakelite micro-balloons	Arcton 6	1·24	7·56	0	4·54	1·098	6·97	0·594	45
						$\times 10$	$\times 10^2$		
			7·48	10	7·85	6·34	1·119	0·597	46
			7·39	20	11·25	4·42	1·71	0·597	47

each family of curves. Within each family the density ratio $(\rho_s - \rho_f)/\rho_f$ or the Grashof number, Gr, varies from curve to curve. The values of these groups corresponding to each curve are listed in Table 1. In all of these runs the ratio of initial bed height to diameter (L_0/D) was maintained at about 2:1. The original gas bed data of this paper were supplemented by data obtained by Lewis *et al.* [12] on the fluidization of glass beads of various sizes by air at atmospheric pressure. In this case the initial bed height/diameter ration was about 10.: 1. These data are recorded in Fig. 6 and the properties listed in Table 3.

Each curve in Fig. 7 represents a given solid fluidized by water for the three different initial bed height/diameter ratios ranging between about 1 : 1 and 3 : 1. These original data were supplemented by those of Wilhelm and Kwauk [13] on the fluidization of glass beads of different

Table 2. Properties of beds fluidized with water
(Data of Simpson and Rodger)

Solid	μ_f (*P*)	*G*	ρ_f (g/cm³)	ρ_s/ρ_f	Gr	ϵ_0	L_0/D	*Run No.*
Glass beads (D) 3910 μ	$1{\cdot}005 \times 10^{-2}$	$1{\cdot}33 \times 10^{6}$	0·998	2·52	$8{\cdot}76 \times 10^{5}$	0·342	0·76	13
						0·348	1·43	12
						0·377	2·41	11
Steel spheres 3160 μ	$1{\cdot}056 \times 10^{-2}$	$1{\cdot}27 \times 10^{7}$	0·998	7·76	$1{\cdot}880 \times 10^{6}$	0·400	0·96	43
						0·408	1·78	42
						0·407	2·84	41
Lead shot 1710 μ	$1{\cdot}005 \times 10^{-2}$	$5{\cdot}07 \times 10^{6}$	0·998	11·22	$4{\cdot}96 \times 10^{5}$	0·383	0·90	10
						0·397	1·98	9
						0·399	2·95	8

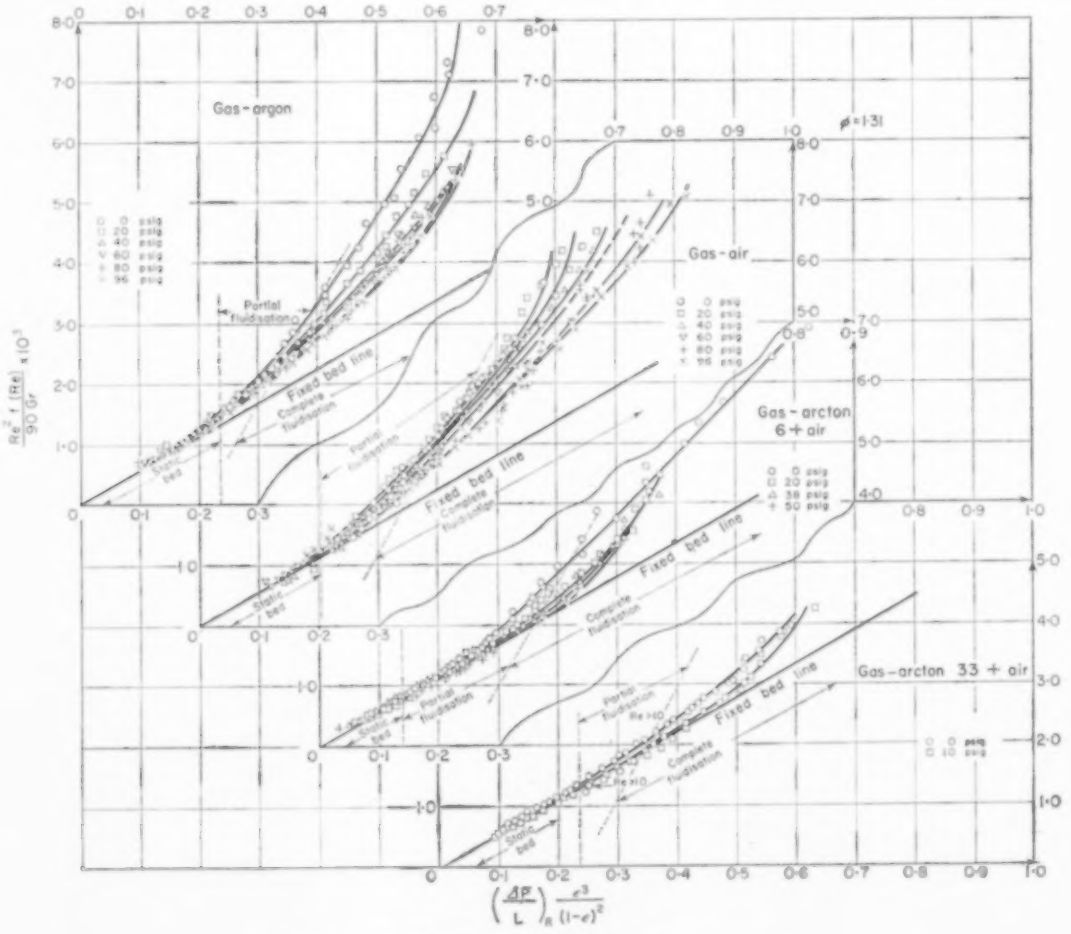

Fig. 3. Fluidization of sand by gases under pressure.

diameters and lead shot by water. These data are shown in Fig. 8 and the values of the corresponding groups are listed in Table 4. The properties of all the solids considered here are listed in Table 5.

Since the displacement of one curve from another in each family was small and since a small error in bed height could have a large effect on the voidage function a large number of readings was taken to define each curve. With the same co-ordinates the curve defined by equation (1) for flow through a fixed bed is a straight line through the origin of slope 5·56. The shape factor ϕ was chosen so that the straight line portion of the fluidization curves corresponding to flow in a packed bed lies along the line defined by equation (1). The values of the shape factors are recorded in Table 5. They appear to be a function of the

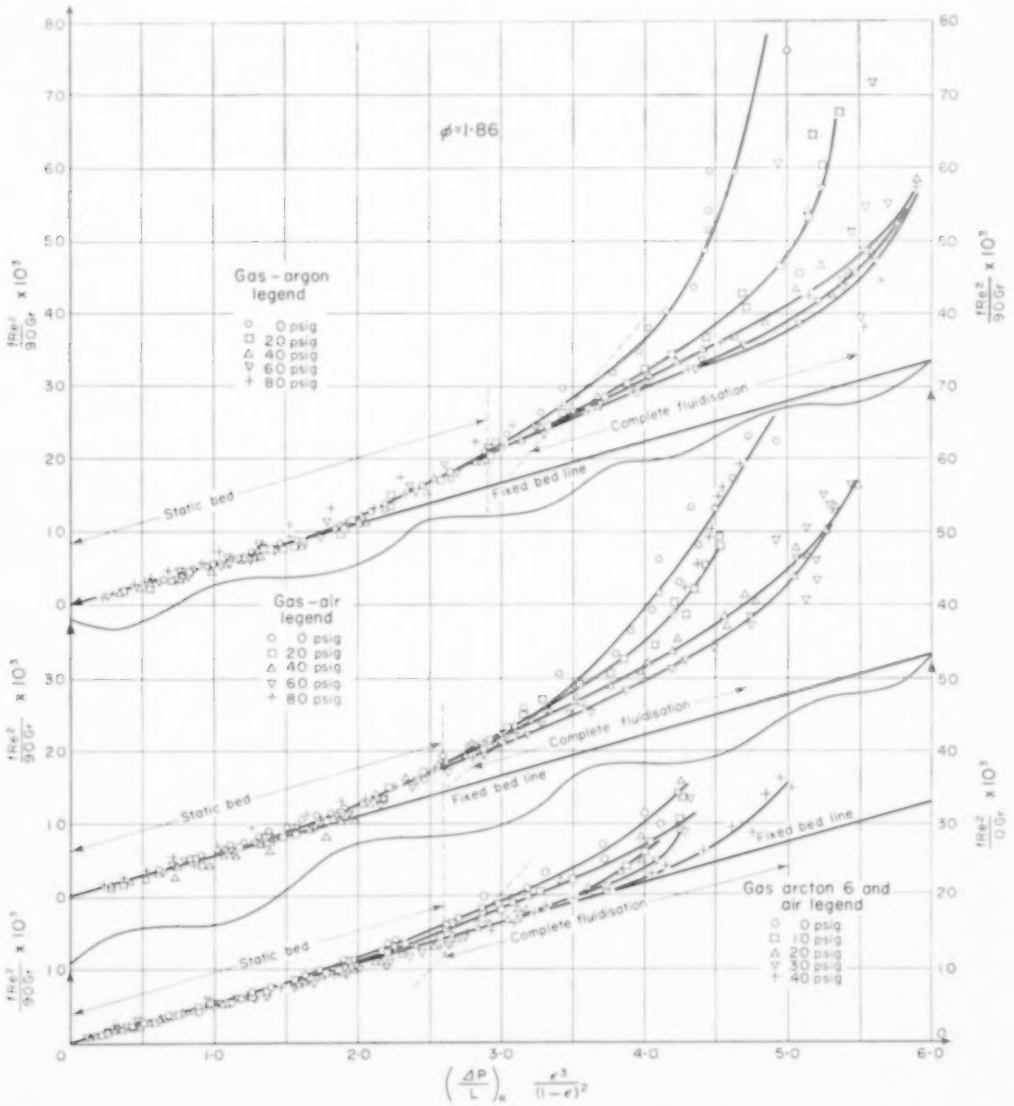

FIG. 4. Fluidization of P.V.C. by gases under pressure.

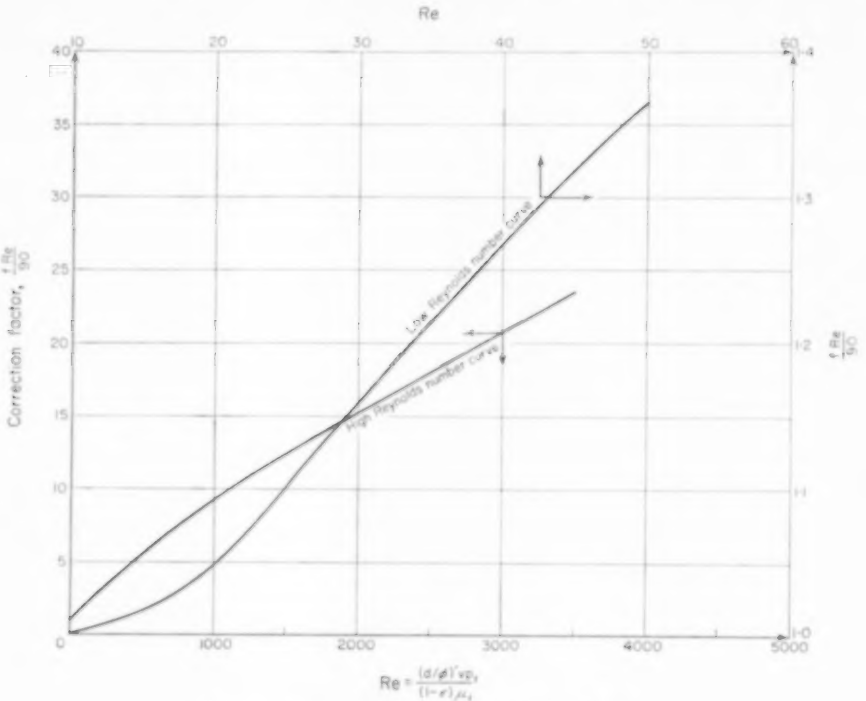

Fig. 5. Correction factor for turbulent flow.

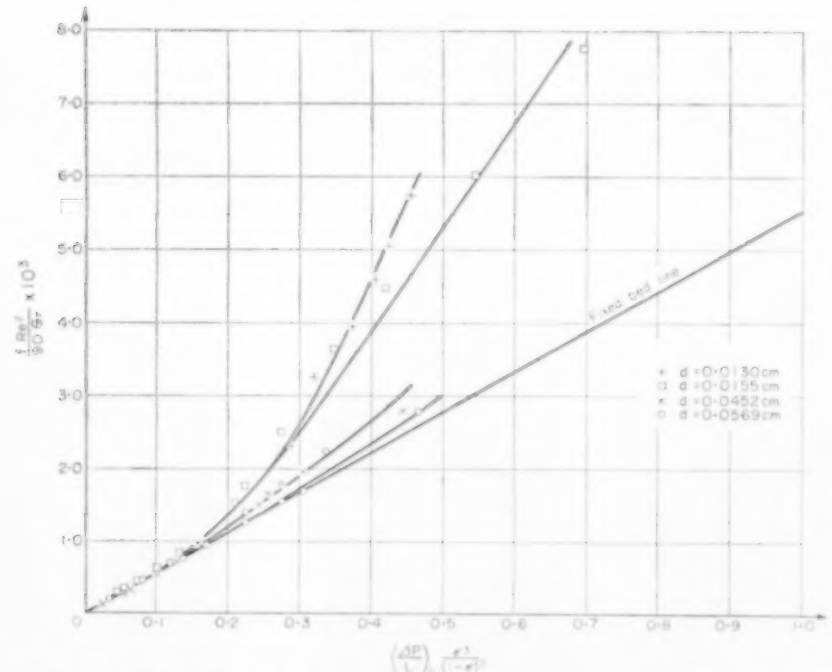

Fig. 6. Fluidization of glass beads by air at 1 atm (data of Lewis *et al.* [12]).

Table 3. Glass spheres fluidized with air
(Data of LEWIS *et al.* [12])

d (μ)	μ_f (P)	G	ρ_f (g/cm^3)	ρ_s/ρ_f	Gr	ϵ_0	L_0/D
130·0	$1{\cdot}80 \times 10^{-4}$	$3{\cdot}975 \times 10^5$	$1{\cdot}205 \times 10^{-3}$	$2{\cdot}05 \times 10^3$	$1{\cdot}945 \times 10^2$	0·398	9·50
155·0	$1{\cdot}80 \times 10^{-4}$	$6{\cdot}88 \times 10^5$	$1{\cdot}205 \times 10^{-3}$	$2{\cdot}045 \times 10^3$	$3{\cdot}39 \times 10^2$	0·380	9·35
452·0	$1{\cdot}80 \times 10^{-4}$	$1{\cdot}625 \times 10^7$	$1{\cdot}205 \times 10^{-3}$	$1{\cdot}995 \times 10^3$	$8{\cdot}15 \times 10^2$	0·388	9·70
569·0	$1{\cdot}80 \times 10^{-4}$	$3{\cdot}10 \times 10^7$	$1{\cdot}205 \times 10^{-3}$	$1{\cdot}995 \times 10^3$	$1{\cdot}588 \times 10^4$	0·401	11·18

VOL. 16 1962

Table 4. Properties of water-fluidized beds
(Data of WILHELM and KWAUK [13])

Solid	μ_f (P)	G	ρ_f (g/cm^3)	ρ_s/ρ_f	Gr	ϵ_0	L_0/D
Glass beads 287 μ	$1{\cdot}00 \times 10^{-2}$	$9{\cdot}92 \times 10^2$	1·000	2·492	$6{\cdot}69 \times 10^2$	0·384	—
Glass beads 510 μ	$1{\cdot}00 \times 10^{-2}$	$2{\cdot}49 \times 10^3$	1·000	2·492	$1{\cdot}675 \times 10^3$	0·384	1·94
Lead shot 1283 μ	$1{\cdot}00 \times 10^{-2}$	$1{\cdot}490 \times 10^6$	1·000	10·79	$1{\cdot}575 \times 10^5$	0·375	1·392
Glass beads 5210 μ	$1{\cdot}00 \times 10^{-2}$	$1{\cdot}845 \times 10^6$	1·000	2·351	$1{\cdot}377 \times 10^6$	0·385	0·825
Socony beads 3280 μ	$1{\cdot}00 \times 10^{-2}$	$1{\cdot}260 \times 10^5$	1·000	1·603	$2{\cdot}085 \times 10^5$	0·368	2·27
Socony beads 4420 μ	$1{\cdot}00 \times 10^{-2}$	$2{\cdot}705 \times 10^5$	1·000	1·603	$4{\cdot}46 \times 10^5$	0·368	2·42

solid alone, as would be expected, and have values of the same order of magnitude as those reported in the literature [9]. The shape factors for the data from the literature were evaluated in a similar way.

EXAMINATION OF THE DATA

It is clear from Figs. 3 and 4 that for a given solid fluidized by a given gas the bed expansion at a given value of the generalized velocity $f\,\mathrm{Re}^2/90\,\mathrm{Gr}$ increases as the gas pressure increases. Each family of curves shows that the effect of decreasing the density ratio $(\rho_s - \rho_f)/\rho_f$ is to increase the bed porosity towards that predicted by the fixed bed line. The effect of fluid viscosity in each of the gas systems is shown by comparing in Figs. 3 and 4 each of the fluidization curves obtained by the various gases with a given solid at a definite value of the ratio $(\rho_s - \rho_f)/\rho_f$. It can be seen that an increase in gas viscosity corresponding to a decrease in G causes the fluidization curve to move away from the fixed bed line.

The effect of the other variables in equation (6) on bed porosity is more difficult to investigate. The study of the effect of particle diameter involving the simultaneous variation of G and $(d/\phi)/D$ and the verification that the effect of solid density ρ_s is adequately described by G and $(\rho_s - \rho_f)/\rho_f$ necessitates the comparison of results on different solids. Then the effect of unknown factors such as the surface properties of

Table 5. Properties of the solids

Source	*Solid*	*Density* ρ_s (g/cm³)	*Particle dia.* (μ)	*Shape factor* ϕ	*Static bed porosity* ϵ_0	*Porosity at complete fluidization* ϵ_2
Simpson and Rodger	Sand	2·631	195·0	1·31	0·39–0·43	0·46–0·48
	PVA	1·201	113·3	1·00	0·39–0·41	0·45–0·47
	Bakelite	0·498	78·9	1·02	0·59–0·62	0·69–0·71
	PVC	1·188	176·4	1·86	0·61–0·65	0·67–0·69
	Glass (A)	2·855	197·9	1·15	0·39–0·43	0·40–0·43
	Glass (B)	2·855	85·8	1·15	0·44–0·46	0·49
	Glass (C)	2·855	313·3	1·07	0·38–0·39	0·40–0·43
	Glass (D)	2·51	3910	1·00	0·34–0·38	0·40
	Steel	7·75	3610	1·00	0·40–0·41	0·42
	Lead	11·21	1710	1·00	0·38–0·40	0·42
Lewis *et al.* [12]	Glass	2·481	130·0	0·79	0·40	0·40
	Glass	2·470	155·0	1·00	0·38	0·38
	Glass	2·410	452·0	1·00	0·39	0·39
	Glass	2·360	569·0	1·00	0·40	0·40
Wilhelm and Kwauk [13]	Glass	2·492	287	0·80	0·38	0·38
	Glass	2·492	510	1·05	0·38	0·38
	Glass	2·351	5210	1·11	0·39	0·39
	Lead	10·79	1283	1·09	0·38	0·39
	Socony beads	1·603	3280	1·00	0·37	0·37
	Socony beads	1·603	4420	1·04	0·37	0·37

the solids are involved. Nevertheless, examination of all the gas/solid data reveals that the solids fall into two distinct classes; those with comparatively small bed expansions comprising the major portion of the data (i.e. sand, glass and PVA) of which Fig. 3 is an example, and those with large bed expansions (i.e. PVC and bakelite spheres) of which Fig. 4 is an example. In the former group complete fluidization starts at a porosity of about 0·45

$$\left(\text{i.e. } \frac{\epsilon^3}{[1-\epsilon]^2} \sim 0{\cdot}3\right);$$

in the latter group complete fluidization only occurs at porosities exceeding 0·68

$$\left(\text{i.e. } \frac{\epsilon^3}{[1-\epsilon]^2} \sim 3{\cdot}1\right).$$

Clearly there must be a profound difference between these two groups of solids apart from density and diameter and this is likely to be associated with the surface properties of the solid, as is discussed below.

It is desirable to reduce the families of curves to one family with each curve defined by a parameter P which from equation (5) may be of the form

$$P \propto \frac{\rho_s - \rho_f}{\rho_f}\,\psi_2\left[G, \frac{(d/\phi)}{D}, \frac{L_0}{D}, \phi, x\right] \qquad (7)$$

For this purpose, the various curves obtained with the gas–solid systems were compared at a constant value of the group $f\,\mathrm{Re}^2/90\,\mathrm{Gr}$ and plots of

$$\log_{10}\frac{\rho_s - \rho_f}{\rho_f} \text{ vs. } \left(\frac{\Delta P}{L}\right)_R \frac{\epsilon^3}{(1-\epsilon)^2}$$

were made. The results for the various gas–solid systems lay along distinct curves which could be superposed by displacing the curves vertically. The amounts $\log_{10}\psi_2$ by which the various curves had to be moved vertically to lie on the curve for the sand–argon runs, chosen because this curve

seemed to be the most reliable, were evaluated. The resultant plot of

$$\log_{10} \psi_2 \left[\frac{\rho_s - \rho_f}{\rho_f}\right] \text{ vs. } \left(\frac{\Delta P}{L}\right)_R \frac{\epsilon^3}{(1-\epsilon)^2}$$

is shown in Fig. 9. This plot was used for evaluating the parameter ψ_2 for the liquid bed data and also the air data of LEWIS *et al.*

It is clear from equation (7) that ψ_2 is a function of five variables. As a first attempt at correlation $\log_{10} \psi_2$ was plotted against $\log_{10} G$ in Fig. 10 for the gas and liquid bed results. The variation of ψ_2 with G shown by the sand, PVA, glass and PVC data is proportional to $G^{-\frac{1}{2}}$, i.e. $\psi_2 \propto \mu_f^2$. The data of LEWIS *et al.* obtained on glass beads fluidized by air and the water bed results for solids of similar densities show the effect of particle diameter and indicate that ψ_2 is proportional to $G^{-0.5}$, i.e. $\psi_2 \propto (d/\phi)^{-1.5}$. This implies that ψ_2 depends on some group other than G containing the diameter term (d/ϕ). Consequently an attempt was made to fit the equation

$$\psi_2 = aG^{-m}\left(\frac{d/\phi}{D}\right)^n \tag{8}$$

to the data of Fig. 10 (excluding the VPC data)

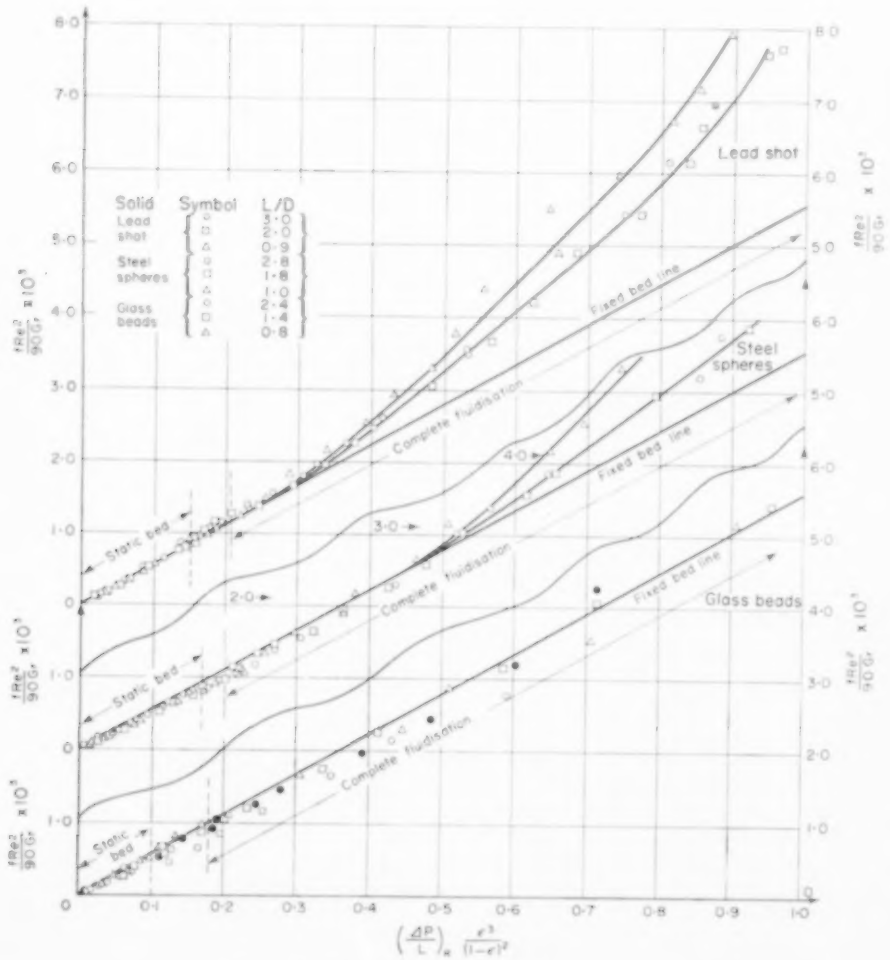

FIG. 7. Fluidization of solids by water.

by the method of least squares. The resultant correlation is shown in Fig. 11 where $\log_{10} \psi_2$ is plotted against

$$\log_{10}\left[G\left(\frac{D}{d/\phi}\right)^{n/m}\right].$$

It was found that $a = 3{\cdot}91 \times 10^{10}$, $m = 1{\cdot}07$ and $n = 1{\cdot}71$, implying that

$$\psi_2 \propto \mu_f^{2{\cdot}14}\,(d/\phi)^{-1{\cdot}5},$$

very close to the first approximation given above. The best parameter that could be used to describe the low expansion data was then given by

$$P = \left(\frac{\rho_s - \rho_f}{\rho_f}\right) G^{-1{\cdot}07} \left(\frac{d/\phi}{D}\right)^{1{\cdot}71} \qquad (9)$$

In order to obtain a family of curves most representative of the low expansion data using the parameter defined by equation (9) $\log_{10} P$ was evaluated for each of the curves and

$$\left(\frac{\Delta P}{L}\right)_R \frac{\epsilon^3}{(1-\epsilon)^2} \text{ for } \frac{f\,\mathrm{Re}^2}{90\,\mathrm{Gr}} =$$

1·5, 3·0, 4·0, 5·0 and 6·0.

The best smooth curve was drawn through each set of points and these curves were used to interpolate values defining the best single family of curves. Fig. 12 represents the fluidization of sand, glass beads and PVA by air, argon, Arcton 6 and Arcton 35, under various pressures, and also glass beads, lead shot, steel spheres and Socony beads fluidized by water. More generally, it can be regarded as representing data on the fluidization by liquids and gases of solids which are completely fluidized at porosities above 0·45

$$\left(\text{i.e. } \frac{\epsilon^3}{[1-\epsilon]^2} > 0{\cdot}3\right).$$

It can be used to predict the porosity function at a given generalized velocity $f\,\mathrm{Re}^2/90\,\mathrm{Gr}$ with an accuracy of ± 10 per cent corresponding to an error in porosity or bed height of about ± 2 per cent. It is based on systems with the following range of properties: $\rho_s = 1{\cdot}201$–$11{\cdot}21$ g/cm^3, $d = 113$–$5210\,\mu$, $\phi = 1{\cdot}00$–$1{\cdot}31$, $D = 2{\cdot}5$–$3{\cdot}0$ in., $\mu_f = 1{\cdot}16 \times 10^{-4}$–$1{\cdot}00 \times 10^{-2}\,P$ and $\rho_f = 1{\cdot}205 \times 10^{-3}$–$1{\cdot}000$ g/cm^3.

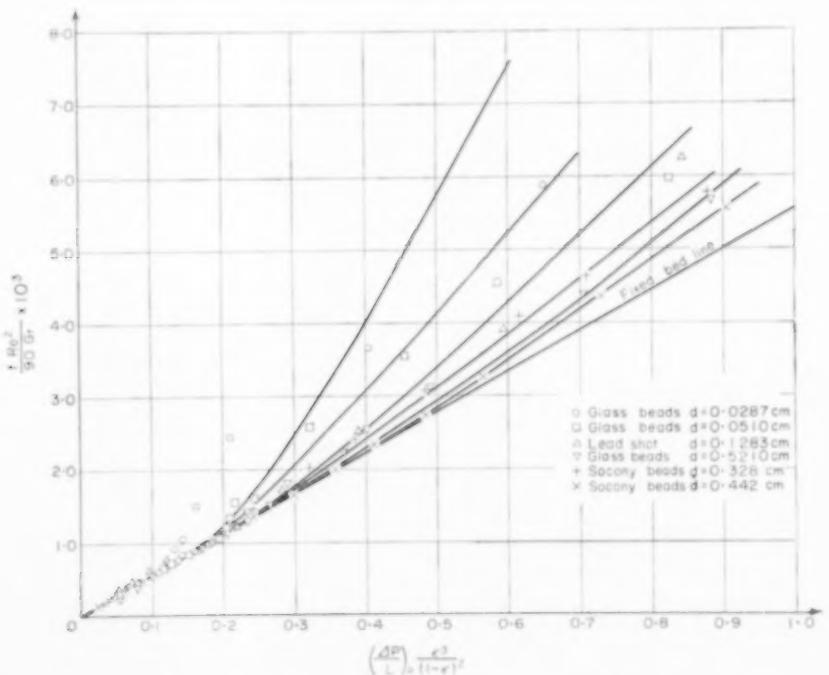

Fig. 8. Fluidization by water (data of Wilhelm and Kwauk [13]).

It can be seen from Fig. 12 that as the parameter P decreases the fluidization lines tend towards the fixed bed line. Since equation(9) can be written as

$$P = \frac{\mu_f^{2\cdot14}}{\rho_f(\rho_s - \rho_f)^{1\cdot4}\, g^{1\cdot07}\,(d/\phi)^{1\cdot80}\, D^{1\cdot71}}$$

this implies that for a given value of the generalized velocity function $f\,\mathrm{Re}^2/90\,\mathrm{Gr}$, bed expansion increases as the fluid viscosity μ_f decreases, the fluid density ρ_f increases and the generalised particle diameter (d/ϕ) increases. This is clearly established by Figs. 3 and 6. In addition, equation (9) implies that bed expansion increases with the net gravitational force on the solid $g(\rho_s - \rho_f)$. This result is in agreement with the data of Fig. 10 where the lines passing through the data for the Socony beads ($\rho_s - \rho_f = 0{\cdot}6$ g/cm^3), the glass beads ($\rho_s - \rho_f = 1{\cdot}5$ g/cm^3), the steel balls ($\rho_s - \rho_f = 6{\cdot}8$ g/cm^3) and the lead shot ($\rho_s - \rho_f \sim 10{\cdot}2$ g/cm^3), lie in the correct order.

Finally Fig. 12 implies that an increase in tube diameter D causes the bed expansion to increase. Since all the experiments reported here were carried out in beds of diameter between $2\frac{1}{2}$ in. and 3 in. the effect of tube diameter D in equation (9) cannot be considered as established. On the other hand, the only other group containing D in equation (7) is the ratio L_0/D. For all the original gas data reported here $L_0/D \sim 2$; for the liquid data $L_0/D \sim 3$, 2 and 1. For the data of Lewis *et al.* $L_0/D \sim 10$ and for the data of Wilhelm and Kwauk $L_0/D \sim 1$–2·5. It can be seen from Fig. 11 that there is no obvious segregation of points in terms of L_0/D.

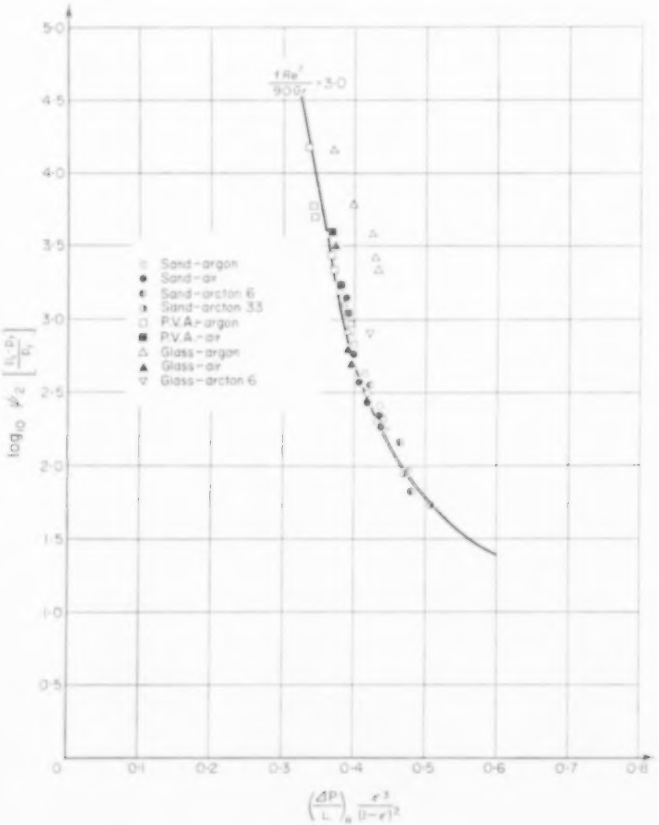

Fig. 9. Coincidence of sand, P.V.A. and glass results.

Effect of surface properties of the solid

So far the only allowance for the surface properties of the solid has been to include the shape factor ϕ as a correction to the measured particle diameter. This factor has not been retained as an independent variable as in equation (7) because it was found possible to correlate the low expansion bed data without explicit allowance for ϕ despite the fact that the solids included in this correlation had shape factors ranging between 1·00 and 1·31. Nevertheless, this correlation is not comprehensive enough to include the high expansion bed data, as exemplified by the PVC results. It seems likely that other properties of the surface, indicated by x in equation (7), must be included in a more general correlation.

What is desired is some measure of interparticle friction obtainable, if possible, from the fluidization data without addition measurements. Such a measure may be given by the porosity ϵ_2 at which fluidization is just complete:

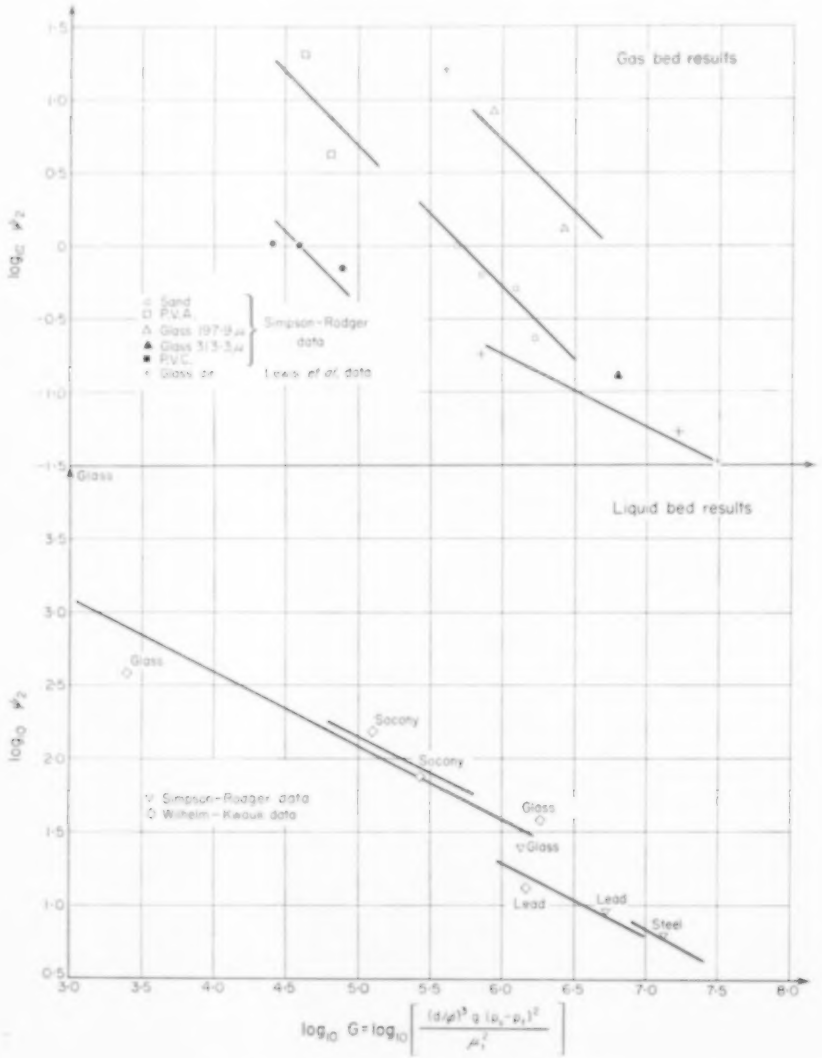

Fig. 10. Dependence of parameter ψ_2 on G.

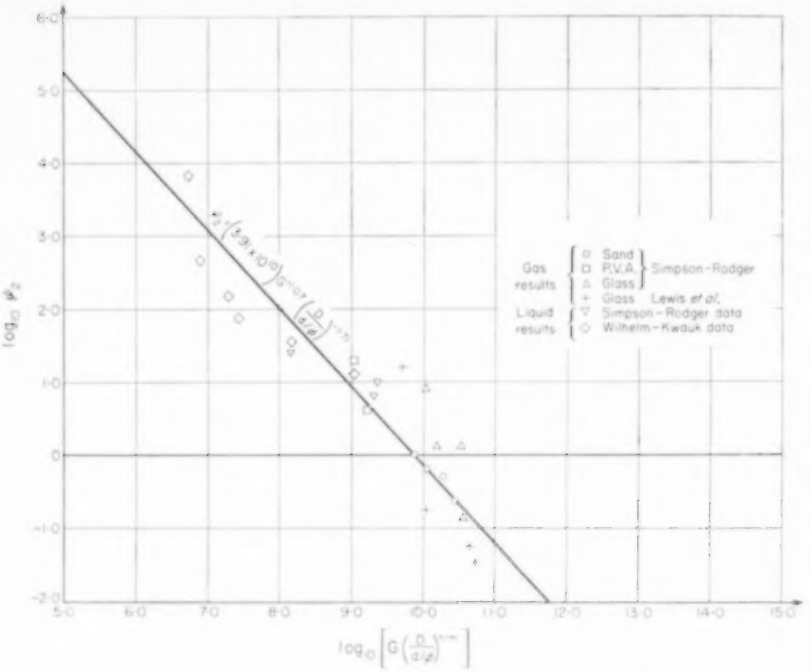

FIG. 11. Correlation of parameter ψ_2 with G and $D/(d/\phi)$.

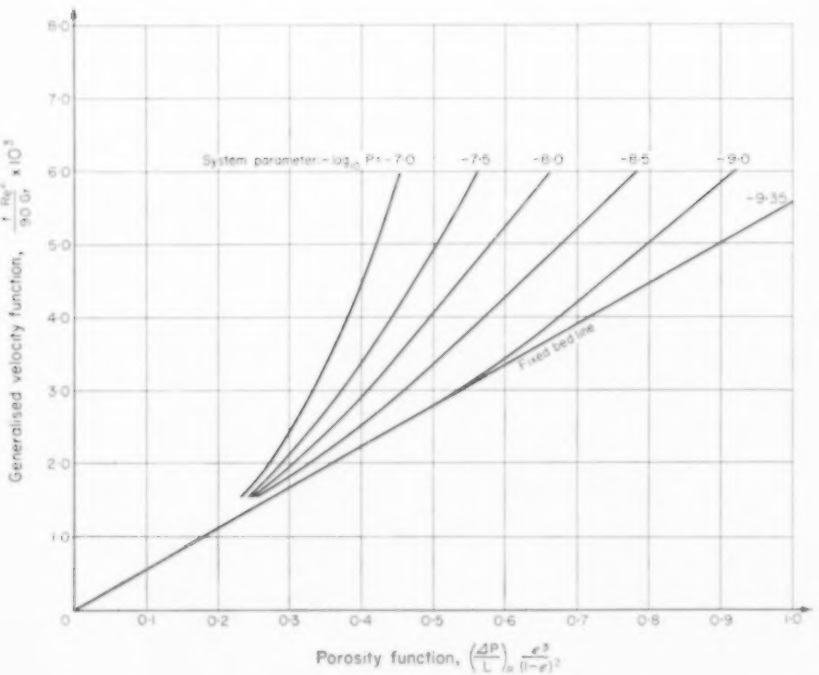

FIG. 12. Generalized bed expansion plot for liquid and gas systems low expansion beds.

$$\text{i.e. } \left(\frac{\Delta P}{L}\right)_R = 1.$$

It will clearly increase as the roughness of the particles increases and can be evaluated along with the shape factor ϕ by measuring pressure drop vs. bed expansion during one fluidization test. The values of ϕ and ϵ_2 for each of the solids studied is shown in Table 5.

An attempt was made to generalize Fig. 12 to include the high expansion data by including ϵ_2 as an additional variable. While the high expansion and low expansion data corresponding to solids with widely different surface properties could now be represented on the same plot, it was considered to be inadequately substantiated. The P.V.C. porosity functions were about 20 per cent higher than those of the general correlation and the results obtained on the bakelite micro-balloons fluidized by Arcton 6 scattered badly. Great difficulty was experienced in fluidizing these micro-balloons smoothly because of channelling.

All subsequent discussion is devoted to the correlation given in Fig. 12 which is reliable for low expansion beds, i.e. $\epsilon_2 = 0{\cdot}45$. However, this correlation is incomplete and more work is required to establish the effect of particle roughness and tube diameter.

Extrapolation of the data to the fixed-bed line

The critical values of the parameter P at which the fluidized bed has the same porosity as an expanded bed of fixed particles submitted to the same generalized velocity can be found from Fig. 12 by extrapolating along constant values of the generalized velocity function $f\,\mathrm{Re}^2/90\,\mathrm{Gr}$ to the fixed bed line. The resultant values of P in terms of the porosity ϵ are shown in Fig. 14, by the solid line. This curve can be considered as giving a critical porosity for a given value of the parameter P above which the flow through the fluidized beds tends to form bubbles. It can be considered as a stability line separating ideal particulate fluidization from incipient aggregative fluidization.

Bubble velocity in fluidized beds

It is now necessary to introduce two unsubstantiated but reasonable assumptions. In

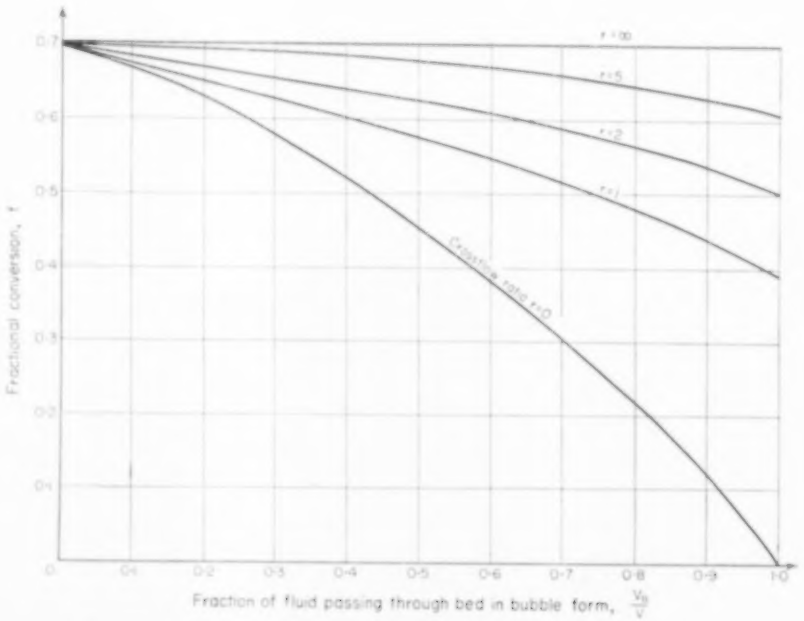

Fig. 13. Effect of bubble formation and cross-flow in the fractional conversion of a first-order heterogeneous reaction in a fluidized bed.

the first, it is assumed that an aggregatively fluidized bed consists of two phases, bubbles and an emulsion phase in which the particles are uniformly dispersed. Let the porosity of the latter phase be ϵ_1, the number of bubbles per unit volume be n and the mean bubble volume be v. Then

$$nv = \frac{\epsilon - \epsilon_1}{1 - \epsilon_1} \tag{11}$$

where ϵ is the mean porosity of the fluidized bed as recorded in Fig. 12. If it is assumed that the superficial velocity of the fluid in the emulsion phase is V_1, that the velocity of rise of a bubble of volume v is u_v and that the volumetric flow rates through the two phases are additive, then the total superficial velocity V of the fluidized bed is given by

$$V = nvu_v + (1 - nv)\, V_1 \tag{12}$$

Substituting equation (11) into (12) and writing in dimensionless form

$$\frac{1}{\mathrm{Gr}}\left(\frac{(d/\phi)\, u_v\, \rho_f}{\mu_f}\right) = \left(\frac{\mathrm{Re}}{\mathrm{Gr}} - \frac{\mathrm{Re}_1}{\mathrm{Gr}}\right)\left(\frac{(1 - \epsilon_1)(1 - \epsilon)}{\epsilon - \epsilon_1}\right) \tag{13}$$

where the groups are defined above and the Reynolds number for the flow through the emulsion phase

$$\mathrm{Re}_1 = \frac{(d/\phi)\, V_1\, \rho_f}{(1 - \epsilon_1)\, \mu_f}$$

can be evaluated from equation (1) with $\epsilon = \epsilon_1$.

Equation (13) gives the mean bubble velocity u_v in terms of the known physical properties of the fluidized bed, the Reynolds number of the over-all flow, the mean porosity ϵ of the bed and the porosity ϵ_1 of the emulsion phase.

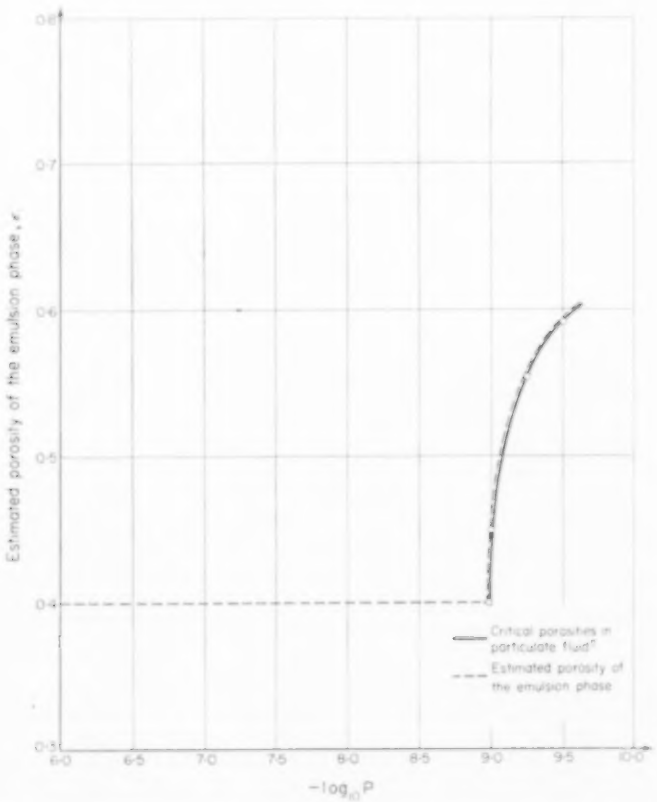

FIG. 14. Critical porosity of the emulsion phase low expansion beds.

As will appear later it is contended that there is no essential difference between a liquid fluidized bed and a gas fluidized bed; only a gradual transformation from ideal, particulate fluidization to full aggregative fluidization. The literature's use of the word particulate is vague. In general, when no bubbles are observed in the fluidized bed it is said to fluidize particulately. In the following, a bed is said to fluidize in an *ideally* particulate manner when its fluidization curve lies along the fixed bed line. This constitutes a quantitative definition of ideally particulate fluidization. It is shown below that some systems fluidize with such small bubbles that they are not obvious to the observer. According to our definition this bed would be said to fluidize particulately, but *not* in an *ideally* particulate manner.

A second assumption is now made that when a bed is fluidized in an ideally particulate manner the fluidization curve will lie along the fixed-bed line in Fig. 12 and that every such system has a critical porosity above which the ideally particulate fluidization will become unstable and bubbles will be formed. This critical porosity can then be identified with the porosity of the emulsion phase. It follows then that the porosity ϵ_1 is a function of P as shown in Fig. 14. However, ϵ_1 cannot be less than ϵ_0, the porosity of the static bed. For those beds which have a value of P yielding a value of porosity in Fig. 14 less than ϵ_0 there will be no range of velocities over which the fluidization can be ideally particulate and the porosity of the emulsion phase will be equal to ϵ_0. Thus for the data of Fig. 12 for which $\epsilon_0 = 0{\cdot}40$, no

VOL 16 196

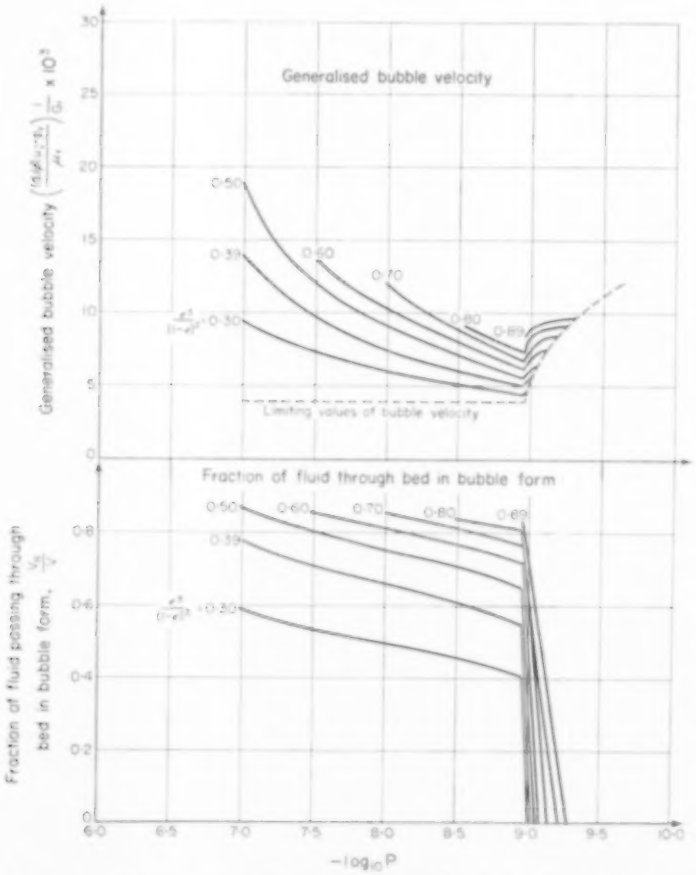

Fig. 15. Bubble characteristics. Low expansion beds. Streamline flow.

system with $\log_{10} P > -8{\cdot}97$ can have ideally particulate fluidization. It is thus possible to estimate the porosity of the emulsion phase by the broken line in Fig. 14.

By combining equations (13) and (1) with Figs. 12 and 14 it is possible to estimate the bubble velocity u_v as a function of the bed porosity ϵ and the parameter P. In particular, when the flow through the bed is streamlined so that

$$\frac{f\,\mathrm{Re}}{90} = \frac{f_1\,\mathrm{Re}_1}{90} = 1$$

the generalized bubble velocity

$$\left(\frac{[d/\phi]\,u_v\,\rho_f}{\mu_f}\right)\frac{1}{\mathrm{Gr}}$$

can be plotted in terms of the parameter P for a series of values of the porosity function $\epsilon^3/(1-\epsilon)^2$ as shown in Fig. 15. It can be seen that as the fluid velocity, and with it the bed porosity, increases the bubble velocity increases. Also the effect of fluid velocity on bubble velocity decreases as P decreases to the value of $\log_{10} P = -8{\cdot}97$. Beyond this point the porosity of the emulsion phase increases as P decreases and the generalized bubble velocity increases slightly at constant bed porosity. It should be noted that as the bed porosity ϵ drops to the emulsion phase value ϵ_1 the generalized bubble velocity in equation (13) tends to the limit

$$\frac{\epsilon_1^3(3-\epsilon_1)}{180\,(1-\epsilon_1)}$$

This lower limit of bubble velocity is shown by the broken line in Fig. 15.

Fraction of fluid through bed in bubble form

If V_B is the volumetric flow rate of fluid through unit cross-section of the bed as bubbles the fraction of fluid through the bed in bubble form as given by an equation similar to (12) and (13) is

$$\frac{V_B}{V} = \left[1 - \frac{V_1/(1-\epsilon_1)}{V/(1-\epsilon)}\right] = \left(1 - \frac{\mathrm{Re}_1/\mathrm{Gr}}{\mathrm{Re}/\mathrm{Gr}}\right) \quad (14)$$

It is thus possible again for streamline flow to plot V_B/V vs. $\log_{10} P$ for a series of values of $\epsilon^3/(1-\epsilon)^2$ as shown in Fig. 15. The fraction V_B/V increases as the bed expands but decreases as P decreases, i.e. as the bed becomes more particulate. When the critical value of P is exceeded the porosity of the emulsion phase increases and the fall of V_B/V to zero value is very rapid.

Since fluid–solid contact in the bubble phase is poorer than in the emulsion phase the ratio V_B/V gives a measure of the efficiency of contact between solid and fluid, at least for the large bubbles encountered in gas beds. If we define along with May [15] the crossflow ratio r as the number of times a bubble rising through the bed exchanges its volume with the surrounding emulsion phase and assume that no reaction takes place between the gas and solid while the gas is inside the bubbles, then for a first order, heterogeneous reaction, the fractional yield f is given by

$$f = 1 - \frac{\exp \alpha}{\beta}\{\beta \cosh \beta - (\alpha + \gamma)\sinh \beta\} \quad (15)$$

where

$$2\alpha = -\left(\frac{\gamma + r}{L - (V_B/V)}\right),$$

$$\beta = \left[\alpha^2 - \frac{\gamma_r}{1-(V_B/V)}\right]^{1/2},\ \gamma = \frac{kM}{V}$$

M is the mass of solid in the bed and k the reaction rate constant. This is a particular case of May's more general equation in which back diffusion is neglected. For piston flow through a packed bed with the same mass of catalyst (i.e. $r = V_B/V = 0$) equation (15) reduced to

$$f = 1 - \exp(-\gamma) \quad (16)$$

If f is chosen to be 0·7 for this fixed bed $\gamma = 1{\cdot}204$. With this conversion as a basis equation (15) has been used to evaluate Fig. 13 in which f is plotted as a function of V_B/V for a series of values of r.

According to Fig. 15 V_B/V can be as high as 0·87. If $r = \infty$ this will have no effect on the fractional conversion. In the extreme case of $r = 0$, f can drop to 0·13. For the laboratory equipment used here $r \sim 1$ in which case $f = 0{\cdot}46$. Unfortunately, no general correlation is available for r in terms of the bed parameters, but Fig. 13 does illustrate why fluidized bed reactors are

necessarily taller than the comparable bed-fixed reactor, at least for gaseous systems.

When air is used to fluidize sand ($d = 195\ \mu$) at atmospheric pressure, $\log_{10} P = -7{\cdot}36$. When the air pressure is 80 p.s.i.g. $\log_{10} P = -8{\cdot}17$. With a bed porosity of 0·5 it can be seen from Fig. 16 that $V_B/V = 0{\cdot}81$ at 1 atm and 0·73 at 80 p.s.i.g., a small but appreciable decrease for a pressure rise exceeding five fold. Apart from advantages that may accrue because of the chemistry of the process, since the crossflow ratio is not likely to change markedly with pressure, little improvement is obtained by carrying out heterogeneous reaction in a fluidized bed under pressure.

Bubble volume, concentration and frequency

It has been found by Davies and Taylor [14] that a large lenticular gas bubble rises through a liquid at a rate given by

$$u_v = a\,(g\,v^{1/3})^{1/2} \tag{17}$$

where $a = 0{\cdot}792$. This equation implies that the drag coefficient of these large bubbles is largely independent of Reynolds number. Davidson *et al.* [6] have found that this equation is applicable to the rise of bubbles injected into quiescently fluidized beds. Since it has been observed that bubbles rising through fluidized beds do appear to be lenticular a final assumption is made that equation (17) can be used as a first approximation to relate the mean bubble velocity u_v to the mean bubble volume v in an aggregatively fluidised bed.

The mean frequency fr with which bubbles of mean volume v appear at the surface of the bed is given by

$$\frac{fr}{A} = nu_v \tag{18}$$

where A is the cross-sectional area of the bed. By combining equations (17), (18) and (11) the mean bubble volume v, the number of bubbles per unit volume n and the bubble frequency fr are given by

$$\frac{a^6}{G^3}\,\frac{v}{(d/\phi)^3} = \left[\frac{(d/\phi)\,u_v\,\rho_f}{\mu_f}\,\frac{1}{\mathrm{Gr}}\right]^6 \tag{19}$$

$$\frac{G^3}{a^6}\,n\left(\frac{d}{\phi}\right)^3 = \left(\frac{\epsilon-\epsilon_1}{1-\epsilon_1}\right)\left[\frac{(d/\phi)\,u_v\,\rho_f}{\mu_f}\,\frac{1}{\mathrm{Gr}}\right]^{-3} \tag{20}$$

$$\frac{fr\,(d/\phi)\,\mu_f\,G^3}{Ag\,(\rho_s-\rho_f)\,a^6} = \left(\frac{\epsilon-\epsilon_1}{1-\epsilon_1}\right)\left[\frac{(d/\phi)\,u_v\,\rho_f}{\mu_f}\,\frac{1}{\mathrm{Gr}}\right]^{-5} \tag{21}$$

For streamline flow the generalized volume, bubble concentration and frequency have been plotted as a function of P for a series of values of G in Fig. 16. It can be seen that as the fluid velocity is increased through a given solid (i.e. P constant), causing the bed to expand, the bubble volume increases, but the bubble concentration and frequency decrease if $\log P < 8{\cdot}97$. Since the bubble volume v is proportional to u_v^6 an increase in fluid velocity in an aggregatively fluidized bed has a much greater effect on bubble volume than on bubble velocity. This agrees with the studies of Yasui and Johanson [4] who found that while the size of bubbles increases with gas velocity, the velocity of the bubbles varies little. The decrease in bubble frequency with gas velocity also agrees with the data of Yasui and Johanson.

Comparison of beds fluidized with liquids and gases

Consider a liquid and a gas fluidized bed with the same value of the parameter P. Since the value of

$$\frac{\mu_f^2}{\rho_f\,(\rho_s-\rho_f)}$$

is larger for a liquid than for a gas (e.g. the value for glass fluidized by water is $5{\cdot}39 \times 10^{-5}$; the value for glass with air at atmospheric pressure is $9{\cdot}54 \times 10^{-6}$) this implies that the particle diameter must be larger for the liquid system than the gas system

$$\left(\text{e.g. } \frac{\text{diameter with water}}{\text{diameter with air}} = 3{\cdot}17\right)$$

These two systems will be represented by the same curve in Fig. 12. If both beds have expanded to the same porosity ϵ then both will have the same generalized velocity $f\,\mathrm{Re}^2/90\,\mathrm{Gr}$. Then for streamline flow in both systems the following relationships are obtained from equations (13), (19), (20) and (21) for the ratio of the bubble

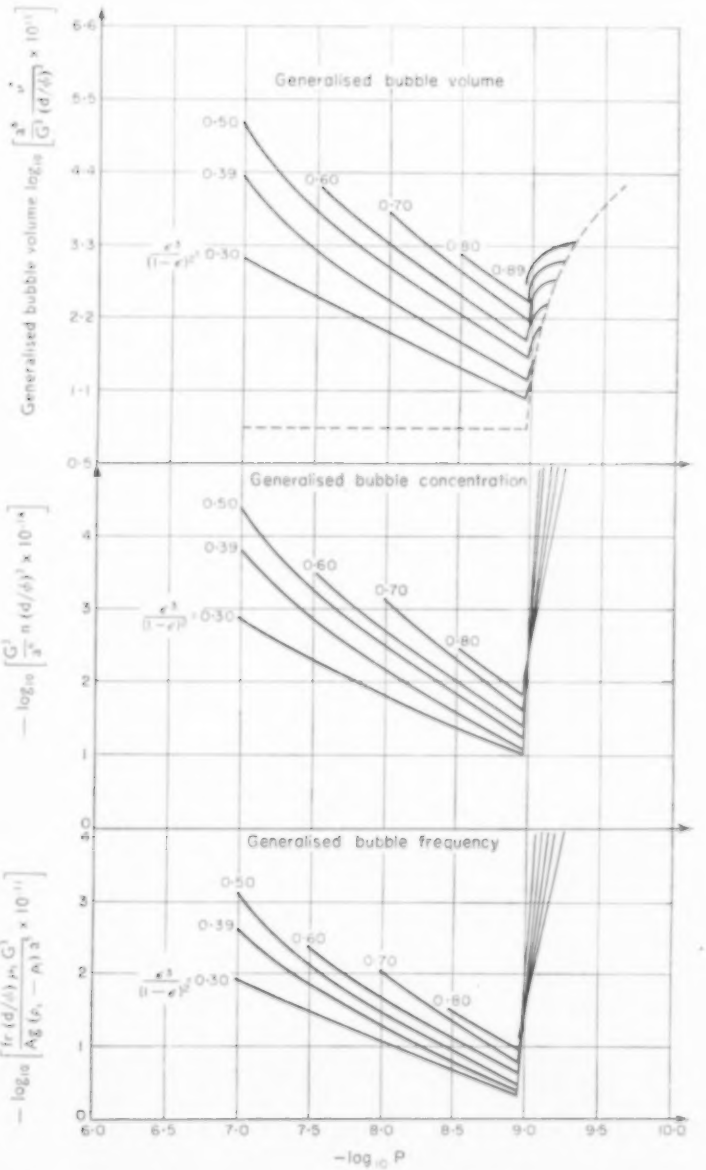

FIG. 16. Bubble characteristics. Low expansion beds. Streamline flow.

characteristics in the gas system (subscript g) to those in the liquid system (subscript l).

$$\frac{u_{cg}}{u_{cl}} = 8{\cdot}44\,; \quad \frac{v_g}{v_l} = 3{\cdot}61 \times 10^5\,;$$

$$\frac{n_g}{n_l} = 2{\cdot}77 \times 10^{-6}\,; \quad \frac{fr_g}{fr_l} = 2{\cdot}33 \times 10^{-5}$$

where the numerical values are for glass beads fluidized by air at 1 atm and water. Thus the velocity of rise of a gas bubble is about 8·4 times that of a liquid bubble at the same bed porosity with the same value of the parameter P, the ratio of linear dimensions of gas to liquid bubbles is 71 : 1 and the ratio of frequencies is $2{\cdot}3 \times 10^{-5}$.

If it is further assumed that the glass beads fluidized with air are of diameter 100 μ then the following parameters can be evaluated for a tube diameter of 6·35 cm.

$$G_g = 2{\cdot}44 \times 10^5\,;$$

$$\frac{\rho_s - \rho_f}{\rho_f} = 2{\cdot}359 \times 10^3\,; \quad \mathrm{Gr}_g = 1{\cdot}035 \times 10^2\,;$$

$$\left(\frac{d/\phi}{D}\right)_g = 1{\cdot}575 \times 10^{-3}\,; \quad \log_{10} P = -7{\cdot}19.$$

If it is further assumed that the mean bed porosity is such that

$$\frac{\epsilon^3}{(1-\epsilon)^2} = 0{\cdot}40$$

then from Figs. 12 and 14

$$\frac{f\,\mathrm{Re}^2}{90\,\mathrm{Gr}} = \frac{\mathrm{Re}}{\mathrm{Gr}} = 4{\cdot}1 \times 10^{-3}$$

(since $\mathrm{Re} = 0{\cdot}424 < 10$); $\epsilon_1 = 0{\cdot}40$. Thus, from Figs. 13 and 16, 100 μ glass beads fluidized by atmospheric air to a mean porosity of $\epsilon = 0{\cdot}48$ should produce bubbles of volume 0·2 cm^3, linear dimension 0·59 cm, rise velocity 0·61 ft/sec, concentration 0·68/cm^3 and frequency 13·8/cm^2 sec. These estimated figures are of the same order of magnitude as those reported by Yasui and Johanson [4] who found bubble velocities ranging between 1 and 2 ft/sec and frequencies between 4 and 12 bubbles per cm^2 sec. The velocities reported by Yasui and Johanson are likely to be too high and the frequencies too low since they are unable to detect bubbles less than $\frac{1}{2}$ in. diameter.

Consider now the larger glass beads fluidized by water to the same porosity but with the particle diameter adjusted to give the same value of the parameter P. Then the 317 μ glass beads should produce bubbles of linear dimension 0·008 cm, concentration $2{\cdot}46 \times 10^5$/cm^3, rise velocity 0·07 ft/sec and frequency $5{\cdot}93 \times 10^5$ cm^2 sec. Although equation (17) is not likely to be applicable to very small bubbles it seems reasonable to conclude that the liquid bed will contain a very large number of small bubbles ($< 0{\cdot}01$ cm) which would not be observed. Thus the gas bed would be observed as fluidizing aggregatively and the liquid bed particulately, but not in the ideally particulate manner according to the definition above.

It is thus suggested that the difference between the type of fluidization observed in liquid systems and gas systems is only one of degree. Both types of fluidization can be represented in the one family of curves. A gas system normally has a comparatively small number of large bubbles rising through the bed; a liquid system may have a large number of small bubbles.

Bubbles in turbulently fluidized beds

The above calculations are only valid when the flow through the bed is ostensibly streamline, i.e. $f\,\mathrm{Re}/90 = 1$ for $\mathrm{Re} \leqslant 10$. For higher Reynolds numbers such as those normally encountered in liquid–solid systems the bubble size, velocity, concentration and frequency cannot be expressed as unique functions of the parameter P and the porosity ϵ. It is necessary to include the independent variable Gr.

Consider the case of lead shot fluidized with water according to the data shown in Table 2. Then $\log_{10} P = -8{\cdot}98$, $\mathrm{Gr}_s = 4{\cdot}96 \times 10^5$ and from Fig. 14 $\epsilon_1 = 0{\cdot}40$. If the porosity of the bed is $\epsilon = 0{\cdot}56$ (i.e. $\epsilon^3/(1-\epsilon)^2 = 0{\cdot}9$) then from Fig. 12

$$\frac{f\,\mathrm{Re}^2}{90\,\mathrm{Gr}} = 5{\cdot}90 \times 10^{-3}\,; \quad \frac{f_1\,\mathrm{Re}_1}{90\,\mathrm{Gr}} = 0{\cdot}99 \times 10^{-3}$$

The turbulent flow correction factor can be evaluated from Fig. 5 as

$$\frac{f\,\mathrm{Re}}{90} = 5{\cdot}64\,;$$

$$\frac{f_1\,\mathrm{Re}_1}{90} = 3{\cdot}24 \text{ and thus}$$

$$\frac{\mathrm{Re}}{\mathrm{Gr}} = 1{\cdot}048 \times 10^{-3},$$

$$\frac{\mathrm{Re}_1}{\mathrm{Gr}} = 0{\cdot}305 \times 10^{-3}.$$

Substituting these values along with the properties listed in Table 2 into equations (11), (13), (15) and (16) we have $u_v = 1{\cdot}17$ ft/sec, $v^{1/3} = 2{\cdot}06$ cm, $n = 3{\cdot}06 \times 10^{-2}$/cm^3 and $fr/A = 1{\cdot}09$/cm^2 sec.

Consequently, when lead shot ($d = 0{\cdot}171$ cm) is fluidized by water bubbles of linear dimension 2·06 cm should be produced. The outside of these lens-shaped bubbles were seen as slits of water in the emulsion phase moving up the walls of the bed. At the top of the bed the spherical tops of the bubbles could be seen easily with the naked eye. The dimensions and frequency of the bubbles appeared to be of the same order of magnitude as those calculated above.

It is emphasized that three assumptions have been made in order to calculate bubble characteristics, viz. that an aggregatively fluidized bed can be treated as made up of bubbles in a uniform emulsion phase, that every particulately fluidized system has a critical porosity above which ideal particulate fluidization breaks down to aggregative fluidization and that the mean bubble velocity in an aggregatively fluidized bed can be related to the mean bubble volume by the Davies–Taylor equation for gas bubbles in a liquid. While the results from these assumptions are reasonable, they are in need of more direct experimental confirmation. Furthermore, all these calculations yield mean values of the bubble characteristics. No allowance has been made for bubble growth by coalescence and no mechanism has been postulated for bubble formation. Also back-mixing or "diffusional" effects in the emulsion phase have been ignored. This seems reasonable since they appear to have little effect on reaction efficiency in a fluidized bed reactor and since back-mixing would certainly vary with the quality of fluidization of the bed. Such an elaboration does not seem useful in view of the limitations of the data given above.

Conclusions

The following conclusions can be summarized from the above work.

1. There is no fundamental difference in mechanism between a liquid fluidized bed and a gas fluidized bed A gas system normally has a comparatively small number of large bubbles and appears to fluidize aggregatively. A liquid system may have a large number of small bubbles and appear to fluidize particulately, but not in the ideal manner defined above.

2. It is possible to represent a wide range of liquid and gas beds on a single correlation relating bed porosity to a generalized velocity function and a parameter P defined in terms of the fluid and solid properties by the equation (9).

3. The surface properties of the solid can play an important part in determining the character of the fluidization.

4. By treating an aggregatively fluidized bed as a two-phase system and making unsubstantiated but reasonable assumptions about the rise of bubbles it is possible to predict bubble velocities frequencies, concentrations and volumes which are in approximate agreement with observation.

Acknowledgement—The authors wish to acknowledge the help of Mr. J. Mitchell of Nobel Division, I.C.I., who designed and constructed the apparatus.

Notation

A = cross-sectional area of the bed
d = particle diameter
d_c = channel diameter
D = bed diameter
f = friction factor ; fractional yield in equation (15)
fr = mean frequency of bubbles of volume v
g = gravitational constant
g_c = unit conversion factor

$$G = \frac{(d/\phi)^3\, g\, (\rho_s - \rho_f)^2}{\mu_f^2} = \mathrm{Gr} \Big/ \frac{\rho_f}{\rho_s - \rho_f}$$

$$\mathrm{Gr} = \frac{(d/\phi)^3\, \rho_f\, g}{\mu_f^2} \cdot \frac{\rho_s - \rho_f}{\rho_f}$$

k = rate constant for first-order heterogeneous reaction
L = bed height
L_0 = initial bed height
M = mass of solid in bed

n = number of bubbles per unit volume

$P = \frac{\rho_s - \rho_f}{\rho_f} G^{-1.07} \left(\frac{d/\phi}{D}\right)^{1.71}$

r = crossflow ratio

$\mathrm{Re} = \frac{(d/\phi)\, V\, \rho_f}{(1-\epsilon)\, \mu_f}$

$\mathrm{Re}_1 = \frac{(d/\phi)\, V_1\, \rho_f}{(1-\epsilon_1)\, \mu_f}$

S_0 = surface area of the particles per unit volume of the particles

u_v = velocity of rise of bubble of volume v

v = mean bubble volume

v = linear velocity of fluid

V = superficial velocity of the fluid

V_1 = superficial velocity of the fluid in the emulsion phase

V_B = volumetric flow rate of fluid through unit cross-section of the bed in bubble form

x = a dimensionless measure of the surface roughness

Δp = pressure drop

ϵ = mean porosity of bed

ϵ_0 = mean porosity of static bed

ϵ_1 = porosity of emulsion phase

ϵ_2 = porosity at which fluidization is just complete

μ_f = fluid viscosity

ρ_f = fluid density

ρ_s = solid density

ϕ = shape factor of particles as recommended by Leva [9].

ψ_1, ψ_2 = functions

References

[1] Othmer D. F. *Fluidization* Reinhold, New York 1956.

[2] Reboux P. *Phenomènes de Fluidisation.* Association Francaise de Fluidisation. Paris 1954.

[3] Leva M. *Fluidization.* McGraw-Hill, London 1959.

[4] Yasui G. and Johanson L. W. *Amer. Inst. Chem. Engrs. J.* 1958 **4** 445.

[5] Rice W. J. and Wilhelm R. H. *Amer. Inst. Chem. Engrs. J.* 1958 **4** 423.

[6] Davidson J. F., Paul R. C., Smith M. J. S. and Duxbury H. A. *Trans. Inst. Chem. Engrs.* 1959 **37** 333.

[7] Carman P. C. *Flow of Gases through Porous Media,* Butterworths, London 1956.

[8] Scheidegger A. E. *The Physics of Flow through Porous Media.* University of Toronto Press 1957.

[9] Leva M. Bureau of Mines, U.S. Government Printing Office Bulletin 504, 1951.

[10] Rose H. E. *Some Aspects of Fluid Flow.* Edward Arnold, London 1951 p. 136.

[11] Brinkman H. C. *Appl. Sci. Res., Hague* 1947 **1A** 27.

[12] Lewis W. K., Gilliland E. R. and Bauer W. C. *Industr. Engng. Chem.* 1949 **41** 1104.

[13] Wilhelm R. H. and Kwauk M. *Chem. Engng. Progr.* 1948 **3** 201.

[14] Davies R. H. and Taylor G. I. *Proc. Roy. Soc.* 1950 **A 200** 375.

[15] May W. G. *Chem. Engng. Progr.* 1959 **55** 49.

Chemical Engineering Science, 1961, Vol. 16, pp. 181 to 188. Pergamon Press Ltd., London. Printed in Great Britain.

Thermodynamics of Chemical Equilibrium—I

Effect of temperature and pressure

C. J. Pings

California Institute of Technology, Pasadena, California, U.S.A.

(*Received* 7 *December* 1959)

Abstract—A general thermodynamic derivation for the temperature and pressure derivatives of the chemical reaction parameter is presented. These derivatives are evaluated for several simple equations of state. Applications are indicated for error analysis, for computation of small changes, for correlation of yield data and for selection of pressures which maximize yield.

Résumé—L'auteur présente une méthode thermodynamique de calcul différentiel permettant d'obtenir les dérivées partielles, par rapport à la température et à la pression, des paramètres caractérisant une réaction chimique. Ces dérivées sont évaluées pour plusieurs équations d'état simples. Application au calcul des erreurs et des faibles variations, aux relations des sonnées sur le rendement, et au choix des pressions qui donnent à ce dernier sa valeur maximum.

Zusammenfassung—Es wird eine allgemeine thermodynamische Ableitung für die Temperatur- und Druckableitungen der chemischen Reaktionsparameter angegeben. Diese Ableitungen sind für mehrere einfache Zustandsgleichungen berechnet. Anwendungsmöglichkeiten werden angegeben für Fehleranalysen, für die Berechnung geringer Änderungen, die Korrelation von Ausbeuteergebnissen und für die Auswahl der Drucke bei maximaler Ausbeute.

Introduction

Expressions for the change in the chemical equilibrium constant with change in thermodynamic state are well known [1, 2, 3]. The equilibrium constant itself can be employed to determine the composition of a system in chemical equilibrium. Changes in state can be translated into changes in equilibrium constant which, in turn, can be translated into changes in composition. However, in many instances, the equilibrium constant is of no interest as such: it is merely evaluated to permit the evaluation of the change in composition or extent of a reaction. There appears to be merit, therefore, in the use of expressions that give directly the latter change.

The purposes of the present paper are

(i) To develop general thermodynamic expressions for the derivatives of reaction extent with respect to temperature and pressure.

(ii) To indicate methods of evaluation of the derivatives for several common equations of state.

(iii) To point out several applications.

Prigogine and Defay [4] have used similar expressions in their general discussion of chemical equilibrium. Davies [5] presents an excellent description of both equilibrium and dynamic displacement of chemical equilibria.

Potter [6] recently discussed the degree of advancement for perfect gas mixtures.

The methods developed here are general and can be extended to non-ideal systems, such as encountered in high pressure synthesis or in liquid state reactions. Subsequent papers will consider the effects of volume change and the equilibrium response to incremental inputs of heat and work.

Thermodynamic Derivations

All of the discussion in the present paper is restricted to a closed system in which only one reaction occurs. This reaction will be denoted by the following equation:

$$\sum_{k=1}^{n} \nu_k A_k = 0 \qquad (1)$$

A_k is here used to represent the chemical formula of the kth component. The ν_k's are the stoichiometric coefficients, which are integers or the ratio of integers. ν_k is positive for the products of a reaction, negative for the reactants and zero for those species present which do not enter into the reaction.

Chemical equilibrium is established for those states that satisfy the following condition [1–4]:

$$\sum_{k=1}^{n} \nu_k M_k \mu_k = 0 \tag{2}$$

This equality is unchanged by dividing by the absolute temperature.

$$\sum_{k=1}^{n} \nu_k M_k \frac{\mu_k}{T} = 0 \tag{3}$$

Differentiating in general terms,

$$\sum_{k=1}^{n} \nu_k M_k \frac{d\mu_k/T}{ds} = 0 \tag{4}$$

Here s is used for parametric representation of changes in state. In considering the variation of μ_k/T it is necessary to take into account derivatives with respect to temperature, pressure and composition parameters. However, in a closed system constrained to paths of chemical equilibrium the mass of but one component can be independently varied. The variations in mass of the remaining constituents are determined by stoichiometric relationship specified by equation (1). The extent of the reaction is frequently represented by ξ [4], which is defined by the following:

$$\frac{d\xi}{ds} = \frac{1}{\nu_1 M_1}\frac{dm_1}{ds} = \frac{1}{\nu_2 M_2}\frac{dm_2}{ds} = \cdots = \frac{1}{\nu_n M_n}\frac{dm_n}{ds} \tag{5}$$

It is convenient to employ ξ as the thermodynamic variable representative of change in composition. Changes in μ_k/T will then be completely determined by changes in T, P and ξ.

$$\frac{d\mu_k/T}{ds} = \left(\frac{\partial \mu_k/T}{\partial T}\right)_{P,\xi}\frac{dT}{ds} + \left(\frac{\partial \mu_k/T}{\partial P}\right)_{T,\xi}\frac{dP}{ds} + \left(\frac{\partial \mu_k/T}{\partial \xi}\right)_{T,P}\frac{d\xi}{ds} \tag{6}$$

Substituting the latter into equation (4):

$$\sum_{k=1}^{n} \nu_k M_k \left(\frac{\partial \mu_k/T}{\partial T}\right)_{P,\xi}\frac{dT}{ds} + \sum_{k=1}^{n} \nu_k M_k \left(\frac{\partial \mu_k/T}{\partial P}\right)_{T,\xi}\frac{dP}{ds} + \sum_{k=1}^{n} \nu_k M_k \left(\frac{\partial \mu_k/T}{\partial \xi}\right)_{T,P}\frac{d\xi}{ds} = 0 \tag{7}$$

The two summations involving derivatives with respect to temperature and pressure can be conveniently expressed in terms of partial enthalpies and partial volumes [2, 3].

$$\sum_{k=1}^{n} \nu_k M_k \left(\frac{\partial \mu_k/T}{\partial T}\right)_{P,\xi} = -\frac{1}{T^2}\sum_{k=1}^{n} \nu_k M_k H_k \tag{8}$$

$$\sum_{k=1}^{n} \nu_k M_k \left(\frac{\partial \mu_k/T}{\partial P}\right)_{T,\xi} = \frac{1}{T}\sum_{k=1}^{n} \nu_k M_k V_k \tag{9}$$

The following substitution is also convenient [1]:

$$\sum_{k=1}^{n} \nu_k M_k \left(\frac{\partial \mu_k/T}{\partial \xi}\right)_{T,P} = R\sum_{k=1}^{n} \nu_k \left(\frac{\partial \ln f}{\partial \xi}\right)_{T,P} \tag{10}$$

Substitution of these expressions into equation (7), followed by rearrangement results in the following:

$$\frac{d\xi}{ds} = \frac{\left[\sum_{k=1}^{n} \nu_k M_k (\bar{H}_k/T)\right](dT/ds) - \left[\sum_{k=1}^{n} \nu_k M_k \bar{V}_k\right](dP/ds)}{RT\sum_{k=1}^{n} \nu_k (\partial \ln f_k/\partial \xi)_{T,P}} \tag{11}$$

Two useful partial derivatives follow directly as special cases of equation (11).

$$\left(\frac{\partial \xi}{\partial P}\right)_T = \frac{-\sum_{k=1}^{n} \nu_k M_k \bar{V}_k}{RT\sum_{k=1}^{n} \nu_k (\partial \ln f_k/\partial \xi)_{T,P}} \tag{12}$$

$$\left(\frac{\partial \xi}{\partial T}\right)_P = \frac{\sum_{k=1}^{n} \nu_k M_k \bar{H}_k/T}{RT\sum_{k=1}^{n} \nu_k (\partial \ln f_k/\partial \xi)_{T,P}} \tag{13}$$

Equations (11), (12) and (13) explicitly relate the change in extent of a reaction to the thermodynamic properties of a mixture. If changes in mole fractions are of primary concern, they may be evaluated as follows. Suppose $m_k(\xi_1)$ is the mass of component k for a value of $\xi = \xi_1$. Then

$$m_k(\xi) = m_k(\xi_1) + \nu_k M_k[\xi - \xi_1], \quad \text{all } k \quad (14)$$

The following equalities hold

$$\frac{d\xi}{ds} = \frac{1}{\nu_k M_k}\frac{dm_k}{ds} = \frac{\sum_{i=1}^{n} m_i}{\nu_k M_k}\frac{dn_k}{ds} = \frac{\sum_{i=1}^{n}(m_i/M_i)}{\nu_k - n_k\sum_{i=1}^{n}\nu_i}\frac{dn_k}{ds}, \quad \text{all } k \quad (15)$$

The first of these equalities follows from the definition of ξ in equation (5). The expressions involving mass fraction and mole fraction are derived in the Appendix.

Using the above expression for change in mole fraction equations (11), (12) and (13) assume the following form:

$$\frac{dn_i}{ds} = \frac{\left\{\left[\sum_{k=1}^{n}\nu_k M_k(H_k/T)\right](dT/ds) - \left[\sum_{k=1}^{n}\nu_k M_k \bar{V}_k\right](dP/ds)\right\}\left\{\nu_i - n_i\sum_{k=1}^{n}\nu_k\right\}}{RT\sum_{k=1}^{n}\nu_k(\partial \ln f_k/\partial\xi)_{T,P}}, \quad \text{all } i \quad (16)$$

$$\left.\frac{dn_i}{dP}\right|_T = \frac{\left[-\sum_{k=1}^{n}\nu_k M_k \bar{V}_k\right]\left[\nu_i - n_i\sum_{k=1}^{n}\nu_k\right]}{RT\sum_{k=1}^{n}\nu_k(\partial \ln f_k/\partial\xi)_{T,P}}, \quad \text{all } i \quad (17)$$

$$\left.\frac{dn_i}{dT}\right|_P = \frac{\left[\sum_{k=1}^{n}\nu_k M_k(H_k/T)\right]\left[\nu_i - n_i\sum_{k=1}^{n}\nu_k\right]}{RT\sum_{k=1}^{n}\nu_k(\partial \ln f_k/\partial\xi)_{T,P}}, \quad \text{all } i \quad (18)$$

If expressions are required for changes in weight fraction equations similar to equations (16), (17) and (18) may be evolved by application of the appropriate equality from equation (15).

Evaluation of the Thermodynamic Properties

The ν_k's and M_k's in equations (11), (12), (13), (16), (17) and (18) are determined by the stoichiometry. For each component, three remaining quantities must be evaluated: $\bar{H}_k$, $\bar{V}_k$ and $(\partial \ln f_k/\partial\xi)$. Since these are all state properties their values are fixed by stipulation of the thermodynamic state of the system. If the system has been well studied these data will be available in graphical and tabular form and the numerical values can be directly substituted into the above equations.

Knowledge of the thermodynamic properties of the system may also be available in the form of an equation of state. If so, the necessary properties may be numerically evaluated and substituted into the above equations. Another approach is to combine the equation of state with the above expressions to yield explicit relations for the composition derivatives in terms of simple state variables. Three useful equations of state are considered below.

If the system is an ideal solution [1] the following equations describe the partial thermodynamic behaviour:

$$\left.\begin{aligned} f_k &= n_k f_k^{\circ} \\ \bar{V}_k &= V_k \\ \bar{H}_k &= H_k \end{aligned}\right\} \quad \begin{matrix}(19)\\ \text{[is]}\end{matrix}$$

For an ideal solution equations (11), (12) and (13) respectively assume the following forms:

$$\frac{d\xi}{ds} = \frac{\left[(\mathbf{m}/RT^2)\sum_{k=1}^{n} \nu_k M_k H_k\right](dT/ds) - \left[(\mathbf{m}/RT)\sum_{k=1}^{n} \nu_k M_k V_k\right](dP/ds)}{\sum_{k=1}^{n}(\nu_k^2/\mathbf{n}_k) - \left[\sum_{k=1}^{n}\nu_k\right]^2} \qquad (20)\ [\text{is}]$$

$$\left(\frac{\partial\xi}{\partial P}\right)_T = \frac{-(\mathbf{m}/RT)\sum_{k=1}^{n}\nu_k M_k V_k}{\sum_{k=1}^{n}(\nu_k^2/\mathbf{n}_k) - \left[\sum_{k=1}^{n}\nu_k\right]^2} = \frac{-(\mathbf{m}/RT)\,\Delta\mathbf{V}}{\sum_{k=1}^{n}(\nu_k^2/\mathbf{n}_k) - \left[\sum_{k=1}^{n}\nu_k\right]^2} \qquad (21)\ [\text{is}]$$

$$\left(\frac{\partial\xi}{\partial T}\right)_P = \frac{(\mathbf{m}/RT^2)\sum_{k=1}^{n}\nu_k M_k H_k}{\sum_{k=1}^{n}(\nu_k^2/\mathbf{n}_k) - \left[\sum_{k=1}^{n}\nu_k\right]^2} = \frac{(\mathbf{m}/RT^2)\,\Delta\mathbf{H}}{\sum_{k=1}^{n}(\nu_k^2/\mathbf{n}_k) - \left[\sum_{k=1}^{n}\nu_k\right]^2} \qquad (22)\ [\text{is}]$$

If it is further assumed that the system obeys the perfect gas laws these three equations become simplified somewhat. In particular, equation (21) becomes

$$\left(\frac{\partial\xi}{\partial P}\right)_T = \frac{-(\mathbf{m}/P)\sum_{k=1}^{n}\nu_k}{\sum_{k=1}^{n}\nu_k^2/\mathbf{n}_k - \left[\sum_{k=1}^{n}\nu_k\right]^2} \qquad (23)\ [\text{is, pg}]$$

Another interesting and useful analytical description of a gas mixture is that provided by the virial equation of state. A low pressure modification of the virial equation provides a satisfactory first-order correction to perfect gas behaviour.

$$Z = \frac{PV}{(R/M)\,T} = 1 + \frac{B(T)}{RT}P \qquad (24)$$

From elementary kinetic theory it may be concluded that the second virial coefficient for mixtures is a quadratic form in mole fractions [7, 8].

$$B(T) = \sum_{i=1}^{n}\sum_{j=1}^{n}\mathbf{n}_i\,\mathbf{n}_j\,B_{ij}(T) \qquad (25)$$

The B_{ij} with like indices are merely the second virial coefficients of the pure components. The B_{ij} with unlike indices are interaction coefficients. HIRSCHFELDER *et al.* [8], GUGGENHEIM [7], and PRAUSNITZ [9] have discussed means of computing the second virial coefficients from either PVT data or from inter-molecular potential data. Combination of the equations (24) and (25) results in the following expression for the behaviour of gas mixtures:

$$Z = \frac{PV}{(R/M)\,T} = 1 + \frac{P}{RT}\sum_{i=1}^{n}\sum_{j=1}^{n}\mathbf{n}_i\,\mathbf{n}_j\,B_{ij}(T) \qquad (26)\ [\text{sm}]$$

For such systems, called simple mixtures [7], the following expressions for the partial thermodynamic behaviour may be derived:

$$V_k = \frac{RT}{M_k P} + \frac{1}{M_k}\sum_{i=1}^{n}\sum_{j=1}^{n}\mathbf{n}_i\,\mathbf{n}_j\left[B_{ik} - B_{ij} + B_{jk}\right] \qquad (27)\ [\text{sm}]$$

$$H_k = H_k^{\infty} + \frac{P}{M_k}\sum_{i=1}^{n}\sum_{j=1}^{n}\mathbf{n}_i\,\mathbf{n}_j \times \frac{d\left\{(1/T)\left[B_{ik} - B_{ij} + B_{jk}\right]\right\}}{d(1/T)} \qquad (28)\ [\text{sm}]$$

$$\ln f_k = \ln \mathbf{n}_k + \ln P + \frac{P}{RT}\sum_{i=1}^{n}\sum_{j=1}^{n}\mathbf{n}_i\,\mathbf{n}_j\left[B_{ik} - B_{ij} + B_{ik}\right] \qquad (29)\ [\text{sm}]$$

For a simple mixture the following expressions then describe the dependence of the reaction parameter on pressure and temperature.

$$\left(\frac{\partial\xi}{\partial P}\right)_T = \frac{(\mathbf{m}/P)\left[RT\sum_{k=1}^{n}\nu_k + 2P\sum_{i=1}^{n}\sum_{j=1}^{n}\mathbf{n}_i\nu_j B_{ij} - P\sum_{k=1}^{n}\nu_k\sum_{i=1}^{n}\sum_{j=1}^{n}\mathbf{n}_i\,\mathbf{n}_j\,B_{ij}\right]}{RT\left[\sum_{k=1}^{n}\nu_k^2/\mathbf{n}_k - \left(\sum_{k=1}^{n}\nu_k\right)^2\right] + 2P\left[\left(\sum_{k=1}^{n}\nu_k\right)^2\sum_{i=1}^{n}\sum_{j=1}^{n}\mathbf{n}_i\mathbf{n}_j B_{ij} - 2\left(\sum_{k=1}^{n}\nu_k\right)\sum_{i=1}^{n}\sum_{j=1}^{n}\mathbf{n}_i\nu_j B_{ij} + \sum_{i=1}^{n}\sum_{j=1}^{n}\nu_i\nu_j B_{ij}\right]} \qquad (30)\ [\text{sm}]$$

$$\left(\frac{\partial \xi}{\partial T}\right)_P = \frac{\mathbf{m}/T\left[\sum_{k=1}^{n} \nu_k M_k H_k^{\circ} + 2P \sum_{i=1}^{n}\sum_{j=1}^{n} \mathbf{n}_i \nu_j \frac{d(B_{ij}/T)}{d(1/T)} - P\left(\sum_{k=1}^{n} \nu_k\right)\sum_{i=1}^{n}\sum_{j=1}^{n} \mathbf{n}_i \mathbf{n}_j \frac{d(B_{ij}/T)}{d(1/T)}\right]}{RT\left[\sum_{k=1}^{n}(\nu_k^2/\mathbf{n}_k) - \left(\sum_{k=1}^{n}\nu_k\right)^2\right] + 2P\left[\left(\sum_{k=1}^{n}\nu_k\right)^2 \sum_{i=1}^{n}\sum_{j=1}^{n}\mathbf{n}_i\mathbf{n}_j B_{ij} - 2\left(\sum_{k=1}^{n}\nu_k\right)\sum_{i=1}^{n}\sum_{j=1}^{n}\mathbf{n}_i\nu_j B_{ij} + \sum_{i=1}^{n}\sum_{j=1}^{n}\nu_i\nu_j B_{ij}\right]} \quad (31)$$ [sm]

The derivatives of the preceding paragraphs are useful in further thermodynamic analysis. For example, they may be used to compute the heat capacity and latent heat of pressure change for a system at chemical equilibrium. The heat received by a system at equilibrium may be related to changes in state variables as follows [4, 10].

$$\frac{\delta q}{ds} = \mathbf{m}\,\mathbf{C}_{P,\xi}\frac{dT}{ds} + \mathbf{m}\,\mathbf{h}_{T,\xi}\frac{dP}{ds} + \sum_{k=1}^{n} \bar{H}_k \frac{dm_k}{ds} \quad (32)$$

or

$$\frac{\delta q}{ds} = \mathbf{m}\,\mathbf{C}_{P,\xi}\frac{dT}{ds} + \mathbf{m}\,\mathbf{h}_{T,\xi}\frac{dP}{ds} + \sum_{k=1}^{n} \nu_k M_k \bar{H}_k \frac{d\xi}{ds} \quad (33)$$

The coefficients appearing in this equation may be defined as follows [4]

$$\mathbf{C}_{P,\xi} = \frac{1}{\mathbf{m}}\left[\frac{\delta q}{dT}\right]_{P,\xi} \quad (34)$$

$$\mathbf{h}_{T,\xi} = \frac{1}{\mathbf{m}}\left[\frac{\delta q}{dP}\right]_{T,} \quad (35)$$

It is sometimes convenient to employ a heat capacity and a latent heat of pressure change that include the effects of shift in chemical equilibrium.

$$\mathbf{C}_P = \frac{1}{\mathbf{m}}\left[\frac{\delta q}{dT}\right]_P \quad (36)$$

$$\mathbf{h}_T = \frac{1}{\mathbf{m}}\left[\frac{\delta q}{dP}\right]_T \quad (37)$$

From equation (33)

$$\mathbf{C}_P = \mathbf{C}_{P,\xi} + \frac{1}{\mathbf{m}}\sum_{k=1}^{n} \nu_k M_k \bar{H}_k \left(\frac{\partial \xi}{\partial T}\right)_P \quad (38)$$

$$\mathbf{h}_T = \mathbf{h}_{T,\xi} + \frac{1}{\mathbf{m}}\sum_{k=1}^{n} \nu_k M_k \bar{H} \left(\frac{\partial \xi}{\partial P}\right)_T \quad (39)$$

If equations (38) and (39) are combined with equations (13) and (12) respectively, the following are obtained:

$$\mathbf{C}_P = \mathbf{C}_{P,\xi} + \frac{(1/T)\left[\sum_{k=1} \nu_k M_k \bar{H}_k\right]^2}{\mathbf{m}\,RT \sum_{k=1}^{n} \nu_k (\partial \ln f_k/\partial \xi)_{T,P}} \quad (40)$$

$$\mathbf{h}_T = \mathbf{h}_{T,\xi} - \frac{\left[\sum_{k=1}^{n} \nu_k M_k \bar{V}_k\right]\left[\sum_{k=1}^{n} \nu_k M_k \bar{H}_k\right]}{\mathbf{m}\,RT \sum_{k=1}^{n} \nu_k (\partial \ln f_k/\partial \xi)_{T,P}} \quad (41)$$

For the ideal solution described by equation (19) these formulae simplify to

$$\mathbf{C}_P = \mathbf{C}_{P,\xi} + \frac{1/RT^2\,[\Delta \mathrm{H}]^2}{\sum_{k=1}^{n}(\nu_k^2/\mathbf{n}_k) - \left[\sum_{k=1}^{n}\nu_k\right]^2} \quad (42)$$ [is]

$$\mathbf{h}_T = \mathbf{h}_{T,\xi} - \frac{(1/RT)[\Delta \mathrm{V}][\Delta \mathrm{H}]}{\sum_{k=1}^{n}(\nu_k^2/\mathbf{n}_k) - \left[\sum_{k=1}^{n}\nu_k\right]^2} \quad (43)$$ [is]

A similar analysis leads to the following expressions for the isothermal and isobaric compressibilities of a system in chemical equilibrium:

$$\left(\frac{\partial \mathrm{V}}{\partial T}\right)_P = \left(\frac{\partial \mathrm{V}}{\partial T}\right)_{P,\xi} + \frac{1}{\mathbf{m}}\sum_{k=1}^{n} \nu_k M_k \bar{V}_k \left(\frac{\partial \xi}{\partial T}\right)_P \quad (44)$$

$$\left(\frac{\partial \mathrm{V}}{\partial P}\right)_T = \left(\frac{\partial \mathrm{V}}{\partial P}\right)_{T,\xi} + \frac{1}{\mathbf{m}}\sum_{k=1}^{n} \nu_k M_k \bar{V}_k \left(\frac{\partial \xi}{\partial P}\right)_T \quad (45)$$

Some Applications

Example A

As an example of an application of these equations consider the following reaction

$$\mathrm{N_2} + 3\mathrm{H_2} \rightarrow 2\mathrm{NH_3}$$

To be specific, it will be assumed that the ammonia synthesis is under consideration with $\mathrm{N_2}$ and $\mathrm{H_2}$ initially present in the stoichiometric ratio. The data are easily summarized by the following:

Component	*Index*	ν_k	$m_k(\xi = 0)$ (Moles)	$m_k(\xi)$ (Moles)
$\mathrm{N_2}$	1	-1	1	$1-\xi$
$\mathrm{H_2}$	2	-3	3	$3-3\xi$
$\mathrm{NH_3}$	3	2	0	2ξ
total (Σ)	—	$\sum_{k=1}^{n} \nu_k = -2$	4	$4-2\xi$

If the system is assumed to be an ideal solution and a perfect gas, the following results from substitution into equation (20)

$$\frac{d\xi}{ds} = \frac{-\left[(-2)/P\right](dP/ds) + (\Delta \mathrm{H}/RT^2)\,(dT/ds)}{[(-1)^2/(1-\xi)] + \left[(-3)^2/(3-3\xi)\right] + (2^2/2\xi) - [(-2)/(4-2\xi)]} \qquad \begin{matrix}(46)\\ \text{[is, pg, ex]}\end{matrix}$$

This simplifies algebraically

$$\frac{d\xi}{ds} = \frac{\xi\,(2-\xi)\,(1-\xi)}{4}\left[\frac{2}{P}\frac{dP}{ds} + \frac{\Delta \mathrm{H}}{RT^2}\frac{dT}{ds}\right] \qquad \begin{matrix}(47)\\ \text{[is, pg, ex]}\end{matrix}$$

A special form of this is the following, which directly relates fractional change in conversion to fractional change in pressure.

$$\frac{d\xi}{\xi} = \frac{1}{2}\,(2-\xi)\,(1-\xi)\,\frac{dP}{p} \qquad \begin{matrix}(48)\\ \text{[is, pg, ex, } T\text{]}\end{matrix}$$

For small changes a useful relationship is thus available.

$$\frac{\Delta\xi}{\xi} \simeq \frac{1}{2}\,(2-\xi)\,(1-\xi)\,\frac{\Delta P}{P} \qquad \begin{matrix}(49)\\ \text{[is, pg, ex, } T\text{]}\end{matrix}$$

A similar equation for the same system may be educed for isobaric variations in temperature.

$$\frac{\Delta\xi}{\xi} = \frac{(2-\xi)\,(1-\xi)}{4}\,\frac{\Delta \mathrm{H}}{RT}\,\frac{\Delta T}{T} \qquad \begin{matrix}(50)\\ \text{[is, pg, ex, } P\text{]}\end{matrix}$$

It is perhaps worth emphasizing that expressions of the form of equations (49) and (50) are particularly useful for estimating either errors or the effect of small changes in the independent variables. Computation of such small changes by iteration of formulae involving the equilibrium constant would likely require considerably more effort.

Example B

As a second example, let a known state of the system be denoted by T_0, P_0, $\xi = 0$, m_{k0}, etc. The problem will be to calculate ξ at a different state for which the system displays new values of temperature and pressure, T_1 and P_1. It will be assumed that the system is adequately described as an ideal solution, equation (20). Then equation (23) may be written in the following form:

$$\int_0^{\xi_1}\left[\sum_{k=1}^{n}\frac{\nu_k^2}{\mathrm{m}_k} - \frac{\left[\sum_{k=1}^{n}\nu_k\right]^2}{\mathrm{m}}\right]d\xi \qquad \begin{matrix}(51)\\ \text{[is]}\end{matrix}$$

$$= \int_{T_0,\,P_0}^{T_1,\,P_1}\left[-\frac{1}{RT}\sum_{k=1}^{n}\nu_k M_k V_k\frac{dP}{ds} + \frac{1}{RT^2}\sum_{k=1}^{n}\nu_k M_k H_k\frac{dT}{ds}\right]ds$$

This can be modified by use of equation (14)

$$\int_0^{\xi_1}\left[\sum_{k=1}^{n}\left[\frac{\nu_k^2}{\mathrm{m}_{k0}+\nu_k\xi}\right]^2 - \frac{\left[\sum_{k=1}^{n}\nu_k\right]^2}{\mathrm{m}_0 + \sum_{k=1}^{n}\nu_k\xi}\right]d\xi = \qquad \begin{matrix}(52)\\ \text{[is]}\end{matrix}$$

$$= \int_{T_0,\,P_0}^{T_1,\,P_1}\left[\frac{\Delta \mathrm{V}}{RT}\frac{dP}{ds} - \frac{\Delta \mathrm{H}}{RT}\frac{dT}{ds}\right]ds$$

$$\ln\prod_{k=1}^{n}\left[\frac{m_{k0}+\nu_k\xi_1}{m_{k0}}\right]^{\nu_k} + \ln\left[\frac{\mathrm{m}_0 + \sum_{k=1}^{n}\nu_k\xi_1}{\mathrm{m}_0}\right]^{\left[\sum_{k=1}^{n}\nu_k\right]^2} \qquad \begin{matrix}(53)\\ \text{[is]}\end{matrix}$$

$$= \int_{T_0,\,P_0}^{T_1,\,P_1}\left[\frac{\Delta \mathrm{V}}{RT}\frac{dP}{ds} + \frac{\Delta \mathrm{H}}{RT^2}\frac{dT}{ds}\right]ds$$

Since ξ is a state property any convenient path may be employed for the evaluation of the integral on the right-hand side of this latter equation: presumably an isobaric path followed by an isothermal path would be used. Since the left-hand side is implicit in ξ an iterative solution

would be required in order to establish a numerical value.

Example C

At a given temperature and for a system of fixed initial composition, is there an optimum pressure which maximizes the extent of a reaction? This can be answered by inspecting $(\partial\xi/\partial P)_T$ for zeroes. For an ideal solution equation (21) can be expressed in terms of the compressibility factor.

$$\left(\frac{\partial \xi}{\partial P}\right)_T = \frac{(\mathbf{m}/P)\sum_{k=1}^{n} \nu_k Z_k}{\sum_{k=1}^{n} (\nu_k^2/\mathbf{n}_k) - \left[\sum_{k=1}^{n} \nu_k\right]^2} = 0 \qquad (54)$$

[is. max or min]

This expression can only be satisfied in a non-trivial way if

$$\sum_{k=1}^{n} \nu_k Z_k = 0 \qquad (55)$$

[is. max or min]

Hence, a point of maximum (or minimum) ξ can be quickly located by determining the zero of equation (55).

Example D

Another interesting result can be derived from equation (11) by considering equilibrium changes at constant ξ.

$$\frac{dP}{dT} = \frac{(1/T)\sum_{k=1}^{n} \nu_k M_k H_k}{\sum_{k=1}^{n} \nu_k M_k V_k} \qquad (56)$$

[ξ]

This has a formal similarity to the Clapeyron equation describing the interrelation of thermodynamic variables along the vapour-pressure curve of a one-component system. If equation (56) is applied to a system that is both ideal and perfect the following results:

$$d \ln P = \frac{dT}{T^2} \frac{\sum_{k=1}^{n} \nu_k M_k H_k}{R \sum_{k=1}^{n} \nu_k} \qquad (57)$$

[ξ, is, pg]

If it is further assumed that the enthalpy change of reaction does not vary with temperature, equation (57) can be integrated to give the following expression, which is identical in form to the Clausius–Clapeyron equation for one-component phase equilibrium:

$$\ln P = C_1 \frac{1}{T} + C_2 \left[\begin{matrix}\xi, \text{ is, pg} \\ \Delta \mathbf{H} = \text{const}\end{matrix}\right] \qquad (58)$$

The assumptions leading to equation (58) are admittedly somewhat stringent. Nevertheless the result may serve as a guide for correlating yield data from bench or pilot plant experiments. At least it suggests that plots of $\ln P$ vs. $1/T$ at constant ξ might be useful for interpolation, or even for modest extrapolation of equilibrium yield data. This could be a particularly worthwhile approach for systems of complicated or unknown stoichiometry, such as those encountered in polymerization or combustion.

Appendix

Derivation of equation (15)

By definition of weight fraction,

$$n_k = \frac{m_k}{\sum_{i=1}^{n} m_i} \qquad (59)$$

Differentiating and substituting from equation (5)

$$\frac{dn_k}{ds} = \frac{1}{\sum_{i=1}^{n} m_i} \frac{dm_k}{ds} = \frac{\nu_k M_k}{\sum_{i=1}^{n} m_i} \frac{d\xi}{ds} \qquad (60)$$

$$\mathbf{n}_k = \frac{m_k/M_k}{\sum_{i=1}^{n} (m_i/M_i)} \qquad (61)$$

[all k]

$$dn_k = \sum_{i=1}^{n} \frac{m_i}{M_i} d\mathbf{n}_k + \mathbf{n}_k \sum_{i=1}^{n} \frac{dm_i}{M_i} \qquad (62)$$

Substituting from equation (5)

$$\nu_k \, d\xi = \sum_{i=1}^{n} \frac{m_i}{M_i} d\mathbf{n}_k + \mathbf{n}_k \sum_{i=1}^{n} \nu_i \, d\xi \qquad (63)$$

$$\frac{d\xi}{ds} = \frac{d\mathbf{n}_k}{ds} \frac{\sum_{i=1}^{n} (m_i/M_i)}{\nu_k - \mathbf{n}_k \sum_{i=1}^{n} \nu_i} \qquad (64)$$

[all k]

Equation (15) then results directly from equations (60) and (64).

Notations

A_k = general molecular symbol for component k
$B(T)$ = second virial coefficient — ft^3/lb.
$B_{ij}(T)$ = contribution to second virial coefficient resulting from interaction of species "i" and "j"
C_1, C_2 = constants
$\mathbf{C}_{p,\xi}$ = isobaric molal heat capacity of system of constant composition — B.Th. U./lb. mole °F
$\mathbf{C}_p$ = isobaric molal heat capacity of a chemically reacting system. — B.Th. U./lb. mole °F
f_k = fugacity of component k — p.s.i.a.
$\mathbf{h}_T$ = latent molal heat of pressure change of a chemically reacting system — B.Th. U./lb. mole p.s.i.
$\mathbf{h}_{T,\xi}$ = latent molal heat of pressure change of a system of constant composition — B.Th. U./lb. mole p.s.i.
H_k = specific enthalpy of component k — B.Th. U./lb.
$\overline{H}_k$ = specific partial enthalpy of component k — B.Th. U./lb.
$\Delta\mathbf{H} = \sum_{k=1}^{n} v_k M_k H_k$, — B.Th. U./lb. mole
M_k = molecular weight of component k
$\mathbf{m}$ = total number of moles
m_k = mass of component k
$\mathbf{m}_k$ = moles of component k
n_k = mass fraction of component k
$\mathbf{n}_k$ = mole fraction of component k
P = pressure — p.s.i.a.
q = heat — B.Th. U.
R = universal gas contant — 10·73147 ft^3 p.s.i./lb. mole °R
s = path parameter
T = absolute temperature — °R
V_k = specific volume of component k — ft^3/lb.
$\overline{V}_k$ = partial specific volume of component k — ft^3/lb.
$\Delta\mathbf{V} = \sum_{k=1}^{n} v_k M_k \overline{V}_k$ — ft^3/lb. mole
Z = compressibility factor — PVM/RT
v_k = stoichiometric coefficient of component k — pure number
μ_k = chemical potential of component k — B.Th. U./lb.
ξ = extent of reaction — lb. mole

Below symbols
$\mathbf{G}$ = molal value of property "G" — G/M

Superscripts
0 = pure substance
∞ = infinite attenuation

Subscripts
i, j, k = refers to components i, j, k
0, 1, 2 = denotes value of property at time or state 0, 1, 2 . . . n

Brackets
[ex] = indicates an example
[is] = indicates an ideal solution
[pg] = indicates a perfect gas
[sm] = indicates a simple mixture

Operators
Σ = summation
$\prod_{i=1}^{n} x_i$ = multiplication ($x_1 x_2 \cdots x_{n-1} x_n$)

References

[1] Lewis G. N. and Randall M. *Thermodynamics.* McGraw-Hill, New York 1923.

[2] Epstein P. S. *Textbook of Thermodynamics.* John Wiley, New York 1937.

[3] Denbigh K. G. *The Principles of Chemical Equilibrium.* Cambridge University Press 1955.

[4] Prigogine I. and Defay R. *Chemical Thermodynamics.* Longmans Green, New York 1954.

[5] Davies R. O. *Rep. Progr. Phys.* 1956 **18** 858.

[6] Potter R. L. *J. Chem. Phys.* 1958 **28** 893.

[7] Guggenheim E. A. *Mixtures.* Oxford University Press 1952.

[8] Hirschfelder J. O., Curtiss C. F. and Bird R. B. *Molecular Theory of Gases and Liquids.* John Wiley, New York 1954.

[9] Prausnitz J. M. *Chem. Engng. Sci.* 1957 **6** 112.

[10] Goranson R. W. *Thermodynamic Relations in Multi-Component Systems.* Carnegie Institution of Washington 1930

Chemical Engineering Science, 1961, Vol. 16, pp. 189 to 201. Pergamon Press Ltd., London. Printed in Great Britain.

Non-steady state behaviour of fixed bed catalytic reactors due to catalyst fouling

G. F. Froment and K. B. Bischoff*

Laboratorium voor Organische Technische Chemie, Rijksuniversiteit Gent, Belgium

(*Received* 27 *January* 1961)

Abstract—The influence of catalyst fouling on the conversion to the product of interest has been studied by coupling a rate equation for the formation of the catalyst fouling compound to the continuity equation for the main product.

Two mechanisms of formation of the catalyst fouling compound have been investigated. In the first, the fouling results from a reaction parallel to the main reaction and, in the second, from a reaction consecutive to the main reaction.

The resulting decrease in activity of the catalyst is accounted for by relating the rate coefficients directly to the carbon content of the catalyst, rather than to time, as has been done until now. Two forms of such a relationship have been used: an exponential and a hyperbolic.

For both mechanisms investigated the carbonaceous material is deposited according to a certain profile: descending in the case of a parallel, ascending in the case of a consecutive mechanism.

The implications of the occurence of such profiles in the carbon content on the rate and temperature profiles are discussed. It is shown that in the case of a descending profile of carbonaceous material the rate and temperature profiles exhibit peak values whose loci travel through the reactor as time increases.

Résumé—Les auteurs étudient l'influence d'un dépôt de carbone sur le taux de conversion d'une réaction conduisant à un produit principal en considérant simultanément l'équation de continuité pour ce produit et une équation exprimant la vitesse de formation du dépôt de carbone.

Deux mécanismes qui peuvent donner lieu à un tel dépôt ont été considérés: d'après le premier le dépôt résulte d'une réaction parallèle à la réaction principale, d'après le second d'une réaction consécutive. La diminution de l'activité du catalyseur est exprimée par une relation entre les coefficients cinétiques d'une part et la teneur en carbone du catalyseur d'autre part, alors que jusqu'à présent on avait plutôt considéré la durée de l'opération. Les relations utilisées dans cet article sont du type exponentiel et hyperbolique.

On montre comment le carbone est déposé selon un profil: décroissant dans le cas du mécanisme parallèle et croissant dans le cas du mécanisme consécutif.

Les conséquences de la présence de ces profils dans la teneur en carbone du catalyseur, sur les profils de vitesse et de température sont discutées. C'est ainsi que lorsque le profil de carbone est décroissant, les profils de vitesse de réaction et de température présentent des pics qui progressent à travers le réacteur en fonction de la durée de l'opération.

Zusammenfassung—Der Einfluss eines kohlenstoffartigen Niederschlages auf den Umsatz zum Hauptprodukt in einem katalytischen Reaktor ist studiert worden durch eine Geschwindigkeitsgleichung um die Bildung des Niederschlages zu kuppeln mit der Kontinuitätsgleichung des Hauptproduktes.

Zwei Mechanismen für die Bildung des Niederschlages sind untersucht worden. Beim ersten war der Abkling das Resultat einer der Hauptreaktion parallelen Reaktion, beim zweiten einer der Hauptreaktion folgenden Reaktion.

Der resultierende Abkling der Aktivität des Katalysators its ausgedrückt worden durch eine Beziehung zwischen den Geschwindigkeitskoeffizienten und dem Kohlenstoffgehalt des Katalysators, vielmehr als mit der Betriebsdauer, wie bisher versucht. Zwei solche Beziehungen, eine exponentielle und eine hyperbolische, sind gebraucht worden. Für beide untersuchten

*Present address: The University of Texas, U.S.A.

Mechanismen wird der Kohlenstoff nach einem gewissen Profil niedergeschlagen: fallend für den Parallel Mechanismus, steigend für den Folgemechanismus.

Die Folge des Bestehens solcher Profile in dem Kohlenstoffgehalt auf die Geschwindigkeits- und Temperaturprofile werden diskutiert. Es wird gezeigt, dass in Fall eines fallenden Profils im Kohlenstoffgehalt die Geschwindigkeit- und Temperaturprofile Spitzen zeigen, deren Platz sich im Reaktor verändert mit zunehmender Betriebsdauer.

1. Introduction

Many chemical reactions of commercial importance are accompanied by side reactions leading to a carbonaceous deposit. This deposit causes a decrease in the activity of the catalyst, termed fouling, which is reflected in a drop in conversion to the product of interest. In order to maintain production rates within the desired limits it is necessary to remove the deposit, i.e. to regenerate the catalyst, either intermittently or, preferably, continuously. Entirely new techniques, such as fluidized or moving bed operations, were developed some twenty years ago, mainly for this purpose.

In spite of these far reaching consequences it seems that catalyst fouling and its influence on the conversion never received the fundamental study one would expect. What has been previously done is to express the drop in conversion empirically vs. process time [1]. The fouling of the catalyst, as measured by its carbon content, has also been related to process time [2–5], but no consideration has ever been given to the effect of the partial pressures of the reacting components. Obviously, the catalyst fouling compound must result in some way either from the reactant or from the product; therefore, it is not justifiable to treat its rate of formation separately from the main reaction.

A more fundamental approach would require the consideration of the mechanisms leading to a set of simultaneous equations expressing the rate of formation of the main product and the catalyst fouling compound.

In addition, a relation would be needed between the amount of deposit and the decrease in conversion. With this type of approach the deposition of catalyst fouling compound is not uniform along the reactor length since the partial pressures of the reacting components vary. If, then, there is a profile, the conversions and selectivities, the temperature distributions and the regeneration transients may be markedly different from those predicted on the basis of uniform fouling. It is the purpose of this paper to draw attention upon such situations.

In the absence of experimental data, especially about the mechanism and the rate of formation of carbonaceous deposits, it seemed justifiable to introduce some simplifying assumptions. These were mainly in the rate equations so that the mathematical treatment remained fairly simple. These simplifications do not affect, however, the general trends revealed by the approach used in this paper.

Also, only isothermal operation has been considered. The coupling of an energy equation to the continuity equations would have required a numerical treatment on an electronic computer and this degree of complexity did not seem justified at the present state of knowledge.

2. The Continuity Equations

We shall assume a flat velocity profile and no diffusion of any sort occuring. Although solid, carbonaceous material is being formed from gaseous compounds, for mathematical simplicity it will also be assumed that both the density and the number of moles remain constant. Then the continuity equation for the reactant, A, may be written, in terms of mole fractions,

$$\frac{\partial y}{\partial t'} + \frac{F}{\epsilon \rho_A \Omega} \frac{\partial y}{\partial z'} = -\frac{\rho_B}{\epsilon \rho_A} r_A \tag{1}$$

When the following dimensionless variables are introduced

$$z = \frac{z'}{d_p} \qquad t = \frac{F}{\epsilon \rho_A \Omega d_p} t' \tag{2}$$

Equation (1) becomes:

$$\frac{\partial y}{\partial t} + \frac{\partial y}{\partial z} = -\frac{\Omega \rho_B d_p}{F} r_A \tag{3}$$

An equation similar to equation (1), where the term containing the feed rate drops out, of course, may be written for the catalyst fouling compound. Since the amount of carbonaceous compound is usually measured by the amount of carbon on the catalyst the equation will be written in terms of carbon. Then the continuity equation for the carbon is

$$\frac{\partial c}{\partial t'} = r_c \tag{4}$$

where the weight of carbon is divided by the weight of catalyst to give a dimensionless variable. When the dimensionless variables defined above are introduced, equation (4) becomes

$$\frac{\partial c}{\partial t} = \frac{\epsilon \rho_A \Omega d_p}{F} r_c \tag{5}$$

Equations (3) and (5) are a pair of coupled, hyperbolic, partial differential equations. Their solution is made easier by using as independent variables z and η, rather than z and t, where

$$\eta = t - z$$

This η is a time-measuring variable that is zero at the displacement front of the flowing material, rather than at zero physical time. In mathematical terms η is the variable along a characteristic of equation (3). Actually, for practical purposes $t \gg z$ – except for very short times, so that $\eta \simeq t$.

In terms of (z, η) equations (3) and (5) may be written

$$\frac{\partial y}{\partial z} = -\frac{\Omega \rho_B d_p}{F} r_A \tag{6}$$

$$\frac{\partial c}{\partial \eta} = \frac{\Omega \rho_A \epsilon d_p}{F} r_c \tag{7}$$

3. Reaction Mechanisms

In equations (6) and (7) the rate terms, r_A and r_c, remain to be specified. Two simple mechanisms will be considered. In the first, the catalyst fouling compound, C, is formed by a reaction parallel to the main reaction.

$$A \xrightarrow{k_1} R$$

$$A \xrightarrow{k_2} C$$

If, for simplicity, both reactions are assumed to be first order with respect to A,

$$r_A = k_1 Py + k_2 Py \tag{8}$$

$$r_c = k_2 Py \tag{9}$$

In the second mechanism the catalyst fouling compound is assumed to be formed by a reaction consecutive to the main reaction,

$$A \xrightarrow{k_1} R \xrightarrow{k_2} C$$

so that, again assuming first-order reactions,

$$r_A = k_1 Py \tag{10}$$

$$r_c = k_2 P(1 - y) \tag{11}$$

In equation (11) $(1 - y)$ represents the mole fraction of R in the gas phase, which is only true in the approximate situation of constant density considered here, of course.

4. Relation Between Rate Coefficients and Carbon Content

The rate coefficients in equations (8)–(11) may be written more explicitly, but still entirely general, as

$$k_1 = k_1^\circ \phi_1 \tag{12}$$

$$k_2 = k_2^\circ \phi_2 \tag{13}$$

where k_1° and k_2° are the values of these coefficients at zero carbon deposition. The ϕ's are functions which may be based on Langmuir–Hinshelwood concepts and, therefore, contain adsorption terms for each component of the reaction mixture. ϕ should be expressed not as a function of time, as has been done previously, but rather as a function of the real variable—the carbon content of the catalyst. First, this choice of variable might allow comparison between different reactions, whereas a correlation with respect to time would be specific for each reaction. Second, when there is a profile in the carbon content the activity of the catalyst varies throughout the reactor, and thus its correlation as a function only of time would be unsatisfactory.

Two specific forms of the ϕ-functions have been considered in this paper. The first form expresses an exponential dependency of the catalyst activity on the carbon deposited. It is based on

the observation that after a very sharp initial decline the conversion to the product of interest decreases more slowly to tend assymptotically to some limiting value, but has no theoretical background whatever. Then,

$$\phi = \exp(-\alpha c)$$

where α is a proportionality factor, to be determined experimentally. The second form expresses a hyperbolic dependency on the carbon deposited.

$$\phi = \frac{1}{1 + Kc}$$

This formula corresponds also to the picture sketched above and may arise from Langmuir–Hinshelwood concepts. For mathematical simplicity, however, only this restricted case, which neglects the adsorption of the components of the main reaction was considered. The constant K is then a sort of adsorption equilibrium constant that expresses the proportionality between the amount of carbonaceous compound deposited, measured as carbon, and the number of active sites fouled*.

5. Catalyst Fouling by a Parallel Reaction Mechanism

When equations (8) and (9) are substituted into equations (6) and (7) respectively, they become

$$\frac{\partial y}{\partial z} = -\frac{\Omega \rho_B d_p P}{F}(k_1 + k_2)\, y \tag{14}$$

$$\frac{\partial c}{\partial \eta} = \frac{\Omega \rho_A \epsilon d_p P}{F} k_2\, y \tag{15}$$

Solutions will be given for both types of activity functions discussed in Section 3.

*A slightly more general hyperbolic function $\phi = 1/(\beta + Kc)$, in which the effect of the adsorption of the main reaction components is partially taken into account by the empirical constant, β, can also be treated by the methods used in this paper. Since it leads to the same general trends as the simpler hyperbolic function, but is more complicated to represent because of the additional parameter, β, it will not be discussed further here.

(a) *Exponential activity function*

For the purposes of this paper there are still two possibilities of interest: both k_1 and k_2 may be affected by the deposition of carbonaceous material on the catalyst (both reactions are catalytic), or only the main reaction is affected. The latter case will be treated here, so that

$$\phi_1 = \exp(-\alpha c)$$

$$\phi_2 = 1$$

Equations (14) and (15) may be written

$$\frac{\partial y}{\partial z} = -a(\exp(-\alpha c) + \gamma)\, y \tag{18}$$

$$\frac{\partial c}{\partial \eta} = by \tag{19}$$

where

$$a = \frac{\Omega \rho_B d_p P}{F} k_1^\circ \tag{20}$$

$$\gamma = \frac{k_2^\circ}{k_1^\circ} \tag{21}$$

$$b = \frac{\Omega \rho_A \epsilon d_p P}{F} k_2^\circ \tag{22}$$

The system of equations (18)–(19) will be solved subject to the boundary conditions that pure A is fed to the reactor, while initially the carbon content of the catalyst is zero:

$$y(0, \eta) = 1 \tag{23}$$

$$c(z, 0) = 0 \tag{24}$$

Then, by differentiating equation (19) with respect to z:

$$\frac{\partial^2 c}{\partial \eta\, \partial z} = b \frac{\partial y}{\partial z} \tag{25}$$

$$= -ab(\exp(-\alpha c) + \gamma)\, y$$

$$= -a(\exp(-\alpha c) + \gamma)\frac{\partial c}{\partial \eta} \tag{26}$$

if equation (26) is integrated with respect to η, it becomes

$$\frac{\partial c}{\partial z} + K(z) = -a\gamma c + \frac{a}{\alpha}\exp(-\alpha c) \tag{27}$$

VOL 16 196

where $K(z)$ is an integration constant. From equation (24), it follows that

$$K(z) = \frac{a}{\alpha} \tag{28}$$

Introducing equation (28) into equation (27) leads to

$$\frac{\partial c}{\partial z} + a\gamma c = \frac{a}{\alpha}\left[\exp(-\alpha c) - 1\right] \tag{29}$$

Equation (29) can now be treated as an ordinary differential equation and directly integrated with respect to z. The boundary condition for equation (29) at $z = 0$ is obtained by combining equation (23) and equation (19)

$$\frac{\partial c(0, \eta)}{\partial \eta} = b$$

from which

$$c(0, \eta) = b\eta + K_1$$

From equation (24), K_1 must be zero so that

$$c(0, \eta) = b\eta$$

In general, equation (29) cannot be solved analytically. For small values of z the function $c(z, \eta)$ can be expanded in a Taylor series in z, however,

$$c(z, \eta) = b\eta + z\left\{-\gamma ab\eta + \frac{a}{\alpha}\left[\exp(-\alpha b\eta) - 1\right]\right\} + \frac{z^2}{2!}\left[-\gamma a - a\exp(-ab\eta)\right]\left\{-\gamma ab\eta + \frac{a}{\alpha}\left[\exp(-\alpha b\eta) - 1\right]\right\} + \ldots. \tag{30}$$

From this and equation (19) $y(z, \eta)$ is derived. This series converges slowly for the case considered in this Section, however. The direct numerical solution of equation (29) is also clumsy, since derivatives of $c(z, \eta)$ must be taken in order to get y. The usefulness of equations (29) and (30) will be shown in the next Section.

In view of this, an approximate solution to the set of equations (18) and (19) was sought. This solution was based on the observation that $\gamma = k_2^\circ/k_1^\circ$ is a small number, since the amount of reactant converted to carbonaceous deposit is very small with respect to the amount converted to the main product. Equation (18) may then be approximated by

$$\frac{\partial y}{\partial z} = -a\exp(-\alpha c)\, y \tag{31}$$

The set of equations (31) and (19) can now be solved analytically, starting with the integration of equation (29) with $\gamma = 0$. The results are

$$y = \left\{1 + \exp(-\alpha b\eta)\left[\exp(az) - 1\right]\right\}^{-1} \tag{32}$$

$$\exp(-\alpha c) = \left\{1 + \exp(-az)\left[\exp(\alpha b\eta) - 1\right]\right\}^{-1} \tag{33}$$

This approximate solution was checked with the series solution derived from equation (30) at values (z, η) where only the first terms in the series were needed. For values of $\gamma = k^\circ_2/k^\circ_1 \leqslant 0{\cdot}02$, the agreement obtained was within 5 per cent, which was satisfactory and sufficient for the purposes of this paper.

It is clearly seen from equations (32) and (33) that y and c are functions of both z and η. These results are plotted in Fig. 1 (a), where the increase of the mole fraction of A, y (or the decrease in conversion) is plotted essentially vs. time at several bed depths, and in Fig. 1 (b), where the carbon profiles are shown at several values of the dimensionless group $\alpha b\eta$. The discussion of these results will be given below, together with those obtained for other particular cases.

(b) *Hyperbolic activity function*

In this case both the main reaction and the side reaction leading to the catalyst fouling compound will be considered to be affected by the fouling, with the restriction that they are both affected in the same way, i.e. their mechanism of formation is identical. Then,

$$\phi_1 = \phi_2 = \frac{1}{1 + Kc}$$

and from equations (14) and (15) combined with equations (12) and (13)

$$\frac{\partial y}{\partial z} = -\frac{ay}{1 + Kc} \tag{34}$$

$$\frac{\partial c}{\partial \eta} = \frac{by}{1 + Kc} \tag{35}$$

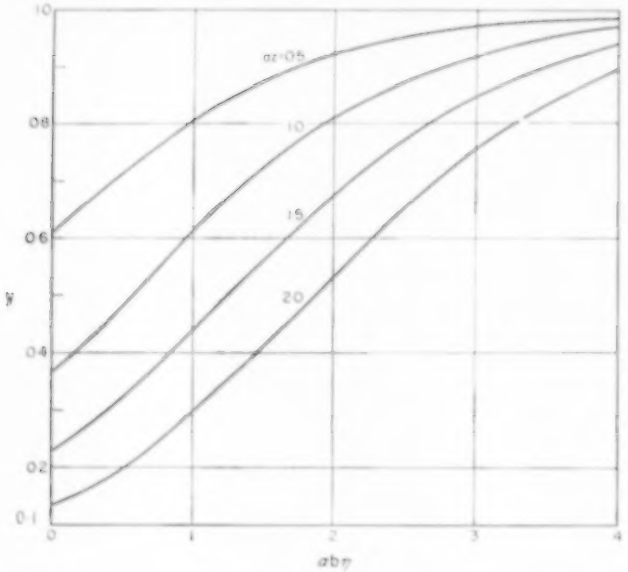

Fig. 1 (a). Reactant Mole fraction vs. time group for parallel reaction mechanism with exponential activity function.

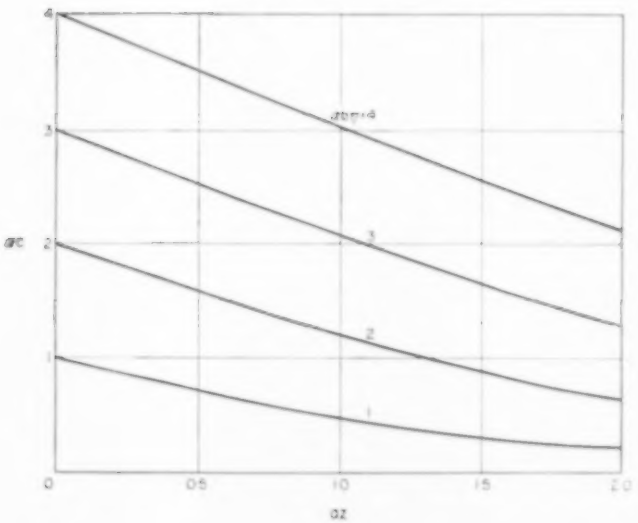

Fig. 1 (b). Carbon profiles for parallel reaction mechanism with exponential activity function.

where a and b are the same combination of variables as in equations (20) and (22) except that k°_1 must be replaced by $k^\circ_1 + k^\circ_2$. The set of equations (34) and (35) may be solved with the boundary conditions given in Section 5 (a), with a procedure used by DU DOMAINE *et al.* [6]. The results are

$$y = \exp\left[-az + (1 + 2K\,b\eta)^{1/2} - 1 - Kc\right] \quad (36)$$

$$Kc\exp(Kc) = \left[(1 + 2Kb\eta)^{1/2} - 1\right] \exp\left[-az + (1 + 2Kb\eta)^{1/2} - 1\right] \quad (37)$$

Fig. 2 (a) shows the increase in y as a function of time at different bed depths and Fig. 2 (b) shows the carbon profile at various $Kb\eta$. These results will also be discussed below. The general trends are the same as in Section 5 (a).

6. Catalyst Fouling by a Reaction Consecutive to the Main Reaction

Substitution of equations (10) and (11) in equations (6) and (7) respectively leads to

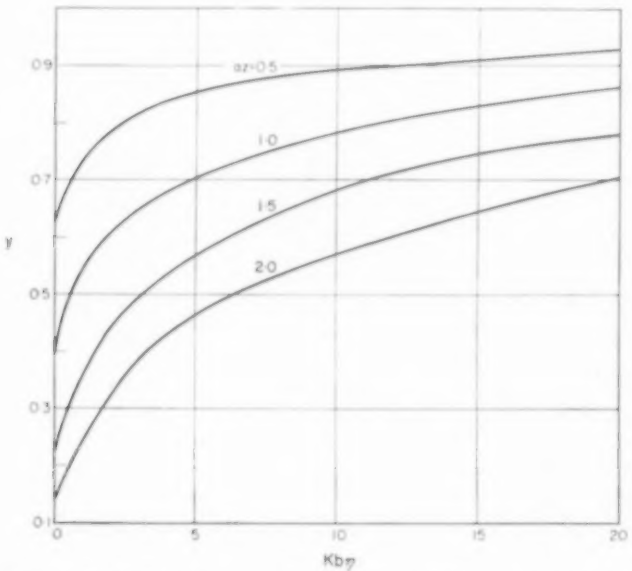

Fig. 2 (a). Reactant mole fraction vs. time group for parallel reaction mechanism with hyperbolic activity function.

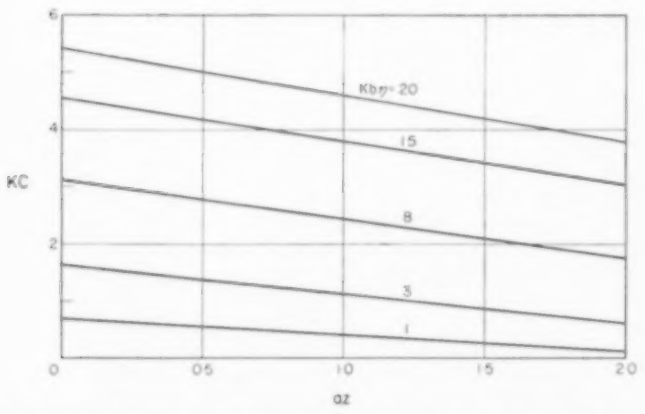

Fig. 2 (b). Carbon profiles for parallel reaction mechanism with hyperbolic activity function.

$$\frac{\partial y}{\partial z} = -\frac{\Omega \rho_B d_p P}{F} k_1 y \qquad (38)$$

$$\frac{\partial c}{\partial \eta} = \frac{\Omega \rho_A \epsilon d_p P}{F} k_2 (1 - y) \qquad (39)$$

For mathematical simplicity only the exponential type of activity function will be considered here, and again it will be assumed that only k_1 is affected. Then

$$\phi_1 = \exp(-\alpha c)$$

$$\phi_2 = 1$$

When equations (12) and (13) are combined with equations (38) and (39) one obtains

$$\frac{\partial y}{\partial z} = -a \exp(-\alpha c)\, y \qquad (40)$$

$$\frac{\partial c}{\partial \eta} = b(1 - y) \qquad (41)$$

where

$$a = \frac{\Omega \rho_B d_p P}{F} k_1^\circ \qquad (42)$$

and

$$b = \frac{\Omega \rho_A \epsilon d_p P}{F} k^\circ_2 \qquad (43)$$

By the following transformations it can be seen that the set of equations (40)–(41) is entirely analogous to the set of equations (18)–(19):

equations (18)–(19)	⟶	equations (40)–(41)
$\exp(-\alpha c)$	⟶	y
y	⟶	$\exp(-\alpha c)$
z	⟶	η
η	⟶	z
αb	⟶	a
a	⟶	$-\alpha b$
γ	⟶	-1

Therefore, the series solution, equation (30), becomes here:

$$\ln y = -az + \eta\{\alpha abz + \alpha b[\exp(-az) - 1]\} + \frac{\eta^2}{2!}[-\alpha b + \alpha b \exp(-az)]\,[\alpha abz + \alpha b[\exp(-az) - 1]] + \ldots \qquad (44)$$

and $c(z, \eta)$ is obtained from

$$\exp(-\alpha c) = \frac{-1}{a}\frac{\partial}{\partial z} \ln y \qquad (45)$$

It was found in this case that when four terms were used the series solution could be used safely up to about $az = 2$, $\alpha b\eta = 2$. When more terms are used the algebra becomes prohibitive as the terms becomes more complex with increasing number. Therefore another solution was sought that would be more convenient for computing profiles at large values of η. It was noticed from the series calculations that, as η gets larger $y(z, \eta) \simeq y(z)$; i.e. y does not change very much with η any more. With this approximation, equation (41) may be directly integrated to give

$$c = b(1 - y)\,\eta \qquad (46)$$

To get the second approximation to y, that makes y a weak function of η, equation (46) is substituted into equation (40) to give

$$\frac{\partial y}{\partial z} = -ay \exp(\alpha b \eta y) \exp(-\alpha b \eta) \qquad (47)$$

Integration of equation (47) leads to

$$\int_1^y \frac{\exp(-\alpha b \eta y')}{y'}\, dy' = -az \exp(-\alpha b \eta) \qquad (48)$$

or

$$ei(\alpha b \eta y) = ei(\alpha b \eta) + \alpha z \exp(-\alpha b \eta) \qquad (49)$$

where

$$ei(x) = \int_x^\infty \frac{\exp(-\lambda)}{\lambda}\, d\lambda \equiv -Ei(-x) \qquad \text{Ref. [7]}$$

Equations (46) and (49) now permit easy calculations of y and αc for large values of η. It was found that the results obtained in this way compare very well with those obtained from the series solution, equations (44) and (45), at $\alpha b\eta = 2$, and since the approximation improves as η increases equations, (46) and (49) may be safely used for $\alpha b\eta > 2$. Equation (44) and equation (45) were used for small η and equations (46) and (49) for large η. Fig. 3 (a) shows the increase in y as a function of time at several bed depths and Fig. 3 (b) shows the carbon profile at several process period lengths.

7. Discussion

(a) *Comparison with available experimental data*

Experimental results on the carbon content of the catalyst as a function of process time have been correlated by formulas of the type

$$c = mt'^{n} \tag{50}$$

This functional form was first presented by Voorhies on the basis of experiments on the cracking of gas oil [4]. Values of the exponent, n, ranging from 0·38 to 0·53 were found, depending on the type of catalyst used. Rudershausen and Watson [2] confirmed this type of correlation for the case of aromatization of *cyclo*hexane and found an exponent $n = 0{\cdot}65$. More recently Tyuryaev *et al.* [3] obtained a value for n of 0·68 for the dehydrogenation of n-butane, and Wilson and Den Herder [5] found $n = 0{\cdot}7$ for a reforming reaction. It should be pointed out that equations like (50) should not be used as a

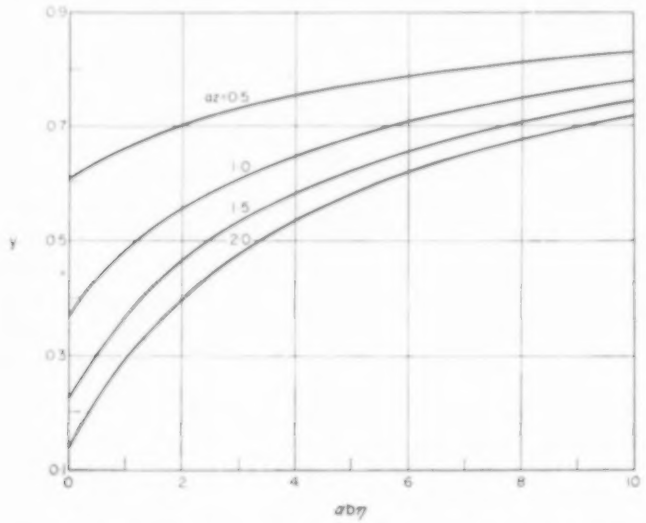

Fig. 3 (a). Reactant mole fraction vs. time group for consecutive reaction mechanism with exponential activity function.

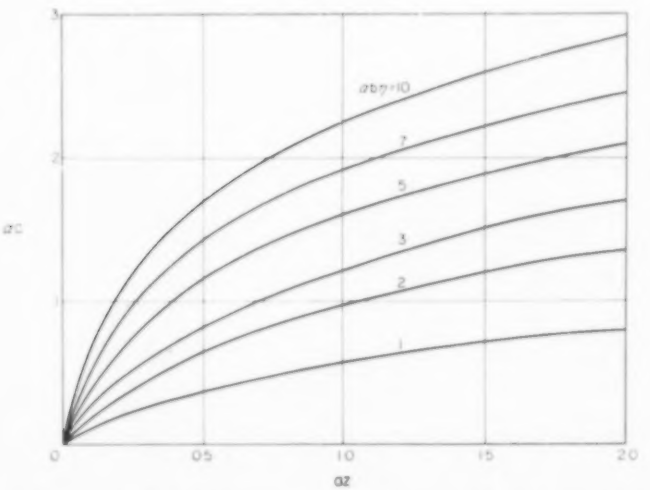

Fig. 3 (b). Carbon profiles for consecutive reaction mechanism with exponential activity function.

basis for establishing a rate equation for the carbon deposition, as has been previously attempted, since no consideration is given to the simultaneously varying partial pressures of the components of the main reaction.

A comparison of the results presented in this paper with equation (50) will now be made, merely to show that the coupled mechanisms considered lead to results that lie in the range of the quoted experimental data. However, in the experimental studies, the carbon content of the catalyst was measured by regeneration *in situ*, or from a well-mixed sample. The carbon contents reported are therefore distance-averaged values, in contrast with the point values given in the Figs. 1, 2 and 3.

$$c_{z\,\mathrm{av.}} = \frac{1}{L'} \int_0^{L'} c\,dz' \tag{51}$$

With this in mind and taking into account that $\eta \simeq t$, equation (51) may be rewritten as

$$c_{z\,\mathrm{av.}} = m'\,\eta^n \tag{52}$$

The $c_{z\,\mathrm{av.}}$ data obtained by graphical integration of the point values given in the Figs. 1, 2 and 3 are presented in Fig. 4 as functions of η, together with equation (52) for $n = 0{\cdot}5$. The exact position of the curves for any one mechanism with respect to another mechanism is indeterminate in this Fig. because different multiplying factors α, K, a and b are used on the axes. In other words, each curve of one mechanism may be shifted with respect to any curve belonging to another mechanism depending on the values of the physical constants α, K, a and b. What is of importance here when different mechanisms are compared are the slopes of the various lines.

The consecutive reaction mechanism with exponential activity function has a slope 1·0 at low values of $\alpha b\eta$ and a slope of 0·5 as $\alpha b\eta$ approaches 4 and beyond. The parallel mechanism with hyperbolic activity function also has a slope of 1·0 for low $Kb\eta$ and approaches 0·5 at about 10. The parallel mechanism with exponential activity function always has a slope of approximately 1·0. These values are in the same range as

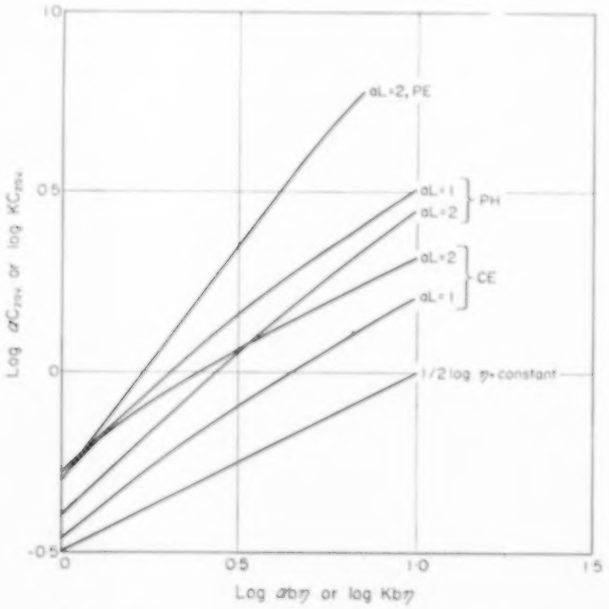

Fig. 4. Distance averaged carbon content vs. time groups.
PE—Parallel reaction mechanism with exponential activity function.
PH—Parallel reaction mechanism with hyperbolic activity function.
CE—Consecutive reaction mechanism with exponential activity function.

those of the experimental studies quoted above. However, it seems that the experimental data are not accurate enough to determine whether or not the slope gradually decreases as time progresses, as indicated by Fig. 4.

The different curves obtained for the same mechanism and activity function for different values of aL also permit some conclusions to be made about the influence of space time* (reciprocal space velocity) since the dimensionless group aL is proportional to this variable. It can be seen that both the point c-values and $c_{z\,av.}$ increase with increasing space time for the consecutive reaction mechanism, but decrease for the parallel mechanism. Only when there is no profile would $c_{z\,av.}$ (in that case also equal to the values at any point) be independent of space time. This is only possible, however, when the rate of formation of the catalyst fouling compound is independent of either the reactant or the product or when parallel and consecutive mechanisms both occur and balance each other in their effect on the carbon profile.

In a real system both reactants and products may form carbonaceous deposits, so that the mechanism would be a combination of parallel and consecutive reactions. Although in general they would not exactly balance each other, the carbon profile would tend to become flat and the space time effect would be less pronounced for such a case. But since a very small amount of carbonaceous material greatly decreases the catalyst activity even a small deviation from a flat

*The term "space time" was proposed by Prof. K. M. Watson in a kinetics course taught at Illinois Institute of Technology.

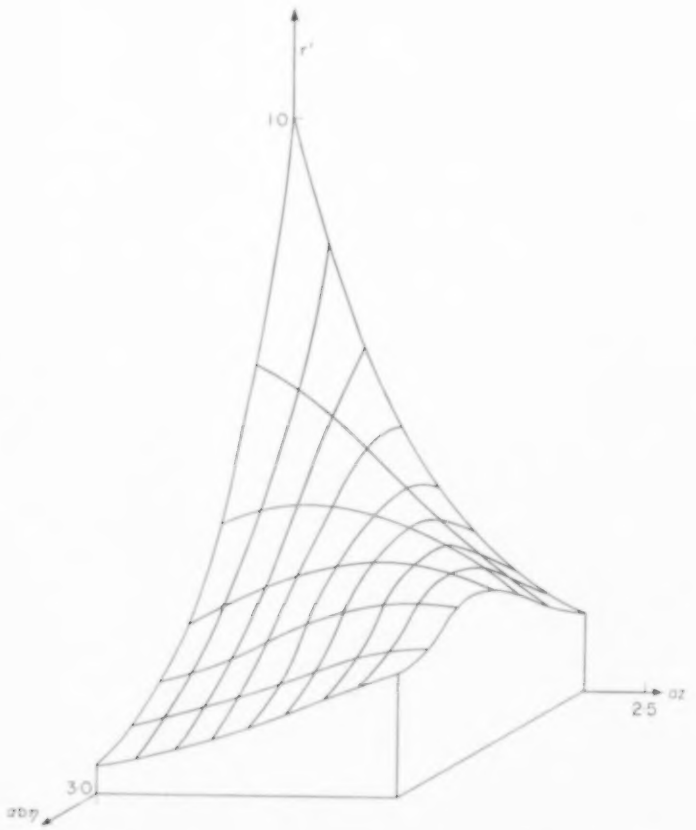

Fig. 5. Rate surface for parallel reaction mechanism with exponential activity function.

profile could have a pronounced effect on the course of the reaction.

Again the conclusion probably is that the method of *in situ* regeneration is not sensitive enough to reveal, by inspection of data obtained at different space times, something about the existence of a profile and therefore about the mechanism and rate of formation. What is needed are careful experiments in which the carbon profile is actually measured.

(b) *Rate profiles*

In the absence of fouling, and for isothermal conditions, the maximum rate of a reaction $A \rightarrow R$ is always at the reactor entrance. This is not necessarily true when the catalyst is fouled, as will be shown in the following.

The parallel reaction mechanism will be discussed first. If, for convenience, the exponential activity function is chosen, the rate of the main reaction, written in dimensionless form, r', is given by

$$r' = \frac{r_A}{k_1^\circ P} = y \exp(-\alpha c) \tag{53}$$

Introducing equations (32) and (33) into (53) leads to

$$r' = \left\{1 + \exp(-az)\left[\exp(+\alpha b\eta) - 1\right]\right\}^{-1} \left\{1 + \exp(-\alpha b\eta)\left[\exp(az) - 1\right]\right\}^{-1} \tag{54}$$

Fig. 5 shows the rate surface, $r'(z, \eta)$. It is seen that a ridge, which is the locus of maximum rates, occurs in the surface.

Whenever the carbon profile is such that it decreases along the reactor length, the locus of maximum rate, and consequently of maximum heat evolution, will travel down the bed as time progresses. If the heat-exchanging conditions are such that a temperature profile is not avoided, which is almost inevitable in practice, then this profile will be continually varying. This may complicate the design of the control system. This conclusion is also valid for the hyperbolic activity function, in fact, for any type of mechanism or any condition that leads to a descending carbon profile. Finally, it may be worthwhile to point out that, for large values of η, the entire reactor, although of plug flow type, operates at a nearly uniform rate.

In the case of an ascending c-profile, which is obtained when the carbonaceous deposit results from a reaction consecutive to the main reaction, the rate, r, is continually decreasing with η in all points of the reactor, except at $z = 0$, where no carbonaceous compound is deposited. A gradually decreasing part of the reactor will then be effective in the conversion to the main product.

Acknowledgement—The authors are indebted to Professors G. Goethals and C. C. Grosjean for valuable discussions. Also, one of the authors (K.B.B.) is grateful to the National Science Foundation of the U.S.A. for financial support in the form of a postdoctoral fellowship.

VOL 16 196

Appendix 1: Determination of Parameters

It can be seen from equation (32) that the parameters can be easily found for the parallel exponential mechanism. If equation (32) is rearranged it becomes

$$\ln\left(\frac{1}{y} - 1\right) = -\alpha b\eta + \ln\left[\exp(az) - 1\right]$$

Therefore, for a fixed z, if $\ln\left[(1/y) - 1\right]$ is plotted against η, the slope is $-\alpha b$ and a (or k_1°) can be found from the intercept. Then if the total carbon is measured at the end of the experiment the value of $\alpha b\eta$ can be calculated for the total time since αb is known, and Fig. 4 used to find $\alpha c_{\text{av.}}$. Then since $c_{\text{av.}}$ has been measured α can be calculated, and from αb the value of b (or k_2°) is found. Thus k_1°, k_2° and α are determined for this mechanism.

Appendix 2: Ranges of Variables

In order to get an idea as to the practical order of magnitude of the variables z and η some experimental data on the dehydrogenation of ethylbenzene was used. The experimental conditions were:

$P = 1$ atm., $\rho_B = 1\,130$ kg/m^3, $F = 0{\cdot}30$ kg/hr,
$\epsilon = 0{\cdot}38$, $\rho_P = 1{\cdot}33$ kg/m^3, $L' = 0{\cdot}084$ m,
$\Omega = 6{\cdot}3 \times 10^{-4}$ m^2, $T = 600$°C

Then

$$aL = \frac{\Omega\,\rho_B\,PL'}{F} k_1^\circ = 0{\cdot}2\,k_1^\circ$$

By a preliminary analysis of the data and ignoring carbon it was found that $k_1^\circ \simeq 10$ atm^{-1} hr^{-1}. Therefore,

$$aL \simeq 2{\cdot}0 \tag{A.1}$$

Also,

$$bt = Pk_2^\circ t' = k_2^\circ t'$$

Since they depend directly on the carbon-forming

mechanism, values of k_2°, α, and K can only be estimated by comparing Figs. 1, 2, 3 and 4 with the experimental data. This was done and the orders of magnitude of the constants are

$$k^\circ_2 \simeq 0{\cdot}01 \text{ atm}^{-1}\text{ hr}^{-1}, \quad \alpha \simeq 100, \quad K \simeq 200$$

For total processing time of the order of 5 hr the values of $\alpha b\eta$ and $Kb\eta$ become

$$\alpha b\eta \simeq \alpha bt = 5 \tag{A.2a}$$

$$Kb\eta \simeq Kbt = 10 \tag{A.2b}$$

The ranges of variables indicated by equations (A.1) and (A.2) determined the values used in the computation for Figs. 1, 2 and 3.

Notation

$a = \dfrac{\Omega \rho_B d_p P k_1^\circ}{F}$ a dimensionless group

$b = \dfrac{\Omega \rho_A \epsilon d_p P k_2^\circ}{F}$ a dimensionless group

c = carbon content of the catalyst, kg carbon/kg catalyst

$c_{av.}$ = distance averaged carbon content, kg carbon/kg catalyst

C = catalyst fouling compound

d_p = particle diameter m

F = feed rate kg/hr

k = rate coefficient $\text{hr}^{-1}\text{ atm}^{-1}$

k° = rate coefficient at $\eta = 0$

K = a type of adsorption equilibrium constant

K_1, K = integration constants

L' = total reactor length

$L = L'/d_p$ = dimensionless total reactor length

m, m' = constants in equations (50) and (52)

M = molecular weight kg/mol

n = exponent in equations (50) and (52)

P = total pressure atm

r_A = rate of disappearance of A hr^{-1}

r_c = rate of production of C hr^{-1}

$r' = r_A/k_1^\circ P$ = dimensionless rate of disappearance of A

t' = time hr

$t = \dfrac{F}{\epsilon \rho_A \Omega d_p} t'$ = reduced time dimensionless

y = mole fraction of A

z' = axial co-ordinate m

$z = z'/d_p$ = dimensionless axial co-ordinate

α = proportionality factor in the exponential activity function

ϵ = void fraction

ρ_A = density of A kg/m^3

ρ_B = bulk density of catalyst kg/m^3

Ω = total cross-section of reactor m^2

$\eta = t - z$ a dimensionless time measuring variable

ϕ = activity function in the rate expression

References

[1] Pozzi A. L. and Rase H. F. *Industr. Engng. Chem.* 1958 **50** 1075.

[2] Rudershausen C. G. and Watson C. C. *Chem. Engng. Sci.* 1955 **3** 110.

[3] Tyuryaev I. Y., Bushin A. N., Mikhailov R. K. and Sarycheva E. A. *Zh. fiz. khim.* 1957 **31** 93.

[4] Voorhies A. *Industr. Engng. Chem.* 1945 **37** 318.

[5] Wilson J. L. and Den Herder M. J. *Industr. Engng. Chem.* 1958 **50** 305.

[6] du Domaine J., Swain R. L. and Hougen O. A. *Industr. Engng. Chem.* 1943 **35** 546.

[7] Jahnke E. and Emde F. *Tables of Functions.* Dover, New York, 1945.

Chemical Engineering Science, 1961, Vol. 16, pp. 202 to 207. Pergamon Press Ltd., London. Printed in Great Britain.

Carbon dioxide absorption in aqueous monoethanolamine solutions

G. Astarita
Istituto di chimica industriale, Via Mezzocannone 16, Napoli, Italy

(*Received* 30 *December* 1960)

Abstract—Experiments have been carried out on the absorption of carbon dioxide in monoethanolamine (MEA) aqueous solutions. A laminar liquid jet absorber was first used, and the results obtained (which covered the contact time range between 0·02 and 0·07 sec), showed good agreement with the penetration theory equations as well as with the kinetics of the mechanism of the chemical reaction which presumably takes place in the liquid phase.

Eventually a disk column absorber was used. The results were reproducible, and have been correlated in compact form by an empirical equation. Interpretation of the data on the basis of the penetration theory equations appears to be only partially successful.

Résumé—Des expériences ont été effectuées sur l'absorption de gaz carbonique dans des solutions aqueuses de monoethanolamines (M E A). On a d'abord employé un absorbeur à écoulement liquide laminaire et les résultats obtenus (comprenant le temps de contact compris entre 0,02 et 0,07 sec) ont été en accord avec les équations de la théorie de la pénétration ainsi qu'avec la cinétique du mécanisme de la réaction chimique qui a probablement lieu en phase liquide.

On a, éventuellement, utilisé une colonne à disques. Les résultats sont reproductibles et ont été rassemblés sous forme d'une équation empirique. L'interprétation des donnése, fondée sur les équations de pénétration apparait comme n'étant que particllement satisfaisante.

Zusammenfassung—Über die Absorption von CO_2 in wässrigen Monoaethanolamin-Lösungen wurden Versuche durchgeführt. Zunächst wurde hierbei ein laminar arbeitender Düsenabsorber benutzt und die erhaltenen Ergebnisse (über einen Kontaktbereich von 0,02 bis 0,07 sec) zeigten eine gute Übereinstimmung sowohl mit den Gleichungen der Penetrationstheorie als auch mit der Kinetik der in der flüssigen Phase vermutlich ablaufenden chemischen Reaktionsmechanismen.

Ausserdem wurde eine Scheiben-Absorbersäule benutzt. Die Ergebnisse waren reproduzierbar und wurden in geschlossener Form durch eine empirische Gleichung korreliert. Die Interpretation der Ergebnisse mit Hilfe der Gleichungen der Penetrationstheorie hatte nur teilweise Erfolg.

Introduction

In the absorption of a slightly soluble gas A in a liquid it is often found useful to add to the liquid phase a component B, which may undergo a chemical reaction with the absorbing gas. This not only increases the capacity of the liquid, defined as the amount of gas which can be dissolved in a given mass of liquid, but furthermore increases the absorption rate itself. The latter effect may be represented by the ratio I of the actual liquid phase absorption coefficient to the value of the same for purely physical absorption under the same hydrodynamic conditions.

The value of I can be theoretically predicted only in a few cases, where the fluodynamics of the liquid phase is well known, and the kinetics of the liquid phase chemical reaction is fairly simple.

On the basis of the well-known penetration theory hypothesis, the average absorption coefficient k°_L for physical absorption in a stagnant liquid can be calculated as [1]

$$k^\circ_L = 2\sqrt{(D_A/\pi t)} \qquad (1)$$

When the absorption process is accompanied by a second-order chemical reaction in the liquid phase a general equation is available only as derived from the film theory by Van Krevelen and Hoftjizer [2]. Integration of the penetration theory equations has not been carried out completely for this case, which is of particular interest

for the carbon dioxide–MEA system, which presumably undergoes a second-order chemical reaction in the liquid phase.

Nonetheless, the exact solution of the problem has been carried out as far as some extreme cases are concerned [3].

Particularly:

Case (a) $T^{1/2} \gg q > 4$, $I = R^{-1} + RB_0/nA_i$ (2)

Case (b) $q \gg T^{1/2} \gg 1$, $I = \sqrt{(\pi\, T/4)}$ (3)

The author has obtained, in previous work with a laminar jet absorber [4] a series of experimental results for the system under consideration, corresponding to high values of T, case (a). The author's data, as well as EMMERT's data obtained with a short wetted-wall column [5], could be well correlated by the empirical equation

$$I = 3{\cdot}78 + 12{\cdot}5\, B_0 \pm 1{\cdot}80 \qquad (4)$$

which has the linear form predicted by equation (2). The numerical values of the coefficients in equation (4) are in reasonable agreement with the values calculated independently for R, n and A_i [6].

As a second step in the investigation of the CO_2–MEA system behaviour experimental data have been collected on a laminar liquid jet absorber in the range of contact times between 0·02 and 0·07 sec. In this range, equation (3) is presumably approximated. To compare experimental results with equation (3) the value of the kinetic constant k needs to be known in order to calculate the values of the dimensionless time T from the defining equation

$$T = kB_0\, t \qquad (5)$$

The value of k should correlate the actual reaction rate at time 0 according to the kinetic equation:

$$r = kB_0\,(CO_2) \qquad (6)$$

The MEA has two functional groups, each one of which may contribute to the over-all reaction taking place in the liquid phase. Possible reactions are [7].

I $CO_2 + NH_2\,ROH = HORNHCOOH$

II $HORNH_2 + H_2O = HORNH^+_3 + OH^-$ (fast)

$CO_2 + OH^- = HCO^-_3$ (slow)

$HCO^-_3 + OH^- = CO^{2}_3{}^-$ (fast)

III $NH_2\,ROH + OH^- = NH_2\,RO^- + H_2O$ (fast)

$CO_2 + NH_2\,RO^- = NH_2\,ROCOO^-$ (slow)

From independent kinetic and equilibrium data on the reactions considered, which have been found in the literature [8–11], it appears that, at time 0, the over-all reaction rate is, at 21·5°C

$$r = (4150 + 270\, B_0{}^{-1/2} + 980\, B_0{}^{1/2})\,(CO_2)\, B_0 \qquad (7)$$

Therefore, the value of k required to fit a second-order rate equation such as (6) is a function of the initial amine concentration. Fortunately, in the range of concentrations investigated k is a weak function of B_0, and an average value of 5400 l/sec gmol can be assumed. Correspondingly, equation (3) becomes

$$I = 64{\cdot}8\,(B_0\, t)^{1/2} \qquad (8)$$

It should be pointed out that equation (8) has been independently calculated as the initial asymptote of the actual data.

Experimental Results

As already stated, in the first part of this work a laminar jet absorber was used, together with a soap-film measuring technique, as already done by other authors [4, 12, 13]. A complete description of the experimental technique employed, as well as the original data, may be found in Ref. [14].

A first series of experimental data has been collected on the physical absorption of CO_2 in water. Results are plotted in Fig. 1, together with the theoretical line calculated from equation (1). The extremely good agreement shown by the data with theory indicates the reliability of the experimental arrangement.

Three series of experiments have been carried out on CO_2 absorption in MEA solutions. The liquid temperature was kept in the range 21–22°C

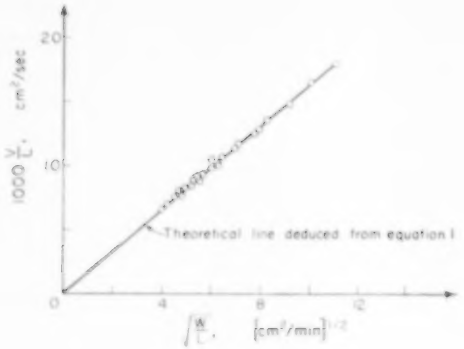

FIG. 1. Physical absorption data.

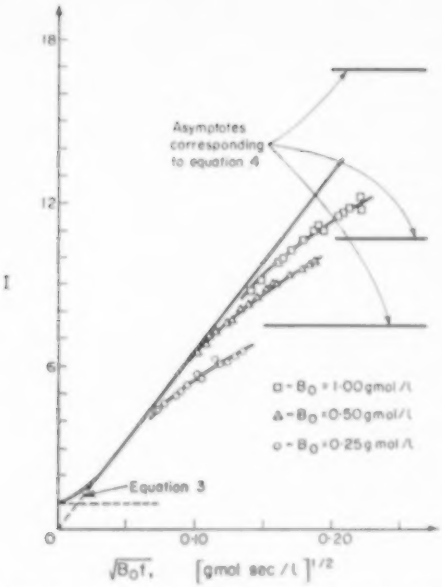

FIG. 2. Liquid jet chemical absorption data.

and recorded for all the runs; data have been corrected to a nominal temperature of 21·5°C. Representative data are plotted in Fig. 2 as I vs. $(B_0\,t)^{1/2}$. In the same Fig. the straight line through the origin corresponds to equation (8). The horizontal straight lines are the final asymptotes as derived from equation (4). The curves drawn through the data points actually appear to tend asymptotically to the line of equation (8), thus indirectly confirming the reaction mechanism assumed. On the whole the experimental results obtained so far seem to indicate that the penetration theory equations correctly represent the behaviour of the system considered, when a second-order reaction mechanism is assumed with $k = 5400$ l/sec gmol at 21·5°C.

Obviously, such a good agreement of experimental data and theory is mainly due to the highly sophisticated absorber used, namely a laminar jet absorber. Peculiar problems arise when the absorption on a packing is considered: in such case, the contact time is no more firmly established, and presumably a whole distribution of contact times has to be considered [15]. Furthermore, the converted amine concentration may build up to an appreciable value, particularly for large packing heights; also in the case in which this does not result in an appreciable CO_2 equilibrium pressure, it nevertheless affects the absorption rate because the depth of penetration of the absorbing component molecules may become of the order of magnitude of the falling liquid layer thickness.

In order to investigate the behaviour of the system in such a situation experiments have been carried out on a laboratory-type disk column. The absorbing element consisted of 28 disks of 1·5 cm diameter, 0·3 cm thickness, threaded on a nylon wire. The disks were made of chemically-roughened lucite. Full details on the experimental arrangement, as well as the original data, may be found in Ref. [16]. A preliminary series of runs has been carried out on the physical absorption rate. The data are in good agreement with those of TAYLOR [17], but not with those of STEPHENS and MORRIS [18]. This might be due to minor geometrical differences in the disks.

The physical absorption rate data, which are plotted as the bottom line of Fig. 3, can be correlated by the equations

$$\mathrm{Re} < 185, \quad N = 4{\cdot}0\ \mathrm{Re}^{-0.40}$$

$$\mathrm{Re} > 185, \quad N = 0{\cdot}96\ \mathrm{Re}^{-0.127}$$

Eventually, five series of experimental runs have been carried out on the CO_2 absorption in MEA solutions, under conditions of no resistance to mass transfer in the gas phase (the gas phase was pure carbon dioxide saturated with water

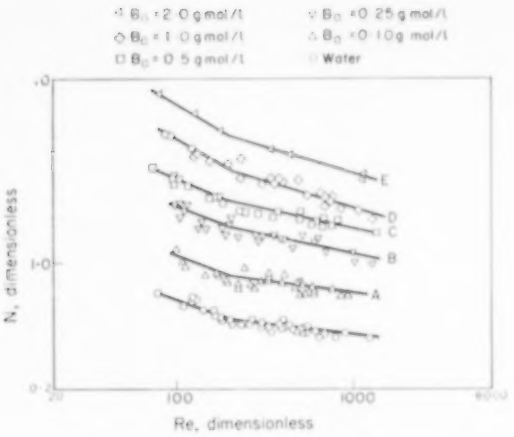

FIG. 3. Disk column absorption data.

vapour). The results are again plotted in Fig. 3, lines *A–E*. The vertical distance between any of these lines and the physical absorption line, which is a measure of I, slightly decreases as Re increases. By cross-plotting the data of Fig. 3 as in Fig. 4 the I values are seen to vary proportionally to B_0 raised to a power of about 0·6, the exponent slightly decreasing with increasing Re values. In other words, the exponent on B_0 increases with contact time.

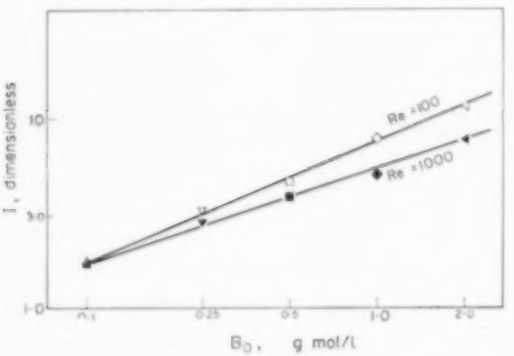

FIG. 4. Absorption increase ratio as a function of amine concentration.

Such behaviour is qualitatively predicted by theory: in fact, the exponent on B_0 should be 0·5 at very low contact times, and 1·0 at very high contact times. The values found experimentally indicate that the conditions prevailing on the disk column are intermediate between cases (a) and (b). It might be interesting to attempt a quantitative testing of this conclusion. An equivalent contact time for the disk column can be roughly evaluated by assuming the following model:

(a) Complete mixing of the liquid phase at the junction between two adjacent disks.

(b) Streamline flow of the liquid along a vertical plane surface of width equal to the mean perimeter of the disks.

For the above-mentioned model values of the various parameters have been calculated for the extreme conditions of the experiments:

Re	B_0 (gmol/l)	t (sec)	$T^{1/2}$	q
100	0·1	0·078	6·5	1·63
	2·0		29·0	32·6
1000	0·1	0·017	3·04	1·63
	2·0		13·6	32·6

The physical absorption results are lower than the values predicted from equation (1) for the assumed model; the values of t and T in the above Table are therefore probably underestimated.

Comparison of the calculated values of $T^{1/2}$ and q indicates that their order of magnitude is roughly the same, thus confirming that the actual conditions are intermediate between cases (a) and (b).

In order to investigate the influence of the driving force A_i on the I values four series of experiments have been carried out at fixed values of B_0 and Re by changing the CO_2 partial pressure in the gas phase. Due to necessary corrections for gas phase mass transfer resistance, and to the different measuring technique which had to be used—namely, electrical conductivity of inlet and outlet liquid was measured—the data for these last series of experiments scatter somewhat more. The best fit of the data was obtained by assuming that the I values varied proportionally to A_i raised to a power of about $-0·6$.

In fact, according to theory, the exponent on A_i should be 0 in case (b), and -1 in case (a); it would therefore be expected that in the case of the disk column the exponent on A_i should be somewhat closer to 0 than the experimental value. The author does not feel that a clear interpretation can be given for this discrepancy.

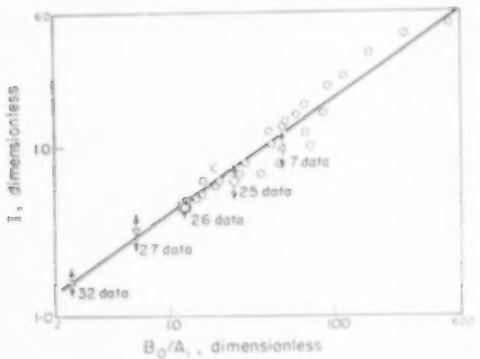

Fig. 5. Over-all correlation of disk column absorption data.

As a first approximation, the exponent on A_i may be assumed constant, and equal to minus the exponent on B_0. In this case, the actual parameter of the phenomenon is the ratio B_0/A_i and all the data obtained can be correlated in compact form by plotting I values vs. the ratio B_0/A_i, as in Fig. 5. In such a plot, all the data points corresponding to one of the five lines A–E of Fig. 3 fall on the same value of the abscissa, and have therefore been represented by a vertical segment, the length of which covers all the values of I observed. The single points on Fig. 5 correspond to experiments carried out with mixed gas phase.

All the data taken on the disk column can be correlated by the empirical equation

$$I = 0{\cdot}875\,(B_0/A_i)^{0{\cdot}67} \qquad (9)$$

which holds in the range investigated. Equation (9), although partially justified on theoretical grounds, has to be considered no more than a correlating equation, which can only very cautiously be extrapolated to different conditions.

Acknowledgments—The author wishes to express his very grateful appreciation of the help received by Dr. H. Kramers, of the University of Delft, who advised the planning of the work and has reviewed the manuscript. The author also acknowledges Mr. Vincenzo Magri and Mr. Stelio Orsini, who collaborated in carrying out the experiments. Complete data may be found in Refs. [14] and [16], or may be obtained from the author.

Notations

A_i	= interface concentration of absorbing gas	gmol/l.
B_0	= initial concentration of reactive solute	gmol/l.
D_A	= diffusivity of absorbing gas	cm²/sec
D_B	= diffusivity of reactive solute	cm²/sec
k	= kinetic constant	l/sec gmol
k'_L	= physical absorption coefficient	cm/sec
k_L	= chemical absorption coefficient	cm/sec
I	= absorption rate increase ratio, k_L/k'_L	—
L	= jet length	cm
n	= stoichiometric coefficient	mol B/mol A
N	= liquid phase NTU	—
q	= concentration parameter $R^2 B_0/nA_i$	—
r	= reaction rate	gmol/l. sec
R	= diffusivity ratio $(D_B/D_A)^{1/2}$	—
Re	= Reynolds number, 4 times the ratio of liquid flowrate per unit perimeter and liquid viscosity	—
t	= Contact time	sec
T	= dimensionless time $kB_0 t$	—
V	= absorption rate	cm³/sec
W	= volumetric liquid flowrate	cm³/sec

References

[1] Higbie R. *Trans. Amer. Inst. Chem. Engrs.* 1935 **31** 365.

[2] Van Krevelen D. W. and Hoftijzer P. J. *Rec. Trav. Chim. Ind.* 1948 **67** 563.

[3] Sherwood T. K. and Pigford R. L. *Absorption and Extraction* McGraw-Hill, New York 1951.

[4] Astarita G., M.Ch.E. Thesis, University of Delaware 1960.

[5] Emmert R. E. Ph.D. Thesis, University of Delaware 1958.

[6] Astarita G. *R. C. Accad. Napoli* 1960 **s4 27**.

[7] Emmert R. E. and Pigford R. L. Personal Communication, July 1959.

[8] Lund V. and Faurholt C. *Dansk Tidsskr. Farm.* 1948 **22** 109.

[9] Pinsent B. R. W., Pearson L. and Roughton F. J. W. *Trans. Faraday Soc.* 1956 **52** 1512.
[10] Bates R. G. and Pinching G. D. *J. Res. Nat. Bur. Stand.* 1951 **46** 349.
[11] Jorgensen E. *Acta Chem. Scand.* 1956 **10** 747.
[12] Njising R. A. T. O. Ph.D. Thesis, University of Delft 1958.
[13] Raimondi P. and Toor H. L. *Amer. Inst. Chem. Engrs. J.* 1959 **5** 86.
[14] Magri V. *Tesi in Ing. Chim., Università di Napoli* 1960.
[15] Danckwerts P. V. *Amer. Inst. Chem. Engrs. J.* 1955 **1** 456.
[16] Orsini S. *Tesi in Ing. Chim., Università di Napoli* 1960
[17] Taylor R. F. and Roberts F. *Chem. Engng. Sci.* 1956 **5** 168.
[18] Stephens E. J. and Morris G. A. *Chem. Engng. Progr.* 1951 **47** 232.

Chemical Engineering Science, 1961, Vol. 16, pp. 208 to 221. Pergamon Press Ltd., London. Printed in Great Britain.

The effect of gas density and gradual vaporization on gas–liquid flow in horizontal pipes

C. J. Hoogendoorn and A. A. Buitelaar
Koninklijke/Shell-Laboratorium, Amsterdam
(Shell Internationale Research Maatschappij N.V., The Hague)

Abstract—In order to elucidate the effect of gas density and gradual vaporization of the flowing fluid in gas–liquid flow in horizontal pipes we have investigated the flow of superheated Freon-11 vapour and water, as well as of flashing Freon-11 in horizontal 15 mm pipes.

The results show that an increase in gas density does not significantly change the transition lines between the different flow patterns in a Kosterin diagram. Only the onset of atomization occurs at lower velocities. The Kosterin diagram also holds for the flow of a vaporizing fluid, except that the transition to froth flow shifts to lower velocities.

The correlation for the pressure drop which we previously gave for lower gas densities was found not to be valid at higher densities. A new correlation is presented in graphical form, giving the pressure drop over a wide range of variables, including gas-to-liquid density ratios of 10^{-3} to 10^{-2}. Tests with flashing Freon showed that the acceleration pressure drop due to the increase in mixture velocity is best calculated with the aid of our previously given hold-up correlation.

Résumé—Afin d'élucider l'influence de la densité du gaz et de la vaporisation graduelle du liquide sur l'écoulement des mélanges gaz–liquide dans des tubes horizontaux, nous avons examiné dans des tubes de 15 mm l'écoulement de la vapeur surchauffée de Freon-11 avec de l'eau, ainsi que du Freon-11 en ébullition.

Les résultats montrent qu'un accroissement de la densité du gaz ne change pas d'une façon significative les lignes de transition entre les différents régimes d'écoulement dans un diagramme Kosterin. Seulement l'atomisation s'amorce à des vitesses inférieures. Le diagramme Kosterin tient également pour l'écoulement d'un fluide en ébullition, à l'exception que l'écoulement avec formation d'écume commence à des vitesses inférieures.

Il a été trouvé que la corrélation que nous avons établie antérieurement pour la chute de pression à des densités de gaz inférieures, ne s'applique pas à des densités supérieures. Une nouvelle corrélation est donnée sous forme d'un graphique représentant la chute de pression sur un large intervalle de variables, comprenant des rapports entre la densité du gaz et du liquide de 10^{-3} à 10^{-2}. Les essais avec le Freon en ébullition montrent que le terme dans la chute de pression qui est attribuable à l'augmentation de la vitesse du mélange peut être calculé de la meilleure façon à l'aide de la corrélation donnée antérieurement pour le holdup.

Zusammenfassung—Um den Effekt von Gasdichte und allmählicher Verdampfung der strömenden Flüssigkeit bei gleichzeitiger Strömung von Gas und Flüssigkeit in horizontalen Rohren zu erklären, haben wir die Strömung von überhitztem Freon-11-Dampf und Wasser sowie von verdampfendem Freon-11 in waagerecht aufgestellten Rohren mit einem Durchmesser von 15mm untersucht.

Die Ergebnisse zeigen, dass eine Zunahme der Gasdichte die Übergangslinien zwischen den verschiedenen Strömungsformen in einem Kosterin-Diagramm nicht wesentlich ändert. Nur tritt die Zerstäubung bei niedrigeren Geschwindigkeiten auf. Das Kosterin-Diagramm gilt auch für die Strömung einer verdampfenden Flüssigkeit, mit dem Unterschied, dass der Übergang zur Schaumströmung bei niedrigeren Geschwindigkeiten stattfindet.

Es hat sich herausgestellt, dass die Beziehung für den Druckabfall, die wir schon früher für niedrigere Gasdichten angaben, bei höheren Gasdichten keine Gültigkeit hat. In Form eines Diagrammes wird nun eine neue Beziehung angegeben, die den Druckabfall über einen weiten Bereich von Variablen gibt, darunter Gas/Flüssigkeit-Dichteverhältnisse von 10^{-3} bis 10^{-2}. Versuche mit verdampfendem Freon zeigten, dass sich der Anteil des Druckabfalls, der auf die Zunahme der Geschwindigkeit des Gemisches zurückzuführen ist, am besten mit Hilfe unserer früheren Holdup-Beziehung ermitteln lässt.

1. Introduction

The simultaneous flow of gas and liquid through pipes is a complicated matter. Up to now a theoretical approach has been impossible and hence this kind of flow has only been investigated in experimental studies. There are, however, so many variables which play a role that it is difficult to cover them all. In a previous publication [1] we gave empirical correlations for pressure drop, hold-up and flow pattern in horizontal pipes. A dimensional analysis was applied to reduce the number of independent variables and it was possible to give correlations over a wide range. However, the dimensionless group representing the influence of gas density could only be studied over a small range. A most important link to technical applications was therefore missing.

Besides, in our former work a systematic study had been made on gas–liquid flow, with a non-condensing gas and a non-vaporizing liquid only, whereas in many practical applications we encounter the flow of a vaporizing medium.

The present article describes the results of experiments on gas–liquid flow in horizontal 15 mm pipes, which were made to study the effect of the two factors that had not been taken into account hitherto. The gas-density effect was found from tests with superheated Freon-11 vapour and water, while vaporization was studied with the flow of flashing Freon-11

Freon-11 (CCl_3F) was chosen, because it is particularly suited to these experiments. Its boiling point is 23·8°C (760 mm Hg), which permits operation at temperatures only little above room temperature and at not too high pressures. Because of its high molecular weight it has a high vapour density. Also, it is a safe liquid with well-known physical properties.

2. Experimental

2·1 *Description of test set-up*

Fig. 1 is a flow sheet of the experimental set-up. For the Freon–Freon experiments liquid Freon-11 is drawn from a storage vessel and pumped through a heater at a sufficiently high pressure to suppress vapour formation, which can be visually checked in a sight-glass just before

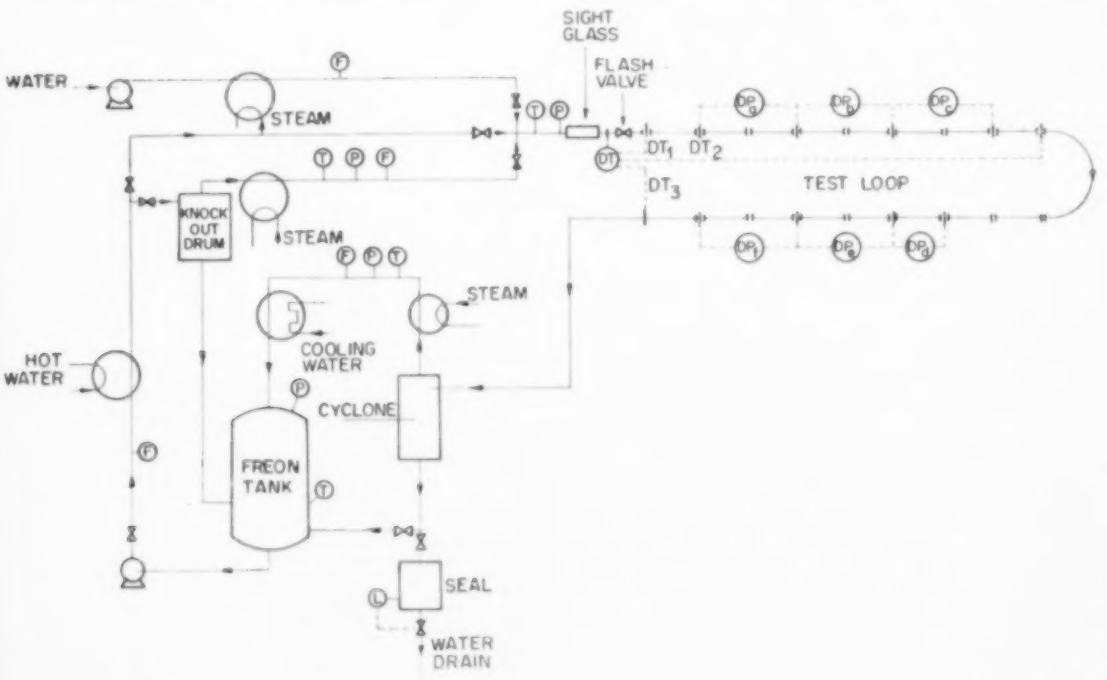

Fig. 1. Flow sheet of Freon installation.

a flash valve. At this point the liquid temperature is also measured accurately (within ± 0·02 °C). Owing to the pressure drop over the flash valve the heated liquid vaporizes partly and flows as a gas–liquid mixture through the test loop. The test loop consists of two parallel parts, each built up from eight sections of 15 mm diameter glass pipes and connected by a 180° bend. The pressure drop over the different pipes in the loop is measured with inverted U-type manometers, filled with liquid and an air cover above it. No vaporization occurred in the manometer legs because the room temperature was always below that in the test sections.

The flow pattern in the test loop is observed visually and classified as indicated in a previous publication [1].

Owing to the vaporization the liquid cools down; at three places in the test section the drop in temperature from its value just before the flash valve is measured. At the end of the test loop the gas–liquid mixture is separated in a cyclone. The liquid is returned to the storage vessel. The vapour is superheated and its flow measured. Finally it is condensed and also returned to the storage vessel.

For the experiments with superheated Freon vapour and water, Freon is partly vaporized in the heater and the gas–liquid mixture separated in a knock-out drum with a large volume to ensure a constant pressure before the test loop. The separated liquid is returned to the storage vessel, the vapour is superheated and its flow measured. Water and vapour are mixed at a temperature well above the saturation temperature, before entering the test loop.

In the experiments the total mass flow velocity was varied between 100 and 3,000 kg/m² sec. The ratio of gas to liquid mass flow rate was between 10^{-3} and $6{\cdot}10^{-2}$.

2.2 *Single-phase friction factors for glass pipes*

The mean diameters of the glass pipes were found by filling them with water and weighing. The results show differences between the pipes of ± 5 per cent. The inner diameter was also measured directly with a feeler. At different cross-sections different values of the diameter were found, most pipes being somewhat conical towards both ends. The mean values came near to those found by weighing. The pressure flanges were all of the same inner diameter; as a result, the joint between the flange and the pipes was not always smooth.

The pressure drops measured over the test sections *a*, *b*, *c*, *d*, *e* and *f* as indicated by the manometers (DP_a, DP_b etc.) in Fig. 1 were used for correlating our results; only for these sections could entrance and end effects be neglected.

Single-phase runs were done to determine the friction factor. Some of the values so found differed from those given for smooth pipes by Moody [2], (see Table 1). Such deviations are probably due to the above-mentioned fact of unsmoothness of the flange-pipe connexion. In the following we have taken for the single-phase friction factor the value found in our experiments.

2.3 *Properties of Freon-11*

The thermodynamic properties of Freon-11 have been published by Benning and McHarness [3]. Their data for the mean temperatures of three series of tests we made are given in Table 2.

2.4 *Determination of fraction vaporized*

The fraction vaporized in the flashing Freon fluid could easily be calculated by writing the energy conservation

Table 1. *Deviations in single-phase friction factor*

Pipe section	*a*	*b*	*c*	*d*	*e*	*f*
% deviation from smooth friction factor	+ 8	− 9	+ 8	+ 2	+ 2	+ 9
Length of section/diameter	52	52	52	26	52	52

Table 2. *Physical properties of Freon-11*

Temperature	(°C)	26	33	45
Vapour pressure	(N/m²)	$1{\cdot}097 \times 10^5$	$1{\cdot}395 \times 10^5$	$2{\cdot}026 \times 10^5$
Density of sat. vapour	(kg/m³)	6·30	7·85	11·20
Density of liquid	(kg/m³)	1470	1460	1440
Dynamic viscosity of vapour	(N s/m²)	$1{\cdot}09 \times 10^{-5}$	$1{\cdot}11 \times 10^{-5}$	$1{\cdot}15 \times 10^{-5}$
Dynamic viscosity of liquid	(N s/m²)	$4{\cdot}20 \times 10^{-4}$	$3{\cdot}95 \times 10^{-4}$	$3{\cdot}58 \times 10^{-4}$
Heat of vaporization	(J/kg)	$1{\cdot}81 \times 10^5$	$1{\cdot}79 \times 10^5$	$1{\cdot}74 \times 10^5$
Specific heat of liquid	(J/kg °C)	871	877	889
Surface tension	(N/m)	$1{\cdot}9 \times 10^{-3}$	$1{\cdot}85 \times 10^{-2}$	$1{\cdot}7 \times 10^{-2}$

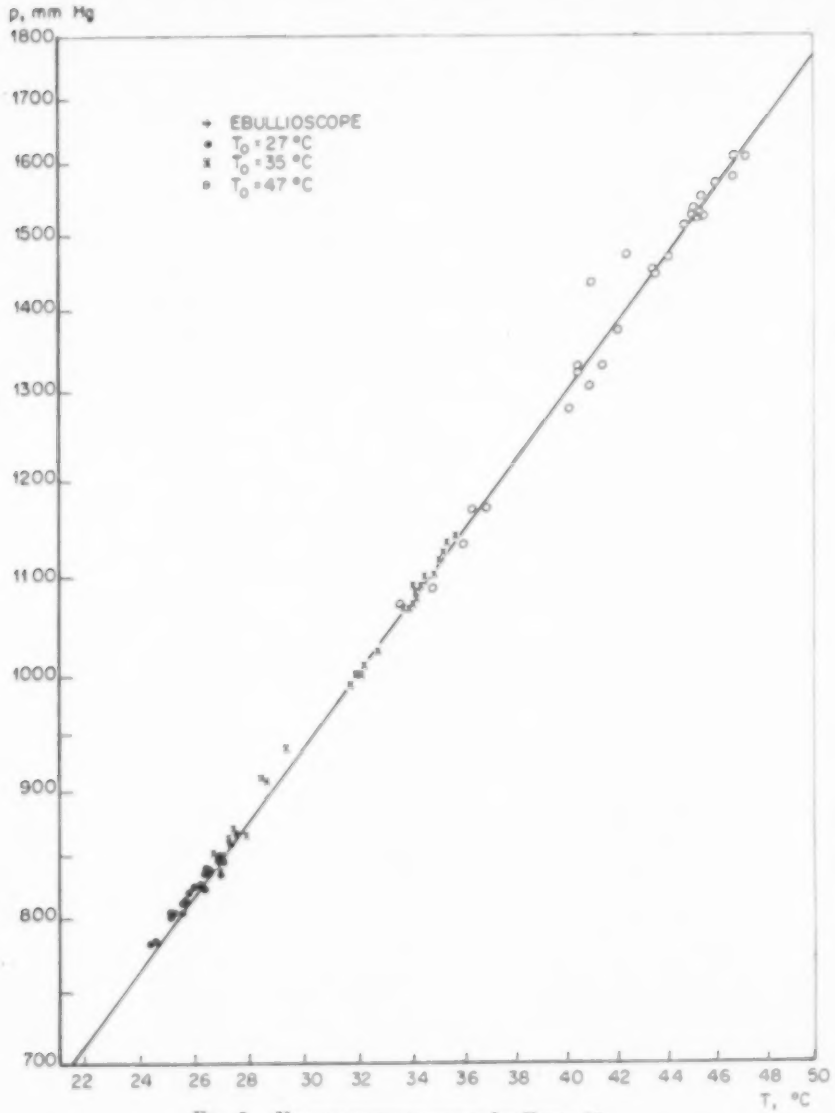

FIG. 2. Vapour pressure curve for Freon-11.

law for point o just before flashing and a point p in the test loop*:

$$M_t\left[\tfrac{1}{2}V_p^2 - \tfrac{1}{2}V_0^2 + H_p - H_{l0}\right] = \Delta Q, \qquad (1)$$

where

$$H_p = H_{lp} + x_p r_p, \qquad (2)$$

which gives

$$x_p = \frac{(\Delta Q/M_t) - \tfrac{1}{2}V_p^2 + \tfrac{1}{2}V_0^2 - H_{lp} + H_{l0}}{r_p}. \qquad (3)$$

*See list of symbols at the end of the paper.

The term representing the change in kinetic energy was in all cases very small (< 0·3 per cent) compared with the change in enthalpy and is further neglected.

The temperature change from o to p being small in our case, we may write

$$x_p = \frac{(\Delta Q/M_t) - c_0(T_p - T_0)}{r_p}. \qquad (4)$$

The rate of heat exchange ΔQ between the flowing fluid and the surroundings is small, but can be taken into account by the procedure described in Appendix I.

For the range of x_p we are interested in ($x_p = 0{\cdot}003$–$0{\cdot}05$), accurate determination of temperature differences between 0·6 and 10°C is necessary. This was done for three points in the test loop with reference to point o, with copper-constantan thermocouples, as described in Appendix II. For intermediate points in the test loop x was found from the pressure at that point and a plot of x_p vs. pressure made by reference to the three above-mentioned points. The total vapour flow leaving the cyclone downstream the test loop could also be found from the pressure. This flow was always within 10 per cent equal to the value measured with the rotameter in the vapour line. The latter value was less accurate as the flow often fluctuated and liquid entrainment vaporized by the superheater would give differences.

The vapour-pressure curve derived from the accurate temperature and pressure determination in the test loop is compared with the values published in the literature [3] in Fig. 2. It is seen that most of our points are in good agreement with the published curve. Two points measured in an ebullioscope, also show good agreement.

3. Discussion of Results

3.1 *Flow pattern*

To analyse the data on flow patterns they have been plotted in Kosterin diagrams (Figs. 3–6) as was done in a previous publication [1]. As the tests were carried out in small-diameter pipes they can be best compared with our data for air and water and for air and gas oil in 24 mm pipes [1]. Fig. 3 shows that the Kosterin diagrams for air–water ($\rho_g/\rho_l = 1{\cdot}5 \times 10^{-3}$) and Freon–water ($\rho_g/\rho_l = 7 \times 10^{-3}$) are in good agreement, especially for the transition from stratified or wave flow to plug or slug flow. A distinct difference is found for the onset of atomization, which occurs here at velocities of 6 – 7 m/sec, as against 10 – 12 m/sec for air. Some data also indicate that the transition to mist/annular

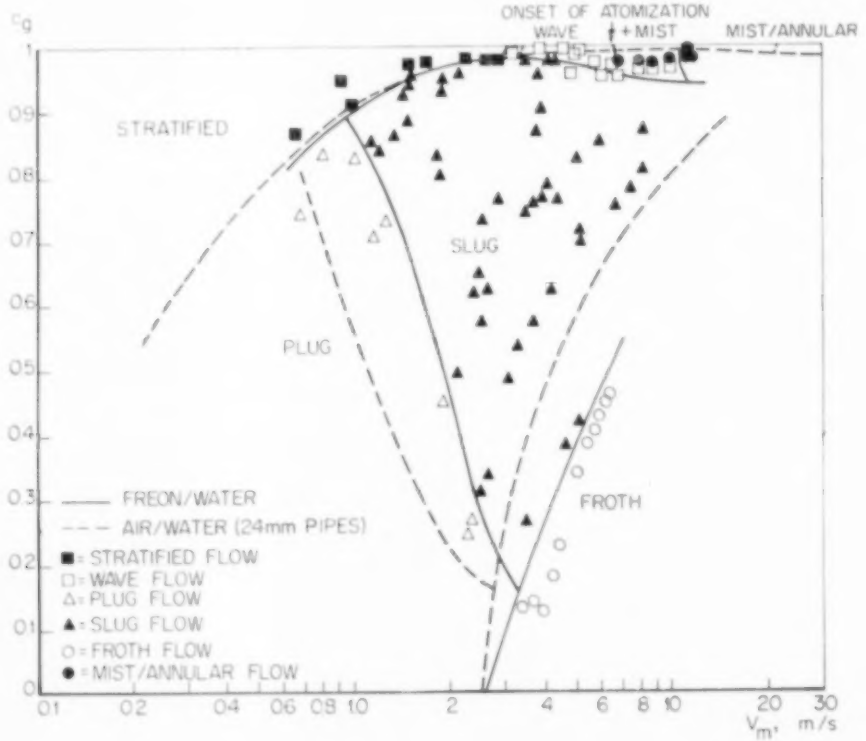

FIG. 3. Kosterin diagram for Freon–water in 15 mm pipes at $\rho_g \simeq 7$ kg/m³.

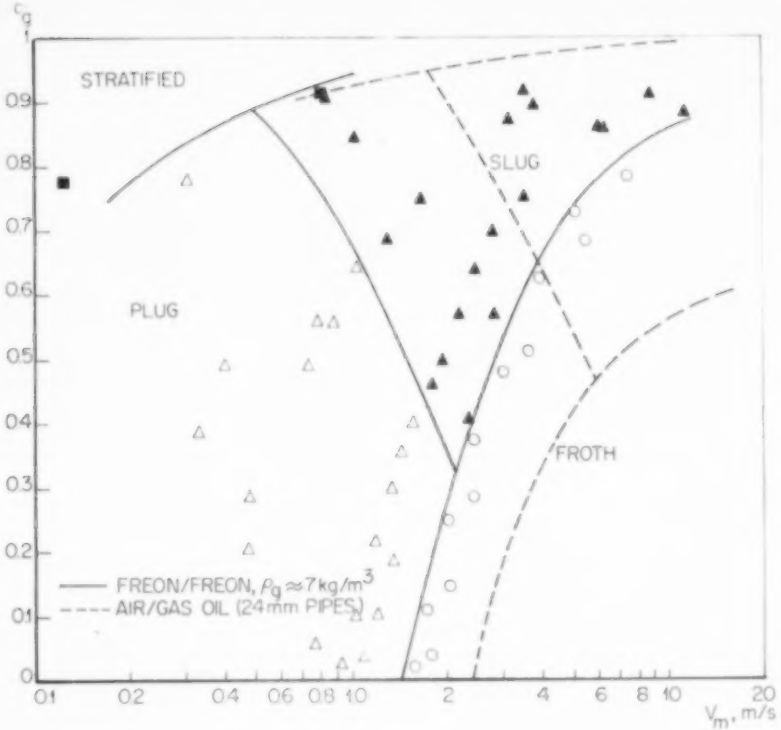

FIG. 4.
Kosterin diagram for flashing Freon in 15 mm pipes at $\rho_g \simeq 7$ kg/m^3.

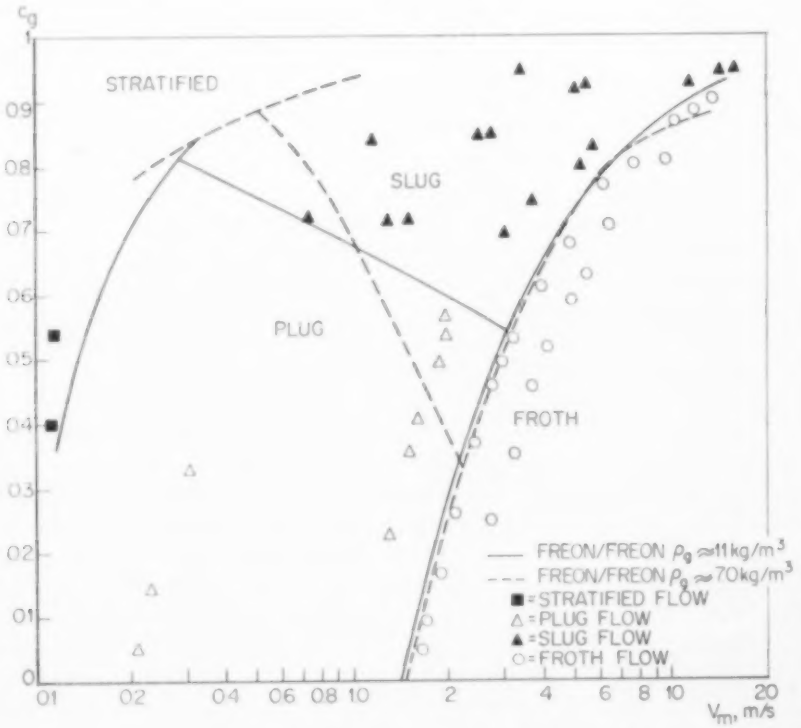

FIG. 5.
Kosterin diagram for flashing Freon in 15 mm pipes at $\rho_g \simeq 11$ kg/m^3.

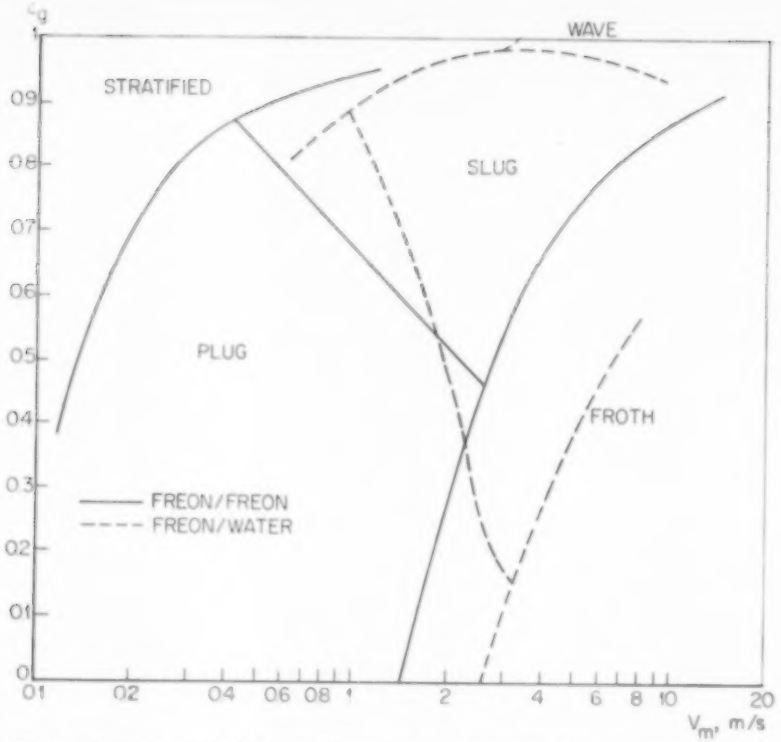

Fig. 6. Comparison of Kosterin diagrams for flashing Freon and for Freon–water.

flow occurs at lower velocities, but they are too few to warrant any conclusion; besides, in small-diameter pipes the whole wall is easily wetted anyhow. The transition from plug to slug flow is always gradual and differences are not significant. For the transition to froth flow a small difference was found.

With Freon–Freon flow (cf. Figs. 4 and 5) the transition to froth flow shifts to much lower velocities (for comparison see Fig. 6). This can be attributed to the fact that the vapour is formed in the liquid as small bubbles. The transition from stratified or wave flow to plug or slug flow is in good agreement with the air–oil data (Fig. 4), but differs markedly from the Freon–water data (Fig. 6). This difference in trend was also found in the air–oil tests compared with the air–water tests and was ascribed to the high surface tension of water, reducing the formation of waves, which retards the onset of slug flow.

The main conclusions are therefore:

1. The Kosterin diagram is not seriously influenced by the gas density in the range of 1 – 12 kg/m³, except that atomization occurs at lower velocities for higher densities.
2. The same Kosterin diagram also holds for a gradually vaporizing medium, except that the transition to froth flow occurs at lower velocities.

3.2 *Pressure drop*

The total pressure drop associated with the flow of flashing Freon is made up of two terms: friction and acceleration. The latter comes in owing to an increase in volumetric flow rate when flashing occurs. It is important especially at high mass velocities (m_t). An approximation of the acceleration pressure loss between two consecutive cross-sections 1 and 2 can be calculated on the basis of different mean velocities of gas and liquid. This gives

$$\Delta p_a = m_t^2 \left[\frac{x_2^2}{\rho_{g2} R_{g2}} - \frac{x_1^2}{\rho_{g1} R_{g1}} + \right.$$
$$\left. + \frac{(1-x_2)^2}{\rho_l (1-R_{g2})} - \frac{(1-x_1)^2}{\rho_l (1-R_{g1})} \right]. \quad (5)$$

Some authors [4-6] compute the acceleration pressure loss from the hypothetical case of no-slip according to the formula:

$$\Delta p_a = m_t^2 \left[\frac{x_2}{\rho_{g2}} - \frac{x_1}{\rho_{g1}} + \frac{x_1}{\rho_l} - \frac{x_2}{\rho_l} \right]. \quad (6)$$

It could be shown that, as long as the total mass velocity m_t does not exceed 500 kg/m² sec, the acceleration pressure loss Δp_a was small enough to be neglected for our experimental data. The total pressure drop is then equal to the

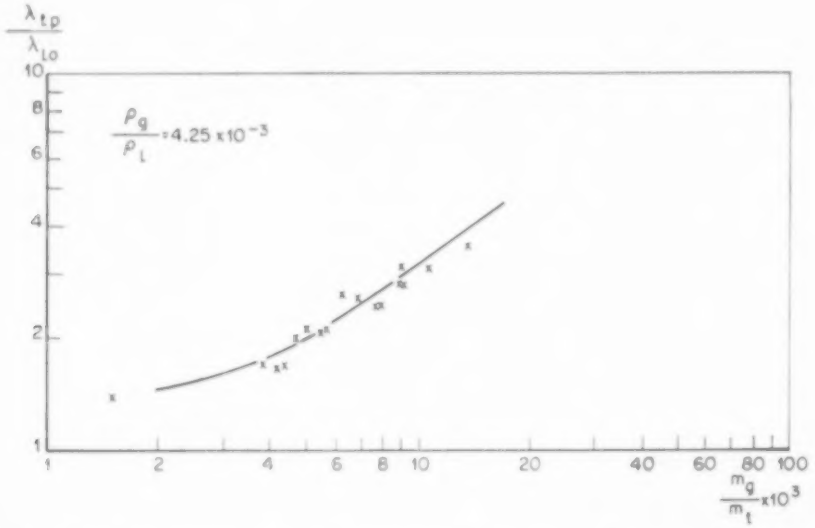

Fig. 7 (a). Two-phase pressure drop coefficient for flashing Freon flow at $m_t = 500$ kg/m² sec.

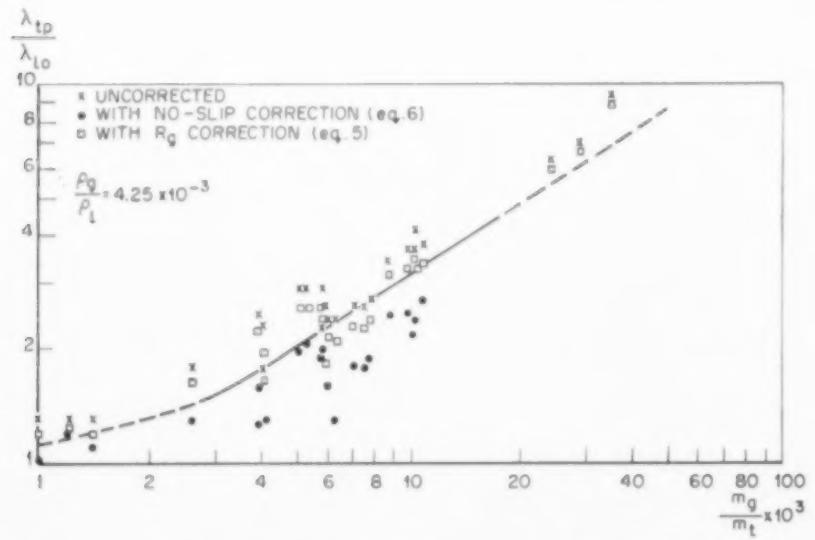

Fig. 7 (b). Comparison of different corrections to λ_{tp} for flashing Freon flow at $m_t = 1100$ kg/m² sec.

friction pressure drop. The friction factors derived from this pressure drop are given in Fig. 7 (a), where

$$\lambda_{lp} = \frac{\Delta p_{lp}}{(\frac{1}{2} m_l^2/\rho_l)(\Delta L/D)}.$$

Fig. 7 (b) shows some results for the total pressure drop, computed for a higher value of m_l, the solid line being taken from Fig. 7 (a). Clearly, the values of $\lambda_{lp}/\lambda_{l0}$, not corrected for acceleration pressure drop, are too high compared with the curve found for low m_l. On the other hand, values corrected with the no-slip method are much too low; for higher values of m_l even negative friction factors were found.

If the exact correction of equation (5) is to be applied the value of R_g must be known. As R_g was not measured in these tests we used as an approximation values derived from the correlation found for air–oil flow in horizontal pipes [1]. This correlation reads

$$\frac{R_g}{1-R_g} = 0{\cdot}60\left[v_{sg}\left(1 - \frac{R_g}{1-R_g}\frac{v_{sl}}{v_{sg}}\right)\right]^{0{\cdot}85}, \quad (7)$$

with v_{sg} and v_{sl} expressed in m/sec. Fig. 8 is a plot of this equation. Fig. 7 (b) shows that the values of $\lambda_{lp}/\lambda_{l0}$ so corrected fit the curve for low m_l very well. Therefore this method was used to correct all pressure-drop measurements for Freon–Freon flow. The results are plotted in Figs. 9 (a – c) as a function of m_g/m_t. In Figs. 10 (a – c) similar plots are presented for the data obtained on Freon–water flow, here Δp_a could be neglected. The solid curves are fitted to the points by the method of least squares.

In a former paper [1], a pressure drop correlation for the plug-, slug- and froth-flow regions was given as

$$\frac{\lambda_{lp}}{\lambda_{l0}} = \left[1 + 230\left(\frac{m_g}{m_t}\right)^{0{\cdot}84}\right]\left[0{\cdot}0138\,\frac{\rho_l}{\rho_g}\right]^a, \quad (8)$$

with

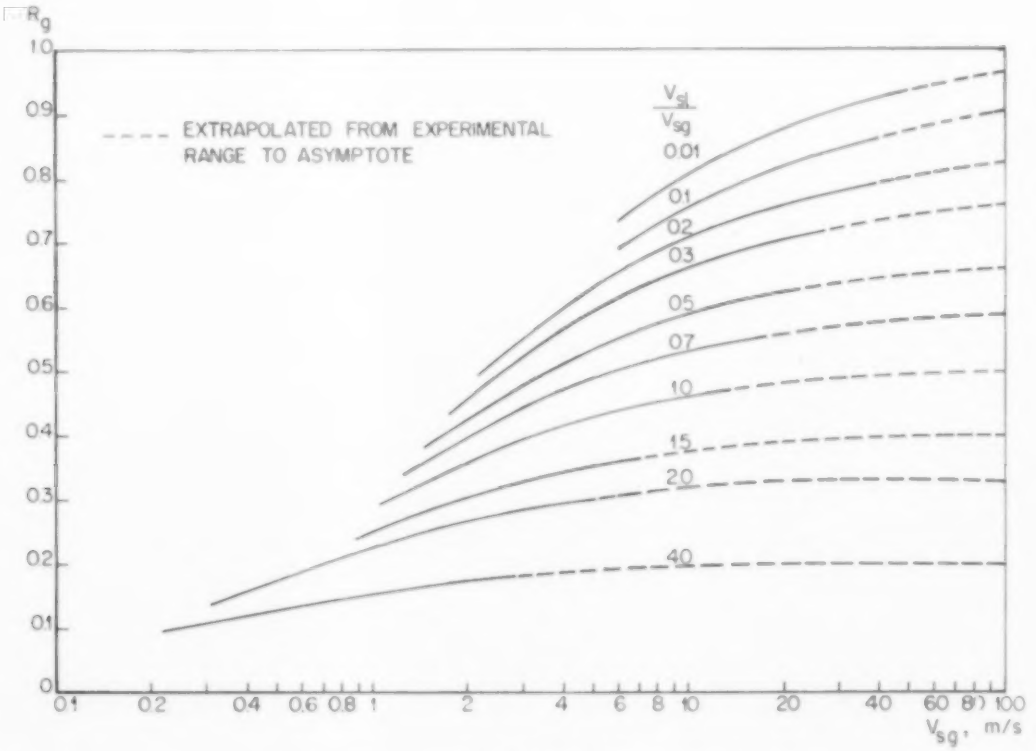

Fig. 8. Hold-up correlation for horizontal two-phase flow.

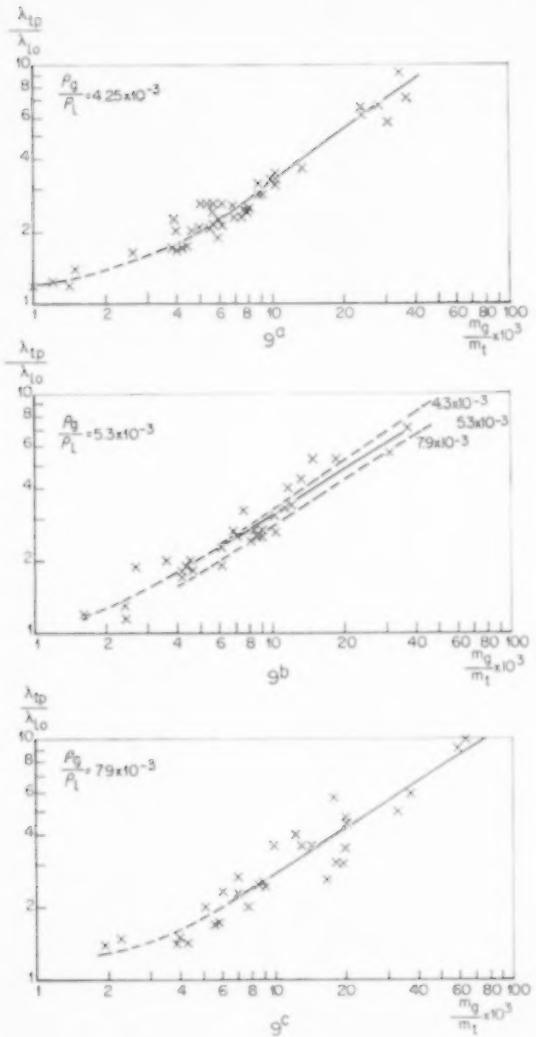

FIG. 9 (a), (b) and (c). Two-phase pressure drop coefficient for flashing Freon in the plug-, slug- and froth-flow regions ($500 < m_t < 2000$ kg/m² sec).

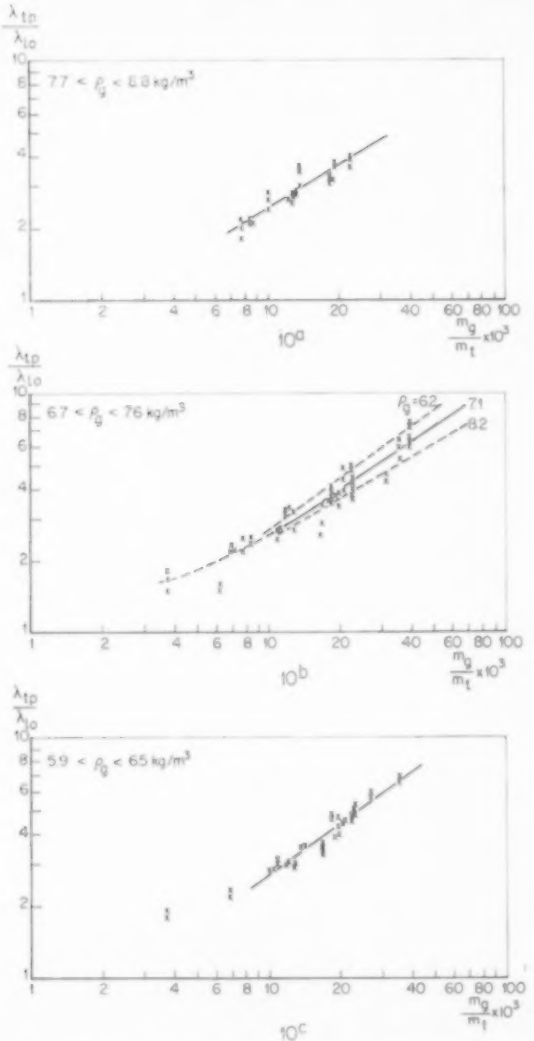

FIG. 10 (a), (b) and (c). Two-phase pressure drop coefficient for Freon–water in the plug-, slug- and froth-flow regions ($330 < m_t < 1450$ kg/m² sec).

$$\lambda_{lo} = f\left(\frac{m_l D}{\eta_l}\right) = f(\mathrm{Re}_{lo}),$$

and

$$x = 9{\cdot}5\left(\frac{m_g}{m_l}\right)^{0{\cdot}5} - 62{\cdot}6\left(\frac{m_g}{m_l}\right)^{1{\cdot}3} \qquad (9)$$

for

$$\mathrm{Re}_{lo} > 3000 \text{ and } m_g/m_t < 0{\cdot}05.$$

Here, f stands for the well-known relation between single-phase friction factor and Reynolds number [2]. This correlation was established for the range $10^{-3} < \rho_g/\rho_l < 3 \times 10^{-3}$, and it was shown [1] that extrapolation to higher gas densities was not permissible.

Our tests described above were all in the plug-, slug- and froth-flow regions and extended the range of values ρ_g/ρ_l to about 9×10^{-3}. The results of these tests are collected in Fig. 11 (a),

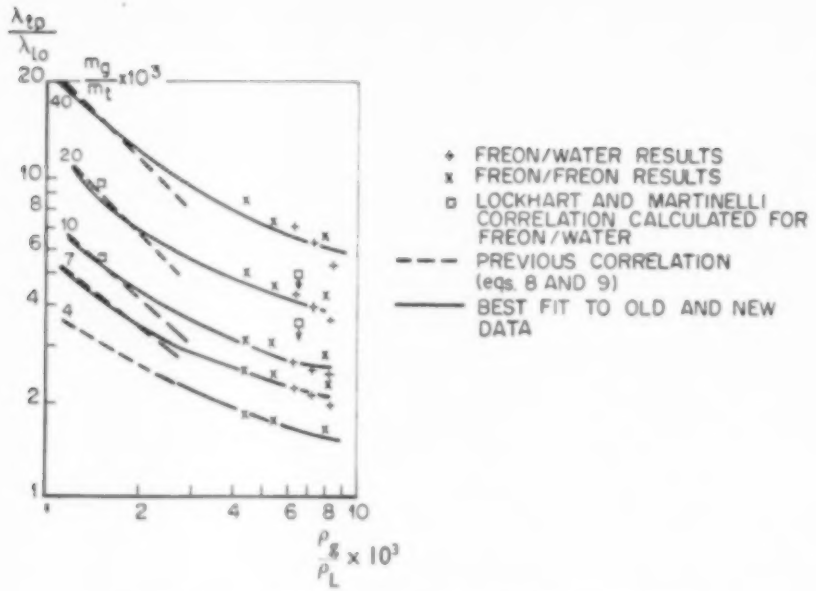

Fig. 11 (a). Effect of gas density on two-phase pressure drop.

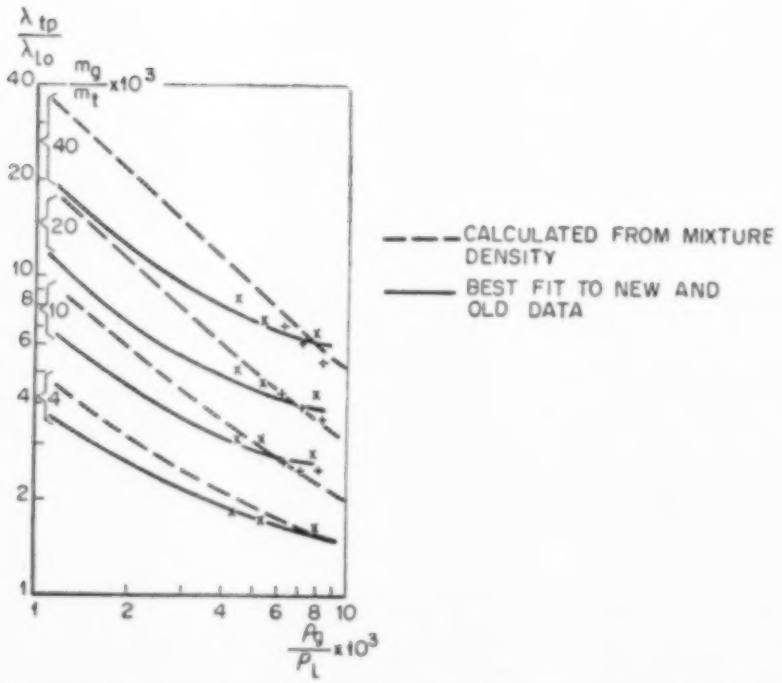

Fig. 11 (b). Comparison of pressure losses calculated from mixture density concept and as measured.

where $\lambda_{tp}/\lambda_{l0}$ is plotted as a function of ρ_g/ρ_l for different values of m_g/m_t. The curves representing equations (8) and (9) have been included for comparison. As expected, the correlation fails at higher gas densities, yielding too low pressure drops. In this Fig. new curves have been drawn that give the best fit to the new data and to the low-density parts of the curves representing (8) and (9). For comparison some values for the two-phase friction factor as calculated from the LOCKHART and MARTINELLI correlation [7] have also been inserted. For low gas densities they are the same as those determined on the basis of our correlation, for higher densities they predict too high pressure losses.

For the calculation of two-phase pressure drop some authors [4, 8] use a "mixture density concept." The flow is then approximated by that of an homogeneous mixture and the single-phase friction law is applied to it. This gives

$$\Delta p_{tp} = \lambda \frac{\Delta L}{D} \frac{1}{2} \frac{m_t^2}{\rho_m}, \qquad (10)$$

where λ can be found from the single-phase friction factor relation with

$$\lambda = f\left(\frac{m_t D}{\eta_l}\right).$$

This means that $\lambda = \lambda_{l0}$, so

$$\frac{\lambda_{tp}}{\lambda_{l0}} = \frac{\rho_l}{\rho_m}.$$

In Fig. 11 (b) the two-phase friction factor so found is compared with our results. For the higher gas densities the approximation is quite good, but for lower density ratios the deviations are very large.

The main conclusions with respect to pressure drop are therefore:

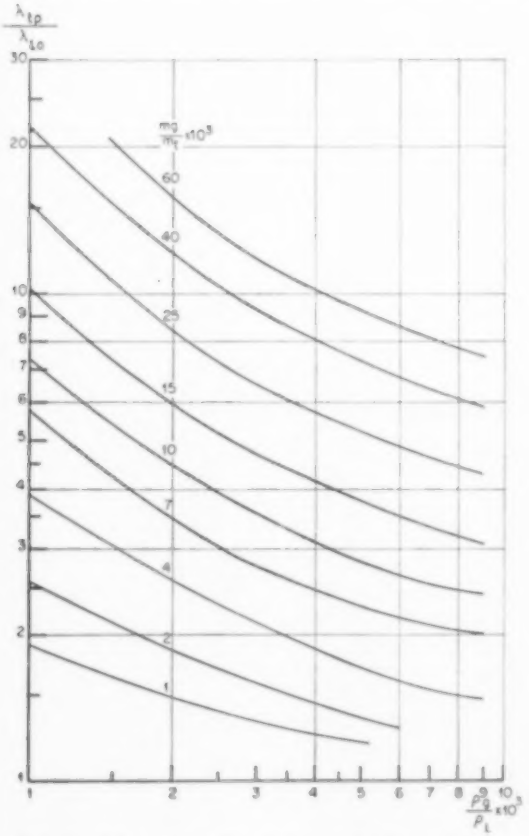

FIG. 12 (a). Correlation between $\lambda_{tp}/\lambda_{l0}$ and ρ_g/ρ_l with m_g/m_t as parameter, holding only for plug-, slug- and froth-flow.

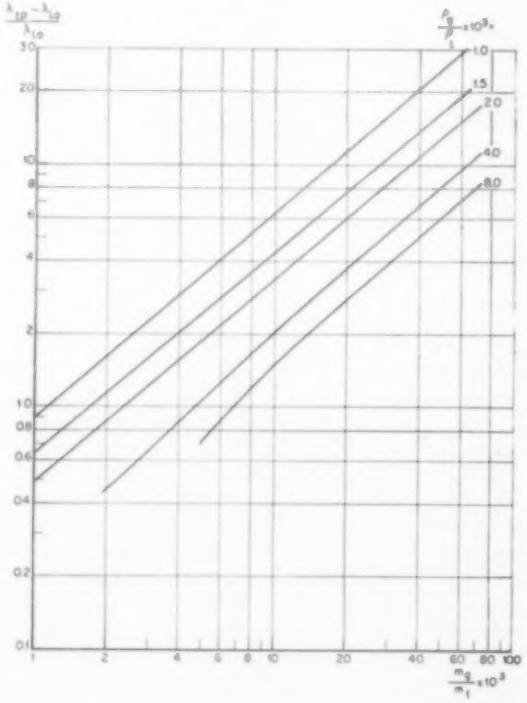

FIG. 12 (b). Correlation between $(\lambda_{tp} - \lambda_{l0})/\lambda_{l0}$ and m_g/m_t with ρ_g/ρ_l as parameter, holding only for plug-, slug- and froth-flow.

1. The correlation for two-phase pressure drop for $m_g/m_t < 0{\cdot}05$ as proposed in a former paper [1] (equations 8 and 9) is only applicable in a narrow range of ρ_g/ρ_l values. Instead of it a new correlation can be given in the form of a graph, shown in Figs. 12 (a) and 12 (b), where $\lambda_{tp}/\lambda_{l0}$ is plotted as a function of (ρ_g/ρ_l) and of m_g/m_t. For convenience this graph is presented in two different ways.

2. For the flow of a vaporizing fluid the pressure drop due to acceleration can best be calculated from equations (5) and (7).

Appendix I

Determination of heat transfer from test loop to surroundings

Experiments were conducted with liquid Freon flowing alone ($x_p = 0$) to estimate the value of ΔQ in equation (4). From these experiments the coefficient of heat transfer from the test loop to the surroundings was found to be 15 ± 3 W/m² °C. This coefficient is wholly determined by the heat transfer at the outer tube wall. When it is computed for free convection we find a value of about 5 W/m² °C. The difference from the measured value may be due to heat losses through the copper manometer connexions as well as to the presence of some forced convection.

With this heat transfer coefficient we computed the value of $\Delta Q/M_t$ in equation [4]. It was mostly between 2 and 5 per cent of the other term in equation (4). Only in some cases, where the temperature in the test section was 20 °C above room temperature, did it increase to more than 15 per cent. In those cases the pipes were insulated for the pressure-drop tests.

Appendix II

Differential temperature measurements

Three copper-constantan thermocouples were used. They had one junction in common, which was immersed in the liquid just before the flash valve. The other three junctions were fitted at the places indicated in the flow sheet (Fig. 1). The junctions were immersed to half-way the pipe diameter to ensure good contact with the liquid. Heat losses through the couple wires are small because the wire diameter is 0·1 mm and the temperature differences are small. As moreover the heat transfer coefficient to the couple junction is large, especially in two-phase flow, the junction temperature is within 0·01 °C equal to that of the liquid.

The couples were calibrated with standard thermometers with an accuracy of 0·01 °C. The measured e.m.f. is given by

$$E = b\,(T_p - T_0) + c\,(T_p - T_0)^2,$$

where b and c are constants. For small values of $(T_p - T_0)$ the second term on the right-hand side can be neglected. The values we found for b are shown in Table 3 in comparison with figures for copper–constantan taken from a handbook [9]. Presumably, the differences are due to a slight difference in composition of the constantan. For the three couples the values found for b were the same to within ± 0·5 per cent ; even after repairing the junction no larger differences were found.

Table 3. E.m.f.'s for copper–constantan as measured and as found from a handbook [9].

T_0 (°C)	b_{measured} (μ V/°C)	b_{handbook} (μ V/°C)
20	36·7	40·3
30	37·6	41·2
40	38·7	42·1

Notation

c_0	= specific heat of liquid at temperature T_0	J/kg °C
c_g	= gas fraction based on volumetric flow	
D	= pipe diameter	m
H_p	= heat content at p	J/kg
H_{l_0}	= heat content of liquid at o	J/kg
H_{l_p}	= heat content of liquid at p	J/kg
ΔL	= pipe length	m
m_t	= total mass velocity	kg/m² sec
m_g	= gas mass velocity	kg/m² sec
M_t	= total mass flow rate	kg/sec
Δp_{tp}	= two-phase pressure drop	N/m²
Δp_a	= pressure drop due to acceleration	N/m²
ΔQ	= heat exchange rate to surroundings	J/sec
Re_{tp}	= two-phase Reynolds number defined by $m_t D/\eta_l$	
R_g	= gas hold-up	
r_p	= heat of vaporization at p	J/kg
T_0	= temperature at o	°C
T_p	= temperature at p	°C
V_0	= velocity at o	m/sec
V_p	= velocity at p	m/sec
v_m	= mixture velocity $= v_{sg} + v_{sl}$	m/sec
v_{sg}	= superficial gas velocity	m/sec
v_{sl}	= superficial liquid velocity	m/sec
x	= fraction vaporized $= m_g/m_t$	
x_p	= fraction vaporized at p	
λ_{l0}	= single-phase friction factor for total mass flowing in liquid phase	
λ_{tp}	= two-phase friction factor defined by $\dfrac{\Delta p_{tp}}{(\frac{1}{2} m_t^2/\rho_l)\,(\Delta L/D)}$	
η_l	= liquid viscosity	N/m² sec
ρ_l	= liquid density	kg/m³
ρ_g	= gas density	kg/m³
ρ_m	= mixture density, defined by : $c_g \rho_g + (1 - c_g)\,\rho_l$	kg/m³

VOL. 16 1962

References

[1] Hoogendoorn, C. J. *Chem. Engng. Sci.* 1959 **9** 205.
[2] Moody L. F. *Trans. Amer. Soc. Mech. Engrs.* 1944 **66** 671.
[3] Benning A. F. and McHarness R. C. *Thermodynamic Properties of Freon-11, Trichloromonofluoromethane, with Addition of other Physical Properties.* Kinetic Chemicals Information Bulletin 1938.
[4] Benjamin M. W. and Miller J. G. *Trans. Amer. Soc. Mech. Engrs.* 1942 **64** 657.
[5] Maker F. L. *Petr. Refin.* 1959 **34** 140.
[6] Rogers J. D. *Amer Inst. Chem. Engrs. J.* 1956 **2** 536.
[7] Lockhart R. W. and Martinelli R. C. *Chem. Engng. Progr.* 1949 **45** 39.
[8] Semyonov N. I. *Dokl. Akad. Nauk SSSR* 1955 **104** 513.
[9] *American Institute of Physics Handbook*, Institute of Physics, New York 1957.

Chemical Engineering Science, 1961, Vol. 16, pp. 222 to 230. Pergamon Press Ltd., London. Printed in Great Britain.

Two-Phase (Gas-Liquid) Flow Phenomena—III

The Calculation of Heat Transfer in a vertical long-tube evaporator

G. H. Anderson, G. G. Haselden* and B. G. Mantzouranis†
Department of Chemical Engineering, Imperial College, Prince Consort Road, London, S.W.7.

(*Received* 7 *December* 1960; *in revised form* 17 *February* 1961)

Abstract—The theory for the upward, annular flow of a liquid in a vertical tube in the presence of a gas or vapour discussed in Part I of this series is developed for the prediction of heat transfer coefficients to a liquid boiling in a vertical tube. The theory is tested on the experimental data of Dengler and Lee.

Résumé—La théorie de l'écoulement annulaire ascendant d'un liquide dans un tube vertical, en présence de gaz ou de vapeur discutée dans la 1ère partie de ce travail est développée ici en vue de prévoir les coefficients de transfert de chaleur pour un liquide en ébullition dans un tube vertical. Cette théorie est vérifiée par les données expérimentales de Dengler et Lee.

Zusammenfassung—Eine Theorie für die aufwärts gerichtete Ringströmung einer Flüssigkeit in einem senkrechten Rohr in Gegenwart eines Gases oder Dampfes, wie in Teil I dieser Serie diskutiert, wird für die Vorausberechnung von Wärmeübergangskoeffizienten an eine Flüssigkeit, die in einem Rohr siedet, entwickelt. Die Theorie wird überprüft mit Hilfe der experimentellen Daten von Dengler und Lee.

Introduction

A review of published work on two-phase heat transfer in vertical tubes covering the period 1935–1957 has been made by Collier [1]. Amongst the significant papers which have appeared since, those of Groothuis and Hendal [2] and Eluhin and Visnev [3] are noteworthy.

The apparatus used in most of these investigations has been equipped to measure only average values of the heat transfer coefficient based on the heat flux for the whole length of the evaporator tube. Since the boiling process will normally produce at least two or three different flow patterns existing over varying regions of the tube it must be concluded that averaged measurements afford a totally inadequate basis for testing theoretical predictions. A satisfactory experimental study must show the relationship between heat flux and temperature difference in every region of the tube. In addition it is necessary to measure the feed rate and condition, the absolute pressure at one end of the tube and the pressure gradient along it. Moreover, all these quantities require to be capable of wide variation.

Of the few authors of studies giving local boiling coefficients Guerrieri and Talty [4] used a natural circulation apparatus which allowed only relatively small variations of liquid feed rate and no direct measurement of it. Coulson and McNelly [5] reported only a few local measurements, most of their published values being average ones. Yoder and Dodge [6] reported a very limited study of a Freon 12–oil mixture covering only low heat fluxes. The most complete work is that of Dengler [7], Dengler and Addoms [8] and Lee [9] in which a radio-active tracer was used to measure liquid hold-up in the tube. As will be seen the main shortcoming of this study is its low precision.

More than a dozen different correlations for the heat transfer coefficients of long-tube evaporators have been proposed. Some of the correlations

*Present address: Chemical Engineering Department, The University, Leeds, 2.
†Present address: 50a Gounari Street, Pireaus, Greece.

Table 1. *Indices of variables in heat tra*

(Equation of the form $h \propto$ undermentioned dimensions, c

Author	*Type of correlation*		*Tube dimensions*		*Operating conditions*			
	Local, l *average*, a	*Convective*, c *nucleate*, n	*Length*, *L*	*Dia.*, *D*	*Mass flow rate*			*Heat flux*
					Feed	*Liquid*	*Vapour*	
Badger [10]	a	n + c						− 0·15
Piret [11]	a	c	0·8	− 1·0				0·80
McNelly [5]	a	c	0·34	− 1·23	0·23			0·34
Mehta [12]	a	n + c			0·155			0·37
Kirschbaum [13]	a	n + c						0·50
Cathro [14]	a	n + c	0·467	− 0·646	0·167			0·334
Guerrieri [4]	l	c		− 1·8		0·395	0·405	
Dengler [8]	l	c		− 1·8		0·35	0·45	
Guerrieri [4]	l	n + c		− 1·16		0·254	0·26	0·357
Dengler [8]	l	n + c		− 1·7		0·35	0·45	
Piret [11]	a	n						0·67
McNelly [5]	a	n						0·69

Note the relationship $q \propto \Delta t^{2\cdot2}$ is equivalent to $h \propto q^{0\cdot545}$.

t transfer equations for long tube evaporators

ns, conditions and properties raised to the powers indicated)

		Fluid properties							
		Liquid				*Vapour*		*Surface tension*	*Latent heat*
	Pressure	μ_L	k_L	ρ_L	C_{pL}	μ_V	ρ_V		
3		− 0·345	0·345		− 0·345		− 0·115	− 2·3	
0		− 0·20	0·40	0·80	1·0		− 0·80	− 0·33	− 0·80
4		− 0·33	0·10	0·25	0·90	0·46	− 0·25		− 0·34
7		− 0·306							
0	0·50	− 0·125	0·50	0·375	0·50		− 0·25	− 0·50	− 0·50
34		− 0·167	0·657	0·32	0·334			− 0·32	− 0·013
		0·355	0·60	0·225	0·40	0·045	− 0·225		
		0·35	0·60	0·25	0·40	0·05	− 0·25		
57	0·357	0·585	0·386	− 0·028	0·258	0·029	− 0·145	− 0·357	0·357
		0·35	0·60	0·25	0·40	0·05	− 0·25	− 0·10	
7		− 0·34	− 0·67	0·16	0·33			− 0·16	− 0·67
9	0·31	0·0	− 0·69	0·33	0·69		− 0·33	− 0·31	− 0·69

*These equations employ additional variables not classified in the table.

Table 2

	Piret and Isbin	McNelly	Kirschbaum		Guerrieri and Talty			
Evaporation (%)	*Average nuclear convection*	*Average nuclear convection*	*Level* 75%	40%	*Tube top nuclear convection*		*Tube mid. nuclear convection*	
50	1325	2470	(1080)	1422	1390	1760	(228)	1160	(—)	1030
10	451	851	(355)	832	620	787	(150)	760	(268)	587

distinguish between the nucleate boiling and forced convection regions whilst others try to cover both. It is difficult to compare them because of the widely varying choice of parameters and the absence in many cases of such vital ones as liquid feed rate. Where the correlations are based on dimensional analysis the various groups are normally evaluated for the conditions at the entry or exit of the tube. By making a number of assumptions it is possible to reduce each of the published equations to a form in which the heat transfer coefficient is expressed as a direct power function of the tube dimensions, the operating variables and the fluid properties. The result of these reductions for a number of equations is shown in Table 1. It might be expected that the more important variables would be the tube dimensions L and D, the feed rate, the heat flux, the liquid viscosity and thermal conductivity. There appears to be little agreement between any of the authors on the significance of these quantities.

Table 2 shows the heat transfer coefficients calculated from these correlations for the case of water vaporizing at atmospheric pressure in a copper tube 6ft long, 0·5 in. i.d., with a feed rate of 50 lb/hr at its boiling point and two heat fluxes (constant over the tube length) corresponding to 50 per cent and 10 per cent vaporization (heat flux density 31,000 and 6200 B.t.u/hr. ft^2 respectively). The various equations agree to the extent of giving higher coefficients for forced convection than for nucleate boiling under these conditions, but it would be difficult in an actual design to know which individual values to use.

It is considered that most of the uncertainties arise from premature attempts to achieve averaged correlations before the significance of the various contributing heat transfer processes is known.

Heat Transfer Mechanisms in a Long-tube Evaporator

To elucidate the process of heat transfer in a long-tube evaporator it is useful to differentiate between the mechanism occurring in at least three zones of the tube. It is assumed that the feed is at its boiling point; if not there will be an entry zone in which either forced convection heat transfer or surface boiling will be operative.

In the first zone the controlling mechanism is nucleate boiling (unless the temperature difference is greater than the critical) and it will be expected that the nature of the tube surface and the purity of the liquid feed (presence of dissolved gases, etc.) will influence the heat transfer coefficient. Since the increase of volume accompanying vaporization at atmospheric pressure is normally in the range 500 – 1000 the evaporation of less than 1 per cent of the feed will cause appreciable changes in the liquid flow condition. The first major change leads to slug flow in which the individual bubbles coalesce to form large bullet-shape volumes of vapour separated by thin slugs of liquid. Further evaporation causes a progressive acceleration of the liquid in the slugs, and in the film covering the tube wall, leading to breakdown of the liquid slugs. This second change leads to annular- or climbing-film flow in which the greater part of the liquid adheres to the tube wall in an upward-flowing film, the remainder being entrained in the vapour. At first the film is heavily rippled due to the influence of the collapsing slugs, but higher up the tube it assumes

a relatively smooth appearance with ripples of only small amplitude.

For long evaporator tubes and large temperature driving forces the liquid film may break down leaving patches of dry wall. Obviously the heat transfer coefficient falls rapidly in these circumstances. Except in cases where the heating medium is at constant temperature (as with condensing steam) burn-out will normally ensue.

It is possible to describe transitional zones between nucleate boiling and slug-flow and between slug-flow and annular-flow, but these transitions are normally achieved rapidly, and the flow patterns within them are indefinite. To describe the heat transfer processes within a long-tube evaporator quantitatively it is obviously desirable to reduce the number of mechanisms requiring separate treatment to a minimum, and for these reasons it appears justifiable to consider only three main zones, namely nucleate, slug-flow and annular-flow. As a further simplification it might be possible to consider slug-flow as a special form of annular-flow since in slug-flow the heating surface is covered by liquid and the main heat transmission is through a thin liquid film. It may be expected that only a small amount of evaporation will occur from the liquid within the slugs, their main influence being a stirring action on the liquid film.

From the above discussion it appears that a quantitative description of the evaporation process in a long-tube evaporator may be built on a consideration firstly of the nucleate boiling region occurring near the inlet of the tube and secondly on an essentially annular-flow region extending over the remainder of the tube. In the latter region it is to be expected that an iterative calculation will be required to allow for the changing film conditions due to evaporation, acceleration and possibly entrainment. Also it will be desirable to have a test available for the onset of dry-wall conditions. When the feed is below its boiling point the entry region of the tube will be calculated as for normal forced convection.

The remainder of this paper is concerned with the extension of the theory of annular flow of liquid and gas in a vertical tube given in parts 1 and 2 of this series [15], to embrace the heat transmission occurring within the annular-flow region of a long-tube evaporator. It is assumed that the flow conditions for a saturated liquid in contact with its vapour are the same as those for a liquid in contact with a permanent gas after appropriate allowance has been made for density and viscosity differences. It is further assumed that the temperature driving force is insufficient to produce nucleation within the liquid film. The equations thus derived will be tested against previously published experimental data.

Heat Transmission Accompanying Annular-film Flow

There is little experimental information available on the variation of pressure gradient and hold-up along the length of an evaporator tube during evaporation. As already mentioned Lee [9], in association with Dengler [7], carried out experiments on the evaporation of water in a 1 in. i.d. vertical copper tube 20 ft long, measuring the local liquid hold-up at four points along the tube by using a radioactive tracer in the form of a soluble salt.

From the local values of total pressure, liquid and vapour flow rates and also their local pressure gradients it was possible to calculate the theoretical value of liquid hold-up by following the interative procedure outlined in Part I of this series [15]. The following assumptions were made:

Constant physical properties across any cross-section, as at the saturation temperature.
Hydraulically smooth surface of the evaporator tube.
No dispersed phase in the vapour stream.

For flow conditions in which it was impossible to obtain agreement between the theoretical and calculated values of y_i^+ whatever reasonable value of R_L was tried, slug flow was considered to prevail. Such flows were at or below the minimum in the plot of pressure gradient against vapour flow.

From the detailed calculations it was seen that, in general, no term in the momentum balances can be neglected, and that the forces required for the acceleration of the vapour and liquid

phases assume increased significance when evaporation is occurring. Unfortunately, the data of LEE do not yield accurate point values of the vapour flow and pressure gradient, and the interference of background radiation rendered the measurement of liquid film thickness unreliable when the liquid hold-up was small.

The measured and calculated values of R_L are compared in Fig. 1. Apart from a few points belonging to the transition region the theoretical values agree with the experimental within the estimated experimental error, but since this is so large it would be unfair to claim that the validity of the theory applied to two-phase flow with heat transfer has been established conclusively. In general the predicted values appear to be low, but this could be attributed to the hydraulic roughness of the evaporator tube.

The analogy between momentum and heat transfer is now used to calculate the heat transfer coefficients for the case of annular flow with heat transfer, but without nucleation on the tube wall, using essentially the treatment of VON KÁRMÁN as quoted by ECKERT [16].

The differential equations describing the momentum and heat transfer in a direction y at any point within a fluid are

$$\tau = (\nu + \epsilon_M)\,\rho\,\frac{du}{dy} \tag{1}$$

$$q = \left(\frac{\nu}{\mathrm{Pr}} + \epsilon_H\right)\rho\,C_p\,\frac{dt}{dy} \tag{2}$$

The terms ν and ν/Pr describe molecular diffusion which predominates in the laminar sublayer, whereas ϵ_M and ϵ_H describe eddy diffusion, important in the turbulent layer; ϵ_M is computed from the velocity distribution and ϵ_H assumed numerically equal to it. The ratio ϵ_M/ϵ_H is believed to vary slightly with y^+ but the variation from unity is not sufficient to cause serious error.

In order to integrate equations (1) and (2) the physical properties of the fluid are assumed to be constant within each layer and the shear stress to vary linearly with y from τ_w to τ_i so that

$$\tau = \tau_w\left[1 + \frac{(\tau_i/\tau_w) - 1}{y_i}\,y\right] \tag{3}$$

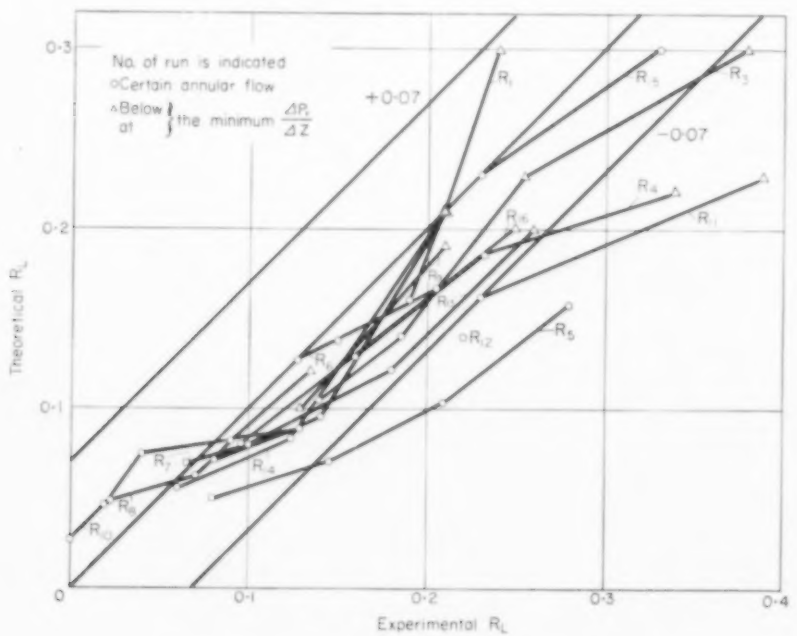

FIG. 1. Results of LEE. Comparison with theory.

The heat flux density q is given by

$$q = q_w \frac{r_w}{r_w - y} = q_w \frac{1}{1 - (y/r_w)} \tag{4}$$

where q_w = heat flux density at the wall.

From equations (2) and (4) we have

$$\int dt = \int \frac{q}{\rho C_p} \cdot \frac{dy}{(\nu/\mathrm{Pr}) + \epsilon_H} =$$

$$\int \frac{q_w}{\rho C_p \nu \left[1 - (y/r_w)\right]} \cdot \frac{dy}{\left[(1/\mathrm{Pr}) + (\epsilon_H/\nu)\right]}$$

Now $y = \frac{\mu y^+}{\rho u^*}$ and $dy = \frac{\mu}{\rho u^*} dy^+$

$$\therefore \Delta t = \int \frac{q_w \mu}{\rho C_p \nu \left[1 - (\mu y^+/\rho u^* r_w)\right] \rho u^*} \cdot \frac{dy^+}{\left[(1/\mathrm{Pr}) + (\epsilon_H/\nu)\right]}$$

Writing $\frac{\rho u^* r_w}{\mu} = \mathrm{Re}^*$ and $\frac{\Delta t}{q_w} \rho C_p u^* \equiv \Delta t^*$

$$\Delta t^* = \int \frac{dy^+}{\left[1 - (y^+/\mathrm{Re}^*)\right]\left[(1/\mathrm{Pr}) + (\epsilon_H/\nu)\right]} \tag{5}$$

Equation (5) can be readily integrated if the variation of ϵ_H/ν with y^+ is known. From (1), substituting the dimensionless forms of y and u we have

$$\frac{\epsilon_M}{\nu} = \frac{\tau}{\rho u^{*2}} \cdot \frac{dy^+}{du^+} - 1 = \frac{\tau}{\tau_w} \frac{dy^+}{du^+} - 1$$

and hence from (3)

$$\frac{\epsilon_M}{\nu} \text{ or } \frac{\epsilon_H}{\nu} = \left(1 + \frac{(\tau/\tau_w) - 1}{y_i^+} y^+\right) \frac{dy^+}{du^+} - 1. \tag{6}$$

By combining (5) and (6) and taking dy^+/du^+ from the universal velocity profile of Von Kármán, the temperature differences Δt_l, Δt_b and Δt_t across the three layers can be calculated in turn.

In the laminar sublayer ϵ_H is taken as negligible n comparison with ν/Pr and (5) becomes

$$\Delta t_l^* = \mathrm{Pr} \int_0^5 \frac{dy^+}{1 - (y^+/\mathrm{Re}^*)}$$

$$= -\mathrm{Pr}\,\mathrm{Re}^* \ln\left(1 - \frac{5}{\mathrm{Re}^*}\right) \tag{7}$$

or if Re^* is large, as it usually is in the annular flow regime,

$$\Delta t_l^* = 5\,\mathrm{Pr} \tag{8}$$

By differentiation of the equation defining flow in the buffer layer

$$\frac{du^+}{dy^+} = \frac{5}{y^+}$$

and hence (6) becomes

$$\frac{\epsilon_M}{\nu} = \left[1 + \frac{(\tau_i/\tau_w) - 1}{y_i^+} y^+\right] \frac{y^+}{5} - 1$$

Thus from (5)

$$\Delta t_b^* = \int_5^{30} dy^+ \Big/ \left(1 - \frac{y^+}{\mathrm{Re}^*}\right) \left[\frac{1}{\mathrm{Pr}} - 1 + \left(1 + \frac{(\tau_i/\tau_w) - 1}{y_i^+} y^+\right) \frac{y^+}{5}\right]$$

Since Re^* is usually $> y^+$ the term $\left[1 - (y^+/\mathrm{Re}^*)\right]$ can be equated to unity and so

$$\Delta t_b^* = \int_5^{30} dy^+ \Big/ \left(\frac{1}{\mathrm{Pr}} - 1\right) + \frac{y^+}{5} + \frac{(\tau_i/\tau_w) - 1}{5 y_i^+} y^{+2} \tag{9}$$

Writing

$$\left(1 - \frac{1}{\mathrm{Pr}}\right) = -\frac{D}{4}$$

and

$$\frac{(\tau_i/\tau_w) - 1}{5 y_i^+} = E$$

(9) integrates to

$$\Delta t_b^* = \left[\frac{1}{(0{\cdot}04 + DE)^{1/2}} \ln \frac{2Ey^+ + 0{\cdot}2 - (0{\cdot}04 + DE)^{1/2}}{2Ey^+ + 0{\cdot}2 + (0{\cdot}04 + DE)^{1/2}}\right]_{y^+=5}^{y^+=30} \tag{10}$$

Equation (10) is presented graphically in Fig. 2 with Pr as the continuous variable and E a parameter.

For the turbulent layer $du^+/dy^+ = 2{\cdot}5/y^+$ and

$$\Delta t_t^* = \int_{30}^{y_i^+} dy^+ \Big/ \left(1 - \frac{y^+}{\mathrm{Re}^*}\right) \left\{\left(1 + \frac{(\tau_i/\tau_w) - 1}{y_i^+} y^+\right) \frac{y^+}{2{\cdot}5}\right.$$

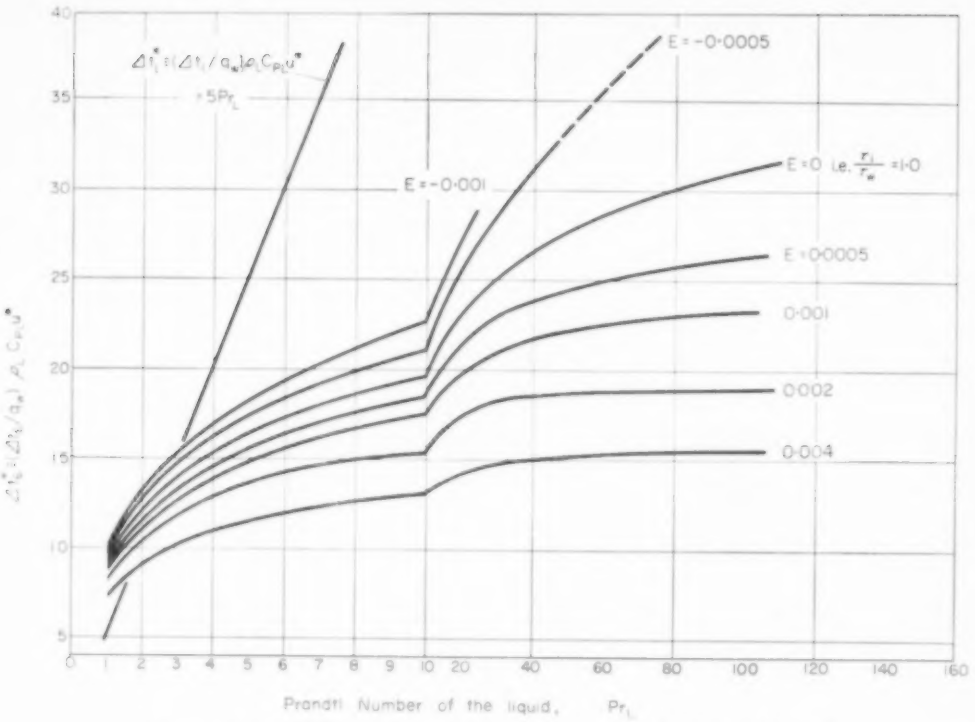

FIG. 2. Temperature drop in "buffer" layer and "laminar sublayer."

which integrates to

$$\Delta t_i^* = 2{\cdot}5\left\{\ln\frac{y_i^+}{30} - \frac{5E\,\mathrm{Re}^*}{5E\,\mathrm{Re}^* - 1}\ln\frac{1+5E\,y_i^+}{1+150\,E} + \frac{1}{5E\,\mathrm{Re}^* - 1}\ln\frac{1-(30/\mathrm{Re}^*)}{1-(y_i^+/\mathrm{Re}^*)}\right\} \quad (11)$$

The evaluation of this equation is laborious but by equating $1-(y^+/\mathrm{Re}^*)$ to unity a simplified form can be obtained.

$$\Delta t_i^* = 2{\cdot}5\ln\frac{y_i^+ + 30\left[(\tau_i/\tau_w) - 1\right]}{30\,\tau_i/\tau_w} \quad (12)$$

This relation is presented in Fig. 3 with y_i^+ as the continuous variable and τ_i/τ_w as parameter. It provides reasonable accuracy when the annular flow regime is well established, but (11) may have to be used as the slug flow regime is approached.

The temperature differences across the three layers are additive, i.e.

$$\Delta t_T = \Delta t_l + \Delta t_b + \Delta t_t$$

or

$$\Delta t_T^* = \Delta t_l^* + \Delta t_b^* + \Delta t_t^* \quad (13)$$

The heat transfer coefficient from tube wall to liquid–gas interface is then given by

$$h = \frac{q_w}{\Delta t_T} = \frac{\rho\,C_p\,u^*}{\Delta t_T^*} \quad (14)$$

This theory breaks down as u^* becomes equal to, or less than, zero, or when nucleation occurs on the tube wall. Providing u^* is positive it may well be applicable to the slug flow regime since the thickness of the turbulent layer has only a small effect on Δt, i.e. a value of y_i^+ corresponding to a much greater value of Re^* than that calculated can be used in such cases without introducing serious error.

In Part I [15] the concept of a "double" velocity profile was put forward, i.e. the gas–liquid interface behaving as would a moving solid–liquid interface. If such is the case then Δt^* over the total y_i^+ would be twice the Δt^* up to the point $y_i^+/2$. It is unlikely that the

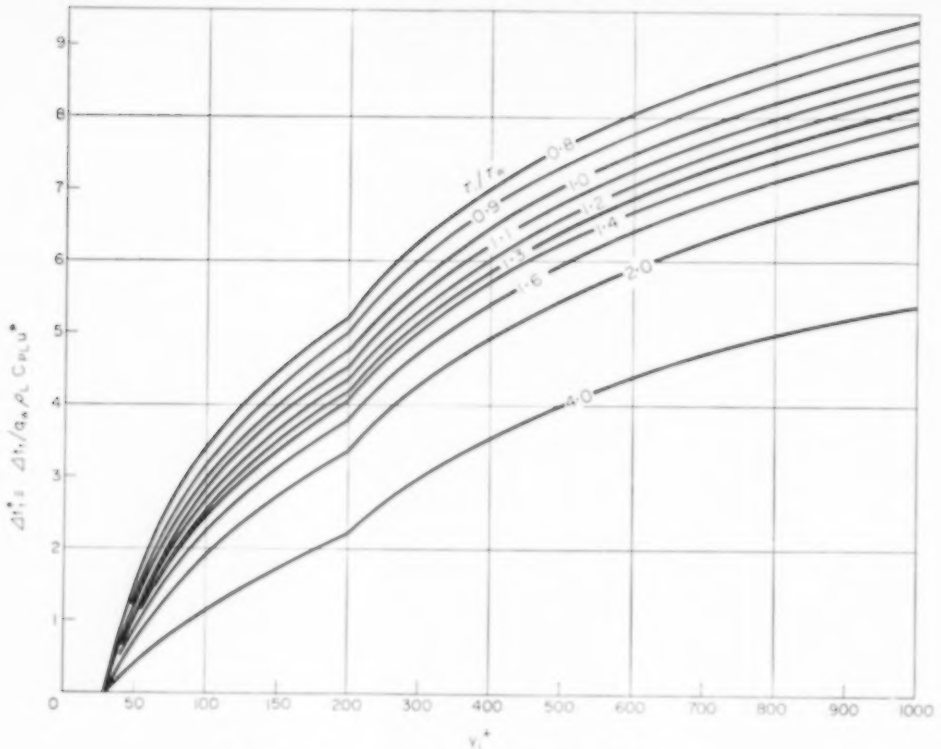

Fig. 3. Temperature drop in "turbulent" layer.

interface is fully damped and so the most likely value of Δt^* lies between those calculated on the "single" and "double" profiles respectively. Furthermore, ripples, which are known to exist on the gas–liquid interface, will probably tend to eliminate temperature gradients in the vicinity of the interface, but since no adequate way of defining these ripples is available their influence remains uncertain.

Testing of Theory Against Experimental Results

The experimental work of Dengler and Addoms [8] and Lee [9] was analysed from the heat transfer aspect in an attempt to confirm the validity of this approach. Although not ideal for this purpose these data are the most useful so far published*. Derived data from the original experimental results are shown in Table 3. All data are point values for the middle of each heating section. The flux density q_w reckoned on the inside tube diameter was obtained from the slope of the curve of vapour fraction vs. distance from the tube base; the contribution of flash vaporization was neglected as its value is small compared with the heat flux through the walls and certainly smaller than the error involved in obtaining q_w. The steam temperature was deduced from the saturation pressure and the wall temperature was taken as the arithmetic average of the readings of the three thermocouples located in the central 2 ft of each heating section, as the point values are so erratic.

The minimum Δt at which nucleation occurs varies with the shear stress at the wall and the nature of the wall surface. In view of the high shear stress and low Δt in most of Dengler's experiments nucleation on the wall is unlikely to have occurred, and the theory is assumed to apply to all his data in which u^* is positive.

The experimental values of Δt_T^* were calculated from equation (14) and compared with those

*It is hoped to publish in Part IV of this series further experimental data in this field.

Table 3. Heat transfer results of DENGLER *and* LEE

Run no.	*Position* $\frac{z}{D}$	q_w (B.t.u/hr ft^2 × 10^{-3})	Δ_t *exp.* (°F)	*Ambiguity in* Δ_t (+ °F −)		h *exp.* (B.t.u/hr ft^2 °F)	*Experimental* Δt_T^* *based on* measured R_L	*Experimental* Δt_T^* *based on* predicted R_L	$\frac{\tau_i}{\tau_w}$	*Theoretical* Δt^* *based on single velocity profile* Δt_l^*	Δt_b^*	Δt_t^*	Δt_T^*
R1	211	96·6	10·6	3·0	2·0	9110	20·3	20·3	1·063	8·15	11·15	8·25	27·55
	166	42·8	8·0	1·5	1·0	5350	29·0	29·1	1·17	7·98	11·0	8·1	27·08
	121	22·5	6·2	1·0	1·0	3630	24·0						
	76	17·1	3·5	0·2	0·2	4880	23·0						
	31	9·6	5·0	2·0	2·0	1920	33·7						
R3	211	116·8	12·2	5·5	2·0	9350	25·3	25·7	1·058	7·87	11·0	8·25	27·02
	166	58·0	7·2	1·0	2·0	8040	22·3	22·3	1·13	7·54	10·8	8·3	26·64
	121	37·0	9·2	3·0	4·0	4020	28·0	27·3	1·60	7·36	10·7	7·58	25·64
	76	29·5	8·4	1·0	1·0	3510	27·8						
	31	20·0	9·4	0·1	0·1	2130	14·8						
R4	211	168·0	21·0	3·0	2·0	8000	37·7	37·2	1·078	7·36	10·7	8·1	26·16
	166	104·3	11·6	3·0	3·0	9160	20·4	20·4	1·11	7·05	10·6	8·35	26·0
	121	65·0	11·2	5·0	3·5	5800	22·9	23·4	1·32	6·95	10·4	8·05	25·0
	76	57·1	12·1	4·0	2·5	4720	23·4						
	31	30·2	12·7	1·0	1·0	2380	24·5						
R5	211	159·3	15·4	7·0	14·0	10350	23·2	22·8	1·082	7·85	11·0	6·35	25·2
	166	105·6	14·0	4·5	3·5	7550	24·5	24·4	1·122	7·45	10·8	6·6	24·85
	121	69·3	14·7	7·0	6·0	4710	27·0	29·0	1·24	7·25	10·6	6·7	24·55
	76	51·0	17·0	7·0	4·0	3000	25·6	30·8	1·35	7·22	10·5	6·55	24·27
	31	27·7	18·0	1·0	1·0	1540							
R6	211	39·8	7·0	1·0	1·5	5680	19·9	19·9	1·322	8·5	11·1	6·2	25·8
	166	28·5	8·0	2·0	1·5	3560	23·5	24·7	1·67	8·4	11·1	5·75	25·25
	121	20·4	5·2	0·5	0·5	3920							
	76	13·0	6·1	0·5	0·5	2130	26·3						
	31	2·8	5·3	1·5	1·5	532	111·0						
R7	211	100·2	14·5	2·0	2·0	6910	26·9	27·1	1·092	8·17	11·1	6·4	25·67
	166	77·5	10·8	2·0	1·0	7180	20·7	20·8	1·171	7·92	11·0	6·5	25·42
	121	47·0	15·0	5·0	8·0	3140	21·0	21·0	2·21	7·82	10·6	5·25	23·67
	76	30·4	13·0	4·0	2·0	2350	32·6						
	31	19·8	12·5	0·5	0·5	1590	45·5						
R8	211	139·0	13·2	5·0	8·0	10500	12·7	15·0	1·056	8·29	11·2	5·2	24·69
	166	72·6	16·1	2·5	5·0	4520	31·9	30·0	1·11	8·07	11·0	5·4	24·47
	121	45·0	17·8	7·0	7·5	2530	29·1	29·7	2·22	8·0	10·4	3·9	22·30
	76	31·1	16·8	6·0	3·0	1850	38·3						

	121	45·0	17·8	7·0	7·5	2530	20·1	29·7	2·22	8·0	10·4	3·9	22·30
	76	31·1	16·8	6·0	3·0	1850	38·3						
	31	24·2	16·2	0·2	0·2	1500	33·0						
R9	211	25·4	8·1	0·5	0·5	2920	18·8	15·9	3·18	8·62	10·3	3·0	22·92
	166	17·6	7·3	1·5	2·0	2120	16·0	19·3	4·21	8·58	10·2	2·0	20·78
	121	14·8	8·5	1·0	1·0	1740							
	76	9·1											
R10	211	158·0	22·0	18·0	18·0	7180	28·1	27·3	0·975	8·06	11·2	4·8	24·06
	166	92·4	17·5	5·5	8·0	5300	36·2	35·3	1·60	7·75	10·9	5·3	23·95
	121	87·0	17·6	13·0	8·0	4950	22·1	37·3	1·17	7·55	10·8	5·4	23·75
	76	27·3	20·5	8·0	4·0	1330	74·6	130·0	1·34	7·46			
	31	6·5	20·9	1·0	1·0	312	171·0						
R11	211	120·0	13·8	1·4	0·6	8700	31·2	31·2	1·16	7·05	10·6	10·0	27·65
	166	80·0	12·1	0·3	0·2	6600	30·2	29·2	1·40	6·95	10·5	9·6	27·05
	121	44·0	8·2	0·3	0·1	5500							
R12	211	206·0	10·5	2·3	3·4	19000	16·1	16·1	1·02	6·95	10·5	10·2	27·65
	166	118·0	14·0	1·0	1·0	8440	13·4	13·4	3·41	6·70	10·4	7·6	24·7
	121	49·1	13·5	0·4	0·4	3640							
R13	211	122·0	12·5	2·5	1·5	9770	17·9	18·0	1·075	9·55	11·8	6·3	27·65
	166	43·9	12·5	2·5	2·0	3500	30·7	31·7	1·32	9·15	11·6	6·1	26·85
	121	23·1	9·7	2·0	2·0	2360	7·4	19·8	3·60	9·05	11·2	3·3	23·55
	76	15·6	10·0	1·0	1·0	1560	50·0						
	31	12·7	7·5	1·0	1·0	1690							
R14	211	112·8	18·3	2·0	2·0	6150	37·3	37·2	1·060	8·85	11·5	6·35	26·7
	166	66·8	16·5	4·0	3·5	4050	40·0	40·4	1·17	8·42	11·2	6·35	25·97
	121	38·9	11·5	5·0	3·0	3380	20·8	20·8	2·14	8·30	10·7	5·0	24·0
	76	25·6	13·5	2·5	2·5	1900	35·7						
	31	13·9	14·0	1·0	1·0	992							
R15	211	39·5	3·4	4·0	2·0	11600	5·3	5·3	2·57	6·98	10·0	5·0	21·98
	166	31·1	11·0	2·0	1·0	2830	3·0	11·7	8·06	6·94	9·4	2·0	19·34
	121	17·0	7·0	3·0	2·0	2425							
	76	6·8	6·5	2·0	2·0	1040	58·4						
	31	5·6	5·3	1·0	1·0	1066							
R16	211	134·5	16·5	3·0	16·0	8150	21·4	21·8	1·03	6·86	10·4	6·95	24·21
	166	95·6	19·0	3·0	3·0	5030	33·5	33·5	1·086	6·75	10·4	7·05	24·10
	121	59·1	14·0	4·5	9·0	4220	8·5	13·1	2·69	6·70	9·8	4·3	20·80
	76	39·4	13·6			2900							
	31	28·1	13·5			2080							

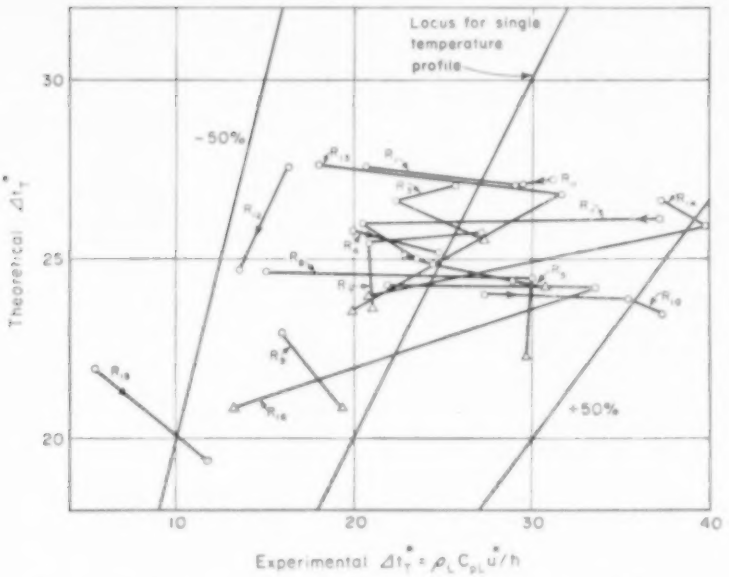

FIG. 4. Heat transfer results of DENGLER. Comparison with theory.

theoretically predicted from (13). In the former u^* could be calculated either from the experimental value of the liquid hold-up R_L or, when annular flow conditions exist, from the predicted hold-up [15], and both values of Δt_T^* are presented in Table 3. The large ambiguity in values has little influence on the value of u^* under annular flow conditions so that the values of Δt_T^* calculated by the two methods agree quite closely.

In view of the ambiguity in the value of Δt and to a lesser extent in the value of q_w, the resulting experimental heat transfer coefficients are estimated to be in general reliable to $\pm$ 50 per cent. Consequently the theoretical values of Δt_T^* are computed using the " single " temperature profile, physical properties constant at the stream temperature and the theoretical y_i^+ based on the " single " velocity profile.

The theoretical and practical values of Δt_T^* are compared graphically in Fig. 4; the scatter appears to be random and is of the same order of magnitude as the estimated experimental error.

CONCLUSION

A method for predicting the point values of temperature head required for a given heat flux in a long-tube evaporator, based on the universal velocity profile, is developed. The heat transfer calculation is based on the assumptions of linear variation of shear stress from the wall to the interface and of constant liquid properties within each layer at any cross-section of the evaporator. The experimental results of DENGLER and LEE are presented in a form suitable for testing this new method. The correspondence between the two is within the range of the experimental error which is considered to be $\pm$ 50 per cent. The need for more accurate experimental data on which to test the method is evident. Such data has now been obtained [17] and will be published shortly.

Acknowledgments—The authors wish to thank Professor D. M. NEWITT in whose department this work was carried out and to acknowledge the generous financial assistance of Shell Internationale Research Mij. N.V.

NOTATIONS

$B = 4\,[(1/\mathrm{Pr}) - 1]$
C_p = specific heat
D = diameter
$E = \dfrac{(\tau_i/\tau_w) - 1}{5y_i^+}$

h = heat transfer coefficient
k = thermal conductivity
L = length
Pr = Prandtl number $\dfrac{C_p\,\mu}{k}$
q = heat flux density
r = radius
R = fraction of cross-section occupied by one phase
Re^* = dimensionless ratio $\dfrac{\rho_L\,u^*\,r_w}{\mu_L}$
t = temperature
Δt^* = dimensionless ratio $\dfrac{\Delta t\,\rho\,C_p\,u^*}{q_w}$
u = velocity
u^* = friction velocity at the wall $(\tau_w/\rho_L)^{1/2}$
u^+ = dimensionless ratio u/u^*
y = distance from tube wall
y^+ = dimensionless ratio $\dfrac{\rho_L\,u^*}{\mu_L}\,y$
z = distance measured along tube in direction of liquid flow
ϵ = eddy diffusivity
μ = viscosity
ρ = density
τ = shear stress
ν = molecular diffusivity $= \mu/\rho$

Subscripts

b = buffer layer
H = heat transfer
i = interface
L = liquid
l = laminar layer
M = mass transfer
T = total
t = turbulent layer
w = wall

References

[1] Collier J. G. U.K. Atomic Energy Authority Report A.E.R.E. CE/R 2496, 1958.
[2] Groothuis H and Hendal W. P. *Chem. Engng. Sci.* 1959 **11** 212.
[3] Eluhin N. K. and Visnev I. P. *Oxygin. Moscow* 1959 **12** 5.
[4] Guerrieri S. A. and Talty R. D. *Heat Transfer Symposium, Kentucky, U.S.A., March* 1955.
[5] Coulson J. M. and McNelly M. J. *Trans. Inst. Chem. Engrs.* 1956 **34** 247.
[6] Yoder R. J. and Dodge B. F. *Proceedings General Discussion on Heat Transfer.* p. 15 Institute of Mechanical Engineers and American Institute Mechanical Engineers 1951.
[7] Dengler C. E. Sc.D. Thesis, Massachusetts Institute of Technology 1952.
[8] Dengler C. E. and Addoms J. N. *Chem. Engng. Progr.* (Symposium Series No. 18) 1956 **52** 95.
[9] Lee G. M.Sc. Thesis, Massachusetts Institute of Technology 1952.
[10] Stroebe G. W., Baker E. M. and Badger W. L. *Trans. Amer. Inst. Chem. Engrs.* 1939 **35** 17.
[11] Piret E. L. and Isbin H. S. *Chem. Engng. Progr.* 1954 **50** 305.
[12] Coulson J. M. and Mehta R. R. *Trans. Inst. Chem. Engrs.* 1953 **31** 208.
[13] Kirschbaum E. *Chem. Ing. Tech.* 1954 **25** 26.
[14] Cathro K. J. and Tait R. W. F. *Austral. J. Appl. Sci.* 1957 **8** 279.
[15] Anderson G. H. and Mantzouranis B. G. *Chem. Engng. Sci.* 1960 **12** 109.
[16] Eckert E. R. G. *Introduction to the Transfer of Heat and Mass.* McGraw-Hill, New York 1950.
[17] Mantzouranis B. G. Ph.D. Thesis, University of London 1959.

Chemical Engineering Science, 1961, Vol. 16, pp. 231 to 241. Pergamon Press Ltd., London. Printed in Great Britain.

Non-Newtonian flow past a sphere*

JOHN C. SLATTERY
Department of Chemical Engineering, Northwestern University, Evanston, Illinois.
and
R. BYRON BIRD
Department of Chemical Engineering, University of Wisconsin, Madison, Wisconsin

(*Received* 9 *January* 1961; *in revised form* 24 *February* 1961)

Abstract—Drag coefficients for spheres moving through five aqueous solutions of carboxymethylcellulose (CMC) were measured. With the assumption that the behaviour of these fluids could be approximated by the Ellis model, two dimensionless correlations for the drag coefficient in terms of a modified Reynolds number and two other dimensionless groups were prepared. The Ellis model is easy to use and provides a much better description of non-Newtonian behaviour than the more commonly used Ostwald–de Waele model. The correlation is of value for the prediction of the settling time of a sphere in a non-Newtonian fluid. The results *seem* to indicate that the behaviours of the CMC solutions studied are independent of the third invariant of the rate of deformation tensor.

Résumé—Cet article traite de la mesure des coefficients de résistance pour des sphères en mouvement dans cinq solutions aqueuses de carboxyméthyl cellulose (CMC). En supposant que le comportement de ces fluides suive approximativement le modèle d'ELLIS, l'auteur propose deux relations sans dimension pour le coefficient de résistance au moyen d'un nombre de Reynolds modifié, et deux autres groupes sans dimensions.

Le modèle d'Ellis est commode à utiliser et donne une bien meilleure description du comportement non–Newtonien que le modèle plus courant d'OSTWALD DE WAELE. La relation est utilisable pour prévoir le temps de sédimentation d'une sphère dans un fluide non-Newtonien. Les résultats semblent indiquer que le comportement des solutions CMC étudiées est indépendant du troisième invariant de la vitesse de déformation du tenseur.

Zusammenfassung—Es wurden Reibungsziffern gemessen für die Bewegung von Kugeln in fünf wässrigen Carboxymethylzellulose (CMC)-Lösungen. Unter der Annahme, dass das Verhalten dieser Flüssigkeiten durch das Ellis-Modell angenähert werden kann, wurden zwei dimensionslose Beziehungen für die Reibungsziffer aufgestellt, die eine modifizierte Reynoldszahl und zwei andere dimensionslose Ausdrücke enthalten. Das Ellis-Modell lässt sich leicht anwenden und liefert eine viel bessere Beschreibung nicht-Newton'schen Verhaltens als das allgemeiner benutzte Ostwald-de Wrele-Modell. Die Beziehung ist brauchbar zur Vorhersage der Absitzzeit einer Kugel in einer nicht-Newton'schen Flüssigkeit. Die Ergebnisse *scheinen* zu zeigen, dass das Verhalten der untersuchten CMC-Lösungen unabhängig von der dritten Invarianten des Tensors der Deformationsgeschwindigkeit ist.

1. NON-NEWTONIAN BEHAVIOUR†

THE EQUATIONS describing the steady motion of an arbitrary isothermal continuum are the equations of continuity and motion:

$$(\rho u^i)_{,i} = 0 \tag{1}$$

$$\rho u^j u_{i,j} = -p_{,i} + v^j_{i,j} + \rho f_i \tag{2}$$

In order to describe the flow of fluids one must first specify a relation between the viscous portion of the pressure tensor v_{ij} and the rate of deformation tensor $d_{ij} = \frac{1}{2}(u_{i,j} + u_{j,i})$.

Recently much attention has been drawn to the relation proposed by REINER [2], by RIVLIN [3] and by PRAGER [4]:

†For the most part we are using the notation of TRUESDELL [1], the only notable exception being that we adopt the symbol u_i for velocity components rather than $\dot{x}_i$. Comma notation stands for covariant differentiation and the summation convention is employed throughout.

*Based on Ph.D. thesis of John C. Slattery.

$$\tau_j^i = \mathscr{G}_0^{\mathbf{v}(\mathbf{d})}\,\delta_j^i + \mathscr{G}_1^{\mathbf{v}(\mathbf{d})}\,d_j^i + \mathscr{G}_2^{\mathbf{v}(\mathbf{d})}\,d_k^i\,d_j^k \quad (3)$$

in which the $\mathscr{G}_\gamma^{\mathbf{v}(\mathbf{d})}$ are functions of the invariants of the d-tensor chosen here to be

$$I_{\mathbf{d}} = d_i^i \quad (4)$$

$$II_{\mathbf{d}} = d_j^i\,d_i^j \quad (5)$$

$$III_{\mathbf{d}} = d_j^i\,d_k^j\,d_i^k \quad (6)$$

Equation (3) is the most general relation between τ_j^i and d_j^i provided that space and time derivatives are not allowed and that $\mathbf{v}$ is an isotropic function of $\mathbf{d}$. Omission of time derivatives in equation (3) is tantamount to excluding viscoelastic phenomena from the theoretical development. One further restriction must be placed on the set of equations (1), (2) and (3), namely that for any real flow the net entropy production rate must be positive.

Specifying the functional dependence of the $\mathscr{G}_\gamma^{\mathbf{v}(\mathbf{d})}$ on $I_{\mathbf{d}}$, $II_{\mathbf{d}}$ and $III_{\mathbf{d}}$ and several phenomenological constants corresponds to selecting a "rheological model." Under certain conditions there must in addition be relations among the derivatives of the $\mathscr{G}_\gamma^{\mathbf{v}(\mathbf{d})}$. Specifically, if $\mathbf{v}$ as a function of $\mathbf{d}$ "admits a potential" $\Gamma^{\mathbf{v}(\mathbf{d})}$, then

$$\tau_j^i = \frac{\partial\,\Gamma^{\mathbf{v}(\mathbf{d})}}{\partial\,d_i^j} \quad (7)$$

and then the following relations among the $\mathscr{G}_\gamma^{\mathbf{v}(\mathbf{d})}$ must hold [2]:

$$\frac{\partial\,\mathscr{G}_0^{\mathbf{v}(\mathbf{d})}}{\partial\,II_{\mathbf{d}}} = \tfrac{1}{2}\,\frac{\partial\,\mathscr{G}_1^{\mathbf{v}(\mathbf{d})}}{\partial\,I_{\mathbf{d}}} \quad (8)$$

$$\tfrac{1}{2}\,\frac{\partial\,\mathscr{G}_1^{\mathbf{v}(\mathbf{d})}}{\partial\,III_{\mathbf{d}}} = \tfrac{1}{3}\,\frac{\partial\,\mathscr{G}_2^{\mathbf{v}(\mathbf{d})}}{\partial\,II_{\mathbf{d}}} \quad (9)$$

$$\tfrac{1}{3}\,\frac{\partial\,\mathscr{G}_2^{\mathbf{v}(\mathbf{d})}}{\partial\,I_{\mathbf{d}}} = \frac{\partial\,\mathscr{G}_0^{\mathbf{v}(\mathbf{d})}}{\partial\,III_{\mathbf{d}}} \quad (10)$$

Similar relations have been given by TRUESDELL [1, p. 133] for a different choice of invariants. We now note that:

(a) For incompressible fluids $u^i{}_{,\,i} = 0$ and $I_{\mathbf{d}}$ vanishes identically. For such fluids we may define $\mathscr{G}_0^{\mathbf{v}(\mathbf{d})}$ to be zero (see TRUESDELL [1, p. 228]).

(b) If, in addition, a potential $\Gamma^{\mathbf{v}(\mathbf{d})}$ exists, and if $\mathscr{G}_2^{\mathbf{v}(\mathbf{d})} = 0$, equation (9) states that $\mathscr{G}_1^{\mathbf{v}(\mathbf{d})}$ depends only on $II_{\mathbf{d}}$ (and *not* on $III_{\mathbf{d}}$).

To date many experimental data have been interpreted in terms of equation (3) with $\mathscr{G}_0^{\mathbf{v}(\mathbf{d})} = \mathscr{G}_2^{\mathbf{v}(\mathbf{d})} = 0$ and $\mathscr{G}_1^{\mathbf{v}(\mathbf{d})}$ a function of $II_{\mathbf{d}}$ alone. (REINER has called these "generalized Newtonian fluids." In TRUESDELL's review article they are called "quasi-linear"). OLDROYD [5, p. 673–674] has cast doubt upon the usefulness of equation (3) by stating that "it has not yet been established that any real liquids behave approximately in this way, with a non-vanishing normal stress coefficient (i.e. $\mathscr{G}_2^{\mathbf{v}(\mathbf{d})}$) and without appreciable elasticity." Nothing is known quantitatively about $\mathscr{G}_2^{\mathbf{v}(\mathbf{d})}$ or about the importance of $III_{\mathbf{d}}$ in $\mathscr{G}_1^{\mathbf{v}(\mathbf{d})}$. It had been hoped that study of the flows non-Newtonian fluids past spheres might give information about these quantities.

In the ensuing discussion we will have occasion to use two empirical models. The first is the widely used but not too realistic Ostwald– de Waele (or "power law") model containing two parameters m and n:

$$\tau_j^i = \left[2m\,(2\,II_{\mathbf{d}})^{(n-1)/2}\right] d_j^i \quad (11)$$

wherein $n < 1$ represents pseudoplastic, $n = 1$ Newtonian and $n > 1$ dilatant fluids. The second is a three-parameter model (ϕ_0, ϕ_1 and α) which has been used by ELLIS [6, p. 246] and more recently by GEE and LYON [7]:

$$d_j^i = \left[\tfrac{1}{2}\,\phi_0 + \tfrac{1}{2}\,\phi_1\,(\tfrac{1}{2}\,II_\tau)^{(\alpha-1)/2}\right]\tau_j^i \quad (12)$$

GEE and LYON have reported that this model is useful for describing the flow of plastic melts, and the experiments of FREDRICKSON [8] and SLATTERY [9] seem to indicate that this model is adequate to describe the steady-state tube flow of carboxymethylcellulose (CMC) solutions. It can be shown using the inversion relations given by TRUESDELL [1, pp. 133–4] that equation (12) reduces to (11) when

$$\phi_0 = 0, \quad m = \left[\frac{1}{\phi_1}\right]^n, \quad n = \frac{1}{\alpha} \quad (13)$$

Note that $\mathbf{d}$ as a function of $\mathbf{v}$ given by equation (12) admits the potential

$$\Gamma^{\mathbf{d}(\tau)} = \phi_0\left[\tfrac{1}{4}\,II_\tau\right] + \phi_1\left[\frac{1}{\alpha+1}\right]\left[\tfrac{1}{2}\,II_\tau\right]^{(\alpha+1)/2} \quad (14)$$

Hence for this model having $\mathscr{G}_2^{\mathbf{d}(\tau)} = 0$ is con-

sistent with having $\mathscr{I}_1^{d\,(v)}$ depend on II_v and *not* on III_v. The experimental results described presently seem to indicate that the flow of CMC solutions *in tubes* and *around spheres* can be fairly well described by equation (12).

2. Previous Work on Flow around Spheres

The following brief tabulation gives references to the sources of literature reviews and mentions specifically some recent works of particular interest in connexion with our work:

Newtonian (theoretical)

(a) Stokes' [10] initial derivation for steady, creeping flow led to the relation $F = 6\pi\mu UR$ which is valid for $Re < 0{\cdot}1$.

(b) Oseen [11] and Goldstein [12] extended Stokes' law taking the inertial terms (i.e. $\rho u^j u_{i,j}$) partially into account; their results are good for $Re < 2$.

(c) Kawaguti [13] made a similar extension to $Re = 50$; see also Proudman and Pearson [14] and Jensen [15].

(d) Hughes and Gilliland [16] surveyed unsteady-state behaviour.

(e) Happel and Byrne [17] treated movement of a sphere within a cylindrical boundary.

(f) Falkenhagen [18] has summarized many other aspects of the theory.

Newtonian (experimental)

(a) Schiller [19] and Muttray [20] summarized data in absence of wall effects.

(b) McNown and Newlin [21] presented results showing effects of a cylindrical container for $10^{-1} < Re < 10^5$.

Non-Newtonian (theoretical)

(a) Tomita [22] presented an expression for the drag force* on a sphere moving very slowly through a fluid characterized by equation (11). Tomita obtained his result by arbitrarily assuming an expression for the stream function which satisfied certain boundary conditions; the constants in this expression were not evaluated using the variational principle described in the paper.

(b) The fluid behaviour model used by Tyabin [23] was not of the form required by equation [3].

(c) Jain [24] examined the conditions under which a symmetric velocity distribution would be obtained for a fluid with

$$\mathscr{I}_1^{v\,(d)} = 2\mu, \quad \mathscr{I}_2^{v\,(d)} = \text{constant} \tag{15}$$

His method was to introduce a suitable artificial external force so that the resulting equations could be integrated; he did not neglect the inertial terms. Having assumed the velocity distribution to be symmetric and the fluid to be subjected to a suitable external force, he concluded that the drag force was not affected by the magnitude of $\mathscr{I}_2^{v\,(d)}$.

(d) Bizzell [25] analysed boundary-layer flow of an Ostwald-de Waele fluid past a sphere and calculated points of separation.

(e) Ziegenhagen, *et al.* [26] have used a variational method to obtain deviations from Stokes' Law for a truncated power series non-Newtonian model; inasmuch as the latter model is inadequate to describe the CMC solutions discussed in this paper, their results cannot be compared with ours.

Non-Newtonian (experimental)

Chase [27], Hirata and Kubo [28] and Sheppard [29] have reported studies on the motion of spheres in non-Newtonian fluids. No attempt was made by these investigators to correlate the flow in this geometry with that in a tube viscometer or rotational viscometer in terms of model parameters.

3. New Experimental Data on Flow of CMC Solutions around Spheres

Two expressions may be written for the force F which acts on a sphere falling at a terminal velocity U in a quiescent fluid of infinite extent. The first expression is the definition of the dimensionless "friction factor" or "drag coefficient" f; the second is the statement of Newton's second law written for the sphere

$$F = \left[\tfrac{1}{2}\rho U^2\right]\left[\pi R^2\right] f \tag{16}$$

$$F = \tfrac{1}{6}\pi D^3 g\,(\rho_{\text{sph.}} - \rho) \tag{17}$$

Elimination of F then gives

$$f = \frac{4}{3}\frac{gD}{U^2}\left[\frac{\rho_{\text{sph.}} - \rho}{\rho}\right] \tag{18}$$

which is the relation used to obtain experimental f values from measurement of the following:

Chem. Engng. Sci. Vol. 16, Nos. 3 and 4, December, 1961.

*One of the authors (J.C.S.) wishes to thank Professor Tomita for his correspondence confirming that Tomita's [22] equation (29) should read

$$F(n) = \frac{n}{n^2 - n + 1} A + \ldots$$

where

$$A = \tfrac{2}{3}\left\{1 - \frac{1}{2n}\left[1 - \frac{(n-1)^2(n+1)}{12}\right] - \frac{(n-1)(n+1)}{10n^2}\left[1 - \frac{(n-1)^2}{6} + \frac{(n-1)^4}{144}\right]\right\}$$

Table 1. *Information regarding* CMC *solution at* 85·0 °F *and experiments performed with them*

Line	*Item*	1	2	3	4	5
1	Solution number	1	2	3	4	5
2	Type of solution*	Low	Low	Medium	Medium	High
3	% CMC by wt.	5·262	4·166	2·565	1·524	0·603
4	Density (g cm^{-3})	1·0188	1·0141	1·0070	1·0025	0·9986
5	Estimated range of $[\frac{1}{2}\Pi_\tau]^{1/2}_{\text{max. sphere}}$ encountered in falling-sphere expts. [equations (28) and (30)] (dyn cm^{-2})	7–1060	8–390	10–705	2–250	3–365
6	Ellis parameter α	1·337	1·170	1·412	1·185	1·707
7	Ellis parameters† ϕ_0 (cm^2 sec^{-1} dyn^{-1})	0·0000	0·1377	0·03830	0·4210	0·2891
8	Ellis parameter† ϕ_1 (cm$^{2\alpha}$ sec^{-1} dyn$^{-\alpha}$)	0·05211	0·3211	0·01810	0·2724	0·02799
9	No. of data points used to establish Ellis parameters	21	22	34	24	26
10	Av. % error‡ in $4Q/\pi R^3$ from equation (32)	2·3	1·6	3·7	5·6	4·9
11	Range $[\frac{1}{2}\Pi_\tau]^{1/2}_{\text{tube wall}} = R\Delta p/2L$ dyn cm^{-2}	8–1010	8–440	17–720	6–300	8–270
12	Av. % error‡ in f from equation (37)	19·4	3·8	13·5	2·4	5·9
13	No. of points compared in line 12	30	7	37	5	24
14	Av. % error‡ in f from Fig. 4	14·5	4·4	6·8	17·2	5·9
15	No. of points compared in line 14	32	49	30	39	41
16	Range of U/D in falling sphere experiments	0·09–45	0·94–81	0·14–40	0·37–93	0·16–98

*Hercules CMC Type 70 C (high viscosity) Lot No. 12708.
Hercules CMC Type 70 premium (medium viscosity) Lot No. 11796.
Hercules CMC Type 70 premium (low viscosity) Lot No. 10550.

†In the tabulation of Ellis-model parameters previously reported [9, p. 79a] column headings ϕ_0 and ϕ_1, should be interchanged.

‡Average of the absolute values of the error [9].

Fluid density ρ

The densities of the five CMC solutions studied are given in Table 1, line 4.

Sphere diameter D

Two sets of spheres were used – steel bearing balls (0·025 in. $< D <$ 0·5 in.) and Christmas tree ornaments, the necks of which had been removed (D = 0·5).

Sphere density $\rho_{\text{sph.}}$

The density of the ball bearings was approximately 7·8 gm cm^{-3}; the density of the glass spheres was varied from approximately 1·0 to 4·9 gm cm^{-3} by filling each with varying amounts of lead shot, a rigid polyurethane foam-in-place liquid resin and paraffin.

Terminal velocity U

Each fluid was studied in three cylindrical containers 4, 5 and 6 in. in diameter and 30 in. high. Approximately 14 in. were allowed between the top of the tube and the measuring section, and 6 in. following the measuring section to the bottom of the tube. For spheres moving

Table 2. *Comparison of impulse counter to frame count on the basis of precision in determination of terminal velocities*

		Average % velocity deviation	*Number of points*
Timing accomplished both by impulse counter and by frame count	Impulse counter	3·0	163
	Frame count	2.0	
Timing done by impulse counter alone		1·8	67
Timing done by frame count alone		0·7	5

slowly a stop watch was used for timing. For spheres moving more rapidly the descent was photographed with an electrically driven 16 mm movie camera. In the latter case fall times could be determined either by counting frames or by noting from the film the readings of a device counting impulses from 60 cycles alternating current; Table 2 compares these two methods. The measuring section itself was composed of three subsections of approximately 6, 11 and 6 cm respectively. From the film average velocities over each of these shorter distances as well as the average velocity over the entire 23 cm were determined. Table 2 gives the maximum per cent deviation of the total average velocity from any one of the three velocities averaged over a portion of the 23 cm; as errors of this magnitude could be introduced in timing and in measuring the fall distance it may be concluded that top and bottom effects were negligible. A comparison of the results for the three cylinders suggested that the effect of the cylindrical boundary could be neglected also.

By far the least accurate quantity entering into the calculation for f is the terminal velocity U. The figure of 2 per cent from Table 2 is believed to represent a conservative estimate of the errors in the terminal velocity for rapidly moving spheres (the frame count velocity was used whenever possible); the error would be much less than one per cent for slow-moving spheres. With these assumptions the error in f would range from about 4 per cent for "fast" spheres to less than 1 per cent for "slow" spheres.

A complete summary of the raw experimental data, and further details are to be found elsewhere [9].

4. New Experimental Data on Flow of CMC Solutions through Capillary Tubes

Two glass viscometers were constructed according to a design sketched in Fig. 1; important dimensions are given in Table 3. The design was a modification of an absolute viscometer used by many workers for Newtonian fluids [30, p. 51]. In operation the viscometers were submerged in a constant temperature bath to a line just below A and B in Fig. 1. Lines from a vacuum system were connected to the two three-way stopcocks, A and B, such that a partial vacuum was drawn on one side while the other side was opened to the atmosphere. By means of a bleed valve pressure differences ranging from 4 in. of water to 25 in. of mercury could be obtained. To operate, the fluid level in the left-hand member was drawn above G, the vacuum connexions reversed so as to cause flow from left to right and the time required for the meniscus fall from G to G′ measured. From this time and the known volume between G and G′ the volume flow rate was calculated. At the end of the run the pressure connexions at A and B could be reversed by means of the three-way stop-cocks, the pressure difference adjusted to a new value and another determination made with the fluid

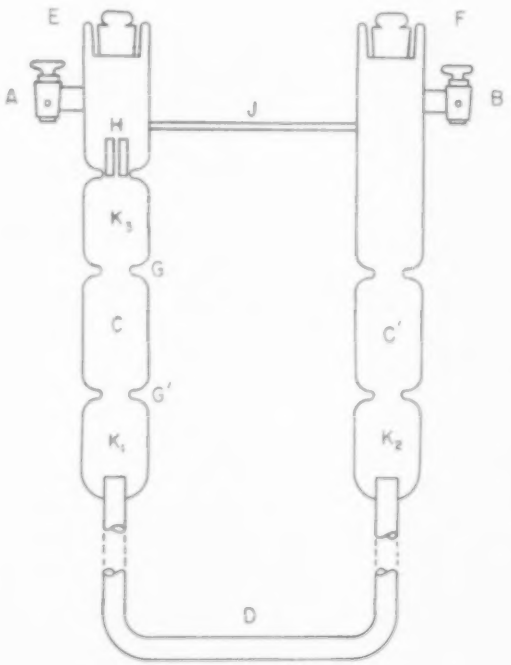

Fig. 1. Capillary-tube viscometer.

flowing in the opposite direction. Runs were 10 min or more apart to allow disturbances in the fluid to be damped out and to allow time for drainage.

Any viscometer used for non-Newtonian fluids should be capable of analysis without resorting to calibrations with Newtonian fluids. From macroscopic mechanical energy balance written for flow between a point 1 in K_1 and a point 2 in K_2 chosen such that the potential energy at point (1) equals that at (2) we obtain [31, p. 211].

$$[p_1 - p_2]Q = E_v + \frac{dK}{dt} + \frac{1}{2}\rho Q \frac{(v^3)_{\text{av.,2}} - (v^3)_{\text{av.,1}}}{v_{\text{av.}}} \quad (19)$$

If we assume that the energy lost due to viscous dissipation outside the capillary tube is negligible compared with that in the tube itself, and if we assume fully developed velocity profiles almost everywhere within the tube,

$$E_v = -2\pi L \int_0^R \tau_{rz}\left[\frac{d u_z}{dr}\right] r\, dr \quad (20)$$

This integral may be evaluated by comparing it with the results of the treatment of RABINOWITSCH [31, p. 68] to obtain

$$E_v = \Delta p\, Q \quad (21)$$

where Δp is the pressure drop over tube D in Fig. 1. Since the flow area of K_1 was made nearly identical with that of K_2,

$$(v^3)_{\text{av.,2}} = (v^3)_{\text{av.,1}} \quad (22)$$

Then for quasi steady-state behaviour

$$\Delta p = p_1 - p_2 \quad (23)$$

But this last assumption means that the pressure difference $(p_1 - p_2)$ is not exactly that read on the manometer $(p_{01} - p_{02})$, for the hydrostatic head changes during the run. The former has been estimated in terms of the latter for Newtonian fluids as [30, p. 73]

$$\Delta p = \frac{2\rho g h}{\ln\left[(p_{01} - p_{02} + \rho g h)/(p_{01} - p_{02} - \rho g h)\right]} \quad (24)$$

A similar calculation for fluids following equation (11) has been carried out [9] to give

$$\Delta p = \frac{[n-1]\left[(p_{01} - p_{02} - \rho g h)^{1/n} - (p_{01} - p_{02} + \rho g h)^{1/n}\right]}{\left[(p_{01} - p_{02} - \rho g h)^{(n-1)/n} - (p_{01} - p_{02} + \rho g h)^{(n-1)/n}\right]} \quad (25)$$

As the parameter n could not be determined until after the data were analysed equation (24) was used to correct the observed pressure difference. The use of equation (24) was further justified since the correction was important only at low stresses, where the fluids approached Newtonian behaviour.

Results from the two viscometers described are presented in Fig. 2. Every effort was made to measure the quantities $R\Delta p/2L$ and $4Q/\pi R^3$ with less than 1 per cent error. Differences obtained on reproducing measurements were less than 1 per cent except at very high and at very low values of the stress at the wall, $R\Delta p/2L$. At the highest stresses errors in measuring short time intervals could account for the differences which ranged as high as 6 per cent. At the lowest

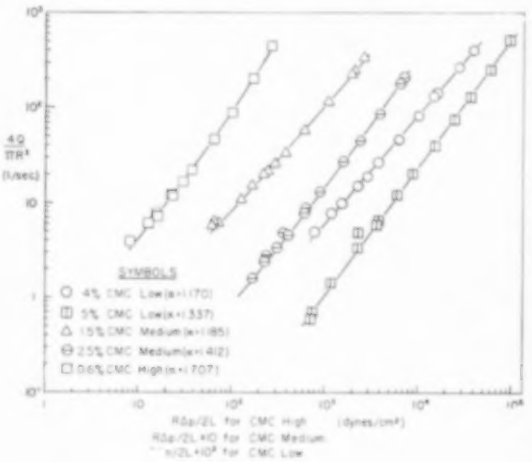

FIG. 2. Comparison of data from capillary-tube viscometers with equation (32).

stresses variations in the small pressure differential over the long period of time required for a run probably were the cause for differences of up to 5 per cent. End effects were neglected in analysing these data; however, they were estimated to be very small. The highest flow rate occurred with the 5 per cent CMC low solution (run 12) for which

$$[\text{Re}_1]_{\text{tube}} = 2R\rho^n \phi_1 \left[\frac{Q}{\pi R^2}\right]^{(2n-1)} = 0.89$$

The "entrance length" for a Newtonian fluid is given by [31, p. 47]

$$L_e = 0.070\, R\, \text{Re}$$

where

$$\text{Re} = \frac{2R\rho}{\mu}\left[\frac{Q}{\pi R^2}\right]$$

Table 3. Dimensions if viscometers (symbols refer to Fig. 1)

	Viscometer no. 1	*Viscometer no. 2*
Length of tube D (cm)	128·27	42·807
Measured average diameter of tube D (cm)	0·6385	0·2104
Factory specified diameter of tube D (cm)	0·6215–0·6469	0·2096–0·2111
Ratio of tube length to measured diameter	200·9	203·5
Volume of C (between lines G and G′) (cm³)	10·271	9·6949
Height (h) of C (between lines G and G′) (cm)	9·0091	8·8999
Approximate volumes of vessels K (cm³)	10	10

VOL. 16 1962

If as an approximation we apply the above for the non-Newtonian problem we find

$$L_e = 0{\cdot}062\ R$$

which is a small fraction of the total length, 407 R (see Table 3).

For a complete tabulation of results and further details see Ref. [9].

5. Behaviour of CMC Solutions

Simple models such as equations (11) and (12) should not be expected to describe the behaviour of a fluid over all ranges of stress. Since the model constants are determined by curve fitting it is important to know the maximum and minimum values of stress occurring in the geometry to be studied. According to Stokes' treatment for a sphere moving slowly through a Newtonian fluid the individual components of stress range from zero at an infinite distance from the sphere to a maximum at the sphere surface, 90° from the direction of flow and

$$\left[\tfrac{1}{2}\,\Pi_v\right]^{1/2}_{\text{max. sphere}} = \frac{3\,\mu\,U}{D} \tag{26}$$

Also from Stokes' development

$$f = \frac{24}{\mathrm{Re}}, \quad \mathrm{Re} = \frac{D\,U\,\rho}{\mu}, \quad \text{for Re} < 0{\cdot}1 \tag{27}$$

Equations (26) and (27) may be combined to obtain

$$\left[\tfrac{1}{2}\,\Pi_v\right]^{1/2}_{\text{max. sphere}} = \frac{U^2\,\rho\,f}{8} \quad \text{for Re} < 0{\cdot}1 \tag{28}$$

From the experimentally determined plot of f vs. Re for Newtonian fluids an empirical relation for f has been suggested [31, p. 194] which is valid for $2 < \mathrm{Re} < 5 \times 10^2$:

$$f = \frac{18{\cdot}5}{\mathrm{Re}^{0{\cdot}6}} \tag{29}$$

Equations (26) and (29) may be combined to obtain the approximate relation

$$\left[\tfrac{1}{2}\,\Pi_v\right]^{1/2}_{\text{max. sphere}} = 3\,U^2\,\rho\left[\frac{f}{18{\cdot}5}\right]^{1{\cdot}067}$$

$$\text{for } 2 < \mathrm{Re} < 5 \times 10^2 \tag{30}$$

For lack of any better criterion the range of $\left[\tfrac{1}{2}\,\Pi_v\right]^{1/2}_{\text{tube wall}} = R\Delta p/2L$ to which an empirical model was fitted was planned to coincide approximately with the ranges of $\left[\tfrac{1}{2}\,\Pi_v\right]^{1/2}_{\text{max. sphere}}$ calculated from equations (28) and (30). The experimental range of $\left[\tfrac{1}{2}\,\Pi_v\right]^{1/2}_{\text{tube wall}}$ and the calculated range of $\left[\tfrac{1}{2}\,\Pi_v\right]^{1/2}_{\text{max. sphere}}$ are given in Table 1, lines 11 and 5 respectively.

For flow through a tube of fluid described by equation (11) (Ostwald-de Waele model) the equation of motion gives [6]

$$\frac{4Q}{\pi\,\mathrm{R}^3} = \frac{4n}{3n+1}\left[\frac{R\,\Delta p}{2Lm}\right]^{1/n} \tag{31}$$

Fig. 2 shows that this model approximates very well the behaviour of the 5 per cent CMC low solution. The other four solutions in Fig. 2 appear to be described by this model at high stresses, while they tend toward Newtonian behaviour at low stresses. An obvious choice for one model which will represent the behaviour of all five solutions is equation (12), (Ellis model); for flow through a tube

$$\frac{4Q}{\pi R^3} = \phi_0 \frac{R\,\Delta p}{2L} + \phi_1 \left[\frac{4}{\alpha + 3}\right]\left[\frac{R\,\Delta p}{2L}\right]^{\alpha} \quad (32)$$

Equation (32) describes power-model behaviour with a Newtonian correction important only at low stresses. On this basis, α was taken as the slope of the log $[4Q/\pi R^3]$ vs. log $[R\Delta p/2L]$ curve at high stresses (large values of $[R\Delta p/2L]$); the two remaining parameters were evaluated by making a least squares fit of equation (32) to the data from the two glass viscometers. Constants determined in this manner are presented in Table 1, lines 6 through 8; the corresponding curves are drawn through the data in Fig. 2. The average error in predicting the experimental data with equation (32) is also given in Table 1, lines 9 and 10.

It should be noted that neither the Ostwald-de Waele model (11) nor the Ellis model (12) specifically account for viscoelastic effects. The solutions used were not tested for viscoelastic behaviour.

6. Correlation for Friction Factors for Flow of CMC Solutions around Spheres

By a dimensional analysis of the equations of continuity and motion and the pertinent boundary conditions, it may be shown [9; 31, p. 107] that for a fluid described by equation (12) the friction factor may be expressed thus:

$$f = f(\mathrm{Re}_1,\ B,\ \alpha) \quad (33)$$

in which α is the dimensionless parameter in equation (12), Re_1 is a Reynolds number referred to ϕ_1:

$$\mathrm{Re}_1 = D^{\alpha}U^{(2\alpha-1)}\rho^{\alpha}\phi_1 \quad (34)$$

and B is a ratio giving the "relative strengths" of ϕ_0 and ϕ_1:

$$B = \frac{\phi_0^{2\alpha-1}\rho^{\alpha-1}D^{2\alpha-1}}{\phi_1} \quad (35)$$

To date no theoretical derivations for f as a function of Re_1, B and α have been made.

The experimental data of Slattery described in Section 3 have been used to obtain experimental correlations. These correlations are expressed not in terms of f but rather the quantity f^* defined by

$$\begin{aligned}\log_{10} f^* = &-2{\cdot}1013\,(\alpha - 1)\\ &-2{\cdot}0303\,(\alpha - 1)^2\\ &+\log_{10} f\left[1 + 1{\cdot}0342\,(\alpha - 1)\right.\\ &+3{\cdot}5017\,(\alpha - 1)\left(\frac{1}{B+1}\right)\\ &-3{\cdot}7789\,(\alpha - 1)\left(\frac{1}{B+1}\right)^2\\ &\left.+1{\cdot}0502\,(\alpha - 1)^2\right] \end{aligned} \quad (36)$$

Two correlations are available:

1. For $\mathrm{Re}_1 < 0{\cdot}1$ the following simple relation holds:

$$f^* = \frac{24}{\mathrm{Re}_1} \quad (37)$$

When $\alpha = 1$ and $B = 0$ this simplifies to the usual Stokes' law. Comparison of equation (37) with experimental data is given in Fig. 3.

2. For $\mathrm{Re}_1 > 0{\cdot}1$ Fig. 4 gives f^* vs. Re_1 for several values of α. The curve $\alpha = 1$ corresponds to the usual Newtonian curve [20, p. 304]. Com-

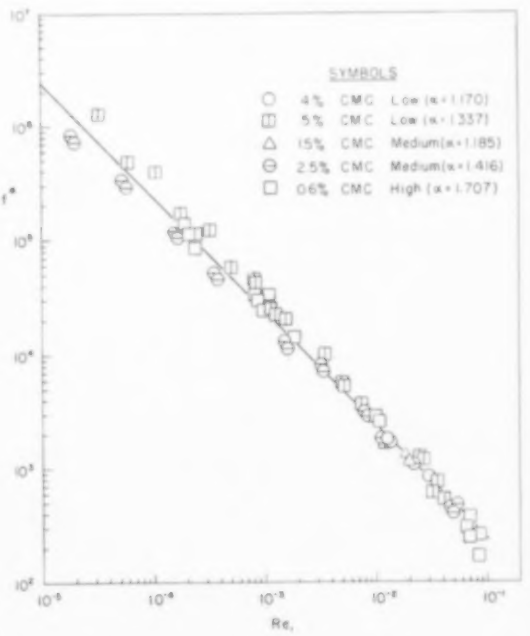

Fig. 3. Comparison of experimental values of f^* with equation (37).

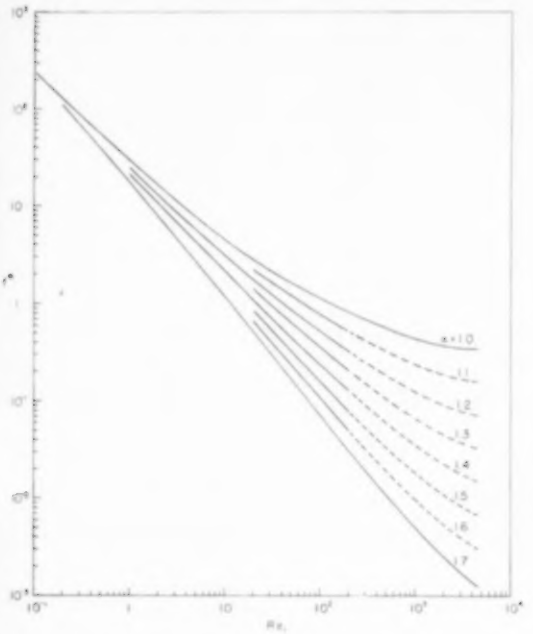

FIG. 4. Graphical correlation of f^*.

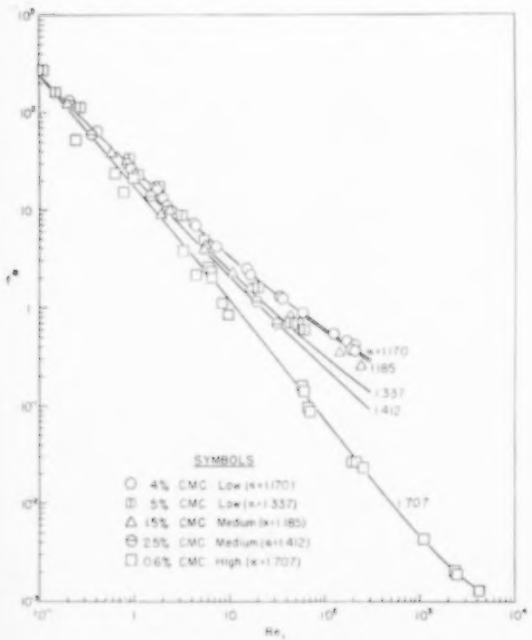

FIG. 5. Comparison of experimental values of f^* with Fig. 4.

parison of Fig. 4 with experimental data is given in Fig. 5.

A more detailed appraisal of the correlations with the data points has been given elsewhere [9]; a summary is given in Table 1, lines 12–15.

For a total of 294 data points the average error in the correlation is slightly more than 10 per cent. This error may be attributed to the following: (1) equation (12) does not describe the volume rate of flow in tubes exactly, as shown in lines 9 and 10 of Table 1; (2) the capillary viscometer used may not be as accurate as some other designs [9, p. 71]; (3) Table 2 indicates that, on the average, failure to reach the terminal velocity and errors in timing accounted for errors of 2 per cent or less in the measured terminal velocity, or errors of 4 per cent or less in the measured friction factor f.

7. Conclusions

1. Equation (37) and Fig. 4 are the only available means for estimating the friction factor for spheres falling in quiescent non-Newtonian fluids whose behaviour can be described by the three-parameter Ellis model, equation (12).

2. Equation (37) and Fig. 4 may be used to estimate friction factors for power-law fluids described by equation (11) by setting $B = 0$, $\alpha = 1/n$ and $\phi_1 = (1/m)^{1/n}$.

3. The use of three-parameter non-Newtonian models for purposes of obtaining experimental correlations has been illustrated for the first time. It is suggested that such an approach will be fruitful for establishing design procedures for flow systems with complex geometries and for heat transfer in such systems.

4. The three-parameter model in equation (37), while still easy to use, provides a better description of the steady-state non-Newtonian behaviour of CMC solutions than does the two-parameter power-law model.

5. We are tempted to conclude *provisionally* that the effects of III_v are small. For creeping flow of a Newtonian fluid it is easy to show that

$$III_v = \left[\frac{\mu U}{D}\right]^3 X \left[\text{function of } \frac{r}{R} \text{ and } \cos\theta\right] \quad (38)$$

In the absence of a better approximation, equation

(38) may be used to suggest the order of magnitude of variations in III_v. As is shown in line 16 of Table 1 the ratio U/D was varied over a very wide range of values. The fact that a reasonably good correlation was obtained without the incorporation of III_v leads us to suspect that the contribution of III_v is small. Additional experiments in simpler geometries will be needed to get further information about the role of III_v, the existence of $\mathscr{G}_2^{d(v)}$, and the importance of viscoelastic effects.

6. Additional experimental work and additional analytical solutions for more sophisticated models (including viscoelasticity) are needed. The present work should be regarded as a first attempt to understand non-Newtonian flow around spheres.

Acknowledgments—The authors wish to thank W. E. STEWART of the University of Wisconsin for his suggestion to check the effect of III_v, E. E. MILLER of the University of Wisconsin for advice concerning photographing the descent of the spheres, L. H. DONCHIN for preparing the graphs and G. G. COTTRELL for assistance with numerical calculations. One of the authors (J.C.S.) is indebted to the Wisconsin Alumni Research Foundation (1956–57, 1958–59) and to the Procter and Gamble Company (1957–58) for financial support of this work. The authors also acknowledge the suggestions for improving the presentation in this manuscript offered by D. W. MCEACHERN, D. M. METER and R. TURIAN of the University of Wisconsin and by A. G. FREDRICKSON of the University of Minnesota.

NOTATION

B = dimensionless group defined by equation (35)

d_{ij} = rate of deformation tensor

D = diameter of sphere

E_v = rate at which energy is dissipated by viscous forces

f = drag coefficient

f^* = modified drag coefficient defined by equation (36)

F = drag force

$\mathscr{G}_\gamma^{v(d)}$ = coefficient in equation (3)

g = acceleration of gravity

h = distance between lines G and G′ (Fig. 1)

K = total kinetic energy in system

L_e = entrance length in tube flow

m, n = parameters of Ostwald–de Waele model, equation (11)

p = pressure

Δp = pressure drop across capillary tube

$(p_{01} - p_{02})$ = pressure difference between A and B in Fig. 1

Q = volume flow rate through capillary tube

r = spherical co-ordinate

R = radius of capillary tube

Re = Reynolds number, $DU\rho/\mu$

Re_1 = modified Reynolds number defined by equation (34)

t = time

U = terminal velocity of sphere

u_j = component of velocity vector

v = component of velocity in direction of flow in capillary-tube viscometer

v_{ij} = viscous portion of pressure tensor

α, ϕ_0, ϕ_1 = parameters of Ellis model, equation (12)

$\Gamma^{v(d)}$ = potential for v_j^i, equation (7)

μ = Newtonian viscosity

ρ = density

I_d, I_v; II_d, II_v; III_d, III_v = Invariants of the viscous portion of the pressure tensor and of the rate of deformation tensor defined by (4), (5) and (6)

REFERENCES

[1] TRUESDELL C. *J. Rat. Mech. Anal.* 1952 **1** 125.
[2] REINER M. *Amer. J. Math.* 1945 **67** 350.
[3] RIVLIN R. S. *Nature, Lond.* 1947 **160** 611.
[4] PRAGER W. *J. Appl. Phys.* 1945 **16** 837.
[5] OLDROYD J. G. *Rheology Theory and Practice* (Edited by EIRICH F. R.) Vol. 1. Academic Press, New York 1956.
[6] REINER M. *Deformation, Strain and Flow.* Interscience, New York 1960.
[7] GEE R. E. and LYON J. B. *Industr. Engng. Chem.* 1957 **49** 956.
[8] FREDRICKSON A. G. Ph.D. Thesis. University of Wisconsin 1959.
[9] SLATTERY J. C. Ph.D. Thesis. University of Wisconsin 1959.
[10] STOKES G. G. *Mathematical and Physical Papers.* Vol. 3 p. 55. Cambridge University Press 1901.
[11] OSEEN C. W. *Ark. Mat. Astr. Fys.* 1910 **6** Nr. 29. As Quoted by GOLDSTEIN [12].
[12] GOLDSTEIN S. *Proc. Roy. Soc.* 1929 A **123** 225.
[13] KAWAGUTI M. *J. Phys Soc., Japan* 1955 **10** 694.
[14] PROUDMAN I. and PEARSON J. R. *J. Fluid Mech.* 1957 **2** 237.

[15] Jensen V. G. *Proc. Roy. Soc.* 1959 **A 249** 346.
[16] Hughes R. R. and Gilliland E. R. *Chem. Engng. Progr* 1952 **48** 497.
[17] Happel J. and Byrne B. J. *Industr. Engng. Chem.* 1954 **46** 1181.
[18] Falkenhagen H. *Handbuch der Experimentalphysik.* Band 4, 1. Teil, S. 47. Akademische Verlagsgesellschaft, Leipzig 1931.
[19] Schiller L. *Handbuch der Experimentalphysik.* Band 4., 2. Teil, S. 339. Akademische Verlagsgesellschaft, Leipzig 1932.
[20] Muttray H. *Handbuch der Experimentalphysik.* Band 4, 2. Teil, S. 235. Akademische Verlagsgesellschaft, Leipzig 1932.
[21] McNown J. S. and Newlin J. T. *Proc. 1st U.S. Nat. Congr. Appl. Mech.* Chicago, 1951 p. 801. American Society of Mechanical Engineers, New York 1952.
[22] Tomita Y. *Bull. J. Soc. Mech. Engrs.* 1959 **2** 469.
[23] Tyabin N. V. *Dokl. Akad. Nauk SSSR* (N.S.) 1953 **88** 57.
[24] Jain M. K. *Z.A.M.M.* 1955 **35** 12.
[25] Bizzell, G. D. M.S. Thesis. Northwestern University 1960.
[26] Ziegenhagen A. J., Bird R. B. and Johnson M. W. Jr. *Trans. Soc. Rheol.* 1961 **5** 47.
[27] Chase G. D. Ph.D. Thesis. Temple University 1955.
[28] Hirata F. and Kubo K. *J. Soc. Chem. Ind., Japan* 1934 **37** 11B.
[29] Sheppard S. E. *Industr. Engng. Chem.* 1917 **9** 523.
[30] Barr G. *A Monograph of Viscometry.* Oxford University Press 1931.
[31] Bird R. B., Stewart W. E. and Lightfoot E. N. *Transport Phenomena.* John Wiley, New York 1960.

Chemical Engineering Science, 1961, Vol. 16, pp. 242 to 251. Pergamon Press Ltd., London. Printed in Great Britain.

The slow motion of a sphere through a viscous fluid towards a plane surface

HOWARD BRENNER
Department of Chemical Engineering, New York University, New York 53, New York

(*Received* 31 *January* 1961)

Abstract—Bipolar co-ordinates are employed to obtain "exact" solutions of the equations of slow, viscous flow for the steady motion of a solid sphere towards or away from a plane surface of infinite extent. Two cases are considered: (i) the plane surface is rigid and fluid adheres to its surface; (ii) the plane is a free surface on which the tangential stresses vanish. Deformation of the surface in the latter case is neglected. Numerical results are provided for the corrections to Stokes' law necessitated by the presence of the plane boundary at a finite distance from the particle. Application of the results to end-effect correlations in the falling-ball viscometer are discussed.

Résumé—Des coordonnées bipolaires sont utilisées pour obtenir des solutions "exactes" des équations relatives à l'écoulement lent et visqueux d'une sphère solide en mouvement uniforme au voisinage ou à distance d'une surface plane infinie. Deux cas sont considérés: (I) La surface plane est rigide et le fluide y adhère; (II) elle est libre et les forces tangentielles disparaissent. On néglige dans ce dernier cas la déformation de la surface. Des résultats numériques sont donnés pour les corrections de la loi de Stokes nécessitées par la présence d'un plan de séparation à une distance finie de la particule. Suit une discussion de l'application des résultats aux relations donnant l'effect des extrémités dans les viscosimètres à chute de bille.

Zusammenfassung—Mit Polarkoordinaten werden "exakte" Lösengun der Gleichungen für langsames viskoses Fliessen für die stationäre Bewegung einer festen Kugel gegen eine ebene, unendlich grosse Oberfläche, oder von ihr hinweg, erhalten. Es werden zwei Fälle betrachtet: (I) Die ebene Oberfläche ist fest und mit Flüssigkeit behaftet; (II) Es liegt eine freie Oberfläche vor, in der die Tangentialspannungen verschwinden. In diesem Fall wird die Verformung der Oberfläche vernachlässigy. Numerische Ergebnisse werden angegeben zur Korrektur des Stokes'schen Gesetzes, die infolge der Gegenwart einer ebenen Grenzfläche in endlicher Entfernung von dem Teilchen notwendig ist. Die Anwendung der Ergebnisse zur Korrektur von Endeffekten im Kugelviskosimeter wird diskutiert.

INTRODUCTION

STOKES' law, for the resistance of a sphere moving slowly through a viscous liquid, finds wide application in the interpretation of low Reynolds number sedimentation phenomena. This well-known relation applies only to fluid media which extend to infinity in all directions. In most real situations, however, the fluid is externally bounded by rigid walls and/or a free surface. The presence of these boundaries at finite distances from the particle necessitate corrections to Stokes' resistance formula.

The case in which a sphere falls along the axis of an infinitely long circular cylinder has been elaborated in great detail by many authors, most notably by HABERMAN and SAYRE [1]. Investigations of this nature emphasize corrections arising from the fact that the fluid is *laterally* bounded. They do not, however, provide insight into the equally interesting case where the fluid is bounded *longitudinally*, that is, perpendicular to the direction of motion of the particle.

In this context we propose to investigate the motion of a spherical particle towards or away from a single plane surface in an otherwise unlimited fluid. Two distinct cases are of interest: (i) the plane surface is rigid as, for example, when it constitutes the bottom of the container in which the particle falls; (ii) the plane is a free surface as, for example, when it corresponds to the interface between a liquid and the atmosphere.

The rigid wall case has been treated by LORENTZ

[2] for the situation in which the sphere radius, b, is small compared to the instantaneous distance, h, of its midpoint from the plane. He finds that the resistance of the particle is greater than would be predicted by Stokes' law by the amount

$$1 + \frac{9}{8}\left(\frac{b}{h}\right) + 0\left[\left(\frac{b}{h}\right)^2\right]$$

It is our intention to provide " exact " solutions of these problems, unrestricted with regard to the ratio b/h.

1. Equations of Motion

We consider here the problem of a solid sphere of radius b moving with constant velocity U towards a plane surface, $z = 0$. The instantaneous distance of the sphere centre from the plane is denoted by h, as depicted in Fig. 1. The origin of co-ordinates, O, is located at the point of intersection of the sphere axis with the plane. Attention is confined to the semi-infinite domain, $z \geqslant 0$.

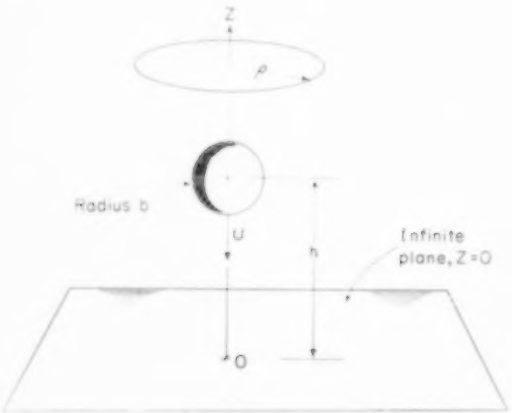

Fig. 1. Schematic sketch.

The fluid motion is, in general, governed by the Stokes–Navier equations,

$$\frac{\partial \mathbf{v}}{\partial t} + \mathbf{v} \cdot \nabla \mathbf{v} + \frac{1}{\rho} \nabla p = \nu \nabla^2 \mathbf{v}$$

and continuity equation,

$$\nabla \cdot \mathbf{v} = 0$$

for incompressible fluids. For sufficiently " slow " motions it is permissible to neglect the quadratic term $\mathbf{v} \cdot \nabla \mathbf{v}$ in comparison to the viscous term, $\nu \nabla^2 \mathbf{v}$. This can be rigorously justified for sufficiently small values of the particle Reynolds number, bU/ν.

The fluid motion is inherently unsteady, since the distance separating the particle from the bounding plane continually changes. However, as is easily established, the time-dependent term in the equations of motion, $\partial \mathbf{v}/\partial t$, becomes negligibly small by comparison to the viscous term for sufficiently small values of the dimensionless group $Ub^2/\nu h$.

Thus, whenever these two dimensionless criteria are met, the equations of motion are of the form

$$\nabla p = \kappa \nabla^2 \mathbf{v}$$

where κ is the fluid viscosity. These are the so-called creeping motion equations. They are to be considered simultaneously with the continuity equation.

Related problems dealing with the slow rotation of two spheres perpendicular to their line of centres [3, 4] and the slow translation of two spheres parallel to their line of centres [5] have been solved exactly in bipolar co-ordinates.

Because the motion is axisymmetrical, the present problem is most readily treated by means of Stokes' stream-function, ψ. In terms of this function the velocity components in cylindrical co-ordinates $[\rho, z]$ are

$$v_\rho = \frac{1}{\rho}\frac{\partial \psi}{\partial z}, \quad v_z = -\frac{1}{\rho}\frac{\partial \psi}{\partial \rho}. \tag{1.1}$$

Neglecting the effects of fluid inertia and the time derivatives of velocity, the differential equation satisfied by the stream-function is [6]

$$\Phi^4(\psi) = 0, \tag{1.2}$$

where the differential operator Φ^2 has the following form in cylindrical co-ordinates:

$$\Phi^2 = \frac{\partial^2}{\partial z^2} + \rho \frac{\partial}{\partial \rho}\left(\frac{\partial}{\rho \partial \rho}\right). \tag{1.3}$$

For the class of problems at hand we describe the fluid motion in bipolar co-ordinates. The bipolar co-ordinates (ξ, η) of a point in a meridian

plane are defined by the conformal transformation [6]

$$z + i\rho = ic \cot \tfrac{1}{2}(\eta + i\xi),$$

or, equivalently, [7]

$$\xi + i\eta = \ln \frac{\rho + i(z + c)}{\rho + i(z - c)},$$

where c is a positive constant. In the present application it is only necessary to consider the situation for which $z \geqslant 0$ and $\rho \geqslant 0$, corresponding to the range of values $\infty > \xi \geqslant 0$, $\pi \geqslant \eta \geqslant 0$. On the basis of the foregoing we find

$$\rho = c \frac{\sin \eta}{\cosh \xi - \cos \eta}, \quad z = c \frac{\sinh \xi}{\cosh \xi - \cos \eta}, \tag{1.4}$$

and thus

$$(z - c \coth \xi)^2 + \rho^2 = (c \operatorname{cosech} \xi)^2,$$

$$z^2 + (\rho - c \cot \eta)^2 = (c \operatorname{cosec} \eta)^2.$$

The surfaces evolved by rotating the curves $\xi =$ constant in the ρ, z plane about the z-axis are therefore a family of spheres of radii $c \operatorname{cosech} \xi$ whose centres lie along the z-axis at the points ($\rho = 0$, $z = c \coth \xi$). When $\xi = 0$ the sphere degenerates into the plane $z = 0$.

If we denote by $\xi = \alpha > 0$ the solid sphere of radius b on which we ultimately wish to satisfy the boundary conditions, then

$$b = c \operatorname{cosech} \alpha.$$

Furthermore, since the centre of this sphere lies at a distance h from the plane $z = 0$, then

$$h = c \coth \alpha.$$

Solving these simultaneously we obtain

$$\alpha = \cosh^{-1}\left(\frac{h}{b}\right) = \ln\left\{\frac{h}{b} + \sqrt{\left[\left(\frac{h}{b}\right)^2 - 1\right]}\right\}, \tag{1.5}$$

and

$$c = b \sinh \alpha. \tag{1.6}$$

A solution of (1.2) in bipolar co-ordinates, suitable for satisfying boundary conditions on the sphere and plane, has been given by STIMSON and JEFFERY [5]. With slight modifications their solution is

$$(\cosh \xi - \mu)^{3/2} \psi = \sum_{n=0}^{\infty} U_n(\xi)\, C_{n+1}^{-1/2}(\mu), \tag{1.7}$$

where for brevity we have put

$$\mu = \cos \eta. \tag{1.8}$$

Here,

$$U_n(\xi) = a_n \cosh(n - \tfrac{1}{2})\xi + b_n \sinh(n - \tfrac{1}{2})\xi + c_n \cosh(n + \tfrac{3}{2})\xi + d_n \sinh(n + \tfrac{3}{2})\xi, \tag{1.9}$$

and $C_{n+1}^{-1/2}(\mu)$ is the Gegenbauer polynomial of order $n + 1$ and degree $-\frac{1}{2}$. These latter functions are related to Legendre polynomials via the relation

$$C_n^{-1/2}(\mu) = \frac{P_{n-2}(\mu) - P_n(\mu)}{2n - 1}$$

The constants a_n, b_n, ... are to be determined from the boundary conditions.

As shown by STIMSON and JEFFERY, the frictional force, F, in the positive z direction, opposing the motion of the sphere is

$$F = \frac{2\pi\kappa\sqrt{(2)}}{b \sinh \alpha} \sum_{n=1}^{\infty} (a_n + b_n + c_n + d_n), \tag{1.10}$$

where κ is the viscosity.

In the subsequent development we shall require an expansion of the term $(\cosh \xi - \mu)^{3/2} \rho^2$ having the same general form as the right-hand side of (1.7). Upon combining (1.4), (1.6) and (1.8), there is obtained

$$\frac{(\cosh \xi - \mu)^{3/2} \rho^2}{b^2 \sinh^2 \alpha} = (1 - \mu^2)(\cosh \xi - \mu)^{-1/2}.$$

But

$$\cosh \xi = \tfrac{1}{2}\left[\exp(\xi) + \exp(-\xi)\right],$$

so that

$$(\cosh \xi - \mu)^{-1/2} = \sqrt{(2)} \exp(\tfrac{1}{2}\xi) \times \times \left[1 - 2\exp(\xi)\mu + \exp(2\xi)\right]^{-1/2}$$

If, in the potential expansion

$$(r_1^2 - 2 r_1 r_2 \mu + r_2^2)^{-1/2} = \sum_{k=0}^{\infty} P_k(\mu) \frac{r_1^k}{r_2^{k+1}},$$

valid for $r_2 > r_1$, we put $r_1 = 1$ and $r_2 = \exp(\xi)$ ($\xi > 0$), then

$$(\cosh \xi - \mu)^{-1/2} = \sqrt{(2)} \sum_{k=0}^{\infty} P_k(\mu) \exp\left[-(k + \tfrac{1}{2})\xi\right].$$

However,

$$(2k + 1)(1 - \mu^2) P_k'(\mu) = (k + 1)(k + 2) C_{k+2}^{-1/2}(\mu) - k(k - 1) C_k^{-1/2}(\mu),$$

from which we find, by appropriately altering the summation indices,

$$(\cosh\xi-\mu)^{3/2}\rho^2=\sqrt{(2)}\,b^2\sinh^2\alpha\sum_{n=1}^{\infty}n(n+1)\left\{\frac{\exp\left[-(n-\tfrac{1}{2})\xi\right]}{2n-1}-\frac{\exp\left[-(n+\tfrac{3}{2})\xi\right]}{2n+3}\right\}C_{n+1}^{-1/2}(\mu) \quad (1.11)$$

which is in the desired form.

2. Solid Plane Surface

Here and in the sequel the fluid motion is referred to a co-ordinate system at rest with respect to the plane. On the hypothesis of no relative motion at fluid solid interfaces the boundary conditions on the surface of the sphere, $\xi=\alpha$, are

$$v_\rho=0,\quad v_z=-U. \quad (2.1)$$

Again, the boundary conditions at the *solid* plane surface, $\xi=0$, are

$$v_\rho=0,\quad v_z=0. \quad (2.2)$$

These can be expressed in terms of the stream function in the following way: By the chain-rule

$$\frac{\partial\psi}{\partial\eta}=\frac{\partial\psi}{\partial z}\frac{\partial z}{\partial\eta}+\frac{\partial\psi}{\partial\rho}\frac{\partial\rho}{\partial\eta}=\rho v_\rho\frac{\partial z}{\partial\eta}-\rho v_z\frac{\partial\rho}{\partial\eta}, \quad (2.3)$$

and

$$\frac{\partial\psi}{\partial\xi}=\rho v_\rho\frac{\partial z}{\partial\xi}-\rho v_z\frac{\partial\rho}{\partial\xi}. \quad (2.4)$$

Thus, on the sphere surface,

$$\left[\frac{\partial\psi}{\partial\eta}\right]_{\xi=\alpha}=\left[\frac{\partial}{\partial\eta}\tfrac{1}{2}U\rho^2\right]_{\xi=\alpha} \quad (2.5)$$

and

$$\left[\frac{\partial\psi}{\partial\xi}\right]_{\xi=\alpha}=\left[\frac{\partial}{\partial\xi}\tfrac{1}{2}U\rho^2\right]_{\xi=\alpha}. \quad (2.6)$$

Since η and ξ are orthogonal the former of these two conditions is satisfied by

$$[\psi]_{\xi=\alpha}=[\tfrac{1}{2}U\rho^2]_{\xi=\alpha} \quad (2.7)$$

As can be verified by direct differentiation the following is entirely equivalent to (2.6) and (2.7):

$$\left[(\cosh\xi-\mu)^{3/2}\psi\right]_{\xi=\alpha}=\left[\tfrac{1}{2}U(\cosh\xi-\mu)^{3/2}\rho^2\right]_{\xi=\alpha}, \quad (2.8)$$

and

$$\left[\frac{\partial\xi}{\partial}(\cosh\xi-\mu)^{3/2}\psi\right]_{\xi=\alpha}=\left[\frac{\partial}{\partial\xi}\tfrac{1}{2}U(\cosh\xi-\mu)^{3/2}\rho^2\right]_{\xi=\alpha}. \quad (2.9)$$

In analogous fashion the evanescence of velocity at the solid plane wall leads us to the boundary conditions

$$\left[(\cosh\xi-\mu)^{3/2}\psi\right]_{\xi=0}=0 \quad (2.10)$$

and

$$\left[\frac{\partial}{\partial\xi}(\cosh\xi-\mu)^{3/2}\psi\right]_{\xi=0}=0. \quad (2.11)$$

The conditions (2.8)–(2.11), in conjunction with (1.7) and (1.11) lead to the following four simultaneous equations to determine the constants $a_n, b_n, \ldots\ldots$:

$$a_n\cosh(n-\tfrac{1}{2})\alpha+b_n\sinh(n-\tfrac{1}{2})\alpha+c_n\cosh(n+\tfrac{3}{2})\alpha+d_n\sinh(n+\tfrac{3}{2})\alpha=\frac{b^2\sinh^2\alpha\,U\,n(n+1)}{\sqrt{(2)}}\left\{\frac{\exp\left[-(n-\tfrac{1}{2})\alpha\right]}{2n-1}-\frac{\exp\left[-(n+\tfrac{3}{2})\alpha\right]}{2n+3}\right\}, \quad (2.12)$$

$$(n-\tfrac{1}{2})\left[a_n\sinh(n-\tfrac{1}{2})\alpha+b_n\cosh(n-\tfrac{1}{2})\alpha\right]+(n+\tfrac{3}{2})\left[c_n\sinh(n+\tfrac{3}{2})\alpha+d_n\cosh(n+\tfrac{3}{2})\alpha\right]=-\frac{b^2\sinh^2\alpha\,U\,n(n+1)}{2\sqrt{(2)}}\left\{\exp\left[-(n-\tfrac{1}{2})\alpha\right]-\exp\left[-(n+\tfrac{3}{2})\alpha\right]\right\}, \quad (2.13)$$

$$a_n+c_n=0, \quad (2.14)$$

and

$$(n-\tfrac{1}{2})b_n+(n+\tfrac{3}{2})d_n=0. \quad (2.15)$$

The solution of this set of equations is

$$c_n=-a_n=\frac{b^2\sinh^4\alpha\,U\,n(n+1)(2n+1)}{\sqrt{(2)}\left[4\sinh^2(n+\tfrac{1}{2})\alpha-(2n+1)^2\sinh^2\alpha\right]}, \quad (2.16)$$

and

$$d_n=-\frac{(2n-1)}{(2n+3)}b_n=-\frac{b^2\sinh^2\alpha\,Un(n+1)}{\sqrt{(2)}\,(2n+3)}\left[\frac{2\sinh(2n+1)\alpha+(2n+1)\sinh 2\alpha}{4\sinh^2(n+\tfrac{1}{2})\alpha-(2n+1)^2\sinh^2\alpha}-1\right] \quad (2.17)$$

If we denote by λ the correction which must be applied to Stokes' law as a result of the presence of the solid wall then

$$F = 6\,\pi\,\kappa\,bU\,\lambda, \tag{2.18}$$

and from (1.10)

$$\lambda = \frac{4}{3}\sinh\alpha\sum_{n=1}^{\infty}\frac{n\,(n+1)}{(2n-1)\,(2n+3)}$$
$$\left[\frac{2\sinh(2n+1)\,\alpha+(2n+1)\sinh 2\,\alpha}{4\sinh^2(n+\tfrac{1}{2})\,\alpha-(2n+1)^2\sinh^2\alpha}-1\right] \tag{2.19}$$

where the parameter α is given in terms of the ratio of sphere radius, b, to the distance of its centre from the plane, h, in equation (1.5). This formula is virtually identical to a similar expression given by STIMSON and JEFFERY [5] for the Stokes' law correction in the case of two equal size spheres falling parallel to their line of centres, except that the lead term in brackets is inverted. Incidentally, as pointed out by FAXÉN [8], there is a typographical error in their manuscript and the multiplier of their expression for λ should be $\frac{4}{3}$ rather than $\frac{2}{3}$.

Using tabulated values of the exponential and hyperbolic functions [9, 10, 11], we have made accurate calculations of λ for values of b/h in the range of interest. These are presented in Table 1.

Table 1. *Stokes' Law corrections for a solid plane, equation* (2.19)

α	h/b	b/h	λ
0	1	1	∞
0·5	1·1276260	0·88681885	9·2517663
1·0	1·5430806	0·64805428	3·0360641
1·5	2·3524096	0·42509603	1·8374749
2·0	3·7621957	0·26580222	1·4128629
2·5	6·1322895	0·16307123	1·2219882
3·0	10·067662	0·099327927	1·1252465
∞	∞	0	1

When the sphere is far removed from the wall it is sufficient to retain only the first term in (2.19) and to neglect $\exp(-\alpha)$ compared to $\exp(\alpha)$. This results in

$$\lambda \simeq 1 + \frac{9}{8}\frac{b}{h}$$

for small b/h, which agrees exactly with the value given by LORENTZ [2] obtained by the method of "reflexions."

3. FREE SURFACE

When the plane, $z = 0$, towards which the sphere falls is a free surface the boundary conditions on the plane are that the normal component of velocity and the tangential stresses vanish:

$$[v_z]_{z=0} = 0, \tag{3.1}$$

and

$$[\widehat{z\,\rho}]_{z=0} = \kappa\left(\frac{\partial\,v_\rho}{\partial\,z}+\frac{\partial\,v_z}{\partial\,\rho}\right)_{z=0} = 0$$

$$[\widehat{z\,\phi}]_{z=0} = \kappa\left(\frac{\partial\,v_\phi}{\partial\,z}+\frac{1}{\rho}\frac{\partial\,v_z}{\partial\,\phi}\right)_{z=0} = 0.$$

The latter equation is automatically satisfied by virtue of the prevailing symmetry. Furthermore, in view of (3.1) the vanishing of the first stress component is assured by setting

$$\left(\frac{\partial\,v_\rho}{\partial\,z}\right)_{z=0} = 0. \tag{3.2}$$

Now,

$$v_z = -\frac{1}{\rho}\frac{\partial\,\psi}{\partial\,\rho} = -\frac{1}{\rho}\left(\frac{\partial\,\psi}{\partial\,\xi}\frac{\partial\,\xi}{\partial\,\rho}+\frac{\partial\,\psi}{\partial\,\eta}\frac{\partial\,\eta}{\partial\,\rho}\right).$$

Since $\xi = 0$ along the plane $z = 0$ then the derivative $\partial\,\xi/\partial\,\rho$ vanishes on this plane and the condition (3.1) is met by $(\partial\,\psi/\partial\,\eta)_{\xi=0} = 0$ or, since ξ and η are orthogonal,

$$(\psi)_{\xi=0} = 0. \tag{3.3}$$

In regard to (3.2) we have from (1.1) that an equivalent condition imposed on the stream function is

$$\left(\frac{\partial^2\psi}{\partial\,z^2}\right)_{z=0} = 0$$

But, with the aid of (3.3) and the relation

$$\frac{\partial^2}{\partial\,z^2}+\frac{\partial^2}{\partial\,\rho^2} = J^2\left(\frac{\partial^2}{\partial\,\xi^2}+\frac{\partial^2}{\partial\,\eta^2}\right),$$

where J is the Jacobian of the transformation,

$$|\,J\,| = \left|\frac{\cosh\xi-\cos\eta}{c}\right|,$$

the vanishing of the tangential stress is easily shown to correspond to

$$\left(\frac{\partial^2 \psi}{\partial \xi^2}\right)_{\xi=0} = 0. \qquad (3.4)$$

The boundary conditions expressed by (3.3) and (3.4) are equivalent to

$$\left[(\cosh \xi - \mu)^{3/2} \psi\right]_{\xi=0} = 0 \qquad (3.5)$$

and

$$\left[\frac{\partial^2}{\partial \xi^2}(\cosh \xi - \mu)^{3/2} \psi\right]_{\xi=0} = 0. \qquad (3.6)$$

From (1.7), these result in the simultaneous equations

$$a_n + c_n = 0 \qquad (3.7)$$

and

$$(n - \tfrac{1}{2})^2 a_n + (n + \tfrac{3}{2})^2 c_n = 0. \qquad (3.8)$$

The surface conditions on the sphere are unaltered from their previous values. Thus, to the above we append equations (2.12) and (2.13). The solution of this set of four simultaneous equations is

$$a_n = c_n = 0, \qquad (3.9)$$

$$b_n = \frac{b^2 \sinh^2 \alpha \, U n (n+1)}{\sqrt{(2)}\,(2n-1)} \left[\frac{4\cosh^2(n+\frac{1}{2})\alpha + 2(2n+1)\sinh^2\alpha}{2\sinh(2n+1)\alpha - (2n+1)\sinh 2\alpha} - 1\right], \qquad (3.10)$$

and

$$d_n = \frac{b^2 \sinh^2 \alpha \, U n (n+1)}{\sqrt{(2)}\,(2n+3)} \left[1 - \frac{4\cosh^2(n+\frac{1}{2})\alpha - 2(2n+1)\sinh^2\alpha}{2\sinh(2n+1)\alpha - (2n+1)\sinh 2\alpha}\right]. \qquad (3.11)$$

The frictional force experienced by the sphere is therefore

$$F = 6 \pi \kappa b U \beta \qquad (3.12)$$

where the Stokes' law correction is

$$\beta = \frac{4}{3} \sinh \alpha \sum_{n=1}^{\infty} \frac{n(n+1)}{(2n-1)(2n+3)} \left[\frac{4\cosh^2(n+\frac{1}{2})\alpha + (2n+1)^2\sinh^2\alpha}{2\sinh(2n+1)\alpha - (2n+1)\sinh 2\alpha} - 1\right] \qquad (3.13)$$

Values of β calculated from the above are presented in Table 2.

When the sphere is far from the free surface, the Stokes' law correction obtained from (3.13) is

$$\beta \simeq 1 + \frac{3}{4}\frac{b}{h}, \qquad (3.14)$$

valid for small b/h.

Table 2. Stokes' law corrections for a free surface, equation (3.13)

α	h/b	β
0	1	∞
0·5	1·1276260	3·98670
1·0	1·5430806	1·97369
1·5	2·3524096	1·4636
2·0	3·7621957	1·247131
2·5	6·1322895	1·1388563
3·0	10·067662	1·0803758
∞	∞	1

Independent confirmation of the present results by a different method of computation is provided by the work of Faxén and Dahl [12]. These authors studied the slow motion of two spheres of unequal size each moving with arbitrary constant velocity parallel to the line of centres, using a successive approximation technique known as the method of "reflexions." If in their treatment the radius of each sphere is b, the centre-to-centre distance is $2h$, and if the spheres move *towards* each other with the same velocity, U, their expression for the frictional drag, F, experienced by either sphere assumes the form

$$\frac{F}{6\pi\kappa bU} = 1 + \frac{3}{4}\left(\frac{b}{h}\right) + \frac{9}{16}\left(\frac{b}{h}\right)^2 + \frac{19}{64}\left(\frac{b}{h}\right)^3 + \frac{93}{256}\left(\frac{b}{h}\right)^4 + \frac{387}{1{,}024}\left(\frac{b}{h}\right)^5 + \frac{1{,}197}{4{,}096}\left(\frac{b}{h}\right)^6 + \frac{5{,}331}{16{,}384}\left(\frac{b}{h}\right)^7 + \frac{19{,}821}{65{,}536}\left(\frac{b}{h}\right)^8 + \frac{76{,}115}{262{,}144}\left(\frac{b}{h}\right)^9 + \cdots\cdots \qquad (3.15)$$

But, when two equal spheres approach one another with the same velocity, the plane midway between them is a plane of symmetry on which the normal velocity and tangential stresses vanish. Thus, (3.13) and (3.15) should be comparable. Values of the Stokes' law correction calculated from (3.15) are presented in Table 3. At the smaller

ratios of h/b this series converges too slowly to yield accurate results. The numbers tabulated are estimated to be correct to about 1 digit in the last significant figure. These results should be compared with those given in Table 2. The agreement is excellent.

Table 3. *Stokes' law corrections for a free surface, equation* (3.15)

h/b	β
1	—
1·1276260	3
1·5430806	1·96
2·3524096	1·4634
3·7621937	1·247126
6·1322895	1·13885607
10·067662	1·080375850
∞	1

4. DISCUSSION

The preceding calculations show that the effect of a stationary obstacle in the path of a particle is to increase the resistance of the latter beyond that which it would experience in an unbounded medium when moving at the same velocity. Alternatively, if a given force (e.g. gravity) be acting the effect is to decrease the sedimentation velocity below that given by Stokes' law. Furthermore, the increased resistance is less in the case of a free surface than in the case of a solid surface, which is unable to yield to the stresses. The inclusion of inertial effects would not, in all probability, modify these qualitative conclusions.

On the other hand, the present results show that for both types of surfaces the resistance is increased by the same amount regardless of whether the particle is moving towards or away from the plane. It is here that the omission of inertial terms in the equations of motion leads, in the general case, to an unrealistic inference. It seems more natural to expect that the resistance be different, according as the sphere is approaching or receding from the surface. Of the two possibilities, the most plausible conjecture is that the resistance suffered by an *approaching* sphere is greatest. This contention can be demonstrated by invoking results from ideal fluid theory [6] which state that a sphere moving perpendicular to a wall is repelled by the wall whether the particle motion is directed towards or away from it, the magnitude of the force being the same in either case. Thus, the forces of inertia hinder the particle in the former case and assist it during the latter. From this we may infer that when inertial effects are sensible the particle resistance is least in the case where the sphere recedes from the surface and vice-versa.

It is a matter of experience that the proximity of a boundary to a moving particle enhances the range of particle Reynolds numbers, Ub/ν, over which the creeping-motion equations provide a valid description of the flow – i.e. the range in which a direct proportionality exists between particle resistance and velocity. For example, in CARTY's [13] experimental study of a ball rolling within a viscous fluid down an inclined plane, this proportionality was observed to persist up to particle Reynolds numbers of about 20. On this basis it is reasonable to expect the present analysis to yield correct values at Reynolds numbers substantially above 0·5, the value normally cited as the upper limit of Stokes' law for an unbounded fluid.

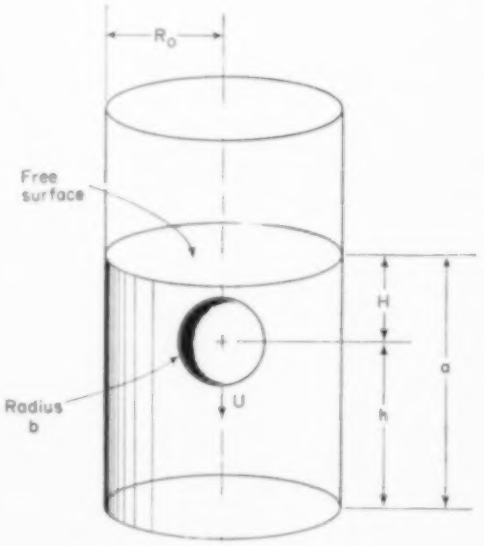

FIG. 2. Falling-ball viscometer.

5. Falling-ball Viscometer

It is of interest to attempt an application of our results to the falling-ball viscometer. In such a device a spherical particle falls along the axis of a circular cylinder, as in Fig. 2. Of importance are the corrections to Stokes' law occasioned by the proximity of the cylindrical boundary, container bottom and free surface to the particle.

Dimensional analysis indicates that the Stokes' law correction resulting from these three effects is of the form

$$\frac{F}{6\pi\kappa bU} = f\left(\frac{b}{R_0}, \frac{b}{h}, \frac{b}{H}\right)$$

Of primary interest is the situation wherein each of the above ratios are small. The separate corrections required for each of the boundaries alone are:

(i) cylindrical boundary correction [1]:

$$f\left(\frac{b}{R_0}, 0, 0\right) = 1 + 2{\cdot}105\left(\frac{b}{R_0}\right) + 0\left[\left(\frac{b}{R_0}\right)^2\right]$$

(ii) container bottom correction:

$$f\left(0, \frac{b}{h}, 0\right) = 1 + \frac{9}{8}\left(\frac{b}{h}\right) + 0\left[\left(\frac{b}{h}\right)^2\right]$$

(iii) free surface correction:

$$f\left(0, 0, \frac{b}{H}\right) = 1 + \frac{3}{4}\left(\frac{b}{H}\right) + 0\left[\left(\frac{b}{H}\right)^2\right]$$

It is tempting to assume that these corrections can be applied separately in the limit, in which event a Taylor series expansion would give

$$\frac{F}{6\pi\kappa bU} = 1 + 2{\cdot}105\left(\frac{b}{R_0}\right) + \frac{9}{8}\left(\frac{b}{h}\right) + \frac{3}{4}\left(\frac{b}{H}\right) + \cdots\cdots \qquad (5.1)$$

This is essentially the point of view adopted by Ladenburg [14] in an oft-cited paper dealing with corrections to the falling-ball viscometer. The conception is, however, fundamentally unsound, as it gives cognizance only to interactions between particle and boundaries while failing to take account of the interactions among the boundaries themselves.

To demonstrate this contention consider the related, but more tractable, problem of a sphere falling between two infinite parallel rigid planes, the motion of the particle being parallel to the walls, as in Fig. 3. Let l_1, and l_2, respectively, denote the distance of each plane from the mid-point of the sphere, and let $2\,l$ be the distance between walls.

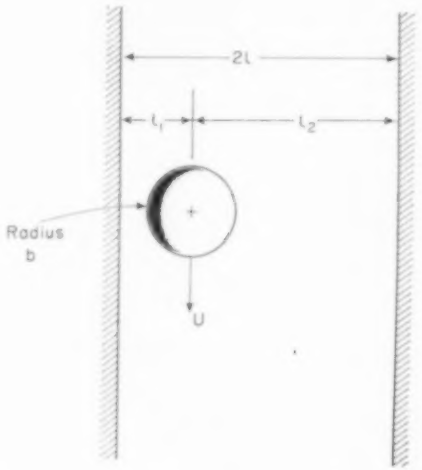

Fig. 3. Sphere falling between parallel planes.

Lorentz [2] provides a solution in the case where a sphere moves parallel to a *single* plane wall, valid for small values of b/l_i.

His correction to Stokes' law is

$$\frac{F}{6\pi\kappa bU} = 1 + \frac{9}{16}\left(\frac{b}{l_i}\right) + 0\left[\left(\frac{b}{l_i}\right)^2\right] \quad (i = 1, 2)$$

Thus, were it correct to simply superimpose the individual corrections, the resistance of a sphere falling between two plane walls would be given by

$$\frac{F}{6\pi\kappa bU} = 1 + \frac{9}{16}\frac{b}{l}\left(\frac{l}{l_1} + \frac{l}{l_2}\right) + 0\left[\left(\frac{b}{l}\right)^2\right] \qquad (5.2)$$

Now, Faxén [15] has obtained a detailed solution of the problem at hand, valid for small b/l. When $l_1 = l_2$ Faxén's solution is

$$\frac{F}{6\pi\kappa bU} = 1 + 1{\cdot}004\,\frac{b}{l} + 0\left[\left(\frac{b}{l}\right)^2\right]$$

while for $l_1 = 3\,l_2$, the coefficient in the above expression becomes 1·3052. The corresponding coefficients derived from (5·2) are 1·125 and 1·500,

respectively. As these differ from the correct values we may infer that it is not generally permissible to superpose individual corrections.

Although the technique of superposing solutions is fundamentally in error, it appears from the two numerical examples cited above that the errors incurred may not be too serious. It therefore appears worthwhile to bring equation (5.1) to fruition, despite its shortcoming. This calculation differs from LADENBURG's [14] principally in that the free surface correction was not known to him. In its stead he utilized the same correction as for a rigid surface.

The instantaneous velocity of the ball is $U' = -dh/dt$. Let h_i and h_f, respectively, denote the initial and final distance of the ball above the bottom of the container and let $a = H + b$ be the depth of liquid in the cylinder. The duration of the experiment is t. Upon substituting into equation (5.1) and performing the necessary integrations, bearing in mind that F is constant, we eventually obtain

$$\frac{F}{6\pi\kappa b\bar{U}} \simeq 1 + 2{\cdot}105\left(\frac{b}{R_0}\right) + \left(\frac{b}{a}\right)\frac{1}{(h_i/a) - (h_f/a)}\left[\frac{9}{8}\ln\frac{(h_i/a)}{(h_f/a)} + \frac{3}{4}\ln\frac{1-(h_f/a)}{1-(h_i/a)}\right] \qquad (5.3)$$

where $\bar{U} = (h_i - h_f)/t$ denotes the average velocity of fall of the ball during the experiment. By way of example, when the speed of fall is timed over the middle third of the length of the viscometer we have $h_i/a = 2/3$ and $h_f/a = 1/3$, whence

$$\frac{F}{6\pi\kappa b\bar{U}} \simeq 1 + 2{\cdot}105\,\frac{b}{R_0} + 3{\cdot}90\,\frac{b}{a}$$

For a typical viscometer whose depth-to-radius ratio, a/R_0, is 10 : 1 this implies that the correction for end-effects will be roughly one fifth of the correction for the cylindrical boundary alone.

Acknowledgements—The author would like to thank JOHN HAPPEL of New York University for his useful suggestions.

NOTATION

a = depth of liquid in viscometer
a_n = coefficient in equation (1.9)
b = radius of sphere
b_n = coefficient in equation (1.9)
c = positive parameter defined by equation (1.6)
c_n = coefficient in equation (1.9)
$C_m^{-1/2}(\mu)$ = Gegenbauer polynomial of order m and degree $-\frac{1}{2}$ with argument μ
d_n = coefficient in equation (1.9)
F = force on sphere
h = distance from sphere centre to plane boundary
h_i = initial distance
h_f = final distance
H = distance from sphere centre to free surface
$i = \sqrt{-1}$ = imaginary number
J = Jacobian of a co-ordinate system transformation
k = summation index
l = one-half distance between walls
l_1, l_2 = distance from sphere centre to walls
n = summation index
p = dynamic pressure of fluid
$P_m(\mu)$ = Legendre polynomial of order m with argument μ
r_1, r_2 = distance from origin to points 1 and 2, respectively
R_0 = cylinder radius
t = time
U = instantaneous velocity of sphere
$\bar{U}$ = average velocity of sphere
$U_n(\xi)$ = function of argument ξ defined in equation (1.9)
$\mathbf{v}$ = fluid velocity vector
v_ρ = velocity component in radial direction
v_z = velocity component in longitudinal direction
z = co-ordinate measured along symmetry axis
$\widehat{z\rho} = \rho$ — component of stress-vector acting across plane z = constant
$\widehat{z\phi} = \phi$ — component of stress-vector acting across plane z = constant

Greek Letters

α = parameter defined by equation (1.5)
β = Stokes' law correction factor for a *free* surface, defined by equation (3.12)
η = bipolar co-ordinate
κ = dynamic viscosity of fluid
λ = Stokes' law correction factor for a *solid* surface, defined by equation (2.18)
$\mu = \cos\eta$
ξ = bipolar co-ordinate
ρ = cylindrical co-ordinate
ρ = density of fluid
ν = kinematic viscosity of fluid
ϕ = azimuthal cylindrical co-ordinate
Φ^2 = differential operator defined by equation (1.3)
ψ = Stokes' stream function

References

[1] Haberman W. and Sayre R. M. *Motion of Rigid and Fluid Spheres in Stationary and Moving liquids inside Cylindrical Tubes.* Report 1143. David W. Taylor Model Basin, U.S. Navy Department, Washington D.C., October 1958.

[2] Lorentz H. A. *Abh. theoret. Phys.* 1907 **1** 23.

[3] Jeffery G. B. *Proc. Lond. Math. Soc.* (Series 2) 1915 **14** 327.

[4] Wadhwa Y. D. *J. Sci. Engng. Res.* India 1958 **2** 245.

[5] Stimson M. and Jeffery G. B. *Proc. Roy. Soc.* 1926 A **111**, 110.

[6] Milne-Thomson L. M. *Theoretical Hydrodynamics* (3rd ed.) pp. 168, 513, 553. Macmillan, New York 1950.

[7] Jeffery G. B. *Proc. Roy. Soc.* 1912 A **87**, 109.

[8] Faxén H. *Z. angew. Math. Mech.* 1927 **7** 79.

[9] *Table of Hyperbolic Sines and Cosines,* Appl. Math. Ser. Nos. 36 (Nov. 30 1953) and 45 (Nov. 15 1955). National Bureau of Standards (U.S. Commerce Department) Washington D.C.

[10] *Tables of the Exponential Function exp (x)* Appl. Math. Ser. No. 14 (June 29 1951). National Bureau of Standards (U.S. Commerce Department) Washington, D.C.

[11] *Tables of the Descending Exponential,* Appl. Math. Ser. No. 46 (Nov. 15 1955). National Bureau of Standards (U.S. Commerce Department) Washington D.C.

[12] Faxén H. and Dahl H. *Ark. Mat., Astron. Fys.* 1925 **19A** No. 13.

[13] Carty J. J. Jr. *Resistance Coefficients for Spheres on a Plane Boundary.* B.S. Thesis, Massachusetts Institute of Technology 1957.

[14] Ladenburg R. *Ann. Phys.* 1907 **23** 447.

[15] Faxén H. *Ann. Phys.* 1922 **68** 89; *Ark. Mat., Astron. Fys.* 1924 **18** No. 29; 1925 **19** A No. 13.

Chemical Engineering Science, 1961, Vol. 16, pp. 252 to 266. Pergamon Press Ltd., London. Printed in Great Britain.

Dynamic control of chemical engineering processes using a method of Lyapunov

R. KOEPCKE and L. LAPIDUS*

IBM Research Centre, Yorktown Heights, New York, U.S.A.

(*Received* 25 *November* 1960 ; *in revised form* 23 *February* 1961)

Abstract—Previous papers from this laboratory have detailed a procedure for controlling dynamic linear chemical processes in an optimum manner. Involved in the method was the use of dynamic programming as developed by BELLMAN and extended by KALMAN and consisted of minimizing a quadratic form of the state or dependent variables of the system. A brief summary of this procedure is presented in a later section of this paper. However, in certain physical situations the method is impractical because of the nature of the inputs which must be used as control variables, i.e. feed compositions must be varied instead of the more natural feed rate.

In the present paper the method of LYAPUNOV is used to extend this dynamic control approach to allow flow rate to be used as a control variable. To illustrate the details a number of different procedures are presented ranging in complexity from a relatively simple approximation to a detailed search routine.

Résumé—Le centre de recherches de l'I.B.M. a étudié dans des articles antérieurs une méthode pour contrôler de façon optimum les procédés chimiques dynamiques et linéaires. Cette méthode utilise la programmation dynamique telle qu'elle a été développée par BELLMAN et étendue par KALMAN et consistant à minimiser la forme quadratique de l'état ou des variables dépendant du système. La dernière partie de cet article donne un résumé de cette méthode. Dans certains cas cette méthode est cependant inutilisable en raison de la nature des données qui doivent être utilisées comme variables de contrôle : ainsi on doit faire varier la composition de l'alimentation plutôt que sa vitesse.

Dans cet article, la méthode de LYAPUNOV est utilisée pour étendre ce contrôle dynamique afin de permettre l'utilisation de la vitesse d'écoulement comme variable de contrôle. Un certain nombre de procédés sont présentés par ordre de complexitré croissante, depuis l'approximation relativement simple jusqu'à la recherche détaillée.

Zusammenfassung—Frühere Arbeiten aus diesem Institut behandelten eine Methode zur Kontrolle dynamischer linearer chemischer Prozesse in optimaler Weise. Dabei wurde die von BELLMAN entwickelte und von KALMAN erweiterte Methode des dynamischen Programmierens angewandt, die darin bestand, dass eine quadratische Form der Zustandsvariablen oder der abhängigen Variablen des Systems auf ein Minimum gebracht wurde. Eine kurze Zusammenfassung dieser Methode wird in einem späteren Abschnitt dieser Arbeit gegeben. Bei gewissen physikalischen Gegebenheiten ist diese Methode jedoch unpraktisch wegen der Natur der Eingangsgrössen, die als Kontrollvariable benutzt werden, zum Beispiel muss die Zulaufzusammensetzung geändert werden, statt logischer die Zulaufgeschwindigkeit.

In der vorliegenden Arbeit wurde die Methode von LYAPUNOV benutzt, um die dynamische Kontrolle zu erweitern, damit die Zulaufbeschwindigkeit als Kontrollvariable benutzt werden kann. Um Einzelheiten zu beleuchten, werden eine Reihe von verschiedenen Verfahren angegeben, die in ihrer Komplexheit von relativ einfachen Annäherungen bis zu speziellen Forschungsmethoden reichen.

*Present Address : Department of Chemical Engineering Princetown University, Princetown, New Jersey, U.S.A.

Statement of Problem

It seems advisable to choose a physical system familiar to chemical engineers which can serve both as a basis for the discussion and for numerical calculations. The particular system chosen is a train of six (6) liquid–liquid countercurrent extraction units with a secondary feed to one of the middle stages (Fig. 1). The solvents are assumed completely immiscible and there is a single solute in the raffinate stream which is to be transferred to the extract stream. The secondary feed is taken from two large reservoirs, each containing a constant, but different, composition of the single solute. The symbols x and y are used to indicate raffinate and extract compositions respectively, F and b are raffinate solvent flow rates and w is the extract solvent flow rate. If H is the hold-up (assumed constant for all stages) of the raffinate phase and h the analogous hold-up of the extract a material balance on any stage leads to the dynamic material balances.

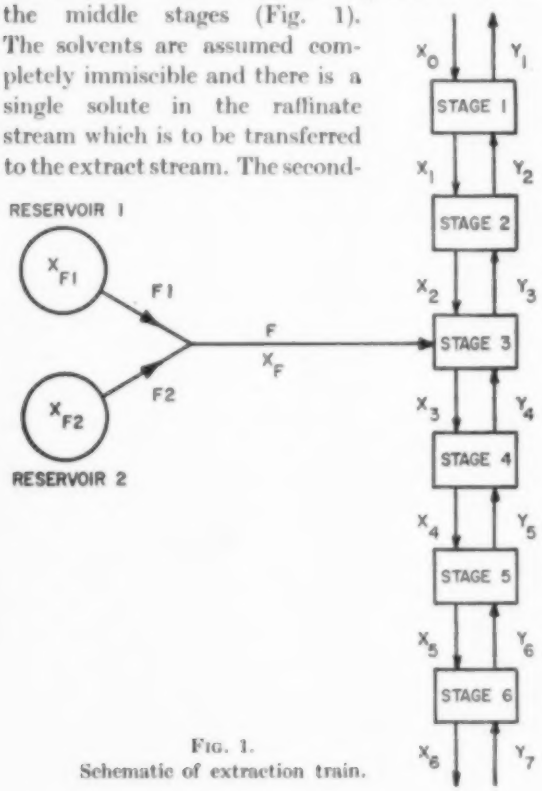

Fig. 1.
Schematic of extraction train.

$$h\frac{dy_n}{dt} + H\frac{dx_n}{dt} = b\left[x_{n-1} - x_n\right] + w\left[y_{n+1} - y_n\right] \qquad n = 1, 2$$

$$h\frac{dy_n}{dt} + H\frac{dx_n}{dt} = b\,x_{n-1} - b^*\,x_n + w\left[y_{n+1} - y_n\right] + Fx_F \qquad n = 3$$

$$h\frac{dy_n}{dt} + H\frac{dx_n}{dt} = b^*\left[x_{n-1} - x_n\right] + w\left[y_{n+1} - y_n\right] \qquad n = 4, 5, 6$$

where $b^* = b + F$. Assuming a linear equilibrium relationship

$$y_n = \alpha\,x_n + \beta$$

and defining

$$d = \frac{b}{a};\quad d^* = \frac{b^*}{a};\quad p = \frac{w\,\alpha}{a};\quad a = h\,\alpha + H$$

the material balance equations can be written in matrix form as

$$\frac{d\mathbf{x}}{dt} = \mathbf{A}\,\mathbf{x} + \mathbf{D}_1\,\mathbf{m}_1 + \mathbf{D}_2\,\mathbf{m}_2$$

In equation (1)

$$\mathbf{A} = \begin{bmatrix} -(d+p) & p & & & & \\ d & -(d+p) & p & & & \\ & d & -(d^*+p) & p & & \\ & & d^* & -(d^*+p) & p & \\ & & & d^* & -(d^*+p) & p \\ & & & & d^* & -(d^*+p) \end{bmatrix}$$

$$\mathbf{x} = \begin{bmatrix} x_1 \\ x_2 \\ \cdot \\ \cdot \\ \cdot \\ x_6 \end{bmatrix}; \quad \mathbf{D}_1 = \begin{bmatrix} d & 0 \\ 0 & \cdot \\ \cdot & \cdot \\ \cdot & \cdot \\ \cdot & 0 \\ 0 & p \end{bmatrix}; \quad \mathbf{D}_2 = \begin{bmatrix} 0 \\ 0 \\ F/a \\ 0 \\ \cdot \\ \cdot \\ 0 \end{bmatrix}; \quad \mathbf{m}_1 = \begin{bmatrix} x_0 \\ \dfrac{y_7 - \beta}{\alpha} \end{bmatrix}; \quad \mathbf{m}_2 = \begin{bmatrix} x_F \end{bmatrix}$$

Note that $\mathbf{m}_1$ and $\mathbf{m}_2$ contain the input streams to the system. Equation (1) may be integrated to yield

$$x(t) = \exp[\mathbf{A}\,t]\,\mathbf{x}(0) + \int_0^t \exp[\mathbf{A}\,(t-\lambda)]\,\mathbf{D}_1\,\mathbf{m}_1\,d\lambda + \int_0^t \exp[\mathbf{A}\,(t-\lambda)]\,\mathbf{D}_2\,\mathbf{m}_2\,d\lambda$$

where [1]

$$\exp[\mathbf{A}\,t] = \sum_{i=0}^{\infty} \frac{(\mathbf{A}\,t)}{i!}$$

$$\mathbf{x}(0) = \mathbf{x}(t), \quad t = 0$$

If it is assumed that the inputs, $\mathbf{m}_1$ and $\mathbf{m}_2$, are changed only at discrete time increments called the sampling times, $t = \tau,\ 2\,\tau,\ 3\,\tau, - - -,\ k\,\tau, - - -$ the integrated equations above can be simplified to the difference form

$$\mathbf{x}(k+1) = \mathbf{\Phi}\,\mathbf{x}(k) + \mathbf{\Delta}_1\,\mathbf{m}_1(k) + \mathbf{\Delta}_2\,\mathbf{m}_2(k) \quad (2)$$

$$k = 0, 1, 2, - - -$$

where

$$\mathbf{\Phi} = \exp[\mathbf{A}\,\tau]$$

$$\mathbf{\Delta}_1 = \left(\int_0^{\tau} \exp[\mathbf{A}\,\lambda]\,d\lambda\right)\mathbf{D}_1$$

$$\mathbf{\Delta}_2 = \left(\int_0^{\tau} \exp[\mathbf{A}\,\lambda]\,d\lambda\right)\mathbf{D}_2$$

To simplify the algebra let us assume that the feed composition x_0 is held constant (thus $\mathbf{\Delta}_1\,\mathbf{m}_1$ is a constant) and control of the system is to be achieved by blending the flows F_1 and F_2 to yield different values of $[x_F]$. On this basis and defining the new variables

$$\mathbf{y}(k) = \mathbf{x}(k) - \mathbf{x}_{ss}$$

$$\mathbf{y}^* = \mathbf{x}_{ss} + [\mathbf{I} - \mathbf{\Phi}]^{-1}\,\mathbf{\Delta}_1\,\mathbf{m}_1$$

$$\mathbf{z}(k) = \mathbf{y}(k) - \mathbf{y}^*$$

where $\mathbf{x}_{ss}$ is a steady-state equilibrium condition of the system, equation (2) is transformed to

$$\mathbf{z}(k+1) = \mathbf{\Phi}\,\mathbf{z}(k) + \mathbf{\Delta}_2\,\mathbf{m}_2(k) \quad (3)$$

$$k = 0, 1, 2, - - -$$

Equation (3) is a difference equation representing the dynamic behaviour of the extraction system.

We now can briefly outline the dynamic programming approach described in previous papers (slight liberties will be taken for purposes of clarity). This objective may be stated in condensed form as finding that set of discrete control signals $\mathbf{m}_2(0), \mathbf{m}_2(1), \ldots\ldots$ which will move the dynamic system represented by equation (3) from an initial state $\mathbf{z}(0)$ to the origin my minimizing the quadratic function

$$\sum_{k=1}^{N} \mathbf{z}^T(k)\,\mathbf{Q}\,\mathbf{z}(k)$$

as $N \to \infty$. When $\mathbf{Q}$ is a positive-definite matrix such as the identity matrix, the iteration pattern [2, 5].

$$\mathbf{P}^{(i)} = \mathbf{\Psi}^{T(N-i)}\,\mathbf{P}^{(i-1)}\,\mathbf{\Psi}^{(N-i)} + \mathbf{Q}$$

$$\mathbf{C}^{(N-1)} = -(\mathbf{\Delta}_2^T\,\mathbf{P}^{(i)}\,\mathbf{\Delta}_2)^{-1}\,\mathbf{\Delta}_2^T\,\mathbf{P}^{(i)}\,\mathbf{\Phi}$$

$$\mathbf{\Psi}^{(N-i)} = \mathbf{\Phi} + \mathbf{\Delta}_2\,\mathbf{C}^{(N-i)}$$

$$\mathbf{P}^{(0)} = \mathbf{Q}$$

$$\mathbf{\Psi}^{(N)} = \mathbf{0}$$

obtained by dynamic programming [6] serves to define the constant matric $\mathbf{C}^{\infty}$ in the equation

$$\mathbf{m}_2(k) = \mathbf{C}^{\infty}\,\mathbf{z}(k) \qquad (4)$$

Using equation (4) and then (3) in a repetitive manner the sequence of optimal control vectors and the values of $\mathbf{z}(k)$ can now be calculated directly. Extension of the method to include other control variables such as the feed composition x_0 follows in a direct manner.

From a realistic and practical point of view, however, it is difficult to visualize control of this physical system by using changes in composition; rather the control would most easily be performed by manipulating the various stream flow rates. From equation (1) it can be seen that if d is used as a control variable the coefficient matrix $\mathbf{A}$ of the dynamic system becomes time-varying. On this basis the method outlined above no longer is adequate since a time-invariant $\mathbf{A}$ is implicit in the development of equation (4).

If both the secondary and the main extract feed rates, F and b (or d), are to be used as control variables equation (1) can be rewritten in the form

$$\frac{d\mathbf{x}}{dt} = \mathbf{A}\mathbf{x} + d\,\mathbf{E}_1\mathbf{x} + \frac{F}{a}\,\mathbf{E}_2\mathbf{x} + d\,\mathbf{D}_3 + \frac{F}{a}\,\mathbf{D}_4 \qquad (5)$$

where

$$\mathbf{A} = \begin{bmatrix} -p & p & & & & & \\ & -p & p & & & & \\ & & -p & p & & & \\ & & & -p & p & & \\ & & & & -p & p & \\ & & & & & -p & p \\ & & & & & & -p \end{bmatrix};$$

$$\mathbf{E}_1 = \begin{bmatrix} -1 & & & & & & \\ +1 & -1 & & & & & \\ & +1 & -1 & & & & \\ & & +1 & -1 & & & \\ & & & +1 & -1 & & \\ & & & & +1 & -1 & \\ & & & & & +1 & -1 \end{bmatrix}$$

$$\mathbf{E}_2 = \begin{bmatrix} 0 & & & & & & \\ & 0 & & & & & \\ & & -1 & & & & \\ & & +1 & -1 & & & \\ & & & +1 & -1 & & \\ & & & & +1 & -1 & \\ & & & & & +1 & -1 \end{bmatrix};$$

$$\mathbf{D}_3 = \begin{bmatrix} x_0^1 \\ 0 \\ 0 \\ 0 \\ 0 \\ 0 \end{bmatrix}; \qquad \mathbf{D}_4 = \begin{bmatrix} 0 \\ 0 \\ x_F \\ 0 \\ 0 \\ 0 \end{bmatrix}$$

and where $(y_7 - \beta)\,\alpha$ is taken as zero (see next Section). Actually equation (5) can be written in a more general form as

$$\frac{d\mathbf{y}}{dt} = \mathbf{D}\,\mathbf{y} + \sum_{i=1}^{r} u_i\left[\mathbf{E}_i\,\mathbf{y} + \mathbf{D}_i\right] \qquad (6)$$

where the u_i, $i = 1, 2, \cdots, r$ are control flow rates and $\mathbf{y} = \mathbf{x} - \mathbf{x}_{ss}$. The control problem of interest now is to find that set of discrete control signals, $\mathbf{u}(0), \mathbf{u}(1), \cdots$, which will move the dynamic system represented by equation (6) (or 5) from an initial state $\mathbf{y}(0)$ to the origin along some optimal path.

Numerical Parameters

To provide a suitable base for subsequent numerical calculations the following parameters were chosen (any convenient set of units may be used).

$w = 60$	$y_7 = 0$ (pure solvent)
$a = 100$	$x_0 = 0{\cdot}0400$
$\alpha = 2{\cdot}20$	$x_F = 0{\cdot}0300$
$\beta = 0$	$F = 50$

In addition to these constant values there is specified that $b_{\text{initial}} = 50$ and $b_{\text{desired}} = 100$. In other words the system of six extraction stages will be at an initial state corresponding to $b = 50$ and the control sequence is to move the system to a new equilibrium state corresponding to $b = 100$. Only the main feed rate is to be used for control in this example; this is merely for convenience sake. Based upon these initial and final conditions and the listed parameters, equation (1) or (5) may be solved in the steady-state, $(d\mathbf{x}/dt = 0)$, to yield

$$\mathbf{x}(0) = \begin{bmatrix} 0{\cdot}0245523 \\ 0{\cdot}0187009 \\ 0{\cdot}0164845 \\ 0{\cdot}0105254 \\ 0{\cdot}0060110 \\ 0{\cdot}0025909 \end{bmatrix};$$

(corresponding to $b = 50$)

$$\mathbf{x}_{ss} = \begin{bmatrix} 0{\cdot}0333450 \\ 0{\cdot}0282850 \\ 0{\cdot}0244595 \\ 0{\cdot}0194628 \\ 0{\cdot}0137847 \\ 0{\cdot}0073323 \end{bmatrix}$$

(corresponding to to $b = 100$)

Lyapunov's Direct Method

As already pointed out the problem of interest here is finding that sequence of inputs $u_1, u_2, - - -$, or $\mathbf{u}(k)$, $k = 0, 1, 2, - - -$ for the dynamic system of equation (6) such that given any arbitrary initial vector $\mathbf{y}(0)$ the system is returned to the origin in some optimum way. "Optimum way" is, of course, an intuitive concept which needs to be precisely defined; it can be practically proposed that a fast response with a minimum overshoot is satisfactory. The overshoot requirements lead to stability considerations, and hence it is natural to define "optimum way" around stability. With this in mind it is a natural approach to establish the control criteria on the basis of Lyapunov's direct method which is the best single technique for the stability analysis of linear or nonlinear processes.

The Appendix to this paper presents many of the pertinent details of the method and thus it is only necessary here to quote some of these results. Briefly, the method is a mathematical abstraction of the simple concept that if the total free energy of a system is always decreasing then that system must be stable. This may be implemented in the present case by finding a scalar function $V(\mathbf{y}) = V(y_1, y_2, - - -, y_n)$ called the Lyapunov function which has the property that the difference $\Delta V(\mathbf{y})$ is minimized over each sampling period by a suitable choice of the $\mathbf{u}(k)$. Note that this consists in the analogous case of the continuous rather than the discrete system of causing the derivative of $V(\mathbf{y})$ to be negative. The function selected here to be used as $V(\mathbf{y})$ is given by

$$V[\mathbf{y}(k)] = \mathbf{y}^T(k)\,\mathbf{Q}\,\mathbf{y}(k) \tag{7}$$

where $\mathbf{Q}$ is a positive-definite matrix. As a consequence

$$\begin{aligned} \Delta V(\mathbf{y}(k)) &\equiv \Delta V(k) \\ &= \mathbf{y}^T(k+1)\,\mathbf{Q}\,\mathbf{y}(k+1) \\ &\quad - \mathbf{y}^T(k)\,\mathbf{Q}\,\mathbf{y}(k) \end{aligned} \tag{8}$$

and using equation (6) with the inputs $u_i = 0$

$$\Delta V(k) = \mathbf{y}^T(k)\,\mathbf{P}\,\mathbf{y}(k) \tag{9}$$

where

$$\mathbf{P} = \boldsymbol{\Phi}^T\mathbf{Q}\,\boldsymbol{\Phi} - \mathbf{Q} \tag{10}$$

$$\Phi = \exp[\mathbf{D}\,\tau]$$

Note that if $\mathbf{P}$ is a negative-definite matrix $\Delta V(k)$ in equation (9) is always negative. As a result the problem becomes one of finding that positive-definite matrix $\mathbf{Q}$ which, when equation (10) is solved, yields a negative-definite matrix $\mathbf{P}$. If this can be accomplished the unforced system, $u_i = 0$, is always stable.

The control criterion of interest can now be stated as:

"Choose the input $\mathbf{u}(k)$ in such a way that the resulting $\Delta V(k)$ is more negative than it would be if the inputs $\mathbf{u}(k)$ were zero. The optimum control vector is that $\mathbf{u}(k)$ which makes $\Delta V(k)$ the most negative."

At this point it is profitable to mention a few important points which motivate such a control criteria. First, the method stresses and establishes stability. A major problem of many designs is to show that if a certain error criteria is minimized the resulting closed-loop system is always stable. By using the present method it is assured that there are no initial conditions which can cause unstability. Second, the method is relatively simple to use assuming suitable computational facilities. The only period of time taken into account in the control is that interval between two successive sampling instants. It is not necessary to consider any past history in order to decide what to do, nor is it necessary to project into the future beyond the bare minimum of one sampling interval. Finally, by solving the problem one

VOL. 16 1962

interval at a time the necessity of an accurate model is greatly reduced. In fact the accuracy of the model is the practical stumbling block to many design approaches which attempt to minimize some criteria over a period of time not warranted by the data used in arriving at the model. It is for these reasons, establishment of stability, simplicity and practicability, that the method of LYAPUNOV is most attractive for establishing a control criteria.

CALCULATING THE OPTIMAL CONTROL VECTOR

There are a number of possible methods which can be used to implement the control strategy defined above for specifying the optimal control vector. In the present section three such possibilities are discussed.

Quantized approximation

The first method is called the quantized approximation and results by starting with equation (6) and noting that for a particular choice of $\mathbf{u}(k)$

$$\mathbf{y}(k+1) = \boldsymbol{\Phi}\,\mathbf{y}(k) + \boldsymbol{\Delta} \qquad (11)$$

where

$$\boldsymbol{\Phi} = \exp\left[\left(\mathbf{D} + \sum_{i=1}^{r} u_i\,\mathbf{E}_i\right)\tau\right]$$

$$\boldsymbol{\Delta} = \sum_{i=1}^{r}\int_{0}^{\tau} u_i \exp\left[\left(\mathbf{D} + \sum_{i=1}^{r} u_i\,\mathbf{E}_i\right)\lambda\right]\mathbf{D}_i\,d\lambda \qquad (12)$$

Substituting (11) into (8) there results

$$\Delta V(k) = \mathbf{y}^T(k)\left[\boldsymbol{\Phi}^T\,\mathbf{Q}\,\boldsymbol{\Phi} - \mathbf{Q}\right]\mathbf{y}(k) + 2\,\boldsymbol{\Delta}^T\,\mathbf{Q}\,\boldsymbol{\Phi}\,\mathbf{y}(k) + \boldsymbol{\Delta}^T\,\mathbf{Q}\,\boldsymbol{\Delta}$$

and letting

$$\begin{aligned}\mathbf{P} &= \boldsymbol{\Phi}^T\,\mathbf{Q}\,\boldsymbol{\Phi} - \mathbf{Q} = \text{square matrix}\\ \mathbf{s} &= 2\,\boldsymbol{\Phi}^T\,\mathbf{Q}\,\boldsymbol{\Delta} = \text{vector}\\ R &= \boldsymbol{\Delta}^T\,\mathbf{Q}\,\boldsymbol{\Delta} = \text{scalar}\end{aligned} \qquad (13)$$

$\Delta V(k)$ becomes

$$\Delta V(k) = \left[\mathbf{P}\,\mathbf{y}(k) + \mathbf{s}\right]^T\mathbf{y}(k) + R \qquad (14)$$

The $\mathbf{P}$ matrix definded in equation (10) is not necessarily the same as $\mathbf{P}$ defined by equation (13), since in the latter case $\boldsymbol{\Phi}$ has been altered by the inclusion of the control vector.

To determine the optimum control vector a possible procedure would be to differentiate equation (14) with respect $\mathbf{u}(k)$, set the result to zero and solve this equation for $\mathbf{u}(k)$. Since this would involve determining the derivative of both $\boldsymbol{\Phi}$ and $\boldsymbol{\Delta}$ with respect to $\mathbf{u}$, and then manipulating the answers, this approach does not seem fruitful. The difficulty is further enhanced when restraints are placed on the $\mathbf{u}$ vector, i.e.

$$b_i \leqslant u_i \leqslant c_i$$

To circumvent these problems, the $\mathbf{u}$'s can be quantized, i.e. the choice of $\mathbf{u}$ can be limited to a finite set selected by some means. Denoting a typical member of that set by u_i, it is easy for a digital computor to calculate a $\mathbf{P}$ matrix, $\mathbf{s}$ vector and the number R defined by equations (13) and denoted as $\mathbf{P}_i$, $\mathbf{s}_i$ and R_i. To illustrate this point let us say that there are two inputs u_1 and u_2 restricted such that

$$-2 \leqslant u_1 \leqslant 3$$

$$-1 \leqslant u_2 \leqslant 1$$

This immediately implies that equation (6) will have the form

$$\frac{d\mathbf{y}}{dt} = \left[\mathbf{D} + u_1\,\mathbf{E}_1 + u_2\,\mathbf{E}_2\right]\mathbf{y} + u_1\,\mathbf{D}_1 + u_2\,\mathbf{D}_2$$

It can then be assumed that adequate control results from using only eighteen possible control vectors; these being generated from the various combinations of using six values of u_1 and three of u_2. For instance the six values of u_1 could be $[-2, -1, 0, 1, 2, 3]$, and the three of u_2 could be $[-1, 0, 1]$. The set of eighteen vectors would then be

$$\begin{bmatrix}3\\1\end{bmatrix};\ \begin{bmatrix}3\\0\end{bmatrix};\ \begin{bmatrix}3\\-1\end{bmatrix};\ \begin{bmatrix}2\\1\end{bmatrix}\ldots;$$

$$\begin{bmatrix}0\\0\end{bmatrix};\ldots;\ \begin{bmatrix}-2\\0\end{bmatrix};\ \begin{bmatrix}-2\\-1\end{bmatrix}$$

with the null vector a member of this set.

On this basis the procedure for calculating the $\mathbf{P}_i$, $\mathbf{s}_i$ and R_i sets would be as follows:

First, determine a $\mathbf{Q}$ matrix, if necessary, using equation (10) with $\mathbf{P} = -\mathbf{I}$ and solving the system

$$-\mathbf{I} = [\exp(\mathbf{D}\,\tau)]^T\,\mathbf{Q}\,[\exp(\mathbf{D}\,\tau)] - \mathbf{Q}$$

Next, use the first control vector of the set to determine $\mathbf{\Phi}_1$ and $\mathbf{\Delta}_1$ by means of equation (12). For the above numbers this means that

$$\mathbf{\Phi}_1 = \exp[\mathbf{D} + 3\,\mathbf{E}_1 + 1\,\mathbf{E}_2]\,\tau$$

$$\mathbf{\Delta}_1 = 3\int_0^\tau \exp\{[\mathbf{D} + 3\,\mathbf{E}_1 + 1\,\mathbf{E}_2]\,\lambda\}\,\mathbf{D}_1\,d\lambda + 1\int_0^\tau \exp\{[\mathbf{D} + 3\,\mathbf{E}_1 + 1\,\mathbf{E}_2]\,\lambda\}\,\mathbf{D}_2\,d\lambda$$

There are a variety of ways to calculate $\mathbf{\Phi}_1$ and $\mathbf{\Delta}_1$ from the above formulae if a digital computer is used. The simplest procedure is to use infinite matrix polynomials, in the form,

$$\exp(\mathbf{A}\,\tau) = \mathbf{I} + \mathbf{A}\,\tau + \frac{\mathbf{A}^2\,\tau^2}{2!} + \ldots = \sum_{i=0}^{\infty} \frac{[\mathbf{A}\,\tau]^i}{i!}$$

$$\int_0^\tau \exp[\mathbf{A}\,\lambda]\,d\lambda = \mathbf{I}\,\tau + \frac{\mathbf{A}\,\tau^2}{2!} + \frac{\mathbf{A}^2\,\tau^3}{3!} + \ldots = \sum_{i=0}^{\infty} \frac{[\mathbf{A}\,\tau]^i}{i!}\,\frac{\tau}{i+1}$$

and only involves matrix multiplication and addition. Once $\mathbf{Q}$, $\mathbf{\Phi}_1$ and $\mathbf{\Delta}_1$ are determined it is possible to use equations (13) to calculate $\mathbf{P}_1$, $\mathbf{s}_1$, and R_1.

Using the next control vector, in this case $[3\,0]^T$, $\mathbf{\Phi}_2$ and $\mathbf{\Delta}_2$ can be calculated in exactly the same way. With these and the same $\mathbf{Q}$, $\mathbf{P}_2$, $\mathbf{s}_2$ and R_2 follow. In like fashion each of the eighteen control vectors can be used and a corresponding $\mathbf{P}$, $\mathbf{s}$ and R evaluated. Now using equation (14) and a particular value of $\mathbf{y}$, eighteen ΔV's can be calculated, i.e.

$$\Delta V_1 = [\mathbf{P}_1\,\mathbf{y} + \mathbf{s}_1]^T\,\mathbf{y} + R_1$$
$$\Delta V_2 = [\mathbf{P}_2\,\mathbf{y} + \mathbf{s}_2]^T\,\mathbf{y} + R_2$$
$$\vdots$$
$$\Delta V_{18} = [\mathbf{P}_{18}\,\mathbf{y} + \mathbf{s}_{18}]^T\,\mathbf{y} + R_{18}$$

From these eighteen scalar values the optimal one is the one which is most negative. If it were, as an example, the fourth ΔV the optimal control values would be $u_1 = 2$ and $u_2 = 1$.

The entire process can be mechanized quite easily since once the system dynamic equations are known the values of the eighteen $\mathbf{P}$'s, $\mathbf{s}$'s and R's can be calculated. Starting with the initial value $\mathbf{y}(0)$ the eighteen ΔV's are evaluated, the most negative chosen and the associated optimal $\mathbf{u}(0)$ applied. From the system dynamics the resulting $\mathbf{y}(1)$ at the end of the first sampling period follows directly. The entire process is repeated to yield $\mathbf{u}(1)$ and $\mathbf{y}(2)$ and then continued in the same manner until $\mathbf{y}_{ss}$ is reached. Note that the calculations are sufficiently complicated that a digital computer is required.

Continuous approximation

Although the present method is as general as the preceding quantized approach it becomes increasingly complicated as the number of inputs increase. However, with only one or two inputs to manipulate and either the range in the values of the inputs not exceedingly large, the method results in great computational simplicity.

The basis of the method is to expand $\mathbf{\Phi}$ and $\mathbf{\Delta}$ as a matrix polynomial in $\mathbf{u}$. If the control vector is a scalar u, i.e. there is only one input, $\mathbf{\Phi}$ in equation (12) can be defined as follows:

$$\mathbf{\Phi} = \exp[\mathbf{D} + u\,\mathbf{E}_1]\,\tau = \sum_{i=0}^{\infty} u^i\,\mathbf{\Psi}_i = \mathbf{\Psi}_0 + u\,\mathbf{\Psi}_1 + u^2\,\mathbf{\Psi}_2 + \ldots$$

where

$$\mathbf{\Psi}_0 = \exp[\mathbf{D}\,\tau]$$

$$\mathbf{\Psi}_i = \sum_{i=1}^{\infty} \mathbf{C}_i\,\frac{\tau^i}{i!} \qquad \begin{cases} \mathbf{C}_1 = \mathbf{E}_1 \\ \mathbf{C}_{i+1} = \mathbf{D}\,\mathbf{C}_i + \mathbf{E}_1\,\mathbf{D}^i \end{cases} \qquad (15)$$

Similarly the expansion for Δ can be written as

$$\Delta = \sum_{i=1}^{\infty} u^i \, \mathbf{U}_i = u \, \mathbf{U}_1 + u^2 \, \mathbf{U}_2 + \ldots\ldots$$

and thus it is possible to rewrite equation (11) in the form

$$\mathbf{y}(k+1) = \boldsymbol{\Psi}_0 \, \mathbf{y}(k) + \sum_{i=1}^{\infty} u^i \, [\boldsymbol{\Psi}_i \, \mathbf{y}(k) + \mathbf{U}_i]$$

$$= \boldsymbol{\Psi}_0 \, \mathbf{y}(k) + \sum_{i=1}^{M} u^i \, [\boldsymbol{\Psi}_i \, \mathbf{y}(k) + \mathbf{U}_i] + \mathbf{E}_M \quad (16)$$

where $\mathbf{E}_M = \sum_{i=M+1}^{\infty} u^i \, [\boldsymbol{\Psi}_i \, \mathbf{y}(k) + \mathbf{U}_i]$.

$\mathbf{E}_M$ may be thought of as the truncation error associated with only retaining M terms in the series expansion.

The control procedure is to substitute equation (16), with $\mathbf{E}_M$ deleted, into equation (9). M is selected either by experimentation or by other considerations. This substitution results in a $2M$-degree polynomial in u which can be differentiated with respect to u and set equal to zero. The roots of the resulting $2M-1$ polynomial can then be determined by standard root-finding techniques. (It is necessary, of course, to determine which of these roots minimize equation (9). However, there are many standard procedures for doing this).

As an illustration of the simplicity that results with this procedure consider the case $M = 1$. Equation (16) now becomes

$$\mathbf{y}(k+1) = \boldsymbol{\Psi}_0 \, \mathbf{y}(k) + u \, [\boldsymbol{\Psi}_1 \, \mathbf{y}(k) + \mathbf{U}_1]$$

where $\boldsymbol{\Psi}_0$ and $\boldsymbol{\Psi}_1$ are given by equation (15) and $\mathbf{U}_1$ is calculated by

$$\mathbf{U}_1 = \left\{ \int^{\tau} \exp[\mathbf{D}\,\lambda] \, d\lambda \right\} \mathbf{D}_1 = \left\{ \sum_{i=0}^{\infty} \frac{(\mathbf{D}\,\tau)^i}{i\,!} \frac{\tau}{i+1} \right\} \mathbf{D}_1$$

Letting $\boldsymbol{\Delta}_1$ denote $\boldsymbol{\Psi}_1 \, \mathbf{y}(k) + \mathbf{U}_1$ there results

$$\mathbf{y}(k+1) = \boldsymbol{\Psi}_0 \, \mathbf{y}(k) + u \, \boldsymbol{\Delta}_1 \quad (17)$$

Differentiating equation (9) with respect to u leads to

$$\frac{d\Delta V(k)}{du} = 2 \frac{d \, \mathbf{y}^T(k+1)}{du} \mathbf{Q} \, \mathbf{y}(k+1)$$

and from equation (17) it can be seen that

$$\frac{d \, \mathbf{y}^T(k+1)}{du} = \boldsymbol{\Delta}_1{}^T$$

Thus setting the derivative of $\Delta V(k)$ to zero

$$\boldsymbol{\Delta}_1{}^T \mathbf{Q} \, \mathbf{y}(k+1) = 0$$

and substituting again from equation (17) finally forms

$$[\boldsymbol{\Delta}_1{}^T \mathbf{Q} \, \boldsymbol{\Psi}_0] \, \mathbf{y}(k) + [\boldsymbol{\Delta}_1{}^T \mathbf{Q} \, \boldsymbol{\Delta}_1] \, u = 0$$

or

$$u = -\frac{[\boldsymbol{\Delta}_1{}^T \mathbf{Q} \, \boldsymbol{\Psi}_0]}{[\boldsymbol{\Delta}_1{}^T \mathbf{Q} \, \boldsymbol{\Delta}_1]} \mathbf{y}(k) \quad (18)$$

It can be seen from equation (18) that the calculations needed to determine the optimal value of u are relatively simple and involve only a few matrix operations. Just as in the quantized approach equation (18) is repeated at each sampling period to develop the sequence of optimal control values.

Without giving any rigorous analysis, a close inspection of equation (18) points out the major problem which can arise in using this procedure. Suppose $\mathbf{y}(k)$ is such that

$$\boldsymbol{\Psi}_1 \, \mathbf{y}(k) = -\mathbf{U}_1$$

In this case $\boldsymbol{\Delta}_1$ and the denominator of equation (18) would be zero; the calculation results in an answer of $u = \infty$. If equation (17) were not an approximation an infinite value of u could be tolerated since $\boldsymbol{\Delta}_1$ would be zero. However, since equation (17) is merely an approximation, such an answer would be disastrous. Various procedures could be used to circumvent this problem. One would be to use a higher order polynomial approximation whenever the denominator of equation (18) was less than a certain amount. Another would be to switch to the quantized approach at this point. In any case, the first-order approximation affords a simple means of arriving

at proper control, providing care is used in its application.

To round off the theory of this Section an analysis of the influence of the ignored $\mathbf{E}_M$ in equation (16) can be made. The results of such analysis show that for any τ, there always exits an M large enough such that if $|u| < |u_{\max}(M)|$ all y's are returned to a circle of size $||\mathbf{y}(M)||$. Further, $|u_{\max}(M)|$ may be arbitrarily large and $||\mathbf{y}(M)||$ may be arbitrarily small. The symbol $||\mathbf{y}||$ denotes the norm of $\mathbf{y}(M)$. Thus by taking enough turns in the expansion the difficulties mentioned in the preceding paragraph can always be eliminated.

Iterative approach

The present method calculates the optimum control vector by an iteration scheme as contrasted to the previous two methods which were direct. The iteration is performed on the polynomial expansion of Φ and Δ given in the preceding Section.

Considering only one input the procedure involving equation (18) can be used to calculate a first approximation, called $u^{(1)}$, to the optimal vector. The iteration now consists of recalculating the variable u in order to obtain a correction to $u^{(1)}$. For this purpose define a new variable $u^{(2)}$ such that

$$u = u^{(2)} + u^{(1)} \tag{19}$$

Substituting (19) into (6) there results (with only one input $u_1 = u$)

$$\frac{d\mathbf{y}}{dt} = (\mathbf{D} + u^{(1)}\,\mathbf{E}_1)\,\mathbf{y} + u^{(2)}\,\mathbf{E}_1\,\mathbf{y} + u^{(1)}\,\mathbf{D}_1 + u^{(2)}\,\mathbf{D}_1$$

The matrix $\mathbf{D} + u^{(1)}\,\mathbf{E}_1$ is a constant matrix (since $u^{(1)}$ has been calculated) and can be denoted as $\mathbf{A}_2$. Similarly the vector $u^{(1)}\,\mathbf{D}_1$ is constant and may be denoted $\mathbf{D}_2$. As a result

$$\frac{d\mathbf{y}}{dt} = [\mathbf{A}_2 + u^{(2)}\,\mathbf{E}_1]\,\mathbf{y} + u^{(2)}\,\mathbf{D}_1 + \mathbf{D}_2$$

This equation is similar in form to (6), (except for the inclusion of the vector $\mathbf{D}_2$), and thus in an analogous fashion it is possible to arrive at a new form for equation (17), i.e.

$$\mathbf{y}(k+1) = \Psi_0\,\mathbf{y}(k) + u^{(2)}\,\Delta_1 + \Delta_2 \tag{20}$$

Note that Ψ_0 and Δ_1 are now different from the corresponding terms of equation (17). Thus Ψ_0 in equation (20) is calculated from

$$\Psi_0 = \exp[\mathbf{D} + u^{(1)}\,\mathbf{E}_1]\,\tau = \exp[\mathbf{A}_2]\,\tau$$

Following the procedure used in determining u_1, a value of $u^{(2)}$ which minimizes $\Delta\,V(k)$ can be obtained. It is

$$u^{(2)} = \frac{\Delta_1^{\,T}\,\mathbf{Q}\,\Psi}{\Delta_1^{\,T}\,\mathbf{Q}\,\Delta_1}\,\mathbf{y}(k) - \frac{\Delta_1^{\,T}\,\mathbf{Q}\,\Delta_2}{\Delta_1^{\,T}\,\mathbf{Q}\,\Delta_1}$$

Redefining the variable u by the equation

$$u = u^{(3)} + [u^{(2)} + u^{(1)}]$$

the procedure just outlined for determining $u^{(2)}$ is repeated. This time $u^{(2)} + u^{(1)}$ is to be considered constant and $u^{(3)}$ is the variable. This process can be repeated until $u^{(N)} \to 0$ at which the time u_{optimum} is equal to $\sum_{i=1}^{N-1} u^{(i)}$. The entire procedure must be applied at each sampling instant.

Actually the procedure outlined using equation (3) and (4) and the iterative sequence between can also be used to solve the present problem. The method is, however, quite inefficient and very time consuming. To briefly outline this method consider equation (5), and suppose that a guess is made of the control value $d^{(1)}$ (the superscript is used to indicate the initial guess). Once this value of $d^{(1)}$ is specified equation (5) is completely determined and may be written in the form of equation (3). The Φ matrix and Δ_2 vector in equation (3) are now known and the iteration pattern can be used to calculate $\mathbf{C}^{\infty}$ and then $m_2(1)$ in equation (4). If $d^{(1)} = m_2(1)$ the guess originally made was correct; if $d^{(1)} \neq m_2(1)$, the guess was wrong and the process is repeated using $d^{(2)} = m_2(1)$. This procedure is continued until finally $|d^{(r)} - m_2(1)| < \epsilon$, some tolerable error. When this criteria has been met the initial value of d, at $t = 0$, is known and equation (5) can be used to advance $\mathbf{x}(0)$ to $\mathbf{x}(1)$. The process of guessing d and iterating is then used again, etc. Note that what is being done is a large search or iteration process per sampling period which in-

cludes a subiteration iteration within the over-all iteration. It would seem obvious that such a procedure would require a large amount of computing time.

From the authors experience in using the three methods outlined above it is possible to make a number of qualitative statements. The quantized approach has the distinct advantage of applying to problems where the inputs may saturate. Its main disadvantage is that fine control is generally lacking. Systems controlled in this fashion are characterized by long tails on their response curves. The continuous approximation is more or less the antithesis of the quantized in that fine control is good but difficulties may be encountered in controlling large perturbations. Thus a combination of the two methods is probably the best to use. The iterative approach has the decided disadvantage of requiring excessive calculation time and thus is not recommended.

VOL. 16 1962

Numerical examples

In the present Section results are given for the numerical use of the above methods as applied to the train of six extraction units defined previously. The resulting data are plotted in Fig. 2.

Using only the quantized approach

Before the quantized approach can be used it is necessary to convert the system dynamic equation (5) to the general form given by (6). Note that in performing this transformation F/a is taken as a constant and that r, the upper limit on the summation of equation (6), is merely 1 since only one control variable is involved. On this basis equation (5) can be written as

$$\frac{d\mathbf{x}}{dt} = \left(\mathbf{A} + \frac{F}{a}\,\mathbf{E}_2\right)\mathbf{x} + d\,\mathbf{E}_1\,\mathbf{x} + d\,\mathbf{D}_3 + \frac{F}{a}\,\mathbf{D}_4 \qquad (5)$$

and at the desired equilibrium point

$$0 = \left(\mathbf{A} + \frac{F}{a}\,\mathbf{E}_2\right)\mathbf{x}_{ss} + d_{ss}\,\mathbf{E}_1\,\mathbf{x}_{ss} + d_{ss}\,\mathbf{D}_3 + \frac{F}{a}\,\mathbf{D}_3$$

Solving for $\mathbf{x}_{ss}$ yields

$$\mathbf{x}_{ss} = -\left[\mathbf{A} + \frac{F}{a}\,\mathbf{E}_2 + d_{ss}\,\mathbf{E}_1\right]^{-1}\left[d_{ss}\,\mathbf{D}_3 + \frac{F}{a}\,\mathbf{D}_4\right]$$

and defining

$$\mathbf{y} = \mathbf{x} - \mathbf{x}_{ss} \qquad \mathbf{D}_1 = \mathbf{D}_3 + \mathbf{E}_1\,\mathbf{x}_{ss}$$

$$u = d - d_{ss} \qquad \mathbf{D} = \mathbf{A} + \frac{F}{a}\,\mathbf{E}_2 + d_{ss}\,\mathbf{E}_1$$

transforms equation (5) into the final form

$$\frac{d\mathbf{y}}{dt} = [\mathbf{D} + u\,\mathbf{E}_1]\,\mathbf{y} + u\,\mathbf{D}_1 \qquad (21)$$

As a first step in the actual computation it is necessary to evaluate $\exp[\mathbf{D}\,\tau]$ by the infinite series expansion. For $\tau = 0{\cdot}20$ the result is (retaining only three decimals)

$$\mathbf{\Phi} = \exp[\mathbf{D}\,\tau] = \begin{bmatrix} 0{\cdot}645 & 0{\cdot}169 & 0{\cdot}022 & 0{\cdot}002 & 0 & 0 \\ 0{\cdot}128 & 0{\cdot}662 & 0{\cdot}163 & 0{\cdot}021 & 0{\cdot}002 & 0 \\ 0{\cdot}012 & 0{\cdot}123 & 0{\cdot}608 & 0{\cdot}156 & 0{\cdot}020 & 0{\cdot}002 \\ 0{\cdot}001 & 0{\cdot}018 & 0{\cdot}177 & 0{\cdot}615 & 0{\cdot}156 & 0{\cdot}200 \\ 0 & 0{\cdot}002 & 0{\cdot}026 & 0{\cdot}176 & 0{\cdot}615 & 0{\cdot}154 \\ 0 & 0 & 0{\cdot}003 & 0{\cdot}026 & 0{\cdot}175 & 0{\cdot}592 \end{bmatrix}$$

The matrix $\mathbf{Q}$ was chosen to be the identity matrix $\mathbf{I}$. As a check to see if this choice is satisfactory the roots of $\mathbf{P}$ in equation (10) were computed using

$$\text{roots}\,[\mathbf{P}] = \text{roots}\left\{\exp[\mathbf{D}^T\,\tau]\,\exp[\mathbf{D}\,\tau] - \mathbf{I}\right\}$$

The values obtained were $-0{\cdot}715$, $-0{\cdot}670$, $-0{\cdot}688$, $-0{\cdot}686$, $-0{\cdot}700$ and $-0{\cdot}813$. Since $\mathbf{P} = \mathbf{P}^T$ and all its roots are negative $\mathbf{P}$ is negative definite. Therefore $\mathbf{Q} = \mathbf{I}$ is allowable.

To perform the quantization the u values were restricted to lie between $2{\cdot}0$ and $-1{\cdot}0$ with ten explicit values

$$2{\cdot}0\,;\ 0{\cdot}5\,;\ 0{\cdot}25\,;\ 0{\cdot}125\,;\ 0{\cdot}0625\,;$$
$$0{\cdot}01325\,;\ 0\,;\ -0{\cdot}05\,;\ -0{\cdot}1\,;\ -1{\cdot}0$$

On the basis of these values the corresponding ten matrices $\mathbf{P}$, vectors $\mathbf{s}$ and scalars R were computed and stored in computer memory. As an example, for $u = 2{\cdot}0$, they were

$$\mathbf{P} = \begin{bmatrix} -0{\cdot}7152 & 0{\cdot}2053 & 0{\cdot}0772 & 0{\cdot}0217 & 0{\cdot}0048 & 0{\cdot}0009 \\ 0{\cdot}2053 & -0{\cdot}6704 & 0{\cdot}2034 & 0{\cdot}0821 & 0{\cdot}0240 & 0{\cdot}0052 \\ 0{\cdot}0772 & 0{\cdot}2034 & -0{\cdot}6882 & 0{\cdot}2150 & 0{\cdot}0901 & 0{\cdot}0247 \\ 0{\cdot}0217 & 0{\cdot}0821 & 0{\cdot}2150 & -0{\cdot}6856 & 0{\cdot}2124 & 0{\cdot}0762 \\ 0{\cdot}0048 & 0{\cdot}0240 & 0{\cdot}0901 & 0{\cdot}2124 & -0{\cdot}7004 & 0{\cdot}1687 \\ 0{\cdot}0009 & 0{\cdot}0052 & 0{\cdot}0247 & 0{\cdot}0762 & 0{\cdot}1687 & -0{\cdot}8139 \end{bmatrix}$$

$$\mathbf{s} = [0{\cdot}0032 \quad 0{\cdot}0037 \quad 0{\cdot}0036 \quad 0{\cdot}0039 \quad 0{\cdot}0037 \quad 0{\cdot}0024]$$

$$R = 0{\cdot}00024$$

At each sampling instant $\mathbf{y}(k)$ was computed from the sampled $\mathbf{x}(k)$ and the known $\mathbf{x}_{ss}$. The ten values of $\Delta V(k)$ were then computed by means of equation (14) using the stored values of $\mathbf{P}$, $\mathbf{s}$ and R and the given $\mathbf{y}(k)$. The value of u corresponding to the most negative such $\Delta V(k)$ was then used for the control signal for the next period. To illustrate, for the initial value of $\mathbf{x}(0)$, $\mathbf{y}(0)$ was computed to be:

$$\mathbf{y}(0) = \mathbf{x}(0) - \mathbf{x}_{ss} = \begin{bmatrix} -0{\cdot}0087822 \\ -0{\cdot}0095841 \\ -0{\cdot}0079750 \\ -0{\cdot}0089374 \\ -0{\cdot}0077737 \\ -0{\cdot}0047414 \end{bmatrix}$$

The ten values $\Delta V(0)$ calculated for this $\mathbf{y}(0)$ are:

$$-30{\cdot}3 \times 10^{-5};\ -12 \times 10^{-5};\ -0{\cdot}3 \times 10^{-5};$$
$$-7{\cdot}7 \times 10^{-5};\ -7{\cdot}0 \times 10^{-5};\ -6{\cdot}6 \times 10^{-5};$$
$$-6{\cdot}2 \times 10^{-5};\ -5{\cdot}6 \times 10^{-5};\ -5{\cdot}0 \times 10^{-5};$$
$$-6{\cdot}3 \times 10^{-5}$$

It is clear that the most negative value is the first, corresponding to an input of $d = 3{\cdot}0$. Proceeding in a like fashion for the other sampling intervals the results shown in Fig. 2 were obtained.

Quantized approach and continuous approximation

The control signal for the continuous method using a first-order approximation can be calculated directly from equation (18). In order to circumvent the problems which arise for large u it was decided to proceed as follows:

(1) Calculate u at the desired sampling period using equation (18). If $|u|$ as calculated by this equation is less than 1·0 this value of u is taken as satisfactory.

(2) If $|u| > 1{\cdot}0$, the programme switched to the quantized method using only the three values of $u = 1{\cdot}0$, 0 and 2·0.

In (1) the use of equation (18) requires the calculation of Ψ_0 and Δ_1. Ψ_0 is merely $\exp[\mathbf{D}\tau]$ as already given and Δ_1 can be calculated using Ψ_1 and $\mathbf{U}_1$ (see equation 17). $\mathbf{U}_1$ results directly from the definition of Φ with $u = 0$ and Ψ_1 from the use of equation (15). In the latter case there results

$$\Psi_1 = \begin{bmatrix} -0{\cdot}112 & -0{\cdot}031 & -0{\cdot}004 & & & \\ 0{\cdot}104 & -0{\cdot}099 & -0{\cdot}028 & -0{\cdot}004 & & \\ 0{\cdot}022 & 0{\cdot}102 & -0{\cdot}090 & -0{\cdot}027 & -0{\cdot}004 & \\ 0{\cdot}003 & 0{\cdot}027 & 0{\cdot}087 & -0{\cdot}092 & -0{\cdot}027 & -0{\cdot}004 \\ & 0{\cdot}004 & 0{\cdot}030 & 0{\cdot}087 & -0{\cdot}092 & -0{\cdot}028 \\ & & 0{\cdot}005 & 0{\cdot}030 & 0{\cdot}084 & -0{\cdot}103 \end{bmatrix}$$

Fig. 2 shows the control achieved by using this approach.

Iterative approach

The use of the iterative approach is felt to be sufficiently direct so that no details of the calculation are necessary. In light of the computation time required for this method (see below) the usefulness of the method is in serious doubt. For this reason also the detailed computations are deleted. The results however are shown in Fig. 2.

Discussion of Results

Fig. 2 contains the results of the three control

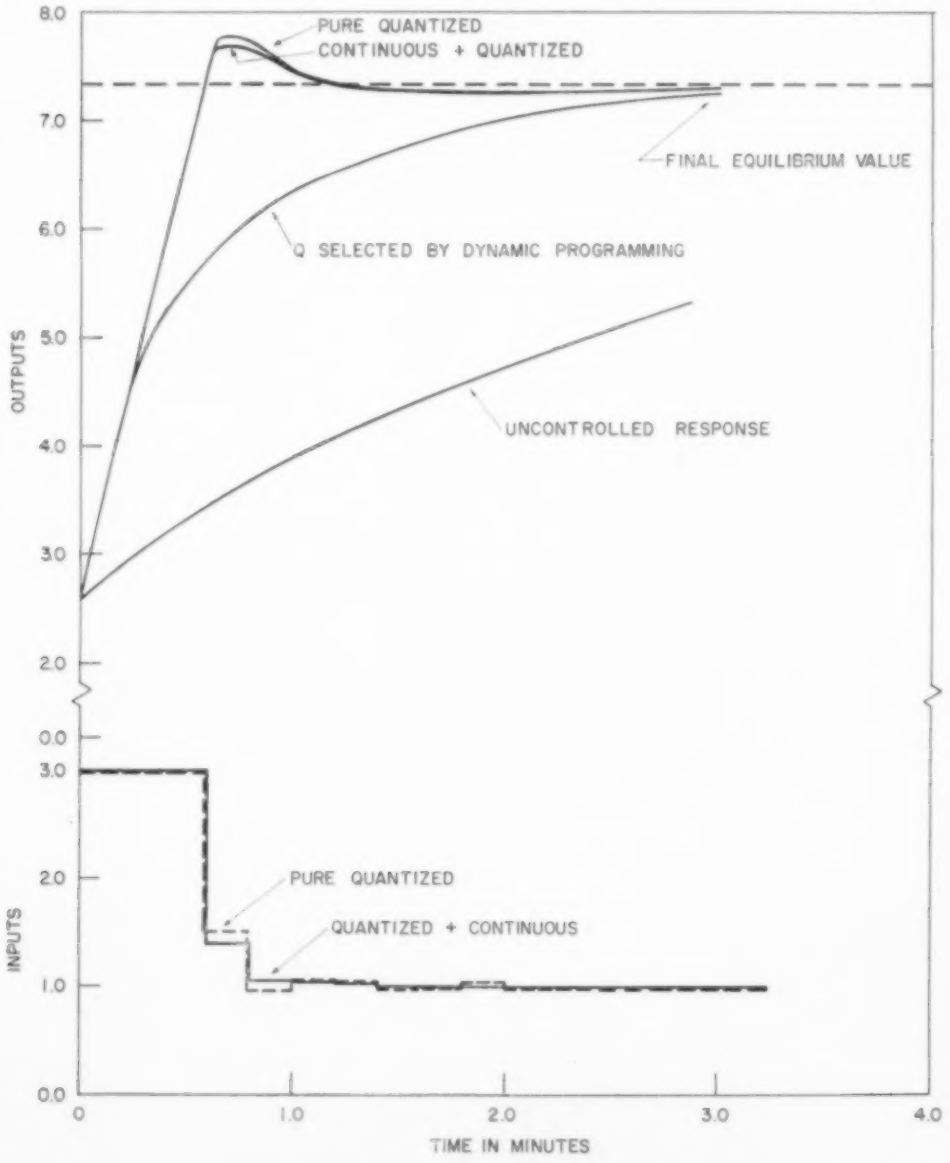

Fig. 2. Dynamic response of extraction train using various control schemes.

methods as applied to the train of six extraction units. The plot shows the exit composition from stage 6, x_6, vs. the time of operation t. Also shown is the normal transient response of the process and the control action for the continuous and quantized approaches.

In any linear process of this type in which the inputs saturate, it is to be expected that for reasonably fast response the inputs will be at one of the limits or at zero. It is seen that this is essentially what occurred for the pure quantized and continuous plus quantized approach. As was expected, the combination approach had a slightly better response over-all than the pure quantized solution. However for large movements in the state space, as here, the difference is not striking. Normal regulatory action at a steady-state would produce more favourable response for the continuous approach.

As far as computational time is concerned, it required about 5 min. on an I.B.M. 704 to compute the proper inputs using the iteration technique described by equation (4) and about 5 sec for either the quantized or the continuous approach. This difference is so great as to make the iteration technique a curiosity rather than a really workable method.

NOTATION

$a = h\,\alpha + H$

b = raffinate (main) solvent flow rate

$b^* = b + F$

$d = b/a$

$d^* = b^*/a$

$d^{(1)}, d^{(2)}, \cdots$ = iteration values of flow rate variable

F = raffinate (secondary) solvent flow rate

F_1 = solvent flow rate from secondary reservoir 1

F_2 = solvent flow rate from secondary reservoir 2

h = extract hold-up for any stage

H = raffinate hold-up for any stage

k = index for sampling period

$p = w\,\alpha/a$

t = time

$u_i, i = 1, 2, \cdots, r$ = generalized control flow rates in equation 6

$u^{(1)}, u^{(2)}, \cdots$ = iteration values of control variables

w = extract solvent flow rate

x_n = raffinate compostion in nth stage

x_F = composition of secondary raffinate feed stream

x_0 = composition of main raffinate feed stream

y_n = extract composition in nth stage

y_7 = composition of extract feed stream

α = parameter in equilibrium expression

β = parameter in equilibrium expression

τ = sampling period

λ = variable of integration

$\mathbf{A}$ = coefficient square matrix of equations 1 and 5

$\mathbf{C}^\alpha$ = matrix in equation (4) obtained by dynamic programming iteration

$\mathbf{D}$ = square matrix in equation (5)

$\mathbf{D}_1$ = matrix of equations (1) and (21)

$\mathbf{D}_2$ = column vector of equation (1)

$\mathbf{D}_3$ = column vector in equation (5)

$\mathbf{D}_4$ = column vector in equation (5)

$\mathbf{E}_1$ = matrix in equation (5)

$\mathbf{E}_2$ = matrix in equation (5)

$\mathbf{E}_M$ = truncation term in series of equations (16)

$\mathbf{I}$ = identity matrix

$\mathbf{m}_1$ = column vector containing inputs equation (1)

$\mathbf{m}_2$ = column vector containing inputs equation (1)

$\mathbf{P}$ = negative-definite matrix of equation (10)

$\mathbf{Q}$ = positive-definite matrix

R = scalar defined by equation (13)

$\mathbf{s}$ = column vector defined by equation (13)

$\mathbf{u}(k)$ = column vector made up of control variables, u_i

$\mathbf{U}_1$ = matrix from equation (16) with $M = 1$

$V(\mathbf{y}) = V(y_1, y_2, \cdots, y_n)$ = scalar of Lyapunov function

$\Delta V(\mathbf{y})$ = difference in Lyapunov function = $= V[\mathbf{y}(k+1) - V\,\mathbf{y}(k)]$

$\mathbf{x}$ = column vector with elements $x_1, x_2, \cdots, x_n$

$\mathbf{x}_{ss}$ = column vector of steady state values of $\mathbf{x}$

$\mathbf{y}(k)$ = column vector of dependent variables at kth sampling period

$\mathbf{z}(k)$ = column vector of dependent variables (equation 3)

$\mathbf{\Phi}$ = square matrix of equation (2)

$\mathbf{\Phi}_1$ = matrix derived from equation (12)

$\mathbf{\Delta}$ = matrix defined by equation (12)

$\mathbf{\Delta}_1$ = matrix of equation (2) and from equation (12)

$\mathbf{\Delta}_2$ = column vector of equation (2)

$\mathbf{\Psi}_0, \mathbf{\Psi}_1, \cdots$ = matrices defined by equation (15)

APPENDIX

Many of the important features of LYAPUNOV's direct method for analysing stability of a physical system can be delineated by a qualitative discussion. Consider a continuous dynamic system which is represented by the set of linear or non-linear differential equations

$$\frac{dy_i}{dt} = f_i(y_1, y_2, \cdots, y_n) \qquad i = 1, 2, \cdots, n \qquad \text{(A.1)}$$

The y_i are the dependent variables of the system. Now suppose that a scalar function $V(\mathbf{y}) = V(y_1, y_2, \cdots, y_n)$ exists near an equilibrium or steady-state point $\mathbf{y}_{ss}$ with the following properties:

I. V is always positive in the neighbourhood of $\mathbf{y}_{ss}$ but at $\mathbf{y}_{ss}$ itself V is zero. This may be expressed as

$$V(\mathbf{y}) > 0, \qquad \mathbf{y} \neq \mathbf{y}_{ss}$$

$$V(\mathbf{y}) = 0, \qquad \mathbf{y} = \mathbf{y}_{ss}$$

II. Near $\mathbf{y}_{ss}$, the derivative of V is always negative and at $\mathbf{y}_{ss}$ itself the derivative is zero. Thus

$$\frac{dV(\mathbf{y})}{dt} < 0, \qquad \mathbf{y} \neq \mathbf{y}_{ss}$$

$$\frac{dV(\mathbf{y})}{dt} = 0, \qquad \mathbf{y} = \mathbf{y}_{ss}$$

LYAPUNOV pointed out that property I corresponds to the stored energy of the dynamic system being a scalar function, always larger than some minimum value which can be taken as zero without loss of generality. In the same manner property II corresponds to the fact that the stored energy is always dissipated, except at $\mathbf{y}_{ss}$ where the energy is a minimum.

The rather obvious conclusion reached by LYAPUNOV was that if a scalar function with properties I and II can be found then the equilibrium state $\mathbf{y}_{ss}$ is a stable state. As a further point of interest we note that since $V(\mathbf{y})$ is an implicit function of t

$$\frac{dV(\mathbf{y})}{dt} = \sum_{i=1}^{n} \frac{\partial V}{\partial y_i} \cdot \frac{dy_i}{dt}$$

$$= \sum_{i=1}^{n} \frac{\partial V}{\partial y_i} \cdot f_i(\mathbf{y}) \qquad \text{(A.2)}$$

Thus once the scalar function is known the derivative can be calculated without actually solving the differential equations (A.1).

Obviously the main problem involved in using LYAPUNOV's method is in finding the scalar function $V(\mathbf{y})$ called the Lyapunov function. When (A.1) is linear $V(\mathbf{y})$ can be calculated in a straightforward manner but when (A.1) is nonlinear there is no clear cut procedure. Thus one must resort to a trial-and-error process of hunting for a Lyapunov function whenever a new system is encountered.

The discussion just presented for analysing stability of a physical system by LYAPUNOV's direct method was quite qualitative and mathematically non-rigorous. Actually there are many subtleties to the method which should be examined carefully. For the most complete discussion in the English literature the paper of KALMAN and BERTRAM [7] is highly recommended.

With this brief description of the continuous case in hand we now turn to the discrete-time dynamic system which is the main concern of the present paper. The following theorem underlies the control strategies proposed.

Theorem 1

"Consider the discrete-time, autonomous dynamic system

$$\mathbf{y}(k+1) = \mathbf{f}[\mathbf{y}(k)] \qquad \text{(A.3)}$$

The nomenclature here is that the vector $\mathbf{y}$ at time $k+1$ is some function of the vector $\mathbf{y}$ at time k. It is implicitly assumed that $\mathbf{f}(\mathbf{0}) = \mathbf{0}$.

Suppose there exists a scalar function $V(\mathbf{y})$, referred to as the Lyapunov function such that $V(\mathbf{0}) = 0$ and

I. $V(\mathbf{y}) > 0, \qquad \mathbf{y} \neq \mathbf{0}$
II. $\Delta V(\mathbf{y}) < 0, \qquad \mathbf{y} \neq \mathbf{0}$
III. $V(\mathbf{y})$ is continuous in $\mathbf{y}$
IV. $V(\mathbf{y}) \to \infty$ as the norm $\mathbf{y} \to \infty$

Under these conditions the system (A.3) is uniformly asymptotically stable in-the-large."

In this theorem $\Delta V(\mathbf{y})$, which corresponds to the derivative in the continuous case, means the difference between $V(\mathbf{y})$ at times $k+1$ and k. Asymptotic stability in-the-large means simply that no matter how much a system is initially perturbed from equilibrium, nor no matter when it is perturbed, it will always return to equilibrium. As a final point note that the form of equation (A.3) corresponds to equation (6) assuming that the system inputs are zero (an autonomous system).

A convenient Lyapunov function for Theorem 1 is the quadratic norm

$$V[\mathbf{y}(k)] = V(k) = \mathbf{y}^T(k)\,\mathbf{Q}\,\mathbf{y}(k) \qquad \text{(A.4)}$$

where $\mathbf{Q}$ is a positive definite-matrix. It can be observed that $V[\mathbf{y}(k)] = 0$ when $\mathbf{y}(k) = \mathbf{0}$ and that conditions I, III and IV of the theorem are satisfied. I is satisfied immediately because $\mathbf{Q}$ is a positive-definite matrix; III is satisfied because the derivative of $V(\mathbf{y})$ exists for all $\mathbf{y}$ and in fact

$$\frac{dV}{d\mathbf{y}} = 2\,\mathbf{Q}\,\mathbf{y}(k)$$

Finally, condition IV is satisfied because $V(\mathbf{y})$ is itself a norm.

It remains only to show that $\mathbf{Q}$ can be so chosen that $\Delta V(k)$ is negative for all k and all $\mathbf{y}$. Note that $\Delta V(k)$ is defined as

$$\Delta V(k) = \mathbf{y}^T(k+1)\,\mathbf{Q}\,\mathbf{y}(k+1) - \mathbf{y}^T(k)\,\mathbf{Q}\,y(k) \qquad \text{(A.5)}$$

In order to shorten the presentation we can seek this $\mathbf{Q}$ for the case of equation (5) or (6) rather than (A.3). The assumption is made that the existence of a steady-state in equation (5) implies that the matrix $\mathbf{D}$ in equation (6) has all its characteristic roots in the left half-plane [7]. Actually the existence of a steady state does not necessarily imply the stability of $\mathbf{D}$, nor will the method to be outlined necessarily fail if $\mathbf{D}$ is not stable. However, for most *practical* cases the assumption is valid and it will be made here in order to avoid the mathematical pathology necessary in such cases. Using equation (6) and its analogy

to equations (1) and (2), $\mathbf{y}(k+1)$ can be determined from $\mathbf{y}(k)$ if the inputs are zero, i.e.

$$\mathbf{y}(k+1) = \exp[\mathbf{D}\,\tau]\,\mathbf{y}(k) = \mathbf{\Phi}\,\mathbf{y}(k)$$

where the $\mathbf{u}(k) = \mathbf{0}$. Using this result in (A.5)

$$\begin{aligned}\Delta V(k) &= \mathbf{y}^T(k+1)\,\mathbf{Q}\,\mathbf{y}(k+1) - \mathbf{y}^T(k)\,\mathbf{Q}\,\mathbf{y}(k)\\ &= \mathbf{y}^T(k)\,[\mathbf{\Phi}^T\,\mathbf{Q}\,\mathbf{\Phi} - \mathbf{Q}]\,\mathbf{y}(k)\\ &= -\mathbf{y}^T(k)\,\mathbf{P}\,\mathbf{y}(k)\end{aligned}$$

where

$$\mathbf{P} = \mathbf{\Phi}^T\,\mathbf{Q}\,\mathbf{\Phi} - \mathbf{Q} \qquad \text{(A.6)}$$

Since all the roots of $\mathbf{D}$ are in the left-hand plane it follows that the magnitudes of the roots of $\mathbf{\Phi}$ in (A.6) are less than one. It is thus possible to use the following theorem, which is a matrix equivalent of the familiar Routh–Hurwitz procedure for determining stability of a differential equation.

Theorem 2

"If the magnitudes of all the roots of a matrix $\mathbf{\Phi}$ are less than one, then for any negative-definite matrix $\mathbf{P}$, equation (A.6) defines uniquely a positive-definite matrix $\mathbf{Q}$."

It should be pointed out that the inverse theorem does not hold. This is, any positive definite matrix $\mathbf{Q}$ does not necessarily define in equation (A.6) a negative definite matrix $\mathbf{P}$. Nevertheless, because of the theorem, it is always possible to find a matrix $\mathbf{Q}$ such that under the assumptions made (the inputs are zero, and the matrix $\mathbf{D}$ is stable) $\Delta V(k)$ in equation (A.5) is always negative. Thus, step II of Theorem I is satisfied. Normally to determine $\mathbf{Q}$ it is possible to make an intelligent guess and use (A.6) to see if $\mathbf{P}$ is negative-definite. If this fails, it is always possible to fall back on the procedure of choosing any negative-definite matrix, say minus the identity matrix set $\mathbf{P}$ equal to this chosen matrix, and then solve the algebraic equations implied by equation (A.6) to determine $\mathbf{Q}$.

Having established a function $V(\mathbf{y})$ which satisfies the the conditions of Theorem I for the autonomous system (the inputs are zero) a control criterion can be defined for choosing the input vector $\mathbf{u}(k)$. The desired control criteria can be stated as follows:

"The input $\mathbf{u}(k)$ is to be chosen in such a way that the resulting $\Delta V(k)$ is more negative than it would be if the input were zero. The optimum control vector is that $\mathbf{u}(k)$ which makes $\Delta V(k)$ most negative."

References

[1] Gantmacher F. T. *The Theory of Matrices*, Vol. 1. Chelsea Publishing Co.

[2] Kalman R. E. and Koepcke R. W. *The Role of Digital Computers in the Dynamic Optimization of Chemical Reactions* IBM Report RC–77 1958.

[3] Kalman R. E., Lapidus L. and Shapiro E. *Chem. Engng. Progr.* 1960 **56** 55.

[4] Lapidus L., Shapiro E., Shapiro S. and Stillman R. E. *Amer. Inst. Chem. Engrs. J.* 1961 **7** 288.

[5] Kalman R. E., Lapidus L. and Shapiro E. *Proc. Joint Symp. Instrument. Comput.* Institution of Chemical Engineers 1959.

[6] Bellman R. E. *Dynamic Programming*, Princeton University Press 1957.

[7] Bertram J. E. and Kalman R. E. *J. Basic Engng.* 1960 **82** 371, 344.

Chemical Engineering Science, 1961, Vol. 16, pp. 267 to 277. Pergamon Press Ltd., London. Printed in Great Britain.

Studies in turbulent mixing—I

Dilution of a jet

D. KRISTMANSON* and P. V. DANCKWERTS

The Department of Chemical Engineering, Pembroke Street, Cambridge.

(*Received* 17 *March* 1961)

Abstract—(a) A photographic method has been used to determine the concentration-distribution of jet-fluid when a circular turbulent jet of liquid mixes with an unlimited liquid environment. The time-average concentration $\bar{a}$ at a point (x, r) is given by

$$\bar{a} = 4{\cdot}78\,\frac{d}{x}\exp -\left(\frac{r}{0{\cdot}135\,x}\right)^2.$$

(b) The process of dilution on the molecular scale of jet liquid by ambient liquid has been studied by using an alkaline jet in an acid environment, both containing an indicator. A plume of blue indicator results: outside the plume all jet fluid has been diluted below some specified concentration, m. It is found that all plumes are the same shape, having a width r at a distance x from the orifice given approximately by

$$\frac{r}{x} = 0{\cdot}32\sqrt{\left(\log_{10} 6{\cdot}41\,\frac{d}{xm}\right)}.$$

The point on the axis at which all jet fluid has been diluted to a concentration m or less is 1·34 times as far from the orifice as the point at which $\bar{a} = m$.

Résumé—(a) Une méthode photographique est utilisée pour déterminer la distribution des concentrations d'un jet fluide, au cours du mélange d'un jet turbulent circulaire avec un liquide environnant non délimité.

En un point (x, r) on a pour température moyenne à

$$a = 4{,}78\,\frac{d}{x}\exp -\left(\frac{r}{0{,}135}\right)^2.$$

(b) La dilution à l'échelle moléculaire d'un jet liquide par un liquide ambiant est étudiée en utilisant un jet alcalin dans un milieu acide, chacun d'eux contenant un indicateur coloré. Il en résulte la naissance d'un cône de coloration bleue. A l'extérieur du cône tout le jet fluide a été dilué au-dessous de la concentration spécifiée m. Tous les cônes ont la même forme, et leur rayon r à une distance x de l'orifice est approximativement donnée par:

$$\frac{r}{x} = 0{,}32\sqrt{\left(\log_{10} 6{,}41\,\frac{\phi}{xm}\right)}.$$

Le point de l'axe à partir duquel tout le jet fluide est dilué à la concentration m où à une concentration inférieure, est à une distance de l'orifice valent 1,34 fois celle correspondant au point pour lequel $\bar{a} = m$.

Zusammenfassung—(a) Es wurde eine photographische Methode benutzt zur Bestimmung der Konzentrationsverteilung eines Flüssigkeitsstrahles für den Fall, in dem ein runder turbulenter Strahl einer Flüssigkeit sich mit einer umgebenden Flüssigkeit unbegrenzter Ausdehnung mischt. Die Konzentration im Zeitmittel $\bar{a}$ im Punkt (x, r) ist gegeben durch

*Present address: The Conslidated Mining and Smelting Company of Canada Ltd., Kimberley, B.C.

$$\bar{a} = 4{,}78\,\frac{d}{x}\exp - \left(\frac{r}{0{,}135\,x}\right)^2.$$

(b) Der Verdünnungsvorgang im molekularen Massstab eines Flüssigkeitsstrahls durch eine ruhende Flüssigkeit wurde mit Hilfe eines alkalischen Strahls in einer sauren Umgebung untersucht, wobei beide einen Indikator enthielten. Ein Büschel mit blauem Indikator entstand, ausserhalb des Büschels war die Flüssigkeit des Strahles stärker als ein spezielle Konzentration m verdünnt. Es wurde gefunden, dass alle Büschel gleiche Gestalt haben, die bei der Weite r im Abstand x von der Düse angenähert gegeben ist durch

$$\frac{r}{x} = 0{,}32\sqrt{\left(\log_{10} 6{,}41\,\frac{d}{mx}\right)}.$$

Der Punkt auf der Achse, bei dem die gesamte Flüssigkeit des Strahls auf eine Konzentration m oder noch weiter verdünnt wird, ist 1,34 mal so weit von der Düse entfernt als der Punkt, bei dem $\bar{a} = m$ ist.

WHEN a turbulent free jet mixes with its environment, the primary result is to intersperse macroscopic elements of the two fluids. Molecular diffusion tends to reduce the resulting variations in concentration between neighbouring regions, but in general the instantaneous concentration of the jet-fluid at any point in the mixing zone fluctuates about its mean value. The more complete the degree of mixing on the molecular scale, the less the fluctuations. More attention has been given to the easier experimental problem of measuring time-average concentrations in the mixing zone than to investigating the degree of "unmixedness" or "segregation." However, when the object of the mixing process is to bring molecules of the two fluids into proximity so that they can react chemically the degree of segregation in the mixing zone is all-important in determining the rate of reaction.

HAWTHORNE *et al.* [1] made some measurements of "unmixedness" in turbulent flames. Since the work reported in the present paper was carried out, ROSENSWEIG *et al.* [2] have reported the results of experiments on concentration-fluctuations in a smoke jet. The decay of temperature fluctuations when a hot jet mixes with a cold environment is an analogous process; CORRSIN and UBEROI [3] have made measurements of these fluctuations.

The experiments reported here were designed to investigate the decay of segregation and the dilution of the jet-fluid in the mixing zone of a liquid jet. The technique used made it unnecessary to measure spatial or temporal concentration fluctuations.

PRINCIPLE OF THE METHOD

We have to make use of the concept of "the concentration at a point" in a region of non-uniform concentration. This concept, like that of "temperature at a point," gives rise to difficulties, but for present purposes it will be sufficient merely to say that a "point" should be taken to mean a region much larger than a molecule, but much smaller than the scale of the smallest concentration "eddies" present.

Suppose the jet consists of water containing a concentration $M(1 - m)$ equivalents per unit volume of alkali, and issues into an environment consisting of water containing a concentration Mm of acid. Both liquids contain the same concentration of an indicator which is blue in alkaline solution and colourless in acid solution. Let the instantaneous concentrations (volume-fractions) of jet-fluid and of ambient fluid at a given point be a, $(1 - a)$ respectively; then if $a = m$ the fluid will be neutral, while if $a > m$ it will be alkaline and blue, while if $a < m$ it will be acid and colourless. The concentration of indicator in the blue form will be the same in all regions where $a > m$ and there will be a sharp surface between blue and colourless fluids, where $a = m$.

The position of the boundary will fluctuate because of turbulence and the segregation of the jet fluid. In general the fluid at a given point will sometimes be blue and sometimes colourless. The fraction of the time, n, for which the fluid at a given point is blue (i.e. the time-average colour density at the point, expressed as a fraction of the colour-density of the blue fluid)

is equal to the fraction of the time for which the concentration of the jet-fluid at the point is greater than m.

In principle it is possible, by taking a time-exposure photograph of the jet, to determine the colour-density at each point; then by varying m one can find the fraction of the time for which the value of a (concentration of jet-fluid) at each point exceeds any given value. With this information it is possible to calculate statistical properties such as $\bar{a}^2$ for each point. This is equivalent to the information obtained by CORRSIN and UBEROI [3] and by ROSENSWEIG *et al.* [2].

VOL. 16 1962

However the mathematical technique for deducing local values of the colour-density from the photographic image of a three-dimensional jet requires experimental measurements of greater accuracy than we were able to obtain. The results were therefore expressed in a cruder but practically useful form. This is described in more detail below. Roughly speaking, it consists of drawing a series of surfaces enclosing the coloured plumes formed with different values of m; outside each it can be said that "almost all" the jet fluid has been diluted to a volume-fraction less than m.

LIMITATIONS OF THE METHOD

Several oversimplifications have been made in this discussion of the principles of the method.

Firstly, it has been assumed that the indicator changes colour abruptly at some value of a. In practice it will be sufficient if the full change takes place over an increment of a very much less than both m and $(1 - m)$. In circumstances typical of our experiments this requirement was generally fulfilled. The full colour of the indicator is developed as the excess concentration of acid changes from about 2×10^{-4} N to zero. In the worst case (the experiment with the smallest value of m) the resulting range of a over which the colour change took place was about 7 per cent of m; in general the error was much smaller.

Secondly, it is assumed that the colour-change adjusts itself instantaneously to the locally prevailing composition. In practice it will be sufficient if the time for the colour-change to take place, in a uniformly-mixed solution containing a slight excess of one reagent, is so small that the colour-distribution is indistinguishable from that which a truly instantaneous change would give. The worst case was the jet with the largest value of m, giving the shortest coloured plume. The time taken for a particle on the axis of the jet to travel the length of the plume was about 4×10^{-2} sec; unless the colour-change reaction takes place in a much shorter time, the plume will be longer and more diffuse than it should be. However, it has been found [4] that the indicator used, bromocresol green, changes colour under these circumstances in less than 10^{-3} sec, and the reaction between acid and alkali is certainly much faster, so in the worst case the measured plume-length will be in error from this cause by less than 2·5 per cent.

Finally, the method is subject to an error, which is difficult to estimate, if the diffusivities of the acid and alkali are unequal. The method purports to follow the mixing of two liquids of known mutual diffusivity, $\mathscr{D}$, by colouring the regions in which the concentration of one fluid is greater than a specified value, m. It can be shown that if both acid and alkali have the same diffusivity in water, $\mathscr{D}$, (which need not be the same as the self-diffusivity of water) the results can be correctly interpreted in this way. However, if their diffusivities are unequal one can only say that the results probably represent the mixing of two fluids with a mutual diffusivity intermediate between the diffusivities of the acid and alkali, and depending on the value of m. Diffusion in a system containing four species of ion is a complicated process, and cannot be described in terms of two diffusivities; but in our experiments the effective diffusivity of the acid was probably substantially greater than that of the alkali. In general the error will not be important if the main object is to compare the behaviour of systems with widely different Schmidt numbers, or if the rate of the mixing process is only weakly dependent on the Schmidt number. In our experiments the effective value of the diffusivity was about 2×10^{-5} cm^2/sec, and the Schmidt number about 500.

Experimental Method

The technique used in these experiments had originally been developed for use in an apparatus made of galvanised iron, in which it was impossible to use either strong acid or strong alkali as the main fluid, because both corrode zinc. A dilute solution (0·02–0·03 N) of borax had therefore been used as the alkali and a solution of hydrochloric acid as the acid. It was convenient to use the same reagents in the experiments described in this paper. The jet fluid was alkaline. The indicator used was bromocresol green, which changes from yellow to blue as the pH changes from 3·8 to 5·4, a range which renders it suitable for use with borax and hydrochloric acid. (In corrosion-resistant equipment it would be simpler to use hydrochloric acid and sodium hydroxide as the reagents and phenophthalein as the indicator; the latter changes from red in alkaline solution to colourless in acid solution, but is not suitable for use with borax).

The absorption spectra of the acidic and basic forms of the indicator were measured. The maximum absorption for the basic (blue) form is at 6150 Å; at this wavelength the acidic (yellow) form absorbs no light. A Wratten 25 (A) filter transmits virtually no light of the wavelengths absorbed by the yellow form and is transparent to wavelengths most strongly absorbed by the blue form; this enables the blue form of the indicator in the mixing zone to be viewed without interference from the yellow form.

Since little light was absorbed by the indicator it was necessary to use a high-contrast plate. Kodak P.200 is the panchromatic plate with the highest contrast available commercially in Great Britain. It is reasonably fast and its characteristic curve has a long linear portion. The plate is not sensitive to wavelengths greater than 6200 Å, while the Wratten 25 (A) filter transmits only wavelengths above 5800 Å. This narrow band ensures that Beer's Law will be obeyed closely.

The working section of the apparatus was illuminated from behind by a pair of 500 W tungsten filament lamps (No. 2 Photofloods). The light was diffused by several sheets of tracing paper. The camera had a lens of 14 in. focal length; this gave an image of adequate size, while the photographs could still be taken from so far away that lines of sight through the mixing zone were practically parallel.

The exposure (3 sec at f 16) was chosen so as to give a satisfactory time-averaged picture and to give optical densities on the developed plate which lay on the linear part of its characteristic curve. Under these circumstances, provided Beer's and Lambert's laws are obeyed,

$$D_0 - D = \varkappa \int b dz, \qquad (1)$$

where D is the optical density of a given point on the image of the plume;

D_0 is the optical density of the exposed plate when there is no plume in the field of view;

$\varkappa$ is a constant depending on the absorption coefficient of the indicator and on the properties of the plate;

$\int b dz$ is the integrated time-average concentration of blue indicator along the line of sight corresponding to the given point on the image.

The constant $\varkappa$ may vary from plate to plate, but will be uniform over a particular plate provided that development is uniform. If absolute concentration measurements are to be made, each plate must be calibrated individually to establish the value of $\varkappa$.

Optical density profiles of plates were obtained with a Joyce Loebel automatic recording densitometer, which gives directly a plot of the optical density.

The apparatus (Fig. 1) was designed to produce a circular jet with a uniform initial velocity-profile, emerging into a stagnant environment uncontaminated with jet-fluid. The Reynolds number, du_0/ν, was to be greater than 10^4. The jet was formed at a shaped orifice $\frac{1}{8}$ in. (0·32 cm) dia. It discharged into a Perspex box 30 in. high and 18 in. square. The box was initially full of liquid, which overflowed at the top during a run. Calculation showed that the velocity of reverse flow due

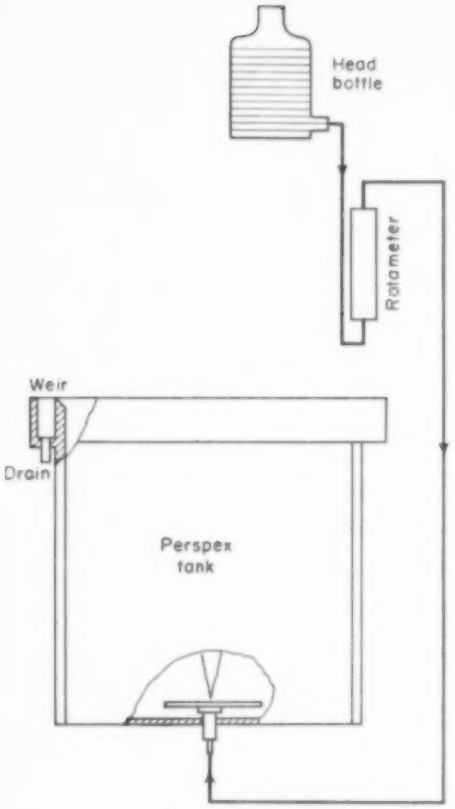

FIG. 1. Apparatus.

to entrainment would be only about 2 per cent of the axial velocity of the jet at $x = 100\,d$, and that in the region of interest the liquid entrained by the jet during the course of a run, would be ambient liquid uncontaminated by jet liquid.

When measuring the spreading of the jet, the jet liquid was a solution of indicator in borax solution, and the tank was filled with water. When measuring dilution of the jet fluid the ambient solution consisted of 0·05 N HCl, and the jet fluid was a solution of borax of concentration $0{\cdot}05\,[(1-m)/m]$ N; both solutions contained 5 mg/l. of bromocresol green.

For calibration purposes a wedge cell containing indicator solution was photographed simultaneously. Since the illumination of the field of view was not uniform, a blank photograph of the apparatus without the jet of blue indicator was taken on the same plate. In applying equation (1) to any point on a photograph of a mixing run, D is the density of the image at this point, and D_0 the background density measured at the corresponding point on the blank photograph.

All measurements were made at a Reynolds number of 12,000.

RESULTS

Spreading of jet

The spreading of a jet of blue indicator solution, with no chemical reaction taking place, was first investigated. It is known from previous work [5] that in fully-turbulent jets (du_0/ν about 10^4 or greater) the time-average concentration (volume fraction) $\bar{a}$ of the jet fluid in the mixing zone is given to a good approximation by an expression of the form:

$$\bar{a}\,(x, r) = A\,\frac{d}{x}\exp - \left(\frac{r}{Bx}\right)^2, \qquad (2)$$

at a point distant r from the axis of the jet on a plane distant x from the origin of the jet (Fig. 2a).

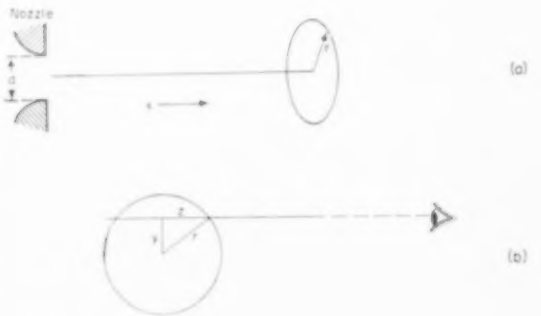

FIG. 2. Co-ordinates of jet.

The constants A and B are the same for all fully-turbulent jets. The best fit is usually obtained when the origin of x is taken to be a few diameters downstream of the actual orifice, but this refinement is not justified by the accuracy of the present work.

If the jet is photographed from a direction at right-angles to its axis, the density of the image at a distance y from the axis (Fig. 2b) is

$$c\int_{-\infty}^{+\infty} \bar{a}\left[x, \sqrt{(y^2+z^2)}\right] dz = cABd\sqrt{(\pi)}\exp -\left[y^2/(Bx)^2\right] \quad (3)$$

where c is the concentration of indicator in the undiluted jet fluid. Thus the density of the photographic image is given by

$$D_0 - D = c\,\alpha\, ABd\sqrt{(\pi)}\exp -\left[y^2/(Bx)^2\right]. \quad (4)$$

The distance from the axis of the image at which the density falls to half the maximum is therefore the same as the distance, $r_{1/2}$, from the axis of the jet at which $\bar{a}$ falls to half the maximum. Thus $r_{1/2}$ can be measured directly from the densitometer trace, and B calculated from the relation

$$\exp -(r_{1/2}/Bx)^2 = \tfrac{1}{2}. \quad (5)$$

The value of α can be determined from density measurements on the image of the wedge cell; the value of $(D_0 - D)$ measured on the centre-line of the image of the jet is (from equation 4) equal to $c\,\alpha\, ABd\sqrt{(\pi)}$, whence A can be determined.

The range of x/d covered was from 8 to 110. The measured values of $r_{1/2}/x$ ranged from 0·095 to 0·126 with a mean value of 0·112, giving $B = 0{\cdot}135$. The results are summarized in Fig. 3 (a). Previously published values of B, or measurements from which B can be calculated [3, 5], range from 0·116 to 0·139 for the spread of temperature and concentration. Most of the published results refer to values of x/d less than 30.

The measured values of A varied from 4·45 to 5·45, with a mean of 4·78. The results are summarized in Fig. 3 (b). Published values [3, 5] range from 4·55 to 5·7 for temperature and concentration.

Dilution of jet fluid

In these experiments the jet fluid was alkaline and the environment acid; the indicator was therefore blue only at those points where the instantaneous concentration of jet-fluid attained values greater than m, and the plume was thus of finite length. The density of the image on the photographic plate at the point (x, y) (Fig. 2b) is

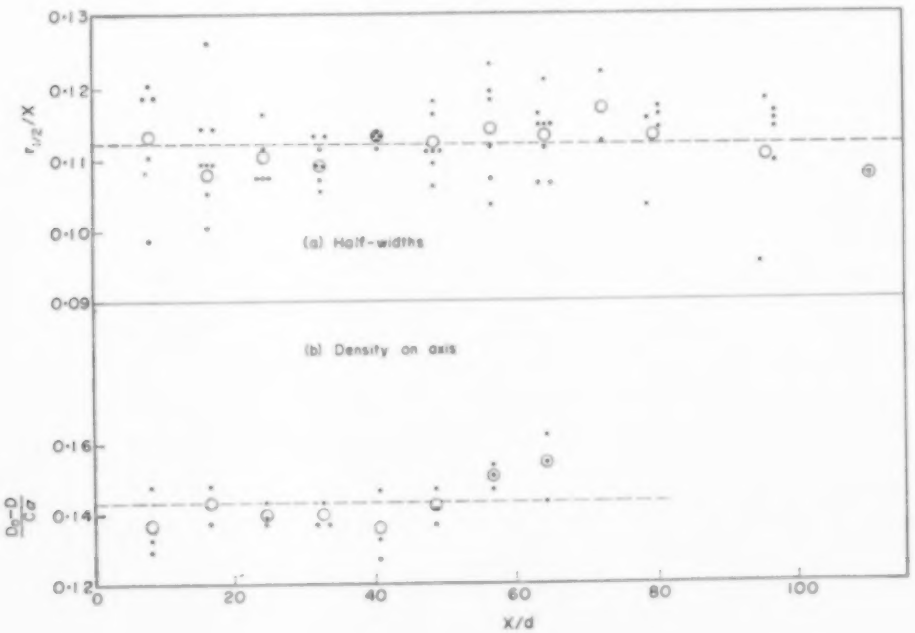

FIG. 3. Results of spreading experiments.

$$c \propto \int_{-\infty}^{+\infty} n\left[x, \sqrt{(y^2 + z^2)}\right] dz$$

where n is the fraction of the time for which the indicator at a given point (x, r) is blue.

In order to recover from this observed quantity the radial distribution of the time-average concentration of blue tracer, $c \cdot n(x, r)$, it is necessary to carry out an elaborate mathematical operation on the transverse density-profile of the image at x. In practice the measurement could not be made with sufficient precision to enable this process to be carried out, and the radial distribution of blue indicator could not be determined.

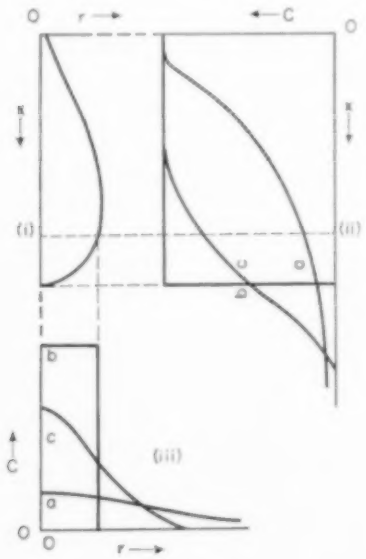

FIG. 4. Time-average colour densities in plumes.

Fig. 4 shows the form of the time-average radial and axial distributions of blue tracer which would be obtained (a) if the jet fluid were completely segregated; (b) if concentration fluctuations were completely smoothed out by molecular diffusion so that the local concentration did not fluctuate with time; and (c) if, as actually occurs, the smoothing process were only partial. In the completely segregated case no reaction occurs and the distribution is the same as in the spreading experiments described above. The completely smoothed plume would have a sharp boundary. The actual plume has a diffuse boundary, but is sharper than the segregated plume. Fig. 5 shows the corresponding forms of the images which would be obtained on the photographic plate. The density-distributions in the images of the completely-segregated and completely-smoothed jets can be calculated from equation (2).

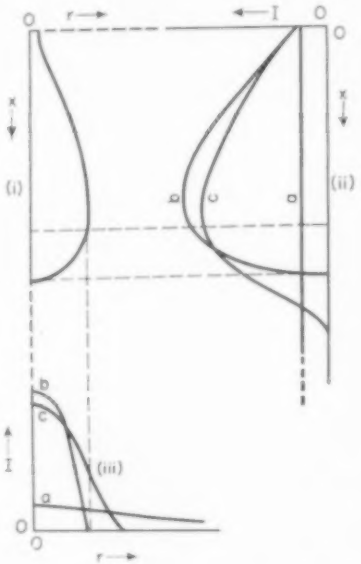

FIG. 5. Relative optical densities in time exposure photographs of plumes.

Inspection of the axial density profiles of the photographs of the plumes showed that the downstream portion was in all cases a straight line for a considerable part of its length, with only a small "tail" (Fig. 6a). Extrapolation of this straight line to zero density gave a point (X) on the axis which may be called "the end of the plume." At this point almost all the jet fluid has been diluted to a concentration m or less. It would be more satisfactory to pick the point at which (say) 99 per cent of the jet fluid has been diluted to a concentration m or less, but without a knowledge of the radial colour-distribution this is impossible.

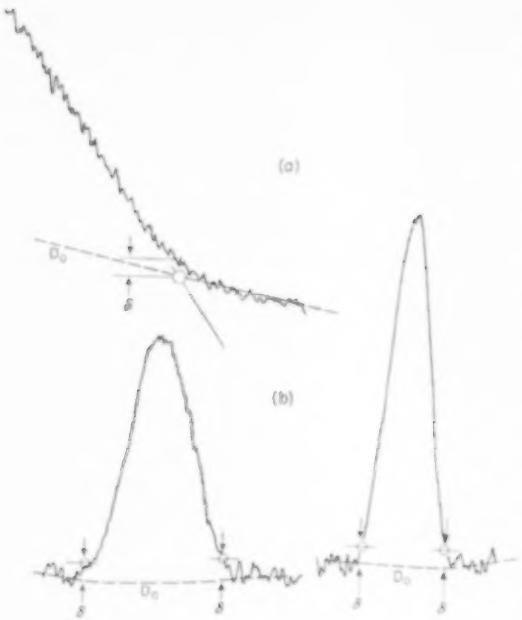

FIG. 6. Specimen density profiles of plumes.

The limit of the plume in other regions of the jet was arbitrarily defined as the point where the optical density of the image had the same value (δ, Fig. 6b) as at the end of the plume. It is thus possible to locate a series of surfaces beyond each of which almost all the jet fluid has been diluted to less than some specified concentration, m.

It is instructive to present the results in such a way as to compare the behaviour of the actual jet with that of a hypothetical "smoothed" jet, in which the concentration at every point is at all times equal to its time-average value. The edge of the smoothed plume is the point at which $\bar{a}$ is equal to m. Thus we find from equation (2) that its width r is given by

$$\frac{r}{L} = B\frac{x}{L}\sqrt{\left(\ln\frac{L}{x}\right)}, \qquad (6)$$

where

$$L = \frac{Ad}{m} \qquad (7)$$

is the length of the smoothed plume. Thus all smoothed plumes can be represented by a single curve with dimensionless co-ordinates r/L, x/L. This is curve A in Fig. 7 (using the value $B = 0{\cdot}135$).

The points representing the limits of the plumes in the actual jet with six different values of m are plotted in the same co-ordinates, calculating L from equation (7) with $A = 4{\cdot}78$. It appears

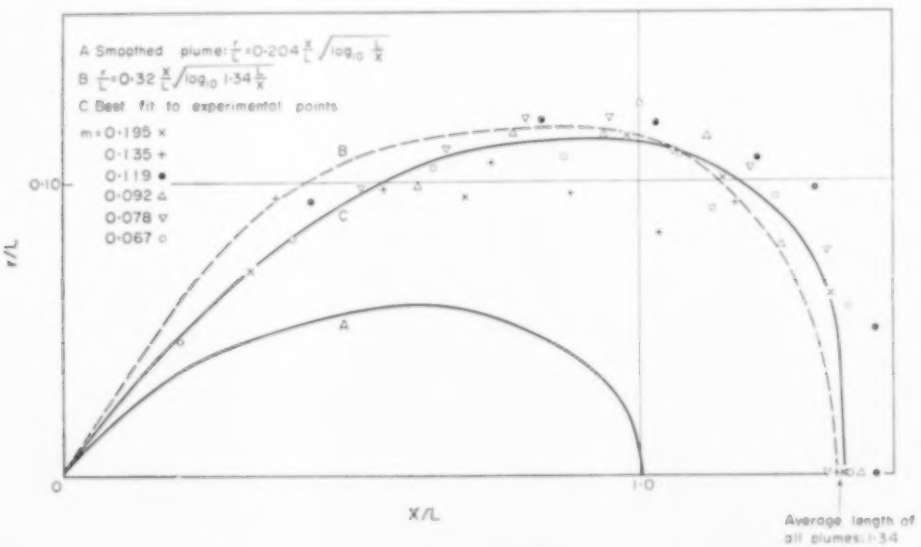

FIG. 7. Plume boundaries.

that the plumes are all similar in shape and that their linear dimensions are proportional to $1/m$. Their shape is given roughly by

$$\frac{r}{L} = 0{\cdot}32\,\frac{x}{L}\sqrt{\left(\log_{10} 1{\cdot}34\,\frac{L}{x}\right)}, \text{ or}$$

$$r = 0{\cdot}32\,x\sqrt{\left(\log_{10} 6{\cdot}41\,\frac{d}{xm}\right)}.$$

In Fig. 8 the length of the plume for various values of m is compared with the length of the smoothed plume. The results can be summarized by saying that the point at which jet-fluid of concentration m disappears is about 1·34 times as far downstream as the point at which the average concentration is m.

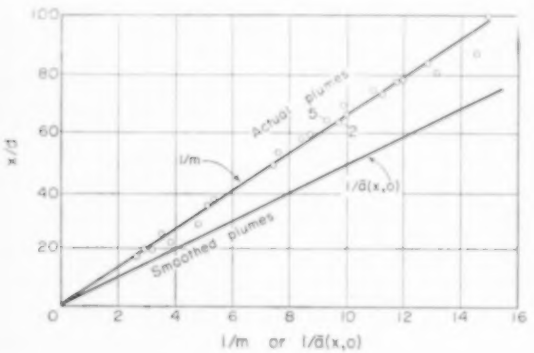

Fig. 8. Plume lengths.

Experiments were carried out to see whether the behaviour of the jet was sensitive to the value of the Reynolds number. The half-angle of a spreading jet, without reaction, was found not to change significantly in the range 2300–12,700. With alkali in jet and acid in ambient fluid, and with $m = 0{\cdot}097$, the length of the plume was found to be independent of the Reynolds number over the range 6500–12,000, although the plume was substantially longer at Reynolds numbers of 4000 and below. All the other experiments described were carried out at a Reynolds number of about 12,000.

Comparison with other Measurements

Comparison may be made with the dissipation of temperature fluctuations in a hot-air jet, as determined by Corrsin and Uberoi [3]. In this case the Prandtl number is 0·7, and the decay of temperature segregation will follow the same pattern as the decay of concentration segregation in a system having a Schmidt number 0·7 (when allowance is made for the reduced density and enhanced spread of a hot jet). These authors report the r.m.s. temperature fluctuation, θ', at various points in the jet. This corresponds to the r.m s. concentration fluctuation

$$a' = \sqrt{[\overline{(a - \bar{a})^2}]} \qquad (8)$$

It is necessary to make some assumption about the distribution of the temperature fluctuations about the mean. We have assumed that the fluctuations are normally distributed about the mean value, $\bar{\theta}$, so that the fraction of the time for which the temperature at the point exceeds a specified value, t, is

$$n = \tfrac{1}{2}\left[1 - \operatorname{erf}\left(\frac{t - \bar{\theta}}{\theta'\sqrt{2}}\right)\right]. \qquad (9)$$

If we imagine those parts of the jet in which the temperature exceeds t to be coloured, we can calculate the time-average optical density distribution in the image of the plume.

It must be emphasized that the assumption of normal distribution of fluctuations may well be wrong, so the conclusions drawn from this calculation must be treated with reserve.

Fig. 9 (a) shows the calculated relative optical densities along the axis of the plume (using the published data for the region $x/d = 15$–20). Using the same procedure to find the "end of the plume" as employed with the photographs of liquid plumes, we find the plume-length to be 1·11 L (L being the distance downstream at which the time-average temperature, $\bar{\theta}$, is equal to the specified temperature, t). This, as would be expected, is less than the value of 1·34 L found for the liquid jets. If the rate of decay of segregation in jets is influenced by diffusion one would expect the relative degree of segregation to be higher at any point in the liquid jet than in the gas jet, thereby giving rise to a longer plume.

Rosensweig, *et al.* [2] used an optical method to measure the fluctuations of smoke-concentration in a jet of smoke-laden air. The Schmidt

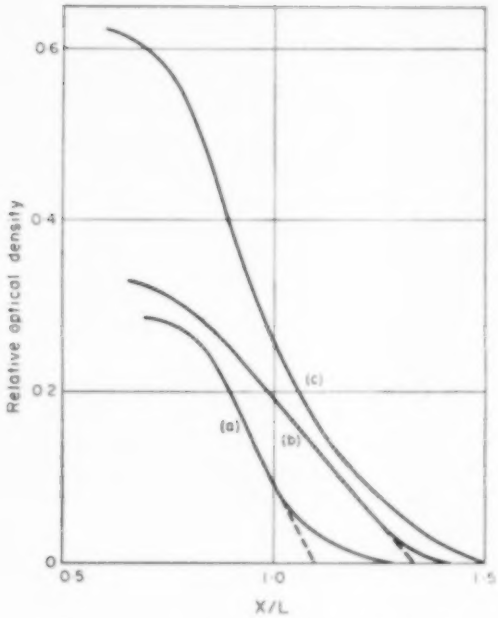

FIG. 9. (a) Synthetic plume for hot-air jet.
(b) Plume in liquid jet.
(c) Synthetic plume for smoke jet.

number in this case was about $5{\cdot}5 \times 10^5$, compared to about 500 for the liquid jet. Their published figures have been used to calculate the profile of the jet having $L = 15\,d$ (the result is not sensitive to the value of L/d chosen). This is shown in Fig. 9 (c). The "synthetic" smoke plume does not cut-off as sharply as the liquid plumes were observed to do. A line drawn through the steepest part of the profile gave an intercept of $1{\cdot}14\,L$. This is actually shorter than the plume-length in water ($1{\cdot}34\,L$), but as can be seen, this is not an appropriate method of locating the "end of the plume" in this case.

A representative liquid plume is tentatively shown at Fig. 9 (b). Unfortunately the plates from which the plume-lengths were determined were not calibrated, so the vertical scale of this profile cannot be directly compared with that of 9 (a) and (c). A vertical scale for (b) has been chosen to fit it in between (a) and (c), where it presumably belongs. The curve for the liquid plume is clearly of different shape from the "synthetic" plumes, suggesting that the assumptions made in calculating the shape of the latter may be at fault. It appears, however, as would be expected, that the plume formed by the smoke jet is effectively longer than the plume of the liquid jet in the sense that a greater proportion of the jet fluid travels a given distance downstream without being diluted to a specified concentration. The fact that the experimentally determined fluctuations in the smoke jet are relatively greater than in the hot-air jet means that the former will give a longer plume, whatever the basis of calculation.

The Reynolds number in the experiments of ROSENSWEIG *et al.* was 26,000 and in those of CORRSIN and UBEROI 52,000, as against 12,000 in our case; but our experiments suggest that this would have little effect on the length of the plume.

Measurements in a hot-air jet specially designed for comparison with those in the liquid jet are now in hand.

CONCLUSIONS

In water, the plumes which indicate the region beyond which the jet fluid has been diluted to a concentration m or less appear to have the same shape for all values of m, and their linear dimensions are proportional to $1/m$. The point on the axis at which almost all the jet fluid has been diluted to a concentration m is about 1·34 times as far downstream from the nozzle as the point at which the time-average concentration is m.

The corresponding figure calculated for a hot-air jet is 1·11. The smoke plume does not appear to have a sharp cut-off, although the calculated profile indicates that it is effectively larger than the plume in water. The plume-lengths are undoubtedly affected by the Schmidt number, although no great reliance can be placed on the quantitative aspect of the comparison between the three systems.

Acknowledgments—The experimental work was carried out in the Department of Chemical Engineering of the Imperial College of Science and Technology. We are indebted to Mr. R. M. WILSON for his help with the calculations on the hot-air and smoke jets. D.K. wishes to express gratitude for the award of an Athlone Fellowship and a grant from the National Research Council of Canada.

Notations

A = constant in equation (2)
a = instantaneous concentration (vol. fraction) of jet fluid
a' = r.m.s. concentration fluctuation
$\bar{a}$ = time-average of a
B = constant in equation (2)
b = concentration of blue indicator
c = concentration of indicator in either form
D = optical density of photographic image
D_0 = background optical density of exposed plate
$\mathscr{D}$ = diffusivity
d = nozzle diameter
L = length of "smoothed" plume = Ad/m
m = value of a which gives neutral mixture
n = fraction of time for which indicator is blue
r = distance from axis of jet
$r_{1/2}$ = concentration half-width of jet
t = specified value of temperature
u_0 = velocity of jet emerging from nozzle
x = distance along axis of jet from nozzle
y = distance of point on photographic image from axis of image
z = distance along line of sight (Fig. 2b)
α = constant in equation (1)
θ' = r.m.s. temperature fluctuation
$\bar{\theta}$ = time-average temperature
δ = optical density of photographic image at edge of plume
ν = kinematic viscosity

$$\mathrm{erf}\,(k) = \frac{2}{\sqrt{(\pi)}} \int_0^k \exp\,(-t^2)\,dt.$$

References

[1] Hawthorne W. R., Weddell D. S. and Hottle H. C. *3rd Symp. Combust. Flame Explos. Phenom.* p. 266. William and Wilkins, Baltimore 1949.
[2] Rosensweig R. E., Hottel H. C. and Williams G. C. *Chem. Engng. Sci.* 1961 **15** 111.
[3] Corrsin S. and Uberoi M. S. NACA Technical Note No. 1865 1959.
[4] Brinkman R., Margaria R. and Roughton F. J. W. *Phil. Trans.* 1933–4 A **232** 65.
[5] Hinze J. O. and V. der Hegge Zijnen B. G. *Appl. Sci. Res.* 1949 A **1** 435; Forstall W. and Gaylord E. W. *J. Appl. Mech.* 1955 **22**, 161; Ruden P. *Naturwissenschaft.* 1933 **21** 375; Squire H. B. *Aircraft Engng.* 1950 **22** 62; Sunavala P. D., Hulse C. and Thring M. W. *Combust. Flame* 1957 **1** 179; Uberoi M. S. and Corrsin S. NACA Report 1142 1953.

Chemical Engineering Science, 1961, Vol. 16, pp. 278 to 286. Pergamon Press Ltd., London. Printed in Great Britain.

Unsteady-state one dimensional countercurrent diffusion of gases

R. F. Dye

Process Development Division,
Phillips Petroleum Company, Bartlesville, Oklahoma, U.S.A.

(*Received* 18 *August* 1960)

Abstract—The problem of one dimensional countercurrent diffusion in porous media is considered. An exact mathematical solution is obtained for unsteady-state diffusion in a porous body separating two well-mixed gas volumes. The development considers that the concentrations in both gas volumes change from their original values ${}_1C_0$ and ${}_2C_0$, to different values ${}_1C(t)$ and ${}_2C(t)$. Unsteady flow in such a system is directly analogous to the unsteady conduction of heat. Experimental apparatus is simple, yet provides for quick and accurate measurement of the quantities necessary for evaluating the flow pattern equation for porous media samples.

Résumé—L'article s'occupe du problème d'une diffusion unidimensionnelle à contre-courant dans des milieux poreux. Une solution mathématique exacte est obtenue pour une diffusion variable dans un corps poreux, séparant deux volumes gaseux bien mélangés. Le traitement considère, que les concentrations de deux volumes gaseux changent de leur valeurs originales, ${}_1C_1$ et ${}_2C_0$, aux valeurs différentes, ${}_1C(t)$ et ${}_2C(t)$. Un courant variable dans un tel système est directement analogue à la conduction variable de la chaleur. L'appareil expérimental est simple, mais permet une mesure rapide et précise de quantités nécessaires pour l'établissement d'une équation typique du courant dans les échantillons de milieux poreux.

Zusammenfassung—Das Problem einer Gegenstromdiffusion in einer Dimension in porösen Mitteln wurde untersucht. Eine genaue mathematische Lösung wurde fur den Fall der nicht stationären Diffusion zweier gut durchgemischten, durch einen porösen Körper getrennten, Gasvolumen abgeleitet. Es wurde angenommen, dass sich die Konzentration beider Gasvolumen von der Ausgangsgrösse ${}_1C_0$ und ${}_2C_0$ auf neue Werte ${}_1C(t)$ und ${}_2C(t)$, beziehungsweise, ändert. Die nicht stationäre Strömung in solchen Systemen entspricht vollständig der nicht stationären Wärmeleitung. Die experimentelle Apparatur is ganz einfach, erlaubt jedoch die schnelle und genaue Bestimmung der notwendigen Grössen fur die Bewertung der Strömungsgleichungen in porösen Proben.

In work reported earlier [1] carbon dioxide and nitrogen gases were allowed to diffuse countercurrently through plugs of compressed potassium perchlorate to study the effect of varying plug porosity and length on the diffusion coefficient. In that work particularly simple experimental apparatus was required for the measurement of the quantities necessary for evaluating effective diffusion coefficients in the porous samples examined. This article develops the exact mathematical solution for the unsteady-state diffusion problem of a porous body as considered in the earlier work, and, subsequently, describes the instrumentation requirements for such a study.

A Statement of the Problem

The problem considered is that of countercurrent diffusion in a porous plug separating two gas volumes, 1 and 2, as shown by Fig. 1. The plug is given a preliminary treatment to justify some statement about the initial distribution–i.e., $C_0(x)$ – in it. Diffusion is allowed to proceed for a definite time and the gas volumes are kept homogeneous by mixing or stirring. The concentrations in 1 and 2 change from their original values, ${}_1C_0$ and ${}_2C_0$, to different values, ${}_1C(t)$ and ${}_2C(t)$, in time t, and from a knowledge of these values the diffusion constant of one of the gases is to be determined as it diffuses into the other.

General Solution of the Problem

Assume for simplicity that the plug is of unit cross-section, and is bounded by planes $x = 0$ and

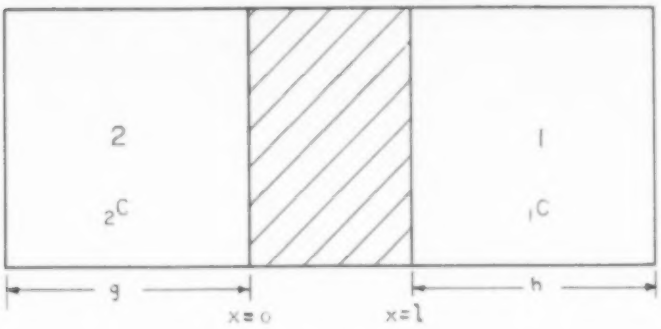

FIG. 1. Diffusion cell.

$x = l$. Homogeneous gaseous mixtures of volumes g and h, and initial concentrations ${}_2C_0$ and ${}_1C_0$ respectively, are in contact with the two sides of the plug. The first extends from $x = 0$ to $x = -g$; the second mixture, in contact with boundary $x = l$, extends to $x = l + h$. The initial distribution of concentration across the medium of "effective" volume, l, is $C_0(x)$. After time t the concentrations in the two gas volumes will be denoted by ${}_2C(t)$ and ${}_1C(t)$, and the distribution in the medium by $C(x, t)$.

The diffusion process considered here can be represented by a partial differential equation (Fick's second law of diffusion):

$$\frac{\partial C}{\partial t} = \frac{D'}{\epsilon}\frac{\partial^2 C}{\partial x^2} \tag{1}$$

The boundary conditions for which equation (1) may be solved are:

(i) $C = C_0(x)$ at $t = 0$ for $0 < x < l$.

(ii) $C(0, t) = {}_2C(t)$; $C(l, t) = {}_1C(t)$ for $t > 0$.

(iii) $C = {}_2C_0$ at $t = 0$ for $-g < x < 0$, and ${}_1C_0$ at $t = 0$ for $l < x < l + h$.

(iv) $$\frac{\partial_2 C}{\partial t} = \frac{D'}{\epsilon g}\left(\frac{\partial C}{\partial x}\right)_{x=0}; \quad \frac{\partial C_1}{\partial t} = -\frac{D'}{\epsilon h}\left(\frac{\partial C}{\partial x}\right)_{x=l}.$$

Equations (iv) express the proportionality of rate of increase of concentration in the gas volumes to rate of supply of concentration changing constituent at the respective boundaries.

The solution of equation (1) can be represented by

$$C = c_1 + c_2 \tag{2}$$

where c_1 and c_2 are solutions which satisfy equation (1). The solution, c_1, which vanishes at $x = 0$ and at $x = l$, and which satisfies equation (i), is given by the known Fourier formula

$$c_1 = \sum_1^{\infty} a_n \exp(-\alpha_n t) \sin\frac{n\pi x}{l} \tag{3}$$

where

$$a_n = \frac{2}{l}\int_0^l C_0(y) \sin\frac{n\pi y}{l}\, dy \tag{4}$$

and

$$\alpha_n = \frac{D' n^2 \pi^2}{\epsilon l^2} \tag{5}$$

Solution c_2, by DUHAMEL's theorem [2], which corresponds to zero initial concentration in the medium and the faces maintained, respectively, in contact with gases of concentrations ${}_2C(t)$ and ${}_1C(t)$ is

$$c_2 = \int_0^t \left\{ {}_2C(\tau)\frac{\partial}{\partial t}F_1(x, t-\tau) + {}_1C(\tau)\frac{\partial}{\partial t}F_2(x, t-\tau)\right\} d\tau, \tag{6}$$

or

$$c_2 = -\int_0^t \left\{ {}_2C(\tau)\frac{\partial}{\partial \tau}F_1(x, t-\tau) + {}_1C(\tau)\frac{\partial}{\partial \tau}F_2(x, t-\tau)\right\} d\tau \tag{7}$$

which may be written

$$c_2 = {}_2C_0\, F_1(x,t) + {}_1C_0\, F_2(x,t) + \int_0^t \left\{ {}_2C'(\tau)\, F_1(x, t-\tau) + {}_1C'(\tau)(x, t-\tau) \right\} d\tau \quad (8)$$

where

$$F_1(x,t) = 1 - \frac{x}{l} - \frac{2}{\pi} \sum_1^\infty \left(\frac{1}{n}\right) \exp(-\alpha_n t) \sin \frac{n\pi x}{l} \quad (9)$$

and

$$F_2(x,t) = \frac{x}{l} + \frac{2}{\pi} \sum_1^\infty \frac{(-1)^n}{n} \exp(-\alpha_n t) \sin \frac{n\pi x}{l}. \quad (10)$$

After substitution of equations (9) and (10) in equation (8) the solution of equation (1) written as $C = c_1 + c_2$ satisfies equations (i) and (ii). After differentiating with respect to x, one may write [3]

$$-l\left(\frac{\partial C}{\partial x}\right) = {}_2C - {}_1C + 2\sum b_n \exp(-\alpha_n t) \cos \frac{n\pi x}{l} + 2\sum \cos \frac{n\pi x}{l} \int \exp\left[-\alpha_n (t-\tau)\right] \times \left[{}_2C' - (-1)^n\, C_1'\right] d\tau$$

where

$$b_n = {}_2C_0 - (-1)^n\, {}_1C_0 - \frac{n\pi a_n}{2}. \quad (12)$$

So equations (iv) now give, respectively

$$-\frac{\epsilon\, lg}{D'}\left(\frac{\partial C_2}{\partial t}\right) = {}_2C - {}_1C + 2\sum b_n \exp(-\alpha_n t) + 2\sum \int \exp\left[-\alpha_n (t-\tau)\right] \times \left[{}_2C' - (-1)^n\, {}_1C'\right] d\tau \quad (13)$$

and

$$\frac{\epsilon\, lh}{D'}\left(\frac{\partial C_1}{\partial t}\right) = {}_2C - {}_1C + 2\sum (-1)^n b_n \exp(-\alpha_n t) + 2\sum \int (-1)^n \exp\left[-\alpha_n (t-\tau)\right] \times ({}_2C' - (-1)^n\, {}_1C')\, d\tau \quad (14)$$

Solution of the problem in the form

$${}_2C(t) = C_\infty - \Sigma \frac{A_i}{\beta_i} \exp(-\beta_i t) \quad (15)$$

$${}_1C(t) = C_\infty - \Sigma \frac{B_i}{\beta_i} \exp(-\beta_i t) \quad (16)$$

[where C_∞ denotes the final uniform concentration of the gaseous solution given by $C_\infty(g+l+h) = ({}_2C_0)\, g + \int_0^l C_0(x)\, dx + ({}_1C_0)\, h$] may be had by substituting, as treated by March and Weaver [4]

$$\frac{\partial C_2}{\partial t} = \Sigma_i A_i \exp(-\beta_i t) \quad (17)$$

$$\frac{\partial C_1}{\partial t} = \Sigma_i B_i \exp(-\beta_i t) \quad (18)$$

in equations (13) and (14), respectively. Equations (13) and (14) will be satisfied identically by substituting equations (17) and (18) if A_i, B_i and β_i satisfy the equations

$$A_i\left[\left(\frac{\epsilon\, lg}{D'}\right) - \frac{1}{\beta_i} + 2\Sigma_n \frac{1}{(\alpha_n - \beta_i)}\right] = B_i\left[-\frac{1}{\beta_i} + 2\Sigma_n \frac{(-1)^n}{(\alpha_n - \beta_i)}\right] \quad (19)$$

$$B_i\left[\left(\frac{\epsilon\, lh}{D'}\right) - \frac{1}{\beta_i} + 2\Sigma_n \frac{1}{(\alpha_n - \beta_i)}\right] = A_i\left[-\frac{1}{\beta_i} + 2\Sigma_n \frac{(-1)^n}{(\alpha_n - \beta_i)}\right] \quad (20)$$

$$b_n = \Sigma_i \frac{A_i - (-1)^n B_i}{(\alpha_n - \beta_i)} \quad (21)$$

If equations (19), (20) and (21) lead to unique values for the numbers A_i, B_i, β_i, equations (17) and (18) will yield the problem solution. Using the formula

$$\tan Z = -\frac{2Z}{(\pi/2)^2 - Z^2} + \frac{2Z}{(3\pi/2)^2 - Z^2} + \frac{2Z}{(5\pi/2)^2 - Z^2} + \cdots \quad (22)$$

and letting

$$Z_i^2 = \frac{\epsilon\, \beta_i\, l^2}{D'} \quad (23)$$

VOL. 16 1962

Equations (19), (20) and (21) become

$$A_i\left(\frac{1}{\gamma_1} - \frac{\cot Z_i}{Z_i}\right) = -B_i\left(\frac{1}{Z_i \sin Z_i}\right) \quad (19')$$

$$B_i\left(\frac{1}{\gamma_2} - \frac{\cot Z_i}{Z_i}\right) = -A_i\left(\frac{1}{Z_i \sin Z_i}\right) \quad (20')$$

$$b_n' = \frac{D'}{\epsilon l^2}\left[{}_2C_0 - (-1)^n\, {}_1C_0 - \frac{n\pi}{l} \times \int_0^l C_0(y) \sin\frac{n\pi y}{l}\, dy = \Sigma_i \frac{A_i - (-1)^n B_i}{n^2\pi^2 - Z_i^2}\right. \quad (21')$$

where

$$\gamma_1 = \frac{l}{g} \text{ and } \gamma_2 = \frac{l}{h} \quad (24)$$

Simultaneous elimination of A_i, B_i, from equations (19′) and (20′) gives

$$Z^2 - (\gamma_1 + \gamma_2) Z \cot Z - \gamma_1 \gamma_2 = 0 \quad (25)$$

The roots of equation (25) give the numbers β_i. By finding the points of intersection of the graphs $y = Z^2 - \gamma_1\gamma_2$ and $y = (\gamma_1 + \gamma_2)$. $Z \cot Z$, one can readily determine the Z's for which real positive values only are taken. From equation (21′), A_i may be had in terms of B_i, β_i and D' and equations (19′) and (20′) can be made to yield B_i in terms of A_i and β_i.

Considering the A's, B's and β's as known, equations (15) and (16) represent the concentrations in the two gas volumes in terms of final uniform concentration C_∞ and t. For time $t = 0$ they become

$${}_2C_0 = C_\infty - \Sigma \frac{A_i}{\beta_i} \quad (26)$$

$${}_1C_0 = C_\infty - \Sigma \frac{B_i}{\beta_i} \quad (27)$$

either of these permits a numerical evaluation of the A_i, B_i. In the ratios $\Sigma(A_i/\beta_i)$, $\Sigma(B_i/\beta_i)$ which appear before the exponential terms of equations (15) and (16), the D' term cancels, since it is a simple multiplier in A_i, B_i and β_i. In all diffusion problems at large values of t, all the exponential terms except the first become small so that if a plot of log $({}_2C - C_\infty)$ against t is made, a curve is obtained such as shown in Fig. 2 in which the curve approaches asymptotically a straight line. The slope of this line is $-\beta_i$. Barrer [5] shows that at small values of t it will not be necessary to take many terms of the exponential series, in solving for A_i and B_i.

By means of equations (15) and (16) for ${}_2C$ and ${}_1C$, the concentration distribution in the plug is found from equations (3) and (6) to be

$$C(x, t) = {}_2C\left(1 - \frac{x}{l}\right) + {}_1C\frac{x}{l} - \frac{2}{\pi}\Sigma_n \frac{1}{n}\sin\frac{n\pi x}{l} \times \Sigma_i \frac{(A_i - (-1)^n B_i)\exp(-\beta_i t)}{(\alpha_n - \beta_i)} \quad (28)$$

which satisfies equation (1) and conditions (i), (ii), (iii) and (iv). This considers that due account is taken of conditions involved in equations (19′), (20′), (21′), (15) and (16). The γ terms associated with these equations are expressions of the ratios of the "effective" porous plug volume to that of respective end containers. The implied assumptions that the diffusion coefficient is independent of concentration and concentration gradient permit this development.

Application of the General Solution

For the case considered here the volume ratios γ_1 and γ_2 are equal to γ and the subscript will be dropped.

Let the positive roots of equation (25) with $\gamma_1 = \gamma_2 = \gamma$ be Z_i where $i = 0, 1, - - - - -$, arranged in order of magnitude. Standard processes for finding the roots of such an equation give

$$Z_0 = (2\gamma)^{1/2}\left(1 - \frac{1}{12}\right)\gamma + \left(\frac{11}{1440}\right)\gamma^2 - - - - - , \quad (29)$$

$$Z_i = i\pi + \frac{2\gamma}{i\pi} - \frac{4\gamma^2}{i^3\pi^3} + - - - , \quad i = 1, 2, - - - . \quad (30)$$

Powers of γ greater than the second may be disregarded since the quantity involved is obviously very small. When $\gamma_1 = \gamma_2$ equations (19′) and (20′) show that

VOL. 16 1962

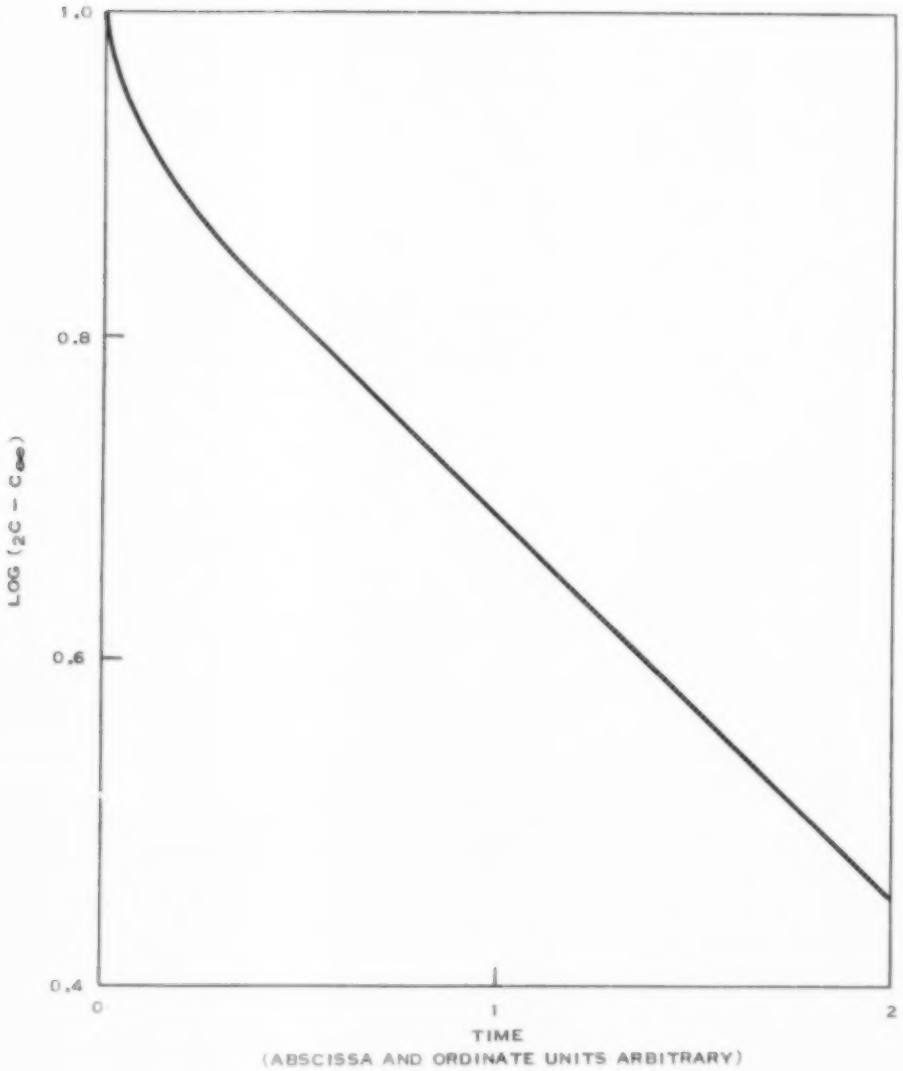

Fig. 2. A typical diffusion rate curve log ($_2C - C_\infty$) vs. time.

$$A_i = (-1)^{i+1} B_i \tag{31}$$

thus the linear equations for A_i become

$$b_n' = \Sigma_i A_i \left[1 + (-1)^{n+1}\right]/(n^2\pi^2 - Z_i^2) \tag{32}$$

The A_i values depend on the initial concentration in the plug, $C_0(x)$. Let us consider that the initial treatment of the plug is such that it is saturated with the gas of container 1 and contains no amount of that constituent of container 2. Then ${}_1C_0 = 0 = C_0(x)$. For this case

$$b_n' = \frac{D'\,{}_2C_0}{\epsilon\, l^2} \tag{33}$$

and equation (32) becomes

$$d_n = \sum_{-1}^{\infty}{}_i\, \alpha_{ni} A_i$$

with

$$d_n = \frac{D'\,{}_2C_0}{\epsilon\, l^2} - \left[\frac{1 + (-1)^n}{n^2\pi^2 - Z_0^2}\right] A_0, \tag{34}$$

and

$$\alpha_{ni} = \left[\frac{1 + (-1)^{n+1}}{n^2\pi^2 - Z_i^2}\right] \tag{35}$$

The solution is

$$A_i = \left(\frac{4\gamma}{i^2\pi^2}\right) A_0 - 2\gamma \left(\frac{D'\,{}_2C_0}{\epsilon\, l^2}\right)\left(\frac{1 - 4\gamma}{i^2\pi^2}\right) \text{ for } i \text{ even}, \tag{36}$$

$$A_i = -2\gamma \left(\frac{D'_2 C_0}{\epsilon l^2}\right)\left(\frac{1 - 2\gamma}{i^2\pi^2}\right) \text{ for } i \text{ odd}. \tag{37}$$

With roots (equation 30) these values of the A_i give

$$\sum_1^{\infty} \frac{A_i}{Z_i^2} = \left(\frac{\gamma}{360}\right) A_0 - \gamma\left(\frac{D'_2 C_0}{\epsilon\, l^2}\right)\left(\frac{1}{3} - \frac{49\gamma}{360}\right), \tag{38}$$

and from equations (26), (27) and (30) and

$$C_\infty - {}_2C_0 = -\left(\frac{{}_2C_0}{2}\right)\left(1 + \frac{\gamma}{2} - \frac{\gamma^2}{4}\right), \tag{39}$$

we get

$$\left(\frac{A_0}{2\gamma}\right)\left(1 + \frac{\gamma}{6} + \frac{\gamma^2}{90}\right) + \left(\frac{D'_2 C_0}{2\,\epsilon\, l^2}\right)\left(1 - \frac{\gamma}{6} + \frac{\gamma^2}{45}\right) = 0 \tag{40}$$

It follows

$$\left(\frac{A_0}{\beta_i}\right) = -\left(\frac{{}_2C_0}{2}\right)\left(1 - \frac{\gamma}{6} + \frac{\gamma^2}{60}\right) \tag{41}$$

$$\left(\frac{A_i}{\beta_i}\right) = -\left(\frac{{}_2C_0}{2}\right)\left(\frac{4\gamma}{i^2\pi^2}\right)\left(\frac{1 - 6\gamma}{i^2\pi^2}\right)$$

for i even or odd, (42)

from which can be obtained

$${}_2C = \frac{{}_2C_0}{2}\left\{1 - \frac{\gamma}{2} + \frac{\gamma^2}{4} + \left(1 - \frac{\gamma}{6} + \frac{\gamma^2}{60}\right) \exp\left[-\frac{2\gamma D' t}{\epsilon\, l^2}\left(1 - \frac{\gamma}{6} + \frac{\gamma^2}{45}\right)\right] + \sum_1^{\infty}{}_i \frac{4\gamma}{i^2\pi^2}\left(1 - \frac{6\gamma}{i^2\pi^2}\right) \exp\left[\frac{-D' t\,(i^2\pi^2 + 4\gamma)}{\epsilon\, l^2}\right]\right\}, \tag{43}$$

$${}_1C = 2\,\frac{C_0}{2}\left\{1 - \frac{\gamma}{2} + \frac{\gamma^2}{4} - \left(1 - \frac{\gamma}{6} + \frac{\gamma^2}{60}\right) \exp\left[\frac{-2\gamma D' t}{\epsilon\, l^2}\left(1 - \frac{\gamma}{6} + \frac{\gamma^2}{45}\right)\right] - \sum_1^{\infty}{}_i (-1)^i \frac{4\gamma}{i^2\pi^2}\left(1 - \frac{6\gamma}{i^2\pi^2}\right)\times \exp\left[\frac{-D' t\,(i^2\pi^2 + 4\gamma)}{\epsilon\, l^2}\right]\right\}, \tag{44}$$

Apparatus and Instrumentation

Fig. 3 shows a schematic diagram for a diffusion apparatus which may be used in the measurement of quantities necessary for evaluation of the diffusion coefficient of a porous sample. All equipment except item C is enclosed in a constant temperature bath. In diffusion tests, pure gases are admitted to the system at points A and B. On entering the system, both gases pass through an electrically-heated preheater C, which may consist of two 20 ft coils of $\frac{1}{4}$ in. copper tubing mounted in an insulated tank of water. Constant temperature is maintained in this tank by means of a thermo-regulator controlling electric current to the heating elements. It is convenient to set this thermo-regulator to maintain the tank temperature at 1–2°F above that of the diffusion system constant temperature bath. Fifteen-foot coils D and E (located within the

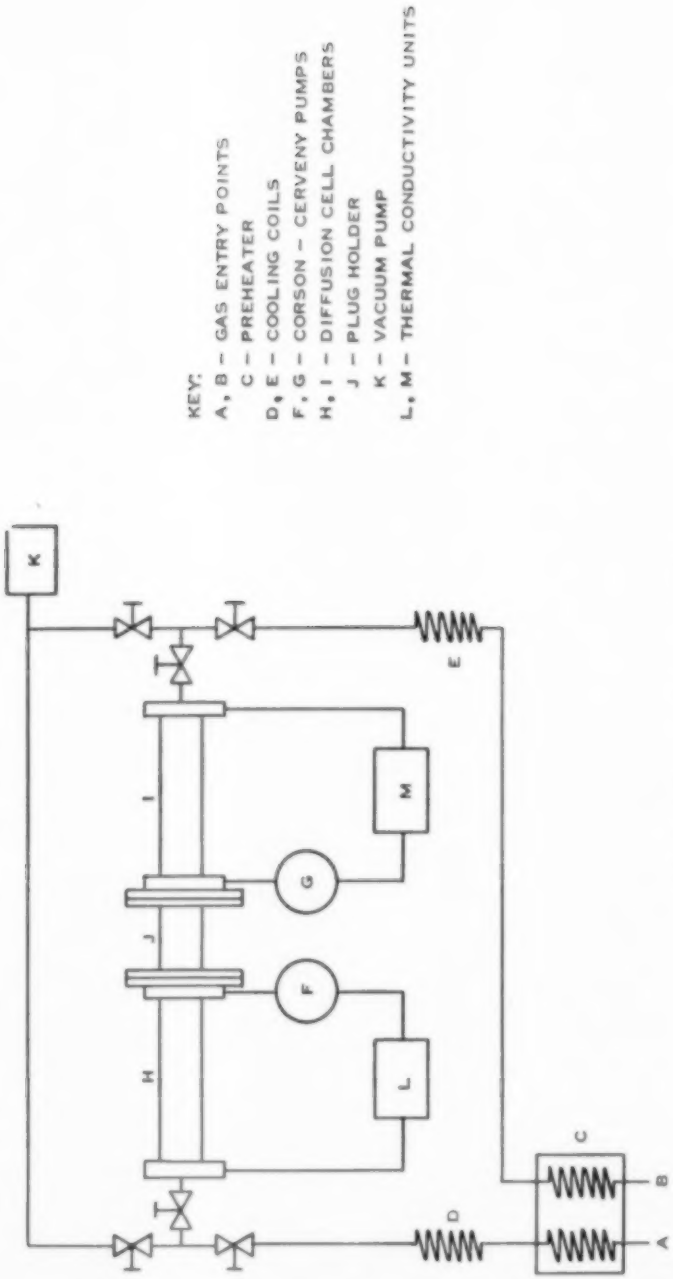

Fig. 3. Schematic diagram of diffusion apparatus.

constant temperature bath), of ¼ in. copper tubing and placed in the lines between the preheater and the diffusion cell proper, will bring the temperature of the gases entering the system down to that of the constant temperature bath.

Construction details of a diffusion cell half and a plug holder are shown by Fig. 4. Dimensions are shown for illustration. When used in experimental work two cell sections are clamped together with the porous plug mounted in the flanged cylindrical holder separating them. This construction provides a definite cell geometry, in that the volumes on both sides of the porous plug enclosed between the cell half and porous medium are equal, and always remains the same irrespective of plug length.

In the course of an experimental run the composition of the gas in each half of the diffusion cell (cell halves are H and I) is observed from time to time by means of a thermal conductivity gas analyser. This instrument measures changes in the thermal conductivity of a gas, and thereby changes in composition, as a function of the change in resistance of a heated platinum filament. The analyser sensing system for this diffusion cell consists of thermal conductivity units L and M. Model 30–S Gow–Mac units perform well in this service. In operation a stream of gas is circulated through each conductivity cell by means of small gas pumps F and G (Corson–Cerveny bellows pumps or other similar units may be used for this purpose), which also maintain homogeneity of the concentrations in the gas chambers. The analyser electrical circuit is that of a Wheatstone bridge with operation based on constant current conditions and degree of bridge unbalance. The conductivity cells are readily calibrated with gases of known composition before conducting a diffusion experiment.

If the constant temperature bath, containing the diffusion cell and thermal conductivity units, is constructed with provisions for both heating and cooling, any temperature within the heating–cooling range of the system may be selected for diffusion runs. However, if only provisions for heating are made (with cooling only by heat-leak) in the bath design, satisfactory diffusion runs may be made at some temperature above the

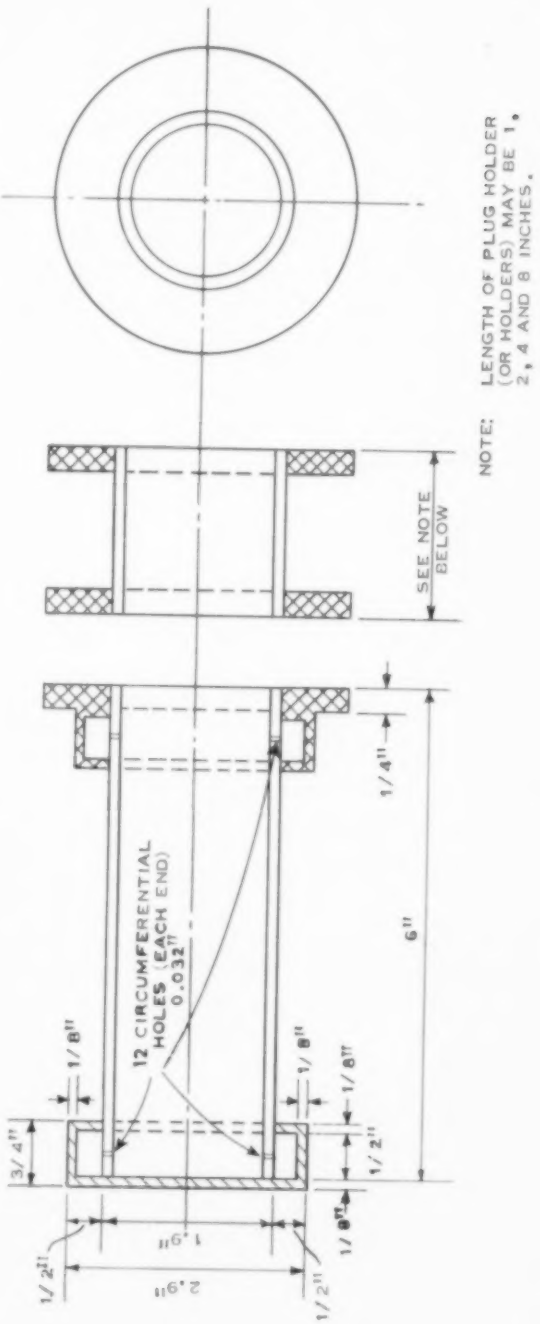

FIG. 4. Construction details of diffusion cell half and plug holder.

ambient, for example, 40 °C (104 °F). Thermal conductivity units are somewhat temperature dependent, but under the conditions of the Dye–DallaValle work [1] it was noted that a 1 °F variation in bath temperature resulted in a negligible change in a gas analysis reading.

Diffusion Test Procedure

Before a diffusion run or test is started, a systematic programme of leak tests should be made to insure satisfactory diffusion cell performance. Reproducible diffusion test data may be insured if the system can be evacuated to approximately 2 mm of mercury. (The schematic diagram shown by Fig. 3 shows manner in which a vacuum pump K may be connected into the system).

It is good practice to conduct two diffusion runs for each porous test specimen of a given length, one with the specimen saturated with one of the two gases used, and another with the specimen saturated with the second gas. This presaturation is necessary to define the concentration distribution in the test specimen at the beginning of diffusion (solution of the problem is greatly simplified when one of the components is uniformly distributed, i.e. when $C_0(x) = C_0$, at $t = 0$). To achieve this preliminary saturation one of the cell chambers must be isolated. This is conveniently done by closing a thin sliding gate fitted to and recessed in one end of the plug holder. This sliding gate is opened at the start of a diffusion run, and during the run composition vs. time is recorded for each cell chamber as determined by the thermal conductivity gas analyser.

Notation

a_n = Fourier coefficient
A_i = characteristic constant in the general solution
b_n = characteristic coefficient
B_i = characteristic constant in the general solution
C = concentration expressed as mole fraction; general solution of equation (1)
c_1, c_2 = particular solutions to equation (1)
C_0 = concentration in porous medium at $t = 0$
${}_1C_0$ = concentration in gas volume 1 at $t = 0$
${}_2C_0$ = concentration in gas volume 2 at $t = 0$
${}_1C(t)$ = concentration in gas volume 1 at time t
${}_2C(t)$ = concentration in gas volume 2 at time t
$C(x, t)$ = concentration in porous medium at distance x and time t
C_∞ = final uniform concentration in system
D = Fick's second law diffusivity (diffusion coefficient)
D' = effective or sought diffusivity for porous medium (related to Fick's second law diffusivity as shown by $D = D'/\epsilon$)
F_1 = Duhamel's theorem function
F_2 = Duhamel's theorem function
g = length and volume of gas container in general solution
h = length and volume of gas container in general solution
i = designates term of a series
l = length and effective volume of porous medium
n = designates term of a series
x = co-ordinate along which diffusion is occurring
t = time
α_n = an expoential index
β_i = a characteristic constant
ϵ = porosity
$\gamma, \gamma_1, \gamma_2$ = volume ratio
τ = time

References

[1] Dye R. F. and DallaValle J. M. *Industr. Engng. Chem.* 1958 **50** 1195.

[2] Carslaw H. S. and Jaeger J. C. *Conduction of Heat in Solids* p. 82, Oxford University Press 1947.

[3] Barnes C. 1934 *Physics* **5** 4.

[4] March H. W. and Weaver W. *Phys. Rev.* 1928 **31** 1072.

[5] Barrer R. M. *Diffusion in and Through Solids* p. 26. Cambridge University Press 1941.

Chemical Engineering Science, 1961, Vol. 16, pp. 287 to 296. Pergamon Press Ltd., London. Printed in Great Britain.

Surface-renewal models in mass transfer

D. D. PERLMUTTER
Chemical Engineering Division,
University of Illinois, Urbana, Illinois, U.S.A.

(*Received* 1 *August* 1960 *in revised form* 10 *February* 1961)

Abstract—Several surface renewal models are developed to describe mass transfer between phases. DANCKWERTS' and HIGBIE's derivations are examined with respect to some alternative eddy residence-time distributions: dead time and multiple capacitance effects are considered. Two other models are based respectively on assumptions of (1) a transient, non-equilibrium interface, and (2) a thin interfacial layer of reduced effective diffusivity. The first of these predicts a maximum in mass transfer rate with respect to system agitation.

Résumé—Plusieurs processus de renouvellement de surface sont exposés pour décrire le transfert de masse entre phases. Les dérivations de DANCKWERTS et HIGBIE sont examinées en tenant compte des temps de résidence et des états tourbillonaires: les temps morts et les nombreux effets de capacité sont considérés. Deux autres processus sont fondés respectivement sur les hypothèses suivantes: (1) Interface non à l'équilibre, transitoire; (2) Couche mince interfaciale de diffusivité effective réduite.

La première de ces hypothèses prévoit un maximum de vitesse de transfert de masse en fonction de l'agitation du système.

Zusammenfassung—Verschiedene Oberflächenerneuerungsmodelle sind entwickelt worden, um den Stofftransport zwischen verschiedenen Phasen beschreiben zu können. Die Ableitungen von DANCKWERTS und HIGBIE wurden bezüglich anderer Verweilzeitverteilung geprüft: Dabei wurden Totzeit und mehrfache Speichereffekte betrachtet. Zwei andere Modelle wurden entwickelt, einmal unter der Annahme einer sich ändernden, nicht im Gleichgewicht befindlichen Grenzfläche, und zum anderen unter der Annahme einer dünnen Grenzschicht mit verminderter Diffusionsfähigkeit. Die erste dieser beiden sagt ein Maximum an Stoffübergang bezüglich der Rührung des Systems voraus.

FOR SOME time it has been clear that the stagnant or laminar film model is an oversimplified description of the mechanism of mass transfer between phases. In particular, it is inadequate in relating mass transfer coefficients to molecular diffusivity, predicting incorrectly a first-order dependence. The experimental evidence favours a square-root dependence, whether in tubular [1] or stirred vessel [2] equipment. Furthermore, as emphasized by HANRATTY [3], this model is not even qualitatively in agreement with observations of the behaviour of a fluid in the immediate neighbourhood of an interface. HANRATTY [3] and DANCKWERTS [4] have each discussed the weaknesses of this model and the merits of a model based on a transient surface, intermittently renewed by fresh eddies from the bulk of solution. TOOR and MARCHELLO [5] have partially reconciled the two models by using the relative age of a surface as a criterion.

There is evidence to suggest that an interfacial resistance to mass transfer may exist, particularly where liquid surfaces are modified by the addition of surface-active agents [6, 7]. DANCKWERTS has shown that this consideration can also be included in the surface-renewal model by using a boundary condition formulated by HIGBIE [8] in conjunction with an assumed eddy residence-time distribution. However, both HIGBIE's and DANCKWERTS' proposals for eddy residence-time distributions have shortcomings: the former does not allow for statistical variation that is known to exist; the latter requires that the most probable eddy have a residence time of zero. DANCKWERTS has already commented on some limitations of his distribution [9]. It is one of the purposes of this paper to offer distributions that seem more acceptable, and to show how they can be related to the two cited above.

But regardless of the residence-time distribution

ambient, for example, 40°C (104°F). Thermal conductivity units are somewhat temperature dependent, but under the conditions of the Dye–DallaValle work [1] it was noted that a 1°F variation in bath temperature resulted in a negligible change in a gas analysis reading.

Diffusion Test Procedure

Before a diffusion run or test is started, a systematic programme of leak tests should be made to insure satisfactory diffusion cell performance. Reproducible diffusion test data may be insured if the system can be evacuated to approximately 2 mm of mercury. (The schematic diagram shown by Fig. 3 shows manner in which a vacuum pump K may be connected into the system).

It is good practice to conduct two diffusion runs for each porous test specimen of a given length, one with the specimen saturated with one of the two gases used, and another with the specimen saturated with the second gas. This presaturation is necessary to define the concentration distribution in the test specimen at the beginning of diffusion (solution of the problem is greatly simplified when one of the components is uniformly distributed, i.e. when $C_0(x) = C_0$, at $t = 0$). To achieve this preliminary saturation one of the cell chambers must be isolated. This is conveniently done by closing a thin sliding gate fitted to and recessed in one end of the plug holder. This sliding gate is opened at the start of a diffusion run, and during the run composition vs. time is recorded for each cell chamber as determined by the thermal conductivity gas analyser.

Notation

a_n = Fourier coefficient
A_i = characteristic constant in the general solution
b_n = characteristic coefficient
B_i = characteristic constant in the general solution
C = concentration expressed as mole fraction; general solution of equation (1)
c_1, c_2 = particular solutions to equation (1)
C_0 = concentration in porous medium at $t = 0$
${}_1C_0$ = concentration in gas volume 1 at $t = 0$
${}_2C_0$ = concentration in gas volume 2 at $t = 0$
${}_1C(t)$ = concentration in gas volume 1 at time t
${}_2C(t)$ = concentration in gas volume 2 at time t
$C(x, t)$ = concentration in porous medium at distance x and time t
C_∞ = final uniform concentration in system
D = Fick's second law diffusivity (diffusion coefficient)
D' = effective or sought diffusivity for porous medium (related to Fick's second law diffusivity as shown by $D = D'/\epsilon$)
F_1 = Duhamel's theorem function
F_2 = Duhamel's theorem function
g = length and volume of gas container in general solution
h = length and volume of gas container in general solution
i = designates term of a series
l = length and effective volume of porous medium
n = designates term of a series
x = co-ordinate along which diffusion is occurring
t = time
α_n = an expocntial index
β_i = a characteristic constant
ϵ = porosity
$\gamma, \gamma_1, \gamma_2$ = volume ratio
τ = time

References

[1] Dye R. F. and DallaValle J. M. *Industr. Engng. Chem.* 1958 **50** 1195.

[2] Carslaw H. S. and Jaeger J. C. *Conduction of Heat in Solids* p. 82, Oxford University Press 1947.

[3] Barnes C. 1934 *Physics* **5** 4.

[4] March H. W. and Weaver W. *Phys. Rev.* 1928 **31** 1072.

[5] Barrer R. M. *Diffusion in and Through Solids* p. 26. Cambridge University Press 1941.

Chemical Engineering Science, 1961, Vol. 16, pp. 287 to 296. Pergamon Press Ltd., London. Printed in Great Britain.

Surface-renewal models in mass transfer

D. D. PERLMUTTER
Chemical Engineering Division,
University of Illinois, Urbana, Illinois, U.S.A.

(*Received* 1 *August* 1960 *in revised form* 10 *February* 1961)

Abstract—Several surface renewal models are developed to describe mass transfer between phases. DANCKWERTS' and HIGBIE's derivations are examined with respect to some alternative eddy residence-time distributions: dead time and multiple capacitance effects are considered. Two other models are based respectively on assumptions of (1) a transient, non-equilibrium interface, and (2) a thin interfacial layer of reduced effective diffusivity. The first of these predicts a maximum in mass transfer rate with respect to system agitation.

Résumé—Plusieurs processus de renouvellement de surface sont exposés pour décrire le transfert de masse entre phases. Les dérivations de DANCKWERTS et HIGBIE sont examinées en tenant compte des temps de résidence et des états tourbillonaires: les temps morts et les nombreux effets de capacité sont considérés. Deux autres processus sont fondés respectivement sur les hypothèses suivantes: (1) Interface non à l'équilibre, transitoire; (2) Couche mince interfaciale de diffusivité effective réduite.

La première de ces hypothèses prévoit un maximum de vitesse de transfert de masse en fonction de l'agitation du système.

Zusammenfassung—Verschiedene Oberflächenerneuerungsmodelle sind entwickelt worden, um den Stofftransport zwischen verschiedenen Phasen beschreiben zu können. Die Ableitungen von DANCKWERTS und HIGBIE wurden bezüglich anderer Verweilzeitverteilung geprüft: Dabei wurden Totzeit und mehrfache Speichereffekte betrachtet. Zwei andere Modelle wurden entwickelt, einmal unter der Annahme einer sich ändernden, nicht im Gleichgewicht befindlichen Grenzfläche, und zum anderen unter der Annahme einer dünnen Grenzschicht mit verminderter Diffusionsfähigkeit. Die erste dieser beiden sagt ein Maximum an Stoffübergang bezüglich der Rührung des Systems voraus.

FOR SOME time it has been clear that the stagnant or laminar film model is an oversimplified description of the mechanism of mass transfer between phases. In particular, it is inadequate in relating mass transfer coefficients to molecular diffusivity, predicting incorrectly a first-order dependence. The experimental evidence favours a square-root dependence, whether in tubular [1] or stirred vessel [2] equipment. Furthermore, as emphasized by HANRATTY [3], this model is not even qualitatively in agreement with observations of the behaviour of a fluid in the immediate neighbourhood of an interface. HANRATTY [3] and DANCKWERTS [4] have each discussed the weaknesses of this model and the merits of a model based on a transient surface, intermittently renewed by fresh eddies from the bulk of solution. TOOR and MARCHELLO [5] have partially reconciled the two models by using the relative age of a surface as a criterion.

There is evidence to suggest that an interfacial resistance to mass transfer may exist, particularly where liquid surfaces are modified by the addition of surface-active agents [6, 7]. DANCKWERTS has shown that this consideration can also be included in the surface-renewal model by using a boundary condition formulated by HIGBIE [8] in conjunction with an assumed eddy residence-time distribution. However, both HIGBIE's and DANCKWERTS' proposals for eddy residence-time distributions have shortcomings: the former does not allow for statistical variation that is known to exist; the latter requires that the most probable eddy have a residence time of zero. DANCKWERTS has already commented on some limitations of his distribution [9]. It is one of the purposes of this paper to offer distributions that seem more acceptable, and to show how they can be related to the two cited above.

But regardless of the residence-time distribution

chosen, the Higbie-Danckwerts model accounts for any interfacial resistance that may exist by using an equivalent mass transfer coefficient. Danckwerts [10] has offered an interpretation of this coefficient, which is developed from the kinetic theory of gases. However, the use of this parameter for liquid–liquid or liquid–solid interfaces (which appear to require it more) is without theoretical justification. Hence, it would seem worthwhile to postulate other ways of interpreting interfacial resistance, especially if the new models predict novel effects or relate to more fundamental parameters. These were the reasons for developing Models II and III in what follows.

Model I

1. *Introduction*

Following Danckwerts [4], consider an eddy of fluid in a turbulent field, which is swept into contact with an interface. For a short time interval the eddy may be treated as of semi-infinite extent. Then

$$\frac{\partial c}{\partial t} = D\,\frac{\partial^2 c}{\partial x^2} \tag{1}$$

$$c = c_B,\ t = 0,\ x > 0 \tag{2}$$

$$c = c_B,\ t > 0,\ x = \infty \tag{3}$$

$$-D\,\frac{\partial c}{\partial x} = k\,(c^* - c),\ x = 0,\ t > 0 \tag{4}$$

Equation (4) defines the interfacial resistance, $(1/k)$, in terms of the equilibrium concentration, c^*. The solution to this set of equations gives the instantaneous surface concentration as

$$c = c_B + (c^* - c_B)\left[1 - \exp\left(\frac{k^2 t}{D}\right)\operatorname{erfc}\left(k\sqrt{\frac{t}{D}}\right)\right] \tag{5}$$

and the instantaneous mass flux as

$$N = k\,(c^* - c_B)\exp\left(\frac{k^2 t}{D}\right)\operatorname{erfc}\left(k\sqrt{\frac{t}{D}}\right) \tag{6}$$

To allow for the spectrum of eddy ages that must exist at any real interface Danckwerts sums the instantaneous fluxes with respect to the assumed eddy-age frequency function*:

$$\phi\,(t) = \frac{1}{\tau}\exp\,(-t/\tau) \tag{7}$$

He obtains the measured mass transfer rate, R, by

$$R = \int_0^\infty N\,\phi\,(t)\,dt \tag{8}$$

$$R = \frac{1}{\tau}\,\mathscr{L}\,[N] = (c^* - c_B)\left[\frac{1}{(1/k) + \sqrt{(\tau/D)}}\right] \tag{9}$$

The corresponding mass transfer coefficient, K, is

$$K = \frac{R}{(c^* - c_B)} = \frac{1}{(1/k) + \sqrt{(\tau/D)}} \tag{10}$$

The solution is equation (30) of Danckwerts' paper [4]. It is evident that the assumed eddy-age frequency function is one of the important components of this model, as indeed Danckwerts has repeatedly emphasized. Higbie's initial postulate was that all eddies have the same residence time, τ; this is equivalent to a constant age distribution:

$$\phi\,(t) = 1/\tau, \qquad 0 < t < \tau \tag{11}$$

or, in terms more familiar in chemical engineering, this may be called the "plug-flow" case. Danckwerts' equation, on the other hand, depends on the idea that all eddies are equally likely to be displaced, regardless of age. This is, after all, the familiar "well-mixed" vessel. The plug-flow and well-mixed character of these two cases can be proved more formally by resort to the work of Zwietering [11]. This author derived the relationships that must exist between the eddy residence-time distribution $[F\,(\theta)$ over a time interval] and the eddy-age frequency function $[\phi\,(t)$ at an instant in time] in a continuous flow system. His equation (8) is as follows in the symbols used here:

$$\phi\,(t) = \frac{1}{\tau}\,[1 - F\,(t)] \tag{12}$$

The distribution function, $F\,(\theta)$, is related to $f\,(\theta)$, the frequency function of residence times, by the definition

$$f\,(\theta) = \frac{dF\,(\theta)}{d\,\theta} \tag{13}$$

Considering the set of eddies in Danckwerts'

*It will be convenient to use the time parameter, τ, instead of its reciprocal, used by Danckwerts.

model to be the elements in a thin (essentially two-dimensional) vessel at the interface, ZWIETERING's relation can be used to show that the age frequency function of equation (7) corresponds to a residence-time frequency function of identical form:

$$f(\theta) = \frac{1}{\tau} \exp(-\theta/\tau) \qquad (14)$$

Equation (14) may readily be identified with the function resulting from analysis of a single well-mixed vessel. This is a convenient description of DANCKWERTS' assumption, for it invites several alternatives for comparison.

VOL. 16 1962

2. *Multiple-capacitance effect*

One of the important contributions of DANCKWERTS' assumption on eddy age distribution is that it takes into account the probabilistic nature of the surface renewal process. But, as noted above, it does not seem reasonable that the most likely eddy residence time be zero, as required by equation (14). One approach to a more satisfactory representation might be to recall that in general, multi-vessel systems tend to compromise between plug-flow and well-mixed models. In the limit, an infinite number of infinitesimal vessels are equivalent to a plug-flow system [12].

If the mass transfer operation is considered to involve two capacitances in series, a suitable residence-time frequency function is

$$f(\theta) = \frac{1}{\tau_2 - \tau_1}\left[\exp(-\theta/\tau_2) - \exp(-\theta/\tau_1)\right] \qquad (15)$$

In a more physical sense this system may be thought of as flow into a well-mixed primary region followed by passage into a well-mixed secondary region. But it should be emphasized that both primary and secondary regions are part of the thin boundary zone composed at any instant of the collection of interface eddies. This zone is in essence a two-dimensional transient reservoir from which mass is transferred by molecular diffusion. As can be seen from Fig. 1 the residence-time frequency function of this two-capacitance model avoids the objection cited above: there is now zero likelihood of finding an eddy with zero residence time, and in fact the most probable residence time (the maximum on the curve) is:

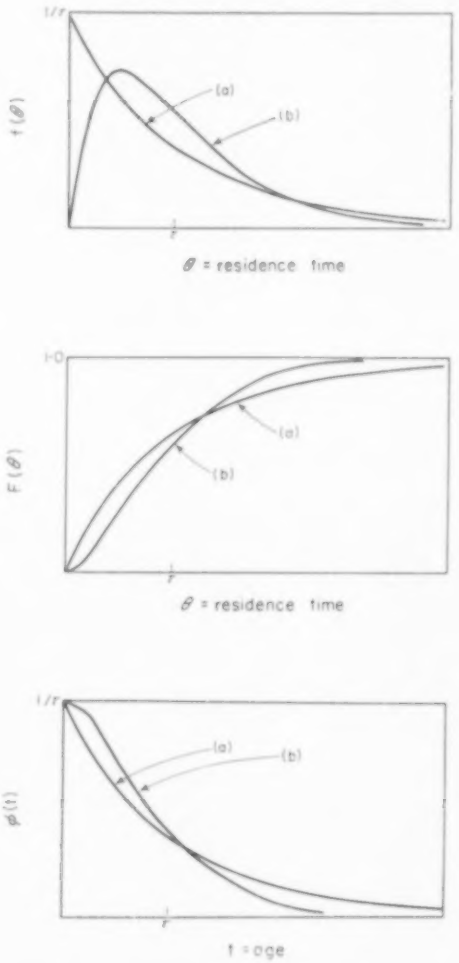

FIG. 1. Distribution and frequency functions for eddies in (a) single- and (b) double capacitance, well-mixed systems.

$$\frac{\tau_1 \tau_2}{\tau_1 - \tau_2} \ln \frac{\tau_2}{\tau_1}, \qquad (16)$$

always greater than zero. It may also be noted from the same Fig., however, that the corresponding eddy-age frequency function, $\phi(t)$, has not been changed as radically in going from the single vessel to the dual vessel model.

Using equations (12) and (13), and returning equation (8) for the mass transfer rate:

$$F(\theta) = 1 + \frac{\tau_1}{\tau_2 - \tau_1} \exp(-\theta/\tau_1) - \frac{\tau_2}{\tau_2 - \tau_1} \exp(-\theta/\tau_2) \quad (17)$$

$$\phi(t) = \frac{1}{(\tau_2^2 - \tau_1^2)} \left[\tau_2 \exp(-t/\tau_2) - \tau_1 \exp(-t/\tau_1)\right] \quad (18)$$

$$K = \frac{1}{(\tau^2_2 - \tau^2_1)} \left[\frac{\tau_2^2}{(1/k) + \sqrt{(\tau_2/D)}} - \frac{\tau_1^2}{(1/k) + \sqrt{(\tau_1/D)}}\right] \quad (19)$$

If both primary and secondary regions have the same mean residence time, $\tau_1 = \tau_2 = \tau/2$:

$$f(\theta) = \frac{4\theta}{\tau^2} \exp(-2\theta/\tau) \quad (20)$$

$$F(\theta) = 1 - \exp(-2\theta/\tau) - \frac{2\theta}{\tau} \exp(-2\theta/\tau) \quad (21)$$

$$\phi(t) = \frac{1}{\tau}\left(1 + \frac{2t}{\tau}\right) \exp(-2t/\tau) \quad (22)$$

$$K = \sqrt{\frac{D}{\tau}} \left\{\frac{(1/K)\sqrt{(D/\tau)} + \frac{1}{8}\sqrt{2}}{[(1/K)\sqrt{(D/\tau)} + (\sqrt{2}/2)]^2}\right\} \quad (23)$$

It is not difficult to extend this development to an n-vessel system by starting with the residence-time frequency function

$$f(\theta) = \frac{n^n \theta^{n-1}}{(n-1)!\,\tau^n} \exp(-n\theta/\tau) \quad (24)$$

The results for various values of n may be considered as successive degrees of compromise between the Higbie and Danckwerts models. For comparison the solutions for $n = 1$, 2 and ∞ are shown in Fig. 2. The $n = \infty$ case is the Higbie solution.

It is abundantly clear from Fig. 2 that the multiple capacitance point of view does not have much promise with regard to interpretation of experimental mass transfer measurements. The three lines in this Fig. never differ by more than about 13 per cent, even in the limit. Evidently, it does not much matter whether the interfacial zone acts as a single well-mixed region, or a plug-flow region, provided that all the fluid in this region is in motion.

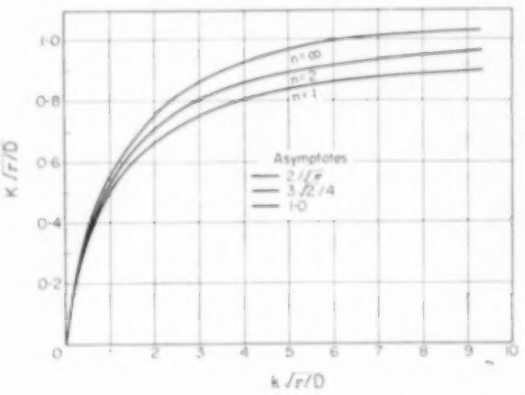

Fig. 2. Mass transfer relations according to model I.

3. *Dead time effect*

A residence-time frequency function with zero intercept can also be arrived at by an alternative approach: that of considering the otherwise well-mixed boundary zone to contain stagnant pockets. Physically, this situation would result from imperfect mixing such as would perhaps be found in the presence of locally laminar flow. Experimental evidence for such a case has been presented by Lynn *et al.* [13], who studied mass transfer over a string of spheres. However, this phenomenon can probably be expected to a greater or lesser extent in any fixed bed containing regions in laminar flow.

To account for stagnant pockets a dead time A, may be added to the single-vessel model by adopting the residence-time frequency function

$$f(\theta) = \begin{cases} 0, & 0 \leqslant \theta < A \\ \frac{1}{\tau} \exp[-(\theta - A)/\tau], & \theta \geqslant A \end{cases} \quad (25)$$

Applying definition (13) gives

$$F(\theta) = \begin{cases} 0, & 0 \leqslant \theta < A \\ 1 - \exp[-(\theta - A)/\tau], & \theta \geqslant A \end{cases} \quad (26)$$

It should be noted that the τ in equation (12)

refers to the *total* mean residence time for the system; consequently, the dead time must be added to the equivalent mixed-vessel parameter. Thus, equation (12) provides

$$\phi(t) = \begin{cases} \dfrac{1}{(\tau + A)} & 0 \leqslant \theta < A \\ \dfrac{1}{(\tau + A)} \exp\left[-(t - A)/\tau\right], & \theta \geqslant A \end{cases} \tag{27}$$

Equations (25), (26) and (27) are shown graphically in Fig. 3. Continuing by the procedure outlined above:

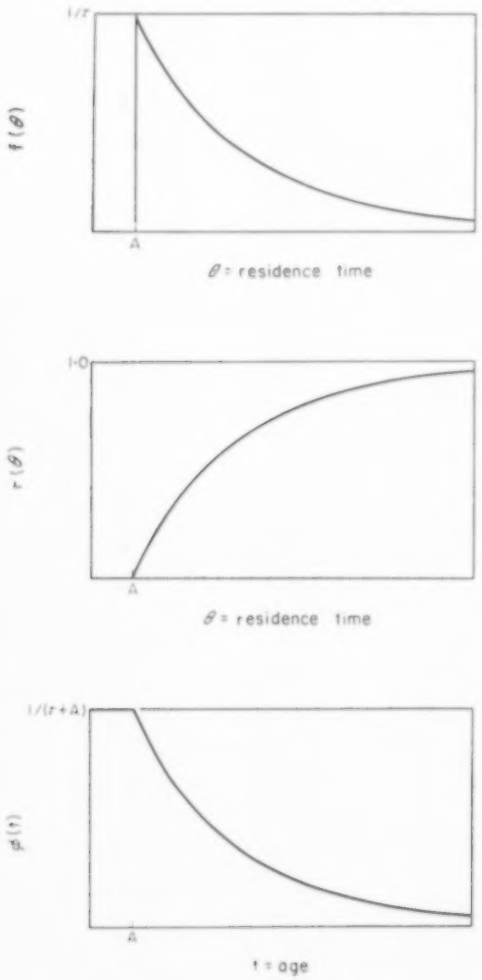

FIG. 3. Distribution and frequency functions for eddies in a single capacitance system with dead time, but otherwise well-mixed.

$$R = \int_0^A \frac{1}{(\tau + A)} N\, dt + \int_A^\infty \frac{1}{(\tau + A)} N \exp\left[-(t - A)/\tau\right] dt \tag{28}$$

$$K = \frac{D}{(\tau + A)\,k}\left[\exp\left(k^2 A/D\right) \operatorname{erfc} k\sqrt{\left(\frac{A}{D}\right)} + 2k\sqrt{\left(\frac{A}{D\pi}\right)} - 1\right] + \frac{k \exp\left(A/\tau\right)}{(\tau + A)\left[\left(k^2/D\right) - \left(1/\tau\right)\right]} \left\{k\sqrt{\left(\frac{\tau}{D}\right)} \operatorname{erfc}\sqrt{\left(\frac{A}{\tau}\right)} - \exp\left[\left(\frac{k^2}{D} - \frac{1}{\tau}\right)A\right] \operatorname{erfc} k\sqrt{\frac{A}{D}}\right\} \tag{29}$$

In the limit as $A \to 0$, equation (29) reduces to the simple equation (10). As $k \to \infty$ (no interfacial resistance), the following simplication is obtained:

$$K = \sqrt{\left(\frac{D}{\tau}\right)}\left[\frac{1}{(A/\tau) + 1}\left\{\frac{2}{\sqrt{\pi}}\sqrt{\left(\frac{A}{\tau}\right)} + \exp\left(A/\tau\right) \operatorname{erfc}\sqrt{\frac{A}{\tau}}\right\}\right] \tag{30}$$

The bracket in equation (30) may be thought of as a correction factor for the dead time, A. This factor is tabulated in Table 1 as a function of the ratio (A/τ). For values of the argument greater than 10, the value of the correction factor may be calculated from the asymptotic equation

$$K = 2\sqrt{\frac{D}{\pi A}} \tag{31}$$

It is interesting to note further that in this limiting case the mass transfer coefficient is a function of dead time, A, but is independent of the first-order mixing parameter, τ. This observation suggests that the Higbie model is equivalent to an all dead time distribution, as indeed it must be.

Equation (29) can also be used to develop the Higbie solution for the case which includes interfacial resistance. In the limit as $(A/\tau) \to \infty$, equation (29) becomes

$$K = \frac{D}{Ak}\left[\exp\left(k^2 A/D\right)\operatorname{erfc} k\sqrt{\left(\frac{A}{D}\right)} + \right.$$
$$\left. + 2k\sqrt{\left(\frac{A}{D\pi}\right)} - 1\right] \quad (32)$$

This solution is actually the $n = \infty$ case of Fig. 2, if the dead time A is identified with the residence time τ.

Unlike the situation described above for the multiple capacitance model, the dead time effect can be very great. Table 1 shows, for example, that the mass transfer rate will be reduced by 50 per cent, if the dead time becomes four times as great as the well-mixed residence time parameter.

Table 1. *Correction factors for dead time* (*single capacitance system, no interfacial resistance*)

$\frac{A}{\tau}$	*Factor from equation* (30)
0	1·00
0·12	0·97
0·25	0·95
0·42	0·90
0·64	0·85
1·00	0·78
1·44	0·71
2·25	0·62
4·00	0·50
6·25	0·42
9·00	0·36

Model II

The presence of an apparent interfacial resistance can be rationalized in another way by postulating a non equilibrium interface condition. Several authors [4, 7] have pointed out that some finite resistance must be expected from this source, as a consequence of the finite velocity of colliding molecules. Attempts at experimental verification of this expectation have produced mixed results. The early evidence supporting interfacial resistance [14] at a gas–liquid interface has been overshadowed by a series of negative findings [7, 15, 16]. Nevertheless, there remains reason to expect such resistance at less mobile boundaries and at boundaries affected by surface-active agents. The former has experimental support in Quinn and Jeannin's findings [17], and the latter are discussed in detail by Harvey and Smith [7]. These ideas may be formalized by writing the boundary condition:

$$c = c_B + (c^* - c_B)(1 - \exp(-\lambda t)), \qquad x = 0,\ t > 0 \quad (33)$$

where the parameter λ is a measure of the rate of equilibration at the interface. Solving equations (1), (2), (3) with boundary condition (33) gives (after Carslaw and Jaeger [18]):

$$\frac{c - c_B}{c^* - c_B} = \operatorname{erfc}\frac{x}{2\sqrt{Dt}} - \frac{\exp(-\lambda t)}{2}\left\{\exp\left[-i\sqrt{\left(\frac{\lambda}{D}\right)}x\right]\right.$$
$$\operatorname{erfc}\left(\frac{x}{2\sqrt{Dt}} - i\sqrt{\lambda t}\right) +$$
$$+ \exp\left[+i\sqrt{\left(\frac{\lambda}{D}\right)}x\right]$$
$$\left.\operatorname{erfc}\left(\frac{x}{2\sqrt{Dt}} + i\sqrt{\lambda t}\right)\right\} \quad (34)$$

The instantaneous mass flux is

$$N = (c^* - c_B)\left[-i\sqrt{(D\lambda)}\exp(-\lambda t)\right.$$
$$\left.\operatorname{erf}(i\sqrt{\lambda t})\right] \quad (35)$$

Proceeding as for Model I, one obtains for the eddy age distribution of equation (7) the result

$$K = \sqrt{\frac{D}{\tau}}\left[\frac{\lambda\tau}{1 + \lambda\tau}\right] \quad (36)$$

It is instructive to rearrange this result in a form directly comparable with equation (10):

$$K = \frac{1}{(1/\lambda\sqrt{D\tau}) + \left[\sqrt{(\tau/D)}\right]} \quad (37)$$

In comparison, it is obvious that the interfacial resistance can be expressed as an equivalent coefficient even in this case. This pseudo-coefficient would be the product: $\lambda\sqrt{D\tau}$. Furthermore, it is clear from equation (37) that an appreciable effect of interfacial resistance will only occur if λ is small enough to make the first denominator term (say) 20 per cent of the

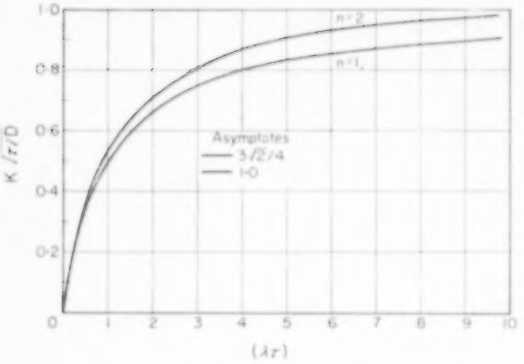

FIG. 4. Mass transfer relations according to model II.

second; that is, if $(1/\lambda) > 0{\cdot}2\ \tau$. Thus, if τ is taken as perhaps 1 sec the time constant of the first-order surface equilibration process $(1/\lambda)$ would have to be at least 0·2 sec. It seems probable then, that experimental measurements would require either a physical arrangement with much smaller τ, or a system with correspondingly smaller λ. This model may also be varied to account for the multiple capacitance or dead time effects discussed for Model I. For example, the result corresponding to the two-vessel residence-time frequency distribution expressed by equation (20) can be written as

$$K = \sqrt{\frac{D}{\tau}}\left[\frac{\sqrt{(2)}\ \lambda\tau\ (10 + 3\ \lambda\tau)}{4\ (2 + \lambda\tau)^2}\right] \qquad (38)$$

For comparison with the results of Model I these solutions are shown in Fig. 4 for the cases of $n = 1$ and 2. The curves for this model are very similar to those obtained for Model I (Fig. 2).

Nevertheless, a very striking difference between Model II and most other mass transfer models can be emphasized by replotting the equations in such a way as to confine the parameter τ to the independent abscissa variable. The mass transfer coefficient then exhibits a maximum, as shown in Fig. 5. Equation (36), for example, predicts

$$K_{max} = 0{\cdot}5\ \sqrt{D\lambda} \text{ at } \lambda\tau = 1 \qquad (39)$$

This behaviour is a consequence of the fact that this model, unlike the others, requires an initial flux of zero:

$$\lim_{t\to 0} N = \lim_{t\to 0}\left\{(c^* - c_B)\left[-i\sqrt{(D\lambda)}\right.\right.$$
$$\left.\left.\exp(-\lambda t)\ \mathrm{erf}\ i\sqrt{\lambda t}\right]\right\} = 0 \qquad (40)$$

One experimental test for this model would, therefore, be a study of mass transfer coefficients for evidence of a maximum with respect to agitation (the parameter τ). As noted above, this effect might only be measurable in systems with small values of λ; i.e. where surface equilibration is relatively slow. SECOR [19] has suggested that such behaviour might be detectable in a crystallization process, where the surface equilibration could be retarded by the

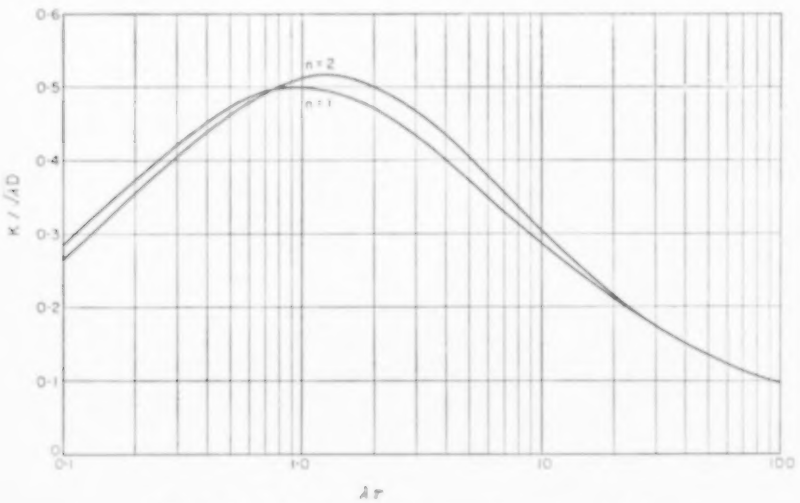

FIG. 5. Mass transfer relations according to model II.

necessity of a molecule finding a suitable crystal position.

MODEL III

Another explanation which has been offered for interfacial resistance attributes the effect to a narrow region adjacent to the interface in which a reduced effective diffusivity is to be found [4]. This is presumed to be due to relatively short-range molecular interactions with the second phase.

As before, consider a semi-infinite eddy, but having a thin surface layer of thickness, L, in which an effective diffusivity, $\mathscr{D}$ is applicable. Assume the surface in contact with the second phase to be in equilibrium with it, and assume equal flux and concentration of solute at both sides of the boundary between the eddy and its thin surface layer. Then following CRANK's equations [20]:

$$\frac{c - c_B}{c^* - c_B} = \sum_{n=1}^{\infty} \alpha^n \left[\operatorname{erfc} \frac{L(2n+1) + x}{2\sqrt{\mathscr{D}t}} - \alpha \operatorname{erfc} \frac{L(2n+1) - x}{2\sqrt{\mathscr{D}t}} \right] \quad (41)$$

$$\text{where } \alpha = \frac{1 - \sqrt{(\mathscr{D}/D)}}{1 + \sqrt{(\mathscr{D}/D)}} \quad (42)$$

The instantaneous flux is

$$N = (c^* - c_B)\sqrt{\left(\frac{\mathscr{D}}{\pi t}\right)} \left[1 + 2\sum_{n=1}^{\infty} \alpha^n \exp\left(-n^2 L^2/\mathscr{D}t\right)\right] \quad (43)$$

Continuing as before, the eddy age distribution function of equation (7) gives the result

$$K = \sqrt{\left(\frac{\mathscr{D}}{\tau}\right)} \left[1 + 2\sum_{n=1}^{\infty} \alpha^n \exp\left(\frac{-2nL}{\sqrt{\mathscr{D}\tau}}\right)\right] \quad (44)$$

which reduces, by the sum for a geometric series, to

$$K = \sqrt{\frac{\mathscr{D}}{\tau}} \left[\frac{1 + \alpha \exp\left(-2L/\sqrt{\mathscr{D}\tau}\right)}{1 - \alpha \exp\left(-2L/\sqrt{\mathscr{D}\tau}\right)}\right] \quad (45)$$

Equation (45) is graphed in Fig. 6 in terms of two dimensionless groups and the parameter, α. It is possible to compare this model with equation (10) of Model I by also showing the latter equation on the co-ordinates of Fig. 6. This may be done by letting

$$k = \frac{\mathscr{D}}{L} \quad (46)$$

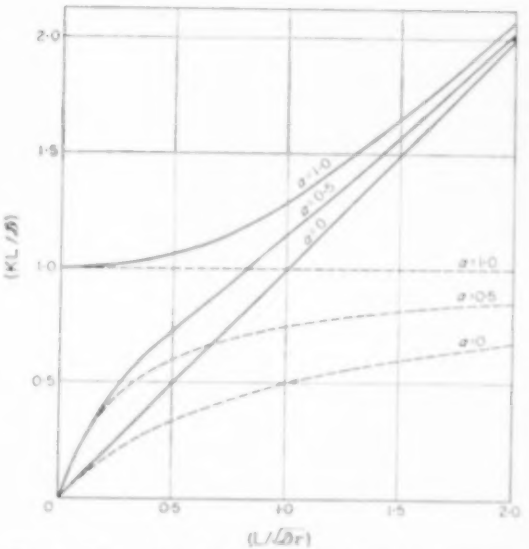

FIG. 6. Comparison of mass transfer models I (broken lines) and III (solid lines).

Making this substitution in equation (10) and using the definition of α given in equation (42)

$$\frac{KL}{\mathscr{D}} = \frac{1}{1 + \left[(1-\alpha)/(1+\alpha)\right](\sqrt{\mathscr{D}\tau}/L)} \quad (47)$$

It is clear from Fig. 6 that the two models become identical for small values of $(L/\sqrt{\mathscr{D}\tau})$ for all values of α; this effect is to be expected as the surface film thins out, or the mean residence time increases to large values. The two models do not give the same result for the limit: $\alpha \to 0$, $(\mathscr{D} \to D)$. In fact, while Model I shows a limit to the mass transfer rate Model III predicts a coefficient increase without limit as the agitation is increased (parameter τ decreased). This difference is a consequence of the Model III equilibrium interface assumption. Model I can only show interfacial equilibrium if $L = 0$.

CONCLUSIONS

Several surface renewal models have been developed to describe mass transfer between

phases. Dead time and multiple capacitance effects were considered.

DANCKWERTS' assumption that all eddies are equally likely to be displaced, regardless of age, is shown to be equivalent to a well-mixed surface zone; HIGBIE's assumption that all eddies have the same residence time is treated as a plug-flow surface zone. The various intermediate cases differ only slightly from one another, as regards predicted mass transfer rates, and the use of multiple-capacitance models does not appear to offer much advantage. On the other hand, a dead-time model which accounts for the existence of local stagnant pockets does predict important differences in mass transfer.

A non-equilibrium interface condition can be described as an exponential time function by using a single "relaxation" parameter. The result predicts a maximum in transfer rate with respect to agitation.

Apparent interfacial resistance can also be interpreted by postulating a narrow (but finite) interface layer of small effective diffusivity. The result agrees with the relations arising from DANCKWERTS' model when either (1) the interfacial layer is especially thin, or (2) the mean residence time is especially large.

Experimental tests of the models described here are made difficult by the inclusion of several parameters, each of which is not subject to straightforward measurement. However, it may be possible to evaluate them from mass transfer experiments by eliminating some, or holding one or more constant. In any case, these equations provide a framework for data correlation which is somewhat more flexible than that conventionally used.

NOTATIONS

A = dead time
c = concentration
c_B = bulk concentration
c^* = equilibrium concentration
D = diffusivity
$\mathscr{D}$ = effective diffusivity in film at interface
$f(\theta)$ = residence-time frequency function
$F(\theta)$ = residence-time distribution function
$i = \sqrt{-1}$
k = reciprocal of interfacial resistance, expressed as a mass transfer coefficient
K = measured mass transfer coefficient
K_{max} = maximum value of K
L = thickness of interfacial film
$\mathscr{L}$ = Laplace transform
N = instantaneous flux
n = the number of vessels in a cascade
R = measured mass transfer rate
t = time
x = distance perpendicular to interface
$\alpha = [1 - \sqrt{(\mathscr{D}/D)}]/[1 + \sqrt{(\mathscr{D}/D)}]$
θ = residence time
λ = equilibration-time parameter
τ = mean residence time
τ_1 = mean residence time for the first vessel
τ_2 = mean residence time for the second vessel
$\phi(t)$ = age frequency function

$$\text{erf}(Z) = (2/\sqrt{\pi}) \int_0^Z \exp(-y^2)\, dy$$

$$\text{erfc}(Z) = 1 - \text{erf}(Z)$$

REFERENCES

[1] SHERWOOD T. K. and HOLLOWAY F. A. L. *Trans. Amer. Inst. Chem. Engrs.* 1940 **36** 39.

[2] JOHNSON A. I. and HUANG C. J. *Amer. Inst. Chem. Engrs. J.* 1956 **2** 412.

[3] HANRATTY T. J. *Amer. Inst. Chem. Engrs. J.* 1956 **2** 359.

[4] DANCKWERTS P. V. *Industr. Engng. Chem.* 1951 **43** 1460.

[5] TOOR H. L. and MARCHELLO J. M. *Amer. Inst. Chem. Engrs. J.* 1958 **4** 97.

[6] BOYE-CHRISTENSEN G. and TERJESEN S. G. *Chem. Engng. Sci.* 1959 **9** 225.

[7] HARVEY E. A. and SMITH W. *Chem. Engng. Sci.* 1959 **10** 274.

[8] HIGBIE R. *Trans. Amer. Inst. Chem. Engrs.* 1935 **31** 365.

[9] DANCKWERTS P. V. *Amer. Inst. Chem. Engrs. J.* 1955 **1** 456.

[10] DANCKWERTS P. V. *Research* 1949 **2** 494.

[11] ZWEITERING Th. N. *Chem. Engng. Sci.* 1959 **11** 1.

[12] KRAMERS H. and ALBERDA G. *Chem. Engng. Sci.* 1953 **2** 173.

[13] Lynn S., Straatemeier J. R. and Kramers H. *Chem. Engng. Sci.* 1955 **4** 63.

[14] Emmert R. E. and Pigford R. L. *Chem. Engng. Prog.* 1954 **50** 87.

[15] Raimondi P. and Toor H. L. *Amer. Inst. Chem. Engrs. J.* 1959 **5** 86.

[16] Scriven L. E. and Pigford R. L. *Amer. Inst. Chem. Engrs. J.* 1958 **4** 439.

[17] Quinn J. A. and Jeannin P. G. *Chem. Engng. Sci.* 1961 **15** 243.

[18] Carslaw H. S. and Jaeger J. C. *Conduction of Heat in Solids*, p. 64. Oxford University Press 1959.

[19] Secor R. M. Suggestion was part of his review of this manuscript.

[20] Crank J. *The Mathematics of Diffusion*, p. 39. Oxford Universtiy Press 1956.

Chemical Engineering Science, 1961, Vol. 16, pp. 297 to 337. Pergamon Press Ltd., London. Printed in Great Britain.

Heat transfer coefficients for boiling mixtures

Experimental data for binary mixtures of large relative volatility

C. V. Sternling and L. J. Tichacek*
Shell Development Company, Emeryville, California, U.S.A.

(*Received* 28 *March* 1961)

Abstract—In the process industries boiling is usually used to separate the components of a mixture. Notwithstanding, published correlations of heat transfer rates in boiling are almost always based on studies on pure substances and involve the tacit assumption that a pure compound and a mixture with the same average properties boil alike. The data presented here show that this assumption is untrue and unsafe.

Heat transfer coefficients were measured in a pool boiler for fourteen binary mixtures. Included were systems which form ideal solutions and systems with strong positive and negative deviations from Raoult's law. The boiling range was larger than 170 °F in all cases.

In these systems with wide boiling range, boiling heat transfer coefficients are smaller, by up to *thirty-fold*, than the appropriate average of the coefficients for the two pure components. This is due to a diffusional resistance which appears when, as a consequence of boiling, the components are partially separated.

Résumé—Dans les procédés industriels on utilise en général la distillation pour séparer les constituants d'un mélange. Cependans les relations publiées sur les vitesses de transfert de chaleur en distillation sont presque toujours fondées sur des études de corps purs avec l'hypothèse tacite qu'un constituant pur, et un mélange avec des propriétés identiques distillent de la même façon. Les données présentées ici montrent que cette supposition est fausse et hasardeuse.

Les coefficients de transfert de chaleur ont été mesurés dans une chaudière pour quatorze mélanges. Dans ces systèmes certains forment des solutions idéales, d'autres manifestent un fort écart positif ou négatif par rapport à la loi de Raoult. L'intervalle entre les températures d'ébullition est supérieur à 170 °F dans tous les cas.

Dans ces systèmes à grands intervalles de distillation, les coefficients de transfert de chaleur à l'ébullition sont plus petits – plus de 30 fois – que la moyenne des coefficients pour les deux composants purs. Ceci est dû à la résistance de la diffusion qui apparait quand les constituants sont partiellement séparés par suite de l'ébullition.

Zusammenfassung—In der Verfahrenstechnik wird das Verdampfen gewöhnlich zum Trennen von Komponenten einer Mischung benutzt. Trotzdem sind die veröffentlichten Wärmeübergangsgeschwindigkeiten für die Verdampfung fast immer auf das Studium reiner Substanzen begründet und schliessen die stillschweigende Annahme mit ein, dass reine Verbindungen und Mischungen unter sonst gleichen Bedingungen auch gleichartig sieden. Die hier veröffentlichten Daten zeigen aber, dass diese Annahme unwahr und unsicher ist.

Wärmeübergangszahlen wurden in einem Verdampfer für 14 binäre Gemische untersucht. Darin waren Systeme eingeschlossen, die ideale Lösungen darstellen und solche, die stark positive und negative Abweichungen vom Raoult'schen Gesetz zeigen. Der Siedebereich war in allen Fällen grösser als 170 °F.

In den Systemen mit grossem Siedebereich waren die Wärmeübergangszahlen bis zu einem dreissigstel kleiner als die durchschnittlichen Werte für die beiden reinen Komponenten. Dies ist durch den Diffusionswiderstand bedingt, der auftritt, wenn im Verlauf der Verdampfung die Komponenten teilweise getrennt werden.

* Present address: Shell Oil Company, Norco, Louisiana.

Purpose and Scope

A major use of boiling is in the separation of components of a liquid mixture. It is rather surprising, therefore, that almost all studies of heat transfer during boiling deal only with pure components. The standard texts on heat transfer present correlations that can be used for mixtures only by tacitly assuming that a mixture boils like a pure component having the same average properties.

In our early attempts to explain boiling theoretically, we suspected that this assumption would be very bad when applied to mixtures of wide boiling range.

The experiments reported here show that this is indeed the case. Consider, for example, the following typical data for boiling of ethylene glycol–water mixtures at one atmosphere pressure.

	Temperature drop required to give $h_b = 400$ B.Th.U/hr ft^2 °F
	°F
Pure water	23
21% v water, 79% glycol	51
Pure ethylene glycol	28

Obviously, an engineer who overlooks this effect of composition on boiling may blunder. By assuming the same vigour of nucleate boiling for a mixture as for a pure component, he may be led to specify a boiler which is too small. Or, attempting to improve operation, he may recommend a change in the wrong direction. For example, ordinarily one would expect that increasing recycle rate to a forced circulation boiler would increase boil-up rates. It has been found, however, that increasing circulation in a glycerol–water evaporator was harmful in at least one case known to the authors. The observed loss in heat transfer is attributable mainly to the suppression of boiling due, in part, to change in feed composition.

In this paper, we present data for pool boiling at atmospheric pressure of binary mixtures with wide boiling range. Since all the common solution types (negative, zero and positive deviations from Raoult's law) were studied, the results are widely applicable. No attempt is made here to explain the results completely. The purpose of this paper is to present the data with only a few explanatory remarks.

Apparatus and Procedure

The electrically heated pool boiler shown in Fig. 1 was used. The sides, top and bottom are of ¼ in. thick aluminium welded to form a chamber with inside dimensions 6 in. wide × 7 in. high × 3 in. deep. Windows of ¼ in. thick pyrex glass were clamped to the open ends of the frame using neoprene caskets. In operation the boiler holds about 1½ l. of liquid.

The heating surface is formed by a 3½ in. length of No. 7 gauge stainless steel hypodermic tubing of O.D. = 0·180 in. and 0·015 in. wall thickness. Lengths of ¼ in. copper tubing were brazed to the stainless steel section and the assembly inserted horizontally through electrically insulating seals in the aluminium walls. The seals were made of bakelite grommets mounted so as to press a teflon gasket against both copper tubing and aluminium frame.

Sixty cycle alternating electric current was passed directly through the heater from the secondary of a specially constructed transformer which was wound to deliver 3 v at 200 A with a maximum of 110 v on the primary. A Variac in the primary circuit regulated the power to the heater. The voltage drop across and current flow through the heater were measured by meters and the power computed as for a resistive load.

For temperature measurement, three thermocouples were placed inside the stainless steel heater – one ¾ in. inboard from the right end, one at the centre, and one ¾ in. from the left end. The thermocouple wires were cloth-covered single strands of 28-gauge iron or constantan wire. The iron-constantan connexion was made by carefully silver soldering a small section of the wire to produce a junction which was as close as possible to a point contact. The thermocouple at the left end of the heater was brought in through the tubing from the right side and vice versa. This placement eliminates most of the error due to conduction along the thermocouple wires. The bare thermocouple junctions were coated with sodium silicate to electrically insulated them against contact with the inside surface of the stainless steel heater. After the thermocouples were placed at their measured positions inside the heater silicon carbide powder was packed inside the heater tube around the thermocouples. Besides preventing movement of the junctions during use, this powder also insures good thermal contact between the thermocouples and the heater tubing and reduces temperature fluctuations. With these precautions in the placement of the thermocouples and by the use of fine thermocouple wire, conduction errors in the thermocouple reading were made negligible. The thermocouple e.m.f.'s were measured on

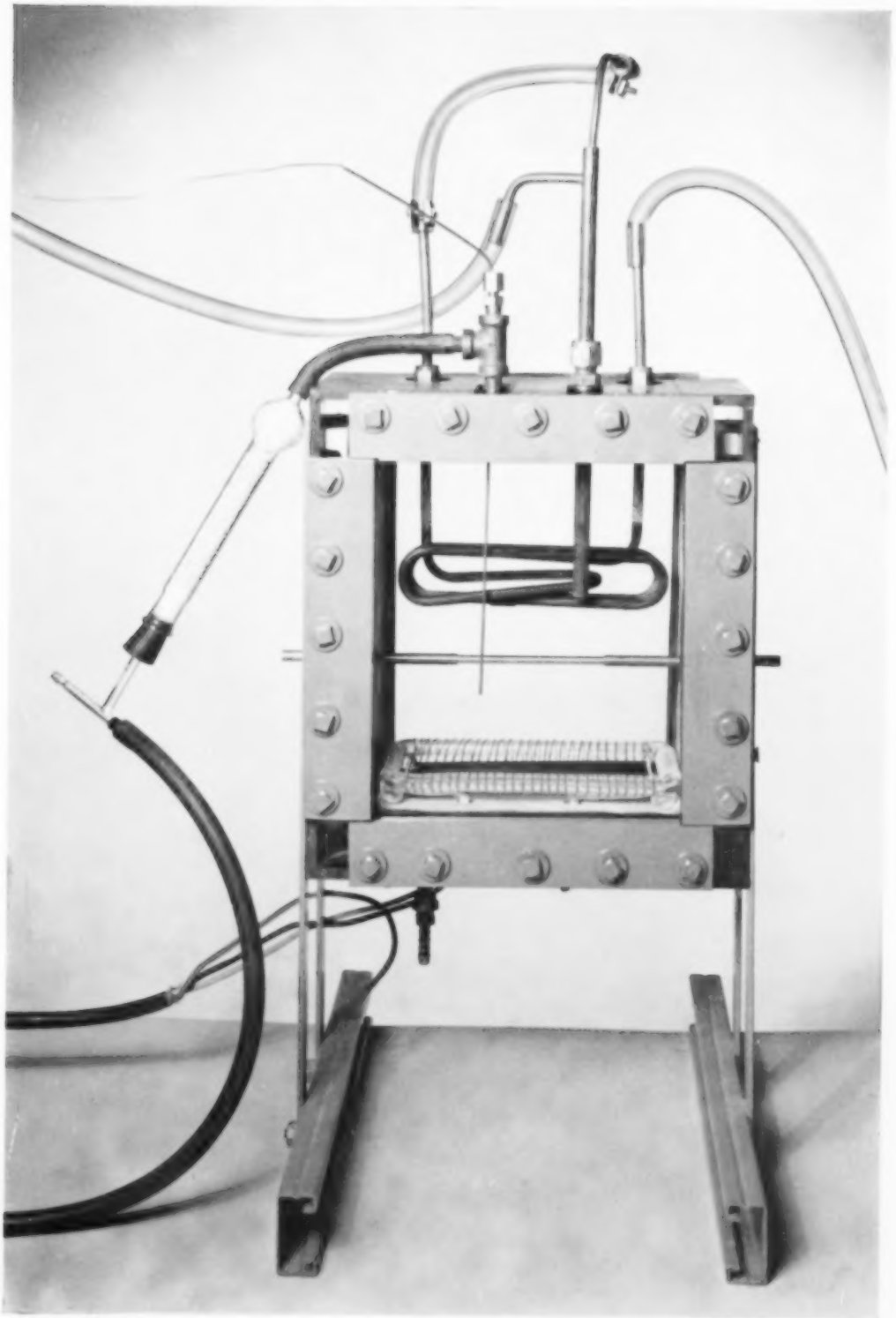

FIG. 1. Boiler.

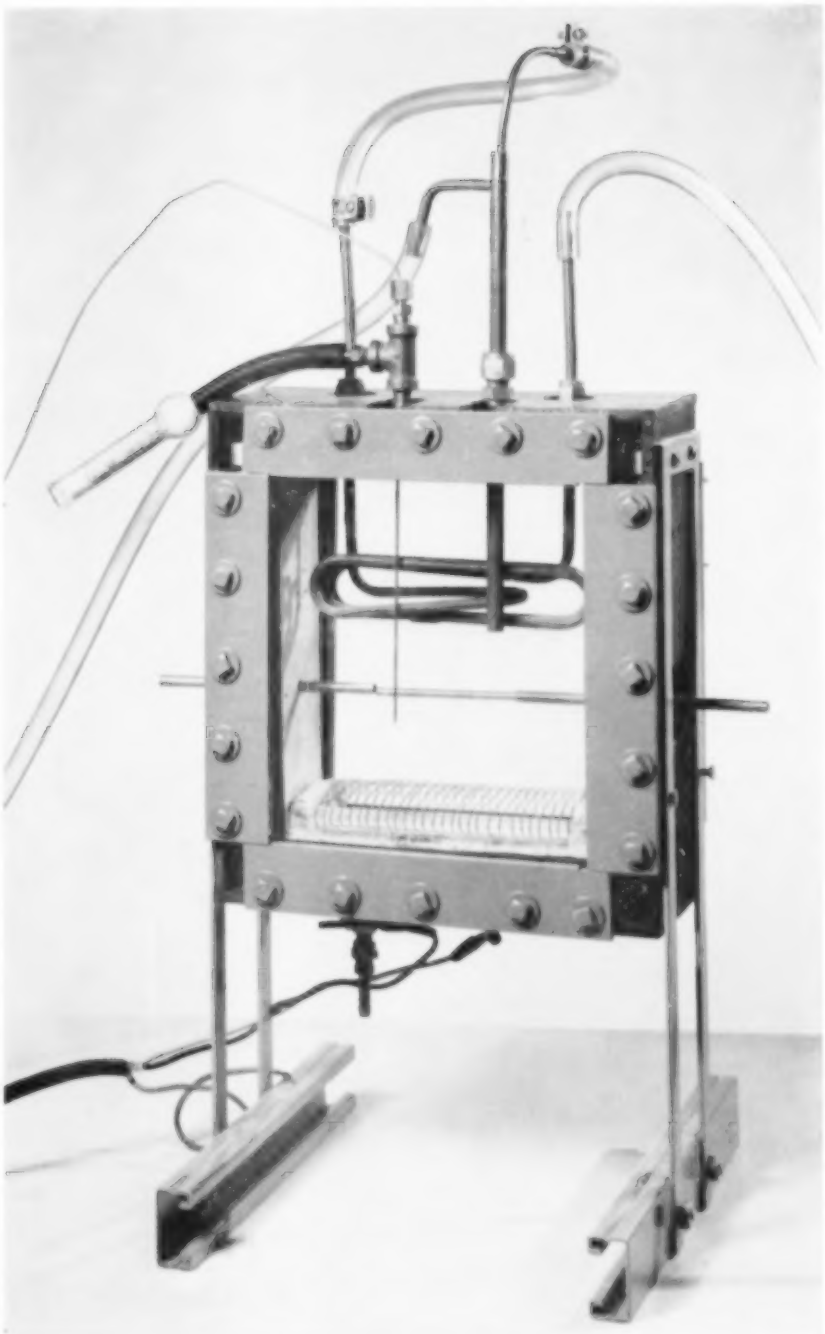

FIG. 2. Photograph of boiler.

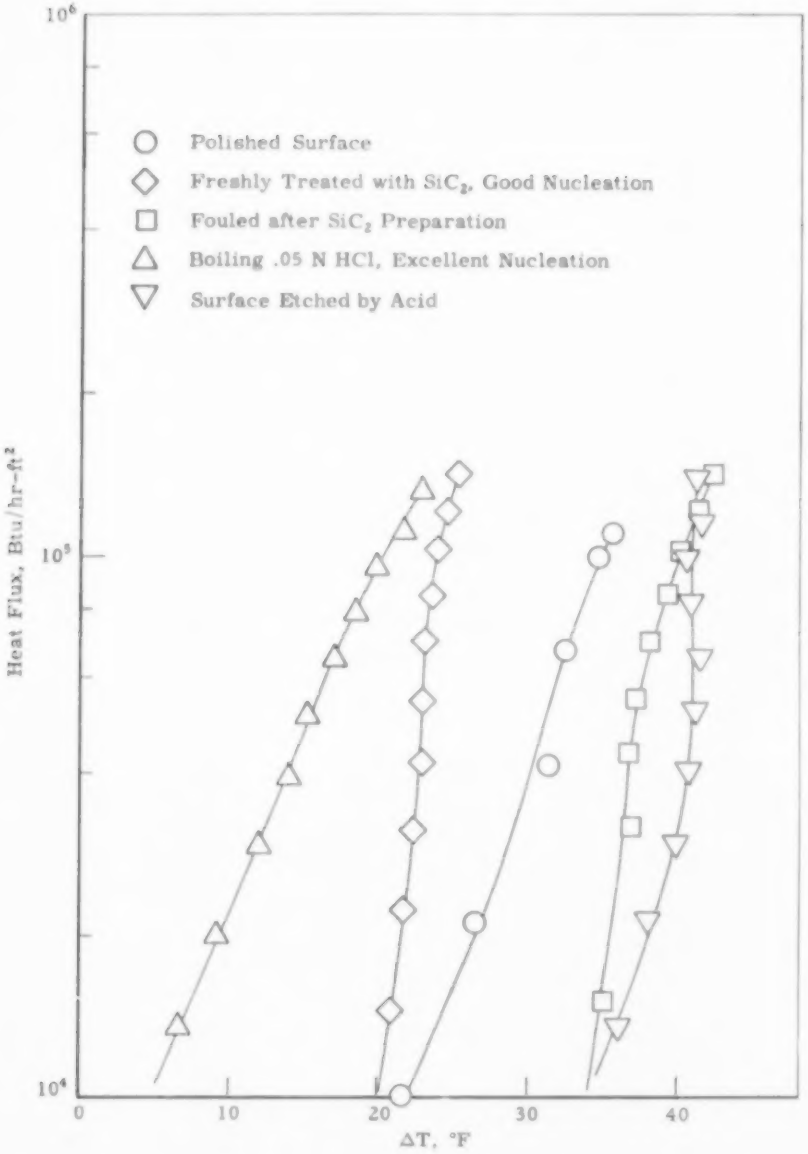

FIG. 8. Comparison of boiling curves for water with varying nucleating conditions.

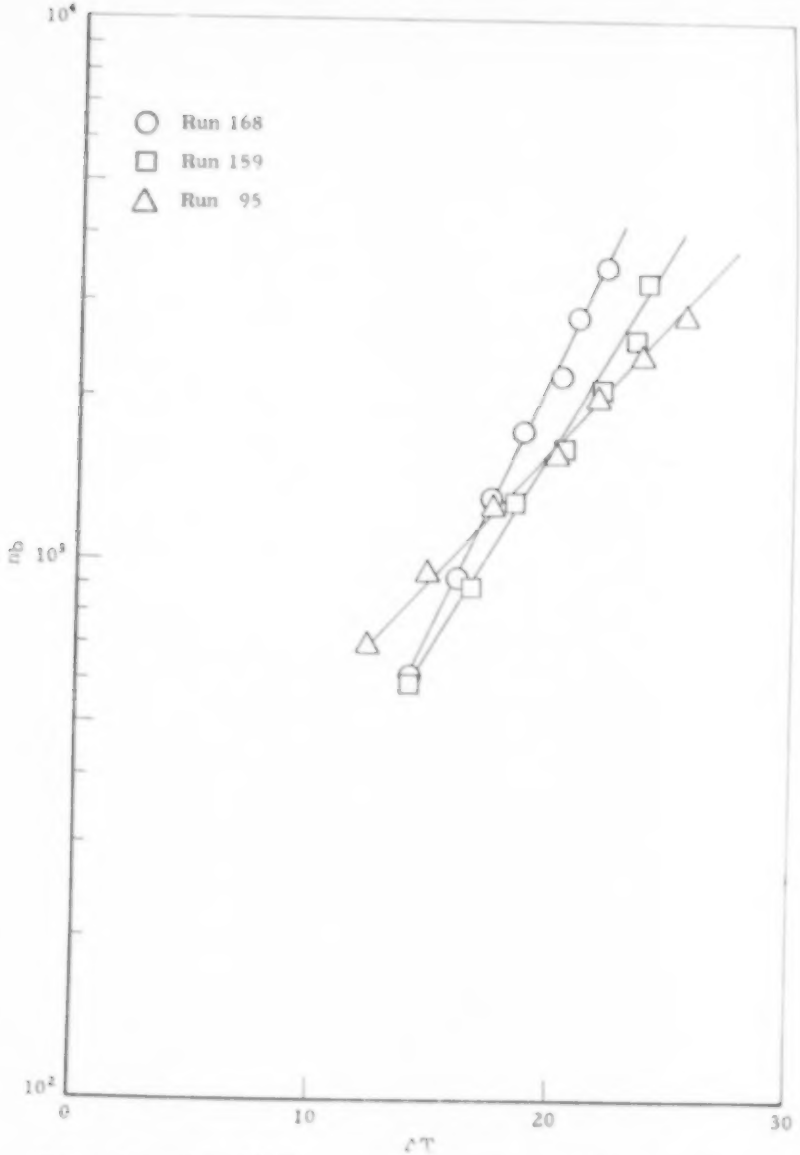

Fig. 4. Comparison of boiling curves for *iso*propanol on different occasions.

a Leeds and Northrup Model 1882 precision portable potentiometer. A large choke was placed in series with the thermocouples to reduce the 60-cycle component. It was found advisable to keep the iron and constantan leads close together to minimize inductive pick-up of 60-cycle current.

Heat losses from the boiler, mainly through the uninsulated glass windows, were large.

When the test heater was operated at low current, the heat losses exceeded heat input from the test heater alone. To prevent the temperature of the liquid from dropping slowly below its boiling point it was necessary to add extra energy through an auxiliary electric heater placed in the bottom of the boiler, as seen in Fig. 1.

The vapour generated by boiling was condensed on a water-cooled coil $\frac{1}{2}$ in. copper tubing placed in the top of the boiling vessel. It contained about 3 ft. of tubing.

Surface Treatment

It is unquestionable that the condition of the

Compound		H_2O
M		18·02
T_{bp}	°F	212·0
T_{cr}	°R	1165
a_0	dyn/cm	152·3
$P_1 \times 10^{-5}$	atm	6·424
a_1	$°R^{-1}$	8978
ρ_1°	g/cm^3	1·347
β_1	$g/cm^3\,°R$	0·00058
c_1°	B.Th.U./lb °F	0·878
b_1	B.Th.U./lb °F °R	0·0002
k_1°	B.Th.U./hr °F ft	0·393
K_1	B.Th.U./hr °F ft °R	10^{-6}
L_1°	B.Th.U./lb	1412·3
j_1	B.Th.U./lb °R	0·658

Table 2. Physical properties of substances used

Formulae: $\rho_1 = \rho_1^{\circ} - \beta T$, $c_1 = c_1^{\circ} + b_1 T$, $k_1 = k_1^{\circ} + K_1 T$, $L_1 = L_1^{\circ} - j_1 T$,
$p_1^{\circ} = P_1 \exp(-a/T)$ $\nu = \nu_0 \exp(\eta/T)$, $\sigma = \sigma_0 (1 - T/T_{cr})$

CH_3OH	I PA	CCl_4	CH_2CCl_2	C_6H_6	*Glycol*	*Glycerine*	DBPh	*Ondina* 17	*Ondina* 133	$n\text{-}C_7H_{16}$	*x* 38 *Resin*
32·04	60·09	153·84	133·42	78·11	62·07	92·09	278·34	335	430	100·20	1320
148·5	180·0	170·2	165·4	176·2	387·3	554	644	548/705	572/835	209·17	
924	930	1001	974	1013	1270	1750	(1407)	1455	1535	972·4	
63·7	42·7	67·5	67·8	71·0	92·0	103·8		54·4	49·7	52·7	
7·645	22·83	0·4734	0·4878	0·623	29·8	193·8	24·2			0·6751	
8235	9369	6786	6743	7010	12746	17005	16220			7432	
1·126	1·123	2·124	1·831	1·191	1·451	1·445	1·20	1·063	1·064	1·9391	1·279
0·000631	0·000632	0·00101	0·000936	0·00059	0·000641	0·00035	(0·0003)	0·000368	0·000366	0·000483	0·000338
0·08	0·49	0·1328	(0·158)	0·058	0·244	0·122	(0·252)	0·168	0·166	0·24	
0·001	0·002	0·00012	(0·0002)	0·0008	0·0006	0·0008	(0·000411)	0·000551	0·000555	0·0005	
0·2311	0·1022	0·1654	(0·1392)	0·1404	0·153	0·164	(0·081)	0·0889	0·0889	0·1636	
0·000202	0·00002	0·00014	(0·00012)	0·00009	0	0	(0)	0·0000234	0·0000234	0·00004	
685	611·1	131·3	150·8	309·3	636	512	116			191·0	
0·35	0·50	0·075	(0·085)	0·22	0·30	0·20	(0)			0·08	

heating surface greatly affects heat flux. To obtain data unobscured by random changes in surface condition requires considerable care. Since the object of this work was to study the effect of liquid composition it is sufficient to be able to make surface that gives reproducible results for a given system. Of course, it would be desirable also to make a surface that gives results reproducible from system to system.

Several treatments of the heater surface were tried. Polishing the heater with fine crocus cloth gave a very smooth surface, but poor nucleation; the boiling was bumpy. Surfaces polished with rough grit cloth were initially very variable and furthermore changed in several days time. Chemical roughening of the surface with a mixture of hydrochloric acid and ferric chloride gave an apparent uniformly rough etching, but the nucleation was poorest of all surfaces tried. Best results were obtained by grinding No. 200 silicon carbide grit against the heater surface with a piece of brass. A relative motion that crushed the particles against the surface appeared preferable to those that scraped the grit along the surface to produce scratches. This treatment was adopted for all data reported here. After a few hours of use the boiling stabilized with relatively good nucleation.

Figs. 3 and 4 illustrate the effects of surface treatment and show why careful preparation of the surface and judicious interpretation of the results are essential. In Fig. 3 data are given for water boiling on several surfaces; in Fig. 4 are data for *iso*propanol boiling on a single surface on different occasions.

Conclusions presented in this report are based solely on intercomparison of results for a single surface taken within a total elapsed operating time of a few hours at most.

Data

The fourteen binary systems studied are listed in Table 1.

Properties of the pure components are shown in Table 2, viscosities for the mixtures in Table 3, and vapour–liquid equilibrium data derived from the measured boiling points in Table 4. Note that we have included systems which obey Raoult's law, e.g. water–glycol, systems with large positive deviations, e.g. IPA–Ondina oil, and systems with large negative deviations, e.g. carbon tetrachloride–Ondina oil.

Original data taken were: mixture composition, heater voltage and current and thermocouple e.m.f.'s for the liquid pool, the right end the centre and the left end of the heater tube. The derived heat transfer coefficients are

Table 1. *Systems studied*

System no.	*More volatile component, A*	*Less volatile component, B*	*Volume % A*
1	Benzene	Ondina No. 17 Oil	100, 90, 80, 60, 40, 20
2	Methyl chloroform	Ondina No. 133 Oil	100, 90, 80, 60, 40, 20
3	Carbon tetrachloride	Ondina No. 133 Oil	100, 90, 80, 60, 40
4	Carbon tetrachloride	Di-*n*-butylphthalate	100, 90, 80, 60, 40, 18, 10, 5
5	*Iso*propanol	Ondina No. 17 Oil	100, 90, 80, 60, 40, 20, 10, 5, 2·5
6	*Iso*propanol	Di-*n*-butylphthalate	100, 90, 80, 60, 40, 20, 10
7	*Iso*propanol	Ethylene glycol	100, 90, 80, 60, 40, 20
8	*Iso*propanol	Glycerine	100, 90, 80, 60, 40, 20, 10
9	Methanol	Ethylene glycol	100, 90, 80, 60, 40, 20
10	Methanol	Glycerine	100, 90, 80, 60, 40, 20
11	Water	Ethylene glycol	100, 70, 50, 21, 11, 3, 0
12	Water	Glycerine	100, 79, 56, 34, 12, 5, 2
13	Methanol	Amyl alcohol	100, 60, 27, 8·5, 0
14	*Iso*propanol	*X*–38 resin	

Table 3. Mixture viscosities v_1 = *volume fraction more volatile component*
$\nu = \nu_0 \exp(\eta/T)$

Component 1 *Component* 2	CH_3OH *glycol*	CH_3OH *glycerine*	IPA *glycol*	IPA *glycerine*	IPA DBPH	IPA *Ondina* 17	CCl_4 DBPH	CCl_4 *Ondina* 133	CH_3CCl_3 *Ondina* 133	*Benzene* *Ondina* 17	H_2O *glycol*	H_2O *glycerine*
v_1	1·00	1·00	1·00	1·00	1·00	1·00	1·00	1·00	1·00	1·00	1·00	1·00
$10^4\ \nu_0$ (ft²/hr)	5·58	5·58	0·259	0·259	0·259	0·259	6·47	6·47	5·31	6·01	1·99	1·99
η (°R^{-1})	2088	2088	4425	4425	4425	4425	1887	1887	2040	2033	2733	2733
v_1	0·90	0·90	0·90	0·90	0·90	0·90	0·90	0·90	0·90	0·90	0·754	0·788
$10^4\ \nu_0$	3·995	3·75	0·284	0·132	0·342	0·302	7·74	6·05	5·77	6·36	1·26	1·29
η	2418	2521	4516	5095	4291	4405	1890	2110	2165	2105	3266	3291
v_1	0·80	0·80	0·80	0·80	0·80	0·80	0·80	0·80	0·80	0·80	0·504	0·555
$10^4\ \nu_0$	3·58	1·72	0·329	0·0732	0·426	0·340	7·40	6·01	6·59	5·85	1·05	0·97
η	2602	3189	4560	5697	4207	4413	2018	2284	2246	2258	3687	3685
v_1	0·60	0·60	0·60	0·60	0·60	0·60	0·60	0·60	0·60	0·60	0·211	0·339
$10^4\ \nu_0$	1·81	0·341	0·305	0·0698	0·643	0·461	5·39	4·53	6·51	6·01	0·760	0·392
η	3272	4639	4819	6227	4066	4422	2480	2835	2647	2459	4319	4640
v_1	0·40	0·40	0·40	0·40	0·40	0·40	0·40	0·40	0·40	0·40	0·1114	0·301
$10^4\ \nu_0$	0·887	0·0651	0·307	0·0543	0·825	0·593	4·50	2·81	4·22	5·04	0·918	0·31
η	3990	6162	5090	6797	4086	4493	2899	3588	3360	2841	4340	4890
v_1	0·20	0·20	0·20	0·20	0·20	0·20	0·18		0·20	0·20	0·0293	0·1186
$10^4\ \nu_0$	0·698	0·0231	0·217	0·0736	1·11	0·810	6·47		2·35	3·50	1·078	0·09
η	4425	7421	5390	6947	4123	4557	3090		4253	3454	4340	6680
v_1				0·10	0·10	0·10	0·10				0·0032	0·0533
$10^4\ \nu_0$				0·0732	1·61	1·23	4·92				1·142	0·0654
η				7083	4092	4446	3315				4340	7222
v_1						0·05	0·05					0·0213
$10^4\ \nu_0$						1·50	3·74					0·0491
η						4469	3580					7737
v_1						0·025						
$10^4\ \nu_0$						1·57						
η						4487						

Table 4. Experimental boiling points and derived Van Laar coefficients

$$\ln \gamma_1 = \frac{A_1}{T}\left[1+\frac{A_1 x_1}{A_2 x_2}\right]^{-2},\quad \ln \gamma_2 = \frac{A_2}{T}\left[1+\frac{A_2 x_2}{A_1 x_1}\right]^{-2}$$

Component 1 *Component* 2	CH_3OH *glycol*	CH_3OH *glycerine*	IPA *glycol*	IPA *glycerine*	IPA DBPh	IPA *Ondina* 17	CCl_4 DBPh	CCl_4 *Ondina* 133	CH_3CCl_3 *Ondina* 133	*Benzene* *Ondina* 17	H_2O *glycol*	H_2O *glycerine*
A_1 (°R^{-1}) A_2 (°R^{-1})	110 132	333 599	571 411	956 946	125 438	728 1457	− 784 − 314	− 8100 − 3240	− 199 − 998	− 600 − 600	0 0	− 361 − 361
v_1 T_{bp} (°F)	1·00 148	1·00 147	1·00 180	1·00 180	1·00 179	1·00 180	1·00 170	1·00 170	1·00 165	1·00 176	1·00 212	1·00 212
v_1 T_{bp}	0·90 151·5	0·90 150	0·90 186	0·90 185	0·90 181·5	0·90 180	0·90 172	0·90 171	0·90 169	0·90 178	0·754 215	0·788 214
v_1 T_{bp}	0·80 154	0·80 152·5	0·80 192	0·80 188	0·80 183	0·80 181·5	0·80 175	0·80 172	0·80 179	0·80 179	0·504 223	0·555 220
v_1 T_{bp}	0·60 165	0·60 158	0·60 203	0·60 192	0·60 186	0·60 183	0·60 184	0·60 179	0·60 176	0·60 186	0·211 251	0·339 234
v_1 T_{bp}	0·40 180	0·40 170	0·40 218	0·40 199	0·40 193	0·40 184	0·40 198	0·40 194	0·40 186	0·40 197	0·1114 274	0·310 238
v_1 T_{bp}	0·20 210	0·20 191	0·20 243	0·20 213	0·20 208	0·20 188	0·18 246		0·20 214	0·20 230	0·293 333	0·1186 279
v_1 T_{bp}				0·10 241	0·10 239	0·10 194	0·10 299				0·0032 375	0·0533 329
v_1 T_{bp}						0·05 212	0·05 368					0·0213 391
v_1 T_{bp}						0·025 264						

Chem. Engng. Sci. Vol. 16, Nos. 3 and 4. December, 1961.

VOL. 16 1962

Table 5. Derived boiling data

Q/A	T_s	ΔT	h	h_c	h_b
System 1. *Benzene–Ondina* 17 *Oil*					
Run 110 100%v benzene					
72,400	209·9	33·9	2138	72	2066
56,900	208·2	32·2	1771	71	1699
44,400	206·0	30·0	1478	70	1408
32,400	202·6	26·6	1219	68	1151
23,200	199·8	23·8	973	66	907
15,100	197·1	21·1	716	64	652
32,200	205·0	29·0	1112	69	1042
8540	193·1	17·1	499	61	439
72,400	210·4	34·4	2105	73	2033
Run 101 100%v benzene					
72,400	208·8	33·5	2164	72	2092
56,900	207·1	31·7	1795	71	1723
44,381	204·8	29·4	1510	70	1440
32,500	202·1	26·7	1215	68	1147
23,200	199·1	23·7	976	66	910
15,100	196·8	21·5	704	64	640
9158	193·5	18·1	504	62	443
32,200	204·8	29·5	1093	70	1023
72,800	209·5	34·1	2133	72	2061
Run 105 90%v benzene					
74,500	248·9	70·9	1050	88	963
58,200	235·4	57·4	1014	83	931
44,900	228·2	50·1	896	80	816
33,200	220·8	42·8	775	77	698
23,400	217·9	39·9	586	76	510
15,100	212·9	34·8	434	73	361
8540	206·5	28·5	299	69	230
32,700	224·5	46·5	704	79	625
74,100	248·1	70·1	1058	88	970
Run 106 80%v benzene					
94,400	312·2	132·9	710	94	616
75,500	285·2	103·9	727	89	639
58,500	263·9	84·6	691	84	608
45,500	254·1	74·7	609	81	527
33,600	247·0	67·6	497	79	418
23,600	240·1	60·8	389	77	312
15,500	233·0	53·6	288	75	213
8420	213·0	33·6	250	66	184
33,400	250·9	71·6	466	80	386
75,500	291·1	111·8	676	90	585
94,400	310·6	131·3	719	94	625

Q/A	T_s	ΔT	h	h_c	h_b
System 1 (*Contd.*)					
Run 107 60%v benzene					
119,900	388·9	203·3	590	97	492
102,000	247·7	162·0	630	90	539
79,000	320·4	134·8	586	86	501
61,900	298·3	112·6	549	81	468
47,400	284·9	99·2	477	78	399
34,800	270·5	84·9	410	75	335
24,800	259·5	73·9	335	72	263
15,600	246·1	60·4	259	68	190
9054	231·6	45·9	197	64	133
34,600	272·6	86·9	398	76	322
79,000	321·8	136·2	580	86	494
119,500	385·1	199·4	599	96	503
Run 108 40%v benzene					
139,000	451·6	255·0	546	94	452
119,000	396·1	199·6	595	87	508
96,700	364·7	168·2	575	82	493
77,600	339·0	142·5	545	78	466
60,700	314·3	117·7	515	74	441
46,900	294·6	98·0	478	70	408
24,200	261·4	64·8	373	63	310
15,600	246·8	50·3	311	59	252
9040	237·4	40·8	222	55	166
33,600	281·0	84·4	399	68	331
78,000	351·1	154·5	503	80	424
139,000	449·2	252·7	551	94	457
Run 109 20%v benzene					
144,000	501·4	271·8	530	86	444
121,000	460·8	231·2	522	82	441
98,600	426·9	197·3	500	78	422
79,000	394·8	165·2	478	74	405
61,900	368·2	138·6	446	70	377
47,400	347·8	118·2	401	67	334
34,600	326·4	96·8	357	63	294
24,400	310·1	80·5	303	60	243
15,800	290·3	60·7	260	55	205
9550	269·7	40·1	238	50	189
33,900	331·7	102·1	332	64	268
79,300	408·4	178·8	444	75	368
146,000	508·5	278·9	522	87	436

Table 5. Derived boiling data — contd.

Q/A	T_s	ΔT	h	h_c	h_b
System 2. Methylchloroform–Ondina 133 Oil					
Run 69 100%v methylchloroform					
65,000	196·4	33·6	1932	57	1875
59,700	196·4	33·7	1774	57	1717
46,300	194·9	32·1	1440	56	1384
33,900	193·3	30·6	1108	55	1053
24,400	192·1	29·3	831	55	776
15,800	189·1	26·3	599	54	546
9400	185·1	22·3	422	51	370
6120	185·5	22·7	269	52	218
4260	181·7	19·0	224	49	175
2610	179·6	16·9	155	48	107
9160	186·0	23·3	393	52	342
33,900	193·3	30·6	1108	55	1053
65,000	197·4	34·7	1875	57	1817
Run 82 100%v Methylchloroform					
63,300	198·0	31·7	2000	46	1954
58,800	197·8	31·4	1851	54	1796
45,200	196·9	30·5	1481	54	1427
33,400	194·6	28·2	1183	53	1130
23,400	195·2	28·8	811	53	758
15,400	192·4	25·9	595	52	543
8910	189·3	22·9	389	50	339
4310	190·7	24·3	177	51	126
2610	187·4	20·9	125	49	75
9160	193·6	27·2	337	53	284
33,400	196·7	30·3	1101	54	1047
63,700	198·8	32·4	1967	55	1912
Run 83 90%v methylchloroform					
71,200	256·8	87·1	817	72	745
60,000	243·7	73·9	812	69	743
46,300	233·1	63·4	730	66	664
33,900	223·5	53·8	629	63	566
23,800	220·1	50·4	472	62	410
15,400	216·1	46·4	333	61	272
8410	209·2	39·5	213	58	155
34,100	242·8	73·1	466	69	398
71,800	262·0	92·2	779	73	706
Run 70 80%v methylchloroform					
80,400	313·7	1440	558	88	471
61,900	294·5	124·7	496	83	413
47,900	280·8	111·1	431	80	351
35,000	270·2	100·5	348	78	271
24,700	254·0	84·3	293	73	220
15,600	241·1	71·4	281	70	149
9520	226·6	56·9	167	65	102
35,700	302·0	132·2	270	85	185
80,400	305·9	136·1	591	86	505
Run 71 60%v methylchloroform					
123,000	413·2	237·5	519	110	419
101,700	386·0	210·3	483	95	388
81,800	354·7	179·0	457	89	368
63,800	326·4	150·7	423	84	339
48,500	307·1	131·2	369	80	289
35,800	282·9	107·2	334	74	260
35,800	285·3	109·6	327	75	252
25,200	268·0	92·3	273	71	202
15,800	248·6	72·9	217	66	151
9690	227·4	51·7	187	59	128
36,700	354·3	179·5	204	89	115
83,200	281·7	207·9	400	94	306
124,500	426·3	253·3	492	102	389
Run 72 40%v methylchloroform					
139,900	476·1	289·7	483	92	391
124,600	445·6	259·3	480	87	393
102,100	410·7	224·4	455	83	372
82,100	380·6	194·3	423	78	344
64,100	359·5	173·2	370	75	295
47,400	338·7	152·4	311	72	239
35,800	318·7	132·4	270	68	202
24,600	296·9	110·6	222	64	158
15,600	273·4	87·1	179	59	120
8680	238·8	52·5	165	51	114
35,800	319·3	132·9	269	68	201
82,100	381·5	195·2	421	78	343
123,700	448·4	262·1	472	88	384
Run 73 20%v methylchloroform					
140,000	553·9	330·5	412	96	316
128,800	523·8	310·4	414	92	323
104,700	475·5	262·1	400	85	315
83,900	433·8	220·4	380	79	302
65,600	402·9	189·5	346	74	272
50,100	380·9	167·5	299	70	229
36,200	358·5	145·1	250	67	183
25,400	335·6	122·2	207	63	145
16,700	312·3	98·9	169	58	111
9540	285·5	72·1	132	52	80
36,700	361·6	148·2	247	67	180
85,900	445·7	232·3	369	80	289
128,000	523·8	310·5	415	92	323

Table 5. Derived boiling data — contd.

Q/A	T_s	ΔT	h	h_c	h_b
System 3. *Carbon tetrachloride–Ondina Oil* 133					
Run 85 100%v carbon tetrachloride					
63,700	202·4	32·7	1949	53	1896
59,100	202·3	32·6	1815	53	1762
45,500	201·0	31·3	1452	52	1400
33,600	200·1	30·4	1106	52	1054
23,800	198·0	28·2	841	51	790
15,600	196·0	26·2	595	50	545
8900	193·1	23·4	382	48	333
33,400	200·0	30·3	1102	52	1050
64,500	203·3	33·5	1924	53	1871
Run 85 90%v carbon tetrachloride					
71,500	279·1	108·0	662	71	591
65,600	266·7	95·7	686	69	617
60,000	252·4	81·3	738	66	672
46,300	238·9	67·9	682	63	619
33,900	227·2	56·2	603	60	543
24,200	221·4	50·3	480	59	421
15,600	220·4	49·3	316	58	258
9000	213·6	42·5	212	56	156
33,600	236·1	65·0	517	62	455
71,800	275·9	104·8	685	70	615
Run 86 80%v carbon tetrachloride					
78,600	352·2	180·2	436	77	359
60,600	308·2	136·2	445	72	373
46,800	286·5	114·4	409	69	340
34,100	266·6	94·5	361	65	295
23,900	253·5	81·4	294	63	231
15,600	241·7	69·7	224	61	163
9000	226·1	54·0	167	57	110
33,900	271·9	99·9	339	66	273
79,000	348·6	176·6	447	77	371
Run 87 60%v carbon tetrachloride					
119,900	441·7	262·5	457	82	375
98,200	398·8	219·6	447	78	370
78,700	374·1	194·9	404	75	329
61,300	348·4	169·2	362	72	290
47,100	330·3	151·1	312	70	242
34,300	308·5	129·4	265	67	198
24,700	299·4	120·3	206	66	140
15,400	278·3	99·1	156	63	93
8900	248·4	69·2	129	57	172
33,900	316·2	137·0	247	68	179
78,300	379·2	200·1	391	76	316
120,000	442·4	263·2	457	82	375

Q/A	T_s	ΔT	h	h_c	h_b
System 3 (*Contd.*)					
Run 88 40%v carbon tetrachloride					
137,600	537·6	344·0	400	101	299
114,300	486·7	293·1	390	94	296
92,800	440·5	246·9	376	87	288
79,300	415·6	222·0	357	84	274
61,900	378·7	185·1	334	78	256
47,400	353·0	159·5	297	74	223
34,600	333·9	140·3	246	70	176
24,400	319·0	125·4	194	67	127
15,600	302·8	109·2	143	64	79
9000	274·8	81·2	111	58	53
34,400	337·7	144·1	238	71	167
79,700	416·7	223·2	357	84	273
13,800	535·3	341·7	403	101	302
System 4. *Carbon tetrachloride–Dibutylphthalate*					
Run 2 2%v carbon tetrachloride					
9800	456·2	60·2	162	62	100
13,900	507·0	111·0	125	73	52
19,300	530·7	134·7	144	78	66
25,900	532·3	136·2	190	78	112
32,900	538·3	142·2	232	79	153
40,700	542·6	146·6	277	79	198
Run 3 3·4%v carbon tetrachloride					
9500	433·6	58·7	162	61	101
13,900	452·1	77·2	181	66	115
19,500	478·2	103·2	189	71	118
25,900	498·7	123·7	209	75	134
32,900	520·4	145·4	226	78	148
41,000	539·5	155·5	264	80	184
50,600	524·5	149·5	339	79	260
41,100	491·1	123·2	334	75	259
32,500	494·8	119·8	271	74	197
25,100	492·3	117·4	214	74	140
Run 4 6·4%v carbon tetrachloride					
95,000	508·5	198·8	478	86	392
81,800	487·4	177·7	460	83	377
69,800	483·9	174·2	401	83	318
58,800	467·5	157·8	372	80	292
49,500	455·2	145·4	341	79	262
39,800	439·9	130·2	306	76	230
31,800	425·2	115·5	276	74	202
24,500	409·8	100·1	245	70	175
18,700	402·4	92·6	202	69	133
13,400	381·0	71·2	187	64	123
8900	360·1	50·4	177	59	118

Table 5. Derived boiling data — contd.

Q/A	T_s	ΔT	h	h_c	h_b
System 4 (*Contd.*)					
Run 5 13·2%v carbon tetrachloride					
94,200	476·8	217·8	432	89	343
80,400	444·7	185·8	433	85	348
67,900	422·1	163·2	416	82	334
57,300	408·2	149·3	384	80	304
47,600	405·2	146·3	325	79	246
38,600	389·8	130·9	295	77	218
30,700	371·4	112·6	273	74	199
24,100	353·3	94·4	256	70	186
18,200	336·4	77·5	234	66	168
13,000	321·7	62·9	207	62	145
8900	303·3	44·4	200	57	143
Run 37 5·0%v carbon tetrachloride					
143,000	565·3	196·8	726	85	641
128,000	553·4	184·9	692	84	608
106,300	532·5	164·1	648	81	567
86,300	518·0	149·5	577	79	498
66,900	505·0	136·5	490	77	413
52,300	492·0	123·6	423	74	349
37,900	475·8	107·4	353	72	281
27,000	462·3	93·8	287	69	218
17,200	451·6	83·1	207	67	140
9700	433·3	64·9	149	63	86
Run 38 9·7%v carbon tetrachloride					
140,000	532·8	234·5	598	92	506
125,000	505·3	207·0	604	89	515
105,000	485·2	186·9	562	86	476
84,200	465·4	167·1	504	84	420
65,900	447·2	148·9	443	81	362
51,000	434·2	135·9	375	79	296
37,200	420·8	122·5	303	76	227
25,900	403·9	105·6	246	73	173
16,600	384·8	86·5	192	69	123
8900	363·6	65·3	136	64	72
36,900	424·6	126·3	293	77	216
85,000	474·4	176·1	483	85	398
Run 39 17·9%v carbon tetrachloride					
143,000	506·1	260·3	550	95	455
123,000	468·4	222·6	554	90	464
102,000	442·5	196·7	521	87	434
82,500	419·7	174·0	474	84	390
64,400	398·8	153·0	420	80	340
49,300	381·1	135·4	364	78	286
36,000	363·6	117·9	305	74	231
25,700	346·1	100·3	257	71	186
15,800	317·1	71·4	221	65	156
8900	295·8	50·1	178	59	119
35,700	367·9	121·1	293	75	217
82,100	427·8	182·1	451	85	366
Run 40 40·2%v carbon tetrachloride					
123,000	434·0	236·4	519	90	429
101,000	404·0	206·4	489	87	402
81,500	375·7	178·2	457	83	374
63,400	357·2	159·7	397	80	317
48,500	340·5	142·9	339	78	261
35,300	323·4	125·8	280	75	205
21,500	302·7	105·1	204	71	133
15,800	276·4	78·8	200	66	134
8700	248·1	50·5	171	58	113
35,000	324·5	127·0	276	75	201
81,100	378·9	181·4	447	83	364
Run 41 59·7%v carbon tetrachloride					
136,000	439·2	255·6	534	91	443
122,000	394·3	210·7	580	86	494
99,800	358·3	174·8	571	82	489
80,100	331·0	147·4	544	78	466
62,600	305·7	122·0	513	74	439
47,700	282·1	98·5	485	70	415
34,900	263·6	79·9	436	66	370
24,600	242·5	58·9	418	61	357
15,800	235·0	51·4	307	59	248
9200	256·6				
34,900	264·9	81·3	429	67	362
80,700	365·2	181·6	444	82	362
Run 42 79·8%v carbon tetrachloride					
117,000	349·3	174·6	668	80	588
94,400	307·8	133·1	709	75	634
75,200	280·9	106·2	708	71	637
58,800	260·8	86·1	683	67	616
45,200	245·5	70·8	639	64	575
32,900	236·3	61·6	534	62	472
19,900	227·7	53·0	375	59	316
15,000	220·1	45·4	330	57	273
9400	211·5	36·8	255	54	201
32,900	242·4	67·7	486	63	423
75,900	297·5	122·8	618	73	545
Run 60 90%v carbon tetrachloride					
96,700	275·1	103·1	937	70	867
77,600	254·9	82·9	936	66	870
60,900	240·6	68·6	888	63	825

Table 5. Derived boiling data — contd.

Q/A	T_s	ΔT	h	h_c	h_b
System 4 (Contd.)					
46,800	230·2	58·1	805	60	745
34,300	223·2	51·1	671	59	612
24,100	219·6	47·6	507	58	449
15,800	214·3	42·3	373	56	317
9000	201·2	29·2	309	51	258
33,900	226·8	54·7	619	60	559
78,300	261·7	89·6	874	68	806
77,300	212·4	43·9	1758	52	1702
71,400	211·3	42·9	1663	56	1607
60,500	209·2	40·8	1482	56	1426
51,400	207·8	39·4	1305	55	1250
43,300	206·3	37·9	1141	55	1086
35,400	204·5	36·1	979	54	925
28,100	202·4	34·0	825	53	772
22,400	201·0	32·6	686	53	633
16,800	198·8	30·4	553	52	501
12,200	196·4	27·9	435	50	385
8200	194·0	25·6	319	49	270
51,700	207·8	39·4	1311	55	1256
61,500	209·2	40·8	1506	56	1450
Run 43 100%v Carbon Tetrachloride					
61,800	202·2	34·1	1811	53	1758
44,100	200·9	32·9	1342	53	1289
Run 44 100%v Carbon Tetrachloride					
63,700	203·6	35·6	1791	54	1737
58,500	203·1	35·1	1668	54	1614
45,200	201·9	33·9	1335	53	1282
33,400	200·1	32·0	1042	52	990
23,600	198·5	30·3	774	52	722
16,400	196·6	28·3	575	51	524
8900	192·4	24·3	366	49	317
33,100	200·1	32·0	1036	52	984
63,700	204·0	35·9	1774	54	1720
System 5. Isopropyl Alcohol–Ondina Oil					
Run 95 100%v *Iso*propyl alcohol					
72,800	205·7	25·4	2869	70	2799
56,900	203·9	23·5	2418	69	2349
44,400	202·0	21·7	2045	67	1978
32,500	200·4	20·0	1621	66	1555
23,200	197·8	17·4	1328	63	1265
14,800	195·0	14·7	1006	60	946
9200	192·6	12·3	747	57	690
32,500	202·0	21·7	1497	67	1430
72,800	205·4	25·0	2907	70	2837
Run 96 90%v *iso*propyl alcohol					
91,300	243·5	63·5	1437	84	1353
73,800	228·7	48·3	1529	78	1451
57,900	216·8	36·8	1573	72	1501
45,200	210·8	30·8	1468	69	1399
33,400	206·0	25·9	1287	66	1221
23,400	202·5	22·5	1040	63	977
15,400	199·5	19·5	793	61	732
8400	198·6	18·6	453	60	393
32,900	206·6	26·6	1237	66	1171
73,800	233·2	53·2	1387	80	1307
91,300	242·5	62·5	1460	84	1376
Run 97 80%v *iso*propyl alcohol					
114,400	306·8	125·2	914	100	814
93,200	274·9	93·3	999	90	909
74,800	253·3	71·6	1045	83	962
59,100	240·7	59·0	1001	78	923
45,700	233·6	51·9	882	75	807
33,600	226·3	44·6	754	72	682
23,800	220·2	38·5	617	69	548
15,600	216·0	24·3	454	66	388
9000	213·2	31·5	286	65	221
33,400	230·4	48·8	684	73	611
74,800	259·8	78·1	958	85	873
114,000	306·8	125·1	915	100	815
Run 98 60% *iso*propyl alcohol					
116,000	402·7	219·7	528	113	415
94,300	347·4	164·4	573	100	473
74,800	298·3	115·3	648	87	561
58,200	257·7	74·7	778	75	703
45,200	233·6	50·6	895	67	828
33,400	219·3	36·3	921	61	860
23,600	212·5	29·5	800	57	743
15,200	206·0	23·0	659	53	606
8900	202·4	19·5	459	51	408
33,000	221·2	38·2	864	62	802
75,200	293·5	110·5	680	86	594
116,000	400·9	217·9	532	112	420

Table 5. Derived boiling data — contd.

Q/A	T_s	ΔT	h	h_c	h_b
System 5 (Contd.)					
Run 99 40%v *iso*propyl alcohol					
119,000	398·3	214·6	555	98	457
96,600	365·9	182·2	530	92	438
77,200	333·2	149·6	516	85	431
60,000	299·7	116·1	516	78	438
45,700	266·3	82·6	553	70	483
33,400	235·7	52·0	642	60	582
23,600	223·1	39·5	597	56	541
15,500	214·5	30·8	502	52	450
9200	209·6	25·9	354	50	304
32,900	235·4	51·7	637	60	577
76,500	330·1	147·0	521	85	436
119,000	404·1	220·5	540	99	441
Run 100 20%v *iso*propyl alcohol					
141,000	430·5	242·9	581	93	488
118,000	391·9	204·3	579	86	493
96,700	361·1	173·4	557	81	476
77,300	337·0	149·3	517	76	441
60,300	317·5	129·6	464	72	392
46,300	299·4	111·8	414	69	345
33,800	275·9	88·2	383	63	320
23,800	251·3	63·7	373	57	316
15,500	227·9	40·3	384	50	334
9400	221·7	34·1	276	47	229
33,400	276·6	89·0	375	63	312
77,300	340·0	152·4	507	77	430
141,000	430·3	242·7	581	93	488
Run 102 10%v *iso*propyl alcohol					
144,000	473·0	279·4	515	90	425
119,000	424·5	230·9	517	83	434
97,400	382·4	188·8	516	77	439
78,000	351·3	157·7	494	72	422
60,600	327·1	133·4	455	68	387
46,800	309·1	115·5	405	64	341
37,300	391·0	97·4	352	61	291
23,800	271·5	77·9	305	57	248
15,000	252·2	58·7	255	52	203
8200	235·5	41·9	195	47	148
34,300	293·9	100·3	342	61	281
78,300	354·8	161·2	485	72	413
144,000	470·5	276·9	519	89	430
Run 103 5%v *iso*propyl alcohol					
9400	293·7	154·2	61	61	0
140,000	510·0	298·6	470	89	381
121,000	466·0	254·5	476	83	393
99,000	430·3	218·8	452	78	374
79,000	397·2	185·8	425	73	352
61,300	365·0	153·6	399	69	330
47,100	341·1	129·6	363	64	299
34,300	315·5	140·0	330	60	270
24,200	295·2	83·7	288	56	232
15,600	275·6	64·2	243	52	191
9000	255·1	43·6	207	46	161
33,900	324·3	112·9	300	62	238
79,700	421·4	210·0	379	77	302
140,000	510·2	298·8	470	89	381
Run 104 2·5%v *iso*propyl alcohol					
142,000	540·8	276·9	511	91	420
123,000	510·5	246·6	500	87	413
101,000	477·3	213·5	472	82	390
80,400	445·1	181·2	444	78	366
63,100	412·6	148·8	424	72	352
48,200	386·0	122·1	395	68	327
35,300	360·8	96·9	364	63	301
24,900	344·7	80·9	308	59	249
15,900	322·8	58·9	270	54	216
9300	303·4	37·5	247	47	200
34,800	367·9	104·1	334	64	270
81,400	469·4	205·5	396	81	315
140,000	547·3	283·4	493	92	401
System 6. Isopropyl Alcohol-di-n-butylphthalate					
Run 130 100%v *iso*propyl alcohol					
74,900	203·8	24·8	3021	70	2951
57,900	202·0	23·0	2514	69	2445
44,900	200·7	21·7	2045	68	1977
32,500	199·1	20·1	1615	66	1549
23,000	197·3	18·3	1259	65	1194
14,900	195·3	16·3	917	63	854
9000	192·8	13·8	657	60	597
Run 131 90%v *iso*propyl alcohol					
91,300	238·6	56·9	1604	86	1518
73,500	226·6	44·9	1634	80	1554
57,900	217·8	36·2	1599	75	1524
44,700	213·1	31·4	1422	72	1350
32,900	207·8	26·1	1259	68	1191
25,200	204·5	22·8	1103	66	1037
15,000	200·7	19·0	787	62	725
8800	200·3	18·6	472	62	410

Table 5. Derived boiling data — contd.

Q/A	T_s	ΔT	h	h_c	h_b
System 6 (*Contd.*)					
Run 132 80%v *iso*propyl alcohol					
115,000	291·2	108·9	1055	105	950
94,000	269·8	86·8	1083	96	987
75,600	256·1	73·1	1033	91	942
59,100	243·9	60·9	970	86	884
45,200	238·9	56·0	807	83	724
33,400	230·8	47·8	698	79	619
23,800	221·5	38·5	618	74	544
15,200	214·4	31·4	483	70	413
8900	206·0	23·0	388	64	324
Run 133 60%v *iso*propyl alcohol					
139,000	373·5	187·5	740	118	622
116,000	341·2	155·2	748	110	638
95,100	313·8	127·8	744	102	642
76,600	294·3	108·3	707	96	611
60,000	285·0	99·0	606	94	512
46,300	275·5	89·5	517	90	427
33,400	262·5	76·5	436	86	350
23,800	260·0	74·0	321	85	236
15,500	245·5	59·5	260	80	180
9160	236·2	50·2	182	76	106
Run 134 40%v *iso*propyl alcohol					
136,000	416·7	223·8	610	110	500
119,000	388·9	195·9	608	105	503
97,800	365·5	172·6	567	100	467
78,700	347·3	154·3	509	96	413
61,300	331·9	139·0	441	93	348
46,900	316·0	123·1	381	89	292
34,100	303·6	110·7	308	86	222
24,000	289·2	96·2	249	82	167
15,500	268·5	75·6	204	76	128
8400	249·2	56·3	158	70	88
Run 135 20%v *iso*propyl alcohol					
138,000	461·1	252·9	547	94	543
121,000	434·1	226·0	534	90	444
100,000	410·4	202·3	495	87	408
80,000	392·2	184·0	435	85	350
62,800	376·1	168·0	373	82	291
48,400	367·7	159·6	304	81	223
35,200	356·9	148·7	237	79	158
24,100	335·5	127·3	190	76	114
15,600	316·6	108·5	144	72	72
9000	285·7	77·5	117	66	51
80,400	406·2	198·0	406	87	319
138,000	429·6	221·4	625	90	535

Q/A	T_s	ΔT	h	h_c	h_b
System 6 (*Contd.*)					
Run 136 10%v *iso*propyl alcohol					
135,000	493·0	253·8	531	95	436
122,000	474·4	235·3	520	92	428
101,000	442·9	203·7	497	88	409
80,700	411·8	172·6	468	82	385
63,100	388·4	149·3	423	79	344
48,500	371·4	132·3	367	76	291
35,500	351·3	112·2	317	72	245
24,800	336·6	97·4	254	69	185
16,100	320·8	81·6	197	66	131
9200	296·2	57·1	160	59	101
35,300	355·6	116·4	303	73	230
81,100	419·7	180·5	449	84	365
135,000	493·7	254·5	529	95	434
System 7. Isoptopyl alcohol–glycol					
Run 119 100%v *Iso*ptopyl alcohol					
74,900	203·9	23·9	3131	70	3061
59,400	203·5	23·5	2530	69	2461
45,700	201·6	21·6	2117	68	2049
33,600	200·4	20·4	1648	67	1581
24,200	198·7	18·7	1292	65	1227
15,400	196·6	16·6	933	63	870
8700	194·3	14·3	607	61	546
33,600	201·2	21·2	1584	68	1516
75,200	204·2	24·2	3105	70	3035
Run 120 90%v *iso*propyl alcohol					
94,800	246·0	59·4	1596	90	1506
75,900	236·1	49·5	1534	85	1449
60,000	226·4	39·7	1511	80	1431
46,600	220·8	34·1	1365	76	1289
34,100	215·1	28·5	1198	73	1125
24,400	212·0	25·4	959	70	889
15,600	209·7	23·1	676	68	608
9000	208·8	22·2	407	67	340
33,600	216·0	29·4	1146	73	1073
75,900	238·1	51·5	1475	87	1388
94 400	247·6	61·0	1547	91	1456
Run 121 80%v *iso*propyl alcohol					
113,000	288·7	96·8	1165	107	1058
92,900	272·8	80·8	1149	101	1048
74,500	260·5	68·6	1086	95	991

Table 5. Derived boiling data — contd.

Q/A	T_s	ΔT	h	h_c	h_b
System 7 (*Contd.*)					
58,500	251·2	59·3	987	91	896
45,200	245·3	53·4	847	88	759
33,600	237·8	45·9	734	84	650
23,800	234·9	42·9	554	83	471
15,300	227·2	35·3	434	78	356
8900	223·0	31·1	286	75	211
32,900	242·8	50·8	648	87	561
112,000	290·4	98·5	1141	108	1033
Run 122 60%v *iso*propyl alcohol					
147,000	339·0	136·2	1078	128	950
136,000	329·1	126·2	1081	125	956
115,000	309·5	106·6	1077	117	960
94,400	292·2	89·3	1056	109	947
75,500	277·6	74·8	1010	103	907
59,400	265·1	62·3	954	97	857
45,700	261·6	58·8	778	95	683
33,600	253·8	50·9	661	91	570
24,000	251·8	49·0	490	90	400
15,100	249·7	46·8	323	85	285
8700	237·2	34·4	251	80	171
33,900	259·6	56·7	597	94	503
76,200	281·0	78·1	976	104	872
147,000	338·9	136·0	1079	128	951
Run 123 40%v *iso*propyl alcohol					
147,000	361·1	142·8	1031	133	898
137,000	351·6	133·2	1031	130	901
115,000	332·8	114·4	1004	123	881
94,400	315·4	97·0	973	116	857
75,600	298·6	80·2	942	109	833
59,400	288·0	69·6	854	105	749
45,800	281·0	62·6	731	101	630
33,900	274·9	56·5	600	98	502
23,800	272·9	54·5	436	97	339
15,500	269·2	50·8	304	95	209
9200	254·1	35·7	257	86	171
33,900	290·1	71·7	472	105	367
75,900	314·7	96·3	789	116	673
143,000	364·5	146·1	975	134	841
Run 124 20%v *iso*propyl alcohol					
137,000	386·5	143·4	957	135	822
119,000	374·7	131·6	905	132	773
97,800	363·6	120·5	812	128	684
79,000	353·6	110·5	715	124	591
62,400	343·3	100·1	623	121	502
47,400	339·9	96·8	489	119	370
34,600	331·8	88·7	390	116	274
24,500	322·2	79·1	310	112	198
15,800	308·0	64·9	243	105	138
8900	291·1	48·0	186	97	89
34,600	348·2	105·1	329	122	207
79,000	379·1	136·0	581	133	448
137,000	389·2	146·0	940	137	803
System 8. Isopropyl alcohol glycerol					
Run 112 100%v *iso*propul alcohol					
74,900	201·1	21·4	3499	69	3430
59,100	201·4	21·7	2718	70	2648
45,500	200·7	21·0	2165	69	2096
33,600	198·9	19·3	1744	68	1676
23,600	197·9	18·2	1294	67	1227
15,000	196·3	16·7	899	65	834
9800	195·2	15·5	630	64	566
33,600	199·0	19·4	1738	68	1670
74,500	201·4	21·7	3427	70	3357
1400	167·7	22·1	64	63	1
2700	183·1	35·8	74	74	0
Run 113 90%v *iso*propyl alcohol					
90,900	236·8	52·1	1745	84	1661
73,500	227·0	42·3	1736	79	1657
57,600	218·8	34·1	1687	74	1613
44,700	211·9	27·3	1636	70	1566
32,900	208·0	23·4	1410	67	1343
23,200	205·8	21·1	1098	65	1033
15,000	203·5	18·9	792	63	729
9000	201·3	16·6	543	61	482
32,900	208·7	24·1	1367	68	1299
73,500	229·5	44·8	1639	81	1558
90,900	240·4	55·7	1631	86	1545
Run 114 80%v *iso*propyl alcohol					
113,000	292·2	104·9	1075	104	971
92,800	269·2	81·9	1133	95	1038
74,900	254·2	66·9	1119	89	1030
58,200	244·6	57·3	1015	84	931
45,500	237·7	50·4	902	81	821
33,400	233·0	45·7	731	73	653
23,400	224·4	37·1	630	74	556
15,500	220·1	32·8	471	71	400
8800	214·1	26·8	328	67	261

Table 5. Derived boiling data — contd.

Q/A	T_s	ΔT	h	h_c	h_b
***System* 8 (*Contd.*)**					
33,200	234·2	46·9	707	79	628
75,200	263·5	76·2	988	93	895
113,000	297·4	110·1	1024	106	918
Run 115 60%v *iso*propyl alcohol					
136,000	352·4	160·1	852	120	732
114,000	328·0	135·8	840	112	728
94,400	302·7	110·4	855	103	752
75,600	282·9	90·6	834	96	738
59,400	267·2	75·0	793	90	703
45,800	257·1	64·9	705	85	620
33,600	251·1	58·9	571	82	489
23,600	248·8	56·5	416	81	335
14,900	241·1	48·8	306	77	229
9200	234·2	41·9	218	74	144
33,700	259·7	67·5	499	86	413
76,300	308·3	116·1	657	105	552
136,000	353·3	161·0	847	120	727
Run 116 40%v *iso*propyl alcohol					
150,000	383·1	183·6	816	145	671
137,000	373·1	173·6	791	140	651
116,000	356·2	156·6	739	133	606
95,100	333·1	133·5	712	122	590
76,300	310·9	111·4	685	112	573
59,700	293·5	94·0	636	104	532
46,300	276·6	77·1	601	96	505
33,900	264·8	65·3	519	89	430
23,800	254·5	54·9	433	84	349
15,100	250·3	50·8	298	81	217
8400	237·6	38·0	221	73	148
33,700	267·0	67·4	499	90	409
77,000	317·7	118·2	651	115	536
145,000	386·8	187·3	774	146	628
Run 117 20%v *iso*propyl alcohol					
145,000	445·7	232·9	622	173	449
120,000	428·7	215·9	557	165	392
98,600	412·0	199·2	495	157	338
80,100	395·2	182·5	439	150	289
62,500	375·1	162·4	385	140	245
48,200	358·6	145·9	330	132	198
35,100	335·6	122·8	285	121	164
25,000	316·3	103·5	241	112	129
16,100	293·3	80·5	200	100	100
9000	266·2	53·5	169	85	84
34,800	244·2	131·4	265	125	140
80,600	415·9	203·2	397	159	238
147,000	348·8	226·0	651	170	481

Q/A	T_s	ΔT	h	h_c	h_b
***System* 8 (*Contd.*)**					
Run 118 10%v *iso*propyl alcohol					
143,000	470·8	230·0	622	186	436
123,000	459·0	218·2	565	180	385
102,000	448·5	207·7	493	175	318
82,500	436·9	196·0	421	170	251
65,300	421·3	180·5	362	162	200
49,800	400·8	160·0	311	152	159
36,500	378·5	137·7	265	141	124
25,600	362·6	121·8	210	132	78
16,400	334·3	93·5	176	118	58
9400	301·0	60·2	156	99	57
36,000	285·0	144·2	250	144	106
82,800	440·6	199·7	414	171	243
141,000	470·9	230·1	614	186	428
System* 9. *Methanol glycol					
Run 75 100%v methanol					
109,000	168·6	20·8	5219	94	5125
89,400	169·5	21·7	4128	95	4033
72,100	169·1	21.3	3386	95	3291
56,600	169·4	21·6	2621	95	2526
44,100	168·2	20·4	2159	94	2065
32,200	169·0	21·2	1519	95	1424
23,000	170·3	22·5	1020	96	924
15,100	175·4	27·6	547	101	446
9200	171·8	24·0	381	98	283
109,000	176·7	28·9	3759	103	3656
89,400	176·2	28·4	3144	102	3042
71,700	175·4	27·6	2596	101	2495
56,600	174·7	26·9	2103	101	2002
44,100	173·4	25·6	1722	99	1623
32,200	172·4	24·6	1311	98	1213
23,200	171·5	23·7	977	98	879
14,800	170·0	22·2	666	96	570
8300	168·5	20·7	401	94	307
4300	182·6	34·8	124	108	16
9000	177·3	29·5	306	103	203
31,700	181·1	33·3	954	107	847
71,700	187·2	39·4	1818	111	1707
107,000	177·9	33·4	3199	106	3093
Run 79 100%v methanol					
108,000	175·8	28·0	3851	102	3749
89,000	175·9	28·1	3168	102	3066
71,700	174·9	27·1	2644	101	2543

Table 5. Derived boiling data — contd.

Q/A	T_s	ΔT	h	h_c	h_b
System 9 (*Contd.*)					
56,300	173·8	26·0	2162	100	2062
43,800	173·1	25·3	1733	99	1634
32,200	172·1	24·3	1326	98	1228
22,800	170·9	23·2	983	97	886
14,800	169·5	21·1	682	95	587
8800	168·1	20·3	433	94	339
8800	167·8	20·0	440	93	347
4200	180·6	32·8	128	106	22
8900	163·2	15·4	577	87	490
31,500	170·3	22·4	1399	96	1303
71,000	175·4	27·6	2573	101	2472
106,000	175·7	27·9	3822	102	3720
Run 80 90%v methanol					
131,000	215·5	63·9	2057	115	1942
111,000	204·4	52·7	2099	109	1990
91,300	196·9	45·3	2017	104	1913
73,500	189·3	37·7	1949	99	1850
57,900	186·2	34·6	1672	97	1575
42,200	185·9	34·3	1230	97	1133
33,200	184·4	32·8	1012	96	916
23,200	187·4	35·8	648	98	550
15,100	181·7	30·0	503	93	410
8400	177·1	25·4	331	90	241
33,200	189·7	38·1	871	100	771
74,200	196·1	44·5	1666	104	1562
132,000	217·9	66·2	1991	116	1875
Run 76 80%v methanol					
152,000	259·9	105·4	1446	145	1301
130,000	243·5	89·1	1460	136	1324
109,000	225·4	70·9	1531	126	1405
89,800	214·5	60·1	1494	120	1374
71,700	209·9	55·5	129	117	12
56,600	201·8	47·3	1196	111	1085
44,100	202·2	47·7	924	111	813
32,200	198·8	44·3	726	109	617
23,000	197·3	42·8	536	108	428
15,000	194·0	39·6	378	105	273
8400	188·1	33·7	249	100	149
32,200	202·7	48·2	668	112	556
72,100	210·7	56·3	1281	117	1164
13,100	245·6	91·1	1436	138	1298
148,000	257·0	102·5	1441	143	1298

Q/A	T_s	ΔT	h	h_c	h_b
System 9 (*Contd.*)					
Run 77 60%v methanol					
150,000	300·2	134·8	1114	159	955
133,000	288·1	122·7	1086	153	933
112,000	272·2	106·8	1048	145	903
91,300	257·6	92·2	990	138	852
73,800	253·0	87·6	843	136	707
57,900	248·3	82·9	698	133	565
44,900	246·7	81·3	552	132	42
33,400	233·8	68·4	488	125	363
23,400	234·2	68·8	339	125	214
15,000	221·7	56·2	266	117	149
8200	205·0	39·6	206	106	100
33,400	247·3	81·8	408	133	275
74,200	265·7	100·3	740	142	598
152,000	305·6	14·01	1084	161	932
Run 78 40%v methanol					
153,000	336·9	156·7	976	162	814
136,000	327·0	146·8	926	158	768
114,000	316·5	136·3	839	153	686
94,400	306·7	136·5	746	149	597
75,500	302·9	122·7	615	147	468
59,400	297·2	117·0	508	145	363
45,700	286·3	106·2	431	140	291
33,600	274·0	93·8	358	134	224
23,800	263·8	83·7	284	129	155
15,100	250·8	70·6	214	122	92
8400	230·7	50·5	166	110	56
33,400	280·9	100·7	331	137	194
76,900	309·2	129·0	596	150	446
155,000	332·4	152·2	1017	160	857
Run 81 20%v methanol					
152,000	365·1	155·6	976	171	805
140,000	360·2	150·8	929	169	760
120,000	347·8	138·3	864	163	701
98,600	339·1	129·6	761	159	602
78,300	330·9	121·4	645	155	490
62,800	326·0	116·5	539	153	386
48,500	325·7	116·3	417	153	264
35,500	315·4	106·0	335	148	187
25,100	306·6	97·1	259	143	116
16,200	290·3	80·9	201	134	67
8900	264·1	54·6	163	118	45
35,300	321·1	111·6	316	150	166
80,100	335·8	126·3	634	158	476
152,000	364·9	155·4	977	171	806

Table 5. Derived boiling data — contd.

Q/A	T_s	ΔT	h	h_c	h_b
System 10. *Methanol glycerine*					
Run 61 100%v methanol					
112,000	174·8	27·3	4081	101	3980
92,500	175·3	27·8	3322	102	3220
74,900	174·4	26·9	2783	101	2682
58,800	173·6	26·2	2245	100	2145
45,500	172·6	25·2	1807	99	1708
33,600	171·8	24·4	1380	98	1282
23,600	170·8	23·4	1008	97	911
15,400	168·8	21·3	723	95	628
8900	165·9	18·4	483	91	392
6000	173·1	25·7	235	100	135
33,400	175·3	27·9	1198	102	1096
74,900	179·2	31·7	2361	105	2256
112,000	179·6	32·2	3481	105	3376
Run 62 10%v glycerine					
155,000	208·8	58·4	2662	117	2545
133,000	197·2	46·7	2841	110	2731
112,000	186·9	36·4	3083	103	2980
92,100	180·7	30·3	3044	99	2945
74,500	176·7	26·3	2835	95	2740
58,900	174·6	24·1	2437	93	2344
45,500	173·1	22·7	2006	91	1915
33,600	171·2	20·8	1618	89	1529
24,000	169·9	19·4	1234	88	1146
15,100	167·7	17·2	878	85	793
8900	166·8	16·4	536	84	452
33,600	173·6	23·1	1453	92	1361
74,800	179·6	29·1	2568	98	2470
133,000	200·5	50·0	2655	113	2542
Run 63 20%v glycerine					
148,000	239·0	86·3	1713	139	1574
135,000	229·4	76·8	1753	133	1620
114,000	215·6	62·9	1805	124	1681
93,600	206·4	53·8	1740	118	1622
75,500	200·8	48·2	1568	114	1454
59,400	196·0	43·4	1368	110	1258
46,000	193·7	41·0	1121	108	1013
33,600	188·1	35·5	948	104	844
24,000	186·8	34·2	700	102	598
15,400	184·0	31·4	493	100	393
9000	180·8	28·2	320	97	223
33,900	196·8	44·2	767	111	656
75,500	206·1	53·5	1413	118	1295

Q/A	T_s	ΔT	h	h_c	h_b
System 10 *(Contd.)*					
Run 64 40%v glycerine					
137,000	306·2	148·1	922	152	770
136,000	300·0	142·0	958	140	809
117,000	289·3	131·2	893	145	748
97,200	281·5	123·4	788	141	647
77,500	270·5	112·4	690	136	554
60,600	263·5	105·4	575	133	442
47,000	256·0	97·9	480	129	351
34,800	250·5	92·4	376	127	249
24,300	241·8	83·7	290	122	168
15,700	225·3	67·2	234	113	121
9000	209·9	51·8	174	104	70
34,500	253·0	94·8	364	128	236
78,600	280·0	121·8	645	140	505
138,000	301·5	143·4	964	150	814
Run 65 60%v glycerine					
148,000	355·3	185·6	799	171	628
142,000	349·2	179·5	791	169	622
119,000	335·2	165·5	722	162	560
98,600	321·3	151·5	650	155	495
79,300	307·2	137·5	577	149	428
62,200	290·2	120·4	516	140	376
47,900	277·3	107·6	445	133	312
35,300	262·7	92·9	379	126	253
24,400	250·0	80·3	303	119	184
15,000	230·7	61·0	245	107	138
7900	213·3	43·6	182	96	86
9800	224·9	55·2	177	104	73
34,800	265·9	96·1	362	128	234
80,700	315·5	145·8	554	153	401
142,000	357·2	187·5	757	172	585
Run 66 80%v glycerine					
147,000	418·7	227·4	648	229	419
123,000	398·9	207·6	594	214	380
101,000	379·4	188·2	538	200	338
82,100	363·2	172·0	478	189	289
64,000	343·1	151·8	422	174	248
49,600	326·6	135·3	366	163	203
36,000	309·4	118·2	304	151	153
25,300	290·7	99·4	255	138	117
15,800	270·0	78·7	200	123	77
8900	243·7	52·4	170	104	66
35,800	308·8	117·5	304	150	154
82,500	375·7	184·5	447	197	250
147,000	425·3	234·1	626	234	392

Table 5. Derived boiling data — contd.

Q/A	T_s	ΔT	h	h_c	h_b
System 11. *Water–ethylene glycol*					
Run 128 95% water					
148,000	236·1	25·6	5784	218	5567
131,000	236·2	25·7	5090	218	4871
111,000	236·1	25·6	4317	218	4100
91,300	236·3	25·8	3539	218	3321
73,800	236·2	25·7	2873	218	2655
58,200	237·3	26·9	2163	220	1943
45,200	236·2	25·7	1759	218	1542
33,200	235·1	24·7	1343	216	1128
23,600	235·1	24·6	958	215	743
15,100	232·4	22·0	688	209	479
9030	228·4	17·9	505	199	306
33,200	236·2	25·7	1290	218	1072
74,200	240·0	29·4	2519	225	2294
131,000	238·3	27·9	4713	222	4491
147,000	237·5	27·0	5428	221	5208
Run 129 90%v water					
149,000	243·8	33·3	4491	253	4238
132,000	243·1	32·6	4044	252	3792
111,000	242·4	32·0	3474	250	3224
91,300	242·3	31·8	2867	250	2618
74,500	242·3	31·8	2341	250	2092
58,200	243·1	32·6	1785	251	1533
45,800	241·9	31·4	1454	249	1205
33,400	241·1	30·6	1090	247	843
24,200	240·3	29·9	809	245	563
15,100	237·1	26·7	567	238	330
9030	229·3	18·8	479	216	263
33,200	242·3	31·9	1040	250	791
74,500	253·6	43·1	1728	273	1456
132,000	245·9	35·5	3720	258	3463
150,000	244·5	34·0	4404	255	4149
Run 54 0·28%w water					
125,000	424·8	49·9	2494	141	2352
103,000	421·9	47·0	2197	139	2057
84,200	419·8	44·9	1877	137	1739
66,500	417·6	42·7	1559	135	1423
51,200	416·7	41·8	1225	134	1091
37,600	414·8	39·8	945	132	812
26,500	411·9	36·9	718	130	588
17,400	407·2	32·2	539	125	414
9650	403·1	28·2	342	121	222
37,100	416·5	41·6	894	134	759
84,200	421·1	46·2	1824	139	1686

Q/A	T_s	ΔT	h	h_c	h_b
System 11. *(Contd.)*					
Run 55 2·64%w water					
142,000	410·0	77·4	1846	160	1686
123,000	403·9	71·3	1735	155	1580
103,000	399·6	67·0	1534	153	1382
82,500	394·4	61·8	1334	148	1185
65,900	391·5	58·9	1119	146	973
50,900	388·0	55·4	920	143	776
37,100	382·9	50·3	738	139	599
26,500	378·0	45·3	585	135	450
16,700	370·8	38·1	439	128	311
9410	363·9	31·3	301	121	180
36,900	385·4	52·8	699	141	558
83,900	395·9	63·3	1325	149	1176
143,000	408·2	75·6	1890	158	1732
Run 56 10·1%w water					
139,000	367·0	93·3	1492	186	1305
119,000	361·7	88·0	1349	182	1166
97,800	355·0	81·3	1204	177	1026
79,000	348·8	75·1	1053	173	880
62,200	341·4	67·7	919	167	752
47,900	337·0	63·3	757	163	594
35,300	331·8	58·1	607	158	448
24,900	325·4	51·7	483	152	330
16,200	318·6	44·9	362	146	216
9030	308·6	34·9	259	135	124
35,000	332·3	58·6	598	159	439
79,300	352·1	78·4	1012	175	837
139,000	366·8	93·1	1495	186	1308
Run 57 19·3%w water					
141,000	340·7	90·0	1567	191	1376
120,000	333·1	82·4	1450	185	1265
99,000	326·4	75·7	1308	179	1129
80,700	321·5	70·8	1141	175	966
63,400	315·4	64·7	981	170	811
49,300	311·9	61·3	805	166	638
36,000	305·9	55·2	651	161	491
25,300	302·9	52·2	485	158	327
16,600	297·9	47·3	351	153	198
9520	288·9	38·2	249	143	106
35,900	309·9	59·2	608	164	443
81,100	325·5	74·8	1084	178	905
141,000	337·6	86·9	1622	189	1434
Run 58 47·65%w water					
138,000	279·3	56·6	2444	235	2209
117,000	275·3	52·6	2225	229	1995
97,100	273·3	50·7	1916	227	1689

Table 5. Derived boiling data — contd.

Q/A	T_s	ΔT	h	h_c	h_b
System 11. (*Contd.*)					
78,700	271·1	48·5	1623	223	1399
61,900	267·1	44·4	1394	217	1178
47,900	267·5	44·8	1070	218	852
35,300	263·3	40·7	868	211	657
24,900	262·8	40·1	622	210	412
15,600	258·4	35·7	436	202	234
8900	250·9	28·1	317	188	129
34,800	266·1	43·4	802	215	587
78,700	270·2	47·5	1656	222	1434
138,000	279·3	56·6	2435	235	2200
Run 59 73·3% w water					
136,000	252·0	37·6	3632	282	3351
116,000	250·3	35·9	3226	278	2948
95,500	250·2	35·8	2671	277	2394
77,600	246·4	31·9	2430	268	2162
60,600	244·9	30·5	1990	264	1726
47,100	244·2	29·7	1584	262	1322
34,600	245·9	31·5	1097	267	830
24,000	243·6	29·2	822	260	561
15,400	241·9	27·5	561	256	305
8900	236·7	22·3	400	241	160
34,300	245·8	31·4	1093	266	827
77,600	247·4	33·0	2352	271	2081
136,000	252·4	37·9	3598	283	3315
System 12. *Water–glycerol*					
Run 18 0·33% w water					
143,000	588·9	84·9	1680	180	1499
125,000	587·6	83·6	1500	180	1320
105,000	579·8	75·8	1381	174	1206
84,600	573·3	69·3	1220	168	1050
67,100	568·6	64·6	1040	166	874
52,300	564·6	60·6	862	163	700
38,300	559·3	55·3	692	158	534
27,300	555·8	51·8	527	155	372
17,000	548·1	44·1	386	148	238
10,300	538·6	34·6	297	139	158
Run 19 1·73% w water					
144,000	503·8	112·6	1281	170	1111
123,000	492·9	101·7	1208	164	1044
102,000	484·1	92·9	1098	159	939
65,300	469·3	78·1	836	150	685
51,100	462·5	71·3	716	146	571
37,200	452·9	61·7	602	139	463

Q/A	T_s	ΔT	h	h_c	h_b
System 12. (*Contd.*)					
26,500	447·8	56·6	469	136	333
16,300	441·9	50·7	322	131	191
9160	424·9	33·8	271	117	155
36,900	453·5	62·4	592	140	452
82,500	477·9	86·7	951	156	795
144,000	504·4	113·2	1274	171	1103
Run 20 4·05% w water					
142,000	452·1	121·1	1172	166	1007
119,000	437·6	106·6	1117	158	958
98,600	426·0	95·0	1038	152	886
79,000	417·1	86·1	917	147	771
63,100	409·6	78·6	803	142	661
48,700	403·1	72·1	676	138	538
35,700	396·4	65·4	546	134	413
25,100	390·9	59·9	420	130	290
16,600	385·6	54·6	304	126	177
9160	379·3	48·3	190	122	68
35,300	394·8	63·8	553	133	420
79,700	416·6	86·7	930	146	784
142,000	445·9	114·9	1236	163	1073
Run 21 9·09% w water					
140,000	402·3	118·7	1176	170	1006
118,000	389·1	105·6	1116	163	953
97,100	377·3	93·8	1035	156	879
78,000	368·7	85·1	916	150	765
61,300	361·7	78·1	784	146	638
47,400	355·7	72·1	657	142	515
34,800	350·9	67·4	516	139	378
24,600	346·2	62·7	392	135	256
15,600	339·6	56·0	279	131	148
8480	325·9	42·4	200	120	80
34,600	349·7	66·1	523	138	385
78,000	366·5	82·9	940	149	791
139,000	398·0	114·5	1216	168	1048
Run 22 18·6% w water					
152,000	383·7	134·7	1129	203	926
136,000	351·5	102·4	1332	182	1149
116,000	343·2	94·1	1229	177	1052
95,100	335·0	85·9	1107	171	936
77,300	328·8	79·8	969	166	802
61,400	322·5	73·4	837	162	675
47,300	318·9	69·9	677	158	518
34,600	314·5	65·4	528	155	373
24,100	311·7	62·6	386	153	233
15,500	306·1	57·1	272	149	124
8910	292·9	43·8	203	137	67

Table 5. Derived boiling data — contd.

Q/A	T_s	ΔT	h	h_c	h_b
System 12. *(Contd.)*					
33,800	315·1	66·1	512	156	357
76,600	327·3	78·2	979	165	814
136,000	350·3	101·2	1343	181	1162
Run 23 40·8%w water					
156,000	298·7	74·0	2107	211	1896
133,000	293·8	69·2	1920	206	1713
112,000	289·7	65·0	1728	202	1526
92,800	286·0	61·4	1513	198	1315
74,900	285·5	60·9	1230	198	1032
59,400	283·6	59·0	1008	196	812
45,700	281·7	57·0	802	193	609
33,600	279·8	55·1	610	191	418
24,000	275·3	50·6	474	186	287
15,400	270·5	45·8	337	181	156
8540	258·0	33·3	256	164	92
33,400	279·1	54·4	613	191	423
75,200	285·9	61·2	1228	198	1030
133,000	294·0	69·4	1921	206	1714
Run 24 67·4%w water					
154,000	270·7	56·6	2720	270	2451
132,000	268·9	54·8	2407	267	2139
111,000	267·5	53·4	2073	265	1808
90,700	265·9	51·8	1752	262	1489
74,200	265·8	51·7	1435	262	1173
58,800	265·0	50·9	1156	261	895
45,500	263·4	49·3	923	258	665
33,400	262·6	48·5	689	257	432
23,600	260·3	46·2	510	253	256
14,800	252·3	38·2	387	239	148
8040	233·5	19·4	415	197	218
Run 28 1·69%w water					
151,000	516·2	125·1	1208	177	1032
134,000	517·2	119·4	1125	177	948
127,000	506·7	115·5	1099	172	927
105,000	493·8	102·6	1028	165	863
85,400	481·8	89·6	953	157	796
67,200	470·3	79·2	849	151	698
51,800	458·6	67·4	768	143	624
37,600	448·1	56·9	662	136	526
26,400	442·2	51·0	517	132	385
16,600	436·4	45·2	367	127	240
8900	422·5	31·4	284	114	170
37,900	447·7	56·6	670	136	534
85,300	478·3	87·1	979	156	823

Q/A	T_s	ΔT	h	h_c	h_b
System 12. *(Contd.)*					
Run 29 4·28%w water					
147,000	456·7	127·4	1150	169	981
139,000	452·8	123·8	1120	167	952
123,000	444·6	117·0	1053	163	890
103,000	432·2	105·6	975	157	819
83,900	421·9	96·0	874	151	723
65,600	410·3	84·6	775	145	631
50,700	400·1	75·6	670	139	531
37,200	388·0	64·0	581	131	450
26,000	379·2	56·2	461	126	336
16,100	370·7	50·1	322	120	201
8530	359·2	40·2	212	112	100
36,900	386·4	64·9	570	131	439
82,800	419·8	93·9	882	150	732
Run 30 9·64%w water					
155,000	407·9	129·3	1195	176	1019
143,000	403·0	124·4	1152	173	979
121,000	390·6	112·0	1082	166	916
101,000	380·9	102·3	982	161	822
82,400	368·1	89·5	921	153	767
63,400	357·2	78·6	807	146	661
49,300	347·9	70·2	702	140	562
35,800	338·7	61·4	582	134	448
25,000	329·4	52·6	474	127	347
15,700	322·0	45·6	344	122	222
8410	311·9	36·6	230	113	117
81,100	367·5	88·9	912	153	759
Run 31 25·5%w water					
140,000	339·1	101·6	1463	200	1263
141,000	338·0	100·5	1404	199	1204
119,000	329·4	91·9	1296	193	1102
98,200	320·7	83·1	1181	186	995
79,000	312·4	75·0	1053	179	874
61,900	306·1	68·6	902	174	728
48,500	300·5	62·9	770	169	610
35,300	293·7	56·2	627	163	464
25,000	286·6	49·1	508	156	352
16,100	281·2	43·7	368	150	218
8910	270·0	32·5	274	137	137
Run 33 28·9%w water					
147,000	319·7	86·3	1700	195	1505
138,000	317·3	83·9	1647	193	1454
117,000	309·8	76·4	1531	187	1344
96,300	302·9	69·5	1385	181	1204
78,000	296·9	63·5	1228	176	1052

Table 5. Derived boiling data — contd.

Q/A	T_s	ΔT	h	h_c	h_b
System 12. (*Contd.*)					
60,600	291·0	57·6	1042	170	871
47,400	286·3	52·9	895	165	730
34,300	281·5	48·1	714	160	553
23,800	276·6	43·2	549	155	394
15,000	262·8	29·4	508	138	370
8170	249·3	15·9	514	116	398
78,300	296·6	63·1	1240	175	1065
Run 34 49·8%w water					
145,000	284·9	64·9	2232	225	2007
136,000	283·4	63·4	2145	224	1921
115,000	278·5	58·4	1973	218	1755
95,100	273·3	55·3	1722	214	1508
74,200	271·4	51·4	1443	209	1234
60,300	270·1	50·0	1206	207	998
46,800	267·9	47·8	979	204	775
34,300	264·7	44·7	768	200	568
23,950	260·9	40·8	588	195	393
15,400	254·4	34·4	450	185	265
8410	246·3	26·3	320	171	149
76,900	273·5	53·4	1439	212	1228
Run 35 74·7%w water					
157,000	263·6	49·8	3159	283	2876
136,000	261·7	48·0	2825	280	2545
115,000	259·2	45·4	2529	275	2254
95,100	256·6	42·8	2221	270	1951
76,900	256·2	42·4	1814	269	1544
60,600	254·9	41·1	1474	267	1207
46,800	254·3	40·6	1155	266	889
34,300	252·8	39·0	879	263	616
24,200	249·2	35·4	682	255	427
24,400	249·1	35·3	690	255	434
15,800	242·5	28·8	549	241	308
8540	234·9	21·2	403	221	182
34,300	253·1	39·3	874	263	610
76,900	255·8	42·0	1830	269	1561
136,000	260·3	46·5	2915	277	2638

System 13. *Methanol–n-ammyl alcohol*

Q/A	T_s	ΔT	h	h_c	h_b
Run 148 100%v *n*-amyl alcohol					
75,900	305·6	32·6	2330	73	2257
59,700	304·4	31·4	1903	72	1831
46,600	302·9	30·0	1554	71	1483
33,900	302·1	29·1	1162	71	1091
24,200	300·3	27·3	884	69	815
15,600	297·3	24·3	641	67	574

System 13. (*Contd.*)

Q/A	T_s	ΔT	h	h_c	h_b
Run 145 91·47%v *n*-amyl alcohol					
92,800	282·6	68·2	1361	87	1274
75,200	275·2	60·7	1238	84	1154
58,800	268·3	53·9	1092	81	1011
45,500	262·2	47·8	952	78	874
33,200	255·2	40·8	814	75	739
23,400	250·4	35·9	650	72	578
15,300	247·4	33·0	463	70	393
8900	242·9	28·4	313	67	246
32,900	261·4	46·9	701	78	623
74,800	279·4	65·0	1151	85	1066
93,200	281·1	66·7	1398	86	1312
Run 146 72·9%v *n*-amyl alcohol					
109,000	253·7	77·9	1403	86	1317
91,000	246·0	70·3	1288	84	1204
72,400	239·1	63·4	1142	81	1061
57,200	233·3	57·6	994	79	915
44,400	226·4	50·7	876	77	799
32,200	220·7	44·9	716	74	642
22,600	215·5	39·8	568	72	496
14,800	209·2	33·5	441	68	373
8300	201·6	25·9	320	64	256
32,000	221·6	45·9	696	74	622
73,100	241·7	66·0	1107	82	1025
10,000	252·5	76·8	1431	86	1345
Run 147 40·1%v *n*-amyl alcohol					
108,000	228·4	71·6	1510	99	1411
89,000	217·8	61·0	1458	95	1363
71,700	209·5	52·8	1359	92	1267
56,300	203·2	46·4	1213	89	1124
44,100	198·5	41·8	1056	86	970
32,200	194·9	38·1	845	84	761
22,600	191·9	35·2	642	83	559
14,600	191·0	34·2	428	82	346
8200	185·2	28·5	286	78	208
31,700	196·4	39·7	800	85	715
71,700	211·8	55·1	1303	93	1210
108,000	227·4	70·6	1526	99	1427

System 14. Isopropyl *alcohol–X* 38 *resin*

Q/A	T_s	ΔT	h	h_c	h_b
Run 156 36%w propanol					
102,000	471·5	276·9	369	127	242
81,700	373·6	179·0	456	90	366
62,500	334·4	139·8	447	77	370

Table 5. Derived boiling data — contd.

Q/A	T_s	ΔT	h	h_c	h_b
System 14. *(Contd.)*					
47,600	311·4	116·8	407	69	338
34,300	283·7	89·1	385	60	325
24,200	258·1	63·5	380	51	329
15,100	238·5	44·0	344	44	300
8800	229·0	34·5	255	40	215
35,000	287·3	92·7	378	61	317
82,400	366·7	172·1	479	88	391
Run 157 66%w propanol					
99,700	304·2	118·9	838	90	748
79,000	281·6	96·3	820	82	738
61,300	263·9	78·6	779	76	703
46,300	247·4	62·1	745	69	676
33,900	237·0	51·7	655	65	590
24,000	229·4	44·1	544	62	482
15,100	225·0	39·7	381	60	321
8700	217·5	32·2	269	56	213
34,300	239·9	54·6	628	66	562
80,100	284·8	99·5	805	84	721
99,700	304·9	119·6	834	91	743
Run 158 82%w propanol					
102,000	376·0	194·7	522	120	402
77,300	246·5	65·1	1187	79	1108
59,700	228·4	47·1	1267	71	1196
45,500	219·1	37·8	1204	67	1137
33,400	214·6	33·3	1004	64	940
23,400	212·6	31·3	747	63	684
15,300	208·8	27·5	556	61	495
8300	206·3	24·9	332	59	273
33,600	218·5	37·2	903	66	837
78,700	246·7	65·4	1203	79	1124
System 15. *n-heptane–Ondina oil*					
Run 90 100%v *n*-heptane					
65,000	235·1	27·3	2382	68	2314
59,700	233·9	26·1	2285	67	2218
46,300	232·4	24·5	1885	66	1819
34,300	230·0	22·2	1548	64	1484
24,200	228·9	21·0	1148	64	1084
15,100	225·4	17·6	860	61	799
8700	222·3	14·5	599	58	541
33,900	232·2	24·4	1389	66	1323
65,000	234·9	27·1	2403	68	2335

Q/A	T_s	ΔT	h	h_c	h_b
System 15. *(Contd.)*					
Run 91 90%v *n*-heptane					
72,800	298·0	86·7	840	86	754
61,200	281·8	70·5	869	81	788
47,100	264·8	53·5	881	75	806
34,800	253·8	42·5	818	70	748
24,800	248·1	36·9	672	68	604
16,100	243·2	31·9	505	65	440
9300	241·6	30·3	306	64	242
34,300	257·3	46·1	745	72	673
72,800	300·0	88·7	821	86	735
Run 92 80%v *n*-heptane					
77,000	338·9	126·1	615	90	525
60,000	302·4	89·7	669	82	587
46,600	286·2	73·4	635	78	557
34,300	273·6	60·8	565	74	491
24,000	263·9	51·1	469	71	398
15,800	260·4	47·6	331	69	262
8900	247·0	34·2	261	64	197
33,900	274·5	61·7	549	74	475
77,300	338·4	125·6	615	90	525
Run 93 60%v *n*-heptane					
102,000	416·6	195·6	522	92	430
81,800	380·3	159·3	513	87	426
64,000	347·3	126·3	507	81	426
49,000	321·7	100·7	487	76	411
36,000	301·1	80·1	450	72	378
25,400	292·8	71·8	353	69	284
16,400	290·7	69·7	236	69	167
9200	278·1	57·1	160	65	95
35,600	305·9	84·8	419	73	346
81,800	383·8	162·7	502	87	415
102,000	418·1	197·1	518	92	426
Run 94 40%v *n*-heptane					
143,000	497·6	255·1	560	90	470
122,000	465·8	223·4	544	87	457
100,000	437·9	195·4	512	83	429
80,400	410·4	167·9	479	80	399
62,500	386·3	143·8	434	76	358
48,200	362·7	120·2	401	73	328
35,300	335·7	93·2	379	68	311
25,000	318·4	76·0	329	64	265
16,300	311·0	68·6	237	62	175
9000	290·8	48·3	187	57	130
37,200	335·5	93·1	399	68	331
80,400	410·4	167·9	479	80	399
142,000	495·0	252·5	564	90	474

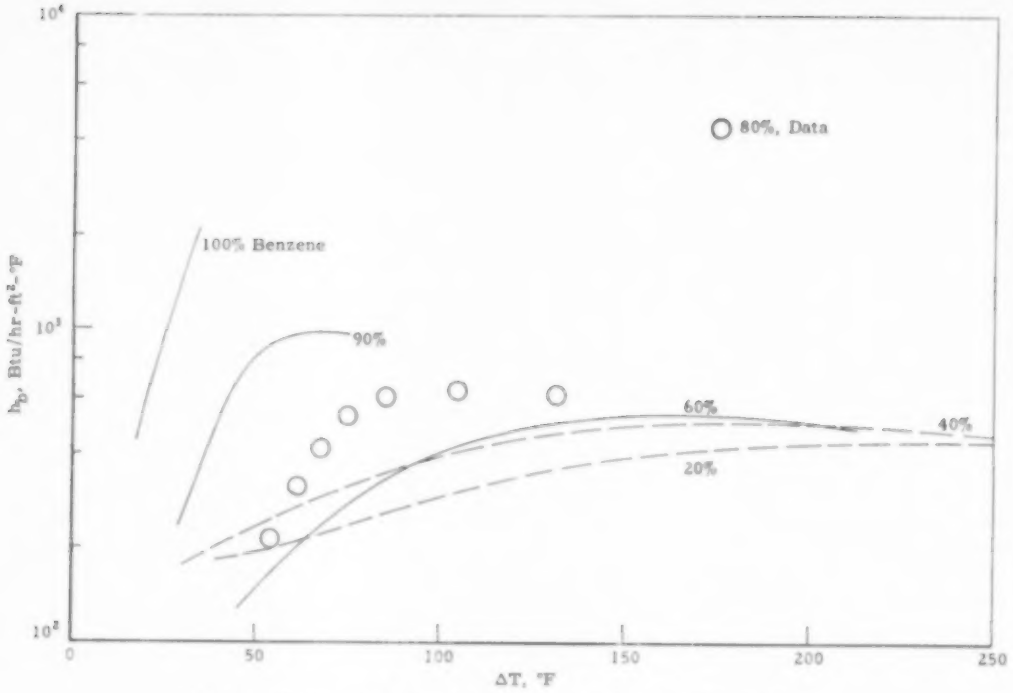

Fig. 5. Boiling data for benzene–Ondina oil, 17 mixtures.

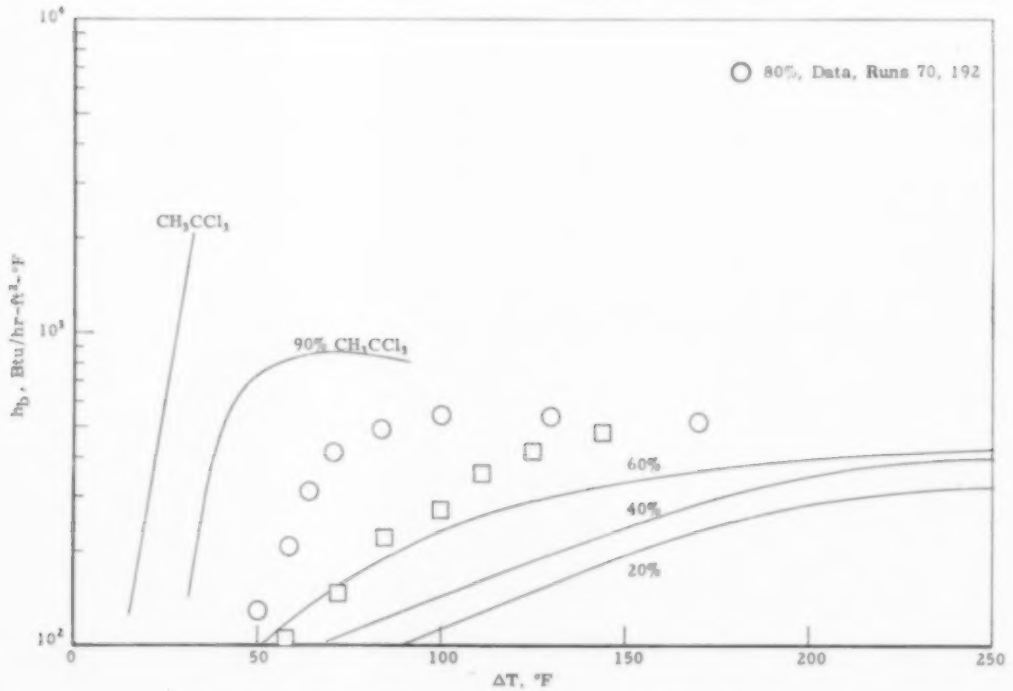

Fig. 6. Boiling data for methylchloroform–Ondina oil, 133 mixtures.

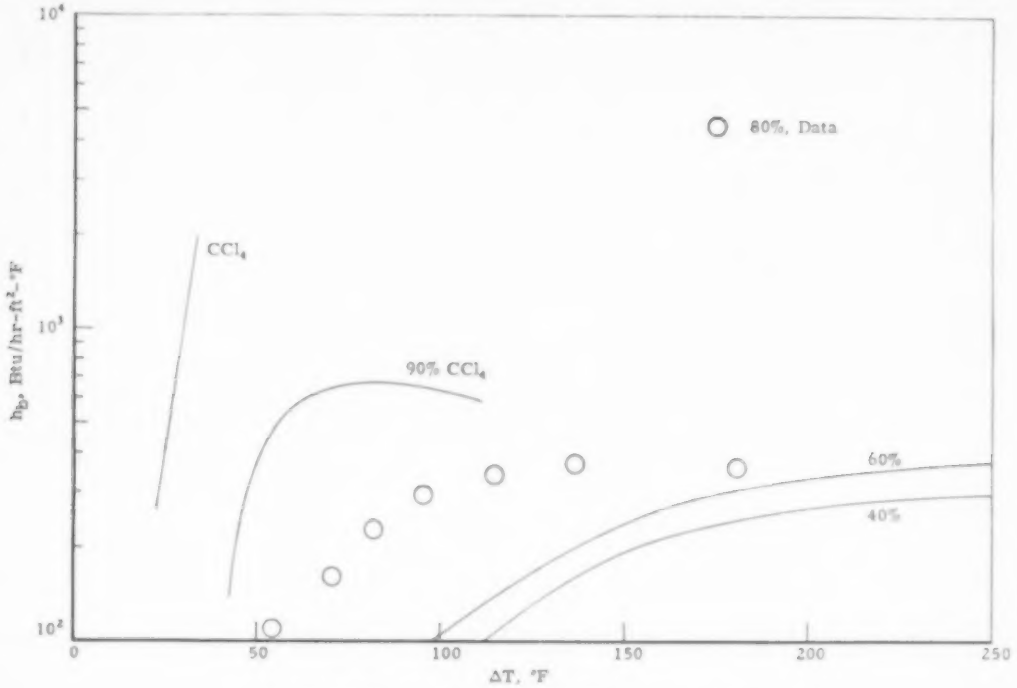

FIG. 7. Boiling data for CCl_4 – Ondina oil, 133 mixtures

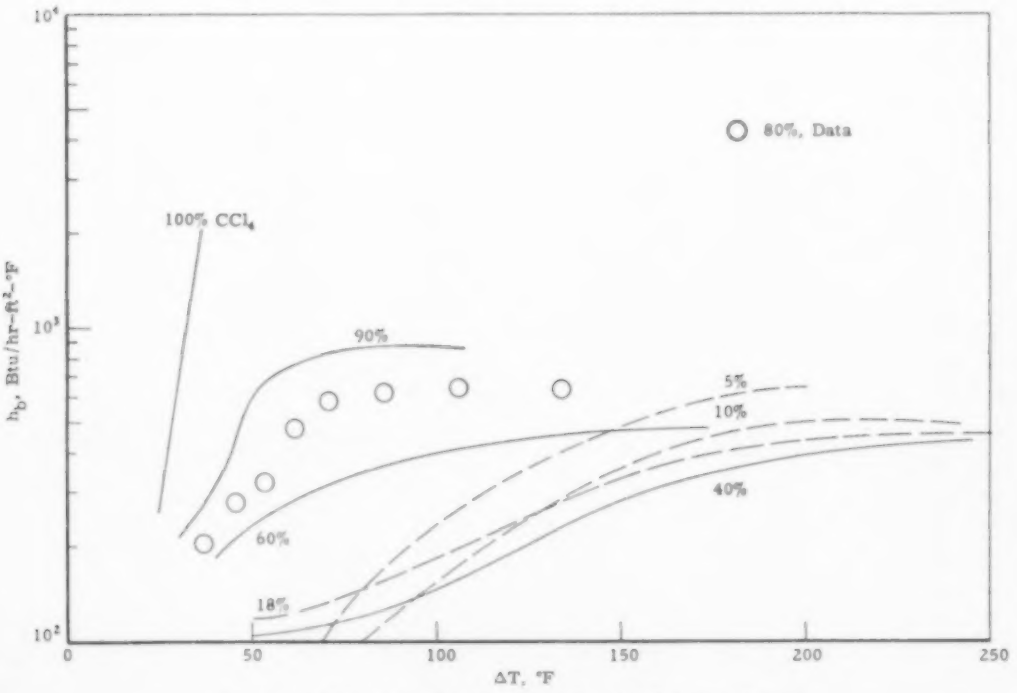

FIG. 8. Boiling data for CCl_4 – di-*n*-butylphthalate mixtures.

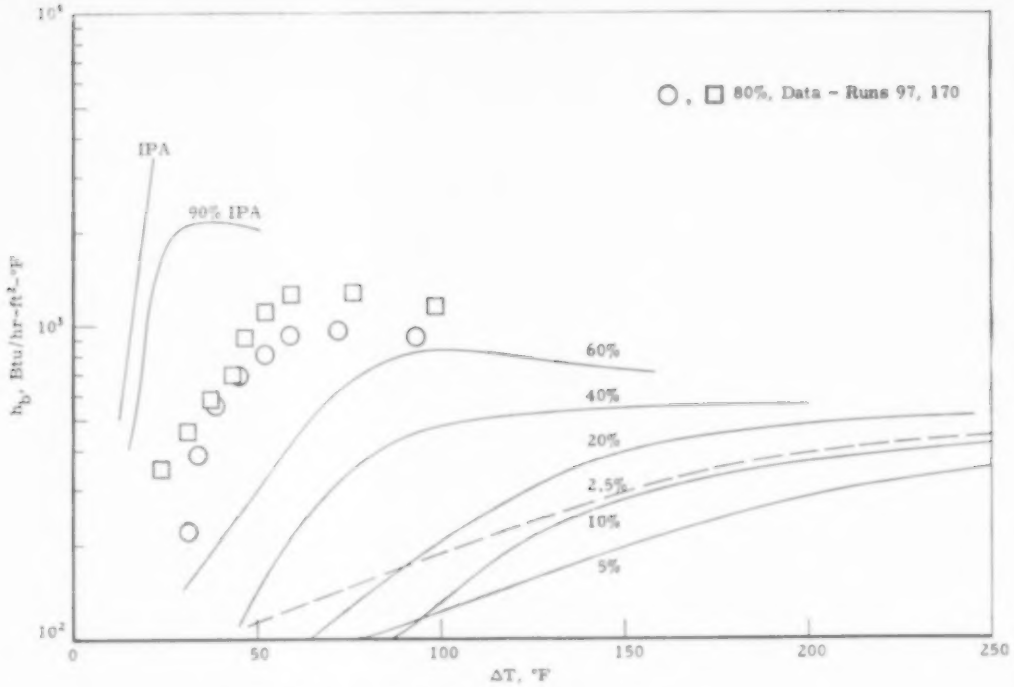

Fig. 9. Boiling data for *iso*propanol–Ondina oil, 17 mixtures.

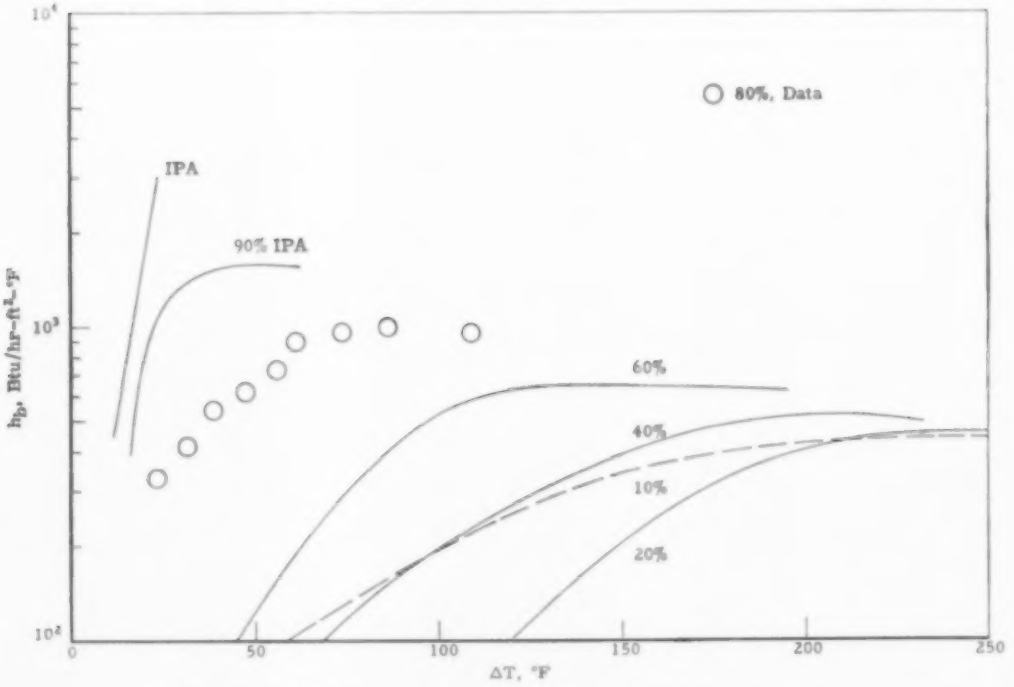

Fig. 10. Boiling data for *iso*propanol–di-*n*-butylphthalate mixtures.

given in Table 5 as functions of temperature difference, Δt. The values reported are time averages. Fluctuations in Δt caused by heating with alternating current are negligible as is shown in the Appendix. Also described in the Appendix are ways for correcting for the temperature drop through the tube wall, for heat losses by longitudinal conduction out the ends of the stainless steel heater tube, and for natural convection. The first two corrections are straightforward, but a few words about the last are apt here.

Natural convection without change of phase would give heat transfer coefficients around 60–150 B.Th.U/hr ft^2 °F for the conditions of these experiments. These rather high values result from the use of a small diameter tube. Obviously, in those runs where the over-all coefficient, h, is only slightly greater than these values, the computed boiling coefficients are worthless. However, for most of the data, h was considerably higher than this and hence the effects of natural convection were small compared to those of boiling.

Now, it has been noted [1] that, within experimental accuracy, heat fluxes due to boiling and various types of convection appear to be additive. To divorce the data from natural convection effects as much as possible the heat transfer coefficients due to natural convection were computed for each run and were *subtracted* from the measured over-all coefficient.

To retain the full accuracy of predictions based on the data presented here a reversed procedure must be used. Heat fluxes due to boiling and due to convection are to be computed separately and then added.

Smoothed graphs of the data are shown in Figs. 5–18. In most cases, points are given for a single composition, near 80% v of component A to show typical scatter.

Discussion of Data

A full explanation of the effect of composition on the boiling of liquids is impossible at this time. In a later paper we plan to present a correlation based on simplified model which enables one to predict boiling coefficients with reasonable accuracy. In this paper, we discuss only certain qualitative features of the boiling curves.

First, note that in all the systems tested, boiling coefficients decrease markedly as material of low volatility (component B) is added to the pure light component, A.

Data for a typical system, water–ethylene glycol, are shown in Fig. 15. As one continues to add glycol, h_b continues to decrease until there is about 10% v water in the mixture. At

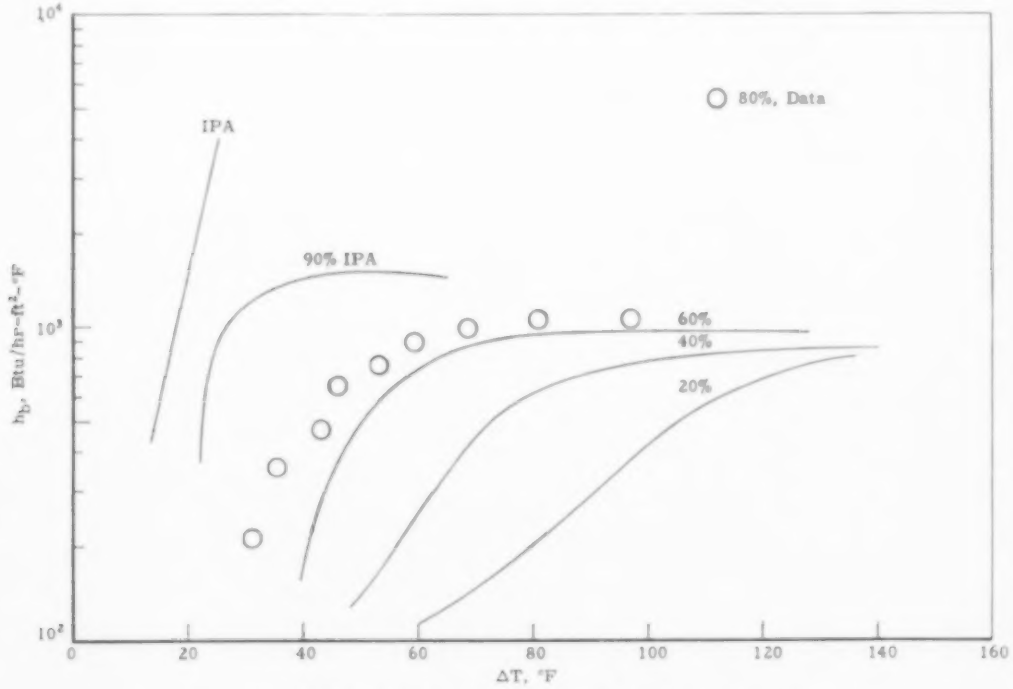

Fig. 11. Boiling data for *iso*propanol–ethylene glycol mixtures.

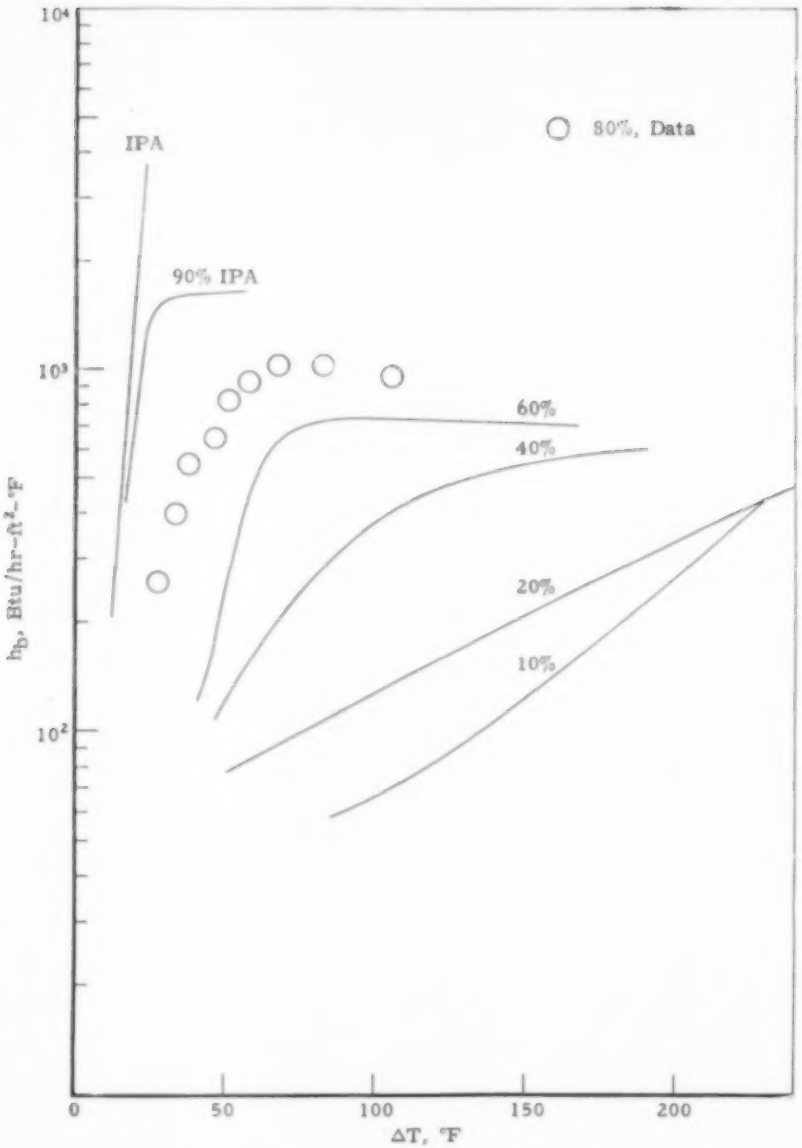

Fig. 12. Boiling data for *iso*propanol–glycerine mixtures.

this composition there is a turnaround, addition of more glycol raises h_b until finally the boiling curve for pure glycol approaches closely to that for pure water.

For most of our systems we did not reach the turnaround composition. To do so would require operating the boiler at an unsafe high temperature. Nevertheless, we think all of our systems will exhibit the turnaround if tested at sufficiently high concentrations.

How are these results to be explained? One might invoke, first, the change in properties, notably viscosity; second, the change in bubble growth rates caused by the varying resistance to mass transfer of the volatile components in diffusing into the growing bubble; and third,

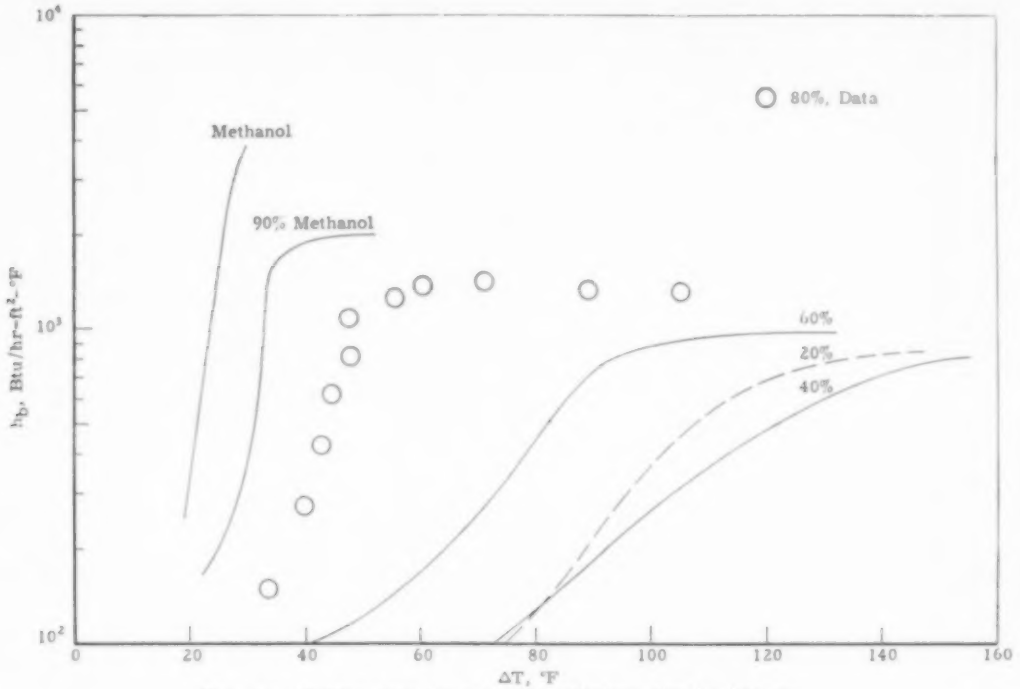

FIG. 13. Boiling data for methanol–ethylene glycol mixtures.

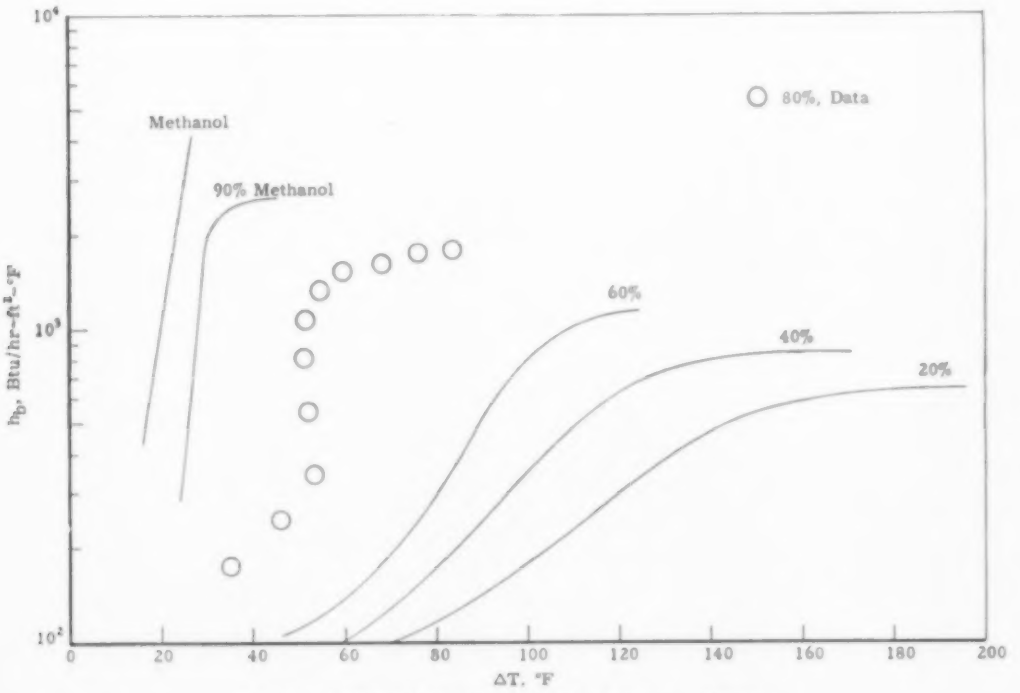

FIG. 14. Boiling data for methanol–glycerine mixtures.

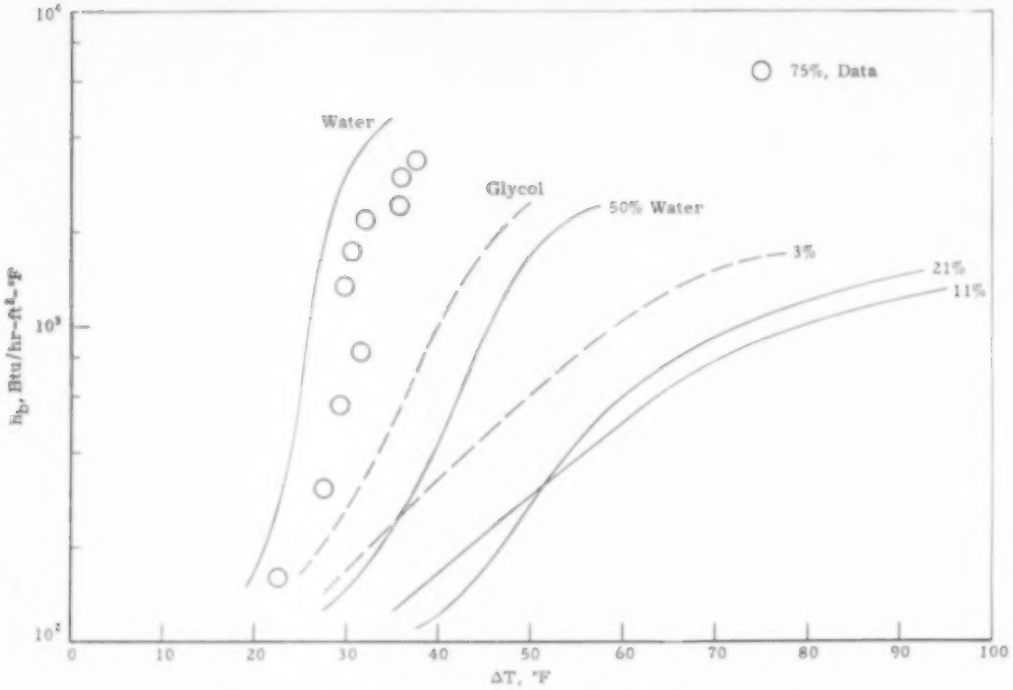

Fig. 15. Boiling data for water–ethylene glycol mixtures.

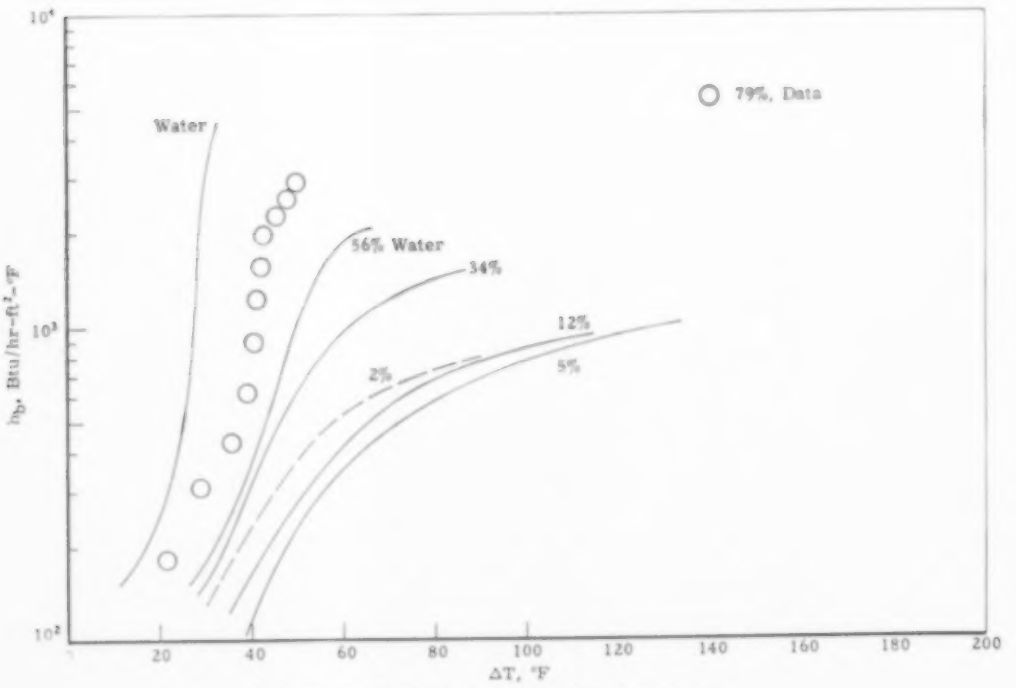

Fig. 16. Boiling data for water–glycerine mixtures.

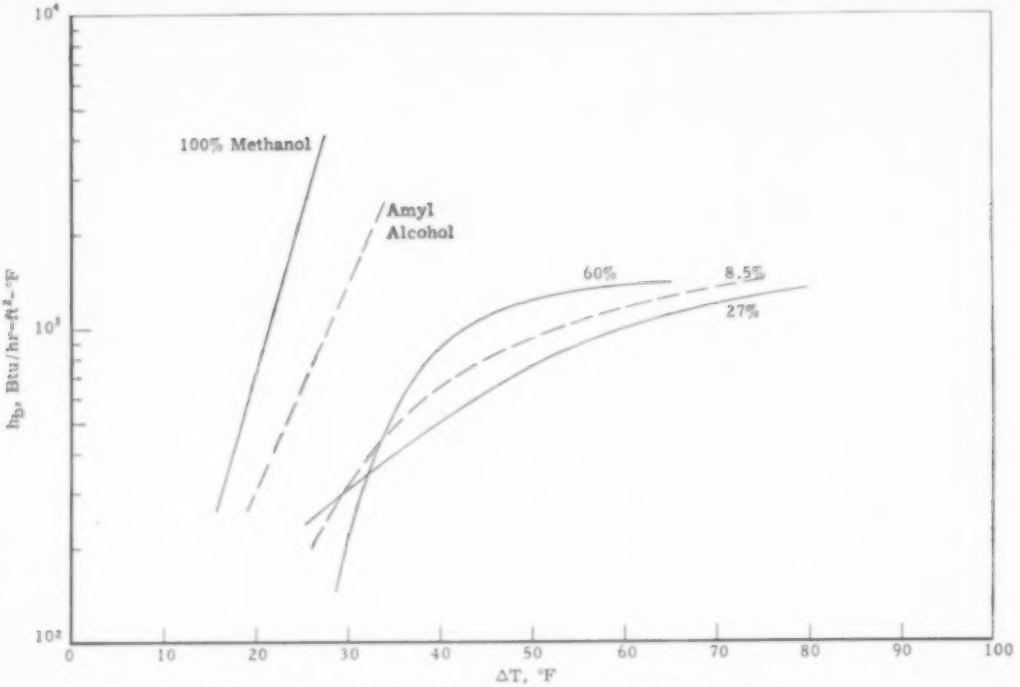

FIG. 17. Boiling data for methanol–amyl alcohol mixtures.

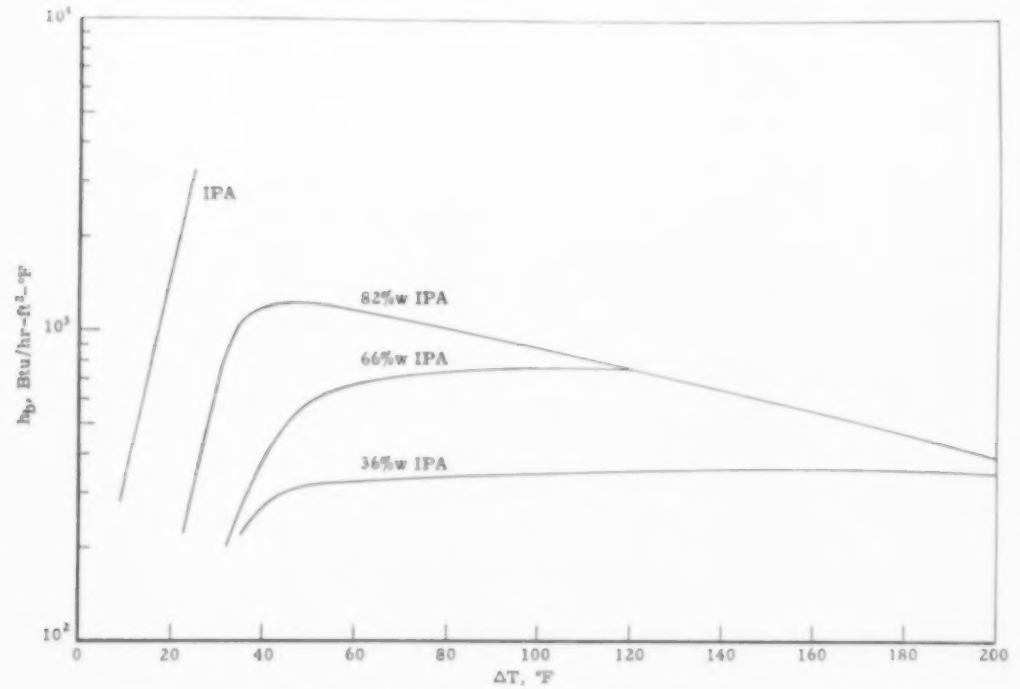

FIG. 18. Boiling data for *iso*propanol–X-38 resin mixtures.

Table 6. Values of F_c derived from data

System 1
Benzene–ondina 17

v_1	Δt at $h_b = 300$	F_c
100	13	1
90	33	2·5
80	59	4·5
60	70	5·4
40	80	6·2
20	104	8·0

System 2. *Methyl chloroform–ondina* 133

v_1	Δt at $h_b \times 300$	F_c
100	20	1
90	35	1·8
80	63	3·2
60	130	6·5
40	180	9·0
20	220	11·0

System 3
CCl_4–*ondina* 133

v_1	Δt at $h_b = 300$	F_c
100	23	1
90	45	2·0
80	100	4·3
60	180	7·8
40	260	11·3

System 4
CCl_4–DBP

v_1	Δt at $h_b = 300$	F_c
100	25	1
90	40	1·6
80	50	2
60	65	2·6
40	156	6·2
10	140	5·6
5	112	4·5

System 5
IPA–*ondina* 17

v_1	Δt at $h_b \times 300$	F_c
100	10	1
90	14	1·4
80	30	3·0
60	50	5·0
40	70	7·0
20	153	15·3
10	160	16
5	210	21

System 6
IPA–DBP

v_1	Δt at $h_b = 300$	F_c
100	9	
90	15	
80	20	
60	75	
40	128	
20	170	
10	136	

System 7
IPA–*glycol*

v_1	Δt at $h_b = 300$	F_c
100	11	1
90	21	1·9
80	34	3·1
60	43	2·9
40	63	5·9
20	92	8·4

System 8
IPA–*glycerine*

v_1	Δt at $h_b \times 300$	F_c
100	11	1
90	14	1·1
80	28	2·2
60	52	4·0
40	83	6·5
20	186	14·3
10	206	15·8

System 8
Methanol–glycol

v_1	Δt at $h_b = 300$	F_c
100	19	1
90	28	1·5
80	40	2·1
60	73	3·8
40	104	5·5
20	96	5·0

System 10
Methanol–glycerine

v_1	Δt at $h_b = 300$	F_c
100	14	1
90	24	1·7
80	44	3·1
60	80	5·7
40	95	6·8
20	120	8·6

System 11
Water–glycol

v_1	Δt at $h_b \times 300$	F_c
100	23	1
75	28	1·2
50	37	1·6
21	51	2·2
11	50	2·2
3	39	1·7
0	31	1·3

System 12
Water–glycerine

v_1	Δt at $h_b = 300$	F_c
100	22	1
79	30	1·4
56	29	1·3
34	39	1·8
12	52	2·4
5	56	2·5
2	45	2·0

System 13
Methanol–amyl alcohol

v_1	Δt at $h_b = 300$	F_c
100	16	1
60	31	1·9
27	29	1·8
8·5	29	1·8
0	20	1·3

System 14
IPA–X 38 *Resin*

v_1	Δt at $h_b \times 300$	F_c
100	9	1
82	25	2·8
66	37	4·1
36	45	5·0

changes in the rate of nucleation, i.e. the case of forming new bubbles on the surface. Probably all three contribute. It is difficult to see, however, how the first two can account for changes in h_b (at constant Δt) of more than about two-fold. We think, therefore, that the rate of nucleation is by far the most important.

In nucleate boiling bubbles form and grow only at definite non-moving sites. Furthermore, as CLARK *et al.* [2] have shown, there is a pithole in the surface at almost every site. Near an active site, the more volatile components in a boiling-liquid mixture are preferentially stripped out to feed the growing bubbles. In time, then, there will accumulate near the pitholes material of low volatility. Unless vigorous mixing is maintained with the bulk liquid the pithole may be clogged with liquid of low volatility. In order to maintain a nucleus of vapour in the hole, the temperature there may have to be raised.

From this explanation, one might guess that the boiling curves for pure components and for mixtures would have similar shape but that the scale of Δt for the mixture would be expanded relative to that for a pure component. As a matter of fact, the curves of Figs. 5–18 may be brought together quite well, at least for heat fluxes below about 30,000 B.Th.U./hr ft², by multiplying Δt by a factor, F_c, characteristic of composition alone.

Table 6 shows values of Δt at $h_b = 300$ B.Th.U./hr ft² °F for all systems and compositions. Also shown are F_c the ratio of the Δt for each case to that for the corresponding pure light component. Figs. 19–23 show how F_c depends on composition. Similar plots could be made for h_b's other than 300. Inspection of the data will show, however, that using any h_b below about 600 would not alter the values of F_c much.

One can estimate the consequences of the depletion effect for any widely boiling binary system as follows. Pick from the systems shown in Table 1 that which is most like the system of interest as regards chemical nature and relative volatility. Read the value of F_c for that system at the appropriate composition from the appropriate diagram (Figs. 5–18). Now simply interpret the scale of temperature differences of the boiling curve of the pure light component as $\Delta t/F_c$.

Table 7. Maximum heat transfer coefficients as function of temperature difference

System	v_1	h_{max}	Δt	$(q/A)_{h_m}$
B–17	90	960	70	67,000
	80	630	97	61,000
	60	530	160	85,000
	40	500	170	85,000
MC–133	90	860	70	60,000
	80	550	110	64,000
CCl_4–133	90	670	80	54,000
	80	370	150	56,000
CCl_4–DBP	90	880	80	70,000
	80	650	110	72,000
	10	510	220	113,000
IPA–17	90	2200	35	77,000
	80	1300	70	91,000
	60	820	95	78,000
	40	550	180	99,000
IPA–DBP	90	1600	50	75,000
	80	1000	90	90,000
	60	640	150	96,000
	40	500	210	105,000
IPA–EG	90	1500	50	75,000
	80	1100	80	88,000
	60	900	90	88,000
	40	840	130	109,000
IPA–G	90	1700	50	85,000
	80	1000	80	80,000
	60	740	90	67,000
M–EG	90	2000	50	100,000
	80	1400	70	98,000
	60	960	120	115,000
M–G	90	2600	50	130,000
	80	1800	80	144,000
	60	1100	130	143,000
	40	840	160	134,000
IPA-resin	6	1200	45	54,000

A second characteristic feature of many to the boiling curves shown in Figs. 5–18 is worth noting. There is a maximum in h_b as a function of Δt. This maximum occurs at a relatively low

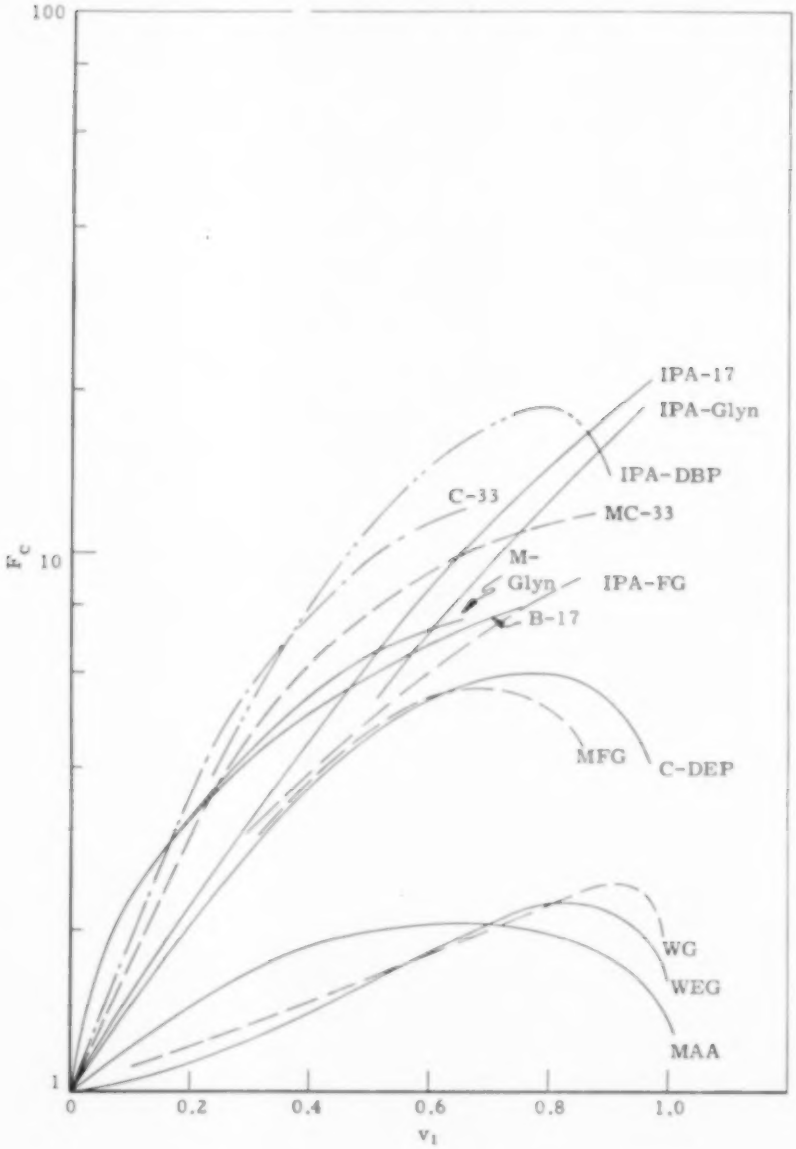

Fig. 19. F_c vs. composition – all systems.

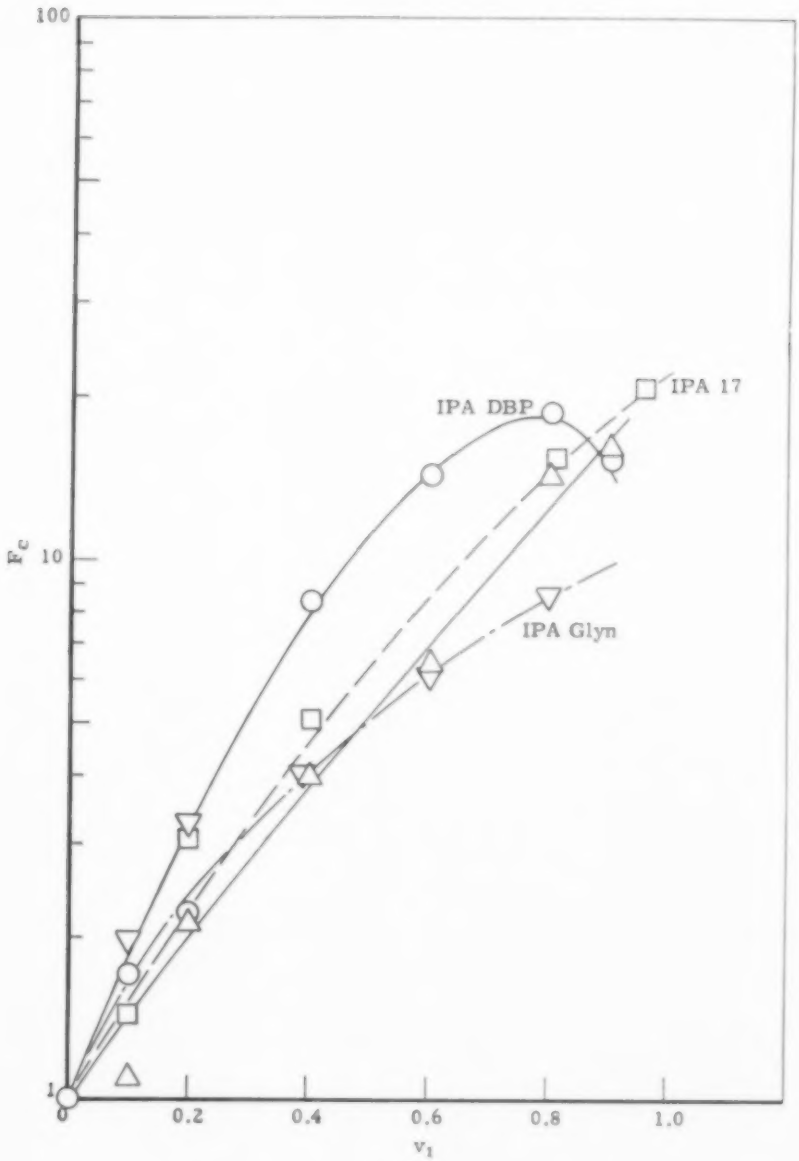

FIG. 20. F_c vs. composition – systems with IPA.

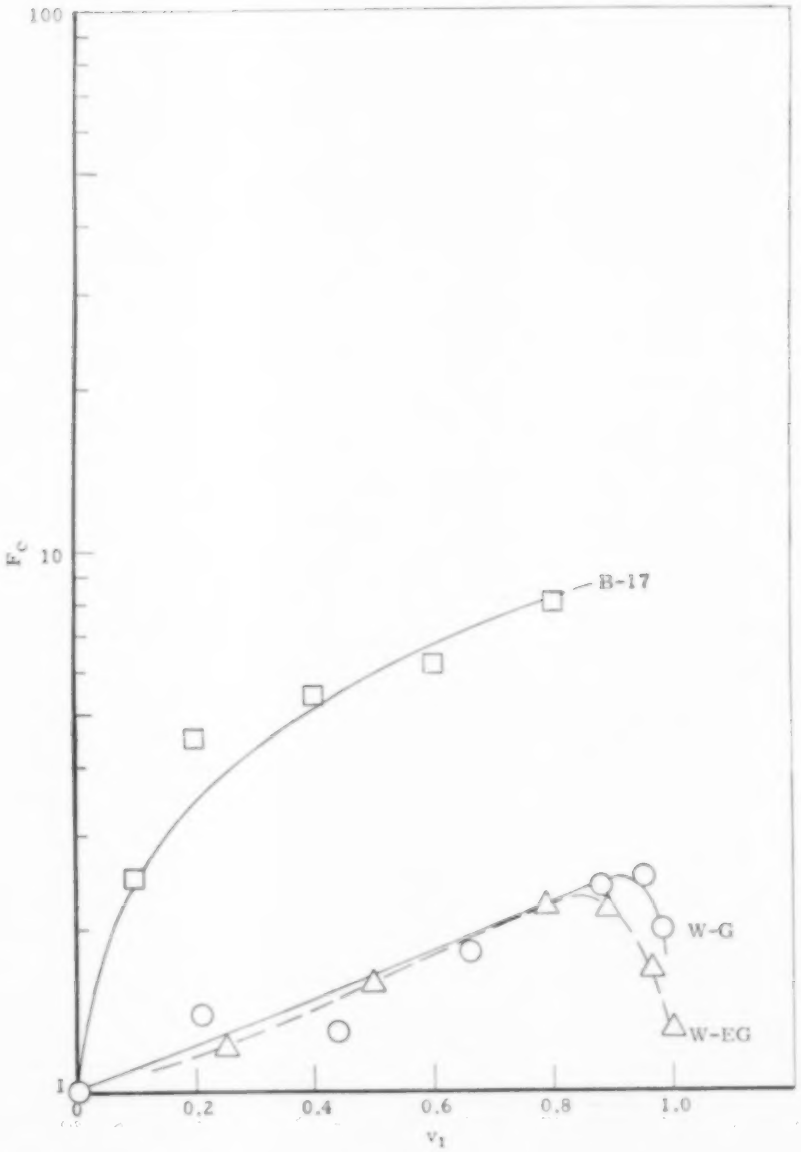

Fig. 21. F_c vs. composition – systems with water and benzene.

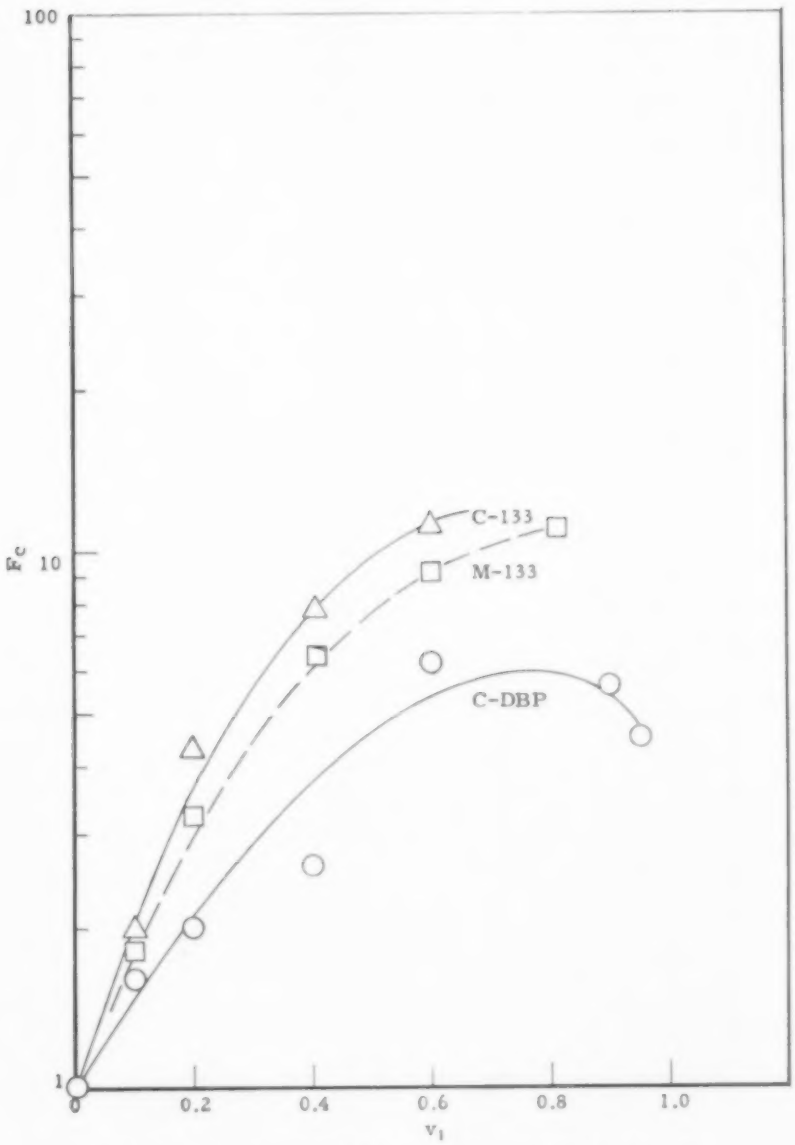

FIG. 22. F_c vs. composition – systems with CCl_4 CH_3CHCl_3.

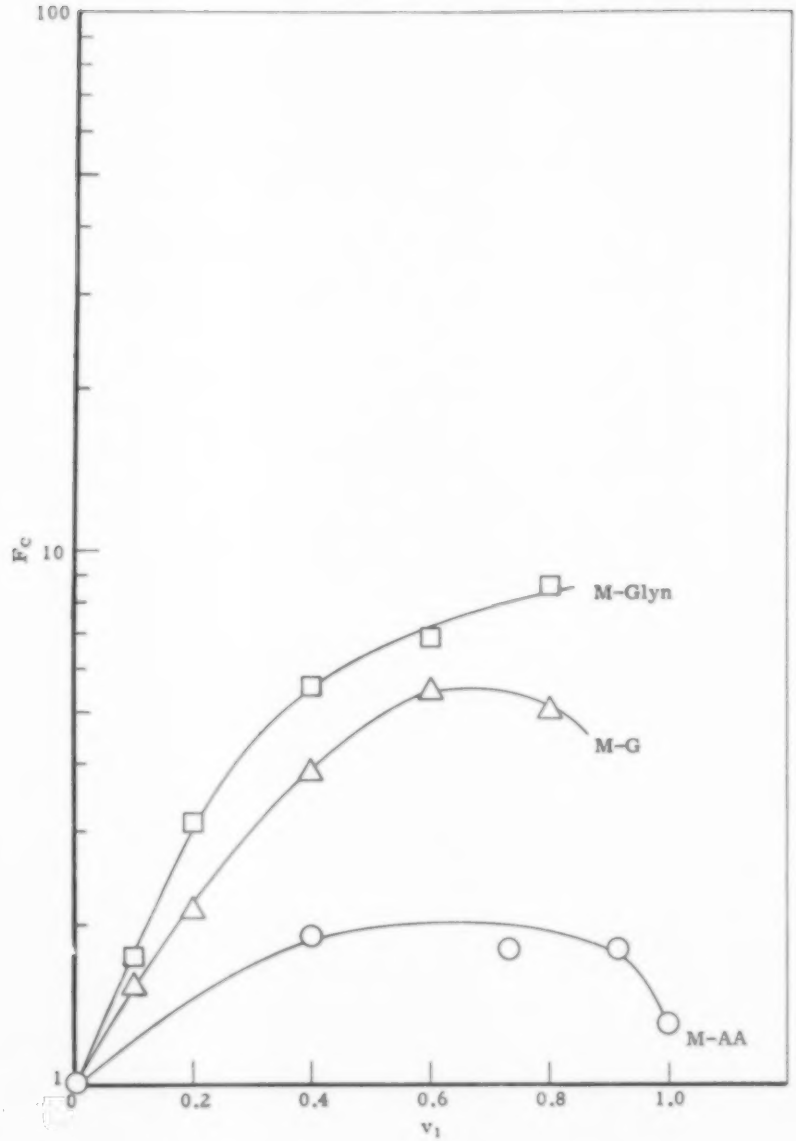

Fig. 23. F_c vs. composition systems with methanol.

heat flux, 50,000–150,000 B.Th.U./hr ft², and must not be confused with the drop-off caused by the transition to film boiling which occurs at a heat flux about ten fold higher. The maxima are most pronounced at low concentrations, 10–20%v. of the heavy component and occur at heat fluxes which are nearly constant in given systems. As seen from Table 7, this q/A varies from about 50,000 B.Th.U/hr ft² for the thick system (IPA–resin) to about 140,000 for the mobile system (methanol–glycerol).

We cannot now explain this effect.

In several of the tests a peculiar type of nucleation which we call *patch boiling* was noted. On the heater were rather large irregular patches of very closely-spaced small bubbles. Between these patches were large areas completely clear of bubbles. It appears that nucleation at a potential site is sometimes favoured by proximity to an active site. Patch boiling was especially noted in the systems methanol–glycol, methanol–glycerol, IPA–Ondina 17, and CCl_4–Ondina 17.

VOL. 16 1962

Appendix

Calculation of boiling heat transfer coefficients from experimental data

At each heat flux during a boiling run the following values were recorded: V, the voltage drop across the heater; I, the current through the heater; E_c, the thermocouple e.m.f. at the centre of the heater; E_L and E_R, the thermocouple e.m.f. at the left and right ends of the heater; E_{liq}, the e.m.f. of a thermocouple submerged in the pool of liquid being boiled. A Datatron computer was used to reduce these data, fed on punched cards, to heat fluxes, temperature differences and heat transfer coefficients.

The centre temperature in °F was calculated from a thermocouple e.m.f. by means of the relation.

$$T_c = 36{\cdot}1 + 33{\cdot}63\,E_c - 0{\cdot}0558\,E_c^2 \qquad (A.1)$$

This formula reproduces the standard thermocouple charts to within ± 0·4 °F over the range 140 °F–500 °F. Errors in ΔT due to using this formula are less than 1 per cent.

The thermal conductivity, k_w at T_c, of the stainless steel heater wall was calculated from

$$k_w = 8{\cdot}83 + 0{\cdot}00417\,T_c \qquad (A.2)$$

The reduction in heat flux caused by longitudinal conduction along the heater was evaluated for a point at the centre of the heater from

$$L/A = 3{\cdot}77\,k_w\,(2E_c - E_L - E_R) \qquad (A.3)$$

This is derived for an assumed parabolic temperature profile along the heater. Since the correction is small, it is not necessary to use a more accurate profile. The coefficient 3·77 incorporates the cross-sectional area of the metal in the heater, the distance between thermocouple locations, the surface area of the heater and the coefficient of proportionality between e.m.f. and temperature. Next, power dissipation per unit surface area of the heater was calculated by

$$\frac{P}{A} = \frac{VI}{0{\cdot}00404} \qquad (A.4)$$

where P/A is in B.Th.U/hr ft². The heat transferred from the surface of the heater to the boiling liquid follows from

$$q/A = (P/A) - (L/A) \qquad (A.5)$$

This heat flux was assumed to be that associated with the surface temperature at the centre of the heater. The temperature difference between the inner and outer surfaces of the heater was calculated from

$$T_w = \frac{(q/A)}{2\,k_w}\,m \qquad (A.6)$$

This was derived for uniform heat generation in the metal which implies that temperature is parabolic in radius. The wall thickness, m, is 0·0012 ft. The temperature at the surface of the heater was then calculated from

$$T_s = T_c - \Delta T_w \qquad (A.7)$$

and this surface temperature is that associated with the heat flux q/A.

The temperature of the liquid, in those runs without sub-cooling, was calculated from the average value of E_{liq} for the boiling data of that run. The temperature difference for boiling heat transfer is then

$$\Delta t = T_s - T_{liq} \qquad (A.8)$$

The liquid heat transfer coefficient was calculated from

$$h = \frac{q/A}{\Delta t} \qquad (A.9)$$

This heat transfer coefficient was then corrected for the effect of free convection around the heater. Because of the small diameter of the heater, this correction was important at low heat fluxes. The natural convection heat transfer coefficient was assumed to vary according to the relationship

$$h_c = A_c\,(\Delta t)^{1/4} \exp\left(\frac{-\epsilon}{T_s + T_{liq} + 920}\right) \qquad (A.10)$$

which is based on the usual equation for natural convection. The coefficient A_c depends on heater diameter, liquid, thermal conductivity, viscosity and coefficient of expansion while ϵ reflects the influence of temperature on the same properties. Both A_c and ϵ were evaluated for each

Table 8. Estimates of amplitude of fluctuations of heater surface temperature caused by use of a.c. heating

Basis: $A = 0{\cdot}01374$ ft^2, $\rho_m = 487$ lb/ft^3, $C_{pm} = 0{\cdot}1$ B.Th.U./lb °F, $f = 120$ c/sec

	Case I 0·18 in. × 0·15 in. *tube* $v/A = 72$ ft		*Case* II 0·004 in. *wire* $v/A = 1000$ ft	
h B.Th.U./hr ft^2 °F	X	*Fluct. amp.* Av. Δt	X	*Fluct. amp.* Av. Δt
100	1510	0·0007	109	0·009
300	505	0·002	36	0·03
1000	151	0·007	10·9	0·09
3000	50·5	0·020	3·6	0·27

mixture tested by fitting equation (A.10) to heat transfer coefficients measured at the lower heat fluxes where there was natural convection but no nucleate boiling.

For boiling runs the boiling heat transfer coefficient was then calculated by

$$h_b = h - h_c \qquad \text{(A.11)}$$

On completion of the calculation, the computer printed the following: q/A, the gross heat flux; T_s, the surface temperature, Δt, the driving force for heat transfer; h, the gross liquid heat transfer coefficient; h_c, the convection heat transfer coefficient; h_b, the boiling heat transfer coefficient.

Temperature Fluctuations caused by the use of Alternating Current

In a resistive element heated by 60 a.c., energy is released as a sine wave at 120 c/sec with amplitude equal to its average value,

$$q = \beta_1 [1 + \sin(2\pi ft)] \qquad \text{(A.12)}$$

Thus, twice in each cycle the power release is zero and twice it is double its average value, β_1. The temperature of the heater surface also fluctuates at the same frequency. However, because of thermal capacity, the phase is shifted and the amplitude lessened.

To estimate the effect of using a.c. on surface temperature we consider a heater of volume v, total surface area A, with heat released uniformly throughout the volume at the rate given by equation (A.12). The temperature inside the heater is assumed uniform at any instant of time. (This requires that $2k_w/hm \gg 1$. In these experiments $2k_w/hm \cong 5$, for $h = 3000$). The heater surface temperature is then given by

$$\Delta t = \frac{\beta_1}{hA}\left\{1 + \frac{\sin(2\pi ft - \tan^{-1} X)}{\sqrt{(1 + X^2)}}\right\} \qquad \text{(13)}$$

where

$$X = \frac{2\pi f \rho_m C_{pm} V}{hA} \qquad \text{(14)}$$

Thus, for a very small h, X is large. The amplitude of the fluctuations approach a limit independent of h, but the average Δt, which is proportional to $1/h$, becomes large. Hence, the ratio of fluctuation amplitude to average Δt approaches zero. On the other hand, for large h or small X the amplitude of the fluctuations approaches the mean value of Δt. Table 8 shows estimated amplitudes for our 0·18 in. O.D. heater. For comparison, also shown are amplitudes for an 0·004 in. wire which is the smallest one used by Rinaldo (see McAdams) [3].

From these calculations, we conclude that it is safe to neglect fluctuations in heater surface temperature for the data presented here, but that in studies which use fine wires this may be risky. In particular, care must be taken in comparing data taken on wires with those for "large" heaters.

Notations

a_1 = constant in vapour pressure formula, Table 3
A = heat transfer area ft^2
A_c = constant in natural convection formula, equation (A-10)
A_1 = van Laar constant, Table 5
A_2 = van Laar constant, Table 5
b_1 = constant in specific heat formula, see Table 3
c_l = liquid specific heat
c_1° = constant in specific heat formula, see Table 3
C_{pm} = metal specific heat, B.Th.U./lb °F
E_c = Thermocouple, e.m.f., at centre v
E_L = thermocouple, e.m.f., at left end v
E_{LIQ} = Thermocouple, e.m.f., for liquid pool v
E_R = thermocouple, e.m.f., at right end v
F_c = ratio of Δt required for a given h_b for a boiling mixture to that required for the pure more volatile component

f = frequency
h = measured heat transfer coefficient for outside of tube B.Th.U/hr °F
h_b = boiling heat transfer coefficient, B.Th.U/hr ft² °F
h_c = natural convection coefficient, B.Th.U/hr ft² °F
h_{max} = maximum h_b with respect to changes in Δt, B.Th.U/hr ft² °F
I = current through heater A
j_1 = constant in latent heat formula, Table 3
K_1 = constant in thermal conductivity formula, Table 3
k_w = thermal conductivity of heater material, B.Th.U/hr ft °F
k_1 = liquid thermal conductivity, B.Th.U/hr °F ft
k_1° = constant in thermal conductivity formula, Table 3
L/A = heat losses out end of heater per unit surface of heater B.Th.U/hr ft²
L_1 = latent heat of vaporization B.Th.U/lb
L_1° = constant in latent heat formula, Table 3
m = heater wall thickness ft
P/A = power dissipated in heater per unit surface of heater B.Th.U/hr ft²
P_1 = constant in vapour pressure formula, Table 3
p_1° = vapour pressure atm
q = rate of energy release in heater, B.Th.U/hr
q/A = heat flux B.Th.U/hr ft²
$(q/A)_{max}$ = maximum nucleate boiling heat flux with respect to changes in Δt, B.Th.U/hr ft²
$(q/A)_{h_m}$ = heat flux corresponding to h_{max} B.Th.U/hr ft²
T = temperature °R
T_{bp} = boiling point °F
T_c = temperature at centre thermocouple °F
T_{cr} = thermodynamic critical temp. °R
T_s = temperature of heater surface °F
T_{liq} = temperature of liquid pool °F
t = time hr
V = voltage drop across heater v
v_1 = volume fraction more volative component
v = volume of metal in heater ft³
$X = 2\pi\rho_m C_{pm} v/hA$
x_1 = mole fraction of more volatile component
x_2 = mole fraction of less volatile component
β = constant in density formula, Table 3
β_1 = amplitude of rate of energy release in heater B.Th.U/hr
γ_1 = activity coefficient of more volatile component
γ_2 = activity coefficient of less volatile component
ΔT_w = temperature drop through heater wall °F
Δt = wall temperature minus boiling point °F
ϵ = constant in natural convection formula, equation A.10
η = constant in viscosity equation, Table 4
ν = liquid kinematic viscosity ft²/hr
ν_0 = constant in viscosity formula, Table 4
ρ_1 = liquid density
ρ_1° = constant in density equation, Table 3
ρ_m = metal density lb/ft³
σ = surface tension, dyn/cm
σ_0 = constant in surface tension formula, Table 3

References

[1] McAdams W. H. *Heat Transmission* p. 391. McGraw-Hill, New York 1954.

[2] Clark H. B., Strenge P. S. and Westwater J. W. *Active Sites for Nucleate Boiling.* Chemical Engineering Progress Symposium Series No. 29, **55** 103 (1959).

[3] McAdams W. H. *Heat Transmission* p. 379. McGraw-Hill, New York 1954.

Chemical Engineering Science, 1961, Vol. 16, pp. 338 to 351. Pergamon Press Ltd., London. Printed in Great Britain.

Some heat transfer characteristics of the two-dimensional laminar incompressible wall jet

WILLIAM H. SCHWARZ and BRUCE CASWELL

Department of Chemical Engineering, Stanford University, Stanford, California, U.S.A.

(*Received* 21 *November* 1960 ; *in revised form* 9 *February* 1961)

Abstract—The heat transfer characteristics of a laminar, incompressible, two-dimensional wall jet with constant physical properties are treated in some detail. Exact solutions have been found when the flow is self-preserving in shape, and the wall temperature is variable and of the form $\Sigma A_n x_n$. These solutions are shown to reduce to the special cases of constant temperature wall ($n = 0$), and constant heat flux ($n = \frac{1}{5}$). Temperature profiles and heat flux rates have been evaluated for a variety of Prandtl numbers.

The laminar wall jet has also been examined by means of the momentum integral technique and the results are compared to the exact solutions for several assumed profiles. Further, a heat transfer expression is obtained for variable starting length of the heated section if the temperature of the wall is constant.

Résumé—Les auteurs traitent en détail les caractéristiques du transfert de chaleur d'un " wall jet " laminaire, incompressible, à deux dimensions et dont les propriétés physiques sont constantes. Des solutions exactes ont été trouvées quand l'écoulement conserve sa forme de lui-même et que la température de la paroi est variable et de la forme $\Sigma A_n x_n$. Ces solutions peuvent s'appliquer aux cas spéciaux de température constante de la paroi ($n = 0$) et à flux thermique constant ($n = \frac{1}{5}$). Les profils de température et les vitesses de flux thermique ont été évalués pour plusieurs nombres de Prandtl.

Le " wall jet " laminaire a été étuidié également par la technique de l'intégrale instantanée et les résultats sont comparés avec les solutions exactes pour plusieurs profils supposés. Ensuite, une expression du transfert de chaleur est obtenue pour une longueur variable de section chauffée si la température de la paroi est constante.

Zusammenfassung—Das Wärmeübergangsverhalten einer inkompressiblen, zweidimensionalen, laminaren Wandströmung mit konstanten physikalischen Eigenschaften wird ziemlich ausführlich behandelt. Exakte Lösungen wurden gefunden für Strömungen, die ihre Form beibehalten und für variable Wandtemperatur, die sich als $\Sigma A_n x^n$ darstellen lässt. Es wird gezeigt, dass sich diese Lösungen auf die Spezialfälle konstanter Wandtemperatur ($n = 0$) und konstanten Wärmestromes ($n = \frac{1}{5}$) zurückführen lassen. Es wurden Temperaturprofile und Wärmestromgeschwindigkeiten für verschiedene Prandtl-Zahlen ermittelt.

Die laminare Wandströmung wurde ausserdem mit einer Methode untersucht, die von der Intergration der Bewegungsgleichung ausgeht, die Ergebnisse werden für mehrere angenommene Profile mit den exakten Lösungen verglichen. Ferner wird ein Ausdruck für den Wärmeübergang bei konstanter Wandtemperatur und variabler Anfangslänge des beheizten Abschnitts erhalten.

1. INTRODUCTION

WHEN a jet of fluid strikes a wall which is submerged in the same fluid, the boundary layer flow which develops is called the wall jet. This name was apparently ascribed by GLAUERT [1], although the type of flow was introduced into the literature by Förthmann [2]. The boundary layer has the characteristic of zero velocity at both the wall and the outer edge, and hence contains a maximum velocity.

The fluid mechanical nature of the incompressible wall jet with constant physical properties has been theoretically examined by GLAUERT [1, 3] for the radial and the two-dimensional cases, including both laminar and turbulant flow. He utilized the concept of self-preservation of the

shape of the velocity profiles with downstream position in order to convert the laminar boundary layer equations into an ordinary, non-linear differential equation. The scaling factors necessary to obtain self-preservation were uniquely determined by showing that a quantity called F, the "exterior flux of momentum flux," was not a function of the downstream direction. There has been no experimental support that the laminar wall jet has a self-preserving form although resemblance of this flow to a combination of a laminar boundary layer on a flat plate with zero pressure gradient and a mixing layer or free jet strongly supports this assumption.

GLAUERT [1] also theoretically examined the turbulent wall jet. This flow has been investigated experimentally by several authors including FÖRTHMANN [2], SIGALLA [4], BAAKE [5], and SCHWARZ and COSART [6]. In general, it has been noted that GLAUERT's solutions are good only as a first approximation. However, the experimental investigations have confirmed the self-preserving nature of the velocity profiles of the turbulent wall jet at least over most of the boundary layer.

The compressible laminar wall jet has been examined by RILEY [7], GLAUERT [3,] and BLOOM and STEIGER [8]. RILEY considered the compressible boundary layer equations (momentum, energy and continuity) for the radial wall jet, and applied the von Mises transformation. The energy equation and the momentum equation are then decoupled by the assumption of a linear variation of viscosity with temperature. RILEY further observed that the flux of exterior momentum flux is an invariant for compressible flow, as well as for incompressible flow, and hence unique values of scaling factors may be obtained with the assumption of similarity or self-preservation of the velocity profiles. An ordinary non-linear differential equation was obtained which is the same as that found by GLAUERT for the incompressible case. The energy equation was solved by numerical methods including viscous dissipation, for similarity conditions when:

(1) The wall is either adiabatic or at constant temperature (T_∞) and the heating is by viscous dissipation ($P = 0{\cdot}73$).

(2) The wall is at a constant temperature, $T_w \neq T_\infty$ and no viscous dissipation.

(3) The jet is initially heated and either the wall is adiabatic or at constant temperature (T_∞). Since the energy equation is linear, the above solutions may be appropriately superposed for various combinations of the conditions.

BLOOM and STEIGER [8] have also treated the compressible laminar wall jet but applied a transformation of variables to the equations of energy and momentum that was utilized by LEVY [9] and LEES [10]. As might be expected, with the assumption of similarity of profiles and that the product of viscosity and density was constant, the governing equations were reduced to two separate ordinary differential equations, which are the same as those obtained by RILEY. The authors then showed that the flux of exterior momentum flux was invariant with downstream position. Further, they solved the energy equation without viscous dissipation for:

(1) Constant temperature wall; $P = 1$; by a numerical scheme.

(2) Variable temperature with a variation of x^n by an asymptotic solution similar to that of SCHUH [11] and LIGHTHILL [12] for n large and P variable.

(3) Variable temperature wall of the form x^n: the heat flux was obtained numerically for various n, $P = 0{\cdot}72$ and $1{\cdot}0$, as well as the enthalpy profiles for $P = 0{\cdot}72$, $n = -\frac{1}{4}$ and $\frac{1}{2}$.

GLAUERT [3] has reviewed the work of RILEY as well as discussed some of the effects of entrainment on the laminar wall jet.

2. THEORY – DEVELOPMENT OF THE EQUATIONS

For an incompressible, steady, two-dimensional flow where the physical properties of the fluid remain constant and the viscous dissipation, pressure gradient and body forces are negligible, the equations of motion, continuity and energy for a Newtonian fluid may be written with the boundary layer approximations as

$$u\frac{\partial u}{\partial x} + v\frac{\partial u}{\partial y} = \nu\frac{\partial^2 u}{\partial y^2} \qquad (1)$$

$$\frac{\partial u}{\partial x} + \frac{\partial y}{\partial v} = 0 \tag{2}$$

$$u\frac{\partial T}{\partial x} + v\frac{\partial T}{\partial y} = \alpha_T \frac{\partial^2 T}{\partial y^2} \tag{3}$$

where ν is the kinematic viscosity (μ/ρ), and α_T is the thermal diffusivity ($k/\rho\, c_p$).

The laminar plane wall jet problem has been solved in exact form by GLAUERT [1, 3] who has expressed his solution in the following form:

$$\psi = \left[40\, F\, \nu\, (x + l)\right]^{1/4} f(\eta) \tag{4}$$

$$F = \nu^2\, U/40 \tag{5}$$

$$u\left[\frac{5F}{2\,\nu\,(x+l)}\right]^{1/2} f'(\eta) \tag{6}$$

$$\eta = \left[\frac{5F}{32\,\nu^2\,(x+l)^3}\right]^{1/4} y \tag{7}$$

$$\frac{\tau_w}{\rho} = \frac{1}{9}\left[\frac{125\, F^3}{8\,\nu\,(x+l)^5}\right]^{1/4} \tag{8}$$

$$v = \frac{1}{4}\left[\frac{40\, F\, \nu}{(x+l)^3}\right]^{1/4}\left[3\,\eta f'(\eta) - f(\eta)\right] \tag{9}$$

The principal assumption was that the flow was self-preserving.

For the two-dimensional wall jet, l may be considered as the location of the virtual origin. The symbol ψ is the stream function which satisfies the continuity equation and hence

$$\frac{\partial \psi}{\partial x} = u\,; \quad -\frac{\partial \psi}{\partial x} = v \tag{10}$$

Also U is some arbitrary constant velocity.

The symbol F represents a quantity found by GLAUERT to be an invariant of the flow with respect to the downstream distance. This quantity plays a similar role in the wall jet problem as the flux of momentum in the free jet problem. The form of F for the plane, incompressible case is given as

$$\frac{d}{dx}\int_0^\infty u^2 \int_0^\infty u\,dy\,dy = 0 \tag{11}$$

or

$$F \equiv \int_0^\infty u^2 \int_0^\infty u\,dy\,dy = \text{constant} \tag{12}$$

The assumption of self-preservation of the shape of the velocity profile allows us to find scaling factors which are functions only of x, the downstream position, for the velocity and the distance from the wall y. From the equations of motion one relation may be obtained which relates the two scales. A second relation that uniquely determines the two scales is obtained from the invariance of F.

A dimensionless temperature may be defined as

$$\tau \equiv \frac{T - T_\infty}{T_w - T_\infty} \tag{13}$$

If the temperature distribution in the boundary layer is self-preserving in shape, then

$$\tau \equiv \tau(\eta) \tag{14}$$

where

$$\eta \equiv y/\delta(x) \tag{15}$$

and

$$\delta(x) \equiv \left[\frac{5\,F}{32\,\nu^3\,(x+l)^3}\right]^{-1/4} \tag{16}$$

For the velocity and the temperature profiles to be fully self-preserving, the length scales both must have the same functional variation with downstream position and hence can differ only by a constant. This constant is at our disposal, since the equations are linear, hence let it be equal to unity.

If the temperature of the wall is non-uniform, then

$$T_w - T_\infty \equiv \theta(x) \tag{17}$$

Now, with equations (6), (7), (9) and (17), equation (3) becomes

$$\tau''(\eta) + P\,\tau'(\eta) f(\eta) - \frac{4\,P\,(x+l)}{\theta(x)}\frac{d\,\theta(x)}{dx} f'(\eta)\,\tau(\eta) = 0 \tag{18}$$

where P is the Prandtl number.

If the temperature profiles are self-preserving, the coefficients in the differential equation cannot be functions of x, therefore

$$\frac{(x+l)}{\theta(x)} \cdot \frac{d\,\theta(x)}{dx} = \text{constant} \tag{19}$$

and hence

$$\theta(x) = \text{constant}\,(x+l)^n \tag{20}$$

Equation (18) may now be written

$$\tau''(\eta) + P\,\tau'(\eta) f(\eta) - 4\,P\,nf'(\eta)\,\tau(\eta) = 0 \quad (21)$$

which is a second-order, ordinary, linear differential equation, subject to the boundary conditions

$$\tau(0) = 1\,; \quad \tau(\infty) = 0 \quad (22)$$

This equation is applicable to any fluid under the stated assumptions except possibly for very low Prandtl numbers. The wall jet has the characteristic of zero velocity outside the viscous boundary layer, if entrainment is excluded. Therefore, at low Prandtl numbers where the thermal boundary layer exceeds the viscous boundary layer heat transfer outside the viscous boundary layer is due to conduction only. It is possible that the boundary layer assumption of gradients in the transverse direction being large compared to the downstream direction is not applicable. This effect would depend on the steepness of the wall temperature variation, and quantitatively is difficult to evaluate.

The function $f(\eta)$ is obtained by solving the ordinary, third-order non-linear differential equation

$$f'''(\eta) + f(\eta) f''(\eta) + 2\left[f'(\eta)\right]^2 = 0 \quad (23)$$

This equation was obtained by Glauert [1] for the laminar wall jet with the assumption that the velocity profiles were self-preserving in shape. The exact solution was given in the form

$$f = g^2\,; \quad f' = 2\,gg'\,; \quad g' = \tfrac{1}{2}(1 - g^3) \quad (24a, b, c)$$

and

$$\eta = \ln \frac{\sqrt{(1 + g + g^2)}}{1 - g} + \sqrt{(3)} \tan^{-1} \frac{g(\eta)}{2 + g(\eta)} \quad (25)$$

The heat flux through the wall is given by

$$q_w(x) = -k \left.\frac{\partial T}{\partial y}\right|_{y=0} \quad (26)$$

or

$$q_w(x) = k \frac{\theta(x)}{\delta(x)} \left[-\frac{d\,\tau(0)}{d\,\eta}\right] \quad (27)$$

Now, if the heat flux through the wall is a constant, equations (16), (20) and (27) give

$$\theta(x) = C(x + l)^{3/4} \quad (28)$$

where C is a constant, and is obtained from

$$\theta(x) = T_w - T_\infty = \frac{q_w}{k}\left[\frac{32\,\nu^3}{5\,F}\right]^{1/4} \left[-\frac{d\,\tau(0)}{d\,\eta}\right]^{-1} (x + l)^{3/4} \quad (29)$$

The expression $\left[-d\,\tau(0)/d\,\eta\right]$ is obtained from the solution of the differential equation (22) with $n = \frac{3}{4}$ and the boundary conditions, equations (22).

A non-uniform wall-temperature which is consistent with the self-preservation principle is of the form of equation (20). The heat transfer characteristics are obtained by solving equation (21) with the appropriate value of n. For this case the heat flux becomes

$$q_w(x) = k\theta(x)\left[\frac{5\,F}{32\,\nu^3 (x + l)^3}\right]^{1/4} \left[-\frac{d\,\tau(0)}{d\,\eta}\right] \quad (30)$$

and $\theta(x)$ is the prescribed wall temperature distribution.

When the temperature of the wall is a constant and not a function of x, then $\theta(x)$ is a constant and therefore $n = 0$. The differential equation will become

$$\tau''(\eta) + Pf(\eta)\,\tau'(\eta) = 0 \quad (31)$$

The heat flux through the wall is given by equation (30) with the appropriate constant for $\theta(x)$ and the derivative $\left[-d\,\tau(0)/d\,\eta\right]$ determined by the solution of equation (31).

3. Solution of the Differential Equation for constant Wall Temperature

The differential equation describing the temperature distribution through the boundary layer when the temperature of the wall is a constant is given by equation (31). This equation may be readily integrated to give:

$$\tau(\eta) - 1 = \tau'(0) \int_0^\eta \exp\left[\int_0^\eta -Pf(\eta)\,d\eta\right] d\eta \quad (32)$$

and

$$-\frac{1}{\tau'(0)} = \int_0^\infty \exp\left[-\int_0^\eta Pf(\eta)\,d\eta\right] d\eta \qquad (33)$$

The temperature distribution and the heat flux at the wall may be obtained by numerically integrating equations (32) and (33).

A more convenient form of solution was obtained by RILEY [7] in the following manner. From equation (25c)

$$dg(\eta) = \tfrac{1}{3}\left[1 - g^3(\eta)\right] d\eta \qquad (34)$$

Then from equations (32) and (33) obtain

$$\tau(\eta) = 3\int_{g(\eta)}^{1} \left[1 - g^3\right]^{P-1} dg(\eta)/3 \int_0^\eta \left[1 - g^3(\eta)\right]^{P-1} dg(\eta) \qquad (35)$$

Transforming variables, let

$$t = 1 - g^3(\eta) \qquad (36)$$

Equation (35) becomes

$$\tau(\eta) = \int_0^t t^{P-1}(1-t)^{-2/3}\,dt \Big/ \int_0^1 t^{P-1}(1-t)^{-2/3}\,dt \qquad (37)$$

where

$$\int_0^1 t^{P-1}(1-t)^{-2/3}\,dt = B(P, \tfrac{1}{3}) \qquad (38)$$

and $B(P, \frac{1}{3})$ is the Beta function, and the first integral in equation (37) is the incomplete Beta function which must be solved by numerical methods or tables. The Beta function may be written in terms of the Gamma functions as

$$B(P, \tfrac{1}{3}) = \frac{\Gamma(P)\,\Gamma(\frac{1}{3})}{\Gamma(P + \frac{1}{3})} \qquad (39)$$

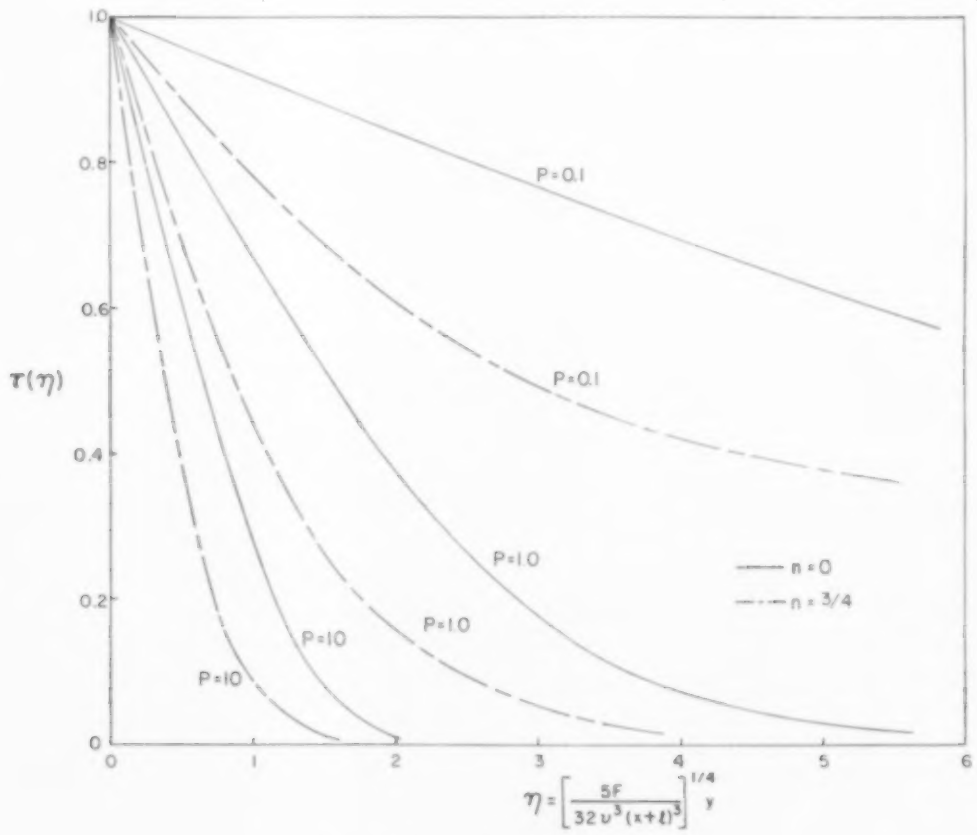

FIG. 1. Temperature distributions.

Table 1. Values of $\left[-d\tau(0)/d\eta\right]$ *for constant wall temperature* ($n = 0$) *and constant heat flux* ($n = \frac{3}{4}$)

P	0·01	0·03	0·10	0·30	0·78	1·0	2·0	5·0	10.0	15·0	50	100	1000
$n = 0$	0·00975	0·02788	0·08019	0·1728	0·2880	0·3333	0·4444	0·6120	0·7886	0·9078	1·369	1·728	3·717
$n = \frac{3}{4}$	0·03709	0·09739	0·1983	0·348	0·493	0·699	0·896	1·151	1·443	1·640	2·47	3·12	6·68

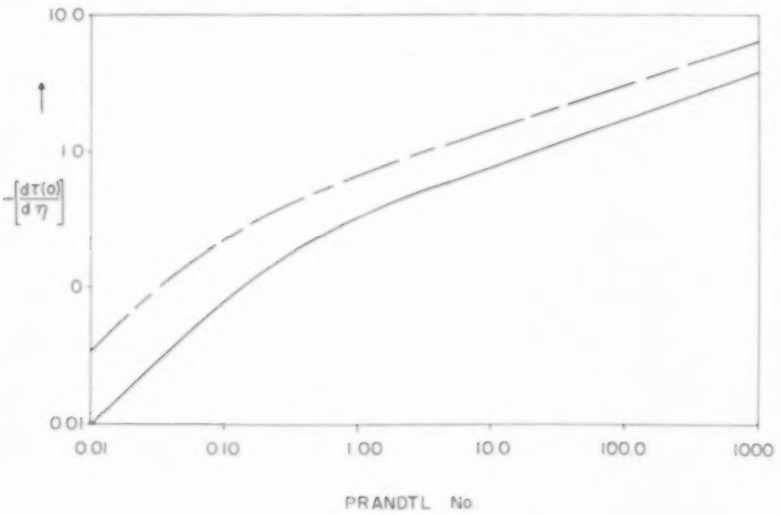

Fig. 2. Plot of $\left[-\frac{d\tau(0)}{d\eta}\right]$ vs. Prandtl number.

In a similar manner, it may be shown that

$$\left[-\frac{d\tau(0)}{d\eta}\right] = \frac{1}{B(P, \frac{1}{3})} = \frac{\Gamma(P + \frac{1}{3})}{\Gamma(P)\,\Gamma(\frac{1}{3})} \quad (40)$$

The temperature distribution as a function of η is plotted in Fig. (1) with the Prandtl number as a parameter. Values of Prandtl number of 0·1, 1 and 10 are shown.

The heat flux through the wall is given by equation (30) or

$$q_w(x) = k(T_w - T_\infty)\left[\frac{5F}{32\nu^3(x + l)^3}\right]^{1/4}\left[-\frac{d\tau(0)}{d\eta}\right] \quad (41)$$

and $\left[-d\tau(0)/d\eta\right]$ is computed by the Gamma functions of equation (40). Values of $\left[-d\tau(0)/d\eta\right]$ are given in Table 1 and shown in Fig. 2 for a variety of Prandtl numbers.

4. A Similarity Solution of the Differential Equation for variable Wall Temperature and Constant Heat Flux

The differential equation for the temperature distribution through the boundary layer, equation (21), may be transformed into a more suitable form using the variables introduced by Glauert to solve the fluid mechanical problem of the laminar wall jet. These variables are given by equation (24). In terms of the variable g the energy equation (21) becomes

$$\frac{1}{g}(1 - g^3)\tau'' + (P - 1)\frac{g^2}{3}\tau' - \frac{8}{3}Pn g\tau = 0 \quad (42)$$

where differentiation is in terms of g. Now, with the transformation

$$t = 1 - g^3 \quad (43)$$

and after some manipulation, equation (42) becomes

$$i(1-t)\tau'' + \left\{(1-P) - \left[(5/3) - P\right]t\right\}\tau' - \\ - \frac{8}{3}Pn\,\tau = 0 \qquad (44)$$

and differentiation is with respect to t. This last equation is in the standard form of the hypergeometric differential equation with solutions (13)

$$\tau(t) = A\,\tau_1(t) + B\,\tau_2(t) \qquad (45)$$

where A and B are constants and

$$\tau_1(t) = F(a, b\,;\, c\,;\, t) \qquad (46)$$

and

$$\tau_2(t) = t^{1-c}F(a-c+1, b-c+1\,;\, 2-c\,;\, t) \qquad (47)$$

$F(a, b\,;\, c\,;\, t)$ represents the hypergeometric series where a, b and c are constants which, in general, are non-integers and

$$c = 1 - P\,;\; a + b + 1 = (5/3) - P\,; \\ ab = 8/3\,Pn \qquad (48)$$

Solving for a:

$$a = -\frac{\left[P - \frac{2}{3}\right]}{2} \pm \\ \pm \frac{1}{2}\sqrt{\left[P^2 - \left(\frac{32\,n+4}{3}\right)P + \frac{4}{9}\right]} \qquad (49)$$

The value of a will be complex when the discriminant is less than zero.

The boundary conditions, equations (22), now become

$$\tau(0) = 0\,; \quad \tau(1) = 1 \qquad (50)$$

Therefore, the constant A is zero and

$$B = \frac{1}{F(a-c+1, b-c+1\,;\, 2-c\,;\, 1)} = \\ \frac{\Gamma(1-a)\,\Gamma(1-b)}{\Gamma(2-c)\,\Gamma(c-b-a)} \qquad (51)$$

The solution now becomes

$$\tau(t) = \frac{\Gamma(1-a)\,\Gamma(1-b)}{\Gamma(2-c)\,\Gamma(c-b-a)}\,t^{1-c} \\ F(a-c+1, b-c+1\,;\, 2-c\,;\, t) \qquad (52)$$

Also, from equations (48), equation (52) may be written as

$$\tau(t) = \frac{\Gamma(1-a)\,\Gamma(1-b)}{\Gamma(1+P)\,\Gamma(\frac{1}{3})}\,t^P \\ F(a+P, b+P\,;\, P+1\,;\, t) \qquad (53)$$

It is of interest to consider the special case of $n = 0$, then

$$\tau(t) = \frac{\Gamma\left[P + \frac{1}{3}\right]}{P\,\Gamma(P)\,\Gamma(\frac{1}{3})}\,t^P \\ F(2/3, P\,;\, P+1\,;\, t) \qquad (54)$$

which is recognized to be the ratio

$$B_t(P, \tfrac{1}{3})/B(P, \tfrac{1}{3})\ [13].$$

This is the same result given before in equation (37) for a constant temperature wall.

Now, in order to compute the heat flux through the wall by equation (30) it is necessary to know $[d\,\tau(0)/d\,\eta]$. It may be shown that

$$\frac{d\,\tau(\eta)}{d\,\eta} = -(1-t)^{2/3}\,t\,\frac{d\,\tau(t)}{dt} \qquad (55)$$

The term $d\,\tau(t)/dt$ will now be determined. Before differentiation, $\tau(t)$, which is given in equation (52), may be written as

$$\tau(t) = \frac{\Gamma(1-a)\,\Gamma(1-b)}{\Gamma(2-c)\,\Gamma(c-b-a)}\,t^{1-c}(1-t)^{c-b-a} \\ F(1-a, 1-b\,;\; 2-c\,;\; t) \qquad (56)$$

Now

$$\frac{d\,\tau(t)}{dt} = \frac{\Gamma(1-a)\,\Gamma(1-b)}{\Gamma(P+1)\,\Gamma(\frac{1}{3})} \\ \left[Pt^{P-1}(1-t)^{1/3}F(1-a, 1-b\,;\, P+1\,;\, t) - \right. \\ - \frac{t^P}{3}(1-t)^{-2/3}F(1-a, 1-b\,;\, P+1\,;\, t) + \\ \left. + t^P(1-P)^{1/3}\frac{dF(1-a, 1-b\,;\, P+1\,;\, t)}{dt}\right] \qquad (57)$$

Then

$$\frac{d\tau(\eta)}{d\eta} = -\frac{\Gamma(1-a)\,\Gamma(1-b)}{\Gamma(P+1)\,\Gamma(\frac{1}{3})}$$

$$\left[Pt^P(1-t)\,F(1-a, 1-b;\ P+1;\ t) - \right.$$

$$-\frac{t^{P+1}}{3}F(1-a, 1-b;\ P+1;\ t) +$$

$$\left. + t^{P+1}(1-t)\frac{dF(1-a, 1-b;\ P+1;\ t)}{dt}\right] \quad (58)$$

When $\eta = 0$, $t = 1$, and equation (58) becomes

$$\left[-\frac{d\tau(0)}{d\eta}\right] = \frac{\Gamma(1-a)\,\Gamma(1-b)\,\Gamma(\frac{2}{3})}{\Gamma(\frac{1}{3})\,\Gamma(P+a)\,\Gamma(P+b)} \quad (59)$$

where a and b are obtained by equations (48) and (49).

For a wall which is maintained at constant temperature, $n = 0$, $b = 0$ and $a = (2/3) - P$, hence

$$\left[\frac{d\tau(0)}{d\eta}\right] = -\frac{1}{B(P, \frac{1}{3})} \quad (60)$$

This result agrees with the previous calculation given as equation (40).

If the temperature distribution along the wall may be represented by a polynomial series in x or

$$T_w - T_\infty = \sum_{n=0}^{N} A_n (x+l)^n \quad (61)$$

then the temperature T of any point in the boundary layer may be determined by

$$T = T_\infty + \sum_{n=0}^{N} A_n (x+l)^n \tau_n(\eta) \quad (62)$$

where $\tau_n(\eta)$ is the solution of the differential equation (21). The boundary conditions are still $\tau(0) = 1$, $\tau(\infty) = 0$. Also the heat transfer from the wall may be found by

$$q_w = k\left[\frac{5F}{32\,\nu^3(x+l)^3}\right]^{1/4} \sum_{n=0}^{N} A_n (x+l)^n \left[-\frac{d\tau(0)}{d\eta}\right] \quad (63)$$

Values of $\left[-d\tau_n(0)/d\eta\right]$ are given in Table 2 for $n = 0$, $\frac{3}{4}$, 1, 2, 3, 4 and for Prandtl numbers of 0·01, 0·73, 7 and 100.

It is readily seen from equation (28) that for a constant heat flux the temperature along the wall must vary as $(x+l)^{3/4}$ or

$$\theta(x) = A_{3/4}(x+l)^{3/4} = T_w - T_\infty \quad (64)$$

where

$$A_{3/4} = \frac{q_w}{k}\left[\frac{5F}{32\,\nu}\right]^{-1/4}\left[-\frac{d\tau_{3/4}(0)}{d\eta}\right]^{-1} \quad (65)$$

Values of $\left[-d\tau_{3/4}(0)/d\eta\right]$ are also given in Table 1, and plotted vs. Prandtl number in Fig. 2. The temperature throughout the boundary layer is given by

$$T = T_\infty + A_{3/4}(x+l)^{3/4}\tau_{3/4}(t) \quad (66)$$

The factor $\tau_{3/4}(t)$ has been evaluated from equation (56) with $n = \frac{3}{4}$, and a and b determined from equations (48) and (49). It is shown in Fig. 1 for Prandtl numbers of 0·1, 1 and 10.

5. Solution by the Momentum Integral Technique

The equation of motion (1) may be integrated with respect to y from zero to infinity and it is found that

$$\frac{d}{dx}\int_0^\infty u^2\,dy = -\frac{\tau_w}{\rho} \quad (67)$$

If the form of the velocity profile is self-preserving, the following functions may be defined

$$\frac{u}{U(x)} \equiv k(\eta);\quad \eta = y/\delta(x) \quad (68)$$

Table 2. Values of $\left[-d\tau_n(0)/d\eta\right]$

P	$n=0$	$n=\frac{3}{4}$	$n=1$	$n=2$	$n=3$	$n=4$
0·73	0·288	0·593	0·6382	0·7994	0·9134	1·002
0·01	0·00975	0·03709	0·4561	0·07718	0·10526	0·1323
7	0·6826	1·268	1·392	1·722	1·959	2·209
100	1·728	3·12	3·388	4·184	4·757	5·218

VOL. 16 1962

where $U(x)$ and $\delta(x)$ are the scaling factors for the velocity and length respectively and are functions of x only. Equation (67) becomes

$$-\frac{\tau_w}{\rho} = \alpha \frac{d}{dx}\left[U^2(x)\,\delta(x)\right] \tag{69}$$

where

$$\alpha = \int_0^\infty k^2(\eta)\,d\eta \tag{70}$$

The shear stress at the wall may also be determined as

$$\frac{\tau_w}{\rho} = \nu \left[\frac{\partial u}{\partial y}\right]_{y=0} \tag{71}$$

Introducing equations (68) into equation (71) obtain

$$\frac{\tau_w}{\rho} = \nu \frac{U(x)}{\delta(x)}\beta \tag{72}$$

where

$$\beta = \frac{dk(\eta)}{d\eta} \tag{73}$$

Equating equation (69) to equation (72) it is found that

$$\frac{\delta(x)}{U(x)}\frac{d}{dx}\left[U^2(x)\,\delta(x)\right] = -\frac{\beta}{\alpha}\nu \tag{74}$$

With an assumed form for the velocity profile $k(\eta)$, values of α and β may be determined. However, equation (74) involves two unknowns $[U(x)$ and $\delta(x)]$. It is then necessary to obtain some other independent relation before $U(x)$ and $\delta(x)$ can be determined explicitely. As mentioned previously, this has been done by GLAUERT who found that the flux of exterior momentum flux was constant or equation (12).

Introducing the self-preserving relations, obtain

$$F = U^3(x)\,\delta^2(x)\,\gamma \tag{75}$$

where

$$\gamma \equiv \int_0^\infty k(\eta)\int_0^\infty k^2(\eta)\,d\eta\,d\eta \tag{76}$$

Now, with equations (74) and (76), obtain

$$\delta(x) = \left[\frac{4(x+l)\beta\nu^{3/4}}{\alpha}\right]\left[\frac{F}{\gamma}\right]^{-1/4} \tag{77}$$

and

$$U(x) = \left[\frac{F}{\gamma}\right]^{1/2}\left[\frac{4(x+l)\beta\nu}{\alpha}\right]^{-1/2} \tag{78}$$

The shear stress at the wall then becomes

$$\tau_w/\rho = \frac{\alpha^5}{\beta\gamma^3 4^5}\left[\frac{F^3}{\theta(x+l)^5}\right]^{1/4} \tag{79}$$

where α, β and γ are given by equations (70), (73) and (76) and a functional form for $k(\eta)$. Several forms for the velocity profile were chosen and are listed in Table 3. The exact form of the shear stress was given by GLAUERT and the results of the integral analysis are compared to that result.

The integral technique may be suitably applied to the heat transfer problem in the following way. First, the energy equation (3) is integrated with respect to y from zero to infinity, and

$$\frac{d}{dx}\int_0^\infty u(T - T_\infty)\,dy = -\alpha_T\left[\frac{\partial T}{\partial y}\right]_{y=0} = \frac{q_w}{\rho C_P} \tag{80}$$

Then, with the definition of τ, equation (13) and the assumption of self-preserving temperature profiles write

$$\tau \equiv \tau(\eta_T);\ \eta_T \equiv y/\delta_T(x) \tag{81a, b}$$

Table 3. Comparison of integral method to exact solution for shear stress

$f(\eta)$	*Range of* η	α	β	γ	$\frac{\tau_w}{\rho}\left[\frac{F^3}{\nu(x+l)^5}\right]^{-1/4}$	% *error*
$1/4\,\eta\exp(-\eta^2/8)$	$0 \leq \eta < \infty$	0·222	0·250	0·101	0·214	3·2
$\sin \eta\,\pi$	$0 \leq \eta \leq 1$	1/2	1·0	0·2676	0·1680	24
$\eta(1-\eta^3)$	$0 \leq \eta \leq 1$	8/105	1	0·00981	0·227	2·7
Exact	$0 \leq \eta < \infty$	—	—	—	0·221	—

Now, the scaling factor for the length $\delta(x)$ is a function only of x, the downstream co-ordinate. This concept of self-preservation of the shape of the temperature profile may actually be too restrictive for the integral solutions. It has been observed that the integral method is often not sensitive to the form of the assumed distribution. If the leading edge of the heated section does not correspond to the origin of the wall jet then exact self-preservation is not possible. However, since the integral method satisfies the equations over the whole layer and not necessarily at the interior, it is possible to apply this technique where the profiles are not self-preserving. This method has been successful in other flows such as the flat plate with pressure gradient.

Introducing the relations (81a, b) into the second term of equation (80) obtain

$$\frac{q_w}{\rho C_P} = \frac{\alpha_T}{\delta_T(x)} \epsilon_1 (T_T - T_\infty) \tag{82}$$

where

$$\epsilon_1 \equiv -\left[\frac{d\,\tau(\eta_T)}{d\,\eta_T}\right]_{\eta_T=0} \tag{83}$$

Similarly these relations are introduced into the left-hand term of equation (80) and it is found that

$$\frac{q_w}{\rho C_P} = (T_w - T_\infty)\frac{d}{dx}\left[U(x)\,\delta_T(x)\right]\int_0^\infty g(\eta)\,\tau(\eta_T)\,d\,\eta_T \tag{84}$$

where $(T_w - T_\infty)$ is constant. Also, define

$$\Delta = \delta_T(x)/\delta(x) \tag{85}$$

hence

$$\eta = \eta_T\,\Delta \tag{86}$$

Further, let

$$\epsilon_2 \equiv \int_0^\infty k(\eta)\,\tau(\eta_T)\,d\,\eta_T \tag{87}$$

Equation (82) may be equated to equation (84), and

$$\delta_T(x)\frac{d}{dx}\left[\epsilon_2\,U(x)\,\delta_T(x)\right] = \alpha_T\,\epsilon_1 \tag{88}$$

Introducing equations (77), (78) and (85) into (88), obtain

$$\Delta(x+l)^{3/4}\frac{d}{dx}\left[\Delta(x+l)^{-1/4}\epsilon_2\right] = \frac{1}{P}\left[\frac{\epsilon_1\alpha}{4\beta}\right] \tag{89}$$

α and β are obtained from the assumed velocity distribution, and ϵ_1 and ϵ_2 are obtained from the assumed velocity and temperature distributions.

Now the local heat flux per unit area at any point on the plate is given by equation (82), with appropriate substitutions, as

$$q_w(x) = k(T_w - T_\infty)\left[\frac{\alpha^3}{4^3\beta^3\gamma}\right]^{1/4}\frac{\epsilon_1}{\Delta}\left[\frac{F}{\nu^3(x+l)^3}\right]^{1/4} \tag{90}$$

where Δ is a function of the Prandtl number and x, and must be evaluated from equation (89).

The local heat transfer coefficient

$$h(x) \equiv q_w(x)/T_w - T_\infty \tag{91}$$

becomes

$$h(x) = k\left[\frac{\alpha}{4^3\beta^3\gamma}\right]^{1/4}\frac{\epsilon_1}{\Delta}\left[\frac{F(x+l)}{\nu^3}\right]^{1/4}(x+l)^{-1} \tag{92}$$

and the local Nusselt number, defined as

$$N_x = \frac{h(x)\,[x+l]}{k} \tag{93}$$

becomes

$$N_x = \left[\frac{\alpha}{4^3\beta^3\gamma}\right]^{1/4}\frac{\epsilon_1}{\Delta}\left[\frac{F(x+l)}{\nu^3}\right]^{1/4} \tag{94}$$

The average Nusselt number, where the starting distance is zero, becomes

$$N_a = \frac{4}{3}\left[\frac{\alpha}{4^3\beta^3\gamma}\right]^{1/4}\frac{\epsilon_1}{\Delta}\left[\frac{F(l+L)}{\nu^3}\right]^{1/4} \tag{95}$$

since the average heat transfer coefficient is given by

$$h_a = \frac{1}{L+l}\int_{-l}^{L} h(x)\,dx \tag{96}$$

and L is the distance from the point $x = 0$, which corresponds to the nozzle outlet or jet axis, for example, to the end of the section.

If the velocity distribution is chosen to be

$$k(\eta) = \eta(1-\eta^2) \quad 0 \leqslant \eta \leqslant 1 \tag{97}$$

and the temperature distribution as

$$\tau(\eta_T) = 1 - \tfrac{3}{2}\,\eta_T + \tfrac{1}{2}\,\eta_T^2 \qquad (98)$$

then when $\Delta < 1$, or for Prandtl numbers greater than one, equation (89) becomes

$$\Delta\,(x+l)^{3/4}\,\frac{d}{dx}\left[(x+l)^{1/4}\,\Delta\left(\frac{\Delta}{10} - \frac{3}{140}\,\Delta^3\right)\right] = \frac{1}{P}\left[\frac{\epsilon_1\,\alpha}{4\,\beta}\right] \qquad (99)$$

Now

$$\alpha = 8/105\,;\ \epsilon_1 = 3/2\,;\ \beta = 1\,;\ \gamma = 0{\cdot}00981 \quad (100)$$

and if $3\,\Delta^4/140 \ll \Delta^2/10$, this equation (99) will become

$$\Delta^3 + \frac{8}{3}\,\frac{d\Delta^3}{dx} = \frac{1}{P}\,\frac{\epsilon_1\,\alpha}{4\,\beta} \qquad (101)$$

With the boundary condition that $\Delta = 0$ when $x = \xi$ (start of heat section), this inhomogeneous, ordinary linear differential may be evaluated as

$$\Delta = \left(\frac{8}{7}\right)^{1/3} P^{-1/3}\left[1 - \frac{\xi + l^{3/8}}{x + l}\right]^{1/3} \qquad (102)$$

Therefore the local heat flux through the wall for Prandtl numbers greater than one, is given by

$$q_w(x) = k\,(T_w - T_\infty)\,0{\cdot}2338\left[\frac{F}{\nu^3\,(x+l)^3}\right]^{1/4} P^{1/3}\left[1 - \frac{\xi + l^{3/8}}{x + l}\right]^{-1/3} \qquad (103)$$

When there is zero starting length, i.e. $\xi = -l$, this equation may be compared to the exact solution, equation (41), rewritten as

$$q_w(x) = k\,(T_w - T_\infty)\,0{\cdot}6287\left[\frac{F}{\nu^3\,(x+l)^3}\right]^{1/4}\left[-\frac{d\,\tau(0)}{d\,\eta}\right] \qquad (104)$$

Values of the approximate expression of equation (104) as well as the exact form are compared for various Prandtl numbers in Table 4. The increasing error at smaller Prandtl number is due to the assumption of $\Delta^3 < 14/3$ used to solve equation (99).

Also shown in Table 4 are values obtained from equation (99) for $\xi = 0$. For this case, Δ is a constant, and equation (99) becomes

$$\Delta^2\left[\frac{\Delta}{10} - \frac{3}{140}\,\Delta^3\right](x+l)^{3/4}\,\frac{d}{dx}\,(x+l)^{1/4} = \frac{1}{P}\left[\frac{\epsilon_1\,\alpha}{4\,\beta}\right] \qquad (105)$$

This reduces to

$$\Delta^3\left[\frac{1}{10} - \frac{3}{140}\,\Delta^3\right] = \frac{24}{210\,P} \qquad (106)$$

The heat flux becomes

$$q_w(x) = 0{\cdot}2444\,k\,(T_w - T_\infty)\left[\frac{F}{\nu^3\,(x+l)^3}\right]^{1/4}\frac{1}{\Delta} \qquad (107)$$

where $1/\Delta$ is a function of the Prandtl number

Table 4. Comparison of exact to approximate methods for solution of heat flux

P	1	2	5	10	15	50	100	1000
Exact $0{\cdot}6287\left[-\frac{d\,\tau(0)}{d\,\eta}\right]$	0·2095	0·2794	0·3848	0·4958	0·5707	0·8607	1·086	2·3369
Approximate Equation (104) $0{\cdot}2338\,P^{1/3}$	0·2338	0·2936	0·3998	0·5037	0·5766	0·8613	1·0852	2·338
Approximate Equation (124) $0{\cdot}2444\ \frac{1}{\Delta}$	0·2085	0·2774	0·3862	0·4949	0·567	0·8554	1·085	2·337

and is found by solving the cubic equation (106). It is seen that better agreement is obtained for Prandtl numbers close to one.

The recommended equations for local heat flux and local heat transfer coefficient with a variable starting length and Prandtl numbers greater than one are given as

$$q_w(x) = Ck\,(T_w - T_\infty)\left[\frac{F}{\nu^3\,(x+l)^3}\right]^{1/4} P^{1/3}\left[1 - \left(\frac{\xi + l}{x + l}\right)^{3/8}\right]^{-1/3} \qquad (108)$$

and

$$h(x, \xi) = C\,\frac{k}{(x+l)}\left[F\,(x+l)/\nu\right]^{1/4} P^{1/3}\left\{1 - \left[(\xi + l)/(x + l)\right]^{3/8}\right\}^{-1/3} \qquad (109)$$

where the constant C has been evaluated from the exact solution as the best fit of the form $CP^{1/3}$ to the function $0{\cdot}6287\left[-d\,\tau(\eta)/d\,\eta\right]$ and $C = 0{\cdot}2216$.

It may be mentioned that these equations can be used to determine the heat transfer or wall temperature for any arbitrary distribution of wall temperature or heat flux respectively, by the classical super-position techniques suggested by Rubesin [14, 15], Chapman and Rubesin [16], Lighthill [12], Klein and Tribus [17] and Eckert [18], Hartnett *et al.* [19] and Eckert *et al.* [20]. These techniques have been applied to the laminar wall jet by Schwarz and Caswell [21].

6. Estimation of F and l

If the two-dimensional wall jet is formed by the scheme shown in Fig. 3 there are several ways of estimating the value of the flux of exterior momentum flux and l, the "virtual origin."

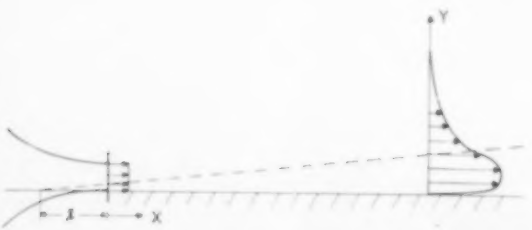

Fig. 3. The tangential two-dimensional wall jet.

At the nozzle outlet, the value of F may be estimated (F_e) from equation (12) and noting that $u = U_n$ = constant where U_n is the uniform velocity of the outlet. Then

$$F_e = \frac{U_n^3}{2}\,d^2 \qquad (110)$$

where d is the nozzle width. This may be re-written as

$$F_e = \tfrac{1}{2}\,U_n\,Q_n^2 \qquad (111)$$

where Q_n is the volume flow at the nozzle per unit width of nozzle ($= U_n\,d$).

If the wall jet, originating at some point $x = -l$, and at $x = 0$ had a flow rate of Q_n and an estimated F_e, an estimated value of l may be computed in the following way:

$$Q = \int_0^\infty u\,dy = \left[40\,F\,(x+l)\,\nu\right]^{1/4} \qquad (112)$$

Then at $x = 0$, $Q = Q_n$ and from equations (111) and (112) it is seen that

$$\frac{l}{d} = 0{\cdot}05\,R_0 \qquad (113)$$

where

$$R_0 = \frac{U_n d}{\nu} \qquad (114)$$

The value of l may also be estimated by assuming that the final form of the developed wall jet acts as if it started at $x = -l$ and at $x = 0$ its maximum velocity is located at $y = d/2$. From equation (7) and $\eta = \eta_{max}$, $y = d/2$, $x = 0$

$$\eta_{max} = 2 = \frac{d}{2}\left[\frac{5\,F_e}{32\,\nu^3\,l^3}\right]^{1/4} \qquad (115)$$

Therefore,

$$l/d = 0{\cdot}0673\,R_0^{1/3} \qquad (116)$$

For the two methods, when $R_0 = 100$, equation (113) gives 5·0 and equation (116) gives 0·312. When $R_0 = 10$, $l/d = 0{\cdot}5$ by equation (113), and 0·1448 by equation (116). For small outlet Reynolds numbers, the two methods give results of the same order of magnitude. However, at the higher Reynolds numbers ($R_0 > 100$) the

VOL. 16 1962

discrepancy becomes considerable. Of the two methods the authors suggest equation (116) to be more reasonable. It is also to be remarked that the laminar wall jet is confined to small Reynolds numbers.

Conclusions

Exact solutions have been obtained for the heat flux and temperature distributions through a two-dimensional, laminar, incompressible wall jet with constant physical properties and negligible viscous dissipation by assuming self-preservation of the velocity and temperature profiles. These results are applicable for wall temperatures which vary as $\sum_n A_n x^n$, and include both the constant temperature wall and the constant heat flux cases. For full similarity, it is necessary that the thermal and momentum boundary layers start identically.

If the wall temperature or heat flux is variable and not of the above form, then approximate methods have been developed to determine the heat transfer characteristics for $P > 1$. Integral methods were used and compared to the exact forms; an error of 10 – 20 per cent is obseved in the heat flux.

Acknowledgements—Financial support for one of the authors (B.C.) by the National Science Foundation is gratefully appreciated.

Notation

a, b, c = constants defined by equations (48)
$B(p, q)$ = incomplete Beta function
$B_1(p, q)$ = complete Beta function
C_p = heat capacity
(η) = dimensionless self-preserving stream function defined by Equation (4)
F = flux of momentum flux, see equation (12)
g = function defined as $g^2 = f$
$h(x)$ = local heat transfer coefficient
k = thermal conductivity
l = distance from starting point of co-ordinate system to the virtual origin
P = Prandtl number $(C_p \mu/k)$
$q_w(x)$ = local heat flux at the wall
t = transformation variable defined as $t = 1 - g^3(\eta)$
T = temperature
T_∞ = temperature at infinity or ambient temperature
T_w = wall temperature
u = velocity in the x or downstream direction
U = arbitrary constant velocity, which is related to F by equation (5)
v = velocity in the y or transverse direction
x = downstream direction measured from the origin, e.g. the stagnation point of an impinging jet or the nozzle of a tangential jet
y = Transverse distance, measured from the wall
α_T = Thermal diffusivity $(k/\rho C_p)$
α = constant defined by equation (70)
β = constant defined by equation (73)
γ = constant defined by equation (76)
Δ = ratio of scaling factor for thermal boundary layer to the momentum boundary layer
$\delta(x)$ = scaling factor for transverse distance y
$F(a, b; c; t)$ = hypergeometric series
ϵ_1 = constant defined by equation (83)
ϵ_2 = constant defined by equation (87)
η_T = dimensionless distance from the wall in the temperature problem
η = dimensionless transverse distance, defined by equation (7)
$\theta(x)$ = function expressing wall-temperature variation
ν = kinematic viscosity, defined as the viscosity of the fluid divided by the density of the fluid (μ/ρ)
ξ = distance from origin of co-ordinate axis to the heated section
τ = dimensionless temperature $= (T - T_\infty)/(T_w - T_\infty)$
τ_w = shear stress at the wall
ϕ = stream function defined in equation (10)

References

[1] Glauert M. B. *J. Fluid Mech*, 1956 **1** 625.
[2] Förthmann E. *Ing. Arch.* 1934 **1** (Translation in NACA Tech. Memo. 1936 789).
[3] Glauert M. B. *Boundary Layer Research* (Edited by Gortler H.) Springer-Verlag, Berlin 1958.
[4] Sigalla A. J. *Roy. Aeronaut.* 1958 **62** 873.
[5] Baake P. *J. Fluid Mech.* 1957 **2** 467.
[6] Schwarz W. H. and Cosart W. P. *J. Fluid Mech.* 1961 **10** 481.

[7] Riley N. *J. Fluid Mech.* 1958 **4** 615.

[8] Bloom M. H. and Steiger M. H. Polytechnic Institute of Brooklyn, Department of Aeronautical Engineering and Applied Mechanics Report 1957.

[9] Levy S. *J. Aero. Sci.* 1954 **21** 459.

[10] Lees L., *Jet Propul.* 1956 **26** 259.

[11] Schuh H. *J. Aero. Sci.* 1953 **20** 146.

[12] Lighthill M. J. *Proc. Roy. Soc.* 1950 A **202** 359.

[13] Erdelyi A. (Editor) *Higher Transcendental Functions.* Vol. 1, pp. 74 and 101. McGraw-Hill, New York 1950.

[14] Rubesin M. W. M.S. Thesis, University of California, Berkeley 1947.

[15] Rubesin M. W. NACA Technical Note 2345 1951.

[16] Chapman D. R. and Rubesin M. W. *J. Aero. Sci.* 1949 **19** 547.

[17] Klein J. and Tribus M. *Heat Transfer Symposium, Ann Arbor* 1952. University of Michigan.

[18] Eckert E. R. G. *Introduction to the Transfer of Heat and Mass.* McGraw-Hill, New York 1950.

[19] Hartnett J. P., Eckert E. R. G., Birkebak R. and Sampson R. L. Technical Report 56–373. Wright Air Development Centre December 1956.

[20] Eckert E. R. G., Hartnett J. P. and Birkebak R. Technical Report 57–315. Wright Air Development Centre May 1957.

[21] Schwarz W. H. and Caswell B. Department of Chemical Engineering Report. Stanford University 1961.

Chemical Engineering Science, 1961, Vol. 16, pp. 352 to 363. Pergamon Press Ltd., London. Printed in Great Britain.

The operating behaviour of multistage systems—I

The steady state

Douglass J. Wilde*
Department of Chemical Engineering, University of California, Berkeley, U.S.A.

(*Received* 12 *May* 1960)

Abstract—Small but constant variations in the composition of the feed to a multistage system produce steady state composition changes at every stage. The relation between these adjacent steady states is investigated theoretically by means of matrix algebra and the theory of continued fractions. Closed form equations for small changes are derived and then analysed to obtain four qualitative conclusions applicable to most practical systems. A proposal is advanced for reducing the need to vary reflux ratio to control product composition.

Résumé—Des modifications faibles mais constantes dans la composition de l'alimentation d'un système polyétagé entrainent pour chaque étage des variations stationnaires de composition.

La relation entre ces états stationnaires adjacents ext examinée théoriquement au moyen de la théorie des matrices et de celle des fractions continues. Dérivation d'équations applicables à de petites variations, dont l'analyse conduit à quatre conclusions qualitatives applicables aux systèmes les plus fréquents. On propose une méthode permettant de diminuer la variation du reflux pour controler la composition du produit.

Zusammenfassung—Kleine aber konstante Abweichungen in der Zulaufzusammensetzung eines mehrstufigen Systems erzeugen eine stationäre Änderung der Zusammensetzung in jeder Stufe. Die Beziehung zwischen diesen benachbarten stationären Bedingungen werden mit Hilfe der Matrizenrechnung und der Theorie der Kettenbrüche theoretisch untersucht. Geschlossene Gleichungen für kleine Änderungen wurden abgeleitet und analysiert, um vier qualitative Folgerungen zu ziehen, die für die meisten praktischen Systeme anwendbar sind. Es wird ein Vorschlag gemacht, der die Notwendigkeit verringert, das Rückflussverhältnis zu ändern, um die Produktzusammensetzung zu kontrollieren.

1. Introduction

Although there is a large body of literature about the *design* of multistage systems such as distillation columns [1] there has been little theoretical investigation of their *operation*. This is not surprising. Operating systems are usually so complicated that it has seemed easier to rely on the experience of human operators familiar with a particular system than to attempt an analysis applicable to many systems. Yet a fundamental theory of the behaviour of operating systems could be of great value to the chemical engineering profession. It could lead to better process control, giving higher product quality and lower consumption of material, labour and energy. It could suggest methods for increasing the capacity of existing equipment without major alterations. It could show how to find causes of improper performance. It could decrease the unproductive time required to adjust to upsets. And most important, it could help the engineer make better, faster decisions about the multistage systems under his supervision, without relying too heavily on expensive computations or the experience of his operating personnel.

Acrivos and Amundson [2] have shown the value of using matrices to describe interacting systems. The particular form of matrix applicable to multistage systems has such a noticeable structure that mathematicians have a name for it—the *Jacobi* matrix [3]. This structure was exploited by Acrivos and Amundson to establish the inherent stability of multistage systems to small pertubations. In this article we investigate the Jacobi structure more deeply, finding that with reasonable simplifying assumptions a great deal of insight can be gained into the operating behaviour of multistage systems.

*Present address: Department of Chemical Engineering, University of Texas, Austin, U.S.A.

This article deals with the steady state composition changes at each stage resulting from a small but constant variation in feed composition. In spite of the simplicity of this case, the results are not without practical application. The engineer in operations is often called upon to predict the effects of a long-term feed change, while the designer may need to evaluate the sensitivity of his steady state design to the quality of the feed. This article gives formulae for finding such nearby steady states without performing new plate-by-plate calculations.

Aside from these direct quantitative applications, the study also shows how a steady state disturbance is propagated away from the source and then returned to the source again. This phenomenon is undesirable from a control standpoint, and we call it *natural feedback* to distinguish it from the feedback generated by control devices. After the steady state characteristics of natural feedback are understood a method for reducing their deleterious effects by holding the reflux composition constant immediately suggests itself.

In developing this theory we use results from several other branches of science with which the reader may wish to become acquainted on his own. The matrix algebra employed is quite elementary and may be found in any text on the subject (cf. FRAZER *et al.* [4]). Interesting topological relations in a multistage system are illustrated by its signal flow graph, a concept borrowed from the electrical engineers by CAMPBELL [5]. The theory of continued fractions, which gives us a basic theorem, is surveyed in WALL's treatise [6].

Research on the implications of natural feedback in multistage systems is continuing. A study of the response to an impulse has just been completed and is now being prepared for publication.

2. THE MATHEMATICAL MODEL

Consider any countercurrent multistage system with or without reflux. For definiteness, we use the notation conventional for distillation columns, although the theory can be applied without significant modification to multistage countercurrent extraction or absorption systems as well. However, when we speak of a "stage," we mean an actual physical stage, not a theoretical stage. Since we are concerned with the operation rather than with the design of such a system, we assume that n, the number of stages, is known. The stages are numbered consecutively from 1 to n, beginning at the "top" of the column, or for more general systems, at the end of system where the reflux is introduced. For systems having no reflux the direction of numbering is unimportant.

Let V_i be the molal flow rate of the "vapour" going from stage i to stage $i-1$, and let L_i be the molal "liquid" rate flowing from stage i to stage $i+1$. The reflux rate will be denoted by L_0, since it flows into stage 1. Select any component of interest and let x_i represent its mol fraction in the "liquid" leaving stage i. Similarly, let y_i be its mol fraction in the "vapour" leaving stage i. In an operating system at steady state all of the L_i, V_i, x_i and y_i are fixed. We shall choose a particular steady state as the *reference state* and say that in the reference state $L_i = L_i^0$, $V_i = V_i^0$, $x_i = x_i^0$, and $y_i = y_i^0$, where L_i^0, V_i^0, x_i^0 and y_i^0 are constants. We shall study systems in which x_i and y_i are permitted to vary about the reference state but where L_i and V_i are assumed constant for all states. For brevity we shall omit the superscripts on L_i and V_i. Define u_i and v_i, the *composition deviations from the reference steady state*, as follows:

$$u_i \equiv x_i - x_i^0 \tag{1}$$

$$v_i \equiv y_i - y_i^0 \tag{2}$$

In each stage i, x_i and y_i are related by some function depending on the phase equilibrium, the rate of mass transfer, the mixing pattern and the presence of leaks or plugged passages. We assume that in the actual column this relation is approximately linear over the range of variation of x_i and y_i. In terms of the composition deviations we have that

$$v_i = \beta_i u_i, \tag{3}$$

where β_i is a constant characteristic of stage i.

There may be side streams leaving the system at any stage. We denote the molal flow rates of "liquid" and "vapour" leaving stage i by L_i^- and V_i^- respectively. These rates are assumed to

be constant and the sidestream compositions are assumed to be the same as x_i and y_i respectively. Similarly there may be fresh material fed to the column at any stage. The molal flow rates of "liquid" and "vapour" feed, symbolized by L_i^+ and V_i^+ respectively, are assumed constant. The feed compositions are x_i^+ and y_i^+, with their deviations u_i^+ and v_i^+ from their reference steady states x_i^{+0} and y_i^{+0} defined as in equations (1) and (2).

A material balance on the component of interest around stage i gives

$$L_{i-1}\,u_{i-1} - (L_i + L_i^-)\,u_i - (V_i + V_i^-)\,v_i + \\ + V_{i+1}\,v_{i+1} + L_i^+\,u_i^+ + V_i^+\,v_i^+ = 0 \quad (4)$$

By rearranging this and using equation (3) we obtain

$$-L_{i-1}\,u_{i-1} + [L_i + L_i^- + \beta_i\,(V_i + V_i^-)]\,u_i \\ - \beta_{i+1}\,V_{i+1}\,u_{i+1} = L_i u_i^+ + V_i v_i^+ \quad (5)$$

We account for the reflux by letting

$$L_0 \equiv V_1 \quad (6)$$

For abbreviation, let

$$a_{i+1} \equiv \frac{\beta_{i+1}\,V_{i+1}}{[L_i + L_i^- + \beta_i\,(V_i + V_i^-)]} \quad (7)$$

$$b_i \equiv \frac{L_{i-1}}{[L_i + L_i^- + \beta_i\,(V_i + V_i^-)]} \quad (8)$$

$$w_i \equiv \frac{(L_i^+\,u_i + V_i^+\,v_i}{[L_i + L_i^- + \beta_i\,(V_i + V_i^-)]} \quad (9)$$

We shall speak of w_i as the *normalized input deviation* at stage i. Using the fact that

$$u_0 \equiv v_1 \equiv \beta_1\,u_1 \quad (10)$$

and

$$V_{n+1} \equiv 0, \quad (11)$$

and making the further abbreviation

$$r \equiv \frac{\beta_1\,V_1}{[L_1 + L_1^- + \beta_1\,(V_1 + V_1^-)]} \quad (12)$$

We can write n equations in the n unknown deviations u_i:

$$\left.\begin{aligned}
(1-r)\;u_1 - a_2\,u_2 - &= w_1 \\
-b_2\,u_1 + u_2 - a_3\,u_3 - &= w_2 \\
-b_3\,u_2 + u_3 - a_4 u_4 &= w_3 \\
&\;\;\vdots \\
\ddots\;-b_{n-1} + u_{n-1} - a_n u_n &= w_{n-1} \\
-b_n\,u_{n-1} + u_n &= w_n
\end{aligned}\right\} \quad (13)$$

3. Natural Feedback

The set of equations (13) describes in algebraic terms the simultaneous relations between the disturbances w_j and the resulting concentration fluctuations u_i. In the next section we shall apply algebraic methods to these equations in order to find out what they mean. Before we do this it is instructive to examine the signal flow graph of a multistage system. This is a graphical representation of the equations (13) which gives topological insight into the interactions of the variables. Fig. 1 shows the signal flow graph applicable here. It is a slight modification of the one given by Campbell [5] who discusses signal flow graphs in some detail. Each circle or *node* represents an equation, while each directed *branch* stands for a a term obtained by multiplying the variable at the tail of the arrow by the constant shown on the arrow. The variable in the node is equal to the sum of all terms whose arrows point to the node. Each branch represents the way in which a disturbance is transmitted from one stage to another.

To be definite let us trace the effects of a positive disturbance w_3 in the concentration of a component in the feed to the third stage. The upset causes both the vapour and the liquid leaving stage 2 to have higher concentrations of the component. This causes the concentration on adjacent stages 2 and 4 to rise. Thus the liquid leaving stage 2 feeds the increase back to stage 3, as does the vapour from stage 4. The disturbance is in fact transmitted in both directions away from

the feed to all stages, which in turn feed corresponding increases back again. This is the phenomenon we shall call *natural feedback*.

The concept of feedback occupies a central position in automatic control theory, for *negative* feedback is often used to correct an input upset [7]. On the other hand natural feedback is *positive* and acutally aggravates any disturbance.

There are two basic mechanisms producing natural feedback. The kind of feedback already described arises from the countercurrent nature of the flow between stages. We shall refer to this type, which occurs in all countercurrent systems, as *countercurrent feedback*. In Fig. 1. the solid branches show the paths of countercurrent feedback. The other kind of feedback occurs only in systems with reflux. As the dashed line of Fig. 1 shows, an upset reaching the first stage disturbs the composition of the reflux, which in turn feeds an upset back to the first stage. This type of feedback will be called *reflux feedback*.

VOL. 16 1962

4. Matrix Representation

The set of linear equations (13) may be expressed more compactly in matrix form. Let the following matrices be defined:

$$\mathbf{A} \equiv \begin{pmatrix} (1-r) & -a_2 & 0 & 0 & \cdots & 0 & 0 & 0 \\ -b_2 & 1 & -a_3 & 0 & \cdots & 0 & 0 & 0 \\ 0 & -b_3 & 1 & -a_4 & \cdots & 0 & 0 & 0 \\ \cdot & \cdot & \cdot & \cdot & & \cdot & \cdot & \cdot \\ \cdot & \cdot & \cdot & \cdot & & \cdot & \cdot & \cdot \\ \cdot & \cdot & \cdot & \cdot & & \cdot & \cdot & \cdot \\ 0 & 0 & 0 & 0 & \cdots & -b_{n-1} & 1 & -a_n \\ 0 & 0 & 0 & 0 & \cdots & 0 & -b_n & 1 \end{pmatrix} \tag{14}$$

$$\mathbf{u} \equiv \begin{pmatrix} u_1 \\ \cdot \\ \cdot \\ \cdot \\ u_n \end{pmatrix} \tag{15}; \qquad \mathbf{w} \equiv \begin{pmatrix} w_1 \\ \cdot \\ \cdot \\ \cdot \\ w_n \end{pmatrix} \tag{16}$$

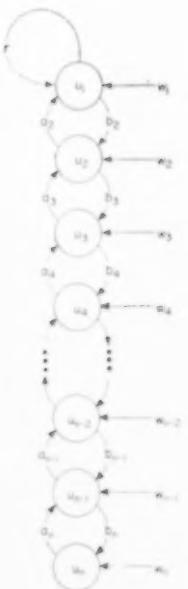

Fig. 1. Signal flow diagram for multistage system.

The matrix representation of equations (13) is

$$\mathbf{A}\,\mathbf{u} = \mathbf{w} \tag{17}$$

Since the matrix A is non-singular, or in other words, since the equations (13) are linearly independent, [2] there is always a matrix $\mathbf{A}^{-1}$, called the inverse of A, such that

$$\mathbf{u} = \mathbf{A}^{-1}\mathbf{w} \tag{18}$$

If $\mathbf{A}^{-1}$ is known it is a simple matter to express the deviations u_i explicitly in terms of the input deviations w_j, for if $\bar{a}_{ij}$ represents the element in the i^{th} row and j^{th} column of $\mathbf{A}^{-1}$, then equation (18) is equivalent to

$$u_i = \sum_{j=1}^{n} \bar{a}_{ij}\, w_j \quad \text{for } i = 1, 2, \ldots, n. \tag{19}$$

The significance of the elements $\bar{a}_{ij}$ of $\mathbf{A}^{-1}$ can be seen clearly by differentiating this equation with respect to a typical input deviation w_j:

$$\frac{\partial u_i}{\partial w_j} = \bar{a}_{ij} \tag{20}$$

Hence the inverse matrix $\mathbf{A}^{-1}$ gives us insight into the complicated relationship between inputs and outputs, for each element $\bar{a}_{ij}$ of $\mathbf{A}^{-1}$ may be viewed as the change in composition of the "liquid" leaving stage i resulting from a unit normalized deviation in the feed to stage j. The constant $\bar{a}_{ij}$ will be called the *gain* of input w_j at stage i. If the gain exceeds unity we say that the disturbance is *amplified*; otherwise we say it is *attenuated*. The $\bar{a}_{jj}$ are known as *self-amplifications*.

Before we can write the inverse $\mathbf{A}^{-1}$ compactly we must introduce two functions by recursive definitions. Let

$$d_j \equiv \begin{cases} 1 - r & \text{for } j = 1 \\ 1 - a_j b_j / d_{j-1} & \text{for } j = 2, 3, \ldots n \end{cases} \tag{21}$$

and

$$e_j \equiv \begin{cases} 1 & \text{for } j = n \\ 1 - a_{j+1} b_{j+1} / e_{j+1} & \text{for } j = 1, 2, \ldots, n-1 \end{cases} \tag{22}$$

In the next section we shall discuss these functions which are known as *approximants* [6] in detail. For now we wish only to use them in our compact representations of the inverse matrix $\mathbf{A}^{-1}$.

There will be two forms of $\mathbf{A}^{-1}$ presented, each giving a different insight into the behaviour of multistage systems. They will be known as the *right inverse* $\mathbf{A}_r^{-1}$ and the *left inverse* $\mathbf{A}_l^{-1}$.

The right inverse $\mathbf{A}_r^{-1}$ is

$$\begin{bmatrix} \frac{1}{d_1 + e_1 - 1}, & \frac{a_2}{d_1(d_2 + e_2 - 1)}, & \frac{a_2 a_3}{d_1 d_2 (d_3 + e_3 - 1)}, \cdots & \frac{a_2 \ldots a_n}{d_1 \ldots d_{n-1}(d_n + e_n - 1)} \\ \frac{b_2}{e_2(d_1 + e_1 - 1)}, & \frac{1}{d_2 + e_2 - 1}, & \frac{a_3}{e_2(d_3 + e_3 - 1)}, \cdots & \frac{a_3 \ldots a_n}{d_2 \ldots d_{n-1}(d_3 + e_n - 1)} \\ \frac{b_2 b_3}{e_2 e_3 (d_1 + e_1 - 1)}, & \frac{b_3}{e_3(d_2 + e_2 - 1)}, & \frac{1}{d_3 + e_3 - 1}, \cdots & \frac{a_4 \ldots a_n}{d_3 \ldots d_{n-1}(d_n + e_n - 1)} \\ \vdots & \vdots & \vdots & \vdots \\ \frac{b_2 \ldots b_n}{e_2 \ldots e_n (d_1 + e_1 - 1)}, & \frac{b_3 \ldots b_n}{e_3 \ldots e_n (d_2 + e_2 - 1)}, & \frac{b_4 \ldots b_n}{e_4 \ldots e_n (d_3 + e_3 - 1)}, \cdots, & \frac{1}{d_n + e_n - 1} \end{bmatrix} \tag{23}$$

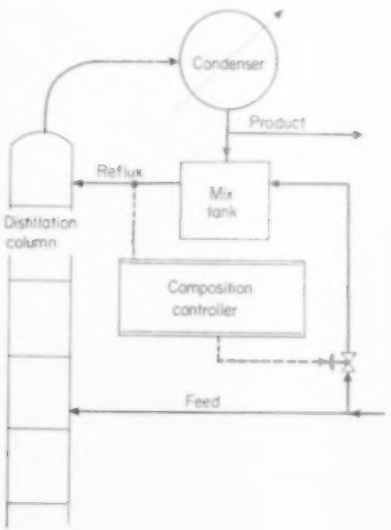

FIG. 2. A system for reducing reflux feedback.

The formulae for its typical elements $\bar{a}_{ij}(r)$ are

$$(d_j + e_n - 1)\,\bar{a}_{ij}(r) = \begin{cases} \prod_{k=i+1}^{n} a_k / d_{k-1} & \text{if } i < j \quad (24a) \\ 1 & \text{if } i = j \quad (24b) \\ \prod_{k=j+1}^{n} b_k / e_k & \text{if } i > j \quad (24c) \end{cases}$$

It can be verified by direct matrix multiplication that $\mathbf{A}_r^{-1}$ is a *right inverse* of $\mathbf{A}$, that is,

$$\mathbf{A}\,\mathbf{A}_r^{-1} = \mathbf{I}, \tag{25}$$

where $\mathbf{I}$ is the n by n unit matrix [2, 4]. However, it is not easy to verify by direct multiplication that $\mathbf{A}_r^{-1}$ and $\mathbf{A}$ are permutable, i.e. that the order of matrix multiplication can be reversed so that

$$\mathbf{A}_r^{-1}\,\mathbf{A} = \mathbf{I} \tag{26}$$

This is why we call $\mathbf{A}_r^{-1}$ the *right inverse*. How-

ever, it is well known [4] that since A is nonsingular, any right inverse satisfying (25) must also satisfy (26) and so we do not need to prove (26) by direct multiplication.

The left inverse matrix $\mathbf{A}_l^{-1}$ is

$$\begin{bmatrix} \frac{1}{d_1+e_1-1}, & \frac{a_2}{e_2(d_1+e_1-1)}, & \frac{a_2a_3}{e_2e_3(d_1+e_1-1)} \cdots, & \frac{a_2\ldots a_n}{e_2\ldots e_n(d_1+e_1-1)} \\ \frac{b_2}{d_1(d_2+e_2-1)}, & \frac{1}{d_2+e_2-1}, & \frac{a_3}{e_3(d_2+e_2-1)} \cdots, & \frac{a_3\ldots a_n}{e_3\ldots e_n(d_2+e_2-1)} \\ \frac{b_2b_3}{d_1d_2(d_3+e_3-1)}, & \frac{b_3}{d_2(d_3+e_3-1)}, & \frac{1}{d_3+e_3-1} \cdots, & \frac{a_4\ldots a_n}{e_4\ldots e_n(d_3+e_3-1)} \\ \vdots & \vdots & \vdots & \vdots \\ \frac{b_2\ldots b_n}{d_1\ldots d_{n-1}(d_n+e_n-1)}, & \frac{b_3\ldots b_n}{d_2\ldots d_{n-1}(d_n+e_n-1)}, & \frac{b_4\ldots b_n}{d_3\ldots d_{n-1}(d_n+e_n-1)} \cdots, & \frac{1}{d_n+e_n-1} \end{bmatrix} \quad (27)$$

The formulae for its typical elements $\bar{a}_{ij}(l)$ are

$$(d_i+e_i-1)\bar{a}_{ij}(l) = \begin{cases} \prod_{k=i+1}^{n} a_k/e_k & \text{if } i<j \quad (28a) \\ 1 & \text{if } i=j \quad (28b) \\ \prod_{k=j+1}^{n} b_k/d_{k-1} & \text{if } i>j \quad (28c) \end{cases}$$

It is easily verified by direct multiplication that $\mathbf{A}_{l-1}$ is a left inverse of A, i.e.

$$\mathbf{A}_l^{-1}\mathbf{A} = \mathbf{I} \quad (29)$$

By the reasoning we used with $\mathbf{A}_r^{-1}$ it happens that $\mathbf{A}_l^{-1}$ is also a right inverse. In fact, the uniqueness of the inverse of any non-singular matrix establishes that

$$\mathbf{A}_r^{-1} = \mathbf{A}_l^{-1} = \mathbf{A}^{-1} \quad (30)$$

The left inverse $\mathbf{A}_l^{-1}$ is the more convenient form for direct computation of the u_i for a given set of w_j. Substitution of the $\bar{a}_{ij}(l)$ into Equation (19) gives

$$u_i = \frac{1}{d_i+e_i-1}\left[\sum_{j=1}^{i-1} w_j \prod_{k=j+1}^{i}\frac{b_k}{d_{k-1}} + w_i + \sum_{j=i+1}^{n} w_j \prod_{k=i+1}^{n}\frac{a_k}{e_k}\right] \quad (31)$$

In this section we have exhibited two forms of the inverse matrix $\mathbf{A}^{-1}$ and given a formula relating the liquid composition deviation at any stage to the set of input composition deviations. These formulae can be used to predict the effects of a small but constant composition change in the feed to an existing multistage system. They may also be employed to investigate the sensitivity of a design to the quality of the feed specified. If the disturbances are of a random character, but occur so slowly that the system has time to adjust to them as they take place, the standard deviation σ_i of each response u_i can be related to the standard deviation τ_j of the upsets w_j and the correlation coefficients ρ_{jk} for each pair of upsets w_j and w_k by well known statistical relations [8] to obtain

$$\sigma_i^2 = \sum_{j=1}^{n}\sum_{k=1}^{n} \rho_{jk}\bar{a}_{ij}\bar{a}_{ik}\sigma_j\sigma_k \quad (32)$$

In order to gain a better understanding of multistage systems we shall seek now to extract simple qualitative principles from the complicated equations derived so far.

5. The Constants a, b, and r

In this section the constants a_i, b_i, and r will be studied. For the sake of initial simplicity we consider first a constant liquid molal overflow system [1] with the value of β_i the same for all stages. Realizing that these assumptions are gross oversimplifications we shall eventually discard them in favour of less restrictive ones. But for the time being let us assume that

$$V_i + V_i^- = V_{i+1} + V_i^+ \quad (33)$$

and

$$L_i + L_i^- = L_{i-1} + L_i^+ \tag{34}$$

Any stage i having neither feed streams nor side streams will be such that

$$V_i^- = V_i^+ = L_i^- = L_i^+ = 0 \tag{35}$$

In this situation Equations (33), (34) and (35), together with definitions (7) and (8) give

$$a_i + b_i = 1 \tag{36}$$

Furthermore, if no stage i has a feed stream or a side stream for $i_1 \leqslant i \leqslant i_2$, then

$$a_i = a_j \tag{37}$$

and

$$b_i = b_j \text{ for all } i_1 \leqslant i,\ j \leqslant i_2 \tag{38}$$

Next consider a stage f which has a feed stream but no side stream, meaning that

$$V_f^- = L_f^- = 0.$$

For purposes of comparison we assume that stages $f-2$, $f-1$, $f+1$ and $f+2$ have neither feed streams nor side streams. Then

$$a_f \equiv \frac{\beta V_f}{L_f^- + \beta V_{f-1}} = \frac{\beta V_{f-1}}{L_{f-2} + \beta V_{f-2}} \equiv a_{f-1}$$

$$a_{f+2} \equiv \frac{\beta V_{f+2}}{L_{f+1} + \beta V_{+1}} =$$

$$= \frac{\beta V_{f+1}}{L_f + \beta (V_f - V_f^+)} > \frac{\beta V_{f-1}}{L_f + \beta V_f} \equiv a_{f+1}$$

$$a_{f+2} = \frac{\beta (V_f - V_f^+)}{L_{f-1} + L_f^- + \beta V_{f-1}} < \frac{\beta V_f}{L_{f-1} + \beta V_{f-1}} \equiv a_f$$

In summary,

$$a_{f-1} = a_f > a_{f+2} = a_{f+3} > a_{f-1} \tag{39}$$

Also

$$b_f \equiv \frac{L_{f-1}}{L_f + \beta V_f} =$$

$$= \frac{L_{f-2}}{L_{f-1} + L_f^+ + \beta V_f^-} < \frac{L_{f-2}}{L_{f-1} + \beta V_{f-1}} \equiv b_{f-1}$$

$$b_{f+1} \equiv \frac{L_f}{L_{f+1} + \beta V_{f+1}} =$$

$$= \frac{L_{f+2} + L_f^+}{L_{f-2} + L_f^+ + \beta (V_{f-2} - V_f^+)} >$$

$$> \frac{L_{f-2}}{L_{f-2} + \beta V_{f-2}} \equiv b_{f-1}$$

$$b_{f+1} \equiv \frac{L_f}{L_{f+1} + \beta V_{f+1}} = \frac{L_{f+1}}{L_{f+2} + \beta V_{f+2}} \equiv b_{f+2}$$

In summary,

$$b_{f+2} = b_{f+1} > b_{f-1} = b_{f-2} > b \tag{40}$$

It is easy to show that

$$a_{f-1} + b_{f-1} = a_{f+2} + b_{+2} = 1 \tag{41}$$

However,

$$a_f + b_f < a_{f+1} + b_{f-1} = 1 \tag{42}$$

and

$$a_{f+1} + b_{f+1} < a_{f+2} + b_{f+2} = 1 \tag{43}$$

Suppose now that s is a stage having a side stream but no feed stream, while stages $s-2$, $s-1$ and $s+2$ have neither. The analysis of this situation takes the same form and it is easy to see that all of the inequalities reverse. That is,

$$a_{s-1} = a_s > a_{s+2} = a_{s+3} > a_{s+1}, \tag{44}$$

$$a_{s+2} = b_{s+1} > b_{s-1} = b_{s-2} > b_s, \tag{45}$$

$$a_{s-1} + b_{s-1} = a_{s+2} + b_{s+2} = 1 \tag{46}$$

$$a_s + b_s > 1, \tag{47}$$

and

$$a_{s+1} + b_{s+1} > 1. \tag{48}$$

It remains to investigate the constant r. Equation (12), which defines r, shows that

$$0 < r < 1.$$

We shall need to decrease the upper bound on r. To do this, we examine the reciprocal of r.

$$\frac{1}{r} = \frac{1}{\beta_1} + \frac{V_1^-}{L_1} + \frac{L_1^-}{L_1} + 1 \tag{49}$$

Notice that the ratio V_1^-/L_1 is the reciprocal of the *reflux ratio* [1]. Equation (49) implies that if

$$\beta_1 \leqslant 1, \tag{50a}$$

then

$$r \leqslant 1/2, \tag{50b}$$

even at total reflux. On the other hand, even if β_1 exceeds unity it will not be much larger than unity in most practical situations, and the term V_1^-/L_1 will usually be large enough to make the right-hand side of (49) at least equal to 2. Hence the conclusion (50b) will be true most of the time,

even when the sufficient condition (50a) does not hold.

6. The Regularity Hypotheses

Certain relations true for the constant molal overflow system with constant β that we have just studied would seem to be true for more general systems. Rather than restrict our analysis to the over-simplified model of the previous section we adopt the following basic postulates, which we shall call *regularity hypotheses*.

A $\quad a_i + b_i \leqslant 1 \qquad$ for all i.

B $\quad r \leqslant \frac{1}{2}$

VOL. 16 1962

Systems for which the regularity hypotheses hold will be called *regular systems*.

The regularity hypotheses may be viewed as simplifying assumptions upon which rigorous proofs of certain interesting properties of multistage systems can be based. We feel that the conclusions drawn from these hypotheses will be valid in practice even when the hypotheses themselves do not strictly hold. Since this is merely a conjecture it may be possible to find a system behaving at variance with our conclusions. We only claim that such a system cannot be regular.

In justification of the regularity hypotheses we point out that in a constant molal overflow system hypothesis A is violated only in the neighbourhood of side streams as equations (36), (42), (43), (47) and (48) have shown. Even in systems with changing overflow the sum $a_i + b_i$ should not deviate from unity by a very large amount. Hypothesis B is merely equation (50b), which we have already justified in Section 5.

The following four conclusions concerning regular systems will be deduced from the regularity hypotheses in the subsequent sections.

(1) Every gain $\bar{a}_{ij}$ is positive.

(2) The self-amplifications $\bar{a}_{jj}$ always exceed unity.

(3) The self-amplifications can reach, but not exceed, $2(n - j + 1)$.

(4) If a stage is added to a system otherwise unchanged all gains will increase.

7. The Approximants d_i and e_i

Now that the ranges of a_i, b_i and r have been circumscribed by the two regularity hypotheses we can turn to the study of d_i and e_i. In order to see the form of these functions more clearly let us expand e_i in terms of the relevant constants a_i, b_i and r, using definition (21).

$$e_i \equiv 1 - \cfrac{a_{i+1}\,b_{i+1}}{1 - \cfrac{a_{i+2}\,b_{i+2}}{1 - \cfrac{}{\ddots \; - \cfrac{a_{n-1}\,b_{n-1}}{1 - a_n b_n}}}}$$

An expression of this form is known as a *continued fraction* f_i when n is infinite; if n is finite e_i is called the n^{th} *approximant* or *convergent* of the full continued fraction f_i. This is the terminology used in Wall's comprehensive work on continued fractions [6]. Although Campbell [5] refers to the approximants as "continued fractions" we prefer to retain the distinction between the finite approximants and the infinite continued fraction.

The f_i are actually special kinds of continued fraction known as "J-fractions." The "J" apparently reflects the fact that tridiagonal matrices such as A, from which the J-fractions are obtained, are called *Jacobi matrices* [3]. In order to prove that our functions e_i converge we make use of a theorem of Paydon and Wall [6, 9] which is a stronger form of a century-old theorem due to Worpitzky (see Wall [6]). In our context the Paydon–Wall theorem is:

Let a_i and b_i be functions of any variables over a domain D in which

$$|a_i b_i| \leqslant c\,(1 - c) \qquad \text{for all } i, \tag{51}$$

where $0 \leqslant c \leqslant \frac{1}{2}$. Then the values z of the continued fraction f_i and its approximants are in the domain

$$\left| \frac{1}{z} - \frac{1}{1 - c^2} \right| \leqslant \frac{c}{1 - c^2} \tag{52}$$

Wall also shows [6] that

$$f_i = \tfrac{1}{2} \tag{53}$$

if and only if

$$a_i b_i = \tfrac{1}{4} \quad \text{for all } i. \tag{54}$$

Hypothesis A, which guarantees that $0 \leqslant c \leqslant \frac{1}{2}$, together with the Paydon–Wall Theorem, equations (53) and (54) and the finiteness of n imply that

$$e_i > \tfrac{1}{2} \tag{55}$$

The least upper bound for e_i is obtained by letting $a_{i+1} b_{i+1}$ approach zero, giving

$$e_i < 1 \quad \text{for } i > 1 \tag{56}$$

The approximants d_i present a problem because the last divisor is $1 - r$ rather than 1. To see this, expand d_i. This difficulty is circumvented by regularity hypothesis B, which, together with the non-negativity of r, implies that

$$\tfrac{1}{2} \leqslant (1 - r) \equiv d_1 \leqslant 1 \tag{57}$$

Hence the quantity $1 - r$ lies in the same range as any continued fraction or approximant satisfying the Paydon–Wall Theorem. We may therefore express $1 - r$ as a continued fraction or approximant. When this is done d_i becomes a continued fraction or approximant satisfying the Paydon–Wall Theorem, so that

$$\tfrac{1}{2} < d_i < 1 \quad \text{for } i > 1. \tag{58}$$

By combining equations (24b), (55), (56) and (58) we obtain

$$1 < \bar{a}_{jj} \equiv \frac{1}{d_j + o_j - 1} \quad \text{for all } j. \tag{59}$$

Since the constants a_i, b_i, d_i and e_i have all been proven positive we see that

$$\bar{a}_{ij} > 0 \quad \text{for all } i, j. \tag{60}$$

This inequality contains conclusion (1) namely, that all gains in a regular system are positive. Conclusion (2), that the self-amplification always exceeds unity, is expressed in equation (59).

Let us now prove conclusion (3), which establishes the following least upper bound for the auto-amplification:

$$\bar{a}_{jj} \leqslant 2\,(n - j + 1). \tag{61}$$

To do this we must prove that

$$e_j \geqslant \frac{n - j + 2}{2\,(n - j + 1)} \tag{62}$$

using mathematical induction on $(n - j)$. To begin, notice that equation (62) is trivially true when $n = j$, by definition (21). Before carrying out the induction we remark that since $a_j b_j$ cannot exceed $\frac{1}{4}$, it follows that

$$e_{j-1} \geqslant 1 - \frac{1}{4e_j} = \frac{4e_j - 1}{4e_j}$$

Then taking equation (62) as the induction hypothesis,

$$e_{j-1} \geqslant \frac{2\,(n - j + 2) - (n - j + 1)}{2\,(n - j + 2)} = \frac{n - (j - 1) + 2}{2\,[n - (j - 1) + 1]},$$

for all j. This completes the induction and establishes the truth of equation (62). Equation (61) follows when the inequalities (57) and (62) are substituted into equation (24b), establishing conclusion (4).

The harmful effect of natural feedback is shown clearly by conclusions (2) and (3). If there were no natural feedback the self-amplification at the disturbance would be exactly unity, and the upset would not be communicated to any other stage. However, in a real system a feed composition disturbance upsets the composition at every stage. Through natural feedback these secondary effects are returned to the feed stage, bringing about an amplification which can become quite large.

8. Addition of a Stage

Consider now the consequences of adding a stage to a regular system. One would expect this to increase the natural countercurrent feedback everywhere in the system and produce higher response coefficients at every stage. We shall show this to be true for any regular system [conclusion (4)].

First we shall examine the effect of an additional stage at the unrefluxed end of the system. Since the constants a_i, b_i, r and hence the constants d_i, are unchanged by this additional stage it is enough to investigate the changes in the self-amplifications $\bar{a}_{jj}$. By showing that the $\bar{a}_{jj}$

always increase we prove that all of the response coefficients must increase, by equations (24a) and (28c). Equation (24b), giving $\bar{a}_{jj}$ as a function of both d_j and e_j, is not convenient for proving this, and it is necessary to express $\bar{a}_{jj}$ entirely in terms of constants d_i. To do this we construct an inverse matrix $\mathbf{A}_d^{-1}$ whose off-diagonal coefficients do not contain any of the e_i. These off-diagonal elements $\bar{a}_{ij}(d)$ are given in terms of the diagonal elements $\bar{a}_{jj}$ by the following combination of equations (24a), (24b), (28b) and (28c).

$$\bar{a}_{ij}(d) = \begin{cases} \bar{a}_{jj} \prod_{k=i+1}^{n} a_k/d_{k-1} & \text{if } i < j \qquad (63a) \\ \bar{a}_{j+1,j+1} \prod_{k=j+1}^{n} b_k/d_{k-1} & \text{if } i > j \qquad (63b) \end{cases}$$

By taking the inner product [4] of the j^{th} row of the matrix $\mathbf{A}$ with the j^{th} column of $\mathbf{A}_d^{-1}$, setting it equal to unity, and rearranging, one obtains the following recurrence relation:

$$\bar{a}_{jj}(d) = \frac{(1 + a_{j-1} b_{j+1} \bar{a}_{j+1,j+1}/d_j)}{d_j}$$

with

$$\bar{a}_{nn} = \frac{1}{d_n}.$$

From this it can be shown by induction that

$$\bar{a}_{jj} = \frac{1 + \sum_{k=1+1}^{n-j} \prod_{l=j+1}^{k} a_l b_l/d_{l-1}d_l}{d_j}$$

We see that $\bar{a}_{jj}$ can indeed by expressed without using any e_i.

Suppose that a new stage, numbered $n+1$, is attached to the unrefluxed end of the system. Then $\bar{a}_{jj}'$, the self-amplification at stage j for the augumented system, is given by

$$\bar{a}_{jj}' = \frac{1 + \sum_{k=1+1}^{n+1-j} \prod_{l=j+1}^{k} a_l b_l/d_{l-1}d_l}{d_j}$$

$$= \frac{\bar{a}_{jj} + \left(\prod_{l=j+1}^{n+1-j} a_l b_l/d_{l-1}d_l \right)}{d_j}$$

Since the second term of this equation is a product of positive factors it follows that

$$\bar{a}_{jj}' > \bar{a}_{jj} \quad \text{for all } 1 \leqslant j \leqslant n. \qquad (64)$$

Hence every self-amplification is increased when a stage is added at the unrefluxed end. Furthermore, by equations (63a) and (63b), all of the response coefficients $\bar{a}_{ij}$ must also increase.

By similar methods it is possible to prove that addition of a stage at the refluxed end also brings about an increase in all of the coefficients of the inverse matrix $\mathbf{A}^{-1}$. The proof requires expressing the $\bar{a}_{jj}$ only in terms of constants a_i, b_i and e_i and then comparing the augmented system with the original system as before. The only complication arises from the fact that all indices advance one unit when a stage is added at the refluxed end. When this is taken into account, the proof goes through as before and will be omitted here. This completes the proof of conclusion (4), which again illustrates the harmful effect of natural feedback.

9. Reflux Feedback

In Section 3, we distinguished between *countercurrent feedback*, present in all multistage systems, and *reflux feedback*, found only in refluxed systems. Since Fig. 1 shows reflux feedback to be positive it might be expected always to have a deleterious effect on the system response. We wish now to examine reflux feedback to see just how bad this effect is.

Consider two systems with identical interstage flows so that they both have the same constants a_i and b_i. However, one system is refluxed while the other is not. This means that the reflux constant r is positive in the former system but zero in the latter. Let the response coefficients in the unrefluxed system be denoted by $\bar{a}_{ij}^{\circ}$ to distinguish them from the $\bar{a}_{ij}$ of the refluxed system. By definition (21) and equations (28a) and (28b) we obtain the following comparison of first stage response in the two systems:

$$\frac{\bar{a}_{1j}}{\bar{a}_{1j}^{\circ}} = \frac{e_1}{(e_1 - r)} \quad \text{for all } 1 \leqslant j \leqslant n. \qquad (65)$$

By hypothesis C and inequality (55), this ratio, never less than unity, can become arbitrarily large at high reflux ratios, although it will remain finite for a finite system. Hence the response at

the first stage can be magnified enormously by reflux feedback no matter where the original disturbance occurs. Similarly, by equation (24c),

$$\frac{a_{i1}}{a_{11}} = \frac{e_1}{(e_1 - r)} \quad \text{for all } 1 < i \leqslant n. \qquad (66)$$

This shows that when the original upset is at the first stage reflux feedback can cause very large responses throughout the system.

The effects of reflux feedback on the other response coefficients are more complicated and we will not investigate them further. However, it is clear from our analysis that in many situations it would be desirable to reduce reflux feedback. In the next section we suggest how this might be accomplished even in a refluxed system.

10. Reduction of reflux feedback

Reflux feedback could be eliminated entirely if it were possible to hold the reflux composition constant in spite of changes in the overhead composition. In a conventional system this is clearly impossible since the reflux is taken directly from the overhead stream.

Suppose, however, that the reflux is a mixture of overhead blended with a small amount of some other material. In principle at least it would be possible to hold the composition of this reflux blend constant and eliminate reflux feedback entirely. Fig. 2 is a schematic diagram of a system for reducing reflux feedback. The controller adjusts the rate at which feed material is mixed with overhead in the well-agitated mix tank in order to hold the blend composition constant. This blend is used as reflux. Notice that such a system can control the fraction of only one of the components at a time, since only two streams are being blended. This limited degree of control may be enough, however, if there is only one component highly sensitive to reflux feedback.

The conventional way of controlling overhead composition is to adjust the reflux ratio, which in turn changes all of the flow rates in the system. Although we have not analysed the secondary effects of these changes it would seem desirable to keep such changes as small as possible. The main advantage of our proposal for reducing reflux feedback is that alterations in the reflux ratio, and hence secondary flow upsets, could be markedly reduced.

On the other hand, there would be a disadvantage to this plan, even if it worked. The reflux would always have a lower quality on the average than in an ordinary system, since a small amount of low grade material would have to be added continuously to the reflux to allow its composition to be controlled. This could require additional stages, especially when the separation is difficult.

11. Reduction of countercurrent feedback

In the preceding section we suggested a method for reducing reflux feedback. The idea of holding composition constant could be applied to any stream. Hence it is possible also to reduce counter-current feedback in this way. The signal flow graph for a system with such a composition controlling device would resemble Fig. 1, except that the branch corresponding to the controlled composition would be removed.

It would of course be more practical to apply this approach to liquid than vapour streams. In a distillation column the most effective composition to control is that of the liquid stream nearest the top, that is, the reflux composition. In leaching, washing and liquid–liquid extraction systems where all of the streams are liquid the signal flow diagram shows that it would be better to control the composition as near as possible to the source of the disturbance. Ideally, the most effective location would be the feed itself, since if the feed composition were constant, there would be no disturbances at all.

12. Concluding summary

A theoretical analysis of the operating characteristics of multistage systems has been undertaken. As a beginning the response of such systems to small changes in steady state feed composition was studied by means of matrix algebra and the theory of continued fractions. The concepts of *natural feedback* and *gain* were introduced, and quantitative expressions for this latter quantity were derived in terms of parameters measurable in the operating system. These *gains* are useful for predicting the effects of

changes in feed on the performance of the system.

The rather complicated gain expressions were analysed further for *regular* systems, defined to be those satisfying two simplifying assumptions known as *regularity hypotheses*. Although the regularity hypotheses were justified on the behaviour of constant liquid molal overflow systems the hypotheses can be applied to almost all practical multistage systems. Four conclusions about gain in regular systems were drawn, namely:

(1) Every gain is positive.

(2) A feed upset is always amplified at the feed stage. This is called auto-amplification.

(3) The auto-amplification at a stage can attain, but not exceed, twice the number of stages from the disturbance to the nearest unrefluxed end, counting the feed stage.

(4) All gains increase when a stage is added to a system otherwise unchanged.

All of these conslusions illustrated the harmful character of natural feedback. A system for reducing natural feedback by holding the reflux composition constant was suggested. Since the proposal involves blending feed with the overhead to control the reflux composition, the improved system control may often be offset by a need for more stages. The plan needs further study.

Research based on this mathematical model is continuing. A study of the response to an impulse input has just been completed and is now being prepared for publication.

References

[1] Robinson C. S. and Gilliland R. R. *Elements of Fractional Distillation*. McGraw-Hill, New York, 1950.

[2] Acrivos A. and Amundson N. R. *Industr. Engng. Chem.* 1955 **47** 1533.

[3] Gantmacher F. R. *Application of the Theory of Matrices*, p. 119 Interscience, New York 1959.

[4] Frazer R. A., Duncan W. J. and Collar A. R. *Elementary Matrices*. Cambridge University Press 1957.

[5] Campbell Donald P. *Process Dynamics* pp. 240–244. John Wiley, New York 1958.

[6] Wall H. S. *Analytic Theory of Continued Fractions*. Van Nostrand, New York 1948.

[7] Tsien H. S. *Engineering Cybernetics*. McGraw-Hill, New York 1954.

[8] Feller W. *An Introduction to Probability Theory—I* p. 216. John Wiley, New York 1957.

[9] Paydon J. F. and Wall H. S. *Duke Math. J.* 1942 **9** 360.

Chemical Engineering Science, 1961, Vol. 16, pp. 364 to 371. Pergamon Press Ltd., London. Printed in Great Britain.

Fluidized-solids reactors with continuous solids feed—I

Residence time of particles in fluidized beds

SAKAE YAGI and DAIZO KUNII
Department of Chemical Engineering, University of Tokyo, Tokyo, Japan

(*Received* 6 *April* 1960; *in revised form* 4 *January* 1961)

Abstract—The distribution of residence times of solid particles is examined in fluidized beds at steady state with continuous feed and discharge of solids, both for beds consisting of a single particle size and for beds consisting of a wide spectrum of particle sizes.

The mean age (residence time in bed) of particles of a given size in the overflow and carryover streams is found in all cases to be given by

$$\bar{\theta} = \frac{1}{(F_1/W)\,\phi + \kappa}$$

where F_1 is the mass flow rate of overflow stream, W is the weight of solids in the bed, ϕ is the ratio of the size distribution function of overflow particles to that within the bed and κ is the elutriation velocity constant of particles whose mean age is being considered.

The constant ϕ is a measure of the degree of vertical segregation of particles within the bed. In most practical situation the bed may be considered to be not segregated, in which case ϕ can be taken to be unity.

For significant carryover of solids the elutriation velocity constant κ controls in determining the average length of stay of particles in the fluidized bed. In all cases the mean age of particles of a given size is the same in both the overflow and carryover streams.

Résumé—La distribution des temps de séjour de particules solides est examiné dans des lits fluidisés en état stationnaire avec une alimentation continue et un soutirage des solides, tous deux pour des lits comportant une seule dimension de particule d'une part et pour des lits se composant d'un large éventail de dimensions de particules d'autre part.

L'âge moyen (temps de séjour dans le lit) des particules d'une dimension donnée dans le trop-plein est donnée dans tous les cas par:

$$\bar{\theta} = \frac{1}{(F_1/W)\,\phi + \kappa}$$

où F_1 est la vitesse du débit massique du trop-plein, W est le poids de solide dans le lit, ϕ est le rapport de la fonction de distribution des dimensions des particules du trop-plein à celle relative aux particules intérieures au lit et κ est la constante de vitesse d'élutriation des particules dont l'âge moyen est pris en considération.

La constante ϕ mesure le degré de sélection verticale des particules à l'intérieur du lit. Dans la plupart des cas le lit peut être considéré comme non sélectif et ϕ est pris égal à l'unité.

Pour des entraînements de solides importants la constante de vitesse d'élutriation κ détermine la durée moyenne de séjour des particules dans le lit fluidisé. Dans tous les cas l'âge moyen des particules d'une dimension donnée est le même dans les courants de trop-plein et d'entraînement.

Zusammenfassung—Die Verweilzeitverteilung von Festoffpartikeln in Wirbelschichten wurde untersucht bei kontinuierlicher Zugabe und Abnahme von Feststoffteilchen sowohl in Schichten mit einhitlicher Teilchengrösse als auch in solchen mit einemw eiten Spektrum von Teilchengrössen.

Das mittlere Alter (Verweilzeit in der Schicht) der Teilchen mit gegebener Grösse im Austrag oder Überlauf kann in allen Fällen ausgedrückt werden durch

$$\bar{\theta} = \frac{1}{(F_1/W)\,\phi + \kappa}$$

wobei F_1 der Durchsatz in Überlaufstrom ist, W ist das Gewicht der Feststoffteilchen in der Wirbelschicht, ϕ ist das Verhältnis der Grössenverteilsungsfunktion der Teilchen im Überlauf zu der in der Schicht, und κ ist die Austragsgeschwindigkeitskonstante der Teilchen, deren

mittleres Alter betrachtet wird. Die Konstante ϕ ist ein Mass für den Grad der vertikalen Segregation der Teilchen im Wirbelbett. In den meisten praktischen Fällen darf man annehmen, dass keine Segregation vorgleigt, wodurch $\phi = 1$ wird. Bei bedeutendem Austrag von Feststoffteilchen bestimmt die Austragsgeschwindigkeitskonstante κ die mittlere Verweilzeit der Teilchen im Wirbelbett. In allen Fällen war das mittlere Alter der Teilchen einer bestimmten Grösse ebensogross in Überlauf wie im Austrag.

VOL. 16 1962

Introduction

The industrial exploitation of a gas–solid reaction by the fluidized-solids technique necessarily requires the extrapolation of the data obtained in small scale laboratory equipment to the larger pilot plant and commercial units.

For continuous operation solids are fed continuously to the fluidized bed and are likewise discharged either through an overflow pipe or by entrainment in the gases. Now the length of stay of particles in the bed determines the extent of reaction of the solids with the gas. However, the length of stay or residence time in the fluidized bed varies from particle to particle. For example some particles are discharged immediately after feeding, while others are discharged only after remaining in the bed for a long time. Hence for the prediction of the extent of chemical reaction it becomes imperative to know the distribution of residence times of the particles in the reactor.

It is this problem, the analysis of the residence time distribution in a fluidized bed, which is to be studied here, both for fluidized beds with uniform particle size and with a wide distribution of particle sizes.

Exit Age-distribution Function and average residence time of Particles of Uniform Size

The residence times within the bed will vary from particle to particle, and knowledge of this distribution of residence times is needed in the calculation of extent of reaction. To find this consider the model of the fluidized bed operated at steady state in which the number of particles fed into the bed within the short time interval $d\theta$ between some definite time θ and $\theta + d\theta$, is $n_0 d\theta$. After an elapsed time θ_p from the instant of feeding of the above particles some particles among them are discharged during the short time interval $d\theta_p$. The number of these particles discharged within $d\theta_p$ is given by [1, 2]

$$(n_0 d\theta) E_1(\theta_p) d\theta_p \qquad (1)$$

where $E_1(\theta_p)$ is defined as " the exit age distribution function for overflow particles."

In fluidized beds it seems reasonable to assume complete mixing for particles with the same diameter, because the average residence time of particles is usually much longer than the time necessary for the mixing of particles after feeding.

Applying the above assumption, the exit age distribution function $E_1(\theta_p)$ is given by [1–3].

$$E_1(\theta_p) = (1/\bar{\theta}) \exp(-\theta_p/\bar{\theta}) \qquad (2)$$

where $\bar{\theta}$ represents the average residence time of particles based upon the number of particles, or

$$\bar{\theta} = N/n_0 = W/F_1 \qquad (3)$$

For particles with comparatively narrow size distribution equation (2) is also applicable, if the following conditions are satisfied:

(a) no carryover particles
(b) complete mixing of the particles.

Measurements of the exit Age-distribution Function for overflow particles

In order to verify the adequacy of equation (2) the exit age distribution function should be measured for overflow particles. The inner diameter of the experimental equipment was 7 cm and the particles were fluidized by air. A summary of both the equipment and operating conditions are shown in Fig. 1 and Table 1. In Fig. 1 the solids were fed continuously to the pneumatic conveying line through the small fluidized feeder and charged into the bottom of the fluidized bed. Particles were discharged at a steady state from the bed through an overflow tube. Besides the main particles sands or coke particles were used as tracer in these experiments. These were chosen because their terminal velocities were practically identical to those of the main particles.

Table 1. *Experimental conditions for measurement of exit age-distribution function for overflow particles* [2]

Particles applied	sand, 50–70 mesh zinc blende, 100–150 mesh
Height of fluidized bed	4·0–10·0 cm
Feed rate of particles	4·8–16·8 cm³/min
Average residence time	6·9–19·8 min
Air velocity, u_g	15·6–35·0 cm/sec
u_g/u_m	0·16–0·23*

*u_m is the terminal velocity of main particles.

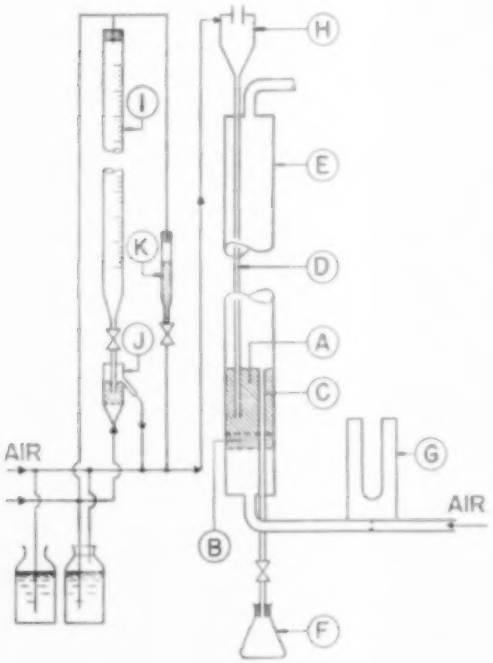

FIG. 1. Experimental apparatus for measurement of exit age-distribution function of overflow particles [2].

A. Fluidized bed. B. Fixed bed as distributor. C. Overflow tube. D. Feed tube. E. Glass tube, I.D. 7 cm. F. Receiver. G. Flowmeter. H. Cyclone collector. I. Hopper of particles. J. Feeder with fluidized bed. K. Tracer particles.

About 6 cm³ of such tracer particles were kept in a small hopper *K* (Fig. 1) and were fed suddenly into the pneumatic line at almost the same feed rate as the main particles. During the short period of feeding of tracer particles the charging of the main particles was stopped automatically and then as soon as the tracer particles were gone the feeding of the main partiles was resumed. Fig. 1 shows the flow-line connexions which were used to assure steady flow of solids through the pneumatic lines immediately after injections of solids [2].

Letting time be measured from the instant of tracer injection, or $\theta_p = 0$, the overflow particles discharged during the short time interval $\Delta\theta_p$ were collected after an elapsed time θ_p. According to the definition the exit age distribution function overflow particles $E_1(\theta_p)$ can be calculated as follows:

$$E_1(\theta_p) = (\Delta Q/Q)/\Delta\theta_p \qquad (4)$$

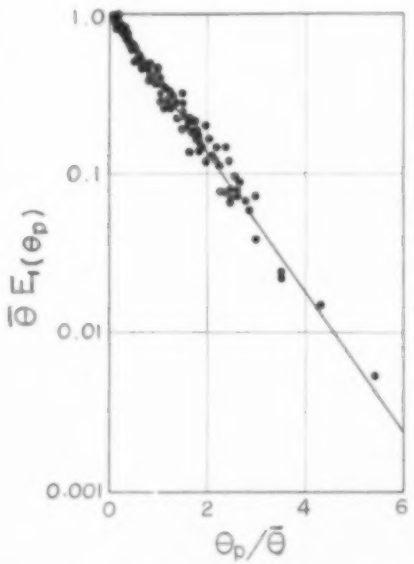

FIG. 2. Comparison of experimental data of $E_1(\theta_p)$ with theoretical equation (2), Ref. [2].

In Fig. 2, all data of $E_1(\theta_p)$ were compared with the theoretical line of equation (2). Close agreement between theory and experiment justifies the assumption of complete mixing of particles in the fluidized bed. Later KAMIYA [4] made similar experiments using particles of $K_2Cr_2O_7$ as the tracer. The amount of tracer in the exit stream was measured by dissolving in water and analys-

ing. KAMIYA's results agreed well with the theoretical line in Fig. 2, serving further to verify the assumption of complete mixing of particles.

ELUTRIATION OF SMALL PARTICLES FROM FLUIDIZED BEDS

When particles with a wide size distribution are fed into fluidized bed in a steady state small particles having terminal velocities less than the superficial gas velocity are elutriated as carryover particles from the fluidized bed. In this case, it is necessary to know the residence times of all sizes of particles in the fluidized bed, especially when high average conversion of product is required. It is incorrect to assume that all small particles which have terminal velocities less than the superficial gas velocity are entrained instantly after their feeding into the fluidized bed. In practice, such small particles are entrained only after staying for comparatively long periods in the bed, these residence times being ample to effect physical or chemical changes in the particles. In connexion with this LEVA [5] made the first experimental work on batch type elutriation.

VOL. 16 1962

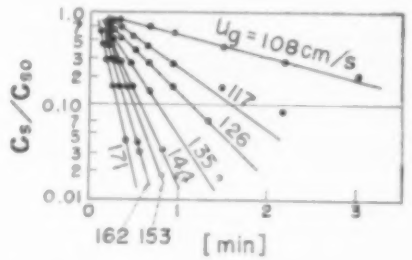

FIG. 3. Examples of experimental data of elutriation velocity constant by YAGI and AOCHI [6].

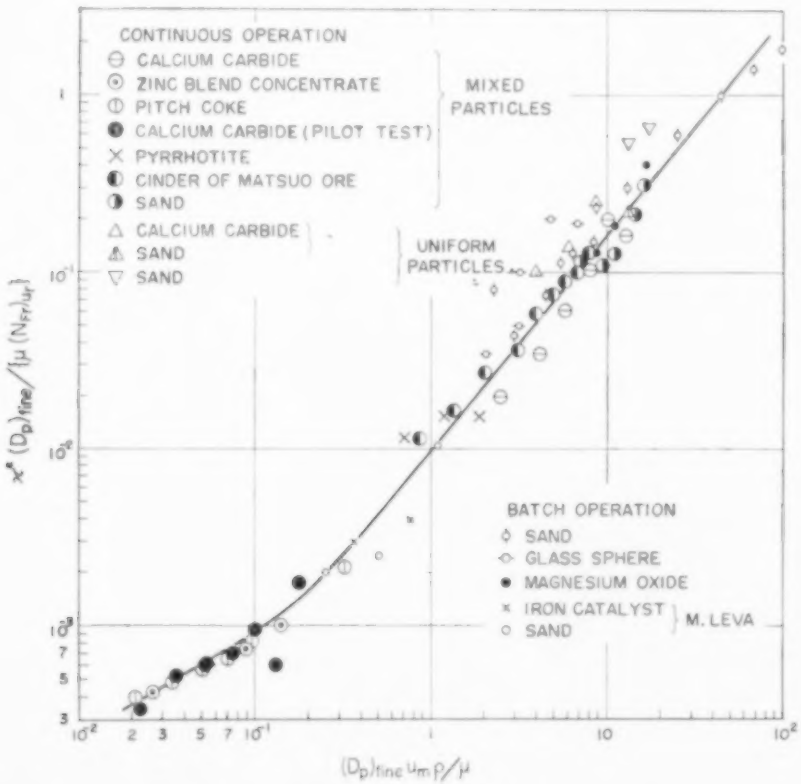

FIG. 4. Correlation for elutriation velocity constant, given by YAGI and AOCHI [6].

YAGI and KUNII [1] defined the "elutriation velocity constant" with the following equation:

$$-\frac{dC_s}{d\theta_p} = \kappa C_s \tag{5}$$

Therefore

$$C_s = S_{s0} \exp(-\kappa \theta_p) \tag{6}$$

The meaning of equation (5) is that the elutriation rate of small particles is proportional to the number of small particles in the fluidized bed, the elutriation velocity constant being the proportionality constant.

YAGI and AOCHI [6] conducted experiments on elutriation phenomena under a wide range of experimental conditions. (Fig. 3). Their data are summarized by the dimensionless correlation shown in Fig. 4, using the following two groups:

$$(D_p)_{\text{fine}}\, u_m\, \rho_g/\mu \text{ and } \kappa^* (D_p)_{\text{fine}}/\{\mu (N_{Fr})_{ur}\} \tag{7}$$

where $\kappa^* = (W/A_T)\,\kappa = (1-\epsilon_c)\, L_c\, \rho_s\, \kappa$ (8)

and

$$(N_{Fr})_{ur} = (u_g - u_m)^2/\{g (D_p)_{\text{fine}}\} \tag{9}$$

The dimensionless correlation in Fig. 4 includes not only the data on batch type elutriation by LEVA [5] but also the data obtained from experiments with continuous feeding. Furthermore, it correlates data on the fluidized roasting of zinc blende with wide size distribution, fluidized gasification of pitch-coke particles and continuous nitrogenation of calcium carbide particles in pilot plant reactor with diameter of 1.0 m. Because of the good fit the correlation in Fig. 4 may well serve as a reasonable pre-estimation of the elutriation velocity constant for design purposes.

ELUTRIATION VELOCITY CONSTANTS IN FLUIDIZED BEDS WITH PARTICLES OF WIDE SIZE DISTRIBUTION

When the feed has a wide size distribution batch type elutriation cannot be used to measure the elutriation velocity constant. In this case it is necessary to operate the fluidized bed at steady state and to feed the particles continuously.

In Fig. 5, which is a model of such fluidized beds, it is assumed that particles do not change their diameter during their stay in the bed, but that the average weight of particles becomes β times that of the raw feed particles, in compliance with the physical or chemical change in the fluidized bed [1].

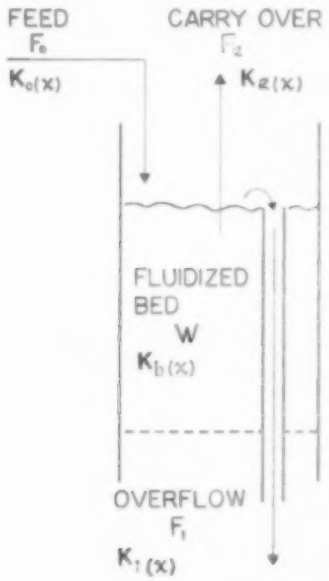

FIG. 5. A model of fluidized bed, particles with wide size distribution

Taking the feed rate of particles to be F_0, the rate of overflow particles F_1, and that of carryover particles entrained by gas stream F_2, the total mass balance gives

$$F_1 + F_2 = \beta F_0 \tag{10}$$

In Fig. 5 $K_0(x)$, $K_b(x)$, $K_1(x)$ and $K_2(x)$ are the size frequency distribution functions for feed particles, for the particles within the fluidized bed, for overflow particles and for carryover particles respectively. Letting the weight of a feed particles of diameter x be w, feed and discharge rates of particles with diameters between x and $x + dx$ can be expressed as follows:

feed rate of particles (number of particles per unit time)

$$n_0 = F_0 K_0(x)\, dx/w \tag{11}$$

overflow rate

$$n_1 = F_1 K_1(x)\, dx/(\beta w) \tag{12}$$

carryover rate

$$n_2 = F_2 K_2(x)\, dx/(\beta w) \tag{13}$$

From the mass balance for particles with diameter between x and $(x + dx)$,

$$n_0 = n_1 + n_2 \tag{14}$$

Extending the application of Equation (5) to any one particle size in bed with wide particle-size distribution,

$$-\frac{dC_s}{d\theta_p} = \kappa C_s = \kappa K_b(x)\, dx \tag{15}$$

Therefore

$$n_2 = W \kappa K_b(x)\, dx/(\beta w) \tag{16}$$

When both the carryover rate F_2 and the size frequency distribution function of carryover particles $K_2(x)$ are measurable the elutriation velocity constant κ for particles with diameter x can be calculated by substituting equation (16) into equation (13).
Thus,

$$\kappa = \frac{F_2 K_2(x)}{W K_b(x)} \tag{17}$$

In addition it may be shown [7] that equation (17) is also valid in cases where the particle diameter changes due to reaction in the fluidized bed.

Furthermore, substituting equations (11), (12) and (16) into equation (14)

$$\kappa = \frac{\beta F_0}{W}\frac{K_0(x)}{K_b(x)} - \frac{F_1}{W}\psi \tag{18}$$

where

$$\psi = \frac{K_1(x)}{K_b(x)} \tag{19}$$

Now ψ is the ratio of size frequency-distribution function of overflow particles to those within the fluidized bed, and for complete mixing within the bed ψ is unity for all values of x. Actually some degree of segregation is likely to occur with large particles below and small particles above. Hence with the overflow pipe near the top of the bed as shown in Fig. 5, ψ may be smaller than unity for large particles and the reverse for small particles. However examination of experimental data will show that the assumption $\bar{\psi} \sim 1$ for all values of x might not lead to any appreciate error in the calculation of residence times of particles for fluidized beds with a wide range of particle sizes.

Exit Age-distribution functions and average residence times for fluidized bed consisting of a wide range of particle sizes

In the model of the continuous fluidized bed shown in Fig. 5, θ is the general time variable while θ_p is the time measured from the instant of feeding of a marked group of particles with wide size distribution into the fluidized bed. Consider that these marked particles are fed into the bed in the time interval between θ and $\theta + d\theta$ and let their stay within the bed be studied. Among the marked particles, the number of particles with diameter between x and $(x + dx)$ is $n_0\, d\theta$. In the short time interval $d\theta_p$ after an elapsed time θ_p some fraction of the marked particles are discharged through overflow pipe or with the flowing gas stream. Now among the marked particles of diameter between x and $(x + dx)$, the number of overflow and carryover particles discharged during $d\theta_p$ may be expressed as $-d\eta_1$ and $-d\eta_2$ respectively. Hence the total decrease of such marked particles is

$$-d\eta = -(d\eta_1 + d\eta_2) \tag{20}$$

where η is the total number of marked particles with diameter between x and $(x + dx)$, remaining in the fluidized bed after the elapsed time θ_p. Now if the total number of particles with diameter between x and $(x + dx)$ in the fluidized bed is

$$N = W K_b(x)\, dx/(\beta w) \tag{21}$$

then the fraction of marked particles with diameter between x and $(x + dx)$ among these N particles is η/N.

Therefore, the number of marked particles discharged from the fluidized bed as overflow and carryover particles is given as follows:
for overflow particles

$$-d\eta_1 = (n_1\, d\theta_p)(\eta/N) \tag{22}$$

for carryover particles

$$-d\eta_2 = (n_2\, d\theta_p)\,(\eta/N) \tag{23}$$

where $n_1\, d\theta_p$ and $n_2\, d\theta_p$ are total number of particles with diameter between x and $x + dx$, which are discharged in the overflow and carryover in the short time interval $d\theta_p$.

Substituting equations (10), (12), (13), (19), (22) and (23) into equation (20), integrating with respect to θ_p and noting that $\eta = n_0\, d\theta$ at $\theta_p = 0$ gives

$$\eta = (n_0\, d\theta)\exp\left[-\left\{(F_1/W)\psi + \kappa\right\}\theta_p\right] \tag{24}$$

Now for any particular particle size the exit age-distribution function for overflow particles $E_1(x, \theta_p)$ is given by

$$-d\eta_1 = (n_0\, d\theta)\, E_1(x, \theta_p)\, d\theta_p \tag{25}$$

Combining with equations (22) and (24)

$$E_1(x, \theta_p) = (F_1/W)\psi \exp\left[-\left\{(F_1/W)\psi + \kappa\right\}\theta_p\right] \tag{26}$$

Similarly, with equations (16), (23) and (24) the exit age distribution function for carryover particles $E_2(x, \theta_p)$ is found to be

$$E_2(x, \theta_p) = \kappa \exp\left[-\left\{(F_1/W)\psi + \kappa\right\}\theta_p\right] \tag{27}$$

Now the mean age $\bar{\theta}$ of these particular overflow particles of size between x and $(x + dx)$ is given by

$$\bar{\theta} = \frac{\int_0^{\theta_p=\infty} \theta_p\, n_0\, d\theta\, E_1(x, \theta_p)\, d\theta_p}{\int_0^{\theta_p=\infty} n_0\, d\theta\, E_1(x, \theta_p)\, d\theta_p} \tag{28}$$

Combining with equation (26) and integrating gives

$$\bar{\theta} = \frac{1}{(F_1/W)\psi + \kappa} \tag{29}$$

For carryover particles an expression identical with equation (29) is obtained, even though the distribution function $E_2(x, \theta_p)$ must be used instead of $E_1(x, \theta_p)$. Hence it becomes clear that the average residence time of overflow particles is theoretically the same as that of carryover particles having the same diameter.

For coarse particles with terminal velocities larger than the superficial gas velocity of the fluidized bed the elutriation velocity constant should be zero, and equation (29) should simplify to

$$\bar{\theta} = (W/F_1)\,\psi \sim W/F_1 \tag{30}$$

On the other hand for small particles which have terminal velocities much smaller than the superficial gas velocity the elutriation velocity constant κ controls and equation (29) reduces to

$$\bar{\theta} \sim 1/\kappa \tag{31}$$

As an illustration the average residence times will be calculated, applying the experimental data of YAGI and KUNII [1] for the fluidized roasting of zinc blende concentrate in a bed of 9·8 cm I.D.

Experimental conditions:

static bed height	:	$L_c = 14{\cdot}1$ cm
weight of the bed	:	$W = 1100$ g
overflow rate	:	$F_1 = 11$ g/min
superficial gas velocity	:	$u_g = 45$ cm/sec
$x = 80\ \mu$		$\kappa = 0{\cdot}01$ min^{-1}
$x = 20\ \mu$,		$\kappa = 0{\cdot}4$ min^{-1}

Substitution of the above values into equation (29) assuming $\psi = 1$ gives

$x = 80\ \mu$, $\bar{\theta} = 50$ min ; $x = 20\ \mu$, $\bar{\theta} = 2{\cdot}4$ min

In commercial-sized fluidized roasters a large fraction of the particles are elutriated in the carryover ; nevertheless conversion is high. Consequently it is reasonable to expect that the average residence times of such small particles is larger than the time necessary for their roasting.

In industrial plants beds are higher than that in the previous illustration by about 5 to 10 times, so it might be valuable to discuss roughly the effects of bed height on the residence time of small particles. Fig. 4 shows that κ^* is a constant at given fluidizing conditions. Hence for constant diameter, equation (8) shows that

$$\kappa \propto L_c^{-1} \tag{32}$$

Hence for tall narrow beds carryover of any sized particle is small, while for short large diameter beds carryover of that sized particle is great. It is estimated that the average residence time for small particles increases in proportion to the bed height for the same fluidization conditions.

Substitution of equation (18) into (29) gives

$$\bar{\theta} = \frac{W}{\beta F_0} \frac{K_b(x)}{K_0(x)} \tag{33}$$

When numerical values of the elutriation velocity constant are available the ratio of overflow particles to total feed particles can be calculated. By combining equations (16) and (18) integration results in the final expression for carryover and overflow rates as follows:

$$\frac{F_2}{\beta F_0} = 1 - \frac{F_1}{\beta F_0} = \int_0^{x=x_{max}} \frac{K_0(x)\,\kappa}{(F_1/W)\psi + \kappa}\,dx \tag{34}$$

Conclusion

Exit age-distribution functions are used to study the residence times of particles in fluidized beds. Theoretically it was shown that the average residence times for a given particle size is the same in both the carryover and overflow streams.

Chemical Engineering Science, 1961, Vol. 16, pp. 372 to 379. Pergamon Press Ltd., London. Printed in Great Britain.

Fluidized-solids reactors with continuous solids feed—II

Conversion for overflow and carryover particles

SAKAE YAGI and DAIZO KUNII
Department of Chemical Engineering, University of Tokyo, Tokyo, Japan

(*Received* 6 *April* 1960; *in revised form* 4 *January* 1961)

Abstract—Based upon the simple model of particles which keep their diameters almost constant during reaction with the gas flowing in the fluidized bed, and applying the exit age-distribution functions obtained in Part I, equations for the conversion of product particles were derived.

For chemical reaction controlling:

$$y = \frac{3}{\phi} - \frac{6}{\phi^2} + \frac{6}{\phi^3}\{1 - \exp(-\phi)\}$$

For gas diffusion through solid phase controlling:

$$y = 1 - \frac{1}{5}\phi + \frac{19}{420}\phi^2 - \frac{41}{4620}\phi^3 + \ldots.$$

where y is the conversion of particles of diameter x, ϕ is the ratio of time required for complete conversion of one particle of diameter x to the average residence time of the particle.

The above equations are applicable to both overflow and carryover particles, hence the conversion for overflow particles must be equal to that for carryover particles for a given particle size.

The mean value of the conversion y can be given as follows:

for overflow stream

$$y_1 = \int_0^{x=x_{max}} y\,K_1(x)\,dx$$

for carryover stream

$$y_2 = \int_0^{x=x_{max}} y\,K_2(x)\,dx$$

where $K_1(x)$ and $K_2(x)$ represent the size frequency distribution functions for the overflow and carryover particles respectively.

Résumé—En s'appuyant sur les modèles simples de particules qui conservent des diamètres pratiquement constants pendant la réaction avec le gaz circulant dans le lit fluidisé, et en appliquant les fonctions de distribution du temps de séjour obtenues dans la 1ère partie de cet article, on établit les équations pour la conversion des particules produites.

Quand la vitesse est contrôlée par la réaction chimique:

$$y = \frac{3}{\phi} - \frac{6}{\phi^2} + \frac{6}{\phi^3}\{1 - \exp(-\phi)\}$$

Quand la vitesse est contrôlée par la diffusion du gaz à travers la phase solide:

$$y = 1 - \frac{1}{5}\phi + \frac{19}{420}\phi^2 - \frac{41}{4620}\phi^3 + \ldots.$$

Dans ces équations y représente la conversion des particules de diamètre x, ϕ le rapport du temps nécessaire pour la conversion complète d'une particule de diamètre x, au temps de séjour moyen la particule.

Les équations ci-dessus sont applicables aussi bien à des particules entrainées qu'à des particules déversées. La conversion pour les particules déversées peut donc être appliqué aux particules entrainées, pour une dimension de particule donnée.

La valeur moyenne de la conversion y peut être exprimée ainsi. Pour un trop plein :

$$y_1 = \int_0^{x=x_{max}} y\, K_1(x)\, dx$$

Pour un entrainement

$$y_2 = \int_0^{x=x_{max}} y\, K_2(x)$$

Avec $K_1(x)$ et $K_2(x)$ représentant les fonctions de distribution de fréquence des dimensions respectivement pour les particules déversées et pour les particules entrainées.

Zusammenfassung—Auf Grund eines einfachen Modells für Teilchen, die ihren Durchmesser während einer in einer Gas durchströmten Wirbelschicht ablaufenden Reaktion praktisch unverändert behalten, und durch Anwendung einer Verweilzeit-Verteilungsfunktion der austretenden Teilchen, die im 1 Teil erhalten worden war, wurden Gleichungen für die Umwandlung der Produktteilchen entwickelt.

Für einen durch die chemische Reaktion geschwindigkeitsbestimmten Schritt :

$$y = \frac{3}{\phi} - \frac{6}{\phi^2} + \frac{6}{\phi^3}\{1 - \exp(-\phi)\}$$

Für einen durch Diffusion in der Feststoffphase geschwindigkeitsbestimmten Schritt

$$y = 1 - \frac{1}{5}\phi + \frac{19}{420}\phi^2 - \frac{41}{4620}\phi^3 + \ldots.$$

wobei y die Umsetzung der Teilchen vom Durchmesser x, ϕ das Verhältnis darstellt von der Zeit, die erforderlich ist, um ein Teilchen vom Durchmesser x völlig umzusetzen, zu der mittleren Verweilzeit des Teilchens.

Die obigen Gleichungen sind sowohl für den Überlauf als auch für den Austrag anwendbar, da der Umsatz der überlaufenden Teilchen gleich dem der ausgetragenen Teilchen bei einem bestimmten Korndurchmesser sein muss.

Für den mittleren Umsatz im Überlauf gilt :

$$y_1 = \int_0^{x=x_{max}} y\, K_1(x)\, dx$$

Für den Austrag gilt :

$$y_2 = \int_0^{x=x_{max}} y\, K_2(x)\, dx$$

wobei $K_1(x)$ und $K_2(x)$ die Korngrössen-Verteilungsfunktion für den Überlauf und den Austrag bedeuten.

VOL. 16 1962

Introduction

The extent of reaction of a particle is a function of its size and length of stay within the reactor, and since these factors may differ from one particle to another, the conversion is not necessarily the same for all particles discharged from the bed. In other words, conversion is low for particles discharged just after their feeding into the bed, but is equal to 100 per cent for particles which have remained within the bed longer than some definite time, i.e. the necessary time for complete reaction. Hence, in the overflow or carryover products, there are some particles which have quite low conversions despite the fact that the average conversion of products may be high.

Based upon the exit age distribution functions

previously obtained (Part I), conversions of the overflow and carryover particles were analysed for reaction of solids with flowing gas.

Time required for complete Conversion of a Particle

Hellinkx [8] followed the progress of combustion of oil shale by quenching and examination of the individual particles. He found that unburnt cores existed which gradually decreased in diameter as reaction proceeded. Finally these unburnt cores disappeared leaving a comparatively dense solid particle of approximately the same diameter as the original unreacted particle.

This mode of combustion occurs not only in oil shale particles but also in a wide range of materials such as coal shale [8] with much ash, and pyrrhotite or zinc blende particles [9, 10].

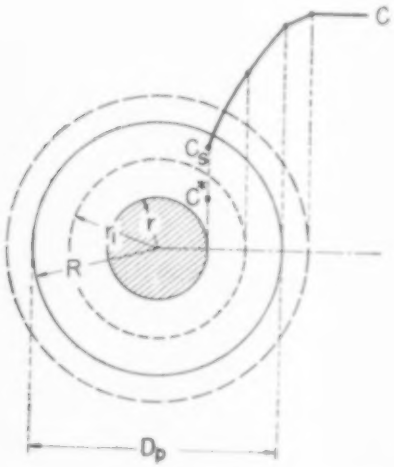

Fig. 1. Model of single particle, in which solid phase remains around the unreacted core. $D_p = x$.

When a particle remains in the solid phase throughout reaction (Fig. 1), the time necessary for complete conversion is given by [7]:

$$\theta_0 = \frac{x}{2\,\alpha\,k\,(C - C^*)} \tag{1}$$

where

$$\frac{1}{k} = \frac{1}{k_c} + \frac{1}{k_d} \tag{2}$$

and

$$k_d = 12\,D_{cs}/x \tag{3}$$

k is the over-all rate coefficient of reaction, k_c is the rate coefficient for the chemical reaction step, α is the volume of solid phase which reacts with unit mol of reactant gas, C and C^* are concentrations of reactant gas in the gas stream and that corresponding to equilibrium on the reaction surface respectively. In equation (2) k_p can be considered to be the mean rate coefficient diffusion of reactant gas through the solid phase. The mass transfer coefficient of the boundary layer has been compared with the value of k_d, and it was concluded that the mass transfer resistance in the boundary layer was negligible compared to the resistance within the particle for the case where the solid phase remains after reaction [7].

The relation between the elapsed time and the radius of unreacted core has been shown as follows [7]:

for chemical reaction controlling:

$$\theta_p/\theta_0 = 1 - 2r/x \tag{4}$$

for diffusion through solid phase controlling:

$$\theta_p/\theta_0 = 1 - 3\,(2r/x)^2 + 2\,(2r/x)^3 \tag{5}$$

Applying the above two equations the decrease of unreacted core radius can be shown as in Fig. 2, where line B is for the case where the chemical reaction rate is comparable with diffusion in the solid phase. This calculation was made with the

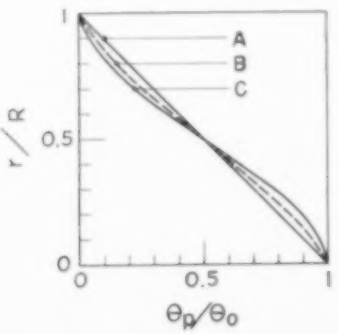

Fig. 2. Decrease of diameter of unreacted core with time, in case of single particle shown in Fig. 1.

original equations of Ref. [7]. Since line C is not much different from line A equation (4) can be applied approximately for particles exhibiting both chemical reaction and diffusion effects. Such an approximation may well be made for the complicated phenomenon occuring in fluidized beds.

Effective concentration of reactant gas and contact efficency of particles with gas stream

When a gas–solid reaction occurs in a fluidized bed the concentration of reactant in the gas stream decreases with increasing distance from the bed entrance. Hence, the mean value of the concentration C_{av} of the reactant gas within the bed is less than the concentration C_0 in the inlet gas. On the other hand, each particle of solid moves haphazardly throughout the bed during its reaction period. Hence, each particle contacts gas of varying composition. Consequently it seems reasonable to take the average values of reactant gas concentration C_{av} in determination of the effective driving force for the conversion of solids.

According to theoretical analysis [3, 12] the distribution of the reactant gas concentration with respect to the height of the fluidized bed is determined by both the rate coefficient of reaction and the axial diffusion coefficient $\overline{D}$. For example, consider the fluidized gasification of coke particles [11] with carbon dioxide under the following conditions, i.e. diameter of coke particles 0·2 mm, flow rate of carbon dioxide 5·17 cm/sec (N.T.P., superficial), average void fraction 0·6, temperature 1,400 °K.

The overall rate coefficient of reaction is taken from Ref. [11], and the value of the axial diffusion coefficient is calculated from the following recommended relation for fluidized beds of laboratory scale: [12]

$$\overline{u}\, L_b/2\, \overline{D} = 1$$

Fig. 3 shows the calculated lines for reactant gas concentration for the assumptions of plug flow, complete mixing flow and for $\overline{u}\, L_b/2\, D = 1$. As may be seen the concentration distribution in the fluidized bed lies between those of the plug flow and the complete mixing flow. Therefore, in order to get an accurate value for the average reactant gas driving force it is necessary to measure the concentration distribution as a function of bed height or to pre-estimate the numerical value of the axial diffusion coefficient. However, as shown in Fig. 3, for conversions of reactant gas less than 60 per cent the difference in the effective concentration driving forces between an actual fluidized bed and plug flow is minor. For instance, in Fig. 3,

$$(\Delta C_{av})_{plug} : (\Delta C_{av})_{fluidized} : (\Delta C_{av})_{comp.\ mixed} = 1 : 0{\cdot}92 : 0{\cdot}80$$

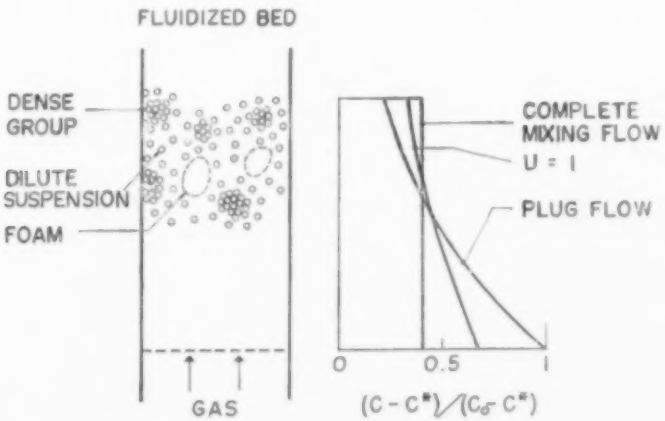

Fig. 3. A model of fluidized bed. $U = \overline{u}\, L_b/2\, \overline{D}$.

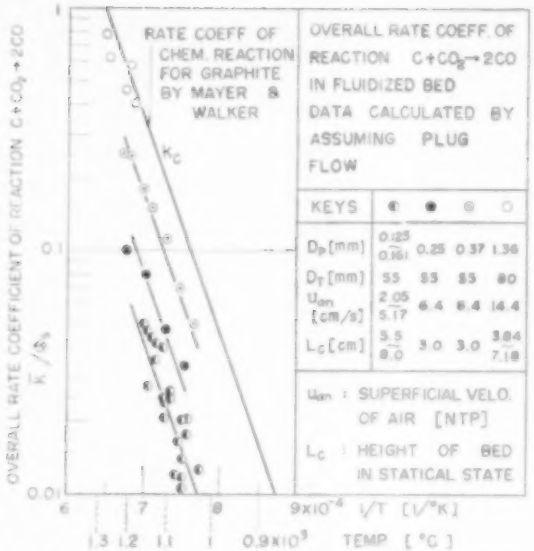

Fig. 4. Examples of data for over-all rate coefficient of reaction $C + CO_2 = 2CO$ in fluidized bed [11].

Gas–solid system consisting of small particles

are apt to agglomerate densely, in which case the gas stream flows upward in the form of "bubbles." Under such conditions, it becomes difficult for each particle to always contact non-stagnant gas having the driving force for conversion. The smaller the particles and the higher the rate coefficient of reaction, the more serious the above phenomenon becomes in affecting the total rate of conversion in a fluidized bed. Shen and Johnstone [13] studied this problem, and as a measure of this phenomenon they introduced the transfer coefficient of turbulent diffusion between the solid and gas phases. Yagi and Kunii [11] conducted studies on the gasification of coke particles, and obtained the data for the over-all rate coefficient of gasification k, some of which is shown in Fig. 4, where ϕ_s is the shape factor. In Fig. 4, k approaches the rate coefficient of chemical reaction for large particles, but the smaller the particles become the more the values of k decrease. Hence, the introduction of what may be called at this point "the contact efficiency of particles in a fluidized bed" δ seems reasonable.

$$\delta = \frac{\text{surface area of particles contacting the gas stream}}{\text{total surface area of particles in the fluidized bed}}$$

and for chemical reaction controlling for each particle:

$$\delta = \frac{\text{over-all rate coefficient of reaction based upon the total surface area of particles}}{\text{rate coefficient of chemical reaction}}$$

Hence, δ represents the effective contact of the particles with the main gas stream in the fluidized bed. The numerical value of δ includes presumably the effect of turbulent diffusion in the fluidized bed. Applying the above values, the time necessary for complete conversion of one particle in the fluidized bed can be written as:

$$\theta_b = \theta_0/(\Phi\,\delta) \tag{6}$$

where Φ represents the ratio of the mean effective gas concentration driving force to the driving force of incoming fresh gas, or

$$\Phi = \Delta C_{av}/(C_0 - C^*) \tag{7}$$

Conversion for overflow particles of uniform size

Consider systems in which particles remain solid with diameters essentially unchanged during reaction. The number of particles discharged from a fluidized bed during the short time interval $d\theta$ is $n_0 d\theta$. Among them, the number of particles with ages between θ_p and $\theta_p + d\theta_p$ can be obtained by the exit age distribution function for overflow particles, i.e. equation (2) of Part I. Therefore, the volume of the unreacted cores in the particles is

$$(n_0\,d\theta_p)\,E_1(\theta_p)\,d\theta\left\{(4/3)\,\pi\,r^3\right\} \tag{8}$$

where r is the radius of the unreacted core in a spherical particle with diameter x. Hence, the total volume of unreacted cores in the particles fed into the bed during $0 \leqslant \theta_p \leqslant \theta_b$ can be obtained by integrating the above equation. Then, the mean value of the conversion y can be calculated as follows: [2]

$$y = 1 - \frac{\text{(total volume of unreacted cores in overflow particles)}}{\text{(total volume of overflow particles)}}$$

$$= 1 - \frac{(n_0\, d\,\theta) \int_0^{\theta_p = \theta_b} (4/3)\,\pi\, r^3\, E_1\,(\theta_p)\, d\,\theta_p}{(n_0\, d\theta)\,(4/3)\,\pi\,(x/2)^3}$$

$$= 1 - \int_0^{\theta_p = \theta_b} (2r/x)^3\, E_1\,(\theta_p)\, d\,\theta_p \qquad (9)$$

Substitution of equations (4) or (5), and (2) of Part I, in equation (9) gives:

for chemical reaction controlling:

$$y = (3/\phi) - (6/\phi^2) + (6/\phi^3)\{1 - \exp(-\phi)\} =$$
$$= 1 - (1/4)\,\phi + (1/20)\,\phi^2$$
$$- (1/120)\,\phi^3 + (1/840)\,\phi^4 - \ldots\ldots \qquad (10)$$

and for diffusion in solid phase controlling:

$$y = 1 - (1/5)\,\phi + (19/420)\,\phi^2$$
$$- (41/4620)\,\phi^3 + 0{\cdot}00149\,\phi^4 - \ldots\ldots \qquad (11)$$

where ϕ is the ratio of time necessary for complete conversion θ_b referred to the mean residence time of the particles θ, i.e. $\phi = \theta_b/\theta$. If the value ϕ is less than unity, the terms above ϕ^3 can be neglected. If $\phi < 0{\cdot}5$ it is sufficient to take only the term for ϕ.

Conversion for overflow and carryover particles with wide size distribution

Consider those particles which remain as comparatively dense solids after conversion and keep their diameter almost constant. In Fig. 5 of Part I those particles are discharged in both the overflow and carryover. Marking the overflow particles discharged during the short time interval $d\,\theta$ at any instant, the number of particles having their diameter between x and $(x + dx)$ is $n_1\, d\,\theta$. Among them, there are incompletely converted particles with unreacted cores of radius r which are of age between θ_p and $\theta_p + d\,\theta_p$. Hence, from equation (26) of Part I, the number of the incompletely coverted particles is given by

$$(n_0\, d\theta_p)\, E_1\,(x, \theta_p)\, d\theta$$

and the mean conversion y for particles with diameter x is given by

$$y = 1 - \frac{(n_0 d\,\theta) \int_0^{\theta_p = \theta_b} (4/3)\,\pi\, r^3\, E_1\,(x, \theta_p)\, d\theta_p}{(n_1\, d\theta)\,(4/3)\,\pi\,(x/2)^3} \qquad (12)$$

Substitution of equations (12), (13), (14), (26) of Part I and equations (4) or (5) into equation (12) gives results which are identical with equations (10) and (11). In this case, y and $\phi = \theta_b/\theta$ should be the values for particles with diameter x.

The conversion y for carryover particles can be calculated in a similar manner with the exception that n_2 and $E_2\,(x, \theta_p)$ are to be used in place of n_1 and $E_1\,(x, \theta_p)$ in equation (12). The result of the calculation shows that the conversion for carryover particles is identical with that of overflow particles for the same particle diameter, equations (10) and (11). Experimental verifications of these theoretical predictions are presented in Part III.

Now the mean value for the conversion for overflow and carryover streams of wide size distribution is found simply as follows:

for the overflow stream

$$y_1 = \int_0^{x = x_{max}} y\, K_1\,(x)\, dx \qquad (13)$$

for the carryover stream

$$y_2 = \int_0^{x = x_{max}} y\, K_2\,(x)\, dx \qquad (14)$$

Factor Φ for average driving force

In a fluidized bed with particles of uniform diameter the particles fed into the bed react with reactant gas during their stay and discharge

through the overflow pipe. Since the mixing is very violent in the fluidized bed, it is assumed that any particle has the same probability of being found in one location as another, in other words the bed is uniform in composition of solid. Also at steady state as shown in Fig. 5 [1], the number of particles within the bed having an unreacted core of radius r is constant.

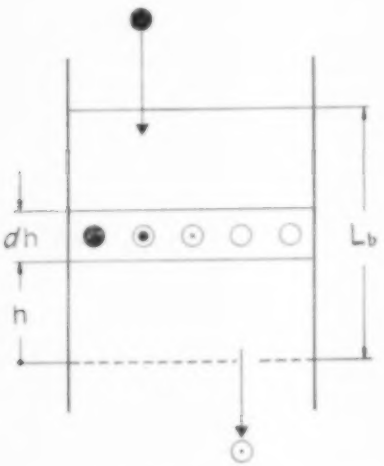

FIG. 5. Model of fluidized bed of particles with uniform size.

Now a particle with unreacted core of radius r needs reactant gas as follows:

$4 \pi r^2 (dm^*/d\theta_p)$ mols per particle, per unit time

Since particles having an unreacted core of radius r have an age between θ_p and $\theta_p + d\theta_p$ their number remaining in the bed can be calculated from equation (2) of Part I, as follows:

$$\eta = (n_0 \, d\theta_p) \exp(-\theta_p/\bar{\theta}) \tag{15}$$

Now the number of these particles within the infinitesimal volume of bed of height dh is $\eta (dh/L_b)$. However, in general, only δ fraction of the total surface area of solids contact the reactant gas. Hence, the quantity of reactant gas necessary for particles having an unreacted core of radius r and located in the infinitesimal bed height dh is given by

$$d(dV) = (4 \pi r^2)(dm^*/d\theta_p) \eta (dh/L_b) \delta$$

for diameters of unreacted cores ranging from 0 to x,

$$dV = \int_0^{\theta_p = \theta_b} (4 \pi r^2)(dm^*/d\theta_p) \eta (dh/L_b) \delta$$

$$= (4 \pi n_0 \delta/L_b) \, dh \int_0^{\theta_p = \theta_b} r^2 (dm^*/d\theta_p) \exp(-\theta_p/\bar{\theta}) \, d\theta_p \tag{16}$$

Substitution of the original equations for both $dm^*/d\theta_p$ and the general relation between r and θ_p into equation (16) results in the following expression (17). Details of the calculation may be found elsewhere [1, 2].

$$dV = \frac{F_0 y}{\pi \rho_s L_b \Phi} \frac{C - C^*}{C_0 - C^*} dh \tag{17}$$

At first, assuming piston flow, the mass balance taken in the infinitesimal volume having the height dh gives

$$GC = G(C + dC) + dV \tag{18}$$

Substitution of equation (17) into equation (18) results in the following equation, for which the boundary condition is $C = C_0$ at $h = 0$,

$$(C - C^*)/(C_0 - C^*) = \exp(-Bh) \tag{19}$$

where $B = F_0 y / \{\pi \rho_s G L_b (C_0 - C^*) \Phi\}$

The mean value of the driving force ΔC_{av} in the bed is found from equation (19) to be

$$\Delta C_{av}/(C_0 - C^*) = \Phi = \{1 - \exp(-BL_b)\}/(BL_b) \tag{20}$$

Elimination of B from equation (20) results in

$$\Phi = (y/e)/\{-\ln[1 - (y/e)]\} \tag{21}$$

where y is the mean conversion for overflow particles and e is the "gas consumption factor" defined as follows:

e = (volume flow of gas entering the fluidized bed)/(stoichciometrical flow of gas needed for the complete conversion of the feed particles).

The details of above elimination may be found in Refs. [1, 2].

Next, for the case of complete mixing flow the concentration of the reactant gas should be constant through the fluidized bed, and should be equal to that of the outlet gas. Hence, a mass balance yields

$$\Phi = 1 - (y/e) \tag{22}$$

Fig. 6 shows values of Φ as a function of y/e for both piston and complete mixing flow. The percentage difference in Φ values between these two extremes of gas flow is small for y/e, smaller than 0·4–0·5. However, as y/e becomes larger then 0·6, the difference increases more quickly.

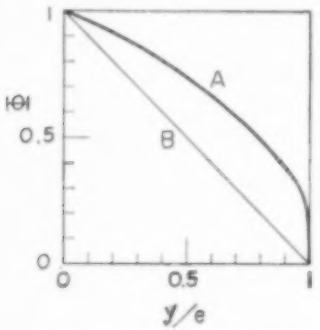

Fig. 6. Correction factor Φ.
A Plug flow B Complete mixing flow.

For systems with a wide size distribution of particles, the particles having diameters between x and $(x + dx)$ are marked among those particles which have been fed into the bed during the short time interval $d\theta$ at any instant. Integration for the total range of diameters results in the following equation instead of equation (17).

$$dV = \int_0^{x=x_{max}} d(dV) = \frac{F_0 \bar{y}}{\pi \rho_s L_b \Phi} \frac{C - C^*}{C_0 - C^*} dh \tag{23}$$

where y is the over-all conversion which includes both the overflow and carryover particles. The final equations for Φ are identical with those found for a uniform particle size, with the single exception that y is to be used in place of y.

Conclusion

Applying the exit age-distribution function obtained in part I, theoretical equations for the conversions of both overflow and carryover particles are obtained for fluidized solid reactors. The analysis is based on the assumption that during reaction the particles remain as solids with unchanging diameters.

Chemical Engineering Science, 1961, Vol. 16, pp. 380 to 391. Pergamon Press Ltd., London. Printed in Great Britain.

Fluidized-solids reactors with continuous solids feed—III

Conversion in experimental fluidized-solids reactors

SAKAE YAGI and DAIZO KUNII

Department of Chemical Engineering, University of Tokyo, Tokyo, Japan

(*Received* 6 *April* 1960; *in revised form* 4 *January* 1961)

Abstract—Experimental data from gas–solid fluidized reactor systems are analysed on the basis of the theoretical treatment of Parts I and II. The following systems are treated:

(a) Roasting of pyrrhotite and zinc blende particles with uniform size.
(b) Roasting of zinc blende concentrate with wide distribution of size.
(c) Distillation of sulphur with two-stage fluidized reactor.
(d) Nitrogenation of calcium carbide.

Close agreement between theory and experiment is obtained.

Résumé—En se basant sur la théorie présentée dans les parties I et II de cet article, les auteurs analysent les données expérimentales pour des réacteurs gaz solide à lit fluidisé.

Les systèmes suivants ont été étudiés:

(a) Grillage de particules de pyrrhotine et de blende de taille uniforme;
(b) Grillage de blende concentrée avec large distribution de dimensions;
(c) Distillation de sulfures dans des réacteurs fluidisés à deux étages;
(d) Fixation d'azote sur le carbure de calcium.

Il y a bon accord entre les expériences et la théorie.

Zusammenfassung—Experimentelle Daten eines Gas-Feststoff-Wirbelschicht-Reaktors wurden auf Grund der theoretischen Ableitung des 1 und 2 Teiles dieser Arbeit untersucht. Dabei wurden folgende Systeme behandelt:

(a) Röstung von Magnetkies und Zinkblende gleicher Korngrösse.
(b) Röstung von Zinkblende-Konzentraten mit grossen Kornspektrum.
(c) Destillation von Schwefel in einem 2-Stufen-Wirbleschicht-Reaktor.
(d) Kalkstickstoffbildung aus Karbid.

Dabei wurde gute Übereinstimmung zwischen Theorie und Experiment erzielt.

INTRODUCTION

FLUIDIZED reactors have recently been used for a variety of gas–solid reactions because of their several well-known advantages. When the fluidized-solids technique is selected for some chemical reaction of solid particles with gas design calculation for pilot or industrial scale plants should be made using the experimental data obtained in model reactors of small scale.

In order to make sure of the utility of the previously obtained theoretical equations for above purpose, they should account for any data in experimental reactors of small scale. Hence, several kinds of fluidized-solid reactors were fabricated and experimental data were analysed with authors' theoretical equations.

Furthermore, above theoretical equations could be applied for the fluidized-solids reactors of the other different chemical reactions, as long as the solid particles would remain hard solid phase after reactions, for instance, reduction of iron ore, calcination of limestone, carbonization of coal, vaporization of shale oil, regeneration of fluid catalyst, etc.

For particles which decrease their diameters in compliance with the chemical reaction, for

example, in case of combustion or gasification of coke particles, extended theoretical and experimental works should be consulted [7].

Roasting of Pyrrhotite particles of uniform size

Yagi and Takagi [14] made fundamental experimental studies on the fluidized roasting of pyrrhotite particles of uniform size, using the experimental roaster shown in Fig. 1.

$$4\,Fe_7S_8 + 53\,O_2 \rightarrow 14\,Fe_2O_3 + 32\,SO_2$$

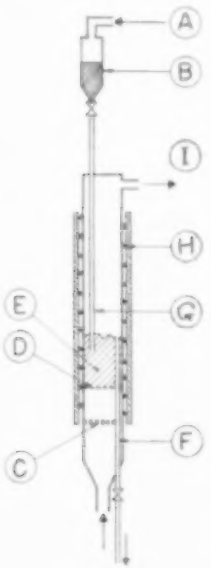

Fig. 1. Experimental reactor for roasting of sulphide ore used by Yagi and Takagi [14].
A. Air. B. Hopper. C. Perforated plate. D. Screen. E. Fluidized bed. F. Overflow tube. G. Feed tube. H. Nichrome heater. I. Gas outlet.

The ranges of experimental conditions are shown in Table 1. The particles of pyrrhotite ore remain in the hard solid state throughout reaction, hence the simplified model for uniform particles developed in Part II may be applied to this situation. For the same range of experimental conditions, Yagi *et al.* [10] roasted pyrrhotite particles in fixed beds, in which particles were dispersed with asbestos fibres. From their experimental data numerical values of the time necessary for complete conversion of single pyrrhotite particles were obtained.

These numerical values showed θ_0 to be dependent on particle diameter as follows:

$$\theta_0 \propto x^{1.5}$$

In contrast, equations (1–3) of Part II from theory predict that for chemical reaction controlling:

$$\theta_0 \propto x \qquad (1)$$

while for diffusion in the solid phase controlling:

$$\theta_0 \propto x^2 \qquad (2)$$

As the experimentally found diameter dependency lies between the two theoretical predictions, it is reasonable to expect that both mechanisms offer resistance to conversion of pyrrhotite particles under the above conditions. Since the difference between equations (10) of Part II for chemical reaction controlling and Equation (11) of Part II for diffusion controlling is not large equation (10) can be employed to approximate the data. Furthermore, values of Φ must be obtained. However these depend on flow type.

According to the discussion in Part II, the concentration distribution in the gas was approximated by plug flow here. This assumption is not

Table 1. Ranges of experimental conditions in fluidized roasting of pyrrhotite particles [14]

Composition of ore (%)	Fe	Cu	SiO_2	MgO	Al_2O_3	CaO	S
	55·95	0·31	4·19	0·61	0·71	0·62	36·27
Diameter of reactors	5·3 and 7·7 cm I.D.						
Temperature	620–900 °C						
Particle diameter	0·088–0·949 mm						
Gas velocity, u_g	7·8–208 cm/sec						
Average residence time	8·9–101 min						
Residual sulphur	0·09–21·6 %						

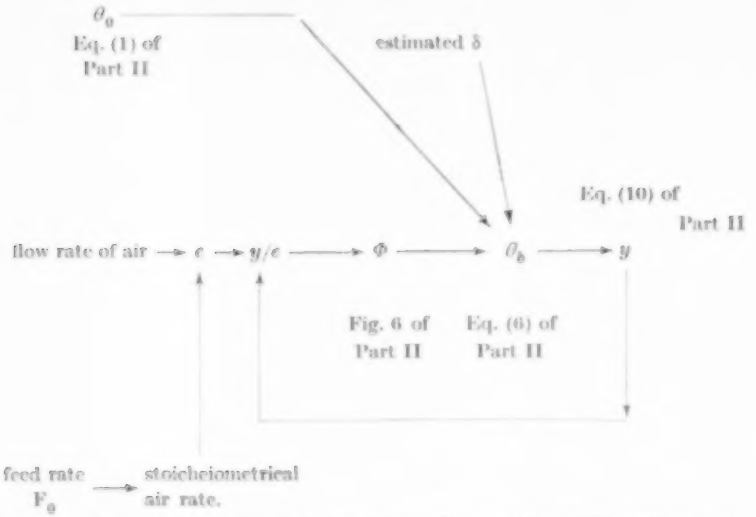

Fig. 2. Procedure of analysis for conversion y for overflow particles with uniform size.

critical, because for small changes in gas concentration difference in flow type does not appreciably effect the results under the present experimental conditions.

Knowing the numerical values of both c and θ_0 conversion y can be decided from Fig. 6 of Part II and equations (6) and (10) of Part II by means of trial and error method. Fig. 2 shows the schematic procedure of calculation for each estimated value of δ. For the system under study values of δ between 0·84 and 1·0 fit the data quite well. The results of calculations are compared with the experimental data in Figs. 3 and 4.

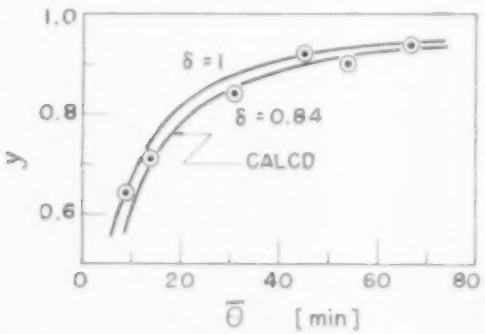

Fig. 3. Conversion y vs. average residence time $\bar{\theta}$.
D_p = 0·551 mm, 800 °C.
Pyrrhotite 0·262 g/sec, air rate 910 cm³/sec.

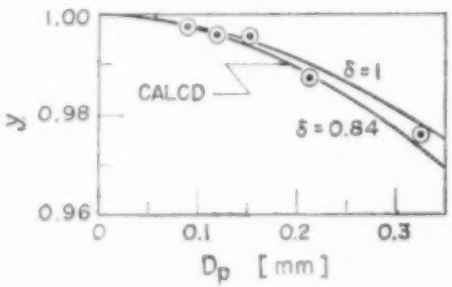

Fig. 4. Conversion y vs. particle diameter [2].
Pyrrhotite, 800 °C ; $\bar{\theta}$ = 60 min.

Roasting of zinc blende of uniform size

Fig. 5 shows the equipment for the roasting of zinc blende particles of uniform size as employed by Yagi, *et al.* [15]. Raw particles were fed into the fluidized bed continuously by the use of small fluidizing feeder. Continuous discharge of overflow particles was also used to insure steady state operations. The range of experimental conditions are shown in Table 2.

In contrast with the preceding section the time necessary for complete oxidation of one particle shall be analysed here. According to Kunii [16] chemical reaction is the rate-controlling mechanism under conditions shown in Table 2.

$$ZnS + \tfrac{3}{2}\,O_2 \rightarrow ZnO + SO_2$$

Table 2. Ranges of experimental conditions in fluidized roasting of zinc blende particles [9].

Composition of ore (%)	Zn	Fe	Cu	Pb	Cd	S
Hosokura	38·8	15·2	0·30	1·0	0·30	35·8
Ikuno	50·13	7·76	2·70	1·46	0·40	29·99

Diameter of reactor	5·0 cm
Temperature	700–900 °C
Particle size	100–200 mesh
Gas velocity, u_g	19·4–35 cm/sec
Average residence time	4·9–113 min
Residual sulphide sulphur	0·27–8·75%
Oxidation (conversion) y	72·4–99·4%

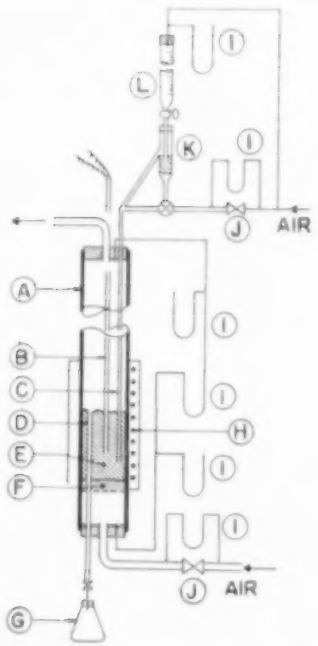

Fig. 5. Experimental reactor for roasting of zinc blende with uniform size [9].
A. Refractory tube. B. Thermocouple well. C. Feed tube. D. Overflow tube. E. Fluidized bed. F. Fixed bed distributor. G. Receiver of cinder. H. Nichrome heater. I. Manometer. J. Flowmeter. K. Feeder with fluidized bed. L. Hopper.

Hence, for $\phi < 0{\cdot}5$, equation (10) reduces to

$$y \sim 1 - \tfrac{1}{4}\phi = 1 - (\tfrac{1}{4})(\theta_b/\bar{\theta}) = 1 - (\tfrac{1}{4})(\theta_0/\delta)(1/\Phi\bar{\theta}) \qquad (3)$$

It may be reasonable to expect that θ_0/δ remains constant for a fixed particle diameter and operating temperature. With this assumption y should be linear in $1/\Phi\bar{\theta}$. From the straight lines obtained in Fig. 6, the assumption of constant θ_0/δ is verified and the time necessary for complete conversion of one particle can be found.

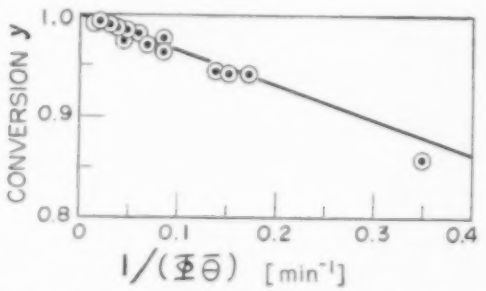

Fig. 6. Conversion factor of overflow particles y vs. $1/(\Phi\bar{\theta})$. Hosokura ore, $D_p = 0{\cdot}11$ mm, 900 °C. $\epsilon = 1{\cdot}08 - 3{\cdot}2$.

Using the same method of calculation mean values of θ_0/δ for various particle size were caclulated as tabulated in Table 3. Figs. 7, 8 and 9 compare actual conversion factors with those predicted using the mean value of θ_0/δ of Table 3 and with equation (3).

Table 3. Necessary time for complete conversion of zinc blende particles

	(mm)	(°C)	θ_0/δ (min)
Hosokura ore	0·11	900	1·28
Ikuno ore	0·126	800	4·0
Ikuno ore	0·089	800	3·8
Ikuno ore	0·089	750	14·0
Ikuno ore	0·089	700	20·0

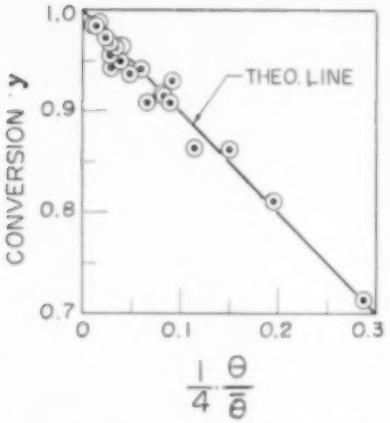

FIG. 7. Conversion of overflow particles y vs. $(1/4)\theta_b/\bar{\theta}$, Ikuno ore, D_p = 0·089, 0·126 mm, 700, 750, 800 °C [9].

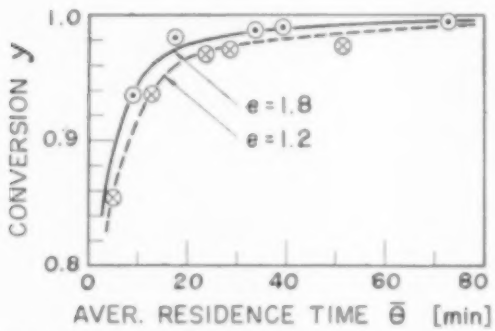

FIG. 8. Comparison of calculated values of y with experimental data, Hosokura ore, D_p = 0·11 mm, 900 °C.

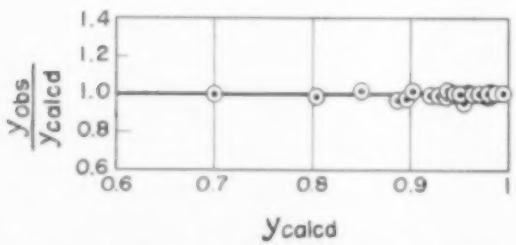

FIG. 9. Comparison of calculated values of y with experimental data, zinc blende, Hosokura and Ikuno ore, 700, 750, 800, 900 °C [9].

ROASTING OF ZINC BLENDE CONCENTRATE WITH WIDE SIZE DISTRIBUTION

YAGI *et. al.* [15] roasted zinc blende concentrate with a wide size distribution in the fluidized-solid roaster shown in Fig. 10. The characteristics of the raw particles and the ranges of experimental conditions are summarized in Table 4. The size frequency distribution function of the feed is shown in Fig. 11. In cases such as this the size-frequency distributions for the overflow and carryover particles are not necessarily equal. However, they will follow the mechanism previously described.

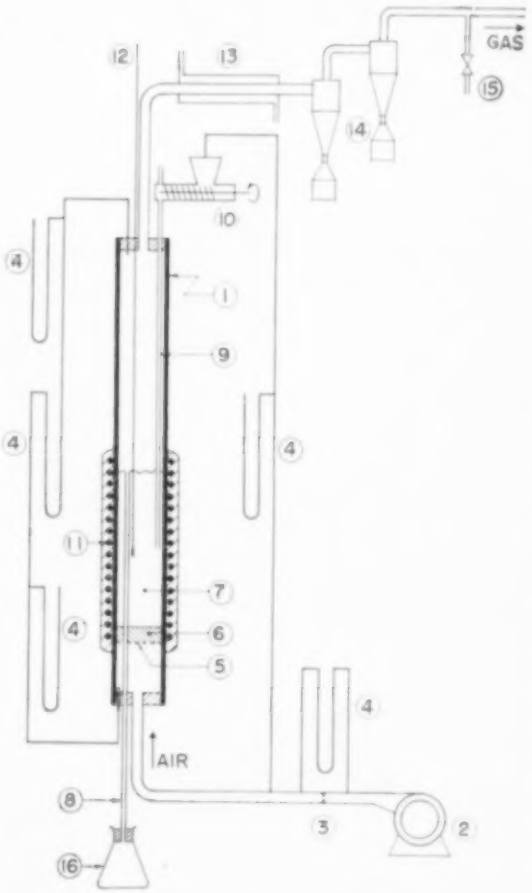

FIG. 10. Experimental reactor used for roasting of zinc blende concentrate [15].

1. Refractory tube I.D. 9·8 cm, height 1 m. 2. Blower. 3. Orifice flowmeter. 4. Mamometer. 5. Screen. 6. Fixed bed as distributor. 7. Fluidized bed. 8. Overflow tube. 9. Feed tube. 10. Feeder. 11. Heater. 12. Thermocouple. 13. Water cooler. 14. Cyclone collector. 15. To gas sampler. 16. Overflow particles.

Table 4. Ranges of experimental conditions in fluidized roasting of zinc blende concentrate with wide size distribution [15].

Composition of ore (%)		Zn 50·5	Fe 8·5	Cu 2·9	Pb 1·4	Cd 0·4	S 30·4
Diameter of reactor		9·8 cm I.D.					
Temperature		700–900 °C					
Weight of bed, W		604–3081 g					
Feed rate of particles, F_0		6·5–25·8 g/min					
Air velocity, u_g		12–45 cm/sec					
Height of fluidized bed		10–42 cm					
Percentage of sulphur dioxide in the produced gas		8·3–11·3%					
Residual sulphur							
overflow	total sulphur	1·1–9·4%					
	sulphide sulphur	0·4–2·5%					
carryover	total sulphur	2·7–11·8%					
	sulphide sulphur	1·3–7·2%					

Equations (17), (18), (19) and (34) of Part I show the interrelationships between the size distribution functions of feed, carryover and overflow particles. Examples of typical size distributions found experimentally for the carryover and overflow are shown in Fig. 12. Comparison of these Figs. 11 and 12 clearly shows the difference in size distribution between feed, carryover and overflow streams.

In order to analyse the experimental data the numerical values of the modified elutriation velocity constant κ^* were calculated from the measured size distributions, by means of equation (18) of Part I, where ψ was assumed to be unity. The relationship between κ^*, particle diameter and velocity are shown in Fig. 13. These data have been added to the general correlation shown in Fig. 4 of Part I. Knowing κ^* allows calculation of the average residence time of particles with diameter x from equations (8) and (29) of Part I. Also the average residence time can be calculated directly from the size frequency distribution functions by means of equation (33) of Part I. One example of the residence time thus determined

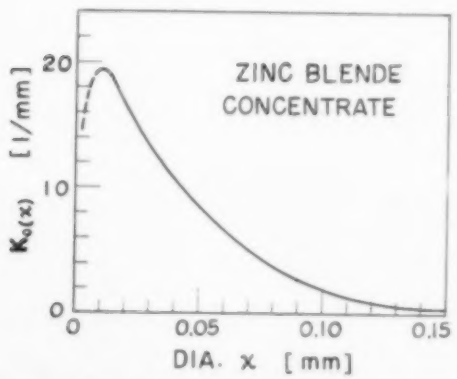

FIG. 11. Size-frequency distribution function of zinc blende concentrate used [15].

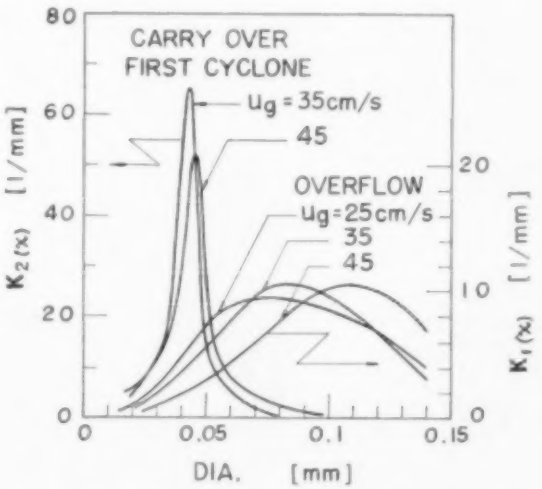

FIG. 12. Size-frequency distribution functions of overflow and carryover particles [15].

may be seen in Fig. 14, and shows that even small particles have fairly long residence times, for example, 30 min for 40 μ particles.

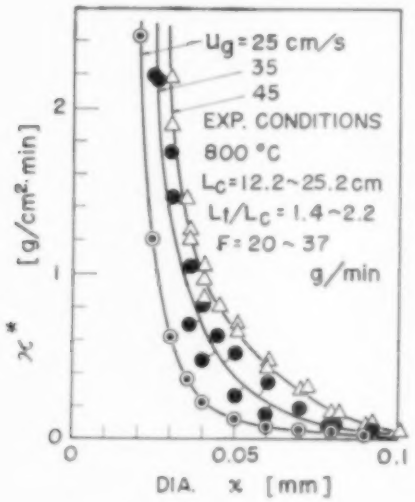

FIG. 13. Modified elutriation velocity constant κ^* obtained from roasting of zinc blende concentrate [15].

Fig. 13 compares the conversions of overflow and carryover particles for the same diameter. Examination shows that within the accuracy of experimental procedures there is no appreciable difference in conversions of overflow and carryover particles. As shown by equations (13) and (14) of Part II the difference between the average conversions of overflow and carryover streams originates in the difference of size frequency distribution. As stated in equations (1) and (2) for chemical reaction controlling:

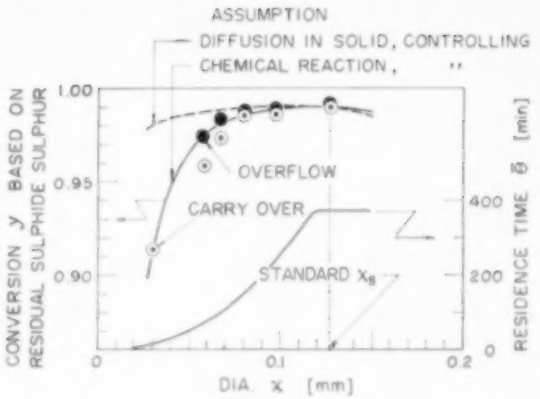

FIG. 14. Comparison of calculated values of conversion y with experimental data [15].
θ: residence time of particles with diameter x mm.
Zinc blende concentrate, 900 °C.

$$\theta_b \propto \theta_0 \propto x \qquad (1')$$

while for diffusion controlling:

$$\theta_b \propto \theta_0 \propto x^2 \qquad (2')$$

Taking $x_s = 0.126$ mm $= 126\ \mu$ as the standard diameter the time necessary for the complete conversion of one particle θ_{bs} with this diameter is calculated as follows:

$$y(x_s) \sim 1 - (1/q)(\theta_{bs}/\bar{\theta}_\cdot) \qquad (4)$$

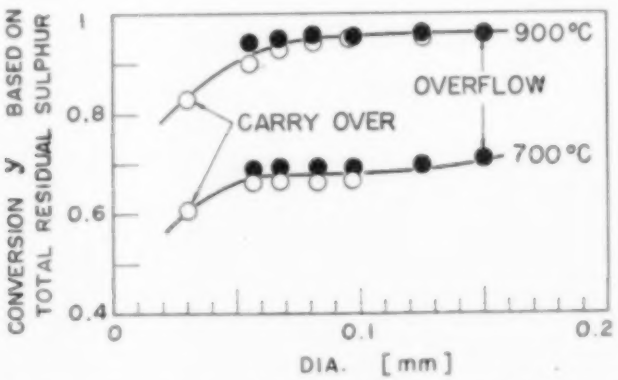

FIG. 15. Conversion y for overflow and carryover particles [15].

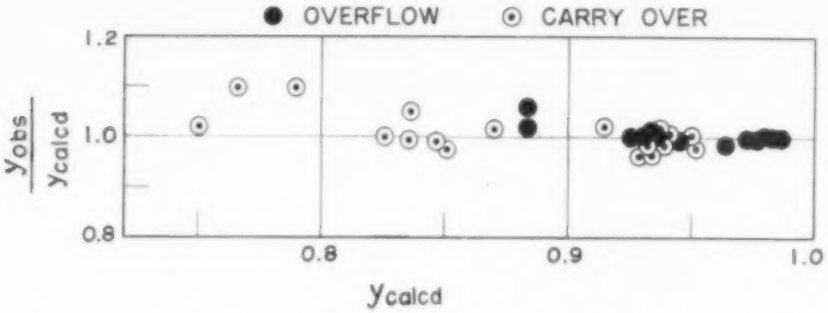

FIG. 16. Comparison of calculated values of conversion y with experimental data.

Here q is 4 for chemical reaction controlling and 5 for solid phase diffusion controlling. Based upon the experimental value of conversion $y(x_s)$ for the standard diameter x_s and applying equations (1′) and (2′), conversions are calculated with equation (3) for each diameter. These are shown in Fig. 14. Fig. 14 shows that the rate controlling mechanism may be determined for small particles, and data indicate that it is the chemical reaction mechanism which controls in the roasting of such fine ore particles. Hence, the conversion for overflow and carryover particles can be written as follows:

$$y_{overflow} = 1 - (\beta F_0/W)(\theta_{bs}/4) \cdot \left[x_s \int_0^{x=x_{max}} K_0(x)(x/x_s)\, d(x/x_s)\right] \quad (5)$$

$$y_{carryover} = 1 - (\beta F_0/W)(\theta_{bs}/4) \cdot \left[x_s \int_0^{x=x_{max}} K_0(x)\{K_2(x)/K_1(x)\}(x/x_s)\, d(x/x_s)\right] \quad (6)$$

Applying the above equations, values of θ_{bs} are calculated. Then from equation (6) of Part II the average value of θ_0/δ is obtained as shown in Table 5.

Comparison of Table 5 with Table 3 indicates that the "contact efficiency of particles in a fluidized bed δ" for a bed consisting of fine particles with a wide size distribution is far less than that value for relatively large particles with uniform diameter.

The calculated values of y by means of Table 5 and equations (5) and (6) agrees closely with experimental data shown in Fig. 16.

Table 5. Necessary time for complete conversion of zinc blende concentrate, θ_0/δ.

Converted to diameter (mm)	0·1			
Temperature (°C)	700	750	800	900
θ_0/δ (min)	72·3	65·3	37·2	10·3

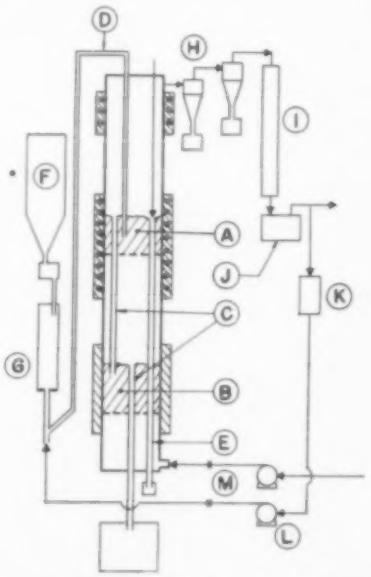

FIG. 17. Experimental reactor for vaporization of sulphur from Matsuo ore [17].
A. Fluidized bed for vaporization of sulphur; I.D. 10 cm. B. Fluidized bed for roasting of pyrite; I.D. 10 cm. C. Overflow tube. D. Feed tube. E. Sampling tube. F. Hopper. G. Feeder. H. Cyclone collector. I. Condenser. J. Scrubbing collector. K. Moisture trap. L. Blowers. M. Flowmeters.

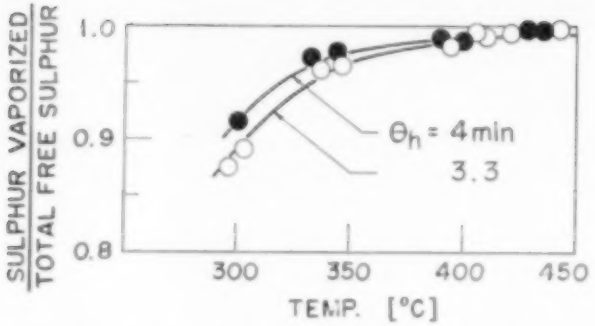

Fig. 18. Vaporization degree of sulphur in upper fluidized bed.

Vapourization of sulphur with two-stage fluidized reactor

A two-stage fluidized-solid reactor was employed for the vapourization of sulphur from pyrite particles containing free sulphur. (Matsuo ore) [17]. In Fig. 17 the raw particles were fed into the upper fluidized bed A and almost all of free sulphur in the particles was vaporized by contacting sulphur dioxide–nitrogen gas of high temperature. From the fluidized bed A the pyrite particles fell into the lower fluidized bed B through the overflow pipe, where they were roasted with the air in order to deliver the necessary heat for the vaporization of sulphur. The conversion for pyrite roasting was fairly high, i.e., 0·87–0·96. Some examples of results for the vaporization of sulphur are shown in Fig. 18.

Assuming the adequacy of equation (10) of Part II, the time necessary for the complete vaporization of sulphur from single particle is calculated. Fig. 19 showing this result indicates a rapid vaporization of sulphur in the fluidized bed.

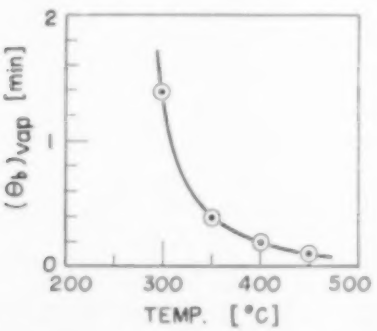

Fig. 19. Necessary time for vaporization of sulphur from Matsuo ore, $D_p = 0{\cdot}22$ mm.

Nitrogenation of Calcium carbide

$$C_a C_2 + N_2 \rightarrow C_a CN_2 + C$$

In order to get the fundamental data for designing a fluidized-solid plant the model reactor with 5·7 cm inner diameter shown in Fig. 20 was employed [18]. Raw particles were fed

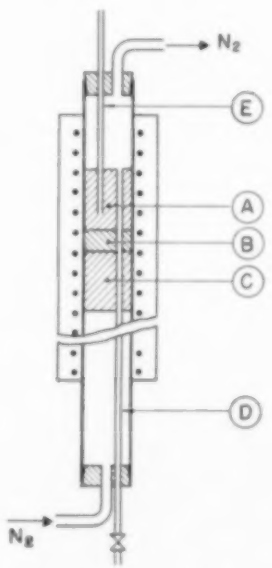

Fig. 20. Experimental reactor for calcium cyanamide [18].
A. Fluidized bed of $CaCN_2$. B. Packed bed of refractory particles. C. Packed bed of activated carbon granules. D. Overflow tube. E. Feed tube.

continuously into the bed by means of screw feeder and pneumatic conveying system. The maximum temperature for suitable fluidization was 1120 °C. One series of experimental data with CaF_2 catalyst (0·3–0·32 per cent of raw material) is analyzed in order to obtain the time necessary for complete conversion θ_b. The results are shown in Fig. 21. In this case, the gas phase is pure nitrogen, hence $\Phi = 1$. Furthermore δ can be assumed unity because the chemical reaction is quite slow [4]. Fig. 21 shows that θ_b is approximately proportional to the particle diameter, indicating that this phenomenon is chemical reaction controlling according to equation (1). Therefore, the temperature dependency of θ_b can be found easily.

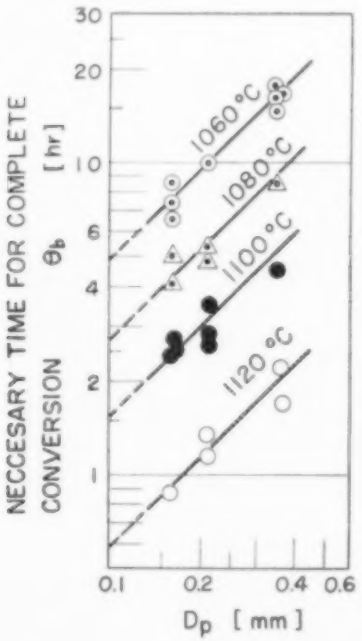

Fig. 21. Necessary time for complete conversion of a particle θ_b, nitrogenation of calcium carbide, catalyst : fluorite (with reactor of 5·7 cm I.D.).

Applying these final results as shown in Fig. 21 the conversions for overflow particles were calculated from equations (1), and (10) of Part II, for a pilot plant with 1 m inner diameter.

This method of analysis is not restricted to systems using CaF_2 catalyst. It has also been applied successfully to systems using KCl, NaCl and $CaCl_2$ catalysts [18]. Considerably good coincidence has been obtained between the estimated values of conversion and the experimental data in the reactors of larger diameters.

Conclusion

Data on conversion factors for product particles obtained for a number of reacting systems under a wide variety of experimental conditions in several experimental fluidized-solid reactors can be analysed satisfactorily with the theoretical equations obtained in Parts I and II.

Close correspondence between theory and the wide range of experimental systems strongly verifies the theory and indicates that it may safely be used for design calculations of equipment and scale-up to large fluidization units.

Acknowledgement—The authors wish to express their appreciation to Prof. O. Levenspiel for his excellent advice and help in the preparation of these papers.

Notation

A_T = sectional area of fluidized bed L^2

C, C_0, C^* = concentration of reactant gas ; arbitrary value, value in inlet flow and equilibrium value on reacting interface, respectively ML^{-3}

ΔC_{av} = average value of driving force for reaction ML^{-3}

C_s, C_{s0} = weight fraction of fine particles ; arbitrary value and initial value, respectively

D_p = particle diameter L

D_{vs} = diffusivity in solid phase $L^2\,T^{-1}$

D = axial diffusion coefficient $L^2\,T^{-1}$

$E_1(\theta_p), E_1(x, \theta_p)$ = exit age-distribution function for overflow stream T^{-1}

$E_2(x, \theta_p)$ = exit age distribution function for carryover stream T^{-1}

e = gas consumption factor

F_0 = mass flow rate of feed rate MT^{-1}

F_1 = mass flow rate of overflow stream MT^{-1}

F_2 = mass flow rate of carryover stream MT^{-1}

G = volume velocity of flowing gas $L^3\,T^{-1}$

g = gravity acceleration $L\,T^{-2}$

h = distance from bottom of bed L

$K_0(x), K_b(x)$, =size frequency distribution function ; for

$K_1(x)$, $K_2(x)$ = feed particles, fluidized bed, overflow particles and carryover particles, respectively L^{-1}

k_c, k_d, $\bar{k}$ = first-order rate coefficient ; of chemical reaction, of diffusion through solid phase and over-all reaction, respectively LT^{-1}

L_c, L_b = height of fluidized bed, in static and fluidized state, respectively L

$dm^*/d\theta_p$ = mass flow rate of reactant gas across the unit area of reaction interface $ML^{-2}T^{-1}$

N = number of particles of size between x and $(x + dx)$

$(N_{Fr})_{ur}$ = modified Froude Number

n_0 = feed rate of particles, number of particles per unit time T^{-1}

n_1, n_2 = discharge rate of particles with diameters between x and $(x + dx)$, number per unit time T^{-1}

Q_0 = weight of tracer particles injected M

ΔQ = weight of tracer particles within collected particles M

R = $D_p/2$ or $x/2$ L

r = radius of reacting interface in solid phase L

u_g, u_m = superficial gas velocity based upon sectional area of bed, terminal velocity of fine particle, respectively LT^{-1}

dV = necessary quantity of reactant gas for particles having unreacted core within the infinitesimal volume $A_T\,dh$ M

W = weight of fluidized bed M

w = weight of one particle with diameter x M

x = particle diameter of particles with wide size distribution L

x_s = diameter of standard particle L

y = conversion of particles with diameter x

y_1, y_2 = average conversions ; of overflow particles and carryover particles respectively

$\bar{y}$ = total conversion of product particles

α = volume of particle corresponding to unit quantity of reactant gas L^3M^{-1}

β = weight ratio of reacted particle to raw particle

δ = contact efficiency of particles with gas stream

ϵ_c = void fraction in statical state

η = number of particles remaining in fluidized bed with diameters between x and $(x + dx)$

η_1, η_2 = number of particles remaining in fluidized bed ; for overflow and carryover particles respectively

θ = time lapse T

θ_b, θ_{bs} = necessary time for complete conversion in fluidized bed for particles with diameter x and for those with diameter x_s respectively T

$\bar{\theta}$ = residence time for particles T

θ_0 = necessary time for complete conversion of one particle in fresh reactant gas T

θ_p = time measured from instance of feeding T

κ = elutriation velocity constant T^{-1}

κ^* = modified elutriation velocity constant $ML^{-2}T^{-1}$

μ = viscosity of gas $ML^{-1}T^{-1}$

ρ_g, ρ_s = density ; for gas and solid particles respectively ML^{-3}

Φ = correction factor for driving force, originating in distribution of reactant gas concentration

ϕ = $\theta_b/\bar{\theta}$

ϕ_s = shape factor

ψ = $K_1(x)/K_b(x)$

$\bar{\psi}$ = mean value of ψ for all values of x

REFERENCES

[1] YAGI S. and KUNII D. *Chem. Engng.* (*Japan*) 1952 **16** 283.

[2] YAGI S. and KUNII D. *J. Chem. Soc., Japan.* (*Industr. Engng. Section*) 1953 **56** 131, 133.

[3] DANCKWERTS P. V. *Chem. Engng. Sci.* 1953 **2** 1.

[4] KAMIYA Y. *Chem. Engng.* (*Japan*) 1955 **19** 412.

[5] LEVA M. *Chem. Engng. Progr.* 1951 **47** 39.

[6] YAGI S. and AOCHI T. Preprint presented at annual meeting of the Society of Chemical Engineers (Japan) in 1956.

[7] YAGI S. and KUNII D. *Proc.* 5th *Inst. Symp. Combustion*, 1955 p. 231. *Chem. Engng* (*Japan*) 1955 **19** 500.

[8] HELLINKX J. R. *Chem. Engng. Sci.* 1954 **3** 209.

[9] YAGI S., KUNII D., NAGANO T. and MINETA N. *J. Chem. Soc.* (*Japan*) (*Industr. Engng. Section*), 1953 **59** 213, 301.

[10] YAGI S., TAKAGI K. and SHIMOYAMA S. *J. Chem. Soc., Japan* (*Industr. Engng. Section*) 1951 **54** 1.

[11] YAGI S., KUNII D., IKEDA Y. and KAMATA T. *Chem. Engng.* (*Japan*) 1955 **19** 402.

[12] YAGI S. and MIYAUCHI T. *Chem. Engng.* (*Japan*) 1953 **17** 382; 1955 **19** 507.

[13] Shen C. Y. and Johnstone H. F. *Amer. Inst. Chem. Engrs. J.* 1955 **1** 349.

[14] Yagi S. and Takagi K. *Chem. Engng.* (*Japan*) 1951 **15** 212, 218, 226.

[15] Yagi S., Kunii D., Nagano T. and Mineta N. *Chem. Engng.* (*Japan*) 1952 **16** 288.

[16] Kunii D. Ph. D. Thesis in Chemical Engineering, University of Tokyo 1958.

[17] Yagi S., Kunii D., Matsuoka T. and Shiba K. *Ann. Report of the Engng. Res. Inst., Fac. Engng., Tokyo Univ,* No. 14, 164 1955.

[18] Yagi S., Kunii D., Shirakawa K., Iwata Y. and Hosaka T. *Ann. Rep. Engng. Inst., Fac. of Engng., Tokyo Univ.*, No. 15, 18 1956.

SELECTION OF CURRENT PAPERS OF INTEREST TO CHEMICAL ENGINEERS

A. K. Ray: Estimation of the critical viscous sub-layer in heat transfer problems. *Appl. Sci. Res.* 1961 A **10** 173–179.

E. M. Sparrow and R. D. Cess: Temperature-dependent heat sources or sinks in a stagnation-point flow. *Appl. Sci. Res.* 1961 A**10** 185–197.

E. H. Wissler and R. S. Schechter: A further note on a diffusion problem with chemical reaction. (See H. A. Lauwerier, *Appl. Sci. Res.* 1959 A8 366) *Appl. Sci. Res.* 1961 A**10** 198–204.

S. C. Gupta: A variational principle for convection of heat in anisotropic media. *Appl. Sci. Res.* 1961 A**10** 229–234.

W. J. Beek and C. A. P. Bakker: Mass transfer with a moving interface. *Appl. Sci. Res.* 1961 A**10** 241–252.

J. Slattery: Flow of a simple non-Newtonian fluid past a sphere. *Appl. Sci. Res.* 1961 A**10** 286–294.

N. C. J. Ros: Flowmeter formulae for critical gas/liquid flow through a restriction. *Appl. Sci. Res.* 1961 A**10** 295–296.

P. Sachs and R. A. K. Long: A correlation for heat transfer in stratified two-phase flow with vaporization. *Int. J Heat Mas Transfer* 1961 **2** 222–230.

M. F. Kazansky, P. P. Latsick and V. N. Oleynikov: Non-stationary temperature and moisture content fields of porous bodies in the convection heat transfer process (i.e. drying porous solids). *Int. J. Heat Mass Transfer* 1961 **2** 231–239.

V. G. Morozov: An experimental study of critical heat loads at boiling of organic liquids on a submerged heating surface. *Int. J. Heat Mass Transfer* 1961 **2** 252–258.

W. R. Schowalter and G. E. Blaker: On the behaviour of impact (i.e. Pitot) tubes at low Reynolds numbers. *J. Appl. Mech.* 1961 **28** 136–137.

J. H. Oxley and J. M. Blocher: Mass and heat transfer during the chemical vapour deposition of metals. *J. Electrochem. Soc.* 1961 **108** 460–464.

R. H. Boll: Calculation of complex equilibrium with an unknown number of phases. *J. Chem. Phys.* 1961 **34** 1108–1110.

G. Houghton, A. S. Keston, J. E. Funk and J. Coull: The solubilities and diffusion coefficients of isobutylene in dimethyl phthalate. *J. Phys. Chem.* 1961 **65** 649–654.

M. Dole: Analysis of the intrinsic viscosity of a polymer undergoing simultaneous cross-linking and degradation. *J. Phys. Chem.* 1961 **65** 700–702.

W. J. Baker and K. R. Keep: The flow of oil and gas mixtures in wells and pipelines: some useful correlations. *J. Inst. Petrol.* 1961 **47** 162–169.

F. C. Haas and A. H. Nissan: Experimental heat transfer characteristics of a liquid in Couette motion and with Taylor vortices. *Proc. Roy. Soc.* 1961 A**201** 215–226.

A. Bournia, J. Coull and G. Houghton: Dispersion of gases in laminar flow through a circular tube. *Proc. Roy. Soc.* 1961 A**201** 227–236.

W. G. Steltz: The critical and two-phase flow of steam. *J. Engng. Power* 1961 **83** 145–154.

G. W. Forman and N. W. Kelly: Cooling-tower fan performance. *J. Engng. Power* 1961 **83** 155–160.

F. A. L. Dullien and M. W. Shemilt: Activity-based diffusion coefficients (i.e. with activity gradient as driving force). *Nature*, Lond. 1961 **190** 526–528.

D. Harrison and L. S. Leung: Bubble formation at an orifice in a fluidized bed. *Nature*, Lond. 1961 **190** 433–434.

P. Barbier: The pneumatic transport of lime. (In French) *Manutention* 1960 **10** 133–138, 147–157.

J. Beranek: The theory of fluidized beds. (In German) *Chem. Tech.* 1960 **12** 515–520.

R. Wenske and D. Gelbin: Multicomponent distillation calculations by a computer. (In German) *Chem. Tech.* 1960 **12** 127–129.

K. Iinoya: Optimum conditions for a pneuamtic conveyor. (In Japanese) *Kagaku Kogaku* 1960 **24** 757–762.

M. James and W. T. Lee: Process control by computer. *Instrum. Pract.* 1961 **15** 305–308.

E. J. Fenech and C. W. Tobias: Mass transfer by free convection at horizontal electrodes. *Electrochim. Acta.* 1960 **2** 311–325.

M. G. Fouad and N. Ibl: Natural convection mass transfer at vertical electrodes under turbulent flow conditions. *Electrochim. Acta* 1960 **3** 233–243.

V. Vanecek: Reactions between granular solids and fluids in continuous reactors. (In Czech.) *Coll. Czech. Chem. Commun.* 1960 **25** 2395–2404.

V. Vanecek, M Markvart and E. Lederer: Fluidized bed drying. (In Czech.) *Chem. Prum.* 1960 **10** 521–525.

R. S. Allan, G. E. Charles and S. G. Mason: The approach of gas bubbles to a gas/liquid interface. *J. Colloid. Sci.* 1961 **16** 150–165.

D. C. Chappelear: Models of a liquid drop approaching an interface. *J. Colloid Sci.* 1961 **16** 186–190.

J. J. VAN DEEMTER and E. T. VAN DER LAAN: Momentum and energy balances for dispersed two-phase flow. *Appl. Sci. Res.* 1961 A **10** 102–108.

D. A. VAN MEEL and H. VERMIJ: A method for flow visualization and measurement of velocity vectors in three-dimensional flow patterns in water models by using colour photography. *Appl. Sci. Res.* 1961 A **10** 109–117.

J. C. MACRAE and W. A. GRAY: Significance of the properties of materials in the packing of real spherical particles. *Brit. J. Appl. Phys.* 1961 **12** 164–171.

W. M. JONES and D. MILLS: Porosity and surface area of a granular bed from measurements of the flow of air through the bed and measurements of the granular shape factors. *Brit. J. Appl. Phys.* 1961 **12** 172–174.

B. P. HUNT: Measurement of the thickness of thin transparent films using fluorescence. *Brit. J. Appl. Phys.* 1961 **12** 175–177.

F. P. BUNDY: Effect of pressure on the e.m.f. of thermocouples. *J. Appl. Phys.* 1961 **32** 483–488.

W. H. REINMUTH: Diffusion to a plane with Langmuirian adsorption. *J. Phys. Chem.* 1961 **65** 473–476.

H. WYCLIFFE: Use of an air bleed when measuring pressure in vacuum processes in which condensable vapours are present. *J. Sci. Instrum.* 1961 **38** 126–129.

D. W. TIMS: A recording flow meter using a radioactive float. *J. Sci. Instrum.* 1961 **38** 145–149.

R. N. CLAYTON: Oxygen isotope fractionation between calcium carbonate and water. *J. Chem. Phys.* 1961 **34** 724–726.

W. J. PANGONIS, W. HELLER and N. A. ECONOMON: Theoretical investigations on the light scattering of colloidal spheres —IX. Lateral scattering at 90° from incident natural and linearly polarized light. *J. Chem. Phys.* 1961 **34** 960–970. X. Scattering ratio and depolarization of light scattered at an angle of observation of 90°. *Ibid.* 1961 **34** 971–979.

A. NARTEN: Fractionation of nitrogen isotopes between nitrosonium salt solutions and nitrogen oxides. *J. Chem. Phys.* 1961. **34** 1056–1057.

P. HERSCH: Localization of ferrous corrosion by azide. *Nature, Lond.* 1961 **190** 250–251.

P. D. BLOORE and J. S. M. BOTTERILL: Similarity in behaviour between gas bubbles in liquid and fluidized solid systems. *Nature, Lond.* 1961 **190** 250–251.

J. W. MULLIN and K. RAVEN: Nucleation in agitated solutions. *Nature, Lond.* 1961 **190** 251.

M. J. COHEN: Two-dimensional gas jets. *J. Appl. Mech.* 1960 **27** 603–608.

W. W. SHORT: Heat transfer and sublimation at a stagnation point in potential flow. *J. Appl. Mech.* 1960 **27** 613–616.

R. H. FOX: An accurate expression for gas pressure drop in high-speed subsonic flow with friction and heating. *J. Appl. Mech.* 1960 **27** 747–748.

P. E. EBERLY and E. H. SPENCER: Mathematics of adsorption for pulse flow through packed columns. *Trans. Faraday Soc.* 1961 **57** 289–300.

N. C. DENO, H. J. PETERSON and E. SACHER: Nitric acid equilibria in water–sulphuric acid. *J. Phys. Chem.* 1961 **65** 199–201.

P. HESTERMANS and D. WHITE: The vapour pressure, heat of vaporization and the heat capacity of methane from the boiling point to the critical temperature. *J. Phys. Chem.* 1961 **65** 362–365.

S. A. RICE and A. R. ALLNATT: Approximate theory of transport in simple dense fluid mixtures. *J. Chem. Phys.* 1961 **34** 409–420.

C. ROSSI and E. BIANCHI: Diffusion of small molecules. *Nature, Lond.* 1961 **189** 822–824.

J. M. BEÉR and R. H. ESSENHIGH: Control of reaction rate in flames. *Nature, Lond.* 1961 **187** 1106–1107.

L. J. CHALLIS, K. DRANSFELD and J. WILKS: Heat transfer between solids and liquid helium—II. *Proc. Roy. Soc.* 1961 A **260** 31–46.

F. L. TEST: The influence of by-pass channels on the laminar flow heat transfer and fluid friction characteristics of shell and tube heat exchangers. *J. Heat Tranfs.* 1961 **83** 39–47.

M. M. CHEN: An analytical study of laminar film condensation—Part 1. Flat plates. *J. Heat Transf.* 1961 **83** 48–54. Part 2. Single and multiple horizontal tubes. *Ibid.* 1961 **83** 55–60.

B. GEBHART: Transient natural convection from vertical elements. *J. Heat Transf.* 1961 **83** 61–70.

F. W. LARSEN and J. P. HARTNETT: Effect of aspect ratio and tube orientation on free convection heat transfer to water and mercury in enclosed circular tubes. *J. Heat Transf.* 1961 **83** 87–93.

J. H. POTTER and M. J. LEVY: The free expansion of dry and moist air. *J. Engng. Ind.* 1961 **83** 97–100.

F. W. G. WARREN: The generation of wave energy at a fluid interface by the passage of a vertically moving slender body. *Quart. J. Roy. Meteorol. Soc.* 1961 **87** 43–54.

M. S. PLESSET and D.-Y. HSIEH: Theory of gas bubble dynamics in oscillating pressure fields. *Phys. Fluids.* 1960 **3** 882–892.

J. R. JONES: Flow of a non-Newtonian liquid in a curve pipe. *Quart. J. Mech. Appl. Math.* 1960 **13** 428–443.

K. WALTERS: The motion of an elastico-viscous liquid contained between coaxial cylinders. (See also J. G. OLROYD, *Quart. J. Mech. Appl. Math.* 1951 **4** 271). *Quart. J. Mech. Appl. Math.* 1960 **13** 444–461.

M. VINOKUR: Kinematical formulation of rotational gas flow. *J. Fluid Mech.* 1960 **9** 533–542.

R. A. Sawyer: The flow due to a two-dimensional jet issuing parallel to a flat plate. *J. Fluid Mech.* 1960 **9** 543–560.

I. Proudman: An example of steady laminar flow at large Reynolds number. *J. Fluid Mech.* 1960 **9** 593–602.

H. W. Liepmann: Gaskinetics and gasdynamics of orifice flow. *J. Fluid Mech.* 1961 **10** 65–79.

W. Eckhaus: Theory of flame-front stability. *J. Fluid Mech.* 1961 **10** 80–100.

B. R. Morton: On a momentum-mass flux diagram for turbulent jets, plumes and wakes. *J. Fluid Mech.* 1961 **10** 101–112.

Y. Chia-Shun: Flow of a homogeneous fluid in a porous medium. *J. Fluid Mech.* 1961 **10** 133–140.

A. McD. Mercer: The growth of the thermal boundary layer at the inlet to a circular tube. *Appl. Sci. Res.* 1960 A **9** 450–456.

W. Squire: A unified theory of turbulent flow—II. (See also *Appl. Sci. Res.* 1959 A **8** 158) *Appl. Sci. Res.* 1960 A **9** 393–410.

W. Squire: A unified theory of turbulent flow—III. *Appl. Sci. Res.* 1961 A **10** 23–44.

P. V. D. Leeden and G. J. Bouwhuis: Tentative rules for shearing stresses in particulate fluidized beds. *Appl. Sci. Res.* 1961 A **10** 78–80.

F. C. Goodrich: The mathematical theory of capillarity—Parts I, II, III. (The shape of fluid interfaces under the conbined action of gravity and surface tension). *Proc. Roy. Soc.* 1961 A **260** 481–509.

P. B. Lorenz: Tortuosity in porous medin. *Nature, Lond.* 1961 **189** 386–387.

J. J. Carberry: Determination of heats of absorption by transient response techniques. *Nature, Lond.* 1961 **189** 391–393.

SELECTION OF CURRENT SOVIET PAPERS OF INTEREST TO CHEMICAL ENGINEERS*

V. I. Brounshtein, L. G. Bykova, V. N. Pokorski, M. A. Ustraikh and M. N. Yablochkina: Experimental examination of the methods for calculation of countercurrent packed and plate columns in the processes of dissolution of a single-component dispersed phase (system toluene–diethylene glycol). *Zh. prikl. Khim.* 1961 **34** 548–557.

I. Ya. Tyurgyaev, A. L. Tsailingold and A. B. Buylov: Effectiveness of gas mixing in a fluidized bed reactor using very fine catalyst particles. *Zh. prikl. Khim.* 1961 **34** 558–564.

V. V. Kafarov and A. S. Bigdorov: Investigation of static pressure of foam on sieve plates. *Zh. prikl. Khim.* 1961 **34** 564–572.

S. K. Ogorodnikov, V. B. Kogan and M. S. Nemtsov: Vapour–liquid equilibrium in systems formed by hydrocarbons and methyl formate. *Zh. prikl. Khim.* 1961 **34** 581–584.

R. V. Kucher, M. A. Korduz and M. E. Teodorovich: On purification of *iso*propylbenzene by adsorption. *Zh. prikl. Khim.* 1961 **34** 598–603.

B. V. Ioffe and O. E. Batagin: Deviations of refractive dispersion of hydrocarbon mixtures from additivity. *Zh. prikl. Khim.* 1961 **34** 603–613.

G. E. Braude and S. F. Shakhova: Solubilities of acetylene and of some higher acetylene hydrocarbons in methanol. *Khim. Prom.* 1961 (3) 177–182.

N. N. Tsyurupa: Determination of size distribution curves for powders. *Khim. Prom.* 1961 (3) 185–190.

N. A. Malafeev, V. A. Malyusov, N. N. Umnik, K. I. Sakodynski and N. M. Zhavoronkov: Determination of coefficients of separation of binary mixtures of tetrachloroalkanes in evaporation under vacuum. *Khim. Prom.* 1961 (3) 196–198.

M. B. Aizenbud and V. V. Dilman: Hydraulics of chemical reactors for gas–liquid systems. *Khim. Prom.* 1961 (3) 199–204.

A. N. Murin: Theory of thermodiffusion columns for the separation of liquids. *Zh. Fiz. Khim.* 1961 **35** 517–520.

D. A. Knyuzev: Calculation of isotope separation factors in ion exchange. *Zh. Fiz. Khim.* 1961 **35** 612–619.

S. M. Khodeeva: Phase equilibria and volume relations in the system acetylene–ammonia at low temperatures. *Zh. Fiz. Khim.* 1961 **35** 629–634.

A. Ya. Deich: Viscosity logarithm and kinematic viscosity in the systems benzene–toluene and *n*-butanol – *tert*-butanol. *Zh. Fiz. Khim.* 1961 **35** 635–637.

V. N. Vigdorovich and A. E. Volpyan: Relation between distribution coefficients expressed by means of concentrations of various components. *Zh. Fiz. Khim.* 1961 **35** 643–646.

M. I. Beigin: Some problems in hydrodynamics of fluidized beds. *Khim. Tekh. Topl. Masel.* 1961 **6** (4) 19–23.

L. A. Bogdanov and M. A. Goldshtik: Effect of wall rotation on the process of separation in a cyclone. *Teploenergetika.* 1961 **8** (4) 58–60.

N. A. Vasilenko and Z. P. Rozenknop: Enrichment of sulphurous gas with simultaneous production of nitrogen fertilizers. *Zh. prikl. Khim.* 1960 **33** 1962–1968.

M. L. Varlamov and O. M. Drobisheva: Investigation of mass transfer and chemisorption in apparatus of venturi type. *Zh. prikl. Khim.* 1960 **33** 2020–2029.

A. I. Rodionov and V. F. Marchenkov: Mass transfer on sieve plates with two types of perforations. *Zh. prikl. Khim.* 1960 **33** 2029–2035.

M. T. Borok: Investigation of the absorption of NO_2, present in microconcentration, by aqueous solutions of salts of aromatic amines. *Zh. prikl. Khim.* 1960 **33** 2035–2042.

A. M. Koganovski and L. A. Stempkovskaya: Adsorption of dissolved substances by a suspended bed of activated charcoal and the gradient of saturation of the bed. *Zh. prikl. Khim.* 1960 **33** 2042–2049.

M. Kh. Kishinevski and L. A. Mochalova: Investigation of the kinetics of extraction in a propeller-stirred tank using the system *n*-heptane–toluene–diethylene glycol. *Zh. prikl. Khim.* 1960 **33** 2049–2056.

B. I. Brounshtein: Method of calculation of the height of counter-current packed and plate columns in the process of dissolution of a one-component dispersed phase. *Zh. prikl. Khim.* 1960 **33** 2056–2062.

E. V. Perov, L. P. Tolmacheva and N. N. Gordeyeva: Solubility of calcium nitrate in nitric acid. *Zh. prikl. Khim.* 1960 **33** 2140–2141.

*To assist readers, translations of any article appearing in the above list can be obtained at a reasonable charge. All orders should be addressed to the Administrative Secretary of the Pergamon Institute at either Headington Hill Hall, Oxford or 122 East 55th Street, New York 22 whichever is more convenient.

E. R. Shenderei, Ya. D. Zelnevski and F. P. Ivanovski: Solubility of carbon dioxide in methylethylketone, ethyl acetate and toluene at low temperatures under pressure. *Khim. Prom.* 1960 (5) 370–374.

D. S. Tsiklis, A. I. Kulikova and L. I. Shenderei: Phase equilibria in the system ethanol–ethylene–water at high temperatures and pressures. *Khim. Prom.* 1960 (5) 401–406.

N. I. Gelperin and V. B. Kvasha: Relationships for the process of mass transfer in rectification cooling of chemical reactors. *Khim. Prom.* 1960 (5) 406–411.

A. Seletski and A. Blyum: Enthalpy – concentration diagram for the system hydrogen – steam. *Khim. Prom.* 1960 (5) 411–413.

L. S. Raginski and A. N. Shirski: Pneumatic pulsator without membrane for pulsed extraction columns. *Khim. Prom.* 1960 (5) 414–419.

B. B. Brandt, L. A. Matov, A. I. Rozlovski and V. S. Khailov: Explosion danger for mixtures of nitrogen oxides with fuel gases and vapours. *Khim. Prom.* 1960 (5) 419–425.

G. B. Narynski: Thermodynamic treatment of experimental data on vapour–liquid equilibrium in the system oxygen –argon. *Zh. Fiz. Khim.* 1960 **34** 1778–1787.

A. N. Nesmeyanov and L. P. Firsova: Determination of equilibrium vapour pressure of solid carbon dioxide. *Zh. Fiz. Khim.* 1960 **34** 1907–1910.

I. A. Rogovaya and M. G. Kaganer: Apparatus for determination of compressibility of gases at pressures up to 200 atm and temperatures from 0 to − 200°C. *Zh. Fiz. Khim.* 1960 **34** 1933–1937.

I. D. Sokolova and V. A. Sokolov: Surface tension of molten salts—I. Technique of measurement. *Zh. Fiz. Khim.* 1960 **34** 1987–1990.

M. G. Kaganer: Investigation of the separation of nitrogen–helium mixtures by diffusion through porous membranes. *Zh. Fiz. Khim.* 1960 **34** 2005–2012.

M. M. Dubinin, M. M. Vyshuyakova, E. G. Zhukovskaya, E. A. Leontev, V. M. Lukyanovich and A. I. Sarakhov: Investigation of the porous structure of solids by sorption methods—V. The application of various methods to the study of the structure of intermediate and micropores of activated carbons. *Zh. Fiz. Khim.* 1960 **34** 2019–2029.

B. S. Petukhov, L. G. Genin and V. L. Malter: Forced convection heat transfer in pipes with internal heat generation within the fluid. *Inzh. Fiz. Zh.* 1960 **3** (9) 3–9.

A. P. Baskakov: The effect of agitation of the material in a fluidized bed on heat transfer between gas and particles. *Inzh. Fiz. Zh.* 1960 **3** (9) 10–16.

V. B. Zenkevich: Application of the similarity method to the study of viscosity of liquid fuels. *Inzh. Fiz. Zh.* 1960 **3** (9) 56–60.

I. V. Krechetov: Development of thermodynamic T–S and H–S diagrams applicable to heat and mass transfer processes. *Inzh. Fiz. Zh.* 1960 **3** (9) 61–64.

A. B. Verzhinskaya and L. N. Novichenok: A new universal method for the determination of thermophysical coefficients. *Inzh. Fiz. Zh.* 1960 **3** (9) 65–68.

A. P. Shushpanov and P. I. Shushpanov: A cylindrical heat source method for determination of thermal properties. *Inzh. Fiz. Zh.* 1960 **3** (9) 74–77.

R. S. Prasolov: Thermal conductivity of a medium with submicroscopic pores. *Inzh. Fiz. Zh.* 1960 **3** (9) 78–82.

G. F. Muchnik: The determination of heat transfer coefficient under quasi-stationary conditions. *Inzh. Fiz. Zh.* 1960 **3** (9) 83–85.

I. L. Lyuboshitis: Determination of optimum conditions for a pneumatic gas dryer operating under variable conditions *Inzh. Fiz. Zh.* 1960 **3** (9) 91–98.

Z. F. Slezenko: A method for measuring the velocity profile of a boundary layer on a non-uniformly heated horizontal flat plate. *Inzh. Fiz. Zh.* 1960 **3** (9) 108–113.

L. D. Meleshko: The determination of the relationship between temperature and crystallization parameters of a substance. *Inzh. Fiz. Zh.* 1960 **3** (9) 114–116.

M. M. Farztdinov: Transmission of heat through a rotating cylinder. *Inzh. Fiz. Zh.* 1960 **3** (9) 117–119.

Ya. Z. Tsypkin: Optimal processes in automatic pulse systems. *Dokl. Akad. Nauk SSSR.* 1960 **134** 308–310.

B. N. Devyatov: General equations describing the interaction of moving media in technical equipment. *Dokl. Akad. Nauk SSSR.* 1960 **134** 639–642.

M. T. Borok: Dependence of the degree of absorption of nitrogen dioxide on its concentration in the gaseous mixture. *Zh. prikl. Khim.* 1960 **33** 1761–1766.

A. G. Morachevski and V. E. Sabinin: Solubility diagrams for the ternary systems caprolactam–water–benzene, caprolactam–water–carbon tetrachloride and caprolactam–water–dichloroethane. *Zh. prikl. Khim.* 1960 **33** 1775–1779.

D. P. Dobochin, L. A. Kachur and O. M. Todes: Model studies of the thermal regime in the process of regeneration of alumina–silicate cracking catalyst. *Zh. prikl. Khim.* 1960 **33** 1779–1783.

I. Ya. Tyuryaev and A. L. Tsailingold: Quantitative characteristics of suspended bed reactors with regard to mixing of solid particles. *Zh. prkl. Khim.* 1960 **33** 1783–1790.

N. M. Zhavoronkov, I. A. Gildenblat and V. M. Ramm: Investigation of mass transfer to a gas stream in packed columns. *Zh. prikl. Khim.* 1960 **33** 1790–1800.

V. P. Postnikov: On heat transfer in a spray scrubber with dispersion of liquid by the gas stream flowing at high velocity. *Zh. prikl. Khim.* 1960 **33** 1801–1808.

B. N. Basargin: On the problem of calculation of mass transfer in rectification columns. *Zh. prikl. Khim.* 1960 **33** 1809–1812.

N. I. Taganov: On the theory of calculation of chemical equipment. *Zh. prikl. Khim.* 1960 **33** 1813–1818.

N. I. Gelperin and N. N. Zelenetski: Vacuum rectification in the production of fragrant substances. *Zh. Vses. Khim. Obshch. Mendeleeva* 1960 **5** (4) 431–437.

M. M. Dubinin, E. G. Zhukovskaya and E. D. Zaverina: On adsorption properties of carbon adsorbents—5. Peculiarities in water vapour sorption by active charcoals in the region of high relative pressures. *Izv. Akad. Nauk SSSR Otd. Khim. Nauk* 1960 (6) 966–975.

L. A. Lovachev: Theory of chain-thermal flame propagation—1. Two active centres. *Izv. Akad. Nauk SSSR, Otd. Khim. Nauk.* 1960 (6) 1022–1029. 2. Two active centres with different diffusion coefficients. *Ibid.* 1960 (7) 1191–1199. 3. Effect of the transfer coefficient on the rate of flame propagation. *Ibid.* 1960 (8) 1354–1357.

B. A. Rudenko, S. S. Yufit, L. N. Ivanova and V. F. Kucherov: The use of gas–liquid chromatography for the analysis of some hydro-carbon mixtures. *Izv. Akad. Nauk Otd. khim. Nauk.* 1960 (7) 1147–1152.

M. M. Dubunin: Theory of physical adsorption of gases and vapours and the adsorption properties of some adsorbents differing in nature and having porous structure. *Izv. Akad. Nauk SSSR, Otd. khim. Nauk.* 1960 (7) 1153–1161.

N. I. Gelperin, B. G. Ainshtein, E. N. Gelperin and S. D. Lvova: Hydrodynamic peculiarities of fluidization of granular materials in conical and conical–cylindrical equipment. *Khim. Tekh. Topl. Masel.* 1960 **5** (8) 51–57.

I. A. Aleksandrov and A. I. Skoblo: Mechanical entrainment of liquid on plates of grid and sieve type. *Khim. Tekh. Topl. Masel* 1960 **5** (9) 42–45.

D. A. Labuntsov: Heat transfer in condensation of steam on a vertical surface under conditions of turbulent flow of the condensate film. *Inzh. Fiz. Zh.* 1960 **3** (8) 3–12.

I. I. Morachevski, R. B. Anognitskaya, E. A. Chumakova and I. G. Bushev: New instruments and methods for studying the mechanism of drying of colloidal capillary-porous materials. *Inzh. Fiz. Zh.* 1960 **3** (8) 13–18.

E. V. Volkov: Rotary movement of a gas in the preaxial zone of a cyclone chamber. *Inzh. Fiz. Zh.* 1960 **3** (8) 26–30.

V. P. Motulevich: Heat transfer and friction of a porous plate in a gas stream during formation of the turbulent boundary layer, with supply of a heterogeneous substance through the pores. *Inzh. Fiz. Zh.* 1960 **3** (8) 31–38.

I. L. Lyuboshits: Investigation of the kinetics of drying in a pneumatic grain dryer of the oscillation type. *Inzh. Fiz. Zh.* 1960 **3** (8) 69–73.

A. T. Nikitin: Temperature distribution in an unbounded hollow cylinder in heat exchange with media of variable temperature at the boundaries. *Inzh. Fiz. Zh.* 1960 **3** (8) 74–77.

M. D. Glinchuk, D. F. Kalinovich, I. I. Kovenski and M. D. Smolin: Method of determining diffusion coefficients in solids. *Inzh. Fiz. Zh.* 1960 **3** (8) 78–81.

A. A. Ots: Motion of particles of variable mass but constant volume. *Inzh. Fiz. Zh.* 1960 **3** (8) 102–106.

I. I. Morozov: Exclusion of aeration of liquids by a turbulent jet. *Inzh. Fiz. Zh.* 1960 **3** (8) 107–109.

L. V. Volodko and D. S. Umreyko: Investigation of mass transfer in colloids. *Inzh. Fiz. Zh.* 1960 **3** (8) 117–119.

T. Misek and J. Hansalek: Transfer of heat and mass in a continuous gas washer. *Chem. Průmysl.* 1960 **10** 346–350. (In Czech.).

P. Szolcsanyi: Minimum particle speed in fluidized beds. *Veszprémi Vegyipari Egyetem Közleményei.* 1958 **2** 41–47. Particle speed range in fluidized beds. *Ibid.* 1958 **2** 49–55. Migration velocity of voids in beds fluidized with a gas stream. *Ibid.* 1958 **2** 85–91. (In Hungarian).

T. Blickle: Particle movement in the fluidized state. *Veszprémi Vegyipari Egyetem Közleményei.* 1958 **2** 323–330. (In Hungarian).

G. D. Efremova and G. G. Leonteeva: Solubility of melamine in solutions of dicyandiamide in liquid ammonia. *Khim. Prom.* 1960 (8) 626–627.

M. S. Nemtsov: Kinetic relationships in the interaction of olefins with sulphuric acid. *Khim. Prom.* 1960 (8) 633–641.

V. M. Platonov, B. G. Bergo, Ya. D. Monko and B. O. Kogan: Calculation of rectification of close-boiling mixtures using a digital computer. *Khim. Prom.* 1960 (8) 656–660.

O. L. Bruk: A general method for calculation of multistage counter-current slurry washers. *Khim. Prom.* 1960 (8) 660–666.

N. S. Torocheshnikov, N. V. Keltsev and Zh. A. Dzharilkanova: New adsorbent for acetylene. *Zh. Vses. Khim. Obshch. Mendeleeva.* 1960 **5** (6) 710–712.

Ya. I. Kogan and Z. A. Burnasheva: Growth and measurement of condensation nuclei in a continuous stream. *Zh. Fiz. Khim.* 1960 **34** 2630–2639.

V. B. Kogan: Method of testing of vapour–liquid equilibrium data of ternary systems with a non-volatile component. *Zh. Fiz. Khim.* 1960 **34** 2834–2837.

S. Sh. Byk and R. P. Kirsanova: Separation of some gaseous hydrocarbon mixtures by diffusion through microporous organic membranes. *Zh. Fiz. Khim.* 1960 **34** 2844.

E. F. Yamschikov: Correction of the refractive index of *n*-pentane. *Zh. Fiz. Khim.* 1960 **34** 2845.

B. P. Konstantinov and L. V. Kotova: The rate of axial mixing in exchange columns for separation of isotopes. *Dokl. Akad. Nauk SSSR.* 1960 **135** 896–898.

B. I. Davidov: Contribution to the statistical dynamics of an incompressible turbulent fluid. *Dokl. Akad. Nauk SSSR.* 1961 **136** 47–50.

A. M. Rozen, V. A. Vasilev, L. P. Gorshkova and A. I. Bezzubova: On the mechanism of processes in packed pulsed columns. *Dokl. Akad. Nauk SSSR.* 1961 **136** 401–404.

M. M. Farztdinov: Measurement of the complex temperature field in walls subjected to convection heating. *Inzh. Fiz. Zh.* 1960 **3** (12) 11–16.

V. I. Ignatyev and N. I. Zvelev: Sedimentation of particles of an aerosol on a cylinder. *Inzh. Fiz. Zh.* 1960 **3** (12) 17–23.

L. A. Kozdoba and V. I. Makhnenko: Electric analogue of non-stationary temperature fields with variable heat generation. *Inzh. Fiz. Zh.* 1960 **3** (12) 24–28.

G. D. Rabinovich: Heat and mass transfer in a bed of moist material. *Inzh. Fiz. Zh.* 1960 **3** (12) 29–34.

J. Ciborowski and B. Steplewski: Investigation of the effect of roughness of material on the rate of drying by infra-red radiation. *Inzh. Fiz. Zh.* 1960 **3** (12) 35–42.

P. V. Tsoi: Heat and moisture transfer during evaporation under boundary conditions of the second type. *Inzh. Fiz. Zh.* 1960 **3** (12) 53–57.

N. I. Gamayunov: Criteria of non-isothermal transfer. *Inzh. Fiz. Zh.* 1960 **3** (12) 58–62.

V. I. Lebedev: Investigation of the effect of the degree of blackness of a medium on heat transfer in a furnace chamber. *Inzh. Fiz. Zh.* 1960 **3** (12) 81–85.

A. E. Alumyae: Effect of moisture movement on heat transfer during determination of thermal coefficients. *Inzh. Fiz. Zh.* 1960 **3** (12) 107–110.

O. M. Todes: Survey of work on fluidization in Poland. *Inzh. Fiz. Zh.* 1960 **3** (12) 123–139.

D. L. Timrot and V. P. Borisoglavski: Experimental investigation of the density of liquid oxygen at temperatures from –190 to –120°C and pressures up to 200 kg/cm² including the saturation curve. *Inzh. Fiz. Zh.* 1961 **4** (1) 3–13

A. S. Predvoditelev: Rates of chemical reactions in turbulent flow—II. *Inzh. Fiz. Zh.* 1961 **4** (1) 14–21.

L. A. Movsesyan: Transient flow of a compressed liquid in long pipelines. *Inzh. Fiz. Zh.* 1961 **4** (1) 22–26.

E. P. Dudikova: Determination of temperature during heat transfer under turbulent conditions. *Inzh. Fiz. Zh.* 1961 **4** (1) 27–30.

V. A. Rabinovich and G. I. Tsoiman: Equation of state and thermodynamic properties of liquid ammonia. *Inzh. Fiz. Zh.* 1961 **4** (1) 31–36.

A. A. Zhukauskas, A. A. Shlanchyauskas and A. P. Yaronis: Investigation of the effect of ultrasonic waves on heat transfer in liquids. *Inzh. Fiz. Zh.* 1961 **4** (1) 58–62.

E. V. Kudryavtsev and N. V. Shumanov: Effect of dimensions and type of solid on the process of non-stationary heat transfer. *Inzh. Fiz. Zh.* 1961 **4** (1) 63–70.

G. P. Stelmakh and V. K. Stolyakov: Heating of a friable material by a solid heat transfer medium. *Inzh. Fiz. Zh.* 1961 **4** (1) 71–75.

I. L. Lyuboshits: Heating of a dispersed material in a radiation heat exchanger. *Inzh. Fiz. Zh.* 1961 **4** (1) 76–81.

V. S. Usenko: Experimental verification of calculated formulae for axially symmetrical filtration. *Inzh. Fiz. Zh.* 1961 **4** (1) 92–97.

V. S. Ermakov, I. P. Zhuk and O. I. Yaroshevich: Calculation of temperatures in heat generating elements of a nuclear reactor under transient conditions. *Inzh. Fiz. Zh.* 1961 **4** (1) 104–108.

Y. Z. Kazavchinski and A. G. Tabachnikov: Equation of state for the stoichiometric mixture of nitrogen and hydrogen. *Inzh. Fiz. Zh.* 1961 **4** (1) 116–119.

K. L. Sheptunov: Dependence of thermal conductivity on temperature difference in friable and monolithic materials. *Inzh. Fiz. Zh.* 1961 **4** (1) 127–130.

G. I. Luzhnov, N. I. Zverev and A. F. Gavrilov: Experimental determination of resistance coefficients in pneumatic transport of pig iron. *Teploenergetika.* 1961 **8** (1) 15–18.

F. P. Kazakevich: Effect of roughness on the aerodynamic resistance of pipe bundles in transverse flow of gas. *Teploenergetika.* 1961 **8** (1) 56–58.

S. I. Kosterin, N. I. Semenov and A. A. Tochigin: Relative velocities in steam-water flow in vertical unheated pipes. *Teploenergetika.* 1961 **8** (1) 58–65.

K. I. Lopatin: Relationships in the process of absorption of hydrogen sulphide and carbon dioxide by solutions of triethanolamine. *Zh. prikl. Khim.* 1961 **34** 265–272.

Yu. P. Karetnikov and V. N. Tarasova: Effect of motion in a solution on incrustation in crystallization of salts. *Zh. prikl. Khim.* 1961 **34** 282–287.

B. G. Rabovski and V. S. Shinyaeva: Correlation of molecular and eddy diffusion in mass transfer in the gaseous phase. *Zh. prikl. Khim.* 1961 **34** 287–291.

M. M. Dubinin: On types of industrial active charcoal for application as adsorbents. *Zh. prikl. Khim.* 1961 **34** 291–299.

I. S. Pavlushenko, N. M. Smirnov and P. G. Romankov: On the effect of mixing on the process of chemical change. *Zh. prikl. Khim.* 1961 **34** 312–319.

S. K. Ogorodnikov, V. B. Kogan and M. S. Nemtsov: Vapour–liquid equilibrium in binary systems formed by hydrocarbons and acetone. *Zh. prikl. Khim.* 1961 **34** 323–331.

I. Ya. Tyuryaev and A. V. Erofeyeva: Kinetic relationships in dehydrogenation of butane in a fluidized catalyst bed. *Zh. prikl. Khim.* 1961 **34** 370–375.

M. P. Susarev: Vapour–liquid equilibrium in the system water – dimethylformamide. *Zh. prikl. Khim.* 1961 **34** 412–415.

T. I. Kunin, A. A. Shutov and L. I. Pankratova: Specific heats of aqueous solutions of mixtures of sulphuric and nitric acids. *Zh. prikl. Khim.* 1961 **34** 451–454.

V. M. Platonov and B. G. Bergo: Calculation of rectification, including thermal interaction of streams, on a large digital computing machine. *Khim. Prom.* 1961 (2) 118–122.

Yu. G. Zelinski and V. V. Kafarov: Hydrodynamic regimes on perforated plates. *Khim. Prom.* 1961 (2) 122–126.

V. A. Chemezov and G. P. Baranov: Investigation of filtration properties of filter aids. *Khim. Prom.* 1961 (2) 127–129.

F. Ya. Revzin: New methods for purification of technical gases from hydrogen sulphide and carbon dioxide. *Khim. Prom.* 1961 (2) 130–133.

A. S. Zheleznyak and A. I. Levin: Azeotropy in binary systems of low molecular monobasic organic acids and water. *Zh. Fiz. Khim.* 1961 **35** 322–326.

V. N. Orlov and A. N. Planovski: Effect of vapour velocity on mass transfer coefficients in vapour and liquid phases for the process of rectification in plate equipment. *Khim. Tekh. Topl. Masel.* 1961 **6** (3) 7–10.

E. Ya. Barsukov and G. S. Enokhin: Methods of removal of entrained dust from cyclones in fluidized bed equipment. *Khim. Tekh. Topl. Masel.* 1961 **6** (3) 36–39.

V. I. Subbotin, P. A. Ushakov and A. V. Zhukov: Investigation of heat transfer in longitudinal flow of water along a pipe bundle with relative pitch of 1·4. *Inzh. Fiz. Zh.* 1961 **4** (3) 3–9.

B. S. Petukhov and F. F. Tsvetkov: Calculation of heat transfer in laminar flow of liquids through pipes at low Peclet number. *Inzh. Fiz. Zh.* 1961 **4** (3) 10–17.

D. M. Apter and Z. F. Chukhanov: Motion of reacting solid particles. *Inzh. Fiz. Zh.* 1961 **4** (3) 26–30.

N. B. Kondukov: Hydrodynamic properties and similarity conditions in unsteady-state fluidization. *Inzh. Fiz. Zh* 1961 **4** (3) 31–38.

M. F. Kazanski: Effect of temperature on the state of adsorbed capillary moisture in the macropores of a dispersed substance. *Inzh. Fiz. Zh.* 1961 **4** (3) 53–57.

G. D. Rabinovich: Transient cooling of a limited volume of fluid. *Inzh. Fiz. Zh.* 1961 **4** (3) 58–63.

G. F. Muchnik: Solution of heat conduction problems by the grid method. *Inzh. Fiz. Zh.* 1961 **4** (3) 72–82.

G. P. Filipova and I. P. Ishkin: Viscosity of air, nitrogen and argon at low temperatures and pressures up to 150 atm. *Inzh. Fiz. Zh.* 1961 **4** (3) 105–109.

M. A. Kaganov, I. S. Lisker and A. F. Chudnovski: Velocity method of determining heat conduction of semiconducting materials. *Inzh. Fiz. Zh.* 1961 **4** (3) 110–112.

L. A. Brovkin: Error of transient methods for the determination of thermal coefficients of hygroscopic substances. *Inzh. Fiz. Zh.* 1961 **4** (3) 127–130.

B. S. Petukhov and A. Ya. Yushin: Heat transfer in laminar and transition regimes of liquid metal flow. *Dokl. Akad. Nauk SSSR.* 1961 **136** 1321–1324.

I. A. Charny, D. S. Vilker, B. I. Mitelman and F. D. Rozenberg: Two-phase supersonic flow. *Dokl. Akad. Nauk SSSR.* 1961 **137** 48.

V. I. Ignatyev and N. I. Zverev: Flow of air, carrying dust, past a cylinder. *Teploenergetika.* 1961 **8** (3) 13–16.

V. I. Tolubinski and V. M. Legki: Heat transfer from compact staggered tube bundles in transverse flow. *Teploenergetika.* 1961 **8** (3) 53–56.

V. P. Isachenko and V. V. Vzorov: Mass transfer in evaporation of water from porous walls contacted with air. *Teploenergetika.* 1961 **8** (3) 57–61.

M. S. Pirogov: Heat transfer to sodium at low Peclet numbers. *Teploenergetika.* 1961 **8** (3) 62–64.